
Rational design of polyfluorinated & enzyme-degradable peptide-based biomaterials

Inaugural-Dissertation
to obtain the academic degree
Doctor rerum naturalium (Dr. rer. nat.)

submitted to the Department of Biology, Chemistry, Pharmacy
of Freie Universität Berlin

by
Suvrat Chowdhary
from Berlin, Germany

April 2023

The research presented in this doctoral thesis was performed under the supervision of Prof. Dr. Beate Koksch from April 2019 until April 2023 at the Institute of Chemistry and Biochemistry in the Department of Biology, Chemistry, Pharmacy of Freie Universität Berlin.

1st reviewer: Prof. Dr. Beate Koksch (Freie Universität Berlin)

2nd reviewer: Prof. Dr. Rainer Haag (Freie Universität Berlin)

Date of defense: 07.09.2023

Declaration of Authorship

I hereby confirm that I have prepared this dissertation entitled “Rational design of polyfluorinated & enzyme-degradable peptide-based biomaterials” solely by myself and independently. All external sources and resources have been specified and correctly cited or acknowledged. This thesis has not been submitted, accepted, rated as insufficient, or rejected in any other doctorate degree procedure.

Berlin, April 2023

Suvrat Chowdhary

Publications

(7) M. F. Khan, **S. Chowdhary**, B. Kokschi, C. D. Murphy, *Biodegradation of amphipathic fluorinated peptides reveals a new bacterial defluorinating activity and a new source of natural organofluorine compounds*, manuscript submitted (14.02.2023).

(6) **S. Chowdhary**, T. Pelzer, M. Saathoff, E. Quaas, J. Pendl, M. Fulde, B. Kokschi, *Fine-tuning the antimicrobial activity of β -hairpin peptides with fluorinated amino acids*, *Pept. Sci.*, **2023**, e24306.
(DOI: 10.1002/pep2.24306)

(5) T. Hohmann[†], **S. Chowdhary**[†], K. Ataka, J. Er, G. H. Dreyhsig, J. Heberle, B. Kokschi, *Introducing Aliphatic Fluoropeptides: Perspectives on Folding Properties, Membrane Partition and Proteolytic Stability*, *Chem. Eur. J.*, **2023**, e202203. --- († = **authors contributed equally**)
(DOI: 10.1002/chem.202203860)

(4) R. Fernandes, **S. Chowdhary**, N. Mikula, N. Saleh, K. Kanevche, H. v. Berlepsch, N. Hosogi, J. Heberle, M. Weber, C. Böttcher, B. Kokschi, *Cyanine Dye Coupling Mediates Self-assembly of a pH Sensitive Peptide into Novel 3D Architectures*, *Angew. Chem. Int. Ed.*, **2022**, e202208647.
(DOI: 10.1002/ange.202208647)

(3) T. Hohmann, M. Dyrks, **S. Chowdhary**, M. Weber, D. Nguyen, J. Moschner, B. Kokschi, *Gram-Scale Asymmetric Synthesis of Fluorinated Amino Acids Using a Chiral Nickel(II) Complex*, *J. Org. Chem.*, **2022**, *87*, 16, 10592–10604.
(DOI: 10.1021/acs.joc.2c00522)

(2) **S. Chowdhary**, R. F. Schmidt, A. K. Sahoo, T. tom Dieck, T. Hohmann, B. Schade, K. Brademann-Jock, A. F. Thünemann, R. R. Netz, M. Gradzielski, B. Kokschi, *Rational design of amphiphilic fluorinated peptides: evaluation of self-assembly properties and hydrogel formation*, *Nanoscale*, **2022**, *14*, 10176–10189.
(DOI: 10.1039/d2nr01648f)

(1) **S. Chowdhary**, J. Moschner, D. J. Mikolajczak, M. Becker, A. F. Thünemann, C. Kästner, D. Klemczak, A.-K. Stegemann, C. Böttcher, P. Metrangolo, R. R. Netz, B. Kokschi, *The Impact of Halogenated Phenylalanine Derivatives on NFGAIL Amyloid Formation*, *ChemBioChem*, **2020**, *21*, 3544–3554.

--- **VIP Paper, Cover image** ---

(DOI: 10.1002/cbic.202000373)

Oral presentations

- *“Der Einfluss fluorierter Aminosäure-Seitenketten auf das Faltung- und Assemblierungsverhalten eines amphipathischen Peptidmotives”*; 19. Deutscher Fluortag, Schmittchen, Germany, 19/09-21/09/**2022**.
- *“Rational Design of Amphiphilic Fluorinated Peptides: Evaluation of Self-Assembly Properties and Hydrogel Formation”*; colloquium of the CRC 1349 “Fluorine-Specific Interactions: Fundamentals and Functions”, Berlin, Germany, 09/12/**2021**.
- *“Development of highly fluorinated self-assembling oligopeptides”*; colloquium of the CRC 1349 “Fluorine-Specific Interactions: Fundamentals and Functions”, Berlin, Germany, 26/10/**2020**.
- *“Mono- and trifluorethylglycin-oligomers: synthesis, conformation, and protease stability”*, network meeting of the CRC 1349 “Fluorine-Specific Interactions: Fundamentals and Functions,” Berlin, Germany, 15/08/**2019**.

Posters

- *“Self-assembly properties of polyfluorinated amphipathic peptides: a systematic study”*; 20th European Symposium on Fluorine Chemistry, Berlin, Germany, 14/08 – 19/08/**2022**.
- *“Rational design of amphiphilic fluorinated peptides: evaluation of self-assembly properties and hydrogel formation”*; 25th Winter Fluorine Conference, Clearwater (Florida), United States of America (USA), 16/01 – 21/01/**2022**.
- *“Rational Design of Amphiphilic Fluorinated Peptides: Evaluation of Self-Assembly Properties, Hydrogel Formation and Biocompatibility”*; colloquium of the CRC 1349 “Fluorine-Specific Interactions: Fundamentals and Functions”, Berlin, Germany, 27/08/**2021**.
- *“Amyloid Formation of Halogenated NFGAIL Variants”*; Tag der Chemie 2021, Berlin, Germany, 06/07/**2021**.
- *“Amyloid Formation of Halogenated NFGAIL Variants”*; 19th European Symposium on Fluorine Chemistry, Warsaw, Poland, 25/08 – 31/08/**2019**. (**Poster Prize**)

Acknowledgments

First and foremost, I would like to thank my doctoral supervisor Prof. Dr. Beate Koksche for the opportunity to work on this doctoral thesis in her laboratories! I greatly appreciate her constant interest and willingness to discuss my research projects. Herzlichen Dank dir für alles, Chefin!

I also thank Prof. Dr. Rainer Haag for being the second supervisor of this dissertation and for the annual project meetings with a multitude of productive feedback!

I would like to thank the Deutsche Forschungsgemeinschaft (DFG) in context of the collaborative research center CRC 1349 "Fluorine-specific interactions" for financial support.

Also, I would like to thank the Koksche group for the productive working environment and the pleasant cooperation over the past years.

Especially, I would like to thank Dr. Jakob Leppkes, Dr. Dorian J. Mikolajczak, Dr. Rita Fernandes, and Michael Dyrks for the delightful joint lab time. I am also grateful to Dr. Allison Berger, Dr. Susanne Huhmann, and Dr. Johann Moschner for the extensive introduction to several methods, assays, and techniques.

Moreover, many thanks go to Dr. Katharina Hellmund for introducing me to the exciting world of peptide-based hydrogels!

In fact, I would like to take this opportunity to deeply thank Thomas Hohmann for the fruitful partnership, as well as countless hours which we spent together in the laboratory, on conference trips, or in the shared office. He was a great lab-mate, whose scientific input led to significant results in our shared projects. Now we're no longer connected through the lab but instead a wonderful friendship that means a lot to me.

Furthermore, I would like to thank my students Tiemo tom Dieck, Gesa H. Dreyhsig, and Tim Pelzer for their experimental support.

This doctoral thesis is the result of several successful collaborations with designated scientists. Therefore, I would like to greatly thank Dr. Boris Schade and Benedikt Kirmayer for countless TEM measurements, analyses, and discussions. I sincerely thank Robert F. Schmidt & Prof. Dr. Michael Gradzielski for the rheological measurements and Dr. Anil K. Sahoo & Prof. Dr. Roland R. Netz for applying MD simulations. Furthermore, I thank Mareike Saathoff & Prof. Dr. Marcus Fulde for the MIC data sets and Dr. Andreas F. Thünemann for executing SAXS measurements. At last, many thanks are dedicated to Dr. Kenichi Ataka & Prof. Dr. Joachim Heberle for SEIRAS experiments.

I would like to extend my sincere thanks to Dr. Mohd Faheem Khan & Prof. Dr. Cormac D. Murphy for ongoing digestion studies on the biodegradability of herein reported polyfluorinated SAPs and their outstanding hospitality during my research stay at the University College Dublin. I really enjoyed this excellent and intensive introduction to micro- and molecular biology!

Also, I need to show my appreciation to all my friends for their continuous support! In particular, I would like to thank my dear friend Daniel Braatz for the many years of friendship and support during my studies and doctoral work!

Most importantly, I am so grateful to my family for their emotional and financial support during the last few years. Their trust in my actions and their permanent encouragement helped me to manage this doctorate.

Finally, I would like to thank my one and only love, Nicole, from the bottom of my heart for all her support, especially during the peak times of the Corona Pandemic and beyond. In the most difficult times, she always stood by my side with pleasant advice and steady confidence. You are the fulfilled dream of my life. Love you so much!

“It's the first page of the second chapter.”

H.P. Baxxter (1998)

Abstract

Amphiphilic peptide-based biomaterials are of great interest for pharmaceutical and biomedical applications and mainly associated with pronounced biocompatibility and biodegradability. In fact, introducing fluorine-containing amino acids into peptides & proteins offers an unique opportunity to enhance their biophysical properties such as membrane permeability. Through its influence on hydrophobicity and polarity, the degree of fluorination dictates the extent of fluorine-specific interactions on peptide folding and stability, intermolecular interactions, and biological activity.

The first study of this doctoral thesis describes the folding, self-assembly, and hydrogelation of single-strand amphipathic peptides with different degrees of fluorination on the amino acid side chains by the iterative incorporation of monofluoroethylglycine (MfeGly), difluoroethylglycine (DfeGly), and trifluoroethylglycine (TfeGly). A combination of experimental and theoretical approaches proved a higher degree of side chain fluorination to promote β -sheet formation and the rheological stability of peptide-based hydrogels in physiological conditions, whereas secondary structure formation was inhibited at a low fluorine content due to fluorine-induced polarity.

In a follow-up study, the selective modification of antimicrobial peptides (AMPs) by fluorinated amino acids was investigated. A β -hairpin-forming peptide motif, whose amphipathic structure enables the targeted disruption of bacterial cell membranes, was therefore examined. Extensive MIC screening with Gram-negative and Gram-positive bacteria confirmed highly fluorinated amino acids such as trifluoroethylglycine (TfeGly) or pentafluoropropylglycine (PfpGly) to strengthen the bioactivity of the AMPs through enhanced intrinsic hydrophobicity without causing a simultaneous increase in toxic & hemolytic properties.

Numerous studies on the singular incorporation of fluorinated amino acids have been published to date, whereas synthetic peptides with larger or exclusive amounts of these building blocks remained unexplored. That drove the motivation for the herein-described development and characterization of so-called "fluoropeptides". In brief, β -sheet to α -helix or fluorine-induced PPII-helix transitions were observed in SDS-supplemented buffer (pH 7.4). *In situ* SEIRAS experiments with POPC:POPG-based membrane models functioned to investigate the fluoropeptide's lipid insertion and (re)folding. Thus, the

highest α -helical secondary structure content was found for the nonfluorinated homooligopeptide and decreased in the order of tri-, di-, and mono-fluorination of the side chains.

An important focus of this doctoral thesis was the evaluation of biodegradability for especially higher polyfluorinated sequences. In fact, all peptides prepared in this work could be hydrolyzed by various proteases regardless of the fluorine content. In cooperation with the University College Dublin, first data on the microbial digestion of fluorinated peptides and individual amino acids could be generated. The enzyme-catalyzed cleavage of the C-F bond on the side chain for both kind of substrates was, for instance, proven by detection of released fluoride ions in solution.

The results of this work will contribute to the rational design and potential application of polyfluorinated peptides, whose enzymatic degradability is going to be of great interest for the future development of fluorinated biomaterials.

Kurzzusammenfassung

Amphiphile peptidbasierte Biomaterialien sind vom großen Interesse für pharmazeutische und biomedizinische Anwendungen und überzeugen zumeist durch ihre Biokompatibilität und Bioabbaubarkeit. Die Einführung von fluorhaltigen Aminosäuren in Peptide & Proteine bietet hierbei die einzigartige Möglichkeit, ihre biophysikalischen Eigenschaften wie etwa die Membranpermeabilität zu verstärken. Insbesondere der Fluorierungsgrad spielt eine entscheidende Rolle, da er durch seinen Einfluss auf die Hydrophobie und Polarität die Gesamtheit fluor-spezifischer Wechselwirkungen auf die Peptidfaltung und -stabilität, intermolekularen Wechselwirkungen und biologische Aktivität steuern kann.

Die erste Studie dieser Doktorarbeit beschreibt die Faltung, Selbstassemblierung und Hydrogelierung von einzelsträngigen amphipathischen Peptiden mit unterschiedlichen Fluorierungsgraden der Aminosäureseitenketten durch den iterativen Einbau von Monofluorethylglycin (MfeGly), Difluorethylglycin (DfeGly) und Trifluorethylglycin (TfeGly). Mittels einer Kombination aus experimentellen und theoretischen Ansätzen konnte gezeigt werden, dass bei physiologischen Bedingungen ein höherer Fluorierungsgrad die Bildung von β -Faltblattstrukturen und die rheologische Stabilität der peptid-basierten Hydrogele fördert, jedoch diese Sekundärstruktur von Peptiden mit niedrigem Fluorgehalt durch die fluor-induzierte Polarität inhibiert wird.

In einer weiteren Studie wurde die gezielte Modifizierung der biologischen Eigenschaften antimikrobieller Peptide (AMP) durch den Einbau fluorierter Aminosäuren untersucht. Hierzu wurde ein β -Hairpin bildendes Peptidmotiv ausgewählt, dessen amphipathische Struktur die zielgerichtete Disruption bakterieller Zellmembrane ermöglicht. Die ermittelten minimalen Hemmkonzentrationen (MHK) gegen verschiedene Gram-negative und Gram-positive Bakterien zeigen, dass hochfluorierte Aminosäuren wie Trifluorethylglycin (TfeGly) und Pentafluorpropylglycin (PfpGly) die Bioaktivität antimikrobieller Peptide durch Erhöhung der intrinsischen Hydrophobie selektiv verstärken können, ohne eine gleichzeitige Zunahme toxischer & hämolytischer Eigenschaften zu verursachen.

Zahlreiche Studien zum singulären Einbau fluorierter Aminosäuren wurden bis dato veröffentlicht, während synthetische Peptide mit größeren bzw. ausschließlichen Mengen dieser Bausteine unerforscht blieben. Dies war die Motivation zur Entwicklung und

Charakterisierung sogenannter "Fluoropeptide". In SDS-beihaltenden Puffer (pH 7.4) wurden, unter anderem, Übergänge von β -Faltblatt Strukturen zu α -Helices oder Fluor-induzierte PPII-Helices beobachtet. *In-situ* SEIRAS-Studien mit POPC:POPG-basierten Membranmodellen dienten zum Studium der Lipidinsertion und (Rück-)Faltung der Fluoropeptide in Abhängigkeit zum gesamten Fluoranteil. Hierbei wurde der höchste Gehalt an α -helikaler Sekundärstruktur für das nichtfluorierte Homooligopeptid bestimmt, welcher in der Reihenfolge der Tri-, Di- und Monofluorierung der Seitenkette abnahm.

Ein wichtiger Schwerpunkt dieser Doktorarbeit war die Bewertung der biologischen Abbaubarkeit für insbesondere höher polyfluorierte Sequenzen. Tatsächlich konnten alle in dieser Arbeit hergestellten Peptide unabhängig vom Fluorgehalt durch verschiedene Proteasen hydrolysiert werden. In Zusammenarbeit mit dem University College Dublin konnten zudem erste Daten zum mikrobiellen Verdau fluorierter Peptide und Aminosäuren generiert werden. Die enzymkatalysierte Spaltung der C-F-Bindung an der Seitenkette für beide Substratarten wurde beispielsweise durch den Nachweis von freigesetzten Fluorid-Ionen in Lösung nachgewiesen.

Die Ergebnisse dieser Arbeit werden zum rationalen Design und potenzieller Anwendbarkeit neuartiger polyfluorierter Peptide beitragen, deren enzymatische Abbaubarkeit von großem Interesse für die künftige Entwicklung fluorhaltiger Biomaterialien sein wird.

Table of Contents

1	Introduction.....	1
2	β-Sheet forming peptides.....	2
	2.1 <i>Self-assembly of amphipathic β-sheet peptides</i>	4
	2.2 <i>Antimicrobial activity of peptide-based β-hairpins</i>	9
	2.3 <i>The D-Phe-[2]Abz β-turn motif.....</i>	13
3	Fluorine – a unique element in peptide engineering	15
	3.1 <i>The nature of the C-F bond - fundamentals and application</i>	16
	3.2 <i>Fluorine in natural compounds and drug development.....</i>	22
	3.3 <i>Biodegradation of fluorinated compounds.....</i>	27
	3.4 <i>The role of fluorine in peptide and protein science</i>	29
	3.5 <i>Synthesis of fluorinated amino acids MfeGly, DfeGly & TfeGly</i>	35
	3.6 <i>Fluorinated peptide-based β-sheet hydrogelators</i>	39
	3.7 <i>Fluorinated antimicrobial peptides</i>	42
4	Effects of fluorinated amino acids on the proteolytic stability of peptides	45
5	Aim of this doctoral thesis	51
6	Published work.....	52
	6.1 <i>Rational design of amphiphilic fluorinated peptides: evaluation of self-assembly properties and hydrogel formation</i>	53
	6.1.1 <i>Individual contributions of authors.....</i>	53
	6.1.2 <i>Rationale and summary of the project.....</i>	54
	6.1.3 <i>Publication and supplementary information</i>	60
	6.2 <i>Fine-tuning the antimicrobial activity of β-hairpin peptides with fluorinated amino acids.....</i>	62
	6.2.1 <i>Individual contributions of authors.....</i>	62
	6.2.2 <i>Rationale and summary of the project.....</i>	63
	6.2.3 <i>Publication and supplementary information</i>	69

6.3	<i>Introducing Aliphatic Fluoropeptides: Perspectives on Folding Properties, Membrane Partition and Proteolytic Stability</i>	71
6.3.1	Individual contributions of authors.....	71
6.3.2	Rationale and summary of the project.....	72
6.3.3	Publication and supplementary information	77
7	Cooperation projects & unpublished work	79
7.1	<i>Biodegradation of fluorinated amphipathic peptides and amino acids (with Prof. Dr. Cormac D. Murphy, University College Dublin)</i>	79
7.2	<i>Cytotoxicity and hemolytic activity of AbuK16, MfeGlyK16, DfeGlyK16 and TfeGlyK16 (unpublished work)</i>	87
8	Experimental section	90
8.1	<i>Overview of experimental & theoretical procedures (Section 6)</i>	90
8.2	<i>General experimental conditions (Section 7.1-2)</i>	91
8.3	<i>Preparation of MfeGly, DfeGly and TfeGly (Section 7.1)</i>	92
8.4	<i>Solid-phase peptide synthesis (Section 7.1-2)</i>	96
8.5	<i>CD spectroscopy (Section 7.1)</i>	97
8.6	<i>Proteolytic digestion studies of amphipathic peptides (Section 7.1)</i>	97
8.7	<i>Microbial degradation of fluorinated peptides and amino acids (Section 7.1)</i>	97
8.8	<i>CCK-8 cytotoxicity assays for the determination of cell viability (Section 7.2)</i>	99
8.9	<i>Hemolytic assay for determining blood-disrupting properties (Section 7.2)</i>	99
9	Summary and outlook	100
10	Bibliography	106

List of abbreviations

6-FAM	6-carboxyfluorescein
[2]Abz	<i>ortho</i> -aminobenzoic acid
[2.3.4.5.6F]Phe	2.3.4.5.6-pentafluorophenylalanine
[2.3.5.6F]Phe	2.3.5.6-tetrafluorophenylalanine
[2.3.5.6F][4I]Phe	2.3.5.6-tetrafluoro-4-iodophenylalanine
[3.5F]Phe	3.5-difluorophenylalanine
[4]Abz	<i>para</i> -aminobenzoic acid
[4F]Phe	4-fluorophenylalanine
AA	amino acid
Abu	α -aminobutyric acid
AMP	antimicrobial peptide
BPTI	bovine pancreatic trypsin inhibitor
BSA	bovine serum albumin
calc.	calculated
CAS	Chemical Abstracts Service
CD	circular dichroism
CR	Congo Red
Cryo-EM	cryogenic electron microscopy
Da	Dalton
DfeGly	difluorethylglycine / (S)-2-amino-4,4-difluorobutanoic acid
DfpGly	difluorpropylglycine / (S)-2-amino-4,4-difluoropentanoic acid
DIC	diisopropylcarbodiimide
DIPEA/DIEA	<i>N,N</i> -diisopropylethylamine (Hünig's base)
DMF	<i>N,N</i> -dimethylformamide
DNA	deoxyribonucleic acid
ECM	extracellular matrix
ESI	electrospray ionization
FA	fluoroacetate
FAA	fluoroacetaldehyde
FDA	U. S. Food and Drug Administration
FL	fluorescence

Fmoc	9- <i>N</i> -fluorenylmethyloxycarbonyl
FPSE	fluorous solid-phase extraction
G'	storage modulus
G''	loss modulus
G_0	plateau storage modulu
GC	gas chromatography
HFA	hexafluoroacetone
HFIP	hexafluoroisopropanol
HfLeu	5,5,5',5',5'-hexafluoroleucine
HfVal	5,5,5',5',5'-hexafluorovaline
HIV	human immunodeficiency viruses
HPLC	high-performance liquid chromatography
HRMS	high-resolution mass spectrometry
IR	infrared
LL-37	cathelicidin (active form)
m/z	mass-to-charge ratio
MD	molecular dynamics
MfeGly	monofluorethylglycine / (S)-2-amino-4-fluorobutanoic acid
MIC	minimal inhibitory concentration
NMR	nuclear magnetic resonance
obs.	observed
PDB	Protein Data Bank
PET	positron emission tomography
PFA	perfluoroalkoxy alkanes
PFAS	per- and polyfluoroalkyl substances
PfpGly	pentafluoropropylglycine (S)-2-amino-4,4,4-trifluoro-4,4-difluoropentanoic acid
pI	isoelectric point
POPC	1-palmitoyl-2-oleoylphosphatidylcholine
POPG	1-Palmitoyl-2-oleoyl-sn-glycero-3-phosphatidylglycerol
PPII	polyproline type II (helix)
PTFE	polytetrafluoroethylene
PVDF	polyvinylidene fluoride

RGD	arginylglycylaspartic acid (Arg-Gly-Asp)
RNA	ribonucleic acid
RP	reversed-phase
SAP	self-assembling peptide
SARS-CoV-2	severe acute respiratory syndrome coronavirus type 2
SAXS	small-angle X-ray scattering
SDS	sodium dodecyl sulfate
SEIRAS	surface-enhanced infrared absorption spectroscopy
SPPS	solid-phase peptide synthesis
T2D	type 2 diabetes mellitus
TEM	transmission electron microscopy
TFE	trifluoroethanol
TfGly	trifluoroethylglycine / (S)-2-amino-4,4,4-trifluorobutanoic acid
TfLeu	5',5',5'-trifluoroleucine
TfMet	trifluoromethionine
TfVal	5',5',5'-trifluorovaline
ThT	Thioflavin T
TIC	total ion chromatogram
TLC	thin-layer chromatography
ToF	time of flight
TSA	tryptic soy agar
TSB	tryptic soy broth
UV	ultraviolet
vdW	van der Waals

The one- and three-letter code for the amino acids were used as recommended by the IUPAC-IUB Joint Commission in Biochemical Nomenclature (JCBN) [*Eur. J. Biochem.*, **1984**, *138*, 9-37].¹

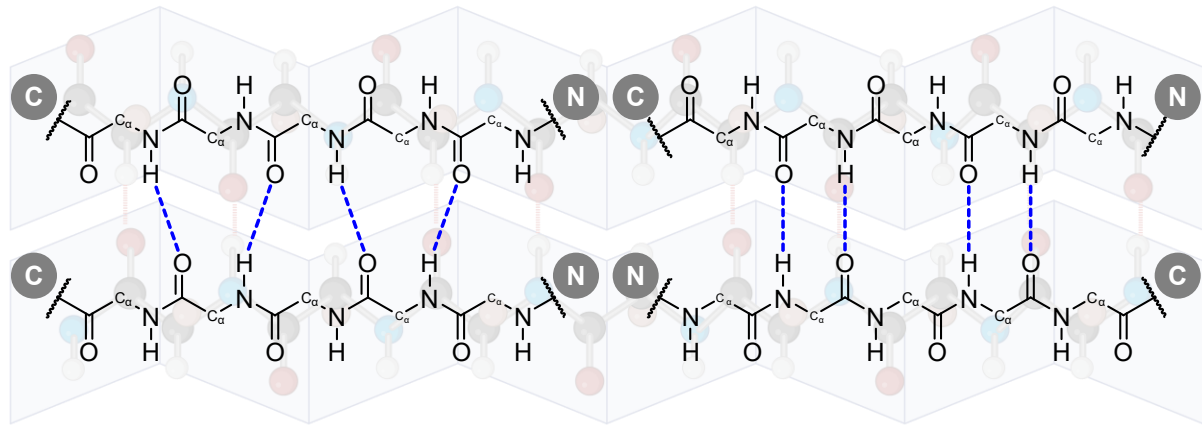
1 Introduction

β -Sheet formation is ubiquitous in peptide & protein-based structures and intermolecular oligomerization, as well as in biological materials such as silk.² Thus, the *de novo* design of advanced β -sheet systems hold immense potentials in pharmaceutical and biomedical research. Engineering the hierarchical self-assembly of supramolecular β -sheet hydrogels, for example, lays the foundation for the tailor-made design of peptide biomaterials with broad applicability in biomedicine.³ On the other hand, optimizing the structural and functional features of synthetic β -hairpin-based antimicrobial peptides (AMPs) is of particular interest for treating a multitude of bacterial infections, but also for overcoming the growing antimicrobial drug resistance by novel therapeutic approaches.⁴ Fluorine, despite its high abundance in our planet's crust, has been foremost neglected by biochemical evolution and is only found in very few natural organic compounds. While the first chemical synthesis of elemental fluorine was reported by Karl O. Christe in 1986, this element has been successfully exploited over decades for the development of novel bio-persistent materials as well as therapeutic drugs.^{5, 6} In peptide and protein engineering, the incorporation of artificial amino acids bearing the highly stable and polar C-F bond is a powerful tool to impart often beneficial effects on folding stability and biological activity, but understanding its impact on peptide and protein properties is yet not complete.⁷

2 β -Sheet forming peptides

β -Sheets belong to the most common secondary structure elements found in peptides and proteins.⁸ They are formed by lateral arrangements of single β -strands in an either parallel or antiparallel orientation which are stabilized by numerous non-covalent forces like hydrogen bonding (between the amide (N=H) and carbonyl (C=O)), hydrophobic or van der Waals interactions. Both alignments differ by an either analog (parallel) or opposite (antiparallel) direction of the β -strands. In parallel β -sheets, the main hydrogen bonds are in an angled shape but perpendicular to the axis of antiparallel β -sheets. The latter case is energetically more favorable and, therefore, for the most part present in native proteins.^{9,10} Tsutsumi *et al.* suggested the statistical amounts on purely parallel β -sheets in proteins to be relatively poor whereas mixed proportions of both parallel and antiparallel are reasonably abundant.^{10,11}

The main characteristics of β -sheet assemblies are illustrated in **Figure 2.1**. In general, intramolecular-formed β -sheets mainly contribute to protein folding and stability as indispensable criterion for biomolecular recognition and activity.¹² For example, nature has evolved the β -turn motif as constitutional signature of antimicrobial peptides (AMPs) like Gramicidin S and Tyrocidine.^{13,14} In contrast, intermolecular β -sheet interactions are not only associated with beneficial protein-protein interactions, but also with protein misfolding and aggregation.¹⁵ Their spontaneous β -sheet assembly into dense amyloidogenic plaques in various tissues is widely associated with neurodegenerative disorders like Parkinson's, Alzheimer's and type II Diabetes (T2D). Moreover, these protein filaments are stated as highly organized due to the cross- β -sheet structure, where the β -strands are aligned perpendicularly to the fibril axis and individual β -sheets along the fibril axis.¹⁶⁻¹⁸ Similar supramolecular architectures are remarkably formed by amphiphilic self-assembling peptides (SAPs). Such fiber networks receive paramount interest as next-generation biomaterials, owing to their ability to form peptide hydrogels with wide ranges of pharmaceutical and biomedical applications like tissue engineering or wound healing.^{19,20}

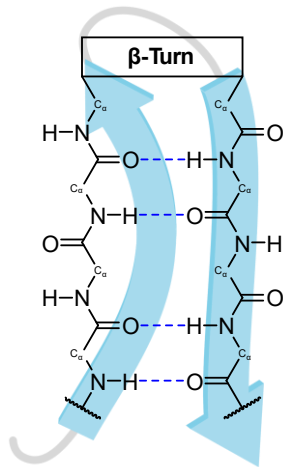


Parallel β-sheet

- Analog direction of β-strands (N- to C-terminus)
- Less stable hydrogen bonds (angled orientation)
- Energetically less favored (least frequent β-sheet configuration)

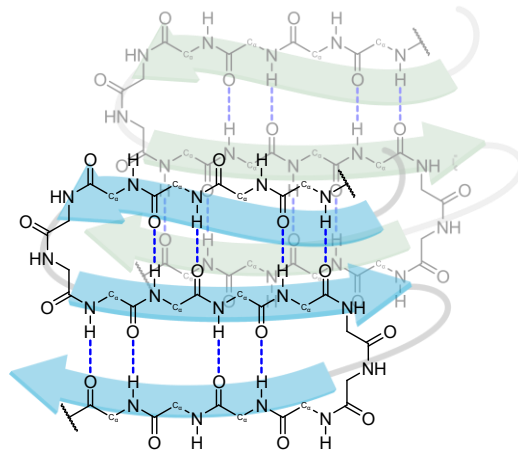
Antiparallel β-sheet

- Opposite direction of β-strands (N- to C-terminus + C- to N-terminus)
- More stable hydrogen bonds (perpendicular to peptide backbone)
- Energetically more favored (most frequent β-sheet configuration)



β-Hairpin (β-turn)

- Antiparallel β-sheet pattern + loop region (stabilized by intramolecular hydrogen bonds)
- Reverse turn (180 °) by four residues (stabilizing hydrogen bond between *i* & *i*+3)
- Structural hallmark of antimicrobial peptides (distinctive structure-function relationship)



Cross-β motif

- Lamination of successive β-sheet layers (intra- and intermolecular hydrogen bonds)
- Repetitive distances of β-sheets and β-strands (intra-strand: 4.7-4.8 Å / inter-strand: 10-12 Å)
- Structural hallmark of amyloid fibrils (associated with neurodegenerative disorders)

Figure 2.1: Main characteristic of parallel and antiparallel β-sheets, β-hairpins and the cross-β motif. Created with BioRender®.¹³

2.1 Self-assembly of amphipathic β-sheet peptides

It has been known for decades that sequential polypeptides with an alternating pattern and higher molecular weight (≥ 5000 Da) can form β-sheets under physiological conditions. First reports in 1975 by Brack *et al.* described *poly*(Val-Lys) to form β-sheet structures at pH 8.8, but to remain disordered at acidic conditions. The necessity of negatively charged salt ions as a shielding effect on the positively charged Lys residues became evident for β-sheet formation. Otherwise, electrostatic repulsions between opposing β-strands can inhibit hydrophobicity-driven self-assembly and maintain the polypeptide in a random coil conformation.²¹ Analog conformational tendencies were reported for alternating polypeptides like *poly*(Tyr-Lys) and *poly*(Glu-Ala).²¹⁻²⁴

The field of self-assembling peptides (SAPs), nevertheless, has undergone a substantial growth by 1990 after Zhang *et al.* located a continuous octad repeat of alternating Ala residues and charged amino acids (Lys and Glu) in the Z-DNA binding yeast protein Zuotin.²⁵ Although its global structure comprises a bundle of four α-helices, examination of a synthesized 16-meric Zuotin_[310-326] by CD spectroscopy revealed the formation of distinctive β-sheet structures. This led to the serendipitous discovery of a naturally occurring SAP which was named EAK-16 (**Figure 2.2**).²⁶

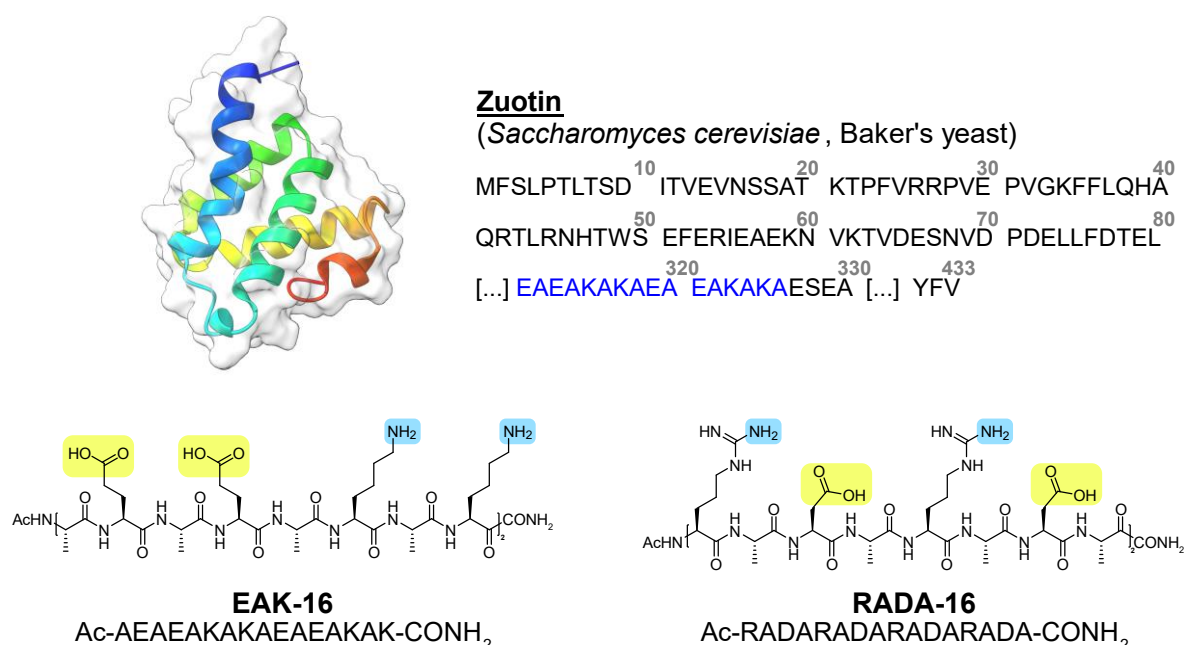


Figure 2.2 Global structure and sequence of Zuotin (PDB ID: 2LWX). Examination of a continuous repeating unit derived from this protein (highlighted in blue) led to the discovery of the first ever reported SAPs EAK-16 and, subsequently, RADA-16.^{26,27}

In further reports from 1995, Zhang *et al.* reported on the *de novo* designed β-sheet hydrogelator RADA-16 (with arginine R and aspartic acid D), whose structural

composition was inspired by the ubiquitous integrin receptor binding site RGD. Both peptides form highly regular nanofibers. Once formed, these macroscopic matrices can entrap large amounts of aqueous solutions (up to 99% (w/v)), are stable towards chaotropic salts and digestive enzymes. Also, these peptide materials can withstand high temperatures up to 90 °C in 1% SDS-solution and, most interestingly, are suitable for the attachment of mammalian cell types.^{26, 28}

The self-assembly into extended β-sheet fiber structures, although being a widespread phenomenon in nature (e.g. curli fibrils in *E. coli*), remains not fully understood till date.²⁹ During the supramolecular fibrillization of amyloidogenic peptides, β-strands are proposed to first self-associate into β-sheets stabilized by hydrogen bonding, hydrophobic, π-π and coulombic interactions and, subsequently, into supramolecular and insoluble fibrils comprising the cross-β motif (**Figure 2.3a**).³⁰⁻³³

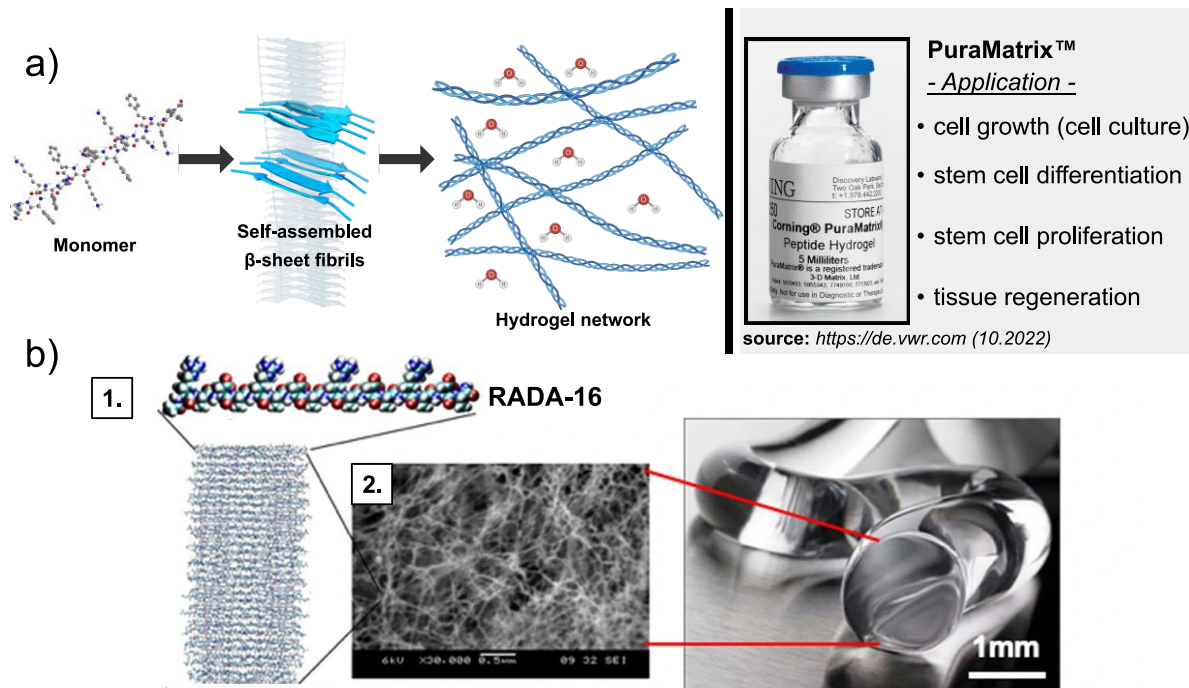


Figure 2.3 a) Proposed model of β-sheet self-assembly based on an amphipathic motif: A monomeric SAP associates into β-sheets and, ultimately, a fibrillary network entrapping large amounts of water (**left**). PuraMatrix™ peptide hydrogel composed of 1% RADA-16 solution (w/v) (**right**). **b)** Formation of RADA-16 based nanofibers: **1.** Self-assembly of a multitude of β-sheet layers **2.** Self-association of a dense fibrillary network (SEM micrograph) into a transparent hydrogel scaffold. Adapted in a modified version from Gelain *et al.* (license: CC BY 4.0). Created with BioRender[®]³⁴⁻³⁶

In case of amphipathic peptides, the hydrophobic residues are proposed to be buried in the interior of β-sheet bilayers while the hydrophilic side chains are exposed to the aqueous medium; this provides a high fluidity and water-content of hydrogel matrices (**Figure 2.3b**). In terms of ionic self-complementary peptides, stabilization of aggregates is driven by ionic interactions between the positively (Glu, Asp) and negatively charged

residues (Lys, Arg). These fibrillary networks offer a broad applicability as biocompatible materials in tissue engineering and wound healing.^{37, 38} For example, a 1%-solution of RADA-16 (w/v) in buffer is commercially available (PuraMatrix™) as extracellular matrix (ECM) mimic for cell culture experiments to support cell growth and differentiation (Figure 2.3a).^{28, 34}

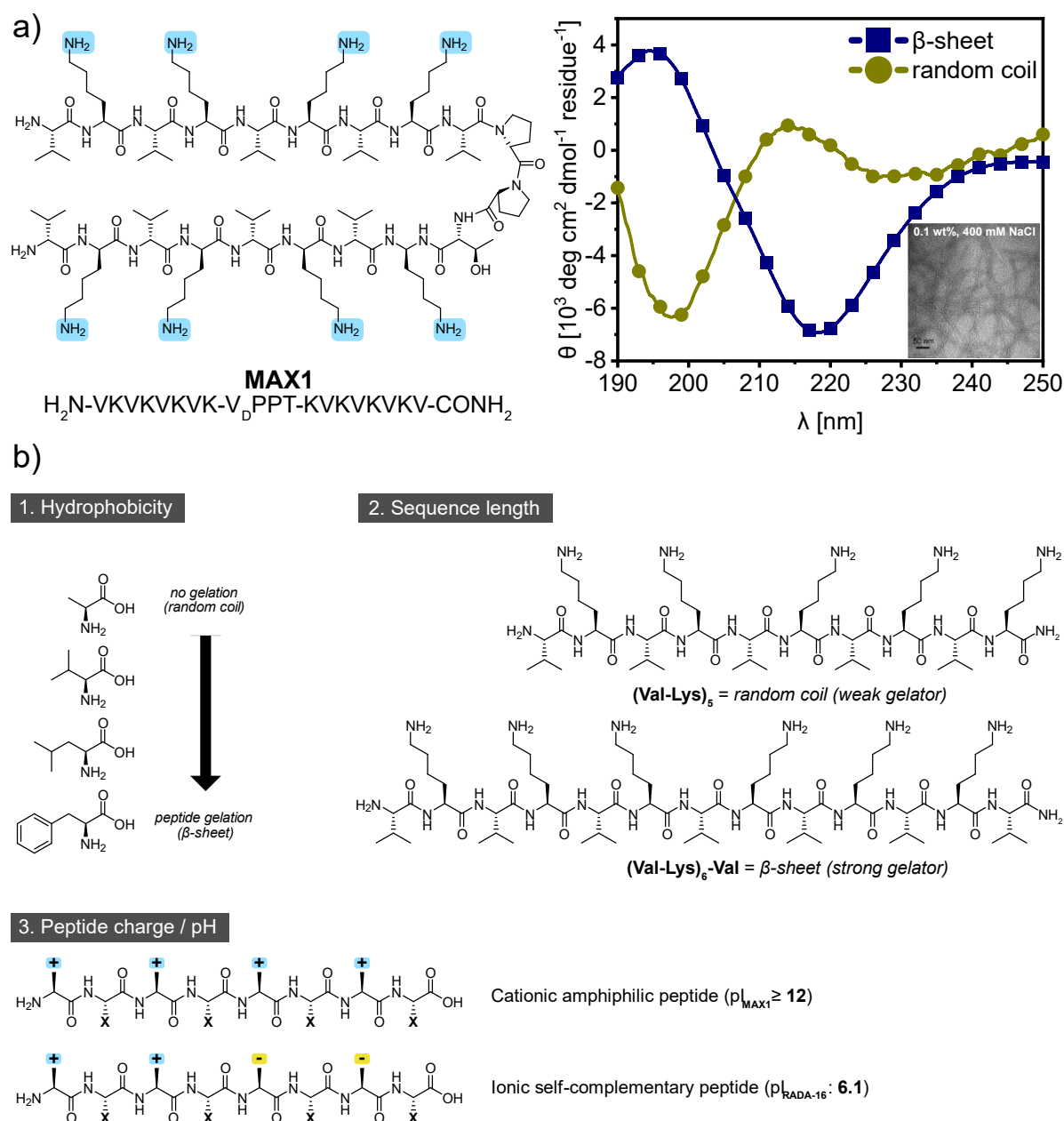


Figure 2.4 a) The cationic amphiphilic peptide MAX1 by Schneider *et al.* undergoes ordered β -sheet assembly (illustrated as paradigmatic CD spectra) into amyloid-like fibrils after addition of ionic strength. TEM micrograph adapted from Ozbas *et al.* with permission (Copyright © 2004 American Chemical Society).³⁹ **b)** Main driving forces of β -sheet formation and supramolecular assembly (hydrogelation).²

A further prominent example of a peptide-based hydrogel is MAX1, a cationic amphiphilic 20-residue sequence described by Schneider and co-workers. This peptide contains a V_DPPPT-β-turn sequence flanked by two (Val-Lys)-repeating units. At neutral or low pH, it exists in a highly soluble but disordered state due to electrostatic repulsion between the charged Lys residues. Application of an exogenous stimulus like a higher pH (about 9.0) or physiological salts (400 mM NaCl) leads to self-triggered peptide folding and assembly into β-sheet structures. Minimizing unfavorable side chain – side chain interactions by ionic strength, therefore, is required to enable the association into highly crosslinked hydrogel networks composed of amyloid-like fibrils as illustrated by TEM micrographs (see **Figure 2.4a**).³⁹⁻⁴¹

Amphipathic peptides have been widely studied for investigating the relationship between peptide β-sheet assembly and hydrophobic properties, sequence length and net charge (**Figure 2.4b**). Bowerman *et al.* probed, for example, the influence of increasing hydrophobicity on a (FKFE)₂ motif by global replacement of Phe with either Ala, Val, Leu, or cyclohexylalanine (Cha) (**Table 2.1**).⁴²

Table 2.1 Peptide sequences, folding pattern (CD) and rheological properties [(XKXE)₂] – Bowerman *et al.*⁴²

Sequence	Π ^a (residue)	CD ^{1*}	G' (Pa) ^{2*}	G''(Pa) ^{2*}
Ac-AKAEAKAE-NH ₂	0.31	random coil	-	-
Ac-VKVEVKVE-NH ₂	1.22	β-sheet	-	-
Ac-LKLELKLE-NH ₂	1.70	β-sheet	-	-
Ac-FKFEFKFE-NH ₂	1.79	β-sheet	208.7 ± 23.9	47.0 ± 9.0
Ac-ChaKChaEChaKChaE-NH ₂ ^{3*}	2.72	β-sheet	217.7 ± 25.5 ^{1*}	29.9 ± 2.5 ^{1*}

^{1*} CD spectroscopy: 4 mM peptide dissolved in water / ^{2*} Rheology: 4 mM peptide dissolved in 40 mM NaCl_{aq}.
^{3*} Peptide was dissolved in a 5% HFIP–water solution to facilitate complete solvation of the Cha-variant.

Secondary structure analysis, microscopic imaging of fibrils, and rheometric analysis of hydrogel formation revealed a correlation between hydrophobicity and assembly behavior. Phe → Ala mutation maintained the peptide as sole random coils, but all remaining sequences formed β-sheet structures. Only the two most hydrophobic variants owning Phe or Cha residues served to form peptide hydrogels, for which higher values of rigidity were determined for the nonaromatic mutant due to the amino acids' hydrophobicity.⁴²

In 2012, Geisler *et al.* provided significant insights into the effects of varying sequence lengths on β-sheet hydrogelation. An extending peptide length by successive elongation

of a single (Val-Lys)-repeating unit led to steady enhancements in β -sheet formation and hydrogelation (see **Table 2.2**).⁴³

Table 2.2 Peptide sequences, folding pattern (CD) and rheological properties [(VK)-motif] – Geisler *et al.*⁴³

Name	Sequence	CD ^{1*}	CD ^{2*}	G' (Pa) ^{3*}
VK9	H ₂ N-VKVKVKVKV-NH ₂	random coil	random coil	1542 ± 143
VK10	H ₂ N-VKVKVKVKVK-NH ₂	random coil	random coil	< 30
Ac-VK10	Ac-VKVKVKVKVK-NH ₂	random coil	β -sheets	~250
VK11	H ₂ N-VKVKVKVKVKV-NH ₂	random coil	β -sheets	1267 ± 48
VK12	H ₂ N-VKVKVKVKVKVKV-NH ₂	random coil	random coil	<30
VK13	H ₂ N-VKVKVKVKVKVK-NH ₂	random coil	β -sheet	6136 ± 254

^{1*} CD spectroscopy: 2 wt% peptide dissolved in water. / ^{2*} CD spectroscopy: 2 wt% peptide dissolved in BTP buffer (pH 7.4).

^{3*} Rheology: 4 wt% peptide dissolved in BTP buffer (pH 7.4).

It becomes apparent that the peptides VK10 and VK12 formed hydrogels with shallow rigidity. The C-terminal Lys residues in both cases were proposed to disturb supramolecular accumulation of β -strands by charge repulsions between the terminal strands. This hypothesis was supported by experimental data obtained for the N-terminal capped Ac-VK10, which formed both β -sheets and comparably stiffer gels than VK10. Significantly larger G' values for VK13-based hydrogels as compared to VK9 and VK11 emphasized a sequence-length dependent self-assembly behavior that facilitates higher amounts of intermolecular contacts and fibrillary cross-links.

The local net charge of an amphipathic peptide plays a tremendous role on its self-assembly behavior. Cationic amphiphilic peptides like MAX1 with an estimated isoelectric point above 12 are highly soluble in aqueous solution and appropriate amounts of salt are required to mask the positively charged Lys residues for inducing peptide assembly.⁴⁴

On the other hand, ionic self-complementary peptides (e.g. RADA-16) possess equal amounts of positively and negatively charged residues, resulting into an isoelectric point of 6.1. In consequence, these SAPs are very prone towards β -sheet fibrillization at a physiological pH range (6-8) and are also less soluble.^{45, 46}

2.2 Antimicrobial activity of peptide-based β-hairpins

Peptides can adopt a multitude of biologically active conformations as a key element for biomolecular recognition. The β-turn motif is one of the most common structural hallmarks in peptides and proteins and allows a stabilization of its pattern by a nearly 180° reverse turn.^{47, 48} Typically, the formation of a β-turn is based on a minimum of four consecutive amino acids (residue i to residue $i+3$) and possesses a characteristic hydrogen bond between the N-H and C=O of residues i and $i+3$.⁴⁹ Common variants of this motif are classified as *type I* and *type II* that differ in the torsion angles of the peptide bond between residues $i+1$ and $i+2$ (see **Figure 2.5a**).⁵⁰ Stabilization of the turn-segment is provided by amino acids with a high β-sheet propensity (Asn, Asp, Trp, Phe) or branched & cyclic structures (Leu, Pro). For instance, the *D-Pro-L-Pro* ($i+1$ & $i+2$) sequence, which is also part of Schneiders' MAX1, forms a type II β-turn structure. Further examples of turn-forming sequences are *Asn-Gly*, *D-Pro-Gly*, *Aib-Gly* and *Aib-D-Pro*.⁵¹ In general, the incorporation of a Gly or Ala residue imparts flexibility of the turn structure by decreasing sterically hindrance between adjacent side chains.^{52, 53} A detailed analysis about the overall β-turn potentials of proteinogenic amino acid was published by Hutchinson *et al.* in 1994.⁵³

The β-hairpin conformation comprises two antiparallel β-strands connected through a β-turn, often containing D- and L-amino acids. Disulfide bridges, cyclization, N-methylation and α,α-dialkylation were located in a large variety of natural occurring β-hairpins to provide protection towards proteolysis.⁵⁴ The structural composition of β-hairpins bears main biofunctionality in protein-protein and protein-DNA/RNA interactions.⁵⁵⁻⁵⁹ The helicase of bacteriophage T7 (gp4), for instance, contains a highly conserved β-hairpin with high proportions of positively charged amino acids that, by binding to the negatively charged phosphate backbone of oligonucleotides, is supposed to act as major site upon intermolecular unwinding in phage DNA replication.⁶⁰ In recent efforts, Nishimura *et al.* developed a RGD-containing peptide with a pH-controlled switch from a disordered state into a bioactive & rigid β-hairpin structure for distinctive internalization to tumor cells enabled through their specific pH.⁶¹

Antimicrobial peptides (AMPs) are a widespread group of small peptides that play a major role in the innate immune defense system of all multicellular organisms, microorganisms, plants, and animals by providing a primary defense against bacterial and viral

infections.⁶² They can be defined as short (10–50 amino acids) amphiphilic peptides with an overall positive charge (generally +2 to +9) and significant amounts ($\geq 30\%$) of hydrophobic residues.^{63, 64} High proportions of cationic residues (e.g. Arg, Lys, His) are designated to mediate electrostatic interactions with bacterial lipids. On the other hand, hydrophobic residues (e.g. Trp, Phe, Leu) can penetrate and, therefore, disorganize the lipid tail region.⁶⁵

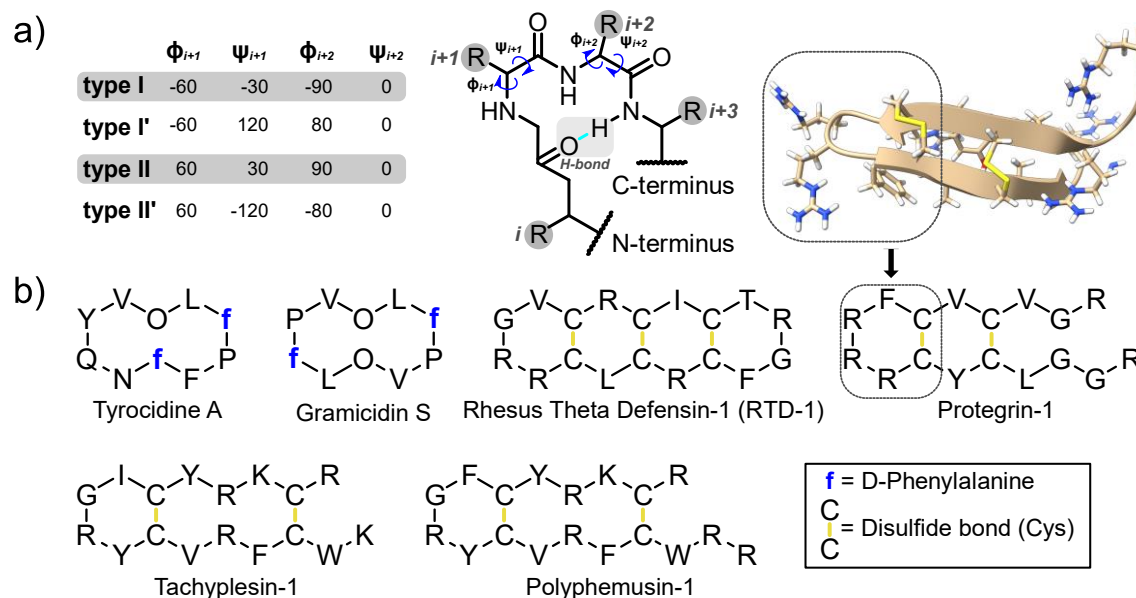


Figure 2.5 a) The structure and classification of β -turns. Type I' and II' β -turns are mirror images of the backbone conformations of type I and type II. The β -turn, thus, is constituted as core segment of a β -hairpin conformation [as shown for Protegrin-1 [(PDB ID: 1PG1)].^{66, 67} **b)** Examples of naturally occurring β -hairpin AMPs.

A multitude of naturally occurring AMPs possesses the β -hairpin conformation (**Figure 2.5b**). Tyrocidine A and Gramicidin S were firstly discovered in 1940 through isolation from *Bacillus brevis*. Both peptides form a β -hairpin structure *via* a *D-Phe-Pro* unit.^{66, 68} A proposed model on the structure-based activity of both peptide antibiotics was provided by Cocklin and co-workers. By means of X-Ray crystallography, the authors identified amphipathic dimers whose hydrophobic patches are oriented towards the membrane interior and the charged residues upward to the aqueous phase.⁶⁸

The illustrated AMPs Rhesus Theta Defensin-1, Protegrin-1, Tachyplesin-1, and Polyphemusin-1 are cyclized either by head-to-tail cyclization and/or disulfide bridges. As illustrated in **Figure 2.5b**, vast majority of these peptides are highly conserved in their amino acid sequence and β -turn units.^{67, 69, 70} Several classes of AMPs were also found to form α -helical structures (e.g. human LL-37 or magainins), but also disordered shapes (e.g. indolicidin) or loop conformations linked by disulfide bridges (e.g. batenecin).^{71, 72}

The mode of action of AMPs can be generally attributed to three key steps: *Attraction*, *Attachment*, and *Insertion*, resulting in the lysis of the bacterial cell membrane (see **Figure 2.6**). The *Attraction* of AMPs to the pathogenic species takes place by allocation of the positively charged residues on the polyanionic microbial cell surfaces. Subsequent permeability of an AMP through the outer cell envelope differs significantly by the microbial species. *Attachment* to the microbial membrane occurs by electrostatic interactions with the anionic components of glycol- and phospholipid head groups. *Insertion* of the AMPs occurs by disruption of physical integrity of cytoplasmic membrane.

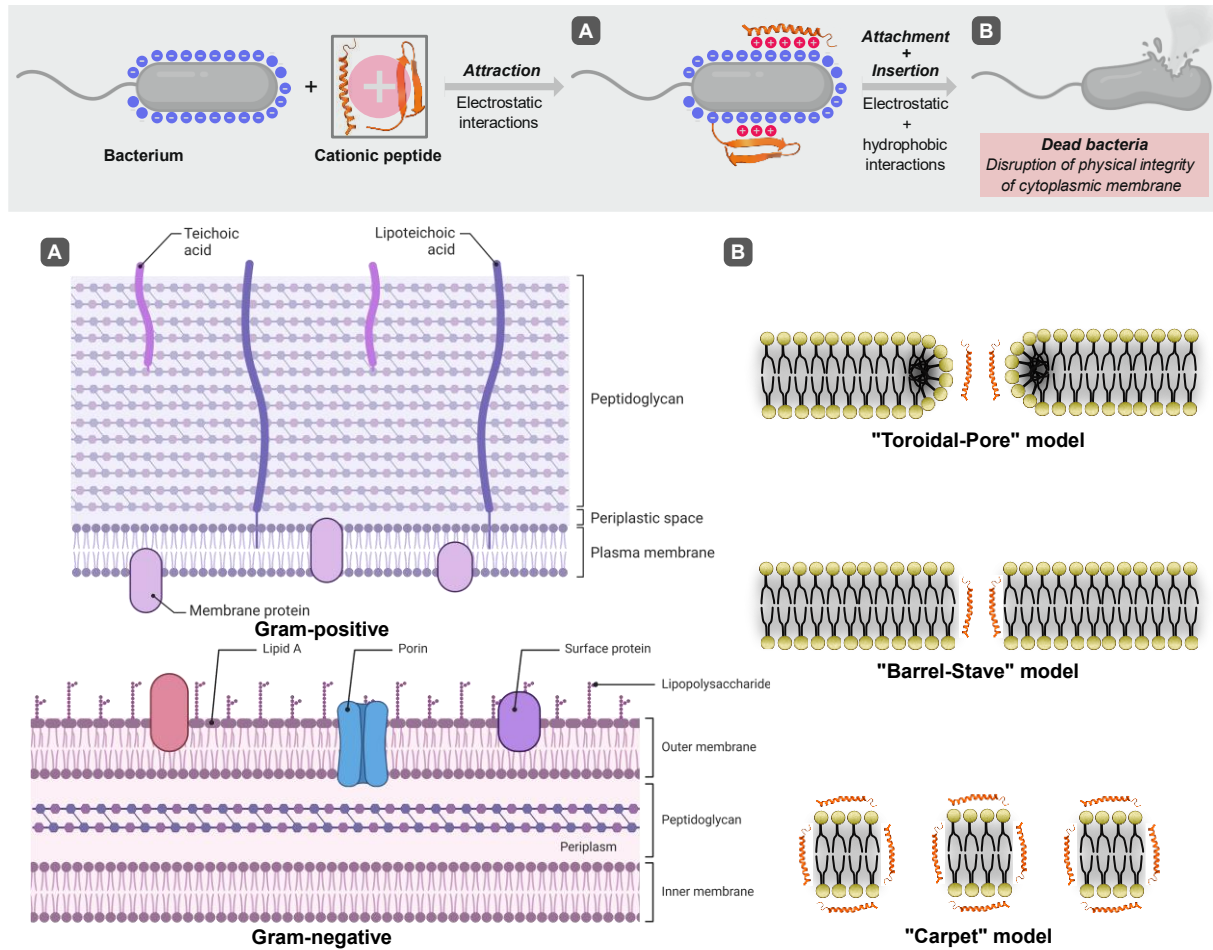


Figure 2.6 Schematic modes of action for bacterial killing mechanisms by AMPs. The outer electrostatic region of the bacterial cell envelopes serves as a primary barrier to AMPs. Several models on perturbation & disruption of the cytoplasmic membrane including pore and carpet formation describe cell lysis by AMP partition into the membrane. Created with BioRender[®].^{73, 74}

The cytoplasmic membrane of Gram-negative bacteria is surrounded by a thin peptidoglycan cell wall and an outer membrane containing a variety of lipopolysaccharides (LPS) functioning as electrostatic network. Gram-positive bacteria lack an outer membrane but are protected by dense layers of cross-linked peptidoglycans. This thick matrix contains negatively charged (lipo)teichoic acids which enable the diffusion of the AMPs by charge attractions. *Insertion* of the AMPs occurs by disruption of

the physical integrity of the cytoplasmic bilayer through hydrophobic interactions with the hydrocarbon-rich lipid-tail region. The partition of the AMP causes membrane pore formation, for which several mechanisms are discussed leading to subsequent cell lysis and death of the pathogenic species.⁷⁵⁻⁷⁷ The “*Toroidal-Pore*” model describes the embedding of the AMPs in the cell membrane followed by formation of ring holes through systemic accumulation with average diameters of 1–2 nm. Second, the “*Barrel-Stave*” model proposes AMPs to penetrate the lipid bilayers as self-associated bundles. Hydrophobic surfaces are interacting with the lipid core of the membrane and their hydrophilic surfaces point inward producing an aqueous pore forming channels for cytoplasmic outflow. The “*Toroidal-Pore*” model, however, foresees the peptides to be always associated with the lipid headgroups even when they are perpendicularly inserted into the lipid bilayer.⁷⁸ In terms of the “*Carpet*” model, the AMPs are arranged parallel to the cell membrane and, once reaching a threshold concentration, disintegrate the lipid bilayer by formation of micellular composites.^{73-75, 79} Beside membrane disruption and subsequent cell lysis, AMPs can also operate on intramolecular mechanisms like inhibition of protein & DNA synthesis with fatal consequences for the bacterial species.⁷³

2.3 The D-Phe-[2]Abz β-turn motif

The development of rigid β-turn mimetics as novel frameworks in biological systems plays a tremendous role in designing synthetic AMPs. The establishment of peptidomimetic turn segments containing D- or β-amino acids, for example, is a frequent approach to improve proteolytic and conformational stability.⁸⁰

In 2017, the research group of Vijayalekshmi Sarojini studied a series of tetrapeptides containing 2-aminobenzoic acid [2]Abz by X-Ray crystallography and NMR spectroscopy. Their rational design was based on the structural composition of the cytotoxic and antiviral cyclic peptide *Asperterrestide A* in which this β-amino acid has been located in the turn-region.^{81, 82} The *de novo* designed linear sequence D-Leu-D-Phe-[2]Abz-D-Ala was found to adopt a planar β-turn stabilized by three hydrogen bonds. Interestingly, the standard $i-i+3$ hydrogen bond was further stabilized by an $i-i+2$ hydrogen bond, as well as an unique intramolecular bond between the amide and carbonyl moiety of [2]Abz (Figure 2.7).⁸²

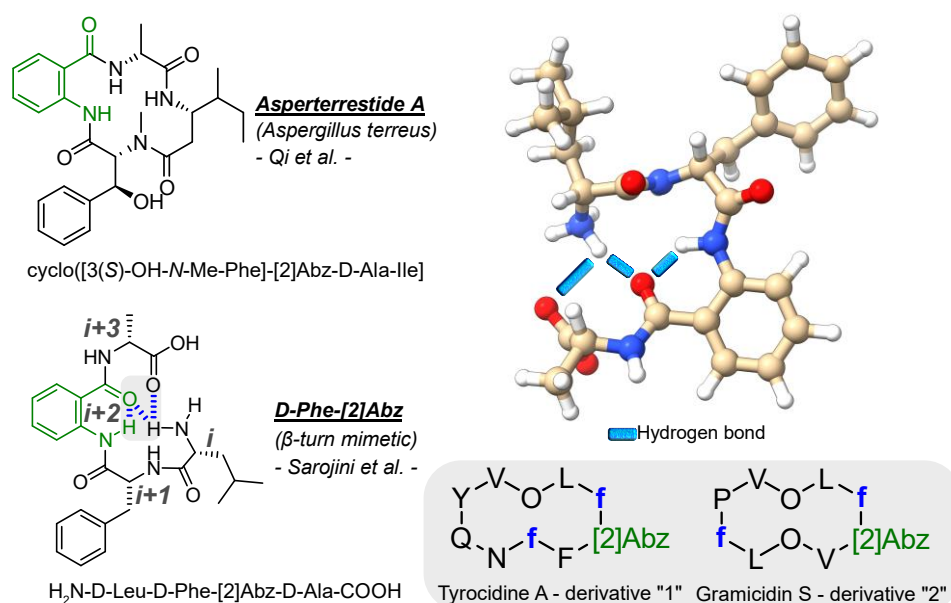


Figure 2.7 Chemical structures of *Asperterrestide A* and the *D-Phe-[2]Abz* unit. The crystal structure of the linear tetrapeptide (PDB ID: 6ANM) revealed three hydrogen bonds (highlighted in blue) to maintain this structure in a β-turn-like conformation. Replacement of the *D-Phe-Pro* β-turn in Tyrocidine A and Gramicidin S with the *D-Phe-[2]Abz* unit retained the β-hairpin structure and antimicrobial activity.^{81, 82}

Unlike traditional β-turn motifs, the rigid and planar framework of the *D-Phe-[2]Abz* motif serves as an universal tool to establish β-hairpin libraries. In a further report, the authors substituted the *D-Phe-Pro* β-turn of both cyclic antimicrobial peptides Tyrocidine A and Gramicidin S with the *D-Phe-[2]Abz* turn motif (see Figure 2.7). Whereby the β-hairpin

conformation was retained for both synthetic analogs, significantly lower hemolytic activities (up to 30-fold) and comparable antimicrobial activities than for Tyrocidine A (**Table 2.3**) were determined. However, the poor solubility of both derivatives “1” and “2” posed a significant problem for therapeutic applicability.⁸³

Table 2.3 Antibacterial activity of Tyrocidine A, AMP analogs “1” and “2” & the acyclic amphiphilic β-hairpins Peptide “2” and “3” – Cameron *et al.*^{83, 84}

Compound	MIC (μM)		
	<i>E. coli</i>	<i>P. aeruginosa</i>	<i>S. aureus</i>
Tyrocidine A	25	100	1.56
Derivative “1” (2017)	50	100	6.25
Derivative “2” (2017)	12.5	25	1.56
Peptide “2” (2018)	3.12	6.25	0.39
Peptide “3” (2018)	25	6.25	0.78

In 2018, Sarojini *et al.* successfully prepared two amphiphilic acyclic β-hairpin peptides (peptide “2” and “3”) bearing the *D*-Phe-[2]Abz motif and high amounts of Arg residues. CD spectroscopy confirmed an existing mixture of disordered structures as well as a distinctive β-hairpin conformations. This was an interesting finding since both peptides, as illustrated in **Figure 2.8**, are devoid of cyclic constraints. Moreover, both peptides provided non-hemolytic properties up to 500 to 800-fold enhanced concentrations than respective MIC values determined for *E. coli*, *P. aeruginosa* and *S. aureus*.⁸⁴ A follow-up work in 2020 focusing on cyclized variants came to somewhat similar structural properties and biological features.⁸⁵

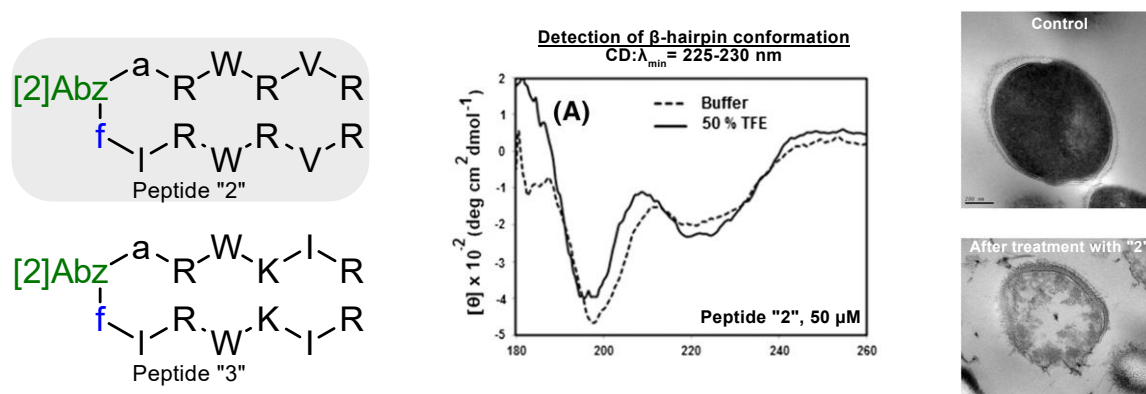


Figure 2.8 Structure of acyclic peptides “2” and “3”. CD spectroscopy in phosphate buffer and trifluoroethanol TFE revealed β-hairpin conformation for peptide “2”. TEM micrographs indicated bacteria death (*S. aureus*) through AMP-induced membrane lysis. Adapted from Sarojini *et al.* with permission (Copyright © 2018 European Peptide Society and John Wiley & Sons, Ltd).⁸⁴

3 Fluorine – a unique element in peptide engineering

Over the last decades, fluorine chemistry has sparked major interest and a continuous growth in novel organofluorine compounds was registered by the Chemical Abstracts Service (CAS).⁸⁶ Marked by a peculiar combination of polarity, nonpolarizability, and hydrophobicity, the C-F bond served in several cases for the development of both very reactive and almost inert compounds and materials with increasing leverage on the multidisciplinary interface of chemistry and biology.⁸⁷ For example, new fluorinated compounds with potential application as electrocatalysts for oxygen reduction reactions or conducting salts were recently reported.⁸⁸⁻⁹⁰ In pharmaceutical research, fluorine is introduced into drug molecules routinely for improving their metabolic stability and binding affinities, but also as a diagnostic probe. The positron-emitting radiopharmaceutical 2-deoxy-2-¹⁸F-fluoro- β -D-glucose (¹⁸F-FDG), for example, is frequently used in positron emission tomography (PET) for the early detection of tumor cells.⁹¹

The site-specific incorporation of fluorinated amino acids into peptides and proteins has generally positive outcomes on their physicochemical properties and biological activity.⁹² Thus, this chapter is devoted to summarizing the main properties of the C-F bond as well as a brief listing of applications, followed by an introduction to fluorinated bioproducts and pharmaceuticals, but also involving the biodegradation aspect of fluorine-containing compounds. The unique potential of fluorinated amino acids as versatile tools in peptide and protein engineering was extensively explored by the Kocsch laboratory and others and will be discussed, including recent approaches on fluorine-directed supramolecular assembly, antimicrobial activity, and proteolytic stability (**Section 4**).^{7, 93-96}

3.1 The nature of the C-F bond - fundamentals and application

Fluorine is a small atom (van der Waals radius: 1.47 Å) and the most electronegative element in the periodic table (χ_p : 3.98). In the case of monofluorinated compounds, the steric constellations compared to carbon-bonded hydrogen are isosteric. The replacement of carbon-bonded hydrogen with a fluorine atom causes only minimal steric perturbations. Also, the van der Waals radius of fluorine is in a similar range as that of an oxygen (1.52 Å) and a hydrogen atom (1.20 Å) (**Table 3.1**).^{97, 98}

Table 3.1: Atomic parameters of the fluorine atom compared to other elements.^{97, 99, 100}

Atom	Ionization Potential (kcal/mol)	Electron Affinity (kcal/mol)	Atom Polarizability (Å ³)	C-X Bond Strength (kcal/mol)	vdW Radii (Å)	Pauling's Electronegativity (χ_p)
H	313.6	17.7	0.66	98.8	1.20	2.20
F	401.8	79.5	0.55	105.4	1.47	3.98
Cl	299.0	83.3	2.18	78.5	1.75	3.16
Br	272.4	72.6	3.05	65.9	1.85	2.96
I	241.2	70.6	4.70	57.4	1.98	2.66
C	240.5	29.0	1.76	83.1	1.70	2.55
O	314.0	33.8	0.82	84.0	1.52	3.44

In a C-F bond, the halogen atom uses a p-orbital to overlap a sp³-hybrid orbital from the carbon atom. The bond strength and length follow an inverse proportional trend: As the van der Waals (vdW) volume increases from F < Cl < Br < I, so does the bond length increase, but the bond strength decrease. Consequently, the C-I bond is the weakest and longest carbon-halogen bond and the halogen itself is a preferred leaving group in, e.g., S_N reactions. The C-F bond, on the other hand, is one of the strongest bonds in organic chemistry.⁸⁷ Due to the high electronegativity of fluorine, the C-F bond is highly polarized, thus undergoing electrostatic or dipolar interactions with surrounding functional groups. Fluorine exerts electronic effects on neighboring groups by withdrawing electron density, leading to changes in pK_a value, Lewis's acidity, and stability of the overall structure. For example, ethanol has a pK_a value of 15.93, while its fluorinated analog 2,2,2-trifluoroethanol (TFE) possesses a value of 12.93. Analogously, trifluoroacetic acid (TFA)

has a smaller pK_a value (0.23) compared to acetic acid (4.76).^{95, 97, 101, 102} Because of high electrostatic attractions between the $C^{\delta+}$ - and $F^{\delta-}$ -atom, the C-F bond has a relatively low polarizability and is accordingly determined as a weak hydrogen bond acceptor. Therefore, $F\cdots H$ -bridges show with 2.0 to 3.2 kcal/mol significantly lower energy values than $O\cdots H$ -bridges (5 to 10 kcal/mol).^{103, 104}

The spatial demand of alkyl residues increases significantly with a growing extent of fluorine substitution. Thus, the vdW volume of a trifluoromethyl group (39.8 Å³) corresponds to that of an ethyl residue (38.9 Å³).^{95, 105} Furthermore, (H → F)-substitution on an aromatic ring leads to an increase in hydrophobicity, whereas terminal mono-, di-, or tri-fluorination of saturated alkyl groups can result into a less lipophilic character.¹⁰¹ Carreira and Müller, for instance, determined lower $\text{Log}P$ values for fluorinated oxetane, propylbenzene and 5-methoxyindole derivatives than for the non-fluorinated analogs (**Figure 3.1a**).^{106, 107} The decrease in lipophilicity is caused by the fluorine-induced molecular dipole, which is schematically illustrated for fluoromethane CH_3F , difluoromethane CH_2F_2 and trifluoromethane CHF_3 in **Figure 3.1b**. The decrease in polarity by higher amounts of fluorine can be rationalized due to a loss of an alternating H-F pattern. This interplay of polarity and lipophilicity are among the most important effects of fluorination and described as “*polar hydrophobicity*” in literature.^{92, 108, 109}

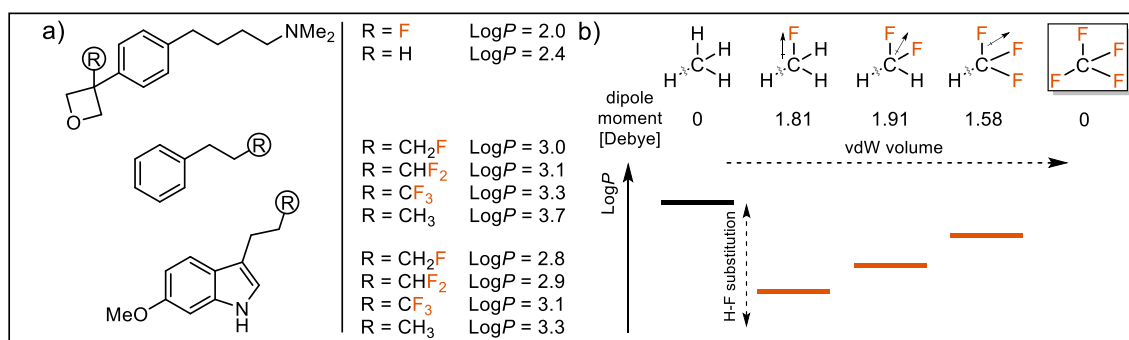


Figure 3.1 a) Chemical structures and reported $\text{Log}P$ values for fluorinated and non-fluorinated oxetane, propylbenzene and 5-methoxyindole derivatives. **b)** Calculated gas-phase dipole moments (vector representation) of methane CH_4 , fluoroethane CH_3F , difluoroethane CH_2F_2 , trifluoroethane CHF_3 and tetrafluoroethane CF_4 . Experimental and theoretical values were adapted from Müller *et al.*^{106, 107}

Perfluorocarbons (PFCs, C_xF_y), e.g. tetrafluoromethane CF_4 , possess a net-zero dipole moment because the individual C-F bond's dipoles cancel each other. The low polarizability of the fluorine atom translates relatively weak intermolecular cohesive forces, low surface energies and refractive indices in fluorinated materials. Thus, PFCs are both hydrophobic and lipophobic and the immiscibility of fluorocarbons with both organic and aqueous solvents is defined as “*fluorous phase*”.¹¹⁰⁻¹¹³ In fact, the application

of PFCs has been well acclaimed in a wide range of fields as the textile industry, material development (e.g. perfluorinated surfactants in firefighting foams)¹¹⁴ and clinical treatments (e.g. fluorinated-tags in drug delivery).^{115, 116}

Polytetrafluoroethylene (PTFE) (Teflon™) is the most popular fluoropolymer till date.¹¹⁷ First discovered in 1938 by DuPont, this material is now frequently used for superhydrophobic coatings, electrical insulation or water separation/purification by specific PTFE membranes.¹¹⁸ Further examples of commonly used fluoropolymers in material and biomedical science and application are Kynar® (polyvinylidene difluoride (PVDF)) and Teflon™ PFA (perfluoroalkoxy alkanes) (**Figure 3.2**). In general, the degree of fluorination and structural pattern of these materials regulates, for instance, the melting temperature, dielectric properties, and polymer mesh size (density).^{119, 120}

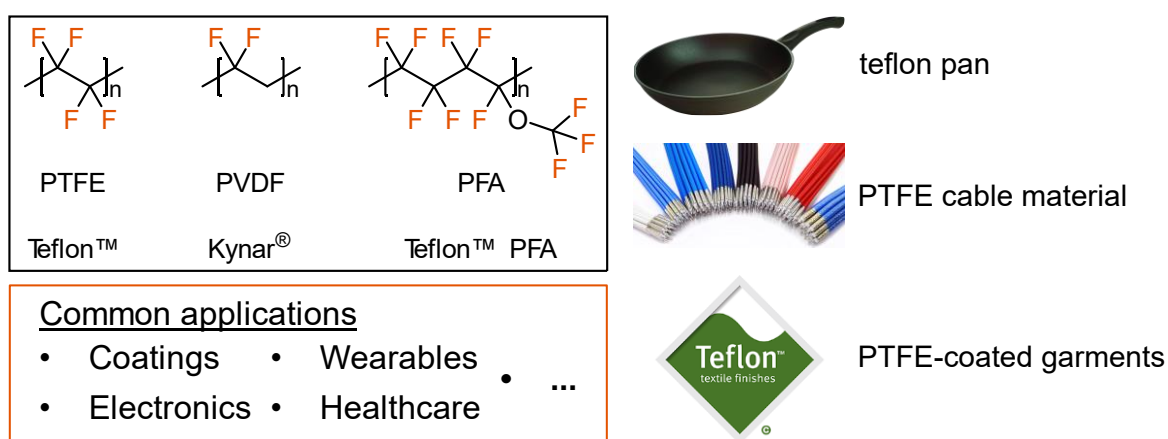


Figure 3.2 Chemical structures of PTFE, PVDF and PFA which are commonly used for ubiquitous industrial applications.¹¹⁹

PFCs have also shown to associate into cellular membranes and, therefore, are widely used as part of carrier systems in the mediated transfer of biomacromolecules like nucleic acids or proteins.^{112, 121}

An impressive breakthrough in fluoroalkyl-based protein delivery was achieved by Cheng and co-workers in 2018. The authors reported on the fabrication of nanoparticles *via* co-assembly of fluoroamphiphiles and albumin (BSA), but also β -galactosidase and saporin. For preparation of protein cargos, polyethylenimine (PEI) was grafted with a wide range of alkanes, cycloalkanes and fluoroalkanes before mixing with FITC-tagged BSA for yielding non-covalent polymer-peptide nanocomplexes. Incubation with HeLa cells resulted in enhanced cellular uptake of fluoroalkyl-decorated cargo systems and confocal images revealed the partition of fluorinated nanocomplexes into the cytosol (**Figure 3.3**).

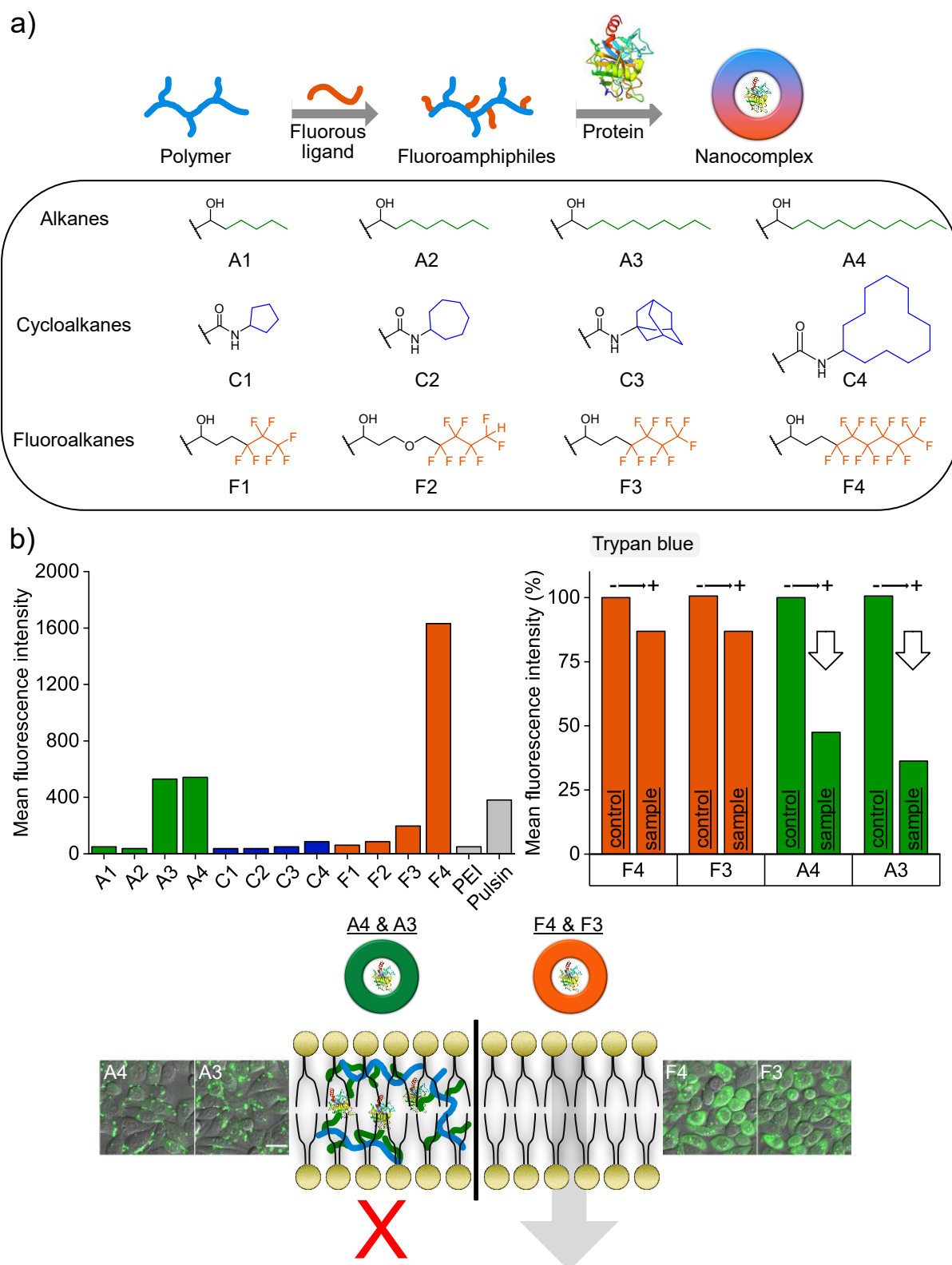


Figure 3.3 a) Fluoroamphiphiles for the non-covalent complexation of BSA-FITC into nanocomplexes. **b)** Cellular uptake was determined by an enhancement of mean fluorescence intensity of HeLa cells transfected with nanocomplexes after trypan blue treatment for quenching BSA-FITC physically adsorbed on the cell membranes. Also, confocal images of HeLa cells treated with polymer/BSA-FITC validated cytosolic protein delivery. In fact, trypan blue quenching resulted into an 80-90% retention of fluorescence intensity when using fluorinated cargos, but a loss of 40% for the non-fluorinated analogs resembling an allocation within the outer membrane. Favorable cytosolic delivery for the fluorinated cargos and a decay of hydrocarbon-conjugated species derived due to superior miscibility with the hydrophobic lipid tail of cellular membranes was suggested by the authors. Adapted in a modified version from Zhang *et al.* (license: CC BY 4.0).¹²²

Moreover, the non-fluorinated analogs were located at the cellular membrane caused by early release of encapsulated proteins. As a proof-of-concept, trypan treatment of the cell revealed a retainment of FITC-based FL intensity of the fluorinated cargo systems (F3, F4) but a significant decrease in FL (about 40%) for the hydrocarbon-equipped complexes (A3, A4).¹²²

In organic chemistry, the narrow miscibility of fluorinated solvents like perfluorohexane (FC-72) with conventional organic solvents received particular interest for developing novel synthetic strategies. Compounds functionalized with perfluorinated groups preferentially dissolve in fluoruous solvents and their partition throughout an organic phase became a standard liquid-liquid extraction technique.^{123, 124} In 2001, Curran and co-workers introduced a fluoruous-tagging strategy by reporting the selective isolation of a library of compounds after multi-step syntheses with prior attached fluoroalkyl-tags through fluoruous chromatography (FPSE).^{125, 126} In 2008, Pohl and co-workers utilized this approach to describe the solution-phase synthesis of mannose tetrasaccharides with a previously reported (C₈F₁₇)-fluoruous-tag (**Figure 3.4**).¹²⁷ After glycosylation, the reaction mixture was transferred on a FPSE-column with selective adsorption of the fluoruous-tagged saccharides and subsequent isolation of the desired product by elution with MeOH.¹²⁸

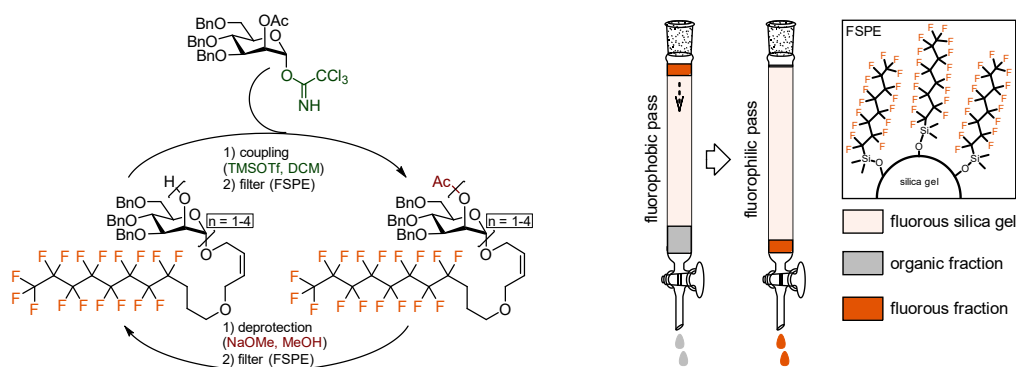


Figure 3.4 Overview of the coupling cycle and strategic selection of protecting groups, fluoroalkyl-linker, anomeric leaving groups and FSPE-based purification for the iterative solution-phase synthesis of mannosides (Pohl *et al.*).¹²⁸

Prior to fluorine-supported carbohydrate synthesis, Mizuno *et al.* demonstrated the synthesis of either C-terminal carboxyl or amidated peptides on a fluoruous support. Peptide coupling proceeded under standard Fmoc-strategy and the C-terminal amino acid was conjugated to a 4-hydroxymethylphenoxyacetyl (HMPA)-type support with a hexakisfluorous chain-type amine (Hfa). This fluoruous-support is developed for the

synthesis of C-terminal carboxyl-groups. After Fmoc deprotection, the Hfa-tagged peptide was selectively isolated through 'fluorous (FC-72) /organic (ACN)' extraction, for which excess reagents remained in the organic solvent. Acidic cleavage from the fluorous support (95% aq. trifluoroacetic acid TFA) finalizes, as demonstrated by the authors, the synthesis of the bioactive peptide Leu-enkephalin Tyr-Gly-Gly-Phe-Leu in notable yields (**Figure 3.5**).^{129, 130}

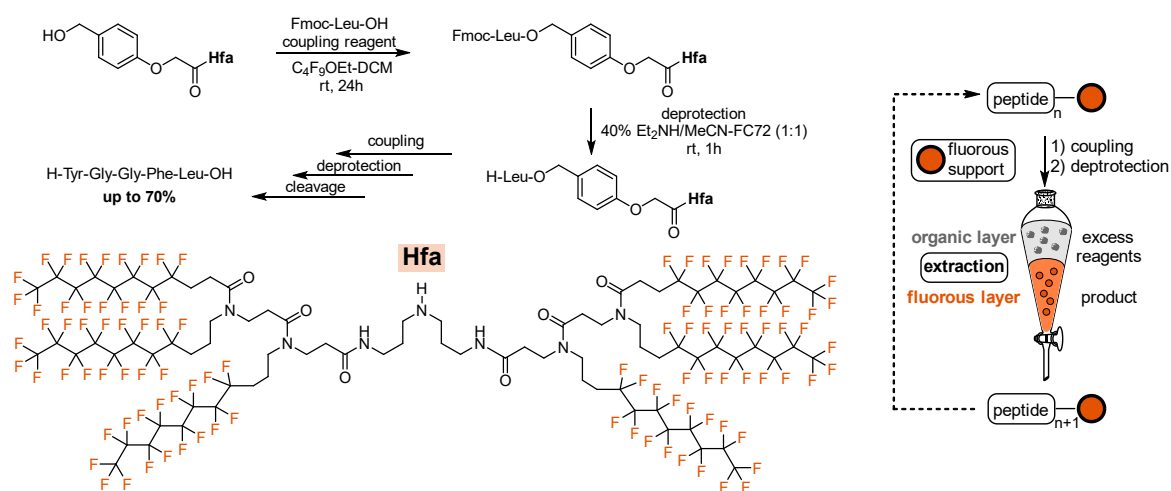


Figure 3.5 Concept of peptide synthesis using fluorous chemistry for the selective extraction of Hfa-linked sequences (Mizuno *et al.*).¹³⁰

3.2 Fluorine in natural compounds and drug development

Fluorine is the 24th most abundant element in the universe.¹³¹ In contrast, the distribution of elements on our planet is somewhat different: Fluorine comprises up to 0.054% of the Earth's crust and is the 13th most common element, more than three times as abundant as chlorine and carbon (both about 0.02%). This element is mostly bound in minerals like CaF₂ (fluorspar), fluorapatite (Ca₅(PO₄)₃F) and cryolite (Na₃AlF₆). Despite its high abundance, fluorine rarely occurs in biomolecules of natural origin, presumably due to the extremely low aqueous solubility of fluorine-containing minerals. For instance, chlorides are much more common in sea water than fluorides (19,000 vs. 1.3 ppm). It is not surprising that, although about 3500 natural occurring organohalogens are reported, only a few organofluorine compounds are identified in the biosphere till date (see **Figure 3.6**).¹³²⁻¹³⁶

Fluoroacetate (**i.**) was the first-ever discovered fluorine-containing natural product. It was initially found in South Africa (1943) as poison in the prostrate shrub *Dichapetalum cymosum* and since then located in several plants in tropical regions.¹³⁷

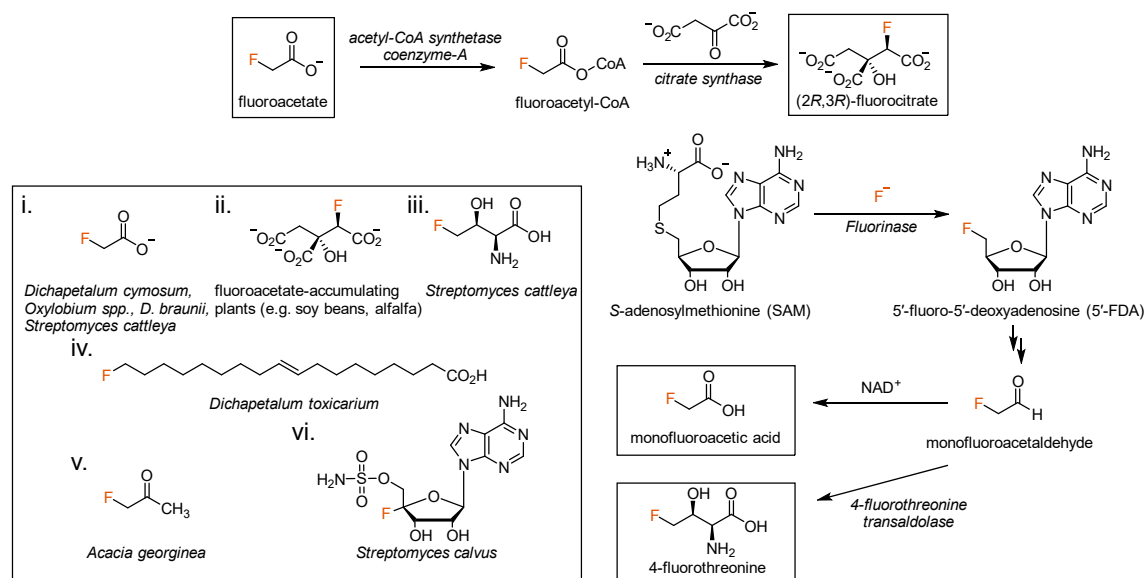


Figure 3.6 Organofluorine compounds **i.** fluoroacetate, **ii.** (2R,3R)-fluorocitrate, **iii.** 4-fluorothreonine, **iv.** ω-fluorooleic acid, **v.** fluoroacetone & **vi.** nucleocidin with schematic metabolic pathways for **ii.** and **iii.**¹³⁸

The high toxicity of this compound is based on the inhibition of the enzyme *aconitase* in the tricarboxylic acid cycle and its reactive metabolites. Biotransformation of fluoroacetate into fluoroacetyl-CoA and, ultimately, (2R,3R)-fluorocitrate (**ii.**) leads to disturbances in citrate transport with fatal consequences for the citrate cycle.¹³⁹ 4-fluorothreonine (**iii.**), the only fluorous amino acid of natural origin discovered so far, was

found in the Gram-positive bacterium *Streptomyces cattleya* but its relevance to metabolic pathways is still unknown. Interestingly, its' *in vitro* antimicrobial activity was discovered in 1986.^{140, 141} The biosynthetic steps leading to this amino acid have been elucidated by Murphy and co-workers. It comprises the conversion of S-adenosyl-L-methionine (SAM) into 5'-fluoro-5'-deoxyadenosine (5'-FDA) by a *fluorinase* enzyme which catalyzes the release of L-methionine by a S_N2-type nucleophilic substitution with fluoride ions at the C_{5'}-residue of SAM. Further metabolization of 5'-FDA into monofluoroacetaldehyde takes place and the latter substrate is, subsequently, converted by the enzyme *4-fluorothreonine transaldolase* (4FTase) into 4-fluorothreonine and monofluoroacetic acid (fluoroacetate) as secondary metabolite.^{142, 143}

In 1964, Ward et al. isolated ω-fluorooleic acid (**iv.**) from the seeds of the West African shrub *Dichapetalum toxicarium*; these ω-fluoro fatty acids are metabolized in the body to produce monofluoroacetic acid (fluoroacetate), and slight exposure can lead to human death. A further fluorinated compound, fluoroacetone (**v.**), was found as a volatile constituent of the native Australian plant *Acacia georginae*.^{144, 145} The last example is nucleocidin (**vi.**), an antimicrobial analogue of adenosine but inappropriate for clinical use due to its cytotoxicity. It was detected in 1956 in culture extracts from the Indian soil bacterium *Streptomyces calvus* and its biosynthetic pathway was described in 2015 by Zhu and co-workers.¹⁴⁶

In contrast to the toxicological potential of fluorinated bioproducts, fluorine-containing pharmaceuticals have been attracting attention for more than half of a century due to a multitude of beneficial effects in drug design and development. As depicted in **Figure 3.7**, systematic fluorination is used on a routine basis to improve and fine-tune pharmaceutical parameters like the pK_a, binding affinity, membrane permeability and metabolic stability. Several excellent reviews by Meanwell and co-workers covering the bigger picture of fluorine in pharmaceuticals have been published during the last few years.^{100, 147, 148} Fluoro-pharmaceuticals containing fluorine atoms or fluorinated functional groups (e.g., trifluoromethyl "CF₃") receive an increasing medicinal importance and belong to the key players in global marketed drugs (about 20%) for several decades.¹⁴⁹ One example describing the outstanding impact of fluorine substitution in medicinal chemistry deals with the development of the cholesterol-absorption inhibitor SCH 58235 (Ezetimibe) (**A**). Comparing to the moderately potent compound SCH 48461, the decoration of two phenyl rings with fluorine substituents proved to circumvent the metabolism of labile sites by Cytochrome P450 monooxygenases.

Application of fluorine in medicinal chemistry

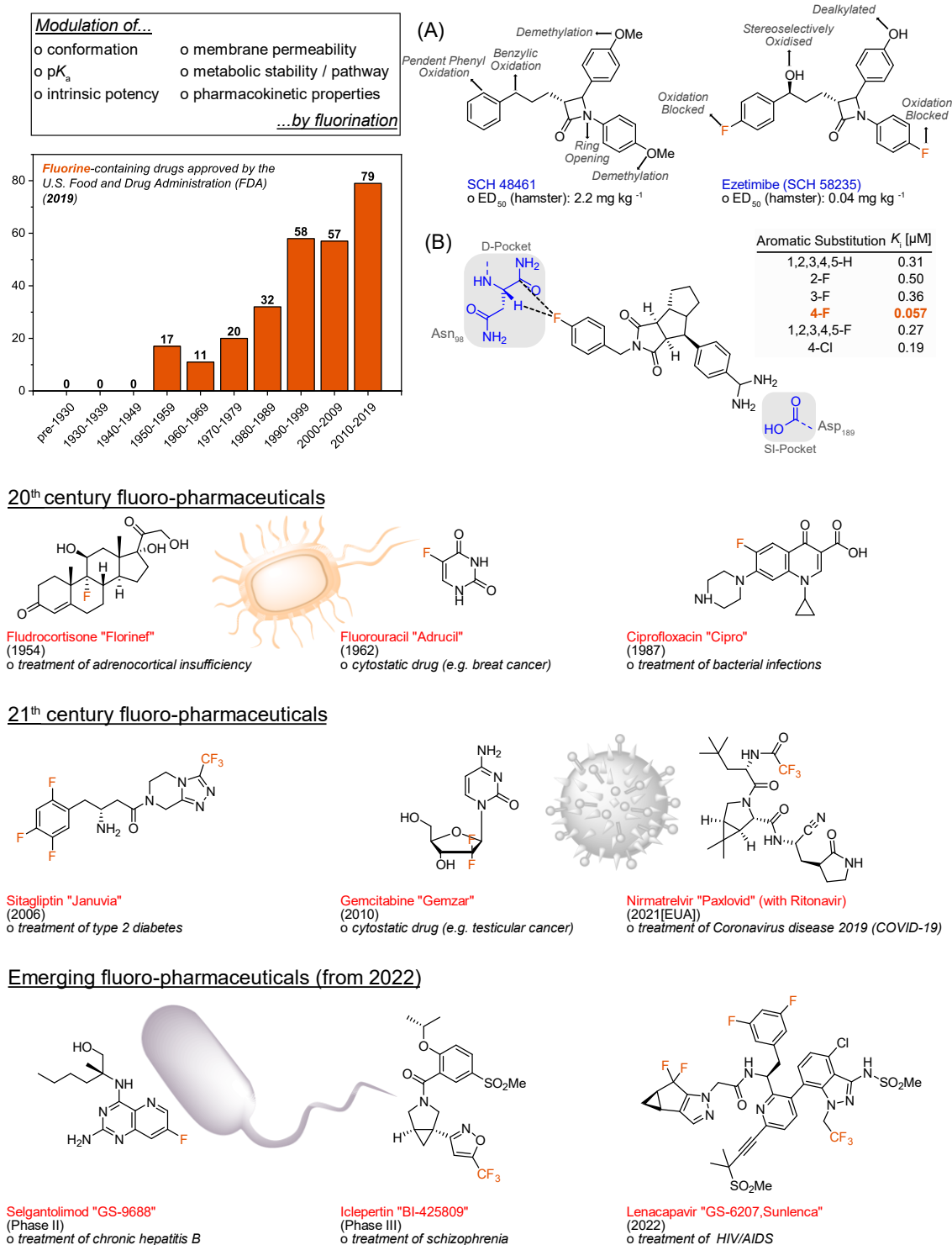


Figure 3.7: The impact of fluorine on medicinal chemistry. A generous number of beneficial effects on physicochemical properties resulted into the successful approval of fluorine-containing drugs by the FDA in the past and present. The implementation of fluorine into drug scaffolds caused a boost in biofunctionality for **(A)** the pharmaceutical agent Ezetimibe and **(B)** a thrombin-inhibitor studied by Diederich and co-workers.^{100, 102, 147, 148, 150-157}

This lead optimization contributed significantly to the metabolic stability and intrinsic potency of Ezetimibe in hamster models.¹⁰² Diederich and co-workers studied the

aromatic substitution of a thrombin inhibitor (**B**) with varying degrees of fluorination. Only the *para*-fluorophenyl mutated inhibitor revealed superior activities than the non-fluorinated drug. X-ray crystal structure analysis of enzyme-inhibitor-complexes revealed favorable dipolar interactions of the C-F group with electrophilic residues in the enzyme's active site as main origin of enhanced activity. In brief, complexation of the 4F-mutant with thrombin generated a close contact of the fluorinated residue with a positively polarized carbon atom (C=O) and the crucial H-C_α atom of Asn98 in the D-pocket.^{154, 158} The successful history of fluoro-pharmaceuticals started in 1954 with the FDA approval of Fludrocortisone and Fluorouracil in 1962.¹⁵⁰ A recent example of fluorine-assisted drug development is constituted by Nirmatrelvir, a peptidomimetic inhibitor of the severe acute respiratory syndrome coronavirus 2 (SARS-CoV-2) main protease 3CL^{pro} developed by Pfizer. In 2021, the FDA issued an emergency use authorization (EUA) on a combined formulation (Paxlovid™) of Nirmatrelvir and Ritonavir, a HIV-1 protease and CYP3A inhibitor, for the treatment and post-exposure prophylaxis of COVID-19.^{153, 159} Upcoming drug candidates like Selgantolimod¹⁵² or Iclepertin¹⁵¹ may open novel therapeutic approaches for the treatment of chronic hepatitis B and schizophrenia.

The development of peptide and protein-based drugs as biocompatible diagnostic agents is becoming increasingly valuable. In 2015, over 220 therapeutic proteins and peptides and 64 antibody-derived drugs were reported to be available on the global pharmaceutical market.^{48, 160} As fluorine substitution is a widespread approach for fine-tuning physicochemical and pharmacokinetic properties in a modality which cannot be achieved by any other element, fluorine-containing amino acids bear promising potentials in drug research.^{150, 161, 162} One example is the anticancer drug Melflufen, a fluorous peptide-drug conjugate (**Figure 3.8a**) supposed for the treatment of multiple myeloma (MM).¹⁶³ Preclinical *in vitro* studies with ovarian cancer (OC) cell lines revealed a significant enhancement of bioactivity than the historical predecessor Melphalan upon introduction of 4-monofluorophenylalanine (OEt-protected).¹⁶⁴ However, Melflufen was provisionally withdrawn from the US market in 2021 after excess deaths in a phase III confirmatory trial.¹⁶⁵ For Ulimorelin, a cyclic-peptide-based ghrelin agonist and prokinetic agent, several structural modifications were tested *via* structure-activity relationship (SAR) screenings and substitution of D-Phe with its 4-fluorinated derivative optimized its pharmacological activity significantly.^{166, 167} When incorporating the aliphatic fluorinated amino acid DfeGly into a prototype inhibitor of the hepatitis C virus NS3, Matassa *et al.* proposed this derivative to act as a potential cysteine-mimetic agent.¹⁶⁸

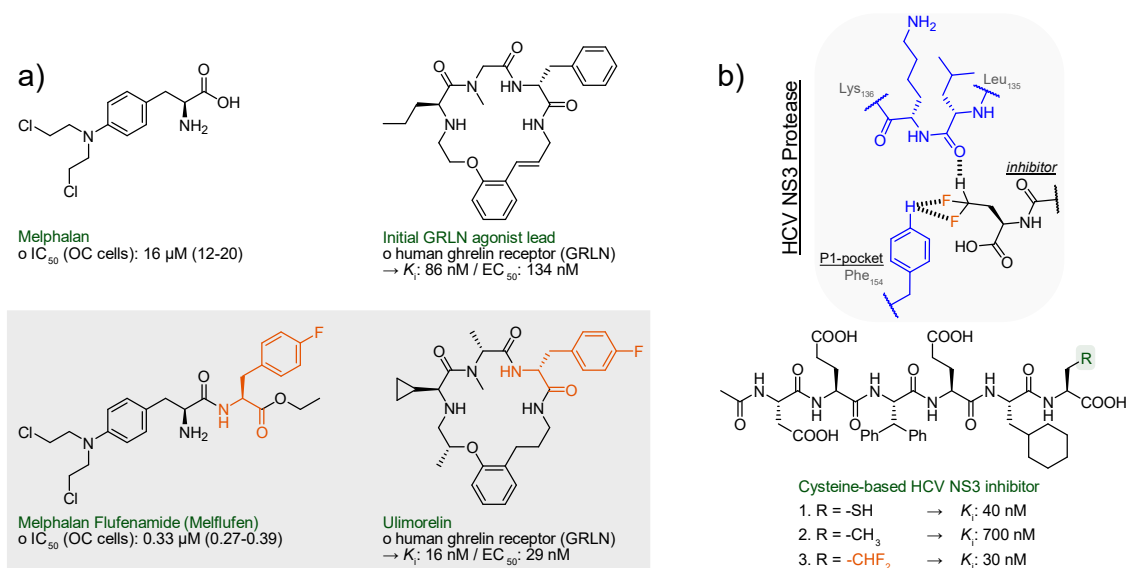


Figure 3.8: **a)** Optimization of pharmacological properties for Melphalan and a prototype GRLN agonist by introduction of fluorinated phenylalanine derivatives. **b)** Optimization of a *de novo* designed HCV NS3 protease inhibitor by accommodation of the substituted fluorinated aliphatic amino acid DfeGly into the P1-pocket of the enzyme as suggested by Matassa and co-workers.¹⁶⁸

They assumed the CF₂H residue as appropriate proton donor with its acidic proton to be closely located to the carbonyl oxygen of Lys136 *via* hydrogen bonding and F⋯H-bridges with the *para*-hydrogen atom of Phe154 (**Figure 3.8b**).¹⁶⁸

In summary, the modification of peptides and proteins with fluorinated analogues of canonical amino acids, as shown in given examples, holds great potentials to confer orthogonal behavior within natural systems.

3.3 Biodegradation of fluorinated compounds

Despite their beneficial physicochemical properties and definite advantages in chemical & biological applications, the chemical inertness and biological persistence of per- and polyfluoroalkyl substances (PFASs) causes an increasing exposure into the biosphere with fatal consequences on ecological and health concerns.^{169, 170} For instance, Ochoa-Herrera *et al.* studied the microbial degradation and toxicity of a diverse range of PFASs like trifluoropentanoic acid, perfluoropropanoic acid and perfluorooctane sulfonate. Only minor inhibition of hydrogenotrophic methanogens in anaerobic biomass up to a PFAS concentration of 500 mg L⁻¹ (resembling barely toxic properties) were detected. However, all selected PFASs were found to be persistent towards microbial degradation over several weeks except for trifluoropentanoic acid which indicated at least 3% total release of fluoride ions.¹⁷¹

Several decades ago, the presence of fluoroacetate in nature and its *in vivo* toxicity raised the question of its biodegradation and biotransformation. In fact, the main class of bacterial proteases catalyzing hydrolytic defluorination is called *fluoroacetate dehalogenase*. The first of its kind was found in 1965 by Peter Goldman in *P. aeruginosa* and achieved the hydrolytic cleavage of fluoroacetate into glycolate and fluoride ions.¹⁷² Further dehalogenases have been also isolated from the soil microbes *F. solani*, *P. fluorescens* and *D. acidovorans*.¹⁷³ Liu *et al.* suggested a two-step reaction mechanism of digestive C-F bond cleavage. It includes an enzyme-acyl complex between a nucleophilic Asp and the C^α-fluoroalkylated residue of fluoroacetate followed by the release of fluoride ions. This ester intermediate is then hydrolyzed by a water molecule activated *via* a basic His to generate the free enzyme and 2-hydroxyacetic acid as digesting product (**Figure 3.9a**).¹⁷⁴ A further defluorinating enzyme, *fluoroacetate-specific defluorinase*, has been found in mammalian animals (e.g. mice & rats) that live in the same area of fluoroacetate-producing plants. Upon lead exposure, fluoride ion release occurs *via* a glutathione-dependent detoxication of fluoroacetate (**Figure 3.9b**).^{173, 175}

Only few case studies on the enzymatic defluorination of fluorinated amino acids have been reported. Donnelly *et al.* determined the enzyme-catalyzed C-F bond cleavage from 4-fluoro-L-glutamic acid in cell extracts of *Streptomyces cattleya*. Analog concentration of fluoride and NH₃ were measured upon digestion, suggesting a deaminase-activity within the cell extract that would contribute to the amino acid's metabolic excretion.¹⁷⁶

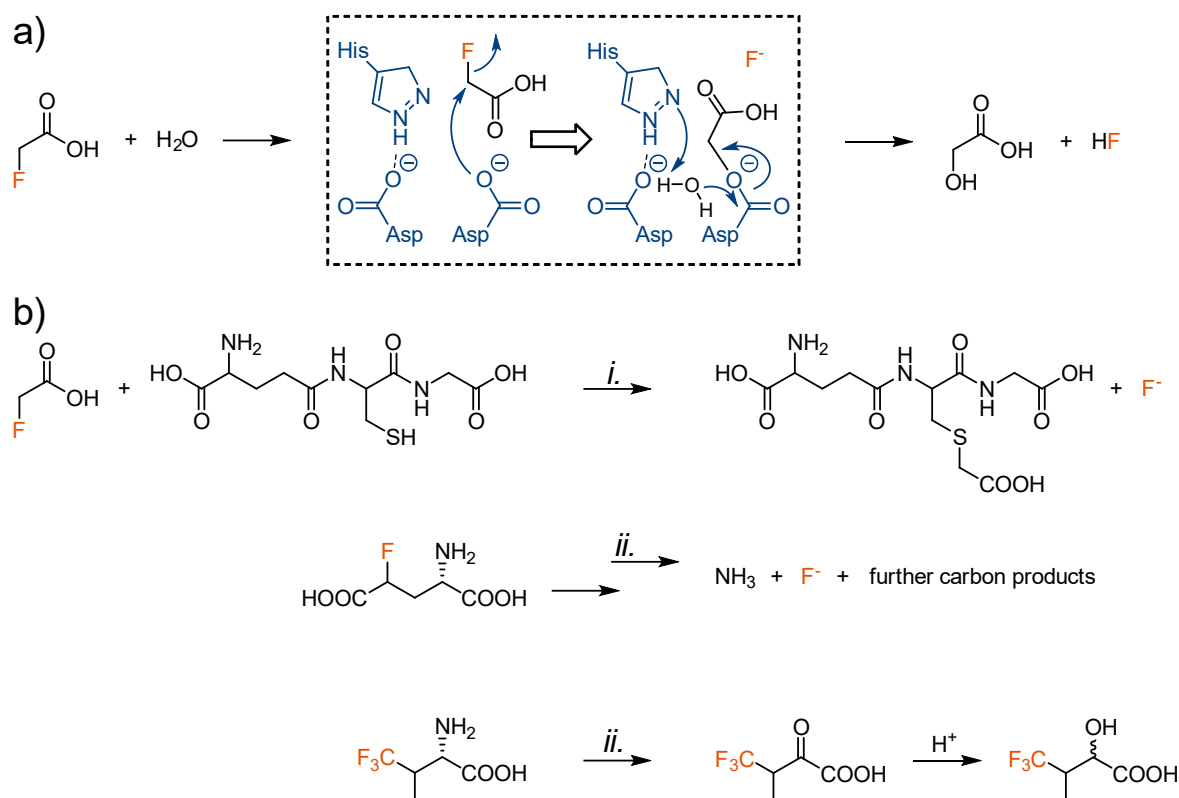


Figure 3.9 a) Hydrolytic defluorination of fluoroacetate through *fluoroacetate dehalogenase* via an Asp-His-Asp catalytic triad. **b)** Further examples of enzyme-catalyzed C–F bond cleavage: **(i.)** *fluoroacetate-specific defluorinase* and **(ii.)** *4-fluoroglutamate dehalogenase/deaminase* – adapted from Murphy and co-workers.^{173, 177}

Similar conclusions on deamination were reported by O'Connor *et al.* when studying the metabolism of racemic TfVal by *B. subtilis*. Interestingly, the authors did not observe any fluoride ion release from the trifluoromethylated side chain, but the substrate rather to be catabolized to 4,4,4-trifluoro-2-hydroxy-3-methylbutanoic acid.¹⁷⁷

The environmental fate of organofluorine compounds is a crucial variable to be evaluated for preventing hazardous outcomes on the worldwide ecosystem. However, only few numbers of living organisms possess suitable mechanisms for the metabolic degradation of fluorinated compounds, which would allow a continuous biological cycling of mineralized fluorides. In fact, nature has been exposed with these chemicals for a comparatively short era of the earth's history and, therefore, requires a much longer period for the evolution of suitable biodegradable processes.^{136, 178}

3.4 The role of fluorine in peptide and protein science

Peptides and proteins own a myriad of natural functions and are responsible for regulating, for instance, biomolecular catalysis, cell signaling and metabolism. Their complex three-dimensional structures and physiological properties are determined by their amino acid sequence. For expanding the overall entity of canonical amino acids, the site-specific incorporation of non-natural and synthetic derivatives belongs to the most common approaches in peptide and protein engineering. Fluorinated amino acids have emerged as valuable building blocks for implementing unique tailor-made properties, like a high chemical & thermal stability. The amount and local position of the fluorinated amino acid in the primary sequence, its spatial demand, and the specific degree of side chain fluorination determines its influence on peptide hydrophobicity, secondary structure formation, supramolecular self-assembly and bioactivity (see **Figure 3.10**).^{7,92} For estimating the hydrophobic nature of fluorinated amino acids, the Koksch laboratory established a RP-HPLC based scale for these synthetic building blocks (**Figure 3.11**).¹⁷⁹ In this plot, the retention time (rt) acts as a dimension of hydrophobicity.^{180, 181}

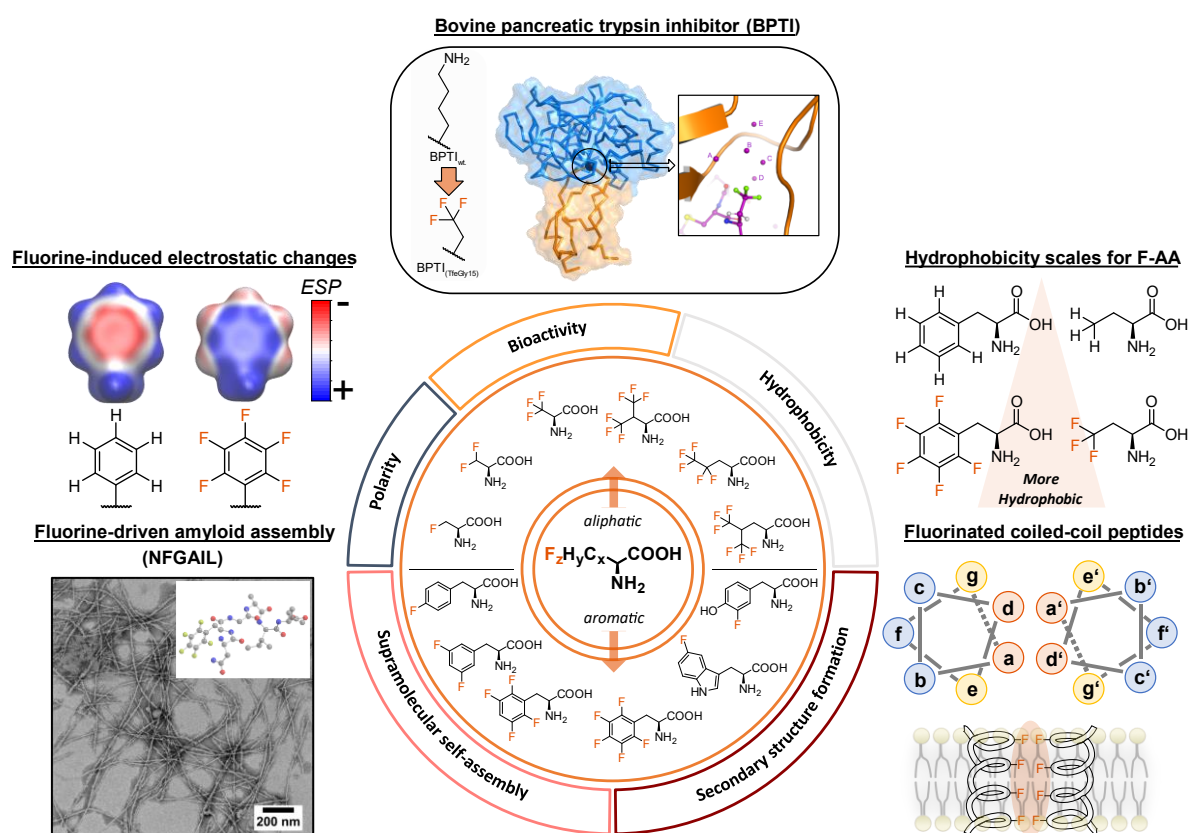


Figure 3.10 Effects of fluorinated amino acids on the intrinsic hydrophobicity, polarity, folding & assembly propensity as well as biological activity of peptide and proteins.⁹²

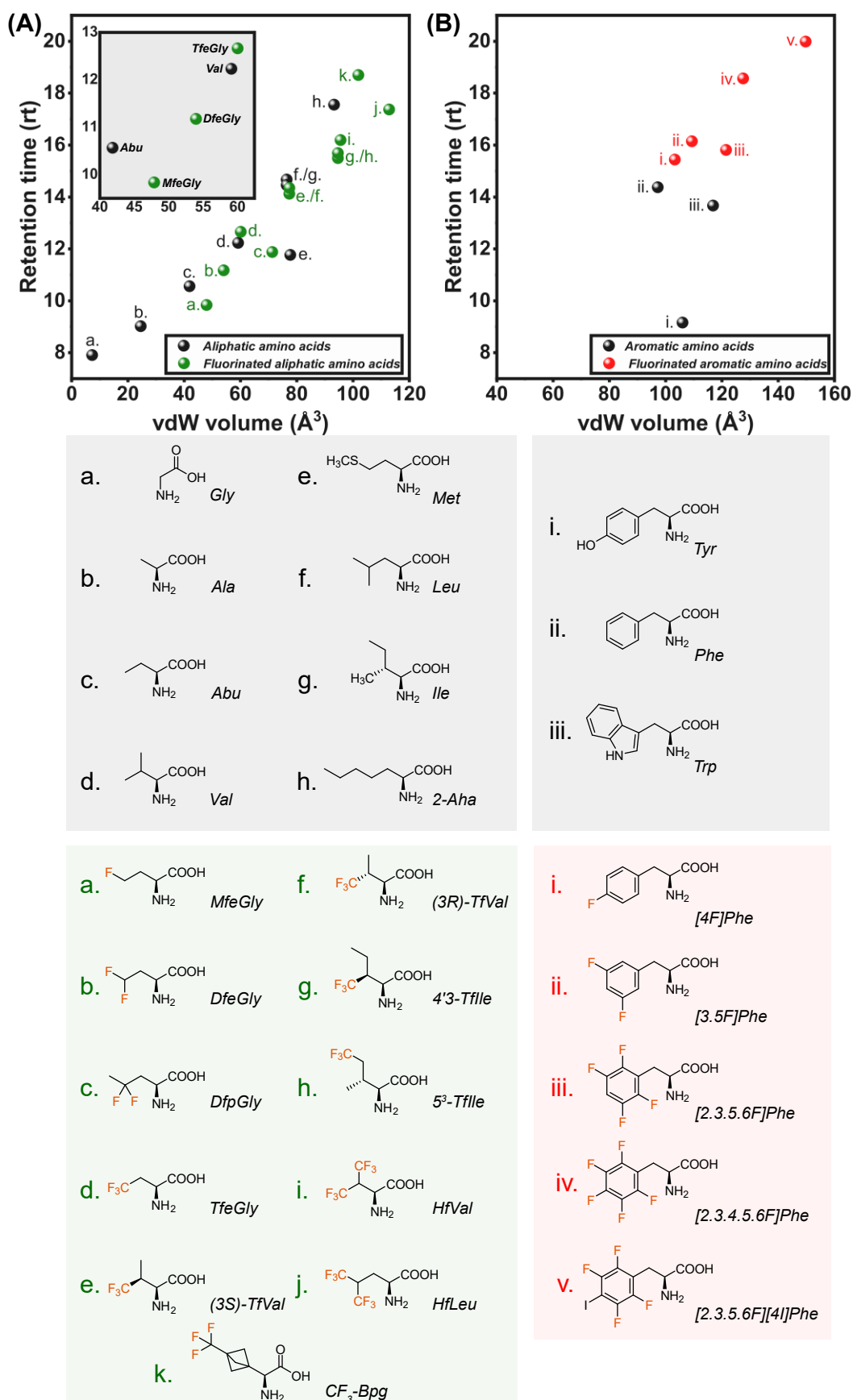


Figure 3.11 Systematic evaluation of **(A)** aliphatic and **(B)** aromatic amino acids (Fmoc-protected for UV detection) and their fluorinated derivatives through a RP-HPLC-based hydrophobicity assay. Retention times of respective Fmoc-amino acids are plotted against the van der Waals volume of the side chains. Types of amino acids are subdivided into aliphatic & aromatic (grey), fluorinated aliphatic (green) and fluorinated aromatic (red).^{182, 183}

Fluorine substitution on aromatic amino acids generally increases the intrinsic hydrophobicity. In the case of aliphatic fluorination, the amino acids Val, Ile and Leu were particularly studied and their non-polar character was mostly enhanced with few exceptions found for monofluorinated side chains (**Figure 3.11**).¹⁸³

The fluorinated amino acids MfeGly, DfeGly and TfeGly derived from the non-natural amino acid Abu are of particular interest since the systematic sequence of terminal side-chain fluorination resembles the series of prior-discussed fluoromethanes (**Section 3.1**). A decrease in non-polar character for MfeGly compared to Abu is stated, whereas DfeGly & TfeGly show enhanced hydrophobicity. Thus, this library of fluorinated Abu comprises isosteric C-H to C-F substitutions (Abu/MfeGly) as well as a CF₃-containing derivative (TfeGly) with similar hydrophobic character and spatial demand than for Val.

For elucidating the effects of fluorination on peptide folding and assembly, coiled-coils were frequently used as model peptides (**Figure 3.12a**). Kumar *et al.*, for example, replaced four Leu residues (a position) and three Val residues (d position) with 5,5,5-trifluoroleucine (TfLeu) and 4,4,4-trifluorovaline (TfVal) in the coiled-coil GCN4 and measured much improved thermodynamical stabilities for the fluorous peptide.¹⁸⁴

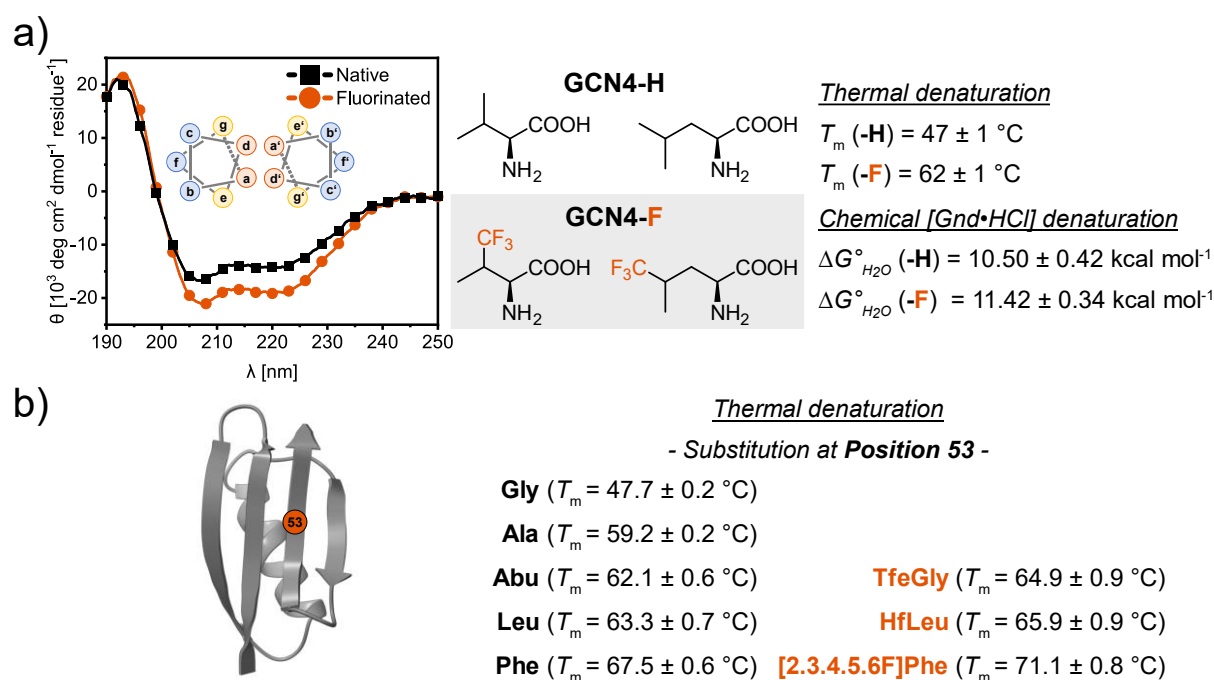


Figure 3.12 a) Replacement of Val and Leu with TfVal and TfLeu within a GCN4-derived peptide enabled higher thermal and chemical stability.¹⁸⁴ **b)** The protein GB1 domain with experimentally determined melting temperatures (T_m) of the main domain (Ala53) and its native & fluorinated derivatives by Cheng and co-workers (PDB ID: 1PGA).^{185, 186}

Several attempts have been made for understanding the effect of fluorinated amino acids on β -sheet formation & stability. In 2009, Chiu *et al.* studied the changes in protein

stability of the β -sheet GB1 domain (56 residues) by fluorination of the solvent-exposed position 53 (Ala) of the internal β -cross-strand. Thermal folding & unfolding experiments revealed the incorporation of TfeGly, HfLeu, and [2.3.4.5.6F]Phe to moderately enhance the thermal stability of this protein when comparing to their native counterparts Gly, Ala, Abu, Leu or Phe (**Figure 3.12b**).¹⁸⁶

β -Sheet based intermolecular interactions are of main relevance in amyloid formation. The fibrillary plaques derived from the human islet amyloid polypeptide (hIAPP), for example, have been identified as potential causing agent in case of T2D.¹⁸⁷ In 2020, the Kokschi laboratory focused on the amyloid core-containing sequence NFGAIL, a fragment derived from hIAPP (residue 22–27) (**Figure 3.13a**). A library of fluorinated NFGAIL variants with varying degrees of aromatic side-chain fluorination was established to probe the role of hydrophobicity and π - π -interactions during amyloid self-assembly. Systematic fluorination enhanced the hydrophobicity of the Phe residues and, at the same time, led to alterations in the electrostatic potential within the aromatic side chains. This approach served to elucidate the necessity of both the hydrophobic nature of the Phe residue and favorable π -stacking geometries (*face-face/edge-face*) through possible perturbations during peptide self-assembly. Experimentally determined lag times by real-time monitoring of NFGAIL amyloid formation revealed a synergy between enhanced hydrophobic properties and accelerated peptide fibrillation, indicating an independency towards π -stacking geometries (**Figure 3.13b**). TEM micrographs confirmed amyloid formation for all sequences with each unique morphologies and fibril diameters (**Figure 3.13c**). The difluorinated mutant N-[3.5F]Phe-GAIL, most interestingly, owned the by far longest lag time (18.16 ± 1.10 h), thereby hinting an elongation of NFGAIL self-assembly upon fluorination. Molecular modelling experiments for [3.5F]Phe and [2.3.5.6F]Phe depicted a facilitated ability of surrounding water molecules to act as both hydrogen bond acceptor and donor. Particularly for [3.5F]Phe, these binding modes result into strong interactions with the aqueous buffer and, therefore, could cause a retardation of amyloid aggregation by diametrical effects based on fluorine-enhanced polarity (**Figure 3.13d**).¹⁸³ In 2015, Ye *et al.* probed the impact of fluorine-specific interactions on protein–protein interactions between the bovine pancreatic trypsin inhibitor (BPTI) and the protease β -trypsin. Their main approach was the substitution of the BPTIs' crucial Lys15 for enzyme inhibition with Abu, DfeGly and TfeGly. In brief, replacement of Lys with Abu (BPTI_(Abu15)) reduced the inhibitory activity, which was comparably restored in case of BPTI_(DfeGly15) and BPTI_(TfeGly15).¹⁸⁸

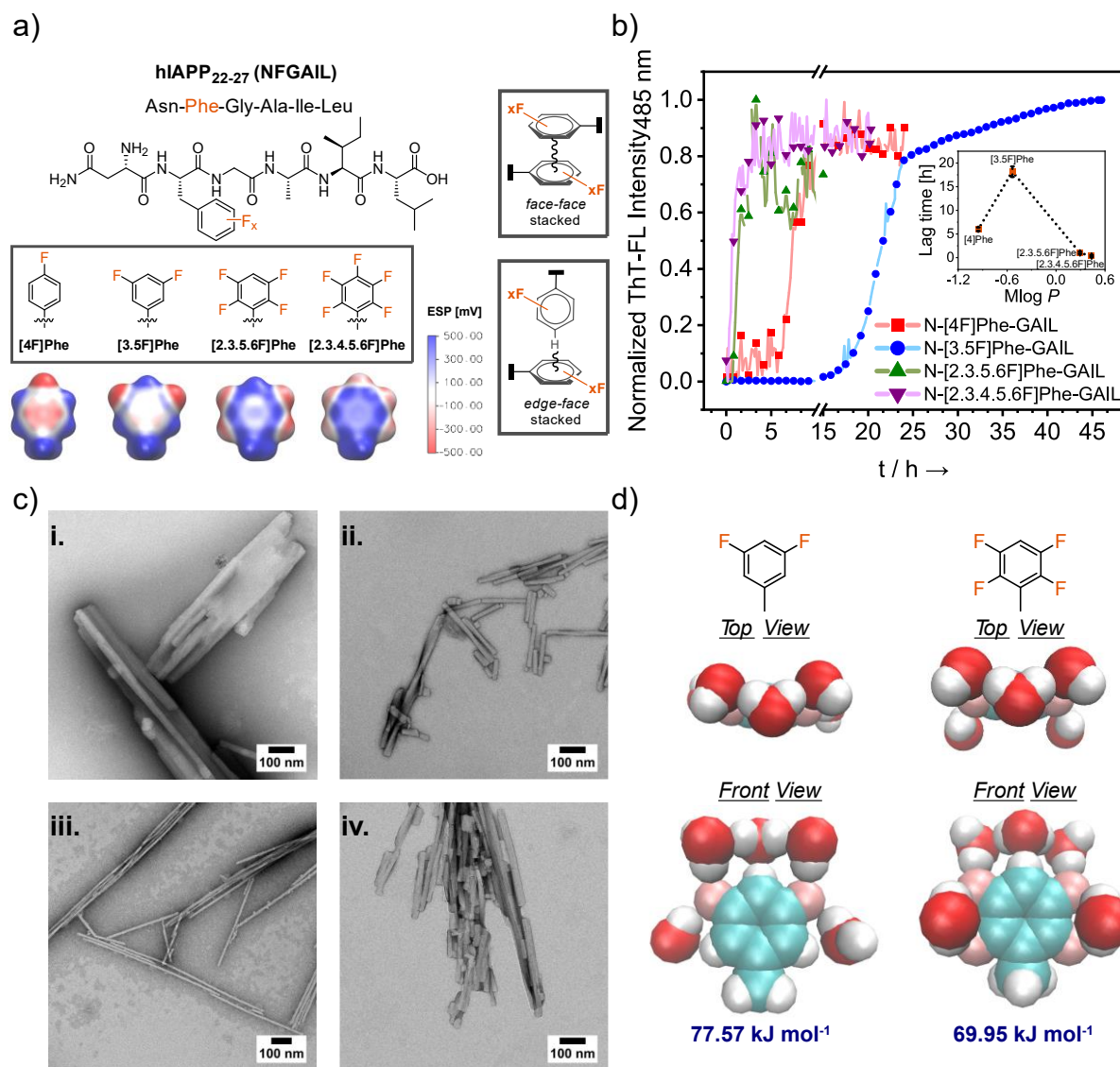


Figure 3.13 Amyloid formation of fluorinated NFGAIL variants: **a)** Chemical structure of the hexapeptide NFGAIL and fluorinated Phe derivatives for probing hydrophobicity and π - π -interactions in amyloid self-assembly. **b)** Thioflavin T based fluorescence assays on amyloid formation with peptides N-[4F]Phe-GAIL [4 mM], N-[3.5F]Phe-GAIL [4 mM], N-[2.3.5.6F]Phe-GAIL [4 mM] and N-[2.3.5.6F]Phe-GAIL [3 mM] dissolved in 10 mM ammonium acetate buffer containing 20 μ M fluorescent dye, pH 7.0 and incubated at 37 °C. **c)** TEM micrographs of NFGAIL solutions after amyloid assembly: **i.** N-[4F]Phe-GAIL, **ii.** N-[3.5F]Phe-GAIL, **iii.** N-[2.3.5.6F]Phe-GAIL and **iv.** N-[2.3.5.6F]Phe-GAIL. **d)** Calculated 5-water clusters for [3.5F]Phe and [2.3.5.6F]Phe based on optimized water-binding geometries. Adapted in a modified version from Chowdhary *et al.* with permission (Copyright © 2020 John Wiley & Sons, Ltd).¹⁸³

In this case, fluorine-induced interactions within the enzymes' active site had beneficial effects on its biofunctionality.^{158, 188} Follow-up investigations by Leppkes *et al.* expanded the library of fluorinated amino acids for the replacement in BPTI at position 15 and probed their inhibitory activity towards the serine protease α -chymotrypsin.¹⁸⁹ Again, BPTI_(Abu15) had a reduced activity than the wild type (**Figure 3.14b**). Comparably enhanced activities found of BPTI_(TfeGly15) and BPTI_(PfpGly15) indicated steric and hydrophobic properties upon side chain fluorination to promote the inhibitor's activity.

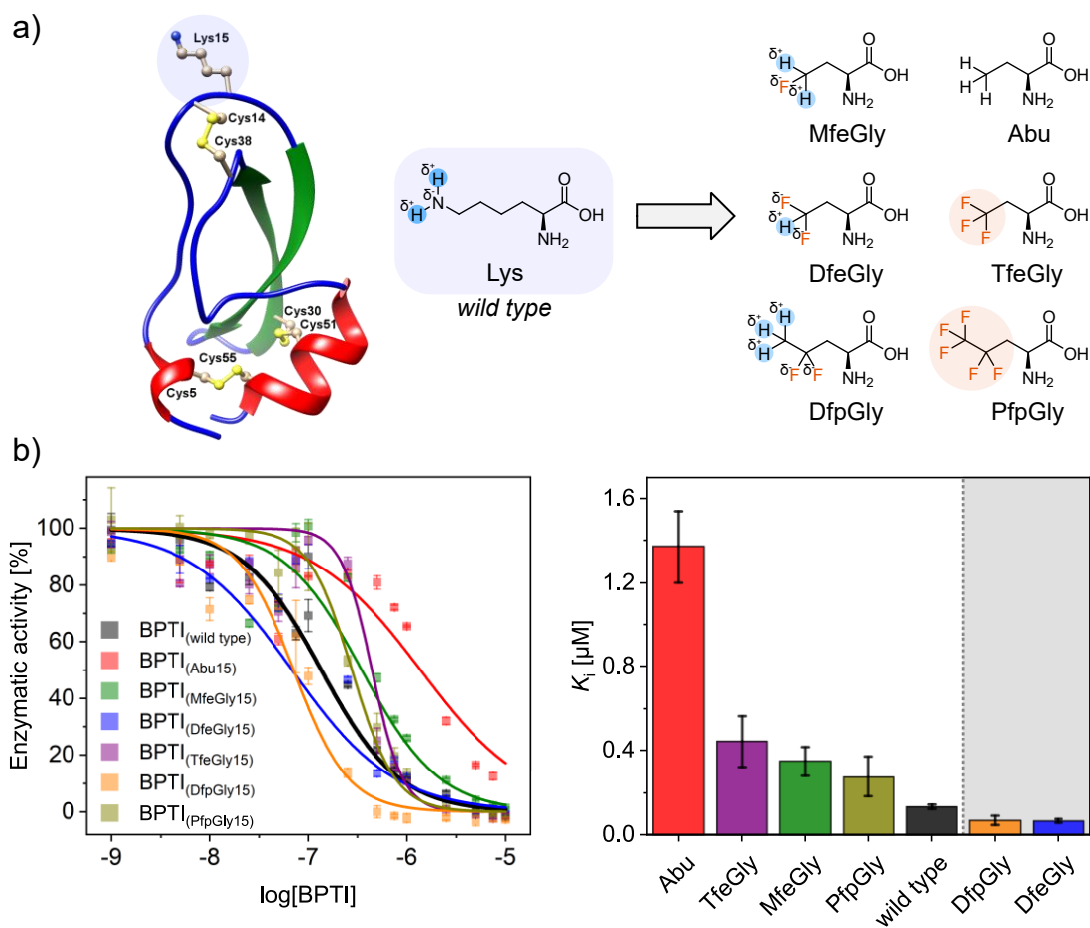


Figure 3.14 a) Site-specific substitution of the P1 position in bovine pancreatic trypsin inhibitor (BPTI) with artificial amino acids possessing either a partially fluorinated (MfeGly, DfeGly, DfpGly) or fully fluorinated fluoroalkyl group (TfeGly, PfpGly). **b)** Inhibition of α -chymotrypsin with fluorinated BPTI variants. Comparison of K_i [μM] reveal enhanced inhibitory activity for BPTI variants bearing both hydrophobic and polar amino acids DfpGly and DfeGly. Adapted from Leppkes *et al.* in a modified version with permission (license: CC BY-NC 3.0).¹⁸⁹

On the other hand, BPTI_(DfeGly15) and BPTI_(DfpGly15) revealed the highest activities among this work. Apparently, the origin of fluorine-induced enzyme-inhibition was considered as a coaction of hydrophobic and polar interactions. Both side chains are more hydrophilic when comparing to TfeGly or, ultimately, PfpGly. Therefore, the superior polarity of partially fluoroalkyl groups in comparison with fluorocarbon (TfeGly) or hydrocarbon derivatives (Abu) was also extensively discussed in recent computational studies by Vila Verde and co-workers.¹⁸⁹⁻¹⁹¹

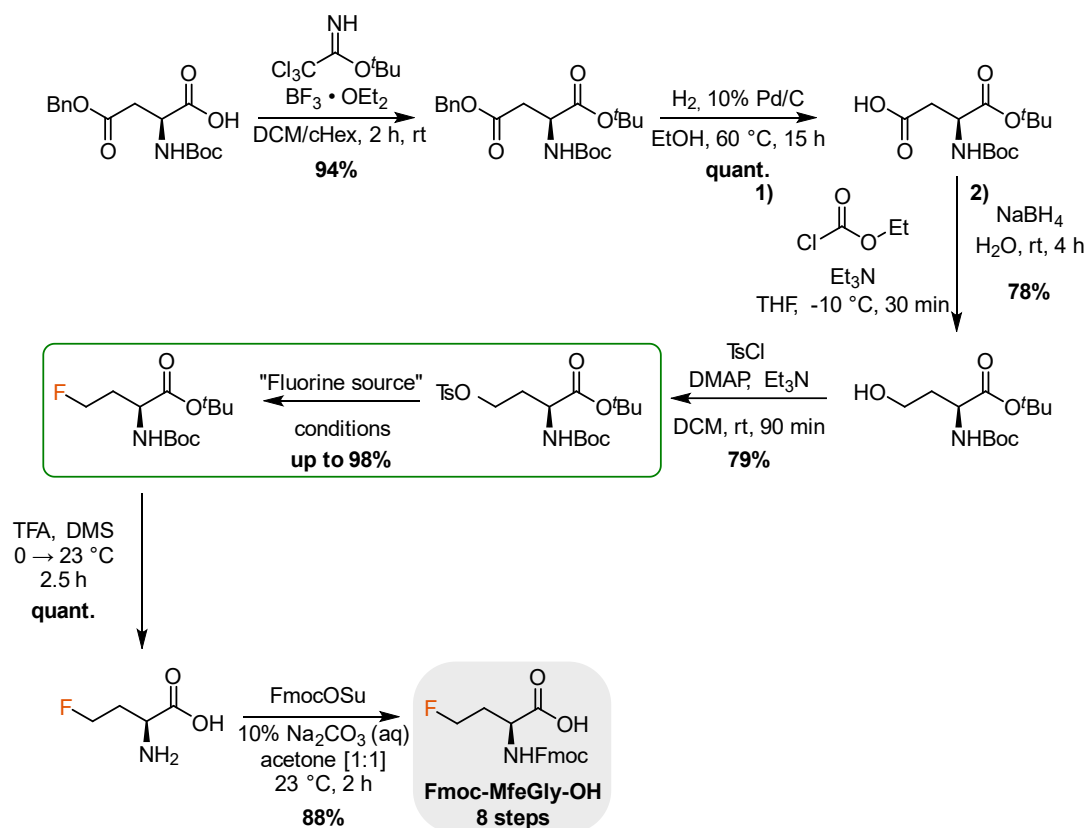
3.5 Synthesis of fluorinated amino acids MfeGly, DfeGly & TfeGly

In this chapter, the standardized synthetic protocols of Fmoc-protected MfeGly, DfeGly and TfeGly are discussed. A selection of synthetic strategies for obtaining fluorinated α -amino acids has been otherwise reviewed in depth by Moschner *et al.* in 2019.¹⁹²

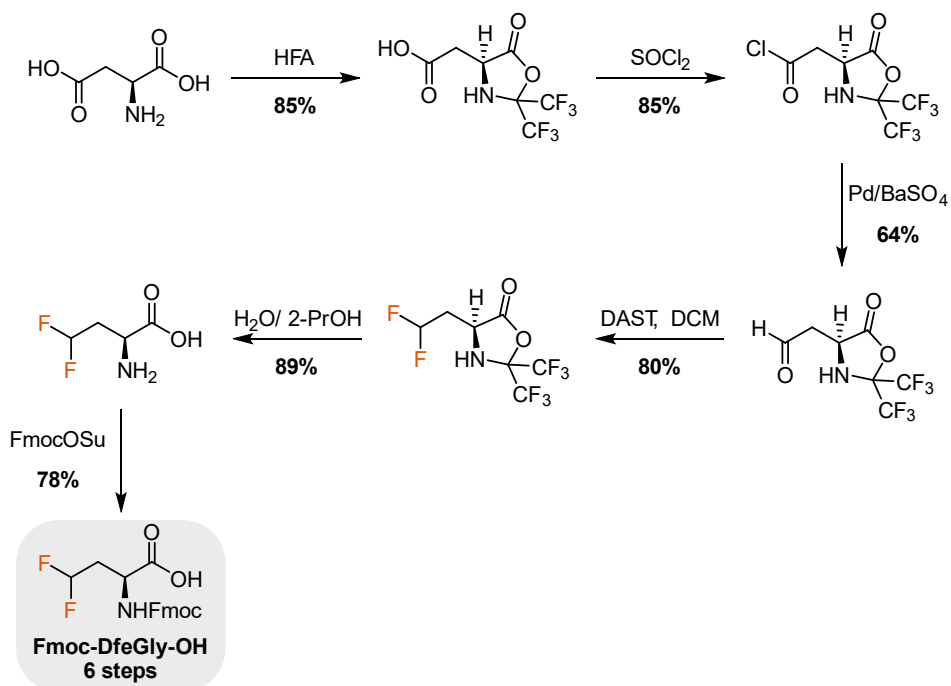
The first enantioselective synthesis of Fmoc-protected MfeGly on the gram scale was published by Leppkes *et al.* in 2020 and comprises an eight-step synthetic route. The synthesis starts with a C-terminal tert-butyl protection of *N*-protected Asp, followed by the hydrogenolysis of the OBn-protecting group of the side chain. This approach enables the selective reduction of the side chain's carboxylic acid to a hydroxyl group through a two-step approach including the preparation of mixed anhydrides with ethyl chloroformate and subsequent treatment with the reducing agent sodium borohydride (NaBH₄). The key step of this strategy is constituted by the nucleophilic fluorination of the tosyl-protected homoserine-derivative for which various fluorination strategies with up to 98% yields (TASF (5 equiv.), Et₃N · 3 HF (1.5 equiv.) in THF/DCM) were tested. At last, the global deprotection of the acid-labile tert-butyl and Boc-functionality followed by the N-terminal Fmoc-protection in basic conditions leads to the isolation of Fmoc-MfeGly-OH in overall yields of up to 50% (**Scheme 3.1**).¹⁹³

For synthesizing the difluorinated variant Fmoc-DfeGly-OH, Burger and co-workers introduced in 1996 a six-step approach starting with the reaction of Asp with hexafluoroacetone HFA to form 2,2-bis(trifluoromethyl)-1,3-oxazolidin-5-one accompanied by the protection of both N- and C-terminal group. Further treatment with thionyl chloride affords the corresponding acid chloride, which is transformed into an aldehyde with Pd/BaSO₄. Again, a nucleophilic fluorination takes place with diethylaminosulfur trifluoride (DAST) as fluorine source, followed by hydrolysis of the HFA-protecting group and Fmoc-protection (**Scheme 3.2**).¹⁹⁴

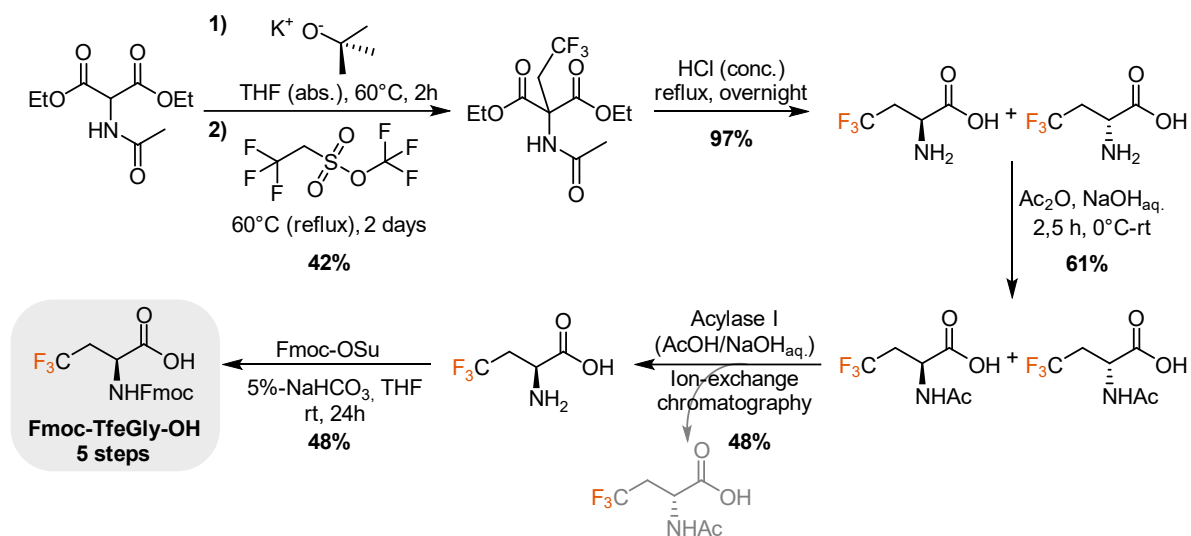
In 1988, Tsushima *et al.* described a chemoenzymatic five-step approach for obtaining Fmoc-TfeGly-OH. The fluorinated side chain is incorporated at first by reaction of diethyl *N*-acetamidomalonate with 2,2,2-trifluoroethyl trifluoromethanesulfonate with prior deprotonation (potassium tert-butoxide KO^{*t*}Bu).¹⁹⁵ Hydrolysis of this intermediate leads to racemic TfeGly, subsequently treated by *N*-terminal acetylation. This step is crucial for the enantioselective isolation of L-TfeGly through Acylase I. Subsequent ion-exchange chromatography and Fmoc-protection results in Fmoc-TfeGly-OH (**Scheme 3.3**).¹⁹⁵



Scheme 3.1 Synthesis of monofluorinated Abu-derivative Fmoc-MfeGly-OH by Leppkes *et al.*¹⁹³



Scheme 3.2 Synthesis of difluorinated Abu-derivative Fmoc-DfeGly-OH by Burger *et al.*¹⁹⁴

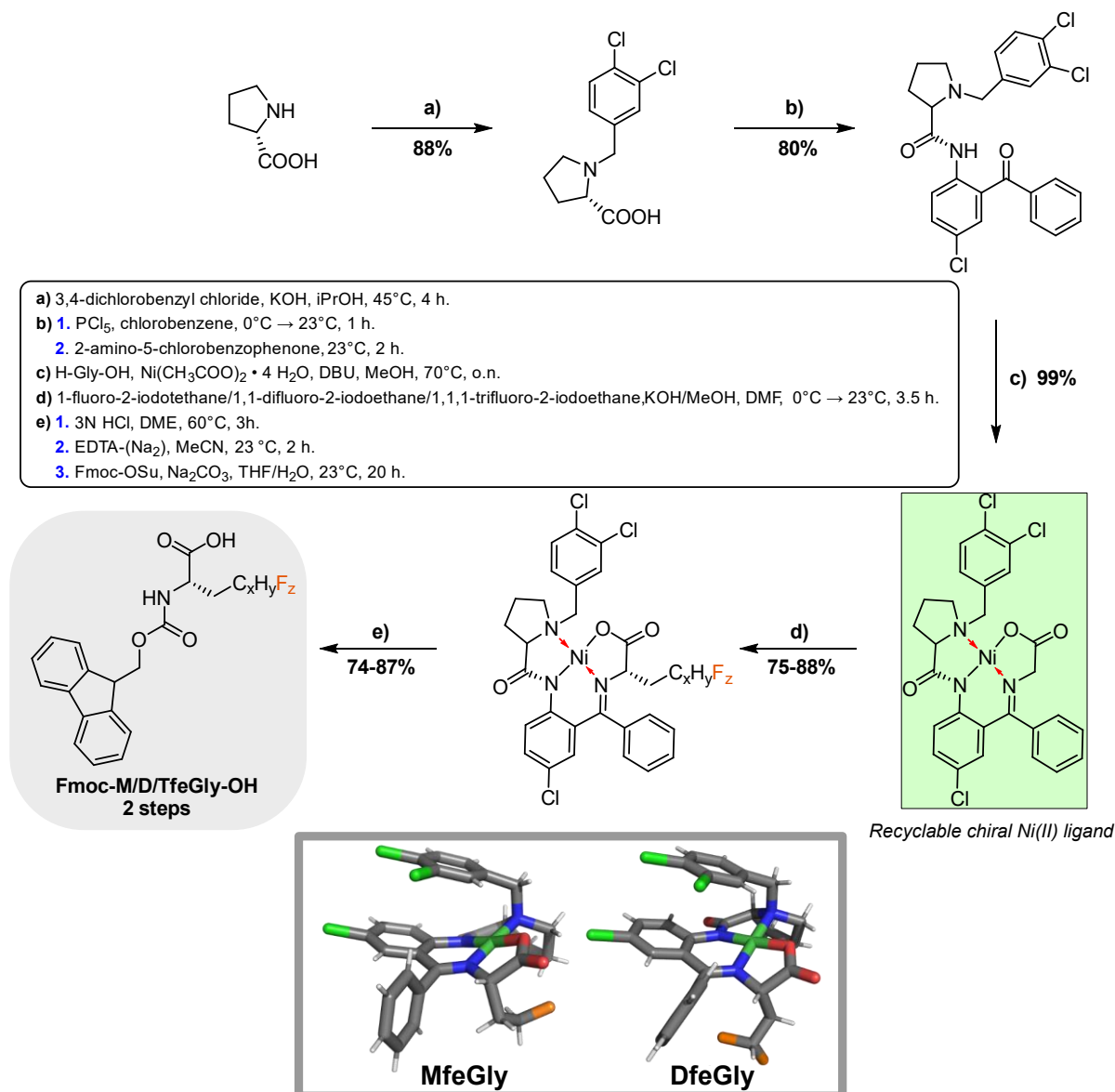


Scheme 3.3 Synthesis of trifluorinated Abu-derivative Fmoc-TfeGly-OH by Tsushima *et al.*¹⁹⁵

Due to equal proportions of the D-enantiomer, however, the enzyme-assisted isolation of L-TfeGly has a theoretical maximum yield of only 50% (**Scheme 3.3**).¹⁹⁵

Most studies focusing on fluorinated peptides or proteins applied the incorporation of only one or a few fluorinated amino acids. This raises the simple but crucial question why synthetic peptides with higher or even exclusive proportions of these building blocks have not been described so far. The most likely answer, as can be taken from the above-discussed protocols for obtaining fluorinated Abu derivatives, is the limited accessibility of tailor-made amino acids. In fact, vast majority of these compounds are not commercially available and require complex multi-synthetic strategies.

Being aware of the emerging necessity on fluorinated amino acids, Soloshonok *et al.* developed a series of chiral Ni(II) complexes for the stereoselective synthesis of such building blocks like, for example, Fmoc-protected TfeGly.¹⁹⁶⁻²⁰¹ As a general procedure, the amino acid Pro is alkylated with 3,4-dichlorobenzyl chloride. To selectively alkylate the amine-moiety, the reaction is carried out in a basic KOH / iPrOH solution. In a further reaction, the intermediate reacts with PCl₅ to form an acid chloride, which enables the formation of an amide bond with the amine-moiety of 2-amino-5-chlorobenzophenone. The formation of the Schiff base as a chelating ligand occurs through the reaction with the amino acid Gly, nickel acetate tetrahydrate and the base DBU. The key step comprises the asymmetric alkylation of the chiral Ni-ligand with a fluorinated alkyl iodide as desired side chain of the amino acid (e.g. C₂H₂F₃I for TfeGly). Hence, X-ray diffraction experiments exposed an unique conformation of the Ni(II) ligand by strong electrostatic attractions between the two chlorinated aromatics in close proximity (**Scheme 3.4**).



Scheme 3.4 Synthesis of Fmoc-MfeGly-OH, Fmoc-DfeGly-OH and Fmoc-TfeGly-OH through an asymmetric and Ni(II)-complex mediated stereoselective synthesis reported by Soloshonok *et al.* and Hohmann *et al.*. The enantioselective alkylation of the Ni(II) complex was further supported by X-ray crystallographic structure determination (shown for the synthesis of MfeGly and DfeGly). The X-ray structures were adapted from Hohmann *et al.* with permission (Copyright © 2022 American Chemical Society).^{197, 198, 200, 202}

This conformation contributes to the main formation of the (*S*)-isomer and steric interferences for the energetically unfavorable (*R*)-alkylation.²⁰¹ Subsequent disassembly in acidic conditions and simultaneous Fmoc-protection finally leads to the isolation of desired products. Recently, the Kocsch laboratory extended this approach for obtaining enantiomerically pure Fmoc-protected aliphatic fluorinated amino acids MfeGly, DfeGly, DfpGly, PfpGly, (*2S,3S*)-TfVal, (*2S,3R*)-TfVal, 5³-(*2S,3R*)-TfIle and 5³-(*2S,3S*)-TfIle.²⁰² In fact, the recovery and recycling of chiral ligands allows an efficient and practical two-step strategy for the generous fabrication of these building blocks on the gram-scale.

3.6 Fluorinated peptide-based β -sheet hydrogelators

The influence of side chain fluorination on peptide β -sheet assembly and hydrogelation has been predominantly studied by substitution of aromatic amino acids with, for the most part, commercially available fluorinated counterparts. Surprisingly, the sum of studies is limited to fluorinated Fmoc-functionalized amino acids, di-, tri- and very few oligopeptides. Two pioneers in this field of research, Bradley L. Nilsson and Hsin-Chieh Lin, have particularly studied low molecular-weight β -sheet hydrogelators for exploring the structure-activity relationships upon fluorination with main focus on supramolecular assembly and potential applicability (**Table 3.2**).^{94, 203}

Table 3.2 Rheological properties of fluorinated Phe-based hydrogelators (G' = storage modulus; G'' = loss modulus). Non-fluorinated peptides (highlighted in yellow) are listed for comparison.

Hydrogelator	c (wt%)	G' (Pa)	G'' (Pa)	Source
Fmoc-F ₅ -Phe	~0.2	3056 ± 71	320 ± 12	B. L. Nilsson (2000) ²⁰⁴
Fmoc-2F-Phe	~0.2	2185 ± 59	154 ± 20	B. L. Nilsson (2010) ²⁰⁵
Fmoc-3F-Phe	~0.2	4219 ± 209	404 ± 39	B. L. Nilsson (2010) ²⁰⁵
Fmoc-4F-Phe	~0.2	443 ± 85	35 ± 16	B. L. Nilsson (2010) ²⁰⁵
Ac-(Cha-Lys-Cha-Lys) ₂ -NH ₂	0.95 (8 mM)	75.6 ± 10.1	24.6 ± 5.5	B. L. Nilsson (2011) ²⁰⁶
Ac-(Phe-Lys-Phe-Lys) ₂ -NH ₂	0.93 (8 mM)	1642.9 ± 19.3	131.7 ± 7.1	B. L. Nilsson (2011) ²⁰⁶
Ac-(F ₅ -Phe-Lys-F ₅ -Phe-Lys) ₂ -NH ₂	1.21 (8 mM)	1961.1 ± 78.6	191.7 ± 6.4	B. L. Nilsson (2011) ²⁰⁶
Fmoc-Phe	~0.2	39 ± 3	5 ± 1	B. L. Nilsson (2016) ²⁰⁷
Fmoc-4F-Phe	~0.2	102 ± 7	9 ± 3	B. L. Nilsson (2016) ²⁰⁷
Fmoc-Phe-DAP	1.5 (33.7 mM)	383 ± 100	59 ± 17	B. L. Nilsson (2019) ²⁰⁸
Fmoc-3F-Phe-DAP	1.5 (33.7 mM)	21311 ± 2057	3973 ± 419	B. L. Nilsson (2019) ²⁰⁸
Fmoc-F ₅ -Phe-DAP	1.8 (33.7 mM)	10776 ± 902	2273 ± 209	B. L. Nilsson (2019) ²⁰⁸
Fmoc-Phe-DAP + Fmoc-F ₅ -Phe-DAP	1.7 (33.7 mM)	17109 ± 1925	2279 ± 163	B. L. Nilsson (2019) ²⁰⁸
Fmoc-2F-Phe-DAP	0.46 (10 mM)	21 ± 2	3.3 ± 0.2	B. L. Nilsson (2022) ²⁰⁹
Fmoc-4F-Phe-DAP	0.46 (10 mM)	1289 ± 110	121 ± 11	B. L. Nilsson (2022) ²⁰⁹
PFB-Phe	1.0	3.0 * 10 ³	1.5 * 10 ²	H.-C. Lin (2014) ²¹⁰
PFB-Phe-Gly	1.0	1.2 * 10 ⁴	1.5 * 10 ³	H.-C. Lin (2014) ²¹⁰
PFB-Phe-Phe	1.0	3.4 * 10 ⁴	8.0 * 10 ³	H.-C. Lin (2014) ²¹⁰
PFB-Phe + PFB-Phe-Phe [1:1]	1.0	3.0 * 10 ³	2.0 * 10 ²	H.-C. Lin (2015) ²¹¹
benzyl-Phe-Phe	≤ 5.0	-	-	H.-C. Lin (2015) ²¹²
4-fluorobenzyl-Phe-Phe	2.0	~5700	~1500	H.-C. Lin (2015) ²¹²
PFB-(FFRGD) (Ca ⁺)	2.0	4.7 * 10 ⁴	8.6 * 10 ³	H.-C. Lin (2022) ²¹³

2F: *ortho*-F; 3F: *meta*-F; 4F: *para*-F; F₅: perfluorinated "[2.3.4.5.6f]Phe"; PFB: perfluorobenzyl

In 2010, the Nilsson group reported side chain fluorination of Fmoc-Phe to support intermolecular assembly *via* hydrophobic and dipole interactions between the aromatic

residues. The degree of aromatic fluorination as well as the local position on the benzyl ring (*ortho*, *meta*, *para*) has been evaluated to specifically strengthen the hydrogel stiffness.^{204, 205, 207} In a further report, global incorporation of [2.3.4.5.6]Phe into a (Phe-Lys)-repeating unit led to higher aggregation rates and rheological stability. Interestingly, cyclohexylalanine (Cha) was found to provide the highest value of peptide hydrophobicity in this work, but also a dramatic loss in hydrogel stability. This circumstance rather indicated π - π interactions than hydrophobicity of each peptide to promote the rigidity of entangled hydrogel networks (**Figure 3.15a**)²⁰⁶.

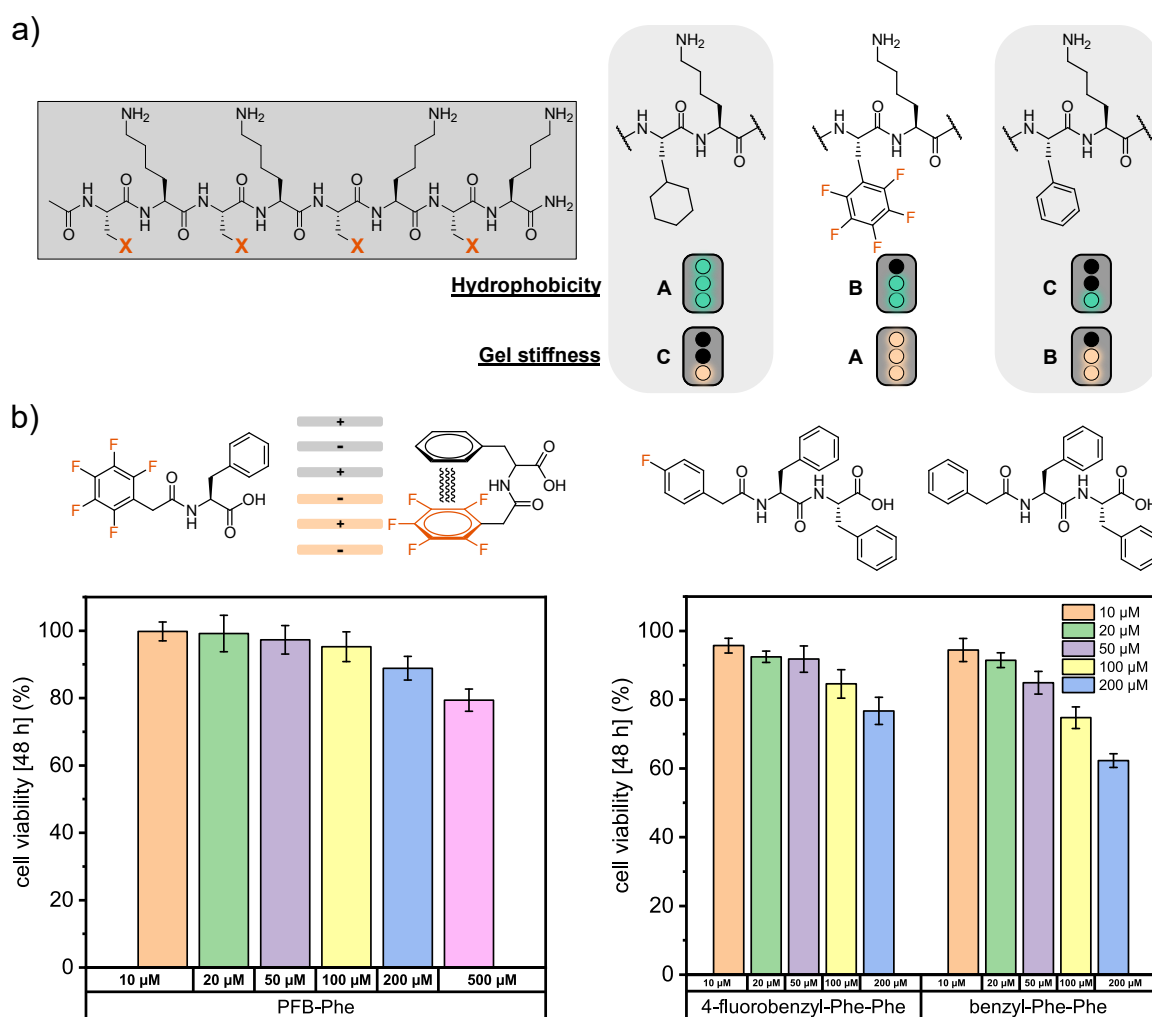


Figure 3.15 a) Trends in hydrophobicity and gel stiffness determined for amphipathic X-Lys sequences (X: Phe, [2.3.4.5.6F]Phe, Cha).²⁰⁶ **b)** Chemical structures, proposed π - π stacking and cell viability data of PFB-Phe, 4-fluorobenzyl-Phe-Phe and benzyl-Phe-Phe. Adapted from Hsu *et al.* and Wu *et al.* in a modified version.^{210, 212}

C-terminal modification of Fmoc-Phe with diaminopropane (DAP) has shown to provide rapid hydrogel formation upon addition of physiological salts. Thus, a 1:1 co-assembled hydrogel of Fmoc-Phe-DAP and perfluorinated Fmoc-^{F5}Phe-DAP displayed higher G' values than the gels composing of exclusively one component, a potential consequence of

attractive π - π interactions by alterations on the electrostatic quadrupole of Phe (**Table 3.2**). Similarly, encapsulation of the aromatic drug Diclofenac yielded the lowest level of drug release for the hydrogel composed of Fmoc-^{F5}Phe-DAP. This supramolecular fluoro-hydrogel, furthermore, succeeded in drug delivery into mice.^{208, 209}

The Lin group worked on perfluorobenzene (PFB)-based hydrogelators (**Figure 3.15b**). These peptide scaffolds were specially designed for exploiting parallel stacking of PFB and the benzyl side chain of Phe, leading to peptide oligomerization, fibril, and hydrogel formation. The rheological strength of the PFB-capped Phe moiety and several dipeptide derivatives of Phe are strongly dependent on both aromaticity and hydrophobicity of the C-terminal amino acid. Further work by Wu *et al.* on 4-fluorobenzyl & benzyl-capped diphenylalanine revealed the fluorinated compound to form a rigid and less toxic hydrogel than the native counterpart which, much more, failed to form stable hydrogel matrices (**Table 3.2**).²¹²

In summary, the effects of fluorine on supramolecular β -sheet assembly, whether based on enhanced hydrophobicity or beneficial alterations in the ESP of an altered σ -framework, has yet been studied for a limited range of aromatic SAPs. The influence of aliphatic fluorinated amino acid on β -sheet hydrogelation, however, has not been studied.

3.7 Fluorinated antimicrobial peptides

The future development of synthetic AMPs is crucial to successfully combat the progressive evolution of antimicrobial resistances. Therefore, the utilization of fluorinated amino acids may anticipate as a useful approach to enhance membrane permeability and, thus, strengthen the non-specific AMP targeting onto the bacterial envelope.²¹⁴

In one of the first-ever reports on fluorinated AMPs, Gimenez *et al.* prepared a library of amphipathic pentapeptides (FKFKF) bearing the fluorinated aromatic derivatives [4F]Phe (fF) and [4-CF₃]Phe (cf3F). Fluorination was found to intensify the antibiotic potency of this peptide against *E. coli* and *S. aureus*, which was attributed to the increased hydrophobicity of the fluorinated derivatives. (Table 3.3).²¹⁵

Table 3.3 Hydrophobicity and antibacterial activity of the alternating pentapeptide “FKFKF” and its fluorinated derivatives - Gimenez *et al.*²¹⁵

Compound	t _R (RP-HPLC) (min)	MIC (µg/mL)	
		<i>E. coli</i>	<i>S. aureus</i>
H-FKFKF-NH ₂	15.0	50	75
H-(fF)K(fF)K(fF)-NH ₂	16.9	37.5	25
H-FK(cf3F)KF-NH ₂	18.1	37.5	25
H-(cf3F)KFK(cf3F)-NH ₂	20.5	37.5	18.75
H-(cf3F)K(cf3F)K(cf3F)-NH ₂	22.6	18.75	4.68

fF: [4]Phe = *para*-fluoro-Phe; cf3F: [4-CF₃]Phe = *para*-trifluoromethyl-Phe

Gottler *et al.* reported on the replacement of all Val and Ile residues in the α -helical AMP Pexiganan (MSI-78, H-GIGKFLKKAKKFGKAFVKILKK-OH) with HfLeu (Table 3.4). The fluorinated peptide (fluorogainin-1) had a significantly less helical content, somewhat similar activities towards a panel of both Gram-positive and Gram-negative strains and omitted blood-cell hemolysis up to a concentration of 250 µg/mL. Contrary results were obtained when substituting both residues Val14 and Val16 in Protegrin-1 (PG-1, H-RGGRLCYCRRRFCVCVGR-NH₂) with HfLeu. Here, fluorination was found to preserve the structural conformation but causing mainly decreased AMP activities, respectively. Also, higher rates of hemolytic activity (100% hemolysis, 7.81 µg/mL) than for the native sequence (44% hemolysis, 7.81 µg/mL) were evaluated. Notably, increased AMP activities against *K. pneumoniae* and *S. aureus* were determined in both studies.^{216, 217}

Table 3.4 Antibacterial activity of Pexiganan (MSI-78), Protegrin-1 (PG-1) and their HfLeu-containing derivatives Fluorogainin-1 and PG-1-FF – Gottler *et al.*^{216, 217}

Strain	MIC (µg/mL)			
	MSI-78	fluorogainin-1	PG-1	PG-1-FF
<i>B. subtilis</i>	< 4	8	25	> 200
<i>K. rhizophila</i>	< 4	8	25	> 200
<i>E. aerogenes</i>	> 250	> 250	6.25	12.5
<i>P. mirabilis</i>	> 250	> 250	> 200	> 200
<i>S. aureus</i>	61	16	25	6.25
<i>K. pneumoniae</i>	> 250	16	-	50
<i>S. sonnei</i>	16	32	12.5	12.5

In 2007, the Kumar laboratory examined a series of HfLeu-substituted versions of the α -helical AMPs buforin-2 (BII1, H-TRSSRAGLQFPVGRVHRLLRK-OH) and magainin-2 (M2, H-GIGKFLHALKKFLKAFLAELMNS-NH₂) (Table 3.5). A library of synthetic AMP derivatives was established, including the buforin-mutant BII1F2 (H-TRSSRAGLQFPVGRVHR-HfLeu-HfLeu-RK-OH) and the magainin-mutant M2F5 (H-GIGKF-HfLeu-HA-HfLeu-KKF-HfLeu-KAF-HfLeu-AE-HfLeu-MNS-NH₂).²¹⁸ Secondary structure analysis revealed higher α -helical contents in both fluorinated buforin and magainin peptides. MIC data of buforin-2 and its variants emphasized the increase in AMP potency to originate from stabilizing effects on peptide folding by fluorine-enhanced hydrophobicity. With regards to the magainin-2 series, exceeding a threshold of hydrophobicity by fluorination resulted in lower MICs and an undesirable increase in hemolytic activity.²¹⁸

Recent studies focused on incorporating fluorinated aromatic amino acids into AMP scaffolds but came to controversial outcomes as well. For example, Setty *et al.* studied a series of fluoro-phenylalanine variants of the AMP Temporin L (TL).²¹⁹

Table 3.5 Antibacterial activity of (fluorinated) buforin and magainin-mutants – Meng *et al.*²¹⁸

Compound	% (9:1 ACN/H ₂ O + TFA) (RP-HPLC) ^{1*}	MIC (µg/mL)		HC ₅₀ (µg/mL) (50% lysis of hRBCs)
		<i>E. coli</i>	<i>B. subtilis</i>	
BII1	31.0	20	10	400
BII1F2	37.0	5	2.5	400
M2	56.5	2.5	2.5	175
M2F5	85.8	40	10	11

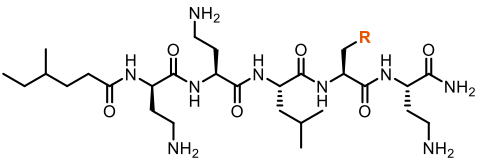
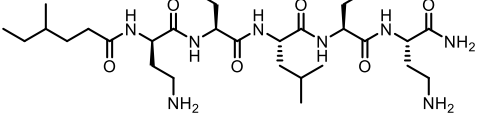
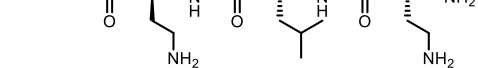
^{1*} Percentages of solvent mixture serves as indicator of hydrophobicity.

Table 3.6 Antibacterial activity of Temporin L (TL) and its fluorinated derivatives – Setty *et al.*²¹⁹

Peptide	Sequence	MIC (μ M)		Helicity (%)
		<i>E. coli</i>	<i>S. aureus</i>	
TL	H-FVQWFSKFLGRIL-NH ₂	3.12	6.25	36.59
TL-2	H-[2.6F]PheVQWFSKFLGRIL-NH ₂	3.12	12.5	7.95
TL-3	H-FVQW[2.6F]PheSKFLGRIL-NH ₂	3.12	25	7.19
TL-4	H-FVQWFSK[2.6F]PheLGRIL-NH ₂	6.25	25	2.29
TL-5	H-[2.6F]PheVQW[2.6F]PheSK[2.6F]PheLGRIL-NH ₂	12.5	25	0.37

As depicted in **Table 3.6**, their MIC data indicated a synergy between antimicrobial potency and folding propensity.²¹⁹ This trend is accompanied by a decrease of α -helical contents through higher degrees of aromatic fluorination. In comparison with native TL, the fluorinated peptides failed to fold into stable helical structures and revealed higher MICs.²¹⁹ Glossop *et al.* came to opposite conclusions on fluorine-imparted AMP potency after investigating the bactericidal activities of fluorophenylalanine-substituted derivatives from the antimicrobial pentapeptide Battacin. All sequences were found to form disordered structures in solution, whereas their antibacterial efficiency was mainly governed by the degree of aromatic fluorination as shown in **Table 3.7**.²²⁰

Table 3.7 Antibacterial activity of (fluorinated) Battacin derivatives – Glossop *et al.*²²⁰

Residue "R"	Peptide motif	MIC (μ g/mL)			
		<i>E. coli</i>	<i>S. aureus</i>	<i>P. aeruginosa</i>	<i>C. albicans</i>
Phe		50	6.3	100	> 100
[4F]Phe		50	6.3	50	100
[2.3.4.5.6F]Phe		12.5	3.1	25	> 100

In conclusion, the incorporation of side chain fluorinated amino acids has shown to alter the inhibitory activity of AMPs against a wide array of pathogenic species with clinical relevance but in varying magnitudes. In fact, current state-of-the-art in this field of research relies on a limited stock of scientific reports published till date.

4 Effects of fluorinated amino acids on the proteolytic stability of peptides

Due to a growing acceptance of synthetic peptides as potential therapeutics together with routinely based fluorine screening on drug candidates, the incorporation of fluorine-containing amino acids into self-assembling or antimicrobial peptides bears exciting perspectives for pharmaceutical applications. The considerably low bioavailability of peptide-based drugs arises from rapid proteolysis.²²¹ Among all peptidases, serine proteases are perhaps the most extensively studied class till date. The spatial structure of a multitude of these proteases owns a pronounced similarity in their active site bearing the so-called catalytic triad “Ser-His-Asp”. Adjacent to the catalytic triad, the subsite pockets are responsible for enzyme-substrate recognition. According to *Schechter & Berger* nomenclature, C-terminal residues of the scissile bond are defined as P1', P2', P3' [...] and residues of the N-terminal side are defined as [...] P3, P2, P1. The S-sites on the protease are listed accordingly. The P1 and P1' residues (accommodated in the S1/S1' subsites) bear the scissile amide bond (**Figure 4.1, top**).^{222, 223} During enzymatic degradation (**Figure 4.1, center**), the close proximity of the negatively charged Asp to the electron rich His strengthens the basicity of the imidazole nitrogen that promotes the nucleophilic attack of an activated Ser on the substrate's carbonyl carbon (i.). This results into a first tetrahedral intermediate (ii.) and, subsequently, a covalent acyl-enzyme (iii.) with release of the C-terminal fragment. Stabilizing the negative charge formed on the tetrahedral transition state is performed by the so-called *oxyanion hole* which are main-chain NH groups alongside the nucleophilic Ser. A further nucleophilic attack by a water molecule causes the generation of a second tetrahedral intermediate (iii.). Release of the N-terminal fragment finally leads to the regeneration of the catalytic site (iv.).^{224, 225}

The specificity of each serine protease is defined by the substrate-binding site's topology in the active center and primarily achieved by substrate recognition in the P1 position. In the S1 subsite of the pancreatic enzyme β -trypsin, for example, the carboxylate group of Asp189 is decisive for substrate binding of cationic charged P1 residues like Lys or Arg (**Figure 4.1, bottom**).²²⁶ In case of the pancreatic α -chymotrypsin, the S1 pocket (Ser189, Gly216, and Gly226) is tailored for large, lipophilic side chains, preferentially accommodating aromatic residues (Phe, Tyr, Trp) as P1 counterparts. The narrow S1 of elastase suits for hydrophobic side chains such as Ala and Val (**Figure 4.1, bottom**).²²⁶

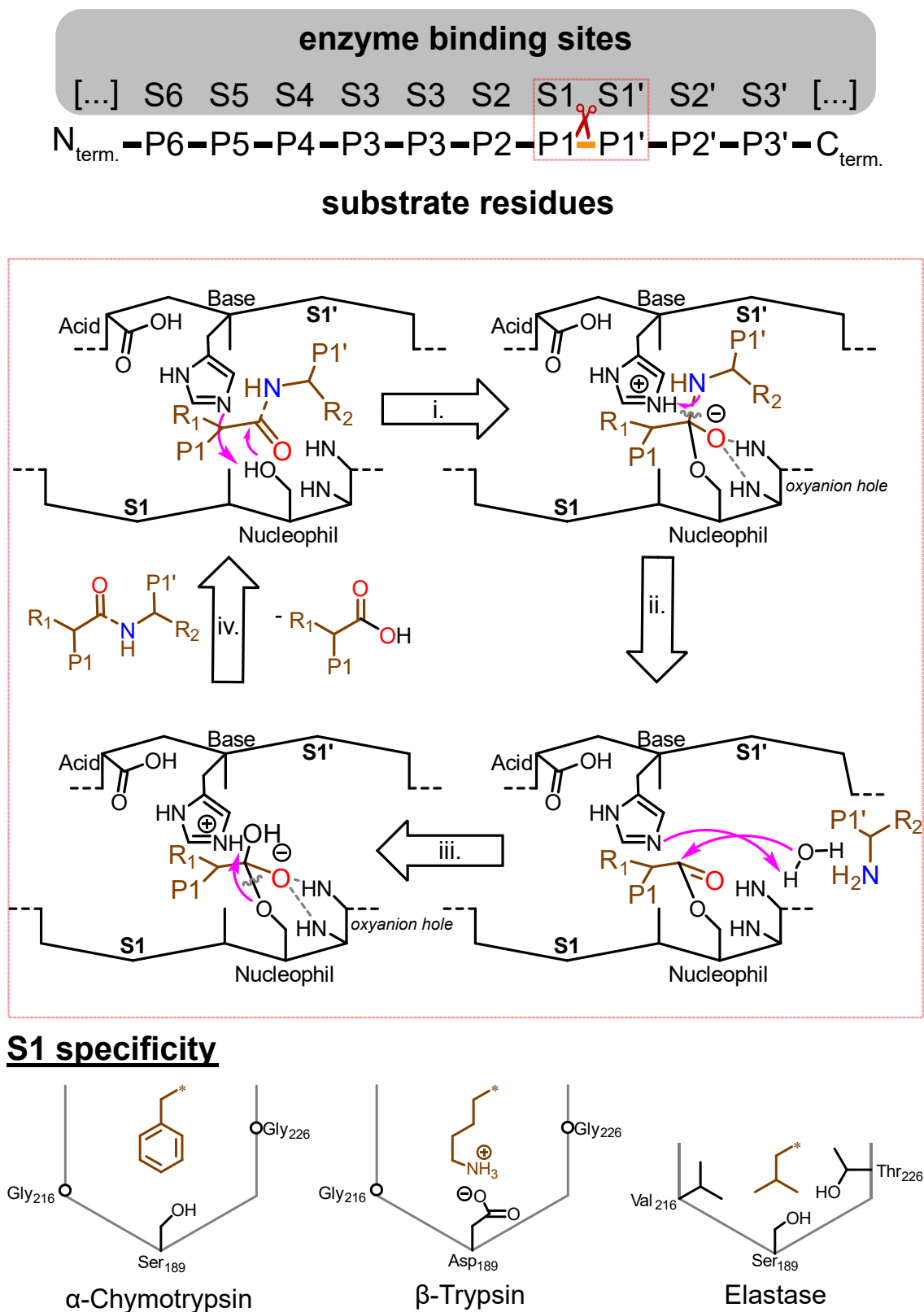


Figure 4.1 Schematic representation of enzyme–substrate interaction according to *Schechter & Berger* nomenclature (**top**).²²³ The catalytic mechanism of serine proteases governed by the catalytic triad is subdivided into: i. first tetrahedral state, ii. enzyme-acyl complex, iii. second tetrahedral state, iv. substrate release and regeneration of the active site (**center**). The unique S1 pockets of α -chymotrypsin, β -trypsin, and elastase determines the enzymes' substrate specificity (**bottom**).²²⁵

Few studies reported on the importance of adjacent P1'-S1' interactions. In 1994, Schellenberger *et al.* accomplished the first large investigation on characterizing the S' subsite specificities of homologous serine proteases including α -chymotrypsin and β -trypsin. Increasing the spatial demand of the P1' residue has shown to favor P1'-S1' interactions in case of α -chymotrypsin. Hydrophobic and unbranched side chains like Met were found to be better accommodated by the S1' subsite than the branched Ile or bulky aromatic amino acids (Trp). Highest rate constants were observed for the cationic amino acids Lys and Arg, explained by electrostatic interactions with the residues Asp35 and Asp64 in the S1' pocket of α -chymotrypsin.^{227, 228} The S1' specificity of β -trypsin is very broad, but with a pronounced preference for hydrophobic residues in P1'. The S3' subsite of both proteases displays a manifold of substrate compatibilities and accommodate D-amino acids as well. Hence, the S3' subsite is reported to overlap the S1' site so that large amino acid residues at P1' or P3' position probably form contacts with both S-pockets. This explains the subsite-similarity in S1' and S3' specificities for both digestive enzymes.^{227, 228}

The incorporation of non-natural amino acids in high proportions is a commonplace strategy to address protease degradation. D- or β -amino acid substitution is frequently reported for disturbing and also prohibiting enzyme-substrate-binding by antagonistic stereochemistry properties. For example, Swanekamp *et al.* determined significantly enhanced rates of proteolytic stability for a (FKFE)₂ hydrogelator sequence against α -chymotrypsin and β -trypsin when substituting L-Phe and L-Lys with their D-enantiomers (Figure 4.2).²²⁹

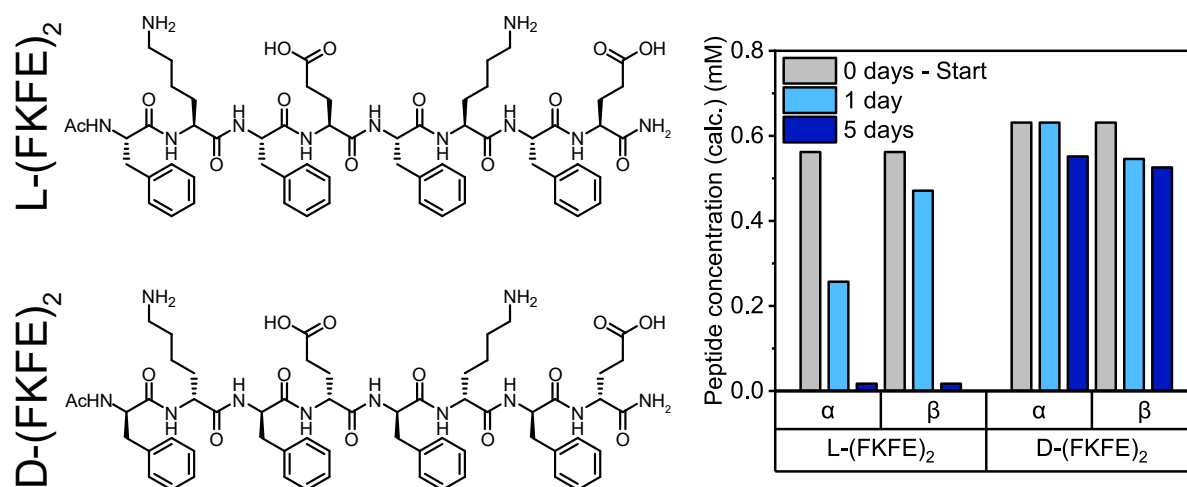


Figure 4.2 Proteolytic degradation of amphipathic peptides L-(FKFE)₂ and D-(FKFE)₂ monitored via RP-HPLC over five days. As reported by Swanekamp *et al.*, the utilization of D-amino acids promoted significantly enhanced stability over proteolytic degradation.²²⁹

In a further study, Mangelschots *et al.* achieved a beneficial enzymatic resistance (up to 120-fold) of a Phe-based hydrogelator by incorporation of β -homophenylalanine.²³⁰ Till date, various design strategies like terminal modifications (acetylation, amidation, *N*-methylation), lipidation, cyclization, glycosylation, and the implementation of peptidomimetics were successfully probed to mask the potential cleavage sites of (bioactive) peptides, thereby impeding the active site of the protease and, finally, proteolytic digestion.²³¹

Replacing an oxidizable C-H group by a strong C-F group onto metabolically labile sites has proven in several cases to increase the bioavailability of drug molecules *in vivo*.¹⁴⁸

In the context of fluorinated amino acids, however, a wide range of published papers focusing on this topic are available till date, describing both an enhanced stability of fluorinated peptides against proteolysis as well as rapid digestion rates in comparison to their native counterparts.^{231, 232} First attempts in 1997 by Kokschi *et al.* explored the site-specific incorporation of C $^{\alpha}$ -(fluoro)alkylated amino acids in five different positions relative to the predominant cleaving site of α -chymotrypsin. Unsubstituted model peptides Z-Ala-Phe-Leu-NH₂ & Z-Phe-Ala-Ala-NH₂ were rapidly hydrolyzed, whereas α,α -disubstituted P1 mutants remained persistent under enzymatic conditions. The steric constraints of both α -methylated and α -trifluoromethylated (α Tfm) side chains led to pronounced retardation of proteolysis by substitutions with both at P2', P2 and even P3. When occupying the P1' position, notably, the (*S,R,S*)-diastereomer of α TfmAla was hydrolyzed rapidly, but the (*S,S,S*)-diastereomer remained persistent similar as the Aib-substituted peptide. Molecular modeling experiments exposed the fluorinated side chain of (*S,R,S*)- α TfmAla to function as electron pair donor for the catalytic Ser195, thereby promoting substrate binding and peptide proteolysis, while the (*S,S,S*)-diastereomer prohibits these favorable interactions by steric hindrance. The absolute configuration of the P1' α Tfm group towards the active site was found to direct enzyme-substrate interactions by polarization effects originating from the α Tfm group (**Figure 4.3**).^{233, 234}

Follow-up work by the Kokschi laboratory focused on the 10-amino acid model peptide FA (**Figure 4.4a**) to probe the substrate specificities (P2, P1', P2') of several proteases by site-specific incorporation of aliphatic fluorine-containing amino acids. Several parameters were stated to significantly affect proteolytic stability like the steric bulk & hydrophobicity of the fluoroalkyl side chain, its proximity to the predominant cleavage site, electrostatic interactions within the enzyme's active site and the specific type of enzyme.²³⁵⁻²³⁷

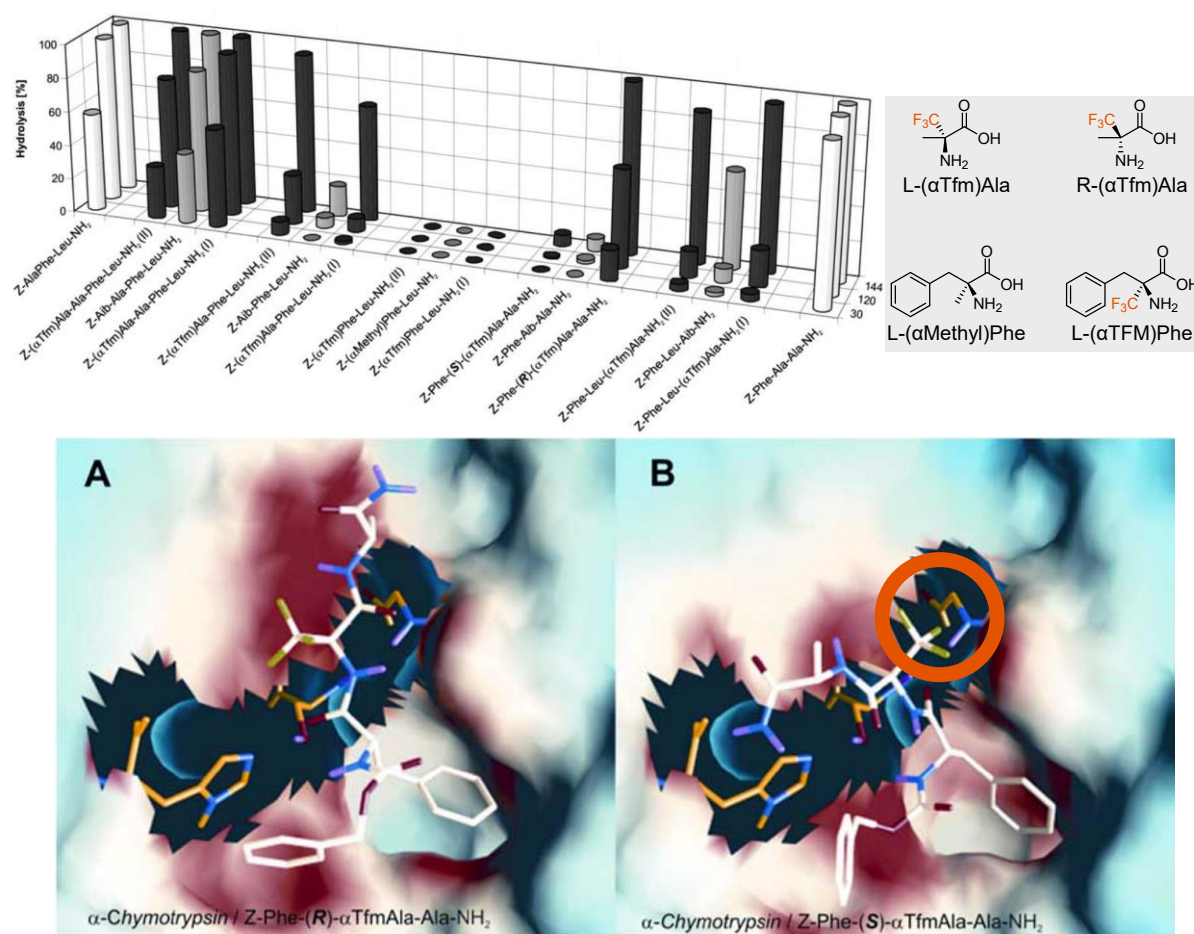


Figure 4.3 Summarized results of the α -chymotrypsin proteolysis study, in which α,α -dimethylated and fluorinated peptides revealed a prolonged stability towards enzymatic hydrolysis comparing to their unsubstituted counterparts. Modelling experiments on the (S,S,S) - and (S,R,S) -diastereomers of α TfmAla emphasized fluorine-driven polarization effects on the catalytic triad to govern peptide proteolysis by conformational changes. Adapted from Smits *et al.* (Copyright © 2006 Bentham Science Publishers Ltd.).²³⁴

When probing the $S1'$ specificity of α -chymotrypsin, Asante *et al.* determined higher rates of peptide hydrolysis for the unbranched and aliphatic amino acids DfeGly and TfeGly as $P1'$ residues than for native Ala (FA). Furthermore, a prolonged proteolytic stability of the Abu-mutant indicated the emergence of fluorine-induced polarization effects in enzyme-substrate recognition. Thus, DfeGly and TfeGly functioned as $P2$ and $P2'$ residues as well.²³⁶ Consequently, fluorine-induced interactions compiled by increased size of the linear side chain, hydrophobicity and fluorine-induced polarity affected the rate of peptide hydrolysis when replacing Ala with fluorinated derivatives from Abu. In contrast, bulky fluorinated amino acids can help to increase the proteolytic stability of peptides by protection of cleavage-relevant peptide bonds (**Figure 4.4b**).²³⁷ Incorporating the branched fluorinated amino acid HfLeu as $P1'$ residue led into higher rates of proteolytic stability against elastase than for α -chymotrypsin.

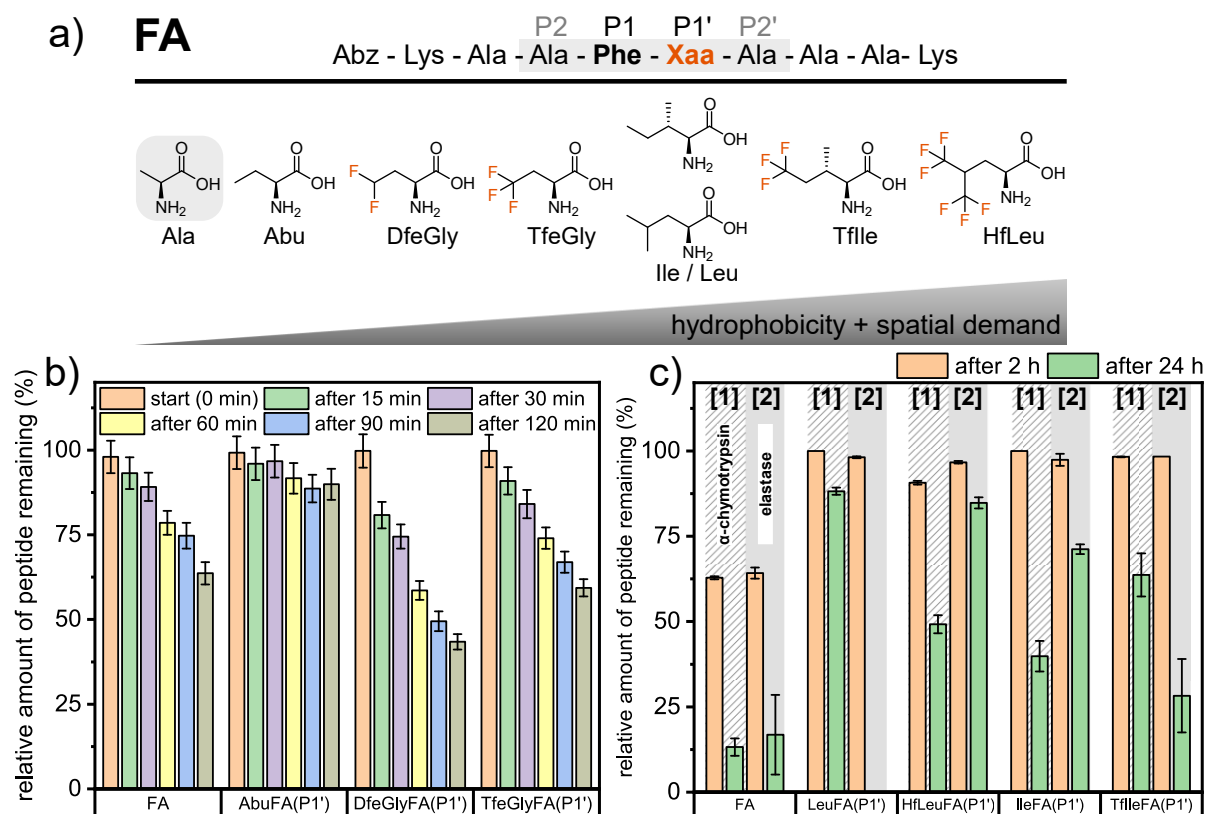


Figure 4.4 a) Substitution of the P1' residue (Xaa) of FA (P1': Ala) with diverse substituents. **b)** Digestion plots of FA variants with α -chymotrypsin. **c)** Digestion plots of FA variants with [1] α -chymotrypsin and [2] elastase. Further experiments focusing on the S2 & S2' specificities were also discussed in depth by Asante *et al.* and Huhmann *et al.* (experimental data were adapted in a modified version) - (Copyright © 2014 Springer-Verlag Wien 2014 & © 2017 Beilstein-Institut).^{236, 237}

Placing Leu as P1' substituent caused complete digestion after 24 h *via* elastase, while Hflleu has shown to counteract proteolysis. Nevertheless, HflleuFA(P1') was more susceptible for digestion by α -chymotrypsin, whereas P1' substituted Leu provided the best protection during 24 h incubation. A reverse trend was observed for Tflle, since the peptide TflleFA(P1') possessed a higher proteolytic resistance towards α -chymotrypsin than IleFA(P1'), whereas the inverted case was determined for elastase.²³⁷ These findings may interdict a general trend on how fluorinated residues impart into the enzymes' active site by P1'-S1' interactions.

In summary, the introduction of fluorinated amino acids serves as a biorthogonal tool to generate either favorable or repulsive interactions with the enzyme's binding site depending on each type of protease. The complex symphony of steric, electronic, and physical properties of each fluorine-containing amino acid and its resulting effects on enzyme-substrate recognition is yet hardly predictable, so that investigations on this research field should be considered as case-by-case scenarios.

5 Aim of this doctoral thesis

The overarching goal of this doctoral thesis is the *de novo* design and characterization of artificial peptides containing high to exclusive amounts of tailor-made fluorinated amino acids. A generous fabrication of the fluorinated building blocks will be achieved by a Ni(II)-complex-based stereoselective synthesis. All peptides will be synthesized *via* SPPS. Initial studies will focus on elucidating the biophysical properties of such polyfluorinated peptides including peptide folding, self-assembly and bioactivity (**Figure 5.1**).

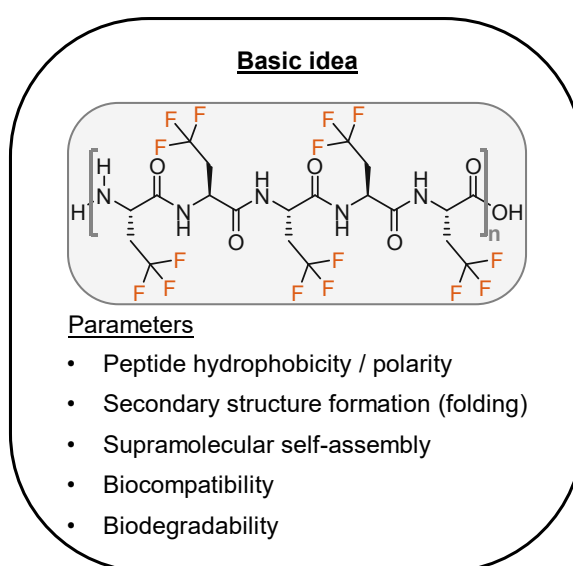
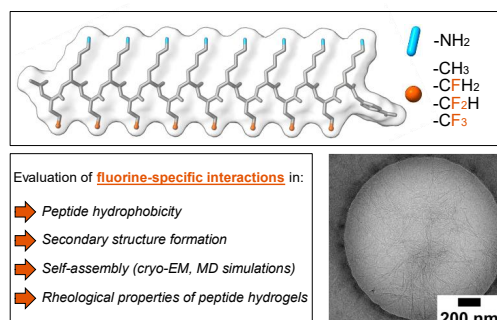


Figure 5.1 Initial considerations about the chemical & biological properties of polyfluorinated peptides.

In general, peptide folding & assembly characteristics will be investigated *via* CD spectroscopy, Thioflavin T fluorescence spectroscopy and cryo-EM / TEM analysis. These experimental approaches will be accompanied by pioneering attempts on exploring the enzymatic degradability of these synthetic & polyfluorinated bio-oligomers.

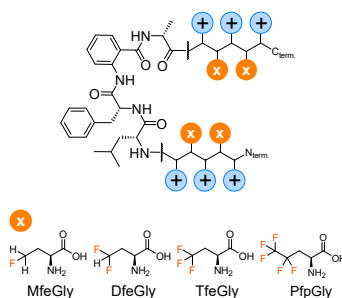
6 Published work

Overview of peer-reviewed publications discussed in this section:

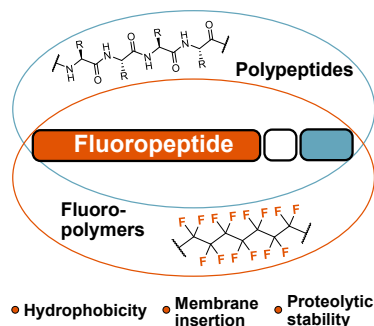


S. Chowdhary, R. F. Schmidt, A. K. Sahoo, T. tom Dieck, T. Hohmann, B. Schade, K. Brademann-Jock, A. F. Thünemann, R. R. Netz, M. Gradzielski, B. Kocsch, *Nanoscale*, **2022**,*14*, 10176-10189.

Fluorinated Antimicrobial Peptides



S. Chowdhary, T. Pelzer, M. Saathoff, E. Quaas, J. Pendl, M. Fulde, B. Kocsch, *Pept. Sci.*, **2023**, e24306.



T. Hohmann[†], **S. Chowdhary**[†], K. Ataka, J. Er, G. H. Dreyhsig, J. Heberle, B. Kocsch, *Chem. Eur. J.*, **2023**, e202203860. († = authors contributed equally)

6.1 Rational design of amphiphilic fluorinated peptides: evaluation of self-assembly properties and hydrogel formation

S. Chowdhary, R. F. Schmidt, A. K. Sahoo, T. tom Dieck, T. Hohmann, B. Schade, K. Brademann-Jock, A. F. Thünemann, R. R. Netz, M. Gradzielski, B. Kokschi, *Nanoscale*, **2022**, *14*, 10176–10189.

Submitted: 25 March 2022; **First published:** 22 June 2022

Published by the Royal Society of Chemistry, London, UK.

The published work is available online - **DOI:** [10.1039/d2nr01648f](https://doi.org/10.1039/d2nr01648f).²³⁸

6.1.1 Individual contributions of authors

Beate Kokschi and **Suvrat Chowdhary** (both FU Berlin) conceived the overall project. **Suvrat Chowdhary** designed and developed concepts and experiments, synthesized, and purified all amino acids and peptides described in this work. **Suvrat Chowdhary** performed HPLC, CD, UV, and FL (staining) experiments. **Suvrat Chowdhary** managed the collaborative network and prepared samples for further experiments by collaboration partners (rheology, SAXS, cryo-EM). **Suvrat Chowdhary** wrote the manuscript. Robert F. Schmidt (TU Berlin) performed rheology experiments and wrote the manuscript. Anil K. Sahoo (FU Berlin, MPIKG Golm) performed MD simulations. Anil K. Sahoo and Roland R. Netz (FU Berlin) analyzed and interpreted MD data and wrote the manuscript. Tiemo tom Dieck (FU Berlin) assisted **Suvrat Chowdhary** in SPPS and circular dichroism experiments. Kerstin Brademann-Jock and Andreas F. Thünemann (both BAM Berlin) performed SAXS measurements and SAXS data analysis. Thomas Hohmann (FU Berlin) provided expertise on the synthesis of fluorinated amino acids. Boris Schade (FU Berlin) performed cryo-EM experiments, analyzed, and interpreted data. Michael Gradzielski (TU Berlin) provided expertise and feedback.

6.1.2 Rationale and summary of the project

So far, the impact of fluorine-specific interactions on peptide β -sheet self-assembly and hydrogelation is scarcely reported. With this work, the first-ever systematic study on polyfluorinated and amphipathic β -sheet SAPs was performed by adjusting the degree of side chain fluorination *via* iterative incorporation of either Abu, MfeGly, DfeGly and TfeGly. This publication provides an extended overview (**Figure 6.1**) on the folding, self-assembly and hydrogelation properties, while further results on the enzymatic / microbial degradability and biocompatibility of the (fluorinated) peptides are discussed in **Section 7**. Moreover, this work includes the gram-scale synthesis of TfeGly, whereas the synthetic protocols for MfeGly and DfeGly were described in follow-up studies (**Section 6.2**).^{202, 238}

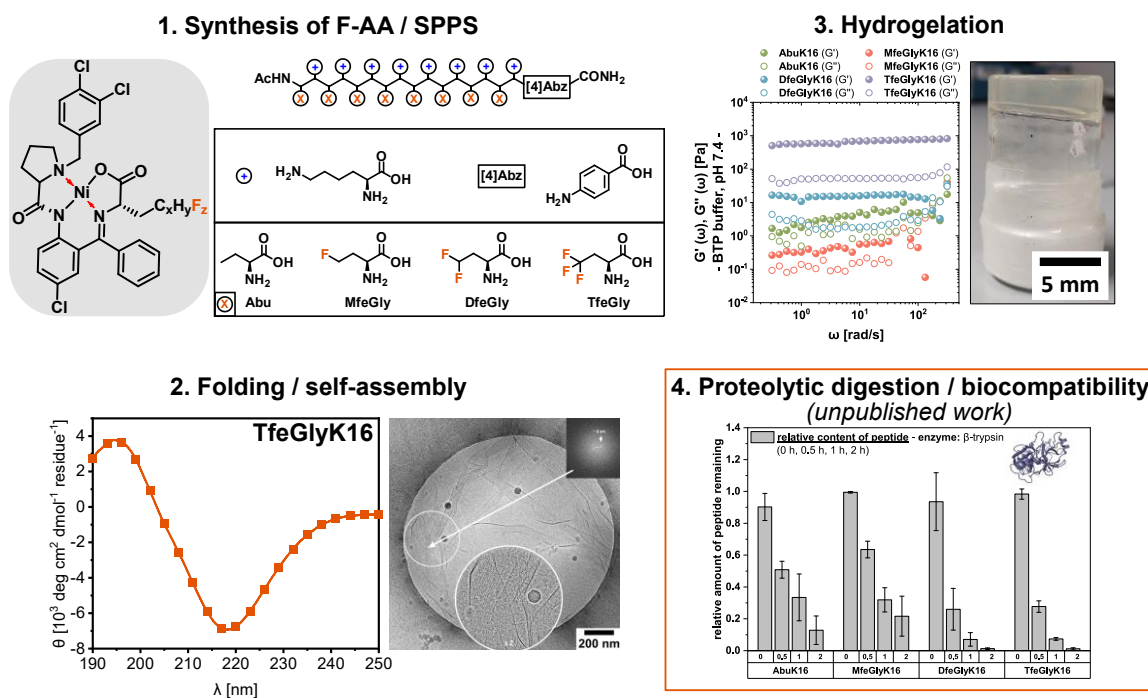


Figure 6.1 Schematic illustration of the project's working plan – “Rational design of amphiphilic fluorinated peptides: evaluation of self-assembly properties and hydrogel formation”.

For determining an appropriate sequence length to study fluorine-enhanced β -sheet formation, a library of amphipathic peptides including Abu and Lys with five (AbuK10) to eight alternating residues (AbuK16) was investigated by CD spectroscopy. In physiological conditions (pH 7.4), only AbuK14 (Ac-(Abu-Lys)₇-[4]Abz-NH₂) and AbuK16 (Ac-(Abu-Lys)₈-[4]Abz-NH₂) formed β -sheets ($\lambda_{\min} = 214\text{--}220$ nm) but all other variants rather polyproline type II-like helices (PPII) ($\lambda_{\max} = 218\text{--}228$ nm & $\lambda_{\min} = 198\text{--}205$ nm). Owing to these results, the fluorinated peptides MfeGlyK16 (Ac-(MfeGly-Lys)₈-[4]Abz-

NH₂), DfeGlyK16 (Ac-(DfeGly-Lys)₈-[4]Abz-NH₂) and TfeGlyK16 (Ac-(TfeGly-Lys)₈-[4]Abz-NH₂) were designed (**Figure 6.2, left**). Chromatographic assays (retention times q) and theoretical calculations on favorable binding motifs of the hydrophobic side chains with water molecules (water interactions energies ΔE_{int}) were conducted to estimate fluorination-induced changes on peptide hydrophobicity and side chain polarity (**Figure 6.2, right**). In fact, incorporation of di- and trifluorinated side chains enhances the hydrophobicity of this scaffold. MfeGlyK16 was found to be more polar, thereby owning the least values of hydrophobicity. It should be mentioned that the decrease in hydrophobicity caused by fluorine-induced polarity corresponds to prior findings on fluorinated methane derivatives discussed in **Section 3.1**.¹⁰⁷

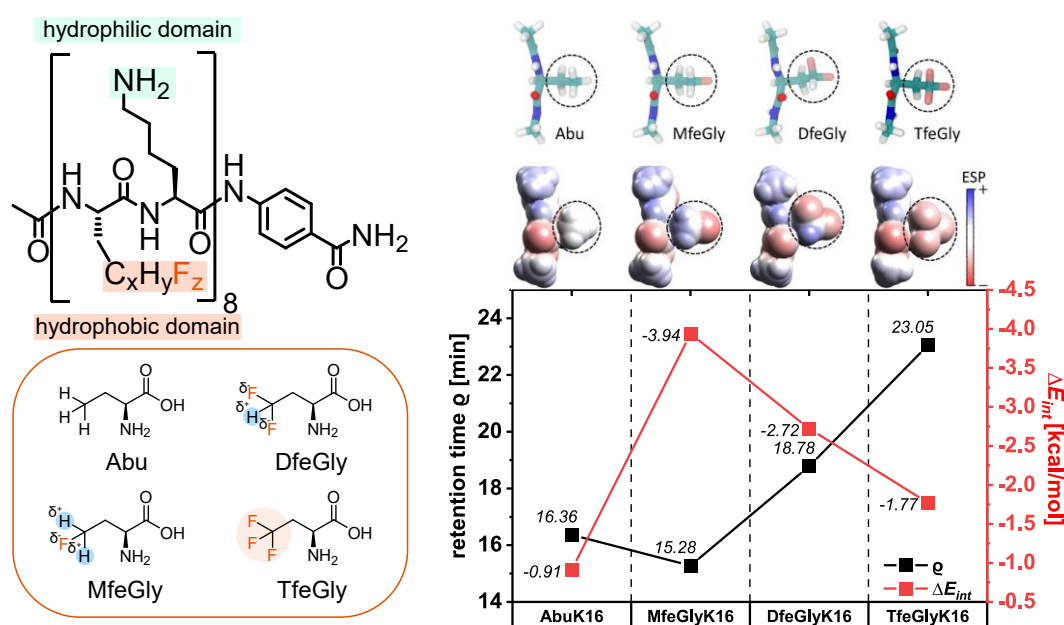


Figure 6.2 Rational design of fluorinated peptides MfeGlyK16, DfeGlyK16 and TfeGlyK16 based on a cationic “Abu-Lys”-repeating unit (AbuK16) (**left**). Retention times q of AbuK16, MfeGlyK16, DfeGlyK16 and TfeGlyK16 as experimental index of intrinsic hydrophobicity plotted against calculated interaction energies ΔE_{int} (HF/6-31G*) of water with an Abu, MfeGly, DfeGly and TfeGly residue (**right**). Geometry optimized structures and ESPs of the hydrophobic amino acids were obtained from quantum mechanical calculations (MP2/6-31G*). Adapted from Chowdhary *et al.* in a modified version (license: CC BY-NC 3.0).²³⁸

CD spectroscopic measurements revealed DfeGlyK16 (0.25 wt%) and TfeGlyK16 (0.1 wt%) to form β -sheet structures at significantly lower concentrations than the solely hydrocarbon-based AbuK16 (2 wt%) at physiological conditions (pH 7.4). No evidence of β -sheet assembly was found for MfeGlyK16 at both physiological and basic buffered conditions (pH 9.0), indicating adverse effects by the polar side chain of MfeGly (**Figure 6.3a**). For deeper insights, MD simulations were applied in which the favored conformational states of two peptide strands of each species at separating inter-peptide distances were probed. In total, the global minimum of potential mean force (PMF) for

MfeGlyK16, very different from the observations for AbuK16, DfeGlyK16 and TfeGlyK16, originates from side chain-side chain interactions of the hydrophobic residues rationalized by intramolecular contact pairs of the strongly polarized fluorine atom (MfeGly) and the adjacent amide bond. The intermolecular assembly of two separate dimers in case of AbuK16, DfeGlyK16 and TfeGlyK16, as illustrated in **Figure 6.3b**, appears to undergo peptide oligomerization. For MfeGlyK16, on the other hand, electrostatic repulsions from the exposing Lys residues on both strands prevent supramolecular assembly. This finding is interpreted as an inhibition of hydrophobicity-driven peptide self-assembly by fluorine-induced polarity (**Figure 6.3b**).

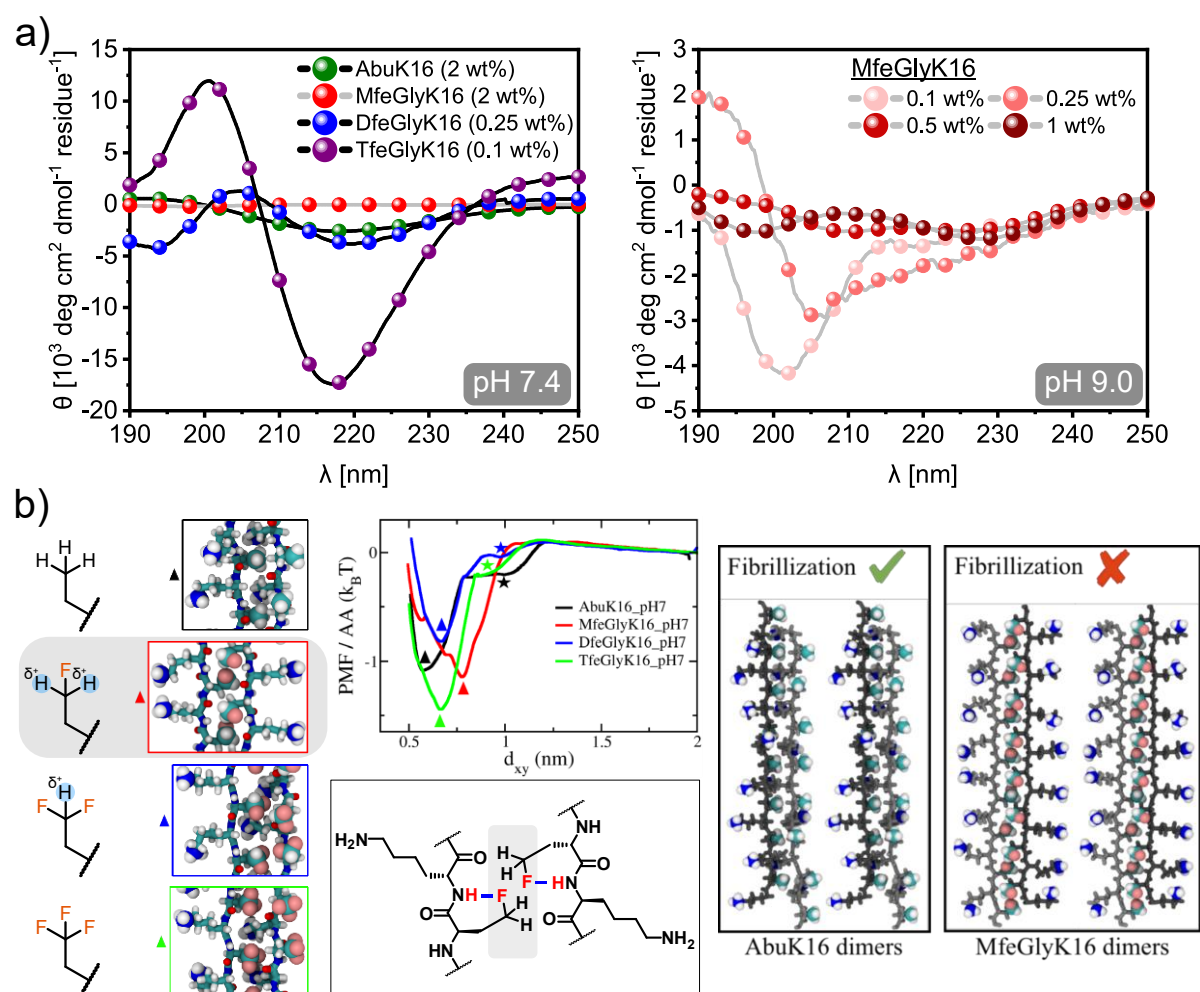


Figure 6.3 a) CD spectra of AbuK16 (2 wt%), MfeGlyK16 (2 wt%), DfeGlyK16 (0.25 wt%) and TfeGlyK16 (0.1 wt%) in 50 mM Bis-tris propane + 150 mM NaCl (pH 7.4) recorded at 37 °C. Additional measurements of MfeGlyK16 in basic conditions (pH 9.0) in varying concentrations provided no evidence on β -sheet formation (indicated by grey-colored lines). **b)** MD simulation results for the amphipathic peptides. The potential of mean force (PMF) per amino acid as a function of inter-strand separation d_{xy} at pH 7 illustrates the free energy profiles of two interacting peptide strands. The intermolecular dimer complexes for AbuK16 and MfeGlyK16 denote an inhibition of oligomerization in case of MfeGlyK16 by electrostatic repulsions of the Lys residues. Adapted from Chowdhary *et al.* in a modified version (license: CC BY-NC 3.0).²³⁸

The β -sheet rich aggregates of AbuK16, DfeGlyK16 and TfeGlyK16 were identified by FL staining experiments using the amyloid-specific dyes Thioflavin T (ThT) and Congo Red

(CR) (**Figure 6.4, top**).^{33, 239} When applying ThT fluorescence spectroscopy to a maximum range of 1 wt% peptide concentration, an up to 180-fold enhancement in FL intensity was observed for TfeGlyK16 and about 9-fold for DfeGlyK16 suggesting the presence of amyloid-like morphologies. Similarly, UV-based staining assays (0.5 wt%) with CR resulted for DfeGlyK16 and TfeGlyK16 to 2.8-fold enhanced values of UV absorbance than for sole CR. By cryo-EM experiments, the amyloid-like morphologies of AbuK16 (2 wt%), DfeGlyK16 (0.25 wt%) and TfeGlyK16 (0.1 wt%) were determined as homogeneous fibrillar strands (**Figure 6.4, bottom**). SAXS measurements served to elucidate the mesoscopic properties of peptide fibrils with average diameters (a • b) in nanometer range (DfeGlyK16 [2 wt%]: 2.9 nm • 4.4 nm / TfeGlyK16 [2 wt%]: 2.9 nm • 3.1 nm). Apparently, fibrillary morphologies were not detected for MfeGlyK16 samples (≤ 2 wt%) which is in absolute agreement to the experimental and theoretical data.

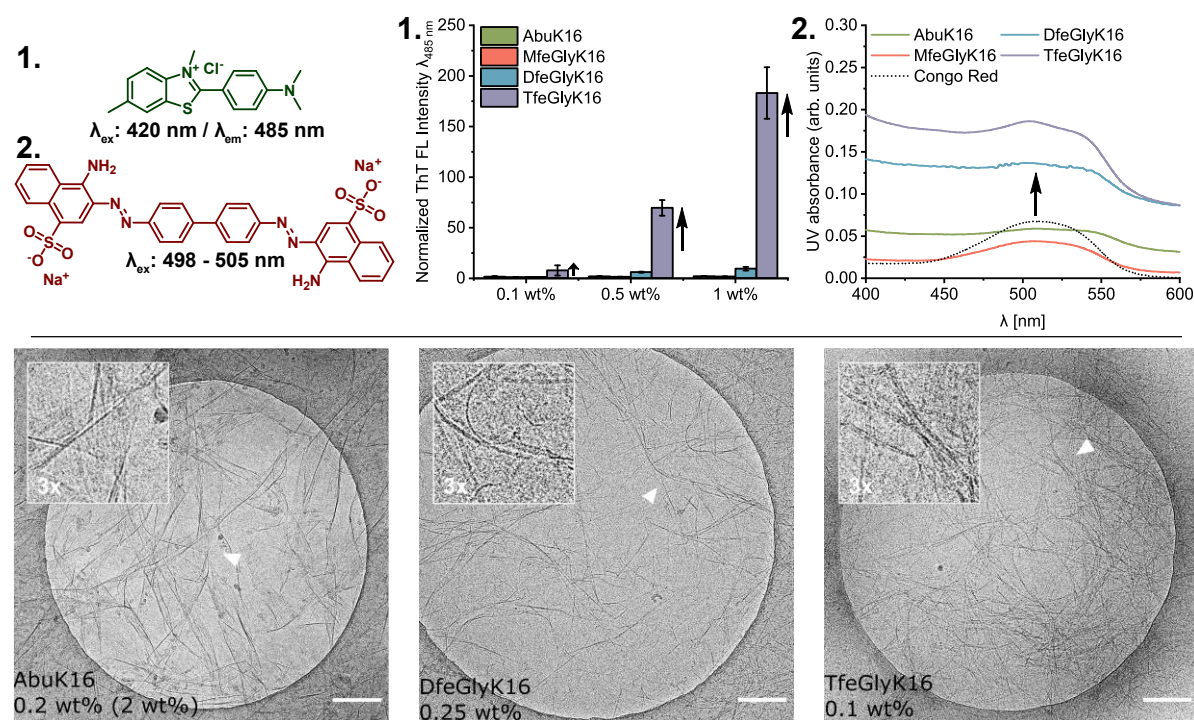


Figure 6.4 Thioflavin T (ThT) fluorescence assay and Congo Red (CR) UV spectroscopic assay for amyloid-like fibril detection **1.** ThT assays of AbuK16, MfeGlyK16, DfeGlyK16 and TfeGlyK16 (0.1 wt%, 0.5 wt%, 1 wt%) incubated for 24 h at 37 °C in 50 mM Bis-tris propane + 150 mM NaCl (pH 7.4) containing 20 μM ThT dye. **2.** CR assays of AbuK16, MfeGlyK16, DfeGlyK16 and TfeGlyK16 (0.5 wt%) incubated for 15 h at 37 °C in 50 mM Bis-tris propane + 150 mM NaCl (pH 7.4) containing 50 μM CR dye. Solely buffered solutions are set as reference samples. For both plots, an increase in FL intensity / UV absorbance (binding to amyloid-like fibrils) is indicated by black arrows (**top**). Cryo-EM micrographs of AbuK16 (2 wt%, diluted to 0.2 wt%), DfeGlyK16 (0.25 wt%) and TfeGlyK16 (0.1 wt%) dissolved in 50 mM Bis-tris propane + 150 mM NaCl, pH 7.4. The scale bar denotes 200 nm (**bottom**). Adapted from Chowdhary *et al.* in a modified version (license: CC BY-NC 3.0).²³⁸

Peptide hydrogels were prepared in both physiological (pH 7.4) and basic (pH 9.0) conditions and their viscoelastic properties were studied by oscillatory rheology.

Calculated plateau storage moduli (G_0) revealed at pH 7.4 the least hydrophobic peptide MfeGlyK16 to form gels with the lowest G_0 value (0.53 Pa, 0.5 wt%) compared to AbuK16-hydrogels (4.81 Pa, 0.5 wt%). Both are mainly softer than matrices formed by DfeGlyK16 (15.3 Pa, 0.5 wt%) and TfeGlyK16 (670 Pa, 0.5 wt%) (**Table 6.1**). This finding is of major importance, as it draws an analogy between hydrogel stiffness and growing amount of fluorine-substitution that promotes amyloid-like β -sheet assembly and hydrogel crosslinking density (ξ). Comparison with the positive control LeuK16 (4869 Pa, 0.5 wt%) assesses TfeGlyK16 to form comparably soft gels with an order of magnitude lower G_0 values because of its less hydrophobic properties than LeuK16 (as estimated *via* q). Lowering the overall Lys charges through a basic buffered environment (pH 9.0) changes the macroscopic properties of the peptide hydrogels. In brief, experimentally determined values of storage moduli G' are much closer than at pH 7.4. The highest increase in G_0 is observed for MfeGlyK16 (209 Pa, 0.5 wt%) and becomes weaker with increasing hydrophobicity (AbuK16, DfeGlyK16). Ultimately, a loss of G_0 by almost one order of magnitude is given for TfeGlyK16 (70 Pa, 0.5 wt%) and LeuK16 (564 Pa, 0.5 wt%). These trends may be attributed, as suggested *via* MD simulations, to main leverages of side chain-neutralization on the assembly and hydrogelation behavior of this peptide library.

Table 6.1 Retention times q , water interaction energies ΔE_{int} , as well as plateau moduli G_0 and mesh sizes ξ measured for all peptide-based hydrogel scaffolds in this project. Adapted from Chowdhary *et al.* in a modified version (license: CC BY-NC 3.0).²³⁸

Name	q [min]	ΔE_{int} (kcal/mol)	c (wt%)	pH	G_0 (Pa)	ξ (nm)	
LeuK16	28.84 \pm 0.025	-	0.5	7.4	4869 \pm 124	9.83 \pm 0.08	
				9.0	564.4 \pm 7.2	20.17 \pm 0.09	
TfeGlyK16	23.05 \pm 0.031	-1.77	0.5	7.4	670 \pm 19	19.05 \pm 0.18	
				9.0	70.24 \pm 1.4	40.4 \pm 0.3	
				0.25	7.4	8.63 \pm 0.79	81.3 \pm 2.5
				0.1	7.4	1.09 \pm 0.12	161.9 \pm 5.7
DfeGlyK16	18.78 \pm 0.044	-2.72	0.5	7.4	15.30 \pm 1.04	67.14 \pm 1.5	
				9.0	554 \pm 15	20.29 \pm 0.18	
AbuK16	16.36 \pm 0.017	-0.91	0.5	7.4	4.81 \pm 0.22	98.72 \pm 1.54	
				9.0	264.1 \pm 5.1	25.98 \pm 0.17	
MfeGlyK16	15.28 \pm 0.075	-3.94	0.5	7.4	0.53 \pm 0.02	205.37 \pm 2.53	
				9.0	208.8 \pm 0.83	28.10 \pm 0.04	

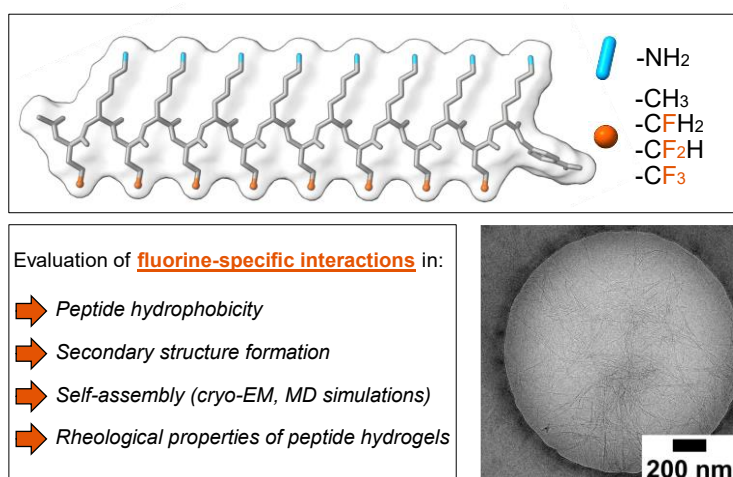
In conclusion, this study constitutes broad principles about the distinct features of aliphatic & polyfluorinated β -sheet forming SAPs with future potentials as peptide-based

biomaterials. A combination of experimental methods, as well as theoretical approaches acted as foundation to explore fluorine-specific interactions on supramolecular self-assembly and hydrogelation in dependency to the degree of side chain fluorination. Thus, fluorine-enhanced hydrophobicity (DfeGly, TfeGly) derived from side chain fluorinated amino acids was demonstrated to promote peptide fibrillation and serves for the preparation of physical hydrogels. Further results on peptide proteolysis and microbial degradation, cytotoxicity and hemolytic activity are discussed in **Section 7**.²³⁸

6.1.3 Publication and supplementary information

Rational design of amphiphilic fluorinated peptides: evaluation of self-assembly properties and hydrogel formation

S. Chowdhary, R. F. Schmidt, A. K. Sahoo, T. tom Dieck, T. Hohmann, B. Schade, K. Brademann-Jock, A. F. Thünemann, R. R. Netz, M. Gradzielski, B. Kocsch, *Nanoscale*, **2022**, *14*, 10176–10189.



DOI: 10.1039/d2nr01648f.

Creative Commons license: [CC BY-NC 3.0](https://creativecommons.org/licenses/by-nc/3.0/)



Cite this: *Nanoscale*, 2022, **14**, 10176

Rational design of amphiphilic fluorinated peptides: evaluation of self-assembly properties and hydrogel formation†

Suvrat Chowdhary,^a Robert Franz Schmidt,^b Anil Kumar Sahoo,^{c,d} Tiemo tom Dieck,^a Thomas Hohmann,^a Boris Schade,^e Kerstin Brademann-Jock,^f Andreas F. Thünemann,^f Roland R. Netz,^c Michael Gradzielski^b and Beate Kokschi^{*a}

Advanced peptide-based nanomaterials composed of self-assembling peptides (SAPs) are of emerging interest in pharmaceutical and biomedical applications. The introduction of fluorine into peptides, in fact, offers unique opportunities to tune their biophysical properties and intermolecular interactions. In particular, the degree of fluorination plays a crucial role in peptide engineering as it can be used to control the characteristics of fluorine-specific interactions and, thus, peptide conformation and self-assembly. Here, we designed and explored a series of amphipathic peptides by incorporating the fluorinated amino acids (2S)-4-monofluoroethylglycine (**MfeGly**), (2S)-4,4-difluoroethylglycine (**DfeGly**) and (2S)-4,4,4-trifluoroethylglycine (**TfeGly**) as hydrophobic components. This approach enabled studying the impact of fluorination on secondary structure formation and peptide self-assembly on a systematic basis. We show that the interplay between polarity and hydrophobicity, both induced differentially by varying degrees of side chain fluorination, does affect peptide folding significantly. A greater degree of fluorination promotes peptide fibrillation and subsequent formation of physical hydrogels in physiological conditions. Molecular simulations revealed the key role played by electrostatically driven intra-chain and inter-chain contact pairs that are modulated by side chain fluorination and give insights into the different self-organization behaviour of selected peptides. Our study provides a systematic report about the distinct features of fluorinated oligomeric peptides with potential applications as peptide-based biomaterials.

Received 25th March 2022,
Accepted 21st June 2022

DOI: 10.1039/d2nr01648f

rsc.li/nanoscale

Introduction

Self-assembling peptides (SAPs) are often composed of an amphiphilic structure motif based on alternating arrangements of hydrophobic and hydrophilic residues.^{1–4} More than two decades ago the first and most prominent variants **EAK16-**

II H₂N-(Ala-Glu-Ala-Glu-Ala-Lys-Ala-Lys)₂-OH and **RADA16-II** H₂N-(Arg-Ala-Arg-Ala-Asp-Ala-Asp-Ala)₂-OH were discovered by Zhang *et al.*⁵ These peptides served as essential motifs to study the hierarchical construction of β -sheet-based macroassemblies.^{2,5–8} Since then, SAPs have attracted paramount interest in biomedical research for their biocompatibility, biodegradability, and biofunctionality. They were utilized in the field of tissue engineering by functioning as extracellular matrix mimics for cell proliferation and wound healing.^{9–14} Their self-assembly is driven by non-covalent interactions such as hydrogen bonding, electrostatic interactions, hydrophobic interactions, aromatic interactions (π - π stacking) and van der Waals forces.^{15–18} A promising approach to produce novel functional peptide-based biomaterials consists of the systematic incorporation of fluorinated amino acids. These non-natural building blocks turned out to be a powerful tool to fine-tune biophysical and chemical properties of peptides and proteins.¹⁹ Fluorine possesses unique properties including a strong inductive effect combined with high electronegativity. The replacement of a single C–H bond with C–F is generally

^aInstitute of Chemistry and Biochemistry, Freie Universität Berlin, Arnimallee 20, 14195 Berlin, Germany. E-mail: beate.kokschi@fu-berlin.de

^bInstitute of Chemistry, Technische Universität Berlin, Straße des 17. Juni 124, 10623 Berlin, Germany

^cDepartment of Physics, Freie Universität Berlin, Arnimallee 14, 14195 Berlin, Germany

^dMax Planck Institute of Colloids and Interfaces, Am Mühlenberg 1, 14476 Potsdam, Germany

^eInstitute of Chemistry and Biochemistry and Core Facility BioSupraMol, Freie Universität Berlin, Fabeckstraße 36a, 14195 Berlin, Germany

^fFederal Institute for Materials Research and Testing (BAM), Unter den Eichen 87, 12205 Berlin, Germany

† Electronic supplementary information (ESI) available. See DOI: <https://doi.org/10.1039/d2nr01648f>



considered to be isosteric.^{20,21} Investigations of the effects of fluorinated amino acids on hydrophobicity,^{22,23} secondary structure formation,^{24,25} protein–protein interactions,^{26,27} amyloid folding kinetics,^{28,29} proteolytic stability,³⁰ the chemical and biological properties of fluorinated peptide-based materials,³¹ and the integration of fluorine into bacteria^{32,33} have been reported by our group. The vast majority of previous studies including our own efforts examining fluorinated amino acids in the context of peptide and protein chemistry were limited to the incorporation of one or only a few of these building blocks. Moreover, the chemical nature and biological features of polyfluorinated peptides with a large proportion of fluorinated aliphatic amino acids have not yet been studied. Thus, we were motivated to address the question of the impact that several of such building blocks would have on fluorine-specific interactions in peptide self-assembly.

The fabrication of polyfluorinated peptides obviously requires generous amounts of fluorinated amino acids.³⁴ Thus, we have recently reported an improved synthetic strategy to obtain the fluorinated amino acid (2*S*)-4-monofluoroethylglycine (**MfeGly**) at the gram scale.³⁵ Moreover, Soloshonok *et al.* developed a general and practical synthetic process to obtain enantiomerically pure Fmoc-protected fluorinated amino acid through an asymmetric and Ni(II)-complex mediated stereoselective synthesis (see Scheme S1 in the ESI†).^{36–39} In current attempts, we have extended this strategy to the synthesis of a diverse range of aliphatic fluorinated amino acids with different side chain patterns.⁴⁰

In this work, we designed an amphipathic motif including lysine and the well-studied non-proteogenic amino acid α -aminobutyric acid (**Abu**), which has been reported as a suitable hydrophobic building block for SAPs.^{41,42} The varying degree of fluorination was adjusted by the iterative incorporation of its derivatives (2*S*)-4-monofluoroethylglycine (**MfeGly**), (2*S*)-4,4-difluoroethylglycine (**DfeGly**) and (2*S*)-4,4,4-trifluoroethylglycine (**TfeGly**). With this peptide library we assessed the impact of fluorine-specific interactions on the intrinsic hydrophobicity, secondary structure formation, self-assembling properties, the morphology of amyloid-like aggregates and the formation of peptide hydrogels. Molecular simulations of the different fluorinated peptides demonstrate that the peptide–peptide interactions are finely tuned by the ability of fluorine atoms to form electrostatic contact pairs with positively partially charged atoms on the backbone and side chains. This ability in turn depends critically on the number of fluorinated substituents, based on which we explain how the fluorination degree controls peptide structure formation.

Results and discussion

Peptide design: estimation of sequence length, hydrophobicity, and fluorine-induced polarity

Our rational design is based on a cationic Abu–Lys repeating unit. A π -system derived from 4-aminobenzoic acid (**[4]Abz**, PABA) was placed on the C-terminus; this building block is a

widely used fluorescent probe and enables precise control over peptide stock concentrations.⁴³ To determine a chain length sufficient for β -sheet formation, we characterized a series of **AbuK**-derived peptides with repeating units ranging from five to eight alternating residues and studied their ability to form secondary structures under physiological conditions *via* CD spectroscopy (Fig. 1a). High peptide concentrations (2 wt%) were chosen to induce peptide self-assembly. As can be seen from the CD spectra, only **AbuK14** (Ac-(Abu–Lys)₇-**[4]Abz**-NH₂) and **AbuK16** (Ac-(Abu–Lys)₈-**[4]Abz**-NH₂) formed β -sheet structures (λ_{\min} = 214–220 nm), whereas the remaining variants (**AbuK10–13**, **AbuK15**) tend to form polyproline type II helices (PPII). This is proven by the characteristic positive and negative maxima at λ_{\max} = 218–228 nm and λ_{\min} = 198–205 nm. The PPII helix comprises an extended left-handed helical structure and was also found for similar Ala–Lys derived SAPs.^{44,45} A further minimum at λ_{\min} = 228–230 nm could hint for a minor population of β -turn like conformations through intramolecular hydrophobic interactions between the **Abu** residues.^{46,47} As the 16-meric **AbuK16** was shown to form β -sheets, we synthesized the polyfluorinated amphipathic peptides **MfeGlyK16** (Ac-(MfeGly–Lys)₈-**[4]Abz**-NH₂), **DfeGlyK16** (Ac-(DfeGly–Lys)₈-**[4]Abz**-NH₂) and **TfeGlyK16** (Ac-(TfeGly–Lys)₈-**[4]Abz**-NH₂) by substitution of **Abu** with each fluorinated derivative according to the eight repeating unit pattern (Fig. 1b).

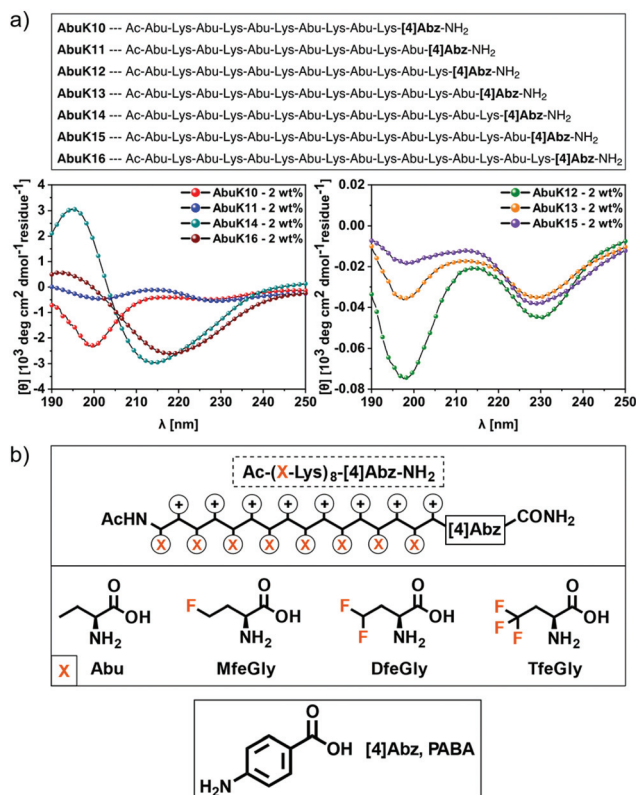


Fig. 1 (a) CD spectra of 2 wt% **AbuK10–AbuK16** in 50 mM Bis-tris propane + 150 mM NaCl, pH 7.4 recorded at 37 °C. (b) Peptide motif (**AbuK16**, **MfeGlyK16**, **DfeGlyK16**, **TfeGlyK16**) and chemical structures of **Abu** and its derivatives **MfeGly**, **DfeGly** and **TfeGly** as well as **[4]Abz**.



Rational design applying fluorinated amino acids in peptide scaffolds crucially depends on a reliable determination of their hydrophobic nature. Estimation of the intrinsic hydrophobicity is indispensable to discuss fluorine-specific interactions for each oligopeptide. In this work, the hydrophobic properties of peptides were determined through a RP-HPLC based assay (Fig. 2a). In general, the hydrophobicity of the peptides increases with the number of fluorine substituents on the individual amino acids. However, **MfeGlyK16** is more polar than **AbuK14** and **AbuK16**, which is in accordance with prior

observed trends in fluorine-induced hydrophobicity with this particular amino acid series.^{28,48} We thus conclude that the origin of the decrease in non-polar character of **MfeGlyK16** lies rather in the physicochemical properties of its side chain than in its overall fluorine content.

Theoretical approaches to determining the hydrophobic nature of fluorinated amino acids emphasized a change in apparent non-polar character through side chain-based interactions in aqueous conditions triggered by fluorination.⁴⁹ To gain deeper insights into the impact of fluorine-specific interactions, we used quantum mechanical (QM) calculations for the residues of **Abu**, **MfeGly**, **DfeGly** and **TfeGly**-derived motifs. The QM geometry optimized structures, their electrostatic potential (ESP) maps and water interaction energies ΔE_{int} for the different types of amino acids are shown in Fig. 2b. The ESP maps reveal different degrees of side chain polarities, the lowest for **Abu** and the highest for **MfeGly**. Interestingly, with further increase in fluorination (**DfeGly**, **TfeGly**), the polarity decreases again. To quantify the hydrophobicity of the side chains, we calculated ΔE_{int} for the different types of amino acids by many initial configurations of an amino acid–water complex for each amino acid type. ΔE_{int} is found to be the smallest for **Abu** ($-0.91 \text{ kcal mol}^{-1}$) and the largest for **MfeGly** ($-3.94 \text{ kcal mol}^{-1}$). Like the side chain polarity, ΔE_{int} decreases with further increase of fluorination: **DfeGly** ($-2.72 \text{ kcal mol}^{-1}$) and **TfeGly** ($-1.77 \text{ kcal mol}^{-1}$). It should be noted that these ΔE_{int} values are smaller than the water–water interaction energy of $-5.85 \text{ kcal mol}^{-1}$, which implies that all these amino acids are hydrophobic. The theoretical values corroborate the experimental trends of peptide hydrophobicity, emphasizing the impact of fluorine-induced polarity changes as seen for **MfeGlyK16**.

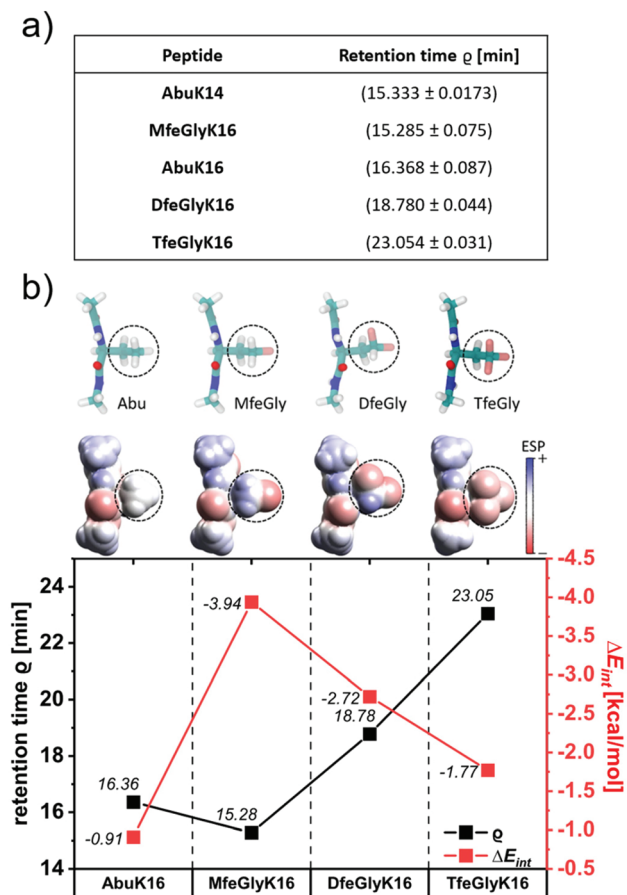


Fig. 2 (a) Retention times ρ of **AbuK14**, **AbuK16**, **MfeGlyK16**, **DfeGlyK16** and **TfeGlyK16** as experimental index of intrinsic hydrophobicity. An increase in ρ corresponds to an enhanced non-polar character of respective peptide. The eluents were (A) $\text{H}_2\text{O} + 0.1\%$ (v/v) TFA and (B) ACN + 0.1% (v/v) TFA by applying a gradient of 5% \rightarrow 40% (B) over 30 min. (b) Geometry optimized structures of different amino acid residues marked with dashed circles with the N-terminal acetyl cap and the C-terminal *N*-methylamide cap obtained from quantum mechanical (MP2/6-31G*) calculations are shown in the ball-stick representation (top row). Atoms are colored according to atom types: carbon (cyan), nitrogen (blue), oxygen (red), hydrogen (white), and fluorine (pink). The corresponding space-filling models are colored according to the calculated electrostatic potential (ESP) showing the varying polarities for the different side chains. The calculated interaction energies ΔE_{int} (HF/6-31G*) of water with an **Abu**, **MfeGly**, **DfeGly** and **TfeGly** side chain are plotted against retention times ρ of **AbuK16**, **MfeGlyK16**, **DfeGlyK16** and **TfeGlyK16**. For comparison, we also calculated the change in ΔE_{int} for water–water interactions ($-5.85 \text{ kcal mol}^{-1}$).

Secondary structure formation of amphipathic peptides

All oligopeptides were studied over a wide concentration range (0.1–1 wt%) by means of CD spectroscopy (Fig. 3). Secondary structure formation was investigated under physiologically buffered (pH 7.4) and basic (pH 9.0) conditions. The results at pH 7.4 show for **AbuK16** and **MfeGlyK16** at concentrations of 0.1–1 wt% (Fig. 3a–d) the typical course of absorption of a PPII-like conformation as discussed for **AbuK**-derived peptides above. Interestingly, the formation of β -sheets was not observed for **MfeGlyK16** at the highest concentration of 2 wt% (Fig. 3d), very different from the observations for **AbuK14** and **AbuK16** (see Fig. 1a). Increasing the degree of fluorination triggers β -sheet formation (≥ 0.25 wt%) for **DfeGlyK16**; for lower concentrations (0.1 wt%) a similar conformation as given for **AbuK16** and **MfeGlyK16** was observed (Fig. 3a–d). A growth in fluorine-content on each individual amino acid increases the hydrophobic nature while, simultaneously, decreasing the polarity and, therefore, promotes β -sheet formation. In this manner, the most fluorinated peptide **TfeGlyK16** was found to form β -sheets at all selected concentrations (Fig. 3a–d).

We further studied these peptides under basic conditions (pH 9.0) (Fig. 3e and f) that promote neutralization of the formal positive charges and, thus, induce β -sheet formation.



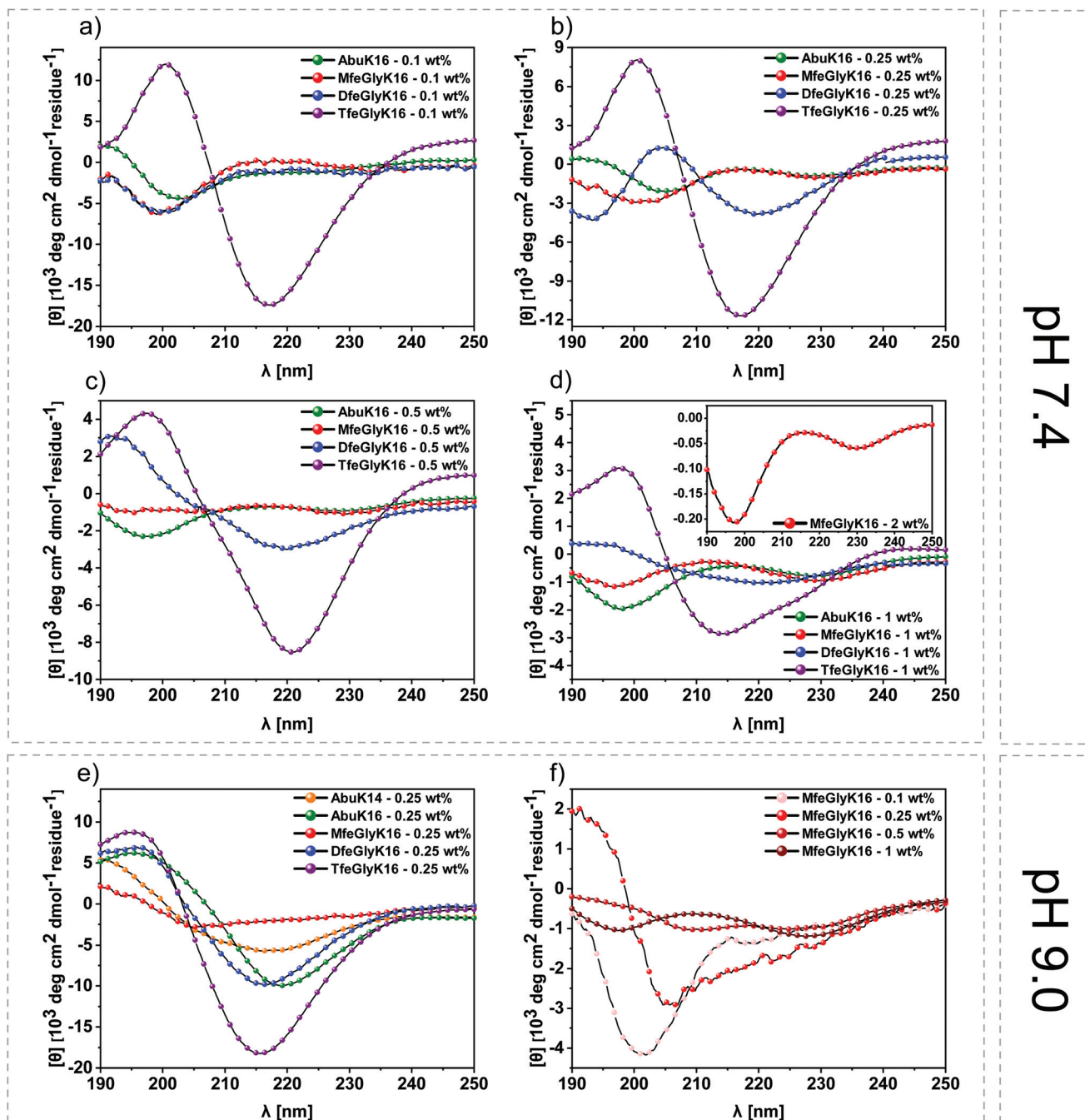


Fig. 3 CD spectra of amphipathic oligopeptides **AbuK16** (green), **MfeGlyK16** (red), **DfeGlyK16** (blue) and **TfeGlyK16** (violet) at (a) 0.1 wt%, (b) 0.25 wt%, (c) 0.5 wt% & (d) 1 wt% (also 2 wt% for **MfeGlyK16**) concentration in 50 mM Bis-tris propane + 150 mM NaCl, pH 7.4 recorded at 37 °C. CD spectra of (e) 0.25 wt% amphipathic oligopeptides **AbuK14**, **AbuK16**, **MfeGlyK16**, **DfeGlyK16** and **TfeGlyK16** and (f) 0.1–1 wt% **MfeGlyK16** in 50 mM Bis-tris propane + 150 mM NaCl, pH 9.0 recorded at 37 °C.

All peptides undergo β -sheet formation at a concentration of 0.25 wt%. Peptides **AbuK14** and **AbuK16** form β -sheets at indicated concentrations at pH 9.0, whereas significantly higher concentrations are necessary under physiological conditions (2 wt%). The only exception in this regard is the variant **MfeGlyK16**, which does not form β -sheets even at higher concentrations of 1 wt% (see Fig. 3f). Comparison of **MfeGlyK16**

with **AbuK14**, both possessing similar values of peptide hydrophobicity, underlines the lack of β -sheet assembly for **MfeGlyK16** due to its side chain properties. Likewise, calculated ΔE_{int} values suggests the residue of **MfeGly** to be better accommodated in a water-exposed environment. We propose this circumstance, phenomenologically, as a notable driving force maintaining **MfeGlyK16** in a PPII-like conformation.



Beside the polar effects of each fluorinated side chain, their intrinsic secondary structure propensities are also crucial factors to understand fluorine-driven peptide folding. As reported by Gerling *et al.* the **MfeGly** side chain possesses the highest helical propensity among its fluorinated derivatives **DfeGly** and **TfeGly**.²⁸ In correlation with the CD data, we suggest a synergistic effect of intrinsic folding propensity and fluorine-induced polarity by multiple incorporation of **MfeGly** causing the folding pattern of **MfeGlyK16**. For this purpose, we executed MD simulations to further elucidate this experimental finding. These theoretical results are discussed below.

Peptide self-assembly and characterization of fluorinated peptide-based hydrogels

Earlier reports demonstrated the supramolecular assemblies of amphipathic peptides to possess similar properties as the cross- β -sheet structure of amyloid fibrils.^{50,51} In order to study structural features of these peptides we used thioflavin T (ThT) fluorescence spectroscopy (Fig. 4a). This dye displays a strong fluorescence upon binding to amyloid-like morphologies caused by rotational immobilization, leading to an increase in fluorescence emission with a maximum at 485 nm. All samples were analyzed after 24 h of incubation time. We additionally studied all solutions by cryo-EM to determine the

morphology of the formed aggregates (Fig. 4b–e). For **AbuK16** and **MfeGlyK16** we did not observe any increase in fluorescence intensity (FL) (range: 0.01–1 wt%). As discussed above, CD spectroscopy at given concentrations confirms our finding that these peptides do not form β -sheets but instead PII helices. In contrast, **DfeGlyK16** shows a 9.5-fold enhanced fluorescence emission (1 wt%) compared to the control sample (ThT-dye in buffer without peptide, fluorescence intensity $FL_{485\text{nm}} = 1.0$), indicating the formation of amyloid-like aggregates. A small increase in FL intensity was observed for **DfeGlyK16** at a minimal concentration of 0.25 wt%, which is also the lowest concentration revealing β -sheet structures in the respective CD spectra. **TfeGlyK16** samples show a dramatic enhancement in fluorescence intensity of up to 180-fold at 1 wt%. Furthermore, the presence of amyloid-like fibrils was confirmed by Congo red (CR) staining experiments (see ESI, Fig. S97[†]). Our results indicate a correlation between the degree of fluorination and the ability to form amyloid-like structures. Cryo-EM studies were performed with those solutions for which a secondary structure pattern or amyloid-like behavior was detected by ThT staining. **DfeGlyK16** (0.25 wt%) (Fig. 4d) and **TfeGlyK16** (0.1 wt%) (Fig. 4e) both form amyloid-like structures. As expected, through CD and ThT staining experiments, **AbuK16** (0.25 wt%) and **MfeGlyK16** (0.25 wt%)

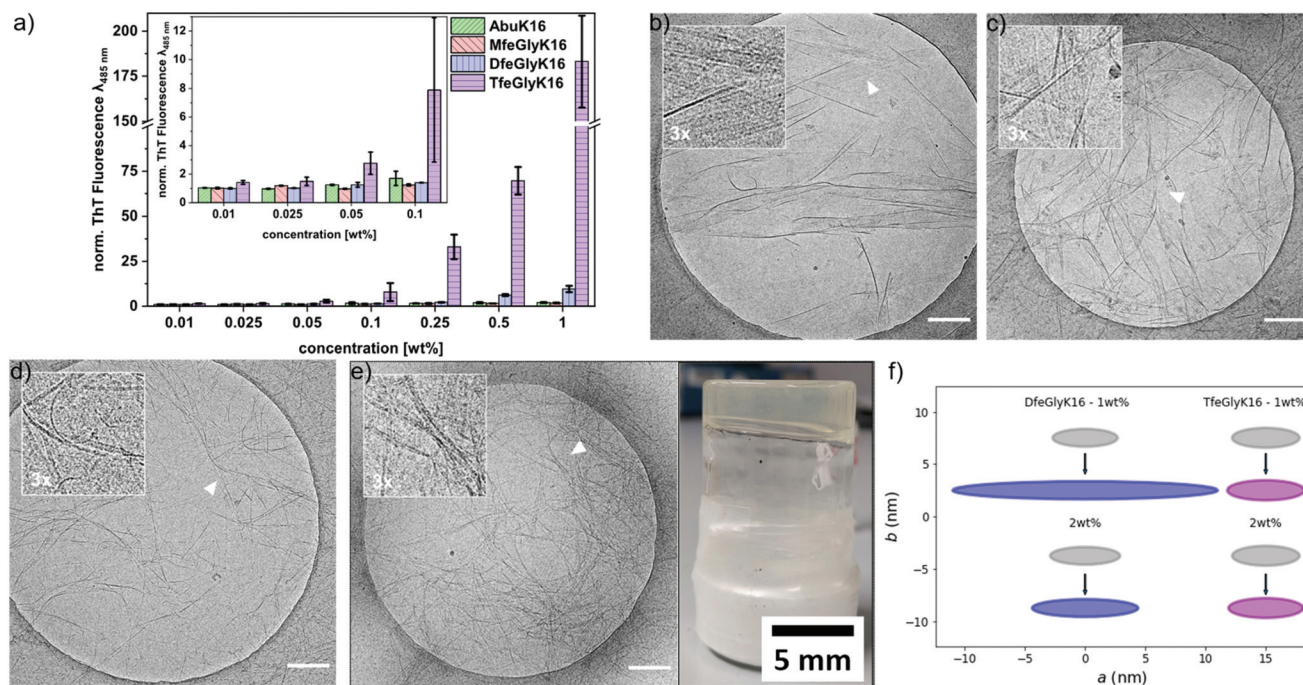


Fig. 4 (a) Thioflavin T assays of **AbuK16** (green), **MfeGlyK16** (red), **DfeGlyK16** (blue) and **TfeGlyK16** (violet) incubated for 24 h at 37 °C in 50 mM Bis-tris propane + 150 mM NaCl containing 20 μM ThT dye, pH 7.4. Fluorescence emission was measured at 485 nm and normalized to a negative control (solely buffer) with a FL intensity of 1.0. Cryo-EM micrographs of (b) **AbuK16** (2 wt%, diluted to 0.2 wt%), (c) **AbuK16** (2 wt%, diluted to 0.2 wt%), (d) **DfeGlyK16** (0.25 wt%) and (e) **TfeGlyK16** (0.1 wt%) + image of a **TfeGlyK16**-based hydrogel at pH 7.4 (0.5 wt%). All samples were dissolved in 50 mM Bis-tris propane + 150 mM NaCl, pH 7.4. Insets display magnified areas of the micrographs indicated by white arrow heads. The scale bar denotes 200 nm for each micrograph. (f) Fibril cross sections corresponding to the SAXS model curves for samples of **DfeGlyK16** and **TfeGlyK16** at concentrations of 1 wt% and 2 wt% obtained through SAXS experiments. The cross-sections are of elliptical shape defined by major and minor semi-axis a and b , respectively. Plotted are the cross-sections derived from SAXS measurement frames $n = 1$ (after 120 seconds (grey ellipses)) and 50 (after 3000 seconds (colored ellipses)). Fibril growth is illustrated by arrows.



did not form any fibrillary structures (see ESI, Fig. S98–S102†). At elevated concentrations of 2 wt%, however, we detected β -sheet formation for **AbuK14** and **AbuK16** by CD measurements (see prior data in Fig. 1a). Cryo-EM of these **AbuK**-derived sequences at 2 wt% concentration revealed narrow ribbons composed of fibrillar strands in a highly regular line pattern (Fig. 4b and c). A similar morphology from assembled fibrils based on a *de novo* designed coiled coil-based amyloidogenic peptide was studied in prior work.⁵² CD data of **MfeGlyK16** at similar concentrations provide a PPII-like structural pattern, and no similar β -sheet assemblies were found in this case. We also applied small-angle X-ray scattering (SAXS) experiments on supposedly amyloid-like fibrils containing solutions of the peptides **AbuK16**, **MfeGlyK16**, **DfeGlyK16** and **TfeGlyK16** over a wide range of concentration (see ESI† for detailed SAXS interpretation). SAXS data from peptides **DfeGlyK16** and **TfeGlyK16** (both 1 wt% and 2 wt%) scale approximately with q^{-1} (**TfeGlyK16**) and q^{-2} (**DfeGlyK16**) at low q -values (see Fig. S111 and S112 in the ESI†). Such scaling behavior indicates a nearly circular cross-section for the fibrils of **TfeGlyK16** (interpreted as circular cylinder) and a flat cross-section for **DfeGlyK16** (interpreted as extended parallelepiped).^{29,53} Data evaluation with both theoretical models in terms of time-resolved experiments [with measurement frames of $n = 1$ (recorded *ca.* 120 s after sample preparation) and $n = 50$ (recorded 3000 s after sample preparation)] revealed an increase of the major semi axis from $a = 2.7$ nm to 11.0 nm for **DfeGlyK16** (1 wt%) and from 2.9 nm to 4.4 nm (2 wt%). In contrast, the short semi-axis of the cross section is

constant at $b = 0.85$ nm. For **TfeGlyK16** an increase of the a -axis from 2.8 nm to 3.2 nm and from 2.8 nm to 3.1 nm at 1 wt% and 2 wt%, respectively, was determined. Here, the short semi-axis of the cross section is constant at $b = 0.95$ nm. An overview on the differences of cross-sections found for both polyfluorinated systems between data frame $n = 1$ and $n = 50$ is given in Fig. 4f.

After having characterized the mesoscopic structure of the different systems, we then turned to studying their macroscopic viscoelastic properties. Here, we performed strain-controlled oscillatory shear rheology measurements with the aim of evaluating the influence of fluorination on the mechanical properties of these gel matrices at pH 7.4 and pH 9.0. Amplitude γ (maximum deformation) sweeps at 1 Hz oscillation frequency were performed before the frequency-dependent measurements to ensure that the value γ of the deformation was always chosen such that the experimental conditions remained in the linear viscoelastic (LVE) regime. As a result, the amplitude γ for the oscillatory measurements was fixed at a value of 0.1%. The frequency sweeps were conducted in an angular frequency range of 0.314 to 314 rad s^{-1} to determine the storage and loss moduli G' and G'' (Fig. 5). First, we investigated the peptides **AbuK16**, **MfeGlyK16**, **DfeGlyK16** and **TfeGlyK16** at physiological conditions of pH 7.4 (Fig. 5a and b). As the non-fluorinated **AbuK16** (0.5 wt%) formed only a low viscous solution at physiological conditions, we established a further reference sample comprising a Leu–Lys repeating unit (**LeuK16**, Ac-(Leu-Lys)₈-[4]Abz-NH₂) to distinguish between the impact of hydrophobicity and fluorine substituents. The Leu–

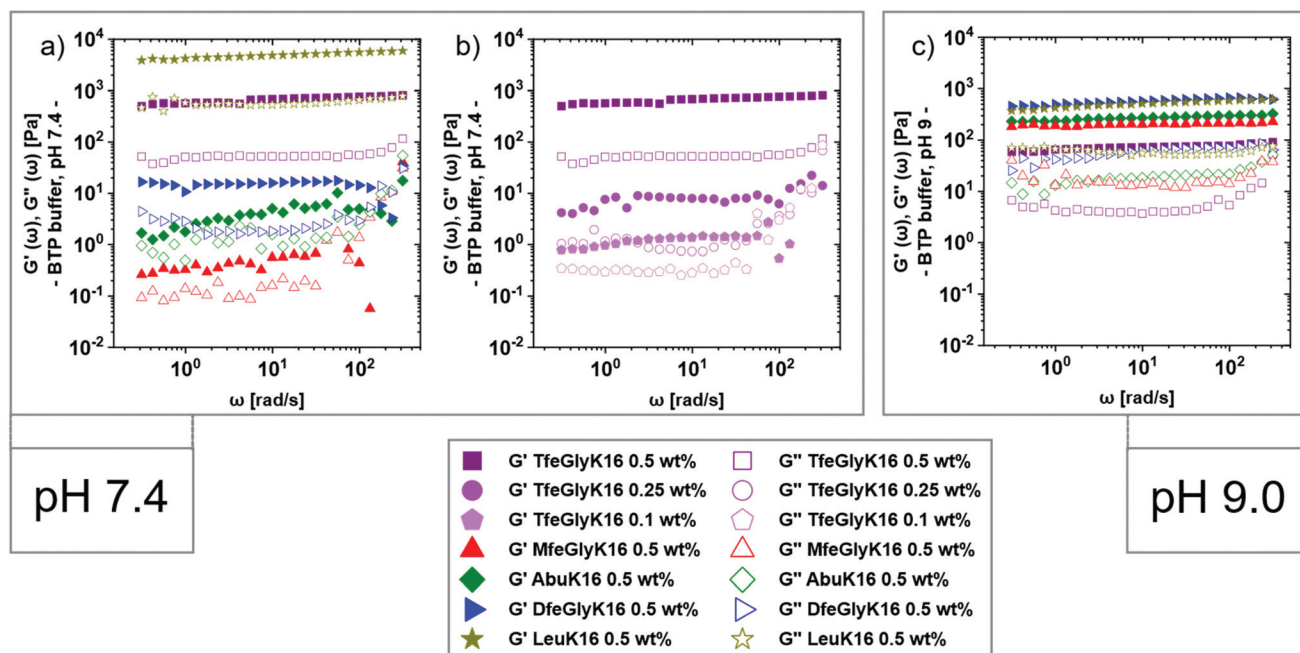


Fig. 5 Storage modulus G' and loss modulus G'' as measured in frequency sweeps ($\gamma = 0.1\%$) at $T = 37$ °C for: (a) the peptides **AbuK16**, **MfeGlyK16**, **DfeGlyK16**, **TfeGlyK16** and **LeuK16** (all 0.5 wt%) at pH 7.4; (b) the peptide **TfeGlyK16** at concentrations of 0.5 wt%, 0.25 wt%, and 0.1 wt% at pH 7.4; (c) the peptides **AbuK16**, **MfeGlyK16**, **DfeGlyK16**, **TfeGlyK16** and **LeuK16** (all 0.5 wt%) at pH 9.0. For sample preparation, freeze-dried peptides were dissolved in 50 mM Bis-tris propane + 150 mM NaCl, either pH 7.4 or pH 9.0.



Lys unit was utilized before by Schneider and co-workers for the development of peptide-based hydrogels.⁵⁴ Through our RP-HPLC assay, we found **LeuK16** ($\rho = 28.84 \pm 0.025$ min) to possess greater hydrophobicity than **TfeGlyK16** (see ESI, Fig. S96†). In the case of **TfeGlyK16** measurements were done also at lower concentrations of 0.25 and 0.1 wt%. These data are given in Fig. 5b and show a very strong reduction of the viscoelastic properties upon dilution, the elastic properties being reduced by a factor of around 80. Finally, for all 0.5 wt% samples we also studied their rheological behavior at pH 9.0 to determine how the change in pH affects the viscoelastic properties of the systems. Looking at Fig. 5c one observes that especially the elastic properties described by G' are now much closer than at pH 7.4. For all samples at pH 7.4 and pH 9.0, G' is at about one order of magnitude larger than G'' , indicating that these are gel-like systems, for which the elastic properties dominate.¹⁷ Both moduli increase somewhat with increasing frequency, thereby showing power law behavior, but with a rather small exponent. The plateau storage modulus G_0 , is of particular interest for gel-like systems. According to classical rubber elasticity theory,⁵⁵ G_0 can be related to the crosslinking density ν of the gel. The crosslinking density can in turn be used to estimate an average mesh size ξ in the system, given as:

$$\nu = G_0/kT = \xi^{-3}$$

where k is the Boltzmann constant and T is the temperature. The respective G_0 values for the peptide gels were determined by taking the average of the storage modulus G' data for $\omega \leq 10^2$ rad s^{-1} . These values and calculated mesh sizes are summarized in Table 1. At pH 7.4 and 0.5 wt% concentration, **MfeGlyK16** (0.53 Pa) shows the lowest G_0 value compared to **AbuK16** (4.81 Pa) and its higher fluorinated variants **DfeGlyK16** (15.30 Pa) and **TfeGlyK16** (670 Pa); the reference **LeuK16** possesses by far the highest value of G_0 , owing largely to a higher degree of hydrophobicity of the side chain compared to **TfeGly**.⁴⁸ Consequently, these experimental data show a consistent analogy to the hydrophobicity trend depicted through our RP-HPLC assay and underline a direct coherence between rheological stiffness and non-polar properties of each

amino acid residue (**MfeGly** < **Abu** < **DfeGly** < **TfeGly** < **Leu**). Thus, the successive addition of fluorine atoms strengthens this hydrogel scaffold at physiological conditions.

An interesting behavior is observed upon increasing the pH from 7.4 to 9.0, which lowers the overall charge of the peptide originating from the Lys residues (Fig. 5c). Upon this change, G_0 increases tremendously for **MfeGlyK16** (209 Pa), **AbuK16** (264 Pa) and **DfeGlyK16** (554 Pa) but drops by almost one order of magnitude for **TfeGlyK16** (70 Pa) and **LeuK16** (564 Pa), thereby bringing all the values closer together. This corresponds to an increase of G_0 by a factor of 394 (**MfeGlyK16**), 55 (**AbuK16**) and 36 (**DfeGlyK16**), but also a reduction of G_0 by a factor of 9.6 (**TfeGlyK16**) and 8.6 (**LeuK16**), respectively. The greatest change in viscoelastic stability is observed for the peptide with the lowest hydrophobicity (**MfeGlyK16**) within this work and becomes weaker with increasing non-polar properties (**AbuK16**, **DfeGlyK16**). This surprising loss in G_0 of **TfeGlyK16**-derived hydrogels was confirmed by further measurements at both pH values with independently prepared samples (see ESI, Fig. S104–106†). As an explanation, we suggest a major leverage of side chain-neutralization on the viscoelastic stability of these supramolecular matrices depending rather on peptide hydrophobicity than on fluorine-specific interactions. An almost equal loss in G_0 value in context of pH change found for **LeuK16** in correlation to **TfeGlyK16** serves as further confirmation of this experimental finding. Hence, the divergence in rheological properties between **DfeGlyK16** and **TfeGlyK16**-based hydrogels is, in particular, an interesting phenomenon as it seems to be triggered by only a single H to F substitution of each amino acid residue.

MD simulations of amphipathic peptides

Finally, we have performed MD simulations of **AbuK16**, **MfeGlyK16**, **DfeGlyK16**, and **TfeGlyK16** in explicit solvent at two different pH values: pH 7 (where for simplicity we assume all Lys residues to be charged) and pH 11 (where we assume all Lys residues to be charge neutral). The aim was to understand how fluorine-specific interactions may modify inter-peptide interactions and thereby control the formation of higher-ordered structures as observed in the above-discussed experiments. Interestingly, we find intra-strand contact pair formations between the fluorine atom of each **MfeGly** residue (**MfeGlyK16**) and backbone hydrogen atoms located on the peptide's amide bonds (Fig. 6a). Such contact pairs are absent in the cases of **DfeGlyK16** and **TfeGlyK16**, whose side chains are randomly oriented as found for **AbuK16** (Fig. 6a). The intra-strand contact pair formation observed for **MfeGlyK16** can be rationalized by the strongly polar **MfeGly** side chain as described before. The free energy profiles of inter-strand interaction as a function of the inter-strand separation for the different peptide types at pH 7 are shown in Fig. 6b, which reveal two distinct minima for each peptide type but **MfeGlyK16**, for which there is only one minimum. The shallow minimum at a larger inter-peptide separation observed for **AbuK16**, **DfeGlyK16**, and **TfeGlyK16** is due to the partially hydrophobic, non-standard (synonymous for **Abu**, **MfeGly**,

Table 1 Results for the plateau modulus G_0 and corresponding mesh sizes ξ

Name	c (wt%)	pH	G_0 (Pa)	ξ (nm)	
LeuK16	0.5	7.4	4869 \pm 124	9.83 \pm 0.08	
		9	564.4 \pm 7.2	20.17 \pm 0.09	
TfeGlyK16	0.5	7.4	670 \pm 19	19.05 \pm 0.18	
		9	70.24 \pm 1.4	40.4 \pm 0.3	
		0.25	7.4	8.63 \pm 0.79	81.3 \pm 2.5
		0.1	7.4	1.09 \pm 0.12	161.9 \pm 5.7
DfeGlyK16	0.5	7.4	15.30 \pm 1.04	67.14 \pm 1.5	
		9	554 \pm 15	20.29 \pm 0.18	
AbuK16	0.5	7.4	4.81 \pm 0.22	98.72 \pm 1.54	
		9	264.1 \pm 5.1	25.98 \pm 0.17	
MfeGlyK16	0.5	7.4	0.53 \pm 0.02	205.37 \pm 2.53	
		9	208.8 \pm 0.83	28.10 \pm 0.04	



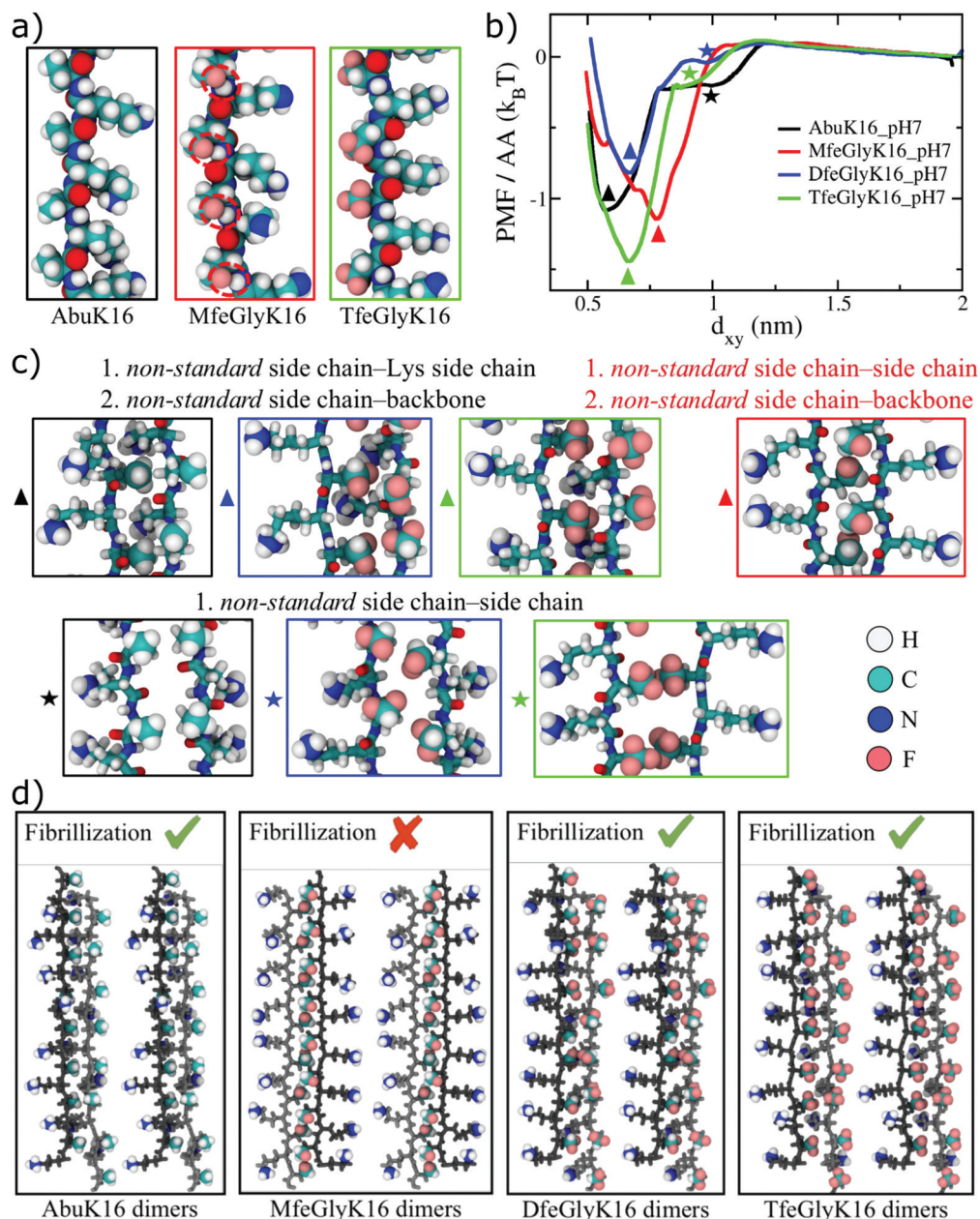


Fig. 6 MD simulation results for amphipathic peptides; water is included in the simulations, but not shown for clarity. (a) Snapshots for representative parts of periodic **AbuK16**, **MfeGlyK16**, and **TfeGlyK16** single strands (taken from umbrella sampling simulations when two strands are far apart) are shown in the space-filling representation and atoms are colored as: H (white), C (cyan), N (blue), O (red), F (pink). Fluorine atoms from **MfeGly** residues and the amide-backbone derived hydrogen atoms form strong intra-strand contact pairs which are marked by red, dashed ellipses. Such contact pairs are not observed for **Abu** and **TfeGly**. (b) The potential of mean force (PMF) per amino acid (AA) as a function of inter-strand separation d_{xy} at pH 7 (charged Lys), depicting the free energy profile of interaction between two peptide strands for side chains with different degree of fluorinations. The global minimum for each peptide type is marked by a triangle, whereas a secondary shallow minimum at a farther distance (when present) is marked by a star symbol. (c) Structures corresponding to free energy minima for each peptide type are shown in ball-stick representation; the terminal group of each side chain is highlighted in the space-filling representation. Atom colors are the same as in (a) and colors of enclosing boxes are the same as colors of the PMF profiles in (b). Dominant binding modes are given at the top of each snapshot. (d) Schematic depicting the possibility of fibrillization of the dimer complex for the different peptide types. One strand of a dimer complex (shown in the ball-stick representation) is colored as light-gray, whereas the other strand is colored as dark-gray. The end groups of side chains from Lys ($-\text{NH}_3^+$), **Abu** ($-\text{CH}_3$), **MfeGly** ($-\text{CFH}_2$), **DfeGly** ($-\text{CF}_2\text{H}$), and **TfeGly** ($-\text{CF}_3$) are highlighted in space-filling representation.

DfeGly and **TfeGly**) amino acid (AA) side chain-side chain interaction, whereas the global minimum at a smaller inter-peptide separation is due to the non-standard AA side chain-

Lys side chain and non-standard AA side chain-backbone interactions (see snapshots in Fig. 6c). In contrast, the minimum free-energy structure of **MfeGlyK16** is due to the



polar, non-standard AA side chain–backbone and non-standard AA side chain–side chain interactions, and the charged Lys residues protrude out to minimize the electrostatic repulsion. Although negative and comparable free energy values for all cases imply that every peptide type can form strongly bounded dimers, the possibility of peptide fibril formation depends on whether two such dimers can in turn form favorable contacts with each other. As depicted in Fig. 6d for **AbuK16**, **DfeGlyK16**, and **TfeGlyK16**, two dimers placed parallel to each other can form favorable contacts between the non-standard AA and Lys side chains (which are found to be important for the stability of a dimer as well). In contrast, two **MfeGlyK16** dimers placed parallel to each other face charged end groups of the Lys residue ($-\text{NH}_3^+$), and thus repel each other. Therefore, higher-order structure formation or fibrillization at pH 7 is predicted to be possible for **AbuK16**, **DfeGlyK16**, and **TfeGlyK16**, but not for **MfeGlyK16**, explaining our experimental findings at physiological conditions. The free energy profiles at pH 11, shown in Fig. S109† (ESI), reveal only one free-energy minimum for each peptide type, the depth of which is more than that of the corresponding peptide type at pH 7. The increased interaction strength is due to the reduced electrostatic repulsion between the two strands, as Lys residues are charge neutral at pH 11. For **MfeGlyK16**, the intra-strand contact pair formations (Fig. 6a) expose the backbone atoms of **MfeGly** amino acids that can form H-bonds with the solvent-exposed backbone atoms of another **MfeGlyK16** strand, resulting in a very compact **MfeGlyK16** dimer with enhanced side chain–side chain interactions (see snapshots in Fig. S109 within the ESI†). These strong cooperative interactions lead to a 2–3 times deeper free energy minimum for **MfeGlyK16** than other peptide types, for which the inter-peptide interactions are dominated by weak backbone–side chain and side chain–side chain contacts. Like at pH 7, for **AbuK16**, **DfeGlyK16**, and **TfeGlyK16**, two dimers placed parallel to each other can form the same favorable contacts as found in the stable structure of a single dimer, and hence the dimer structure can be periodically extended from either side by adding more dimers to produce large-scale peptide fibrils. For **MfeGlyK16**, the dimer structure is the most stable among the different peptide types and the inter-dimer interaction strength is expected to be lower due to the only possible side chain–side chain interaction as backbone atoms in a dimer complex are shielded by **MfeGly** side chains given by intra-strand contact pair formation. Hence, higher-order structures are expected to be less stable for **MfeGlyK16** and would provide an explanation for its structural properties.

Conclusions

In this work, we systematically designed and characterized a library of oligopeptides with high numbers of fluorinated amino acids. The peptides **AbuK16**, **MfeGlyK16**, **DfeGlyK16** and **TfeGlyK16** served as models to evaluate the impact of fluorine-specific interactions in the context of secondary structure formation, peptide self-assembly and hydrogel formation. The

fluorination degree of the aliphatic side chain plays a crucial role in determining the peptide intrinsic hydrophobic properties. This led not only to the observation of different secondary structures such as PPII helices or β -sheets, but also to fluorine-driven self-assembly into ordered nanostructures. On the other hand, we found for **MfeGlyK16** at physiological conditions no evidence of β -sheet assembly, explained by MD simulations that find strong dimer formation preventing peptide fibrillization. Rheological characterization revealed a correlation between the hydrophobic nature of each fluorinated amino acid and an enhanced viscoelastic stability of resulting hydrogel matrices as shown for **MfeGlyK16**, **DfeGlyK16** and **TfeGlyK16** in physiological conditions, but also a loss in mechanical stiffness for the latter variant at pH 9.0. This study firstly established and studied a library of distinctive aliphatic and polyfluorinated SAPs for which fluorine-specific interactions were evinced by significant alterations of intra- and intermolecular interactions. The underlined design principle, the unique properties of the peptides and resulting hydrogel matrices will contribute to the future development of *de novo* designed fluorinated biomaterials.

Experimental section

General methods

^1H -, ^{13}C - and ^{19}F -NMR spectra (see ESI†) were recorded at room temperature using a JEOL ECX 400 (JEOL, Tokyo, Japan), a JEOL ECP 500 (JEOL, Tokyo, Japan) or a Bruker AVANCE III 700 (700 MHz, BRUKER, Billerica, MA, USA). Chemical shifts δ are reported in ppm with the solvent resonance (MeOH-d_4) as the internal standard. HRMS were determined on an Agilent 6220 ESI-TOF MS instrument (Agilent Technologies, Santa Clara, CA, USA). For analysis, the MassHunter Workstation Software Version B.02.00 (Agilent Technologies, Santa Clara, CA, USA) was used. IR Spectra were recorded on an ALPHA II FT-IR spectrometer (Bruker, USA). All NMR and IR spectra were evaluated by using Mnova/Mestrenova (Mestrelab Research, CA, USA). Elemental analysis was proceeded by use of an VARIO EL elemental analyzer (Elementar Analysensysteme GmbH, Langenselbold, Germany). All essential data for compound characterization is placed within the ESI.† All chemicals were purchased from commercial sources (Merck, Sigma-Aldrich, VWR, Fluorochem) and used without further purification. The Fmoc-protected fluorinated amino acid **TfeGly** was synthesised according to literature (see ESI,† chapter “Gram scale synthesis and characterization of fluorinated amino acid Fmoc-TfeGly-OH”). **MfeGly** and **DfeGly** were synthesised by Suvrat Chowdhary and Thomas Hohmann.

Synthesis and purification of peptides

All peptides were synthesized with a microwave-equipped Liberty Blue™ peptide synthesizer (CEM, Matthews, NC, USA). A Rink Amide ProTide™ resin (CEM, Matthews, NC, USA) was utilized and the synthesis was performed either in 0.05 mmol or 0.1 mmol scale using oxyma/DIC as activating reagents



(0.05 mmol scale: 0.5 M oxyma in DMF and 0.25 M DIC in DMF/0.1 mmol scale: 1 M oxyma in DMF and 0.5 M DIC in DMF). Coupling of native Fmoc-protected amino acids occurred in DMF using 5 eq. of substance (for fluorinated amino acids only 1.5 eq. were used) with 5 eq. of activating reagents and double couplings of 4 min coupling time (for fluorinated amino acid: mono coupling of 10 min) at 90 °C. For deprotection of the N-terminus, a 10% piperazine (w/v) solution in EtOH/NMP (1:9) with 0.1 M HOBt was used. Acetylation was done manually in three batches using acetic anhydride (10% v/v) and DIPEA (10% v/v) in DMF (6 mL). All peptides were cleaved from the resin by treatment with TFA/TIPS/H₂O (90/5/5) for three hours using sonication at room temperature. Then the resins were washed with TFA and DCM, and excess of solvents were removed by evaporation. Peptides were dried by lyophilization before purification with preparative reversed phase HPLC. Purification of synthesized peptides was performed on a Knauer low-pressure HPLC system (Knauer GmbH, Berlin, Germany) sold by VWR (Darmstadt, Germany), comprising a LaPrep Sigma preparative pump (LP1200), a ternary low-pressure gradient, a dynamic mixing chamber, a 6-port-3-channel injection valve with an automated preparative 10 mL sample loop, a LaPrep Sigma standard 1-channel-UV-detector (LP3101), a flow cell with 0.5 mm thickness and a 16-port LaPrep Sigma fractionation valve (LP2016). A Kinetex RPC18 endcapped (5 μM, 100 Å, 250 × 21.2 mm, Phenomenex®, USA) HPLC-column was used. A Security Guard™ PREP Cartridge Holder Kit (21.20 mm, ID, Phenomenex®, USA) served as pre-column. As eluents water and ACN, both containing 0.1% (v/v) TFA were applied. HPLC runs were performed with a flow rate of 15.0 mL min⁻¹, UV-detection occurred at 220 nm for respective peptides. Data analysis occurred with an EZChrom Elite-Software (Version 3.3.2 SP2, Agilent). After separation, the purity of the collected fractions was determined by analytical HPLC. Analytical HPLC was carried out on a Chromaster 600 bar DAD-System with CSM software or a Hitachi Primaide™ UV-HPLC system (both from VWR/Hitachi, Darmstadt, Germany). A Kinetex® RP-C18 (5 μM, 100 Å, 250 × 4.6 mm, Phenomenex®, USA) column and a SecurityGuard™ Cartridge Kit equipped with a C18 cartridge (4 × 3.0 mm, Phenomenex®, USA) as pre-column was used. Otherwise, a Luna® RP-C8 (5 μM, 100 Å, 150 × 3 mm, Phenomenex®, USA) column was used. As eluents water and ACN, both containing 0.1% (v/v) TFA were applied. A flow rate of 1 mL min⁻¹ was used and UV-detection occurred at 220 nm or 280 nm for respective peptides. Data analysis was done with EZ Chrom ELITE software (version 3.3.2, Agilent). The resulting pure peptides (>95%) were obtained after lyophilization of the collected fractions. All essential data for the quantification of purified peptides (HPLC data, HRMS spectra) can be found in the ESI (Fig. S37–S91 and Tables S1–S22†).

Lyophilization

To lyophilize the synthesized peptides a laboratory freeze dryer ALPHA 1-2 LD (Christ Gefriertrocknungsanlagen GmbH, Osterode am Harz, Germany) was used.

Sample preparation – exchange of TFA salts

All purified peptides were inevitably obtained as corresponding TFA salts during resin cleavage and subsequent RP-HPLC purification using eluents containing 0.1% TFA. Peptide samples (about 13 mg each) were dissolved in 800 μL Milli-Q-H₂O and transferred on a VariPure IPE exchange column (100 mg, 3 mL) (Agilent Technologies, Santa Clara, CA, USA). These columns were previously washed and pre-conditioned with MeOH (3 × 3 mL) and Milli-Q-H₂O (3 × 3 mL). The resin was additionally washed with Milli-Q-H₂O (500 μL) and the collected peptide fractions were combined. Afterwards, desired samples were lyophilized to obtain the peptide with bicarbonates as counter-ions.

Preparation of peptide stock solutions and self-assembly

Peptide stock solutions were prepared by dissolving lyophilized peptide powder (10–15 mg) in 1,1,1,3,3,3-hexafluoropropan-2-ol [HFIP] (2 mL) and treatment for 15 min in an ultrasound-bath to dissolve preformed aggregates. An aliquot of 10 μL was evaporated and the dried peptide film dissolved in a 6 M guanidine hydrochloride (GndHCl) solution (pH 7.4), resulting into a dilution factor (DL) of 100. These samples were measured *via* UV detection at 280 nm by use of an Eppendorf BioPhotometer plus with semi-micro-VIS Cuvettes (PMMA) 10 × 100 (Eppendorf, Hamburg, Germany). All UV spectra were baseline corrected with a reference spectrum of a sample containing solely buffer solution. The UV absorbance given through the fluorophore *p*-aminobenzoic acid (PABA) at the C-terminus of the peptides at 280 nm was evaluated in triplicates. By use of a calibration curve derived from *p*-aminohippuric acid (PAH) (see ESI, Fig. S92†), the concentration of each stock solution was calculated. If not otherwise stated, all peptide samples were treated following this protocol before each measurement: an aliquot from the HFIP peptide stock solution was taken and evaporated. The dried peptide was then dissolved in respective buffer and vortexed (1 min), sonicated (5 min) and finally ultracentrifuged (1 min) at room temperature.

RP-HPLC assay for estimation of hydrophobicity

The protocol for the RP-HPLC assay was previously established by our group.^{28,29} Peptide samples were dissolved in 250 μL of a mixture of 5% (v/v) ACN in 95% (v/v) Milli-Q-water containing 0.1% TFA and filtered over a syringe filter with 0.2 μm pore size. The overall concentration of each sample was 0.2 mM. The retention times of all samples were determined on a C18 column (Capcell C18, 5 μm) using a LaChrom-ELITE-HPLC-System (VWR International) with UV detection at 280 nm. A linear gradient from 5 to 40% ACN + 0.1% TFA in 30 min was applied at room temperature and all experiments were performed in triplicates.

QM calculations

All QM calculations were performed using Gaussian 16.1.⁵⁶ Abu, MfeGly, DfeGly, and TfeGly-derived motifs, as shown in



Fig. 2b, were taken for QM calculations. Geometry optimizations of these structures were done at the MP2/6-31G* level of theory. Water interaction energies were obtained from the HF/6-31G* single point calculations of the geometry optimized structures. Electrostatic potential maps for the geometry optimized structures were rendered using the Avogadro software.⁵⁷ Dihedral energy scans were performed at the MP2/6-31G* level of theory. Force field parameters and partial atomic charges for the amino acid **Abu** and its fluorinated variants (**MfeGly**, **DfeGly**, and **TfeGly**) were initially obtained from CHARMM36m⁵⁸ and CGenFF⁵⁹ parameters, using the CGenFF program.^{60,61} As there were large penalties for dihedral angles associated with side chain rotations ($C\alpha-C\beta-C\gamma-F$ and $C\alpha-C\beta-C\gamma-H$) and partial atomic charges, new parameters were derived from QM energy scans and water interaction energies, respectively using the FFParm package.⁶² Optimized partial atomic charges and dihedral parameters for the different amino acids are given in the ESI† (Chapter 12).

Equilibrium MD simulations

To study interpeptide interactions, two periodic polypeptide chains, each with the long-axis oriented along the z -direction, with an interaxial distance d_{xy} of 2.5 nm, arranged antiparallel (ap) to each other were considered. Each system was solvated in a rectangular box of size $5 \times 5 \times 5.832$ nm³. If needed, enough counterions (Cl^- ions) were added to charge neutralize the whole system. The simulation box is shown in Fig. S108† (ESI). CHARMM-compatible TIP3P water^{63,64} and ion parameters⁶⁵ were used. The solvated system was subjected to energy minimization using the steepest descent algorithm, for removing any unfavourable contacts. The simulation for each case was performed for 500 ns in the $Np_{xy}L_zT$ ensemble, with L_z per amino acid = 3.6 Å, at $T = 300$ K and $p_{xy} = 1$ bar with periodic boundary condition in xyz directions, using the GROMACS 2020.1 package.⁶⁶ The stochastic velocity rescaling thermostat⁶⁷ with a time constant of $\tau_T = 0.1$ ps was used to control the temperature, while for the pressure control a semi-isotropic Parrinello–Rahman barostat⁶⁸ was used with a time constant of $\tau_p = 1$ ps and a compressibility of $\kappa = 4.5 \times 10^{-5}$ bar⁻¹. The LINCS algorithm⁶⁹ was used to convert the bonds with H-atoms to constraints, allowing a timestep of $\Delta t = 2$ fs. Electrostatics interactions were computed using the particle mesh Ewald (PME) method⁷⁰ with a real-space cut-off distance of 1.2 nm, while van der Waals (VDW) interactions were modelled using Lennard-Jones potentials with a cut-off distance of 1.2 nm where the resulting forces smoothly switch to zero between 1 nm to 1.2 nm.

Umbrella sampling simulations

To calculate the free energy landscape or the potential of mean force (PMF) between two periodic polypeptide chains, the final configuration obtained from the equilibrium MD simulation was first pulled in either direction to generate initial conformations for two polypeptide chains at different interaxial separations. Total 40–50 umbrella windows, with an inter-window spacing of 0.35 Å, were simulated in the $Np_{xy}L_zT$

for 30 ns each. During these simulations, an additional umbrella potential with a spring constant of 10 000 kJ mol⁻¹ nm⁻² was used to restrain the interaxial separation to a given distance. Every 100 fs data was collected, and the last 20 ns simulation data for each window was used to obtain the PMF using the weighted histogram analysis method (WHAM).^{71,72} The *g_wham* module⁷³ of GROMACS was used for performing the WHAM analysis and calculating error bars using the bootstrap method.

CD spectroscopy

Circular dichroism experiments were performed using a Jasco J-810 spectropolarimeter fitted with a recirculating chiller (D-76227, Karlsruhe). Data were recorded using 0.1 mm Quartz Suprasil® cuvettes (Hellma) equipped with a stopper. Spectra were recorded at 37 °C from 190 to 250 nm at 0.2 nm intervals, 1 nm bandwidth, 4 s response time and a scan speed of 100 nm min⁻¹. Baselines were recorded and were subtracted from the data. Each reported CD value represents the average of minimum three measurements. Further CD spectra can be found in the ESI (Fig. S93–S95†).

Congo red (CR) assay for fibril detection

Aliquots of peptide HFIP-stock solutions (0.5 wt%) were dried and then redissolved in 50 mM Bis-tris propane + 150 mM NaCl with addition of 50 μM Congo red (overall pH 7.4). Negative controls were prepared by dissolving corresponding samples in buffer without dye. After dissolution, the standard self-assembly protocol was applied, and all samples were incubated overnight at 37 °C. UV spectra (300–700 nm) were recorded for all samples using a Varian Cary 50 UV-VIS Spectrophotometer (Agilent, USA) and 0.5 mm Quartz Suprasil® cuvettes (Hellma). Experimental data can be found in the ESI (Fig. S97†).

Thioflavin T (ThT) fluorescence assay for fibril detection

A suitable protocol for this assay was recently published by our group.²⁹ Aliquots of peptide HFIP-stock solutions were dried and then redissolved in 50 mM Bis-tris propane + 150 mM NaCl with addition of 20 μM Thioflavin T (overall pH 7.4). The buffer containing ThT was previously filtered over a nylon syringe filter with 0.2 μm pore size. After dissolution, the sample was sonicated for 30 s, transferred on a BRAND® microplate (size: 96 wells, color: black; Sigma-Aldrich), sealed to prevent evaporation and placed in an Infinite® M Nano⁺ plate reader (Tecan Deutschland GmbH, Crailsheim, Germany). ThT fluorescence ($\lambda_{ex} = 420$ nm, $\lambda_{em} = 485$ nm, Z-position: 15 173 nm [manual], gain: 80 [manual], lag time: 0 μs, integration time: 20 μs) was measured after 24 h incubation at 37 °C. The fluorescence intensity at 485 nm was normalized with respect to the negative control solely containing buffer (set as $FL_{int} 1.0$).

Cryogenic electron microscopy (cryo-EM)

Perforated carbon film-covered microscopical 200 mesh grids (R1/4 batch of Quantifoil, MicroTools GmbH, Jena, Germany)



were cleaned with chloroform and hydrophilized by 60 s glow discharging at 10 μA in a EMSCOPE SC500 before 4 μl aliquots of the peptide solution were applied to the grids. The samples were vitrified by automatic blotting and plunge freezing with a FEI Vitrobot Mark IV (Thermo Fisher Scientific Inc., Waltham, Massachusetts, USA) using liquid ethane as cryogen. The vitrified specimens were transferred to the autoloader of a FEI TALOS ARCTICA electron microscope (Thermo Fisher Scientific Inc., Waltham, Massachusetts, USA). This microscope is equipped with a high-brightness field-emission gun (XFEG) operated at an acceleration voltage of 200 kV. Micrographs were acquired on a FEI Falcon 3 direct electron detector (Thermo Fisher Scientific Inc., Waltham, Massachusetts, USA) using the 70 μm objective aperture at a nominal magnification of 28 000, corresponding to a calibrated pixel size of 3.75 \AA per pixel, respectively.

Small-angle-X-ray scattering (SAXS)

SAXS measurement were performed in a flow-through capillary with a Kratky-type instrument (SAXSess from Anton Paar, Austria) at 37 ± 1 $^{\circ}\text{C}$. The SAXSess has a low sample-to-detector distance of 0.309 m, which is appropriate for investigations of liquid samples with low scattering intensities. The measured intensity was converted to absolute scale according to Orthaber *et al.*⁷⁴ The scattering vector q is defined in terms of the scattering angle θ and the wavelength λ of the radiation ($\lambda = 0.154$ nm): thus, $q = 4\pi n/\lambda \sin \theta$. Deconvolution (slit length desmearing) of the SAXS curves was performed with the SAXS-Quant software. Samples analyzed with SAXS were used as prepared, *i.e.* samples were mixed with buffer solution, vortexed for 20 s and filled in the capillary. Curve fitting was conducted with SASfit.⁷⁵

Rheological characterization of amphipathic peptide hydrogels

Before each measurement, peptide samples of **AbuK16**, **MfeGlyK16**, **DfeGlyK16**, **TfeGlyK16** and **LeuK16** were dissolved in 50 mM Bis-tris propane + 150 mM NaCl (either pH 7.4 or pH 9.0), treated as mentioned above and incubated at 37 $^{\circ}\text{C}$ for 24 h. All rheological measurements were performed on an Anton Paar MCR 502 WESP temperature-controlled rheometer in strain-imposed mode at physiological temperature (37 $^{\circ}\text{C}$). For all measurements, a parallel plate geometry with chromium oxide coating was used, with a diameter of 50 mm for the upper rotating plate. The gap size between the plates was set to 175 μm . The sample and geometry were surrounded by a solvent trap to reduce effects of solvent evaporation. Further experimental data can be found in the ESI (Fig. S97[†]).

Author contributions

B. K. and S. C. conceived the overall project. B. K. provided guidance on data analysis, interpretation, and manuscript preparation. S. C. designed and developed concepts and experiments, synthesized, and purified all peptides, performed CD, UV and FL experiments, established and proceeded a RP-HPLC-based

hydrophobicity plot for peptides, prepared samples for further experiments and wrote the manuscript. R. F. S. performed rheology experiments and wrote the manuscript. A. K. S. performed simulations. A. K. S. and R. R. N. analyzed and interpreted data and wrote the manuscript. T. t. D. assisted S. C. in synthesis and purification of peptides and circular dichroism experiments. K. B.-J. and A. F. T. performed SAXS experiments and SAXS data analysis. T. H. provided fluorinated amino acids. B. S. performed cryoEM experiments, analyzed, and interpreted data. R. R. N. and M. G. provided expertise and feedback.

Conflicts of interest

There are no conflicts to declare.

Acknowledgements

S. C., T. H., B. S., R. R. N. and B. K. gratefully acknowledges financial support by the Deutsche Forschungsgemeinschaft (DFG) through the collaborative research center CRC 1349 “Fluorine-Specific Interactions”, project no. 387284271. R. F. S., M. G., and R. R. N. were funded by the DFG grant CRC 1449 “Dynamic Hydrogels at Biointerfaces”, project no. 431232613. We thank Dr Johann Moschner, Dr Katharina Hellmund, Dr Dorian Jamal Mikolajczak, Dr Ana Rita de Lima Fernandes, Dr Allison Berger, and Dr Chaitanya Kumar Thota for fruitful scientific discussions and expertise. We thank Dr Jakob Leppkes for his support during the synthesis of fluorinated amino acids. We would like to acknowledge the assistance of the Core Facility BioSupraMol supported by the DFG. We thank Benedikt Kirmayer for assistance in the preparation of cryo-EM samples and micrographs. A. K. S. and R. R. N. acknowledge support from the Max-Planck MaxWater initiative.

Notes and references

- 1 A. Levin, T. A. Hakala, L. Schnaider, G. J. L. Bernardes, E. Gazit and T. P. J. Knowles, *Nat. Rev. Chem.*, 2020, **4**, 615–634.
- 2 S. Zhang, *Nat. Biotechnol.*, 2003, **21**, 1171–1178.
- 3 J. P. Schneider, D. J. Pochan, B. Ozbas, K. Rajagopal, L. Pakstis and J. Kretsinger, *J. Am. Chem. Soc.*, 2002, **124**, 15030–15037.
- 4 B. Ozbas, J. Kretsinger, K. Rajagopal, J. P. Schneider and D. J. Pochan, *Macromolecules*, 2004, **37**, 7331–7337.
- 5 S. Zhang, T. Holmes, C. Lockshin and A. Rich, *Proc. Natl. Acad. Sci. U. S. A.*, 1993, **90**, 3334–3338.
- 6 S. Zhang, T. C. Holmes, C. M. DiPersio, R. O. Hynes, X. Su and A. Rich, *Biomaterials*, 1995, **16**, 1385–1393.
- 7 F. Gelain, Z. Luo and S. Zhang, *Chem. Rev.*, 2020, **120**, 13434–13460.
- 8 F. Gelain, Z. Luo, M. Rioult and S. Zhang, *npj Regener. Med.*, 2021, **6**, 9.



- 9 C. J. C. Edwards-Gayle and I. W. Hamley, *Org. Biomol. Chem.*, 2017, **15**, 5867–5876.
- 10 V. Castelletto, C. J. C. Edwards-Gayle, F. Greco, I. W. Hamley, J. Seitsonen and J. Ruokolainen, *ACS Appl. Mater. Interfaces*, 2019, **11**, 33573–33580.
- 11 S. Motamed, M. P. Del Borgo, K. Kulkarni, N. Habila, K. Zhou, P. Perlmutter, J. S. Forsythe and M. I. Aguilar, *Soft Matter*, 2016, **12**, 2243–2246.
- 12 P.-X. Zhang, N. Han, Y.-H. Kou, Q.-T. Zhu, X.-L. Liu, D.-P. Quan, J.-G. Chen and B.-G. Jiang, *Neural Regener. Res.*, 2019, **14**, 51–58.
- 13 K. S. Hellmund, B. von Lospichl, C. Böttcher, K. Ludwig, U. Keiderling, L. Noirez, A. Weiß, D. J. Mikolajczak, M. Gradzielski and B. Kokschi, *Pept. Sci.*, 2021, **113**, e24201.
- 14 S. Lee, T. H. T. Trinh, M. Yoo, J. Shin, H. Lee, J. Kim, E. Hwang, Y.-B. Lim and C. Ryou, *Int. J. Mol. Sci.*, 2019, **20**, 5850.
- 15 J. Y. C. Lim, Q. Lin, K. Xue and X. J. Loh, *Mater. Today Adv.*, 2019, **3**, 100021.
- 16 X. Zhao and S. Zhang, *Chem. Soc. Rev.*, 2006, **35**, 1105–1110.
- 17 L. M. De Leon Rodriguez, Y. Hemar, J. Cornish and M. A. Brimble, *Chem. Soc. Rev.*, 2016, **45**, 4797–4824.
- 18 J. Kopeček and J. Yang, *Acta Biomater.*, 2009, **5**, 805–816.
- 19 J. N. Sloand, M. A. Miller and S. H. Medina, *Pept. Sci.*, 2021, **113**, e24184.
- 20 A. A. Berger, J.-S. Völler, N. Budisa and B. Kokschi, *Acc. Chem. Res.*, 2017, **50**, 2093–2103.
- 21 E. N. G. Marsh, *Acc. Chem. Res.*, 2014, **47**, 2878–2886.
- 22 S. A. Samsonov, M. Salwiczek, G. Anders, B. Kokschi and M. T. Pisabarro, *J. Phys. Chem. B*, 2009, **113**, 16400–16408.
- 23 M. Salwiczek, S. Samsonov, T. Vagt, E. Nyakatura, E. Fleige, J. Numata, H. Cölfen, M. T. Pisabarro and B. Kokschi, *Chem. – Eur. J.*, 2009, **15**, 7628–7636.
- 24 S. Huhmann, E. K. Nyakatura, H. Erdbrink, U. I. M. Gerling, C. Czekelius and B. Kokschi, *J. Fluorine Chem.*, 2015, **175**, 32–35.
- 25 T. Vagt, E. Nyakatura, M. Salwiczek, C. Jäckel and B. Kokschi, *Org. Biomol. Chem.*, 2010, **8**, 1382–1386.
- 26 S. Ye, B. Loll, A. A. Berger, U. Mülow, C. Alings, M. C. Wahl and B. Kokschi, *Chem. Sci.*, 2015, **6**, 5246–5254.
- 27 J. Leppkes, N. Dimos, B. Loll, T. Hohmann, M. Dyrks, A. R. Wieseke, B. G. Keller and B. Kokschi, *RSC Chem. Biol.*, 2022, **3**(6), 773–782.
- 28 U. I. M. Gerling, M. Salwiczek, C. D. Cadicamo, H. Erdbrink, C. Czekelius, S. L. Grage, P. Wadhvani, A. S. Ulrich, M. Behrends, G. Haufe and B. Kokschi, *Chem. Sci.*, 2014, **5**, 819–830.
- 29 S. Chowdhary, J. Moschner, D. J. Mikolajczak, M. Becker, A. F. Thünemann, C. Kästner, D. Klemczak, A.-K. Stegemann, C. Böttcher, P. Metrangolo, R. R. Netz and B. Kokschi, *ChemBioChem*, 2020, **21**, 3544–3554.
- 30 S. Huhmann and B. Kokschi, *Eur. J. Org. Chem.*, 2018, **2018**, 3667–3679.
- 31 C. K. Thota, A. A. Berger, B. Harms, M. Seidel, C. Böttcher, H. von Berlepsch, C. Xie, R. Süßmuth, C. Roth and B. Kokschi, *Pept. Sci.*, 2020, **112**, e24130.
- 32 F. Agostini, L. Sinn, D. Petras, C. J. Schipp, V. Kubyshekin, A. A. Berger, P. C. Dorrestein, J. Rappsilber, N. Budisa and B. Kokschi, *ACS Cent. Sci.*, 2021, **7**, 81–92.
- 33 J.-S. Völler, M. Dulic, U. I. M. Gerling-Driessen, H. Biava, T. Baumann, N. Budisa, I. Gruic-Sovolj and B. Kokschi, *ACS Cent. Sci.*, 2017, **3**, 73–80.
- 34 J. Moschner, V. Stulberg, R. Fernandes, S. Huhmann, J. Leppkes and B. Kokschi, *Chem. Rev.*, 2019, **119**, 10718–10801.
- 35 J. Leppkes, T. Hohmann and B. Kokschi, *J. Fluorine Chem.*, 2020, **232**, 109453.
- 36 H. Mei, T. Hiramatsu, R. Takeda, H. Moriwaki, H. Abe, J. Han and V. A. Soloshonok, *Org. Process Res. Dev.*, 2019, **23**, 629–634.
- 37 J. Han, R. Takeda, X. Liu, H. Konno, H. Abe, T. Hiramatsu, H. Moriwaki and V. A. Soloshonok, *Molecules*, 2019, **24**, 4521.
- 38 Y. Nian, J. Wang, H. Moriwaki, V. A. Soloshonok and H. Liu, *Dalton Trans.*, 2017, **46**, 4191–4198.
- 39 T. T. Romoff, A. B. Palmer, N. Mansour, C. J. Creighton, T. Miwa, Y. Ejima, H. Moriwaki and V. A. Soloshonok, *Org. Process Res. Dev.*, 2017, **21**, 732–739.
- 40 T. Hohmann, M. Dyrks, S. Chowdhary, M. Weber, D. Nguyen, J. Moschner and B. Kokschi, ChemRxiv, 2022, this content is a preprint and has not been peer-reviewed.
- 41 R. Gambaretto, L. Tonin, C. Di Bello and M. Dettin, *Biopolymers*, 2008, **89**, 906–915.
- 42 G. D'Auria, M. Vacatello, L. Falcigno, L. Paduano, G. Mangiapia, L. Calvanese, R. Gambaretto, M. Dettin and L. Paolillo, *J. Pept. Sci.*, 2009, **15**, 210–219.
- 43 K. Güçlü, G. Kırışlıoğlu, M. Özyürek and R. Apak, *J. Agric. Food Chem.*, 2014, **62**, 1839–1845.
- 44 A. K. Pandey, K. M. Thomas, C. R. Forbes and N. J. Zondlo, *Biochemistry*, 2014, **53**, 5307–5314.
- 45 T. J. Measey, R. Schweitzer-Stenner, V. Sa and K. Kornev, *Macromolecules*, 2010, **43**, 7800–7806.
- 46 Y. Cho, L. B. Sagle, S. Iimura, Y. Zhang, J. Kherb, A. Chilkoti, J. M. Scholtz and P. S. Cremer, *J. Am. Chem. Soc.*, 2009, **131**, 15188–15193.
- 47 T. J. Measey and R. Schweitzer-Stenner, *J. Am. Chem. Soc.*, 2006, **128**, 13324–13325.
- 48 M. Salwiczek, E. K. Nyakatura, U. I. M. Gerling, S. Ye and B. Kokschi, *Chem. Soc. Rev.*, 2012, **41**, 2135–2171.
- 49 J. R. Robalo and A. Vila Verde, *Phys. Chem. Chem. Phys.*, 2019, **21**, 2029–2038.
- 50 Y. Chen, Y. Hua, W. Zhang, C. Tang, Y. Wang, Y. Zhang and F. Qiu, *Int. J. Nanomed.*, 2018, **13**, 2477–2489.
- 51 A. Bertolani, L. Pirrie, L. Stefan, N. Houbenov, J. S. Haataja, L. Catalano, G. Terraneo, G. Giancane, L. Valli, R. Milani, O. Ikkala, G. Resnati and P. Metrangolo, *Nat. Commun.*, 2015, **6**, 7574.
- 52 M. S. de Freitas, R. Rezaei Araghi, E. Brandenburg, J. Leiterer, F. Emmerling, K. Folmert, U. I. M. Gerling-Driessen, B. Bardiaux, C. Böttcher, K. Pagel, A. Diehl, H. v. Berlepsch, H. Oschkinat and B. Kokschi, *J. Struct. Biol.*, 2018, **203**, 263–272.



- 53 J. Schmitt, V. Calabrese, M. A. da Silva, S. Lindhoud, V. Alfredsson, J. L. Scott and K. J. Edler, *Phys. Chem. Chem. Phys.*, 2018, **20**, 16012–16020.
- 54 I. M. Geisler and J. P. Schneider, *Adv. Funct. Mater.*, 2012, **22**, 529–537.
- 55 P. J. Flory and J. Rehner Jr., *J. Chem. Phys.*, 1943, **11**, 521–526.
- 56 M. J. Frisch, G. W. Trucks, H. B. Schlegel, G. E. Scuseria, M. A. Robb, J. R. Cheeseman, G. Scalmani, V. Barone, G. A. Petersson, H. Nakatsuji, X. Li, M. Caricato, A. V. Marenich, J. Bloino, B. G. Janesko, R. Gomperts, B. Mennucci, H. P. Hratchian, J. V. Ortiz, A. F. Izmaylov, J. L. Sonnenberg, D. Williams, F. Ding, F. Lipparini, F. Egidi, J. Goings, B. Peng, A. Petrone, T. Henderson, D. Ranasinghe, V. G. Zakrzewski, J. Gao, N. Rega, G. Zheng, W. Liang, M. Hada, M. Ehara, K. Toyota, R. Fukuda, J. Hasegawa, M. Ishida, T. Nakajima, Y. Honda, O. Kitao, H. Nakai, T. Vreven, K. Throssell, J. A. Montgomery Jr., J. E. Peralta, F. Ogliaro, M. J. Bearpark, J. J. Heyd, E. N. Brothers, K. N. Kudin, V. N. Staroverov, T. A. Keith, R. Kobayashi, J. Normand, K. Raghavachari, A. P. Rendell, J. C. Burant, S. S. Iyengar, J. Tomasi, M. Cossi, J. M. Millam, M. Klene, C. Adamo, R. Cammi, J. W. Ochterski, R. L. Martin, K. Morokuma, O. Farkas, J. B. Foresman and D. J. Fox, *Gaussian 16 Rev. C.01*, 2016.
- 57 M. D. Hanwell, D. E. Curtis, D. C. Lonie, T. Vandermeersch, E. Zurek and G. R. Hutchison, *J. Cheminf.*, 2012, **4**, 17.
- 58 J. Huang, S. Rauscher, G. Nawrocki, T. Ran, M. Feig, B. L. de Groot, H. Grubmüller and A. D. MacKerell, *Nat. Methods*, 2017, **14**, 71–73.
- 59 K. Vanommeslaeghe, E. Hatcher, C. Acharya, S. Kundu, S. Zhong, J. Shim, E. Darian, O. Guvench, P. Lopes, I. Vorobyov and A. D. Mackerell, Jr., *J. Comput. Chem.*, 2010, **31**, 671–690.
- 60 K. Vanommeslaeghe and A. D. MacKerell, *J. Chem. Inf. Model.*, 2012, **52**, 3144–3154.
- 61 K. Vanommeslaeghe, E. P. Raman and A. D. MacKerell, *J. Chem. Inf. Model.*, 2012, **52**, 3155–3168.
- 62 A. Kumar, O. Yoluk and A. D. MacKerell, Jr., *J. Comput. Chem.*, 2020, **41**, 958–970.
- 63 W. L. Jorgensen, J. Chandrasekhar, J. D. Madura, R. W. Impey and M. L. Klein, *J. Chem. Phys.*, 1983, **79**, 926–935.
- 64 A. D. MacKerell Jr., D. Bashford, M. Bellott, R. L. Dunbrack Jr., J. D. Evanseck, M. J. Field, S. Fischer, J. Gao, H. Guo and S. Ha, *J. Phys. Chem. B*, 1998, **102**, 3586–3616.
- 65 R. M. Venable, Y. Luo, K. Gawrisch, B. Roux and R. W. Pastor, *J. Phys. Chem. B*, 2013, **117**, 10183–10192.
- 66 M. J. Abraham, T. Murtola, R. Schulz, S. Páll, J. C. Smith, B. Hess and E. Lindahl, *SoftwareX*, 2015, **1**, 19–25.
- 67 G. Bussi, D. Donadio and M. Parrinello, *J. Chem. Phys.*, 2007, **126**, 014101.
- 68 M. Parrinello and A. Rahman, *J. Appl. Phys.*, 1981, **52**, 7182–7190.
- 69 B. Hess, *J. Chem. Theory Comput.*, 2008, **4**, 116–122.
- 70 T. Darden, D. York and L. Pedersen, *J. Chem. Phys.*, 1993, **98**, 10089–10092.
- 71 G. M. Torrie and J. P. Valleau, *J. Comput. Phys.*, 1977, **23**, 187–199.
- 72 S. Kumar, J. M. Rosenberg, D. Bouzida, R. H. Swendsen and P. A. Kollman, *J. Comput. Chem.*, 1992, **13**, 1011–1021.
- 73 J. S. Hub, B. L. De Groot and D. Van Der Spoel, *J. Chem. Theory Comput.*, 2010, **6**, 3713–3720.
- 74 D. Orthaber, A. Bergmann and O. Glatter, *J. Appl. Crystallogr.*, 2000, **33**, 218–225.
- 75 I. Bressler, J. Kohlbrecher and A. F. Thünemann, *J. Appl. Crystallogr.*, 2015, **48**, 1587–1598.



Rational Design of Amphiphilic Fluorinated Peptides: Evaluation of Self-Assembly Properties and Hydrogel Formation

Suvrat Chowdhary¹, Robert F. Schmidt², Dr. Anil Kumar Sahoo^{3,4}, Tiemo tom Dieck¹, Thomas Hohmann¹, Dr. Boris Schade⁵, Kerstin Brademann-Jock⁶, Dr. Andreas Thünemann⁶, Prof. Dr. Roland R. Netz³, Prof. Dr. Michael Gradzielski² and Prof. Dr. Beate Kokschi^{1*}

1 Institute of Chemistry and Biochemistry, Freie Universität Berlin, Arnimallee 20, 14195 Berlin, Germany

2 Institute of Chemistry, Technische Universität Berlin, Straße des 17. Juni 124, 10623 Berlin, Germany

3 Department of Physics, Freie Universität Berlin, Arnimallee 14, 14195 Berlin, Germany

4 Max Planck Institute of Colloids and Interfaces, Department of Biomaterials, Am Mühlenberg 1, 14476 Potsdam, Germany

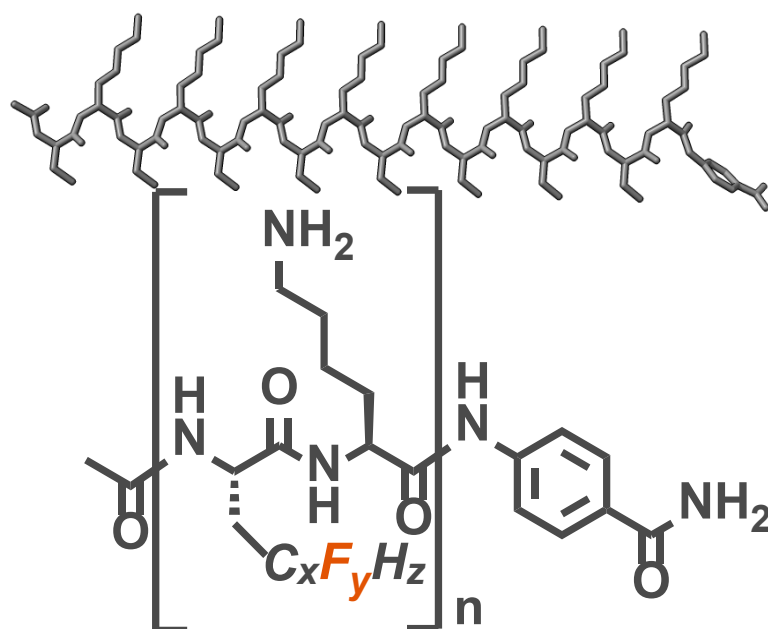
5 Institute of Chemistry and Biochemistry and Core Facility *BioSupraMol*, Freie Universität Berlin, Fabeckstraße 36a, 14195 Berlin, Germany

6 Federal Institute for Materials Research and Testing (BAM), Unter den Eichen 87, 12205 Berlin, Germany

* **Corresponding author:**

Prof. Dr. Beate Kokschi; beate.kokschi@fu-berlin.de; Phone: +49 30 838 55344

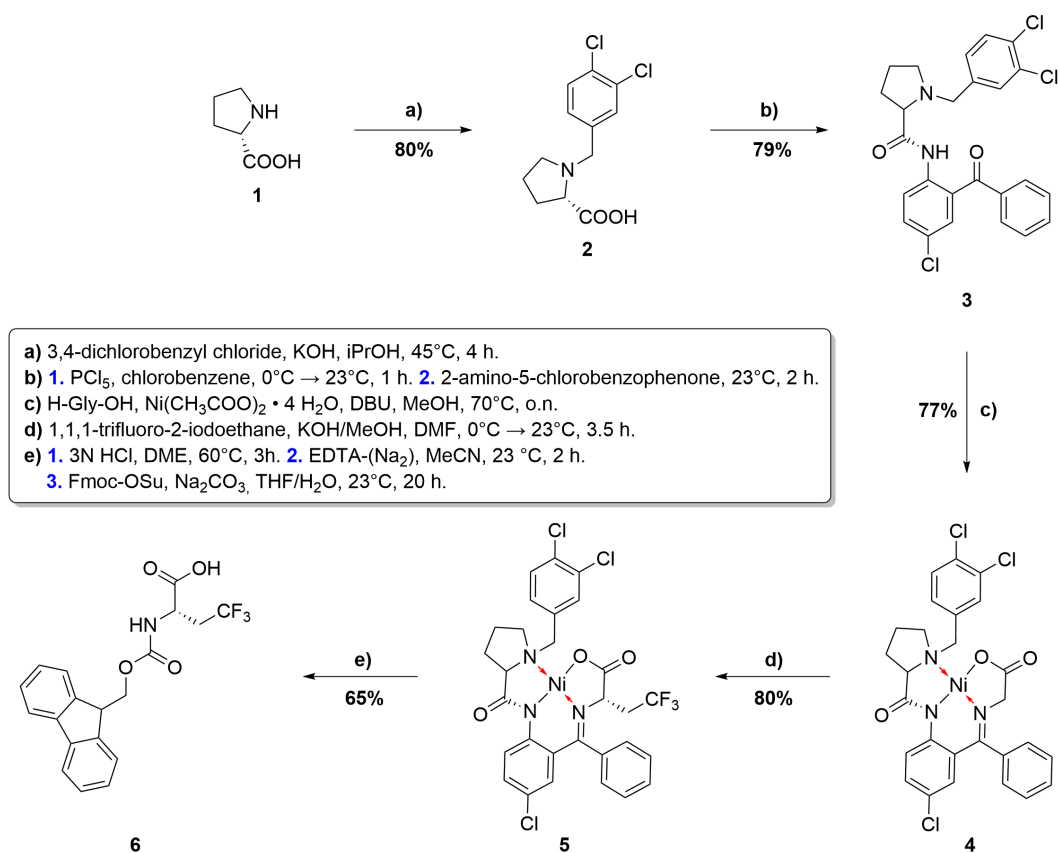
Supporting Information



Content

1. Gram scale synthesis and characterization of fluorinated amino acid Fmoc-TfeGly-OH (6).....	2
1.1 Synthesis of (3,4-dichlorobenzyl)-L-proline (2).....	3
1.2 Synthesis of <i>N</i> -(2-benzoyl-4-chlorophenyl)-1-(3,4-dichlorobenzyl)pyrrolidine-2-carboxamide (3).....	6
1.3 Synthesis of Nickel(II)-[N-[[[5-Chloro-2-[[[(S)-1-[(3,4-dichlorophenyl)methyl]-2-pyrrolidinyl- κ N]carbonyl]amino κ N]phenyl]phenylmethylene]-glycinato(2-)- κ N, κ O] --Glycine-Ni(II) Ligand Complex (4)	9
1.4 Synthesis of the CF ₃ -CH ₂ -alkylated Glycine-Ni(II) Ligand Complex 5.....	12
1.5 Synthesis of Fmoc-TfeGly-OH (6).....	15
2. Fluorinated Fmoc-protected amino acids Fmoc-MfeGly-OH (7) and Fmoc-DfeGly-OH (9)	18
2.1. Characterization of Fmoc-MfeGly-OH (7).....	18
2.2. Characterization of Fmoc-DfeGly-OH (8).....	21
3. Peptide Synthesis: Selected HPLC chromatograms of crude peptides after SPPS	24
4. Peptide Synthesis: Characterization of purified sequences	30
4.1 Peptide sequence: AbuK10	31
4.2 Peptide sequence: AbuK11	33
4.3 Peptide sequence: AbuK12	35
4.4 Peptide sequence: AbuK13	37
4.5 Peptide sequence: AbuK14	39
4.6 Peptide sequence: AbuK15	41
4.7 Peptide sequence: AbuK16	43
4.8 Peptide sequence: MfeGlyK16.....	45
4.9 Peptide sequence: DfeGlyK16.....	47
4.10 Peptide sequence: TfeGlyK16	49
4.11 Peptide sequence: LeuK16.....	51
5. Determination of peptide stock concentrations	53
6. CD spectroscopy: Further results	54
6.1 CD Spectroscopy: AbuK10-16 – water / BTP buffer pH 9 – concentration: 2 wt%	54
6.2 CD Spectroscopy: Salt effects and valency on secondary structure formation (AbuK16, MfeGlyK16, DfeGlyK16, TfeGlyK16).....	55
6.3 CD Spectroscopy: Impact of non-aqueous solvents on secondary structure formation (AbuK16, MfeGlyK16, DfeGlyK16, TfeGlyK16).....	56
7. Characterization of reference sequence LeuK16.....	57
8. Detection of amyloid-like fibrils: Congo red (CR) UV-spectroscopy	58
9. Further cryoEM micrographs (AbuK14, AbuK16, MfeGlyK16, DfeGlyK16, TfeGlyK16)	59
10. Inversion tests of peptide-based hydrogels	62
11. Rheological characterization of aliphatic oligopeptides – Further data.....	63
12. MD simulations of (polyfluorinated) amphipathic peptides.....	65
12.1 Optimized partial charges on Abu	65
12.2 Optimized partial charges on MfeGly	66
12.3 Optimized partial charges on DfeGly.....	67
12.4 Optimized partial charges on TfeGly.....	68
12.5 MD simulations – further data	69
13. Small-angle X-ray scattering (SAXS).....	72
14. References.....	79

1. Gram scale synthesis and characterization of fluorinated amino acid Fmoc-TfeGly-OH (**6**)



Scheme S1: Synthesis of Fmoc-TfeGly-OH (**6**) in gram scale according to Soloshonok *et al.*¹⁻⁹

A five-step synthesis for Fmoc-TfeGly-OH (**6**) was developed and described in literature by Soloshonok *et al.*¹⁻⁹ In the first step of this synthetic route, H-Pro-OH **1** is alkylated with 3,4-dichlorobenzyl chloride. To selectively alkylate the amine and not the C-terminal carboxyl group, the reaction is carried out in a basic KOH / iPrOH solution. The intermediate **2** reacts afterwards with PCl_5 to form the corresponding acid chloride, enabling the formation of an amide bond with the amine side chain of 2-amino-5-chlorobenzophenone and the synthesis of compound **3**. The formation of the Schiff base as a chelating ligand in compound **4** occurs through the reaction of **3** with H-Gly-OH, nickel acetate tetrahydrate and DBU. The following asymmetric alkylation of the chiral Ni-ligand **4** with $\text{CF}_3\text{CH}_2\text{I}$ and subsequent disassembly of compound **5** and simultaneous Fmoc-protection leads finally to the *N*-Fmoc derivative of (2*S*)-4,4,4-trifluoroethylglycine (TfeGly).

1.1 Synthesis of (3,4-dichlorobenzyl)-L-proline (2)

L-Pro-H (**1**) (69.0 g, 0.6 mol, 1 equiv.) and KOH (70.6 g, 1.26 mol, 2.1 equiv) were dissolved in iPrOH (600 mL) at 45 °C. Afterwards 3,4-dichlorobenzyl chloride (91.1 mL, 0.66 mol, 1.1 equiv.) were added and the reaction mixture was stirred for 4 h at 45 °C. For quenching, the pH was adjusted to 5-6 with HCl_{conc.} and MeOH (1000 mL) was added. The reaction mixture was then stirred for 16 h at 45°C and precipitated KCl salts were filtered and washed with a iPrOH/MeOH mixture (3:2). The filtrated solution was concentrated under reduced pressure and the crude product was washed with MeCN (500 mL) for 10 min under gentle stirring. Finally, the product was filtered, washed with MeCN and dried *in vacuo*.

The title compound **2** was obtained as a white solid substance (133.32 g, 0.48 mol, 80%).

¹H NMR (600 MHz, METHANOL-D₄): δ = **7.67** (d, J = 2.2 Hz, 1H), **7.49** (d, J = 8.3 Hz, 1H), **7.38** (dd, J = 8.3, 2.2 Hz, 1H), **4.35** (d, J = 13.0 Hz, 1H), **4.18** (d, J = 12.9 Hz, 1H), **3.79** (dd, J = 9.6, 6.7 Hz, 1H), **3.49 – 3.44** (m, 1H), **3.16 – 3.07** (m, 1H), **2.42 – 2.32** (m, 1H), **2.05 – 1.96** (m, 2H), 1.92 – 1.79 (m, 1H).

¹³C ¹⁰ NMR (151 MHz, METHANOL-D₄): δ = 171.88, 170.55, 168.50, 142.06, 128.74, 127.98, 118.88, 40.90, 22.62.

IR (ATR): ν = 3059.34, 2974.98, 2858.70, 1603.14, 1526.06, 1477.04, 1386.78, 1374.44, 1308.48, 1145.31, 1022.05, 835.23, 813.93, 663.51, 651.15, 496.65, 489.81, 400.90 cm⁻¹.

Elemental analysis [CHN] (%) = Anal. Calcd for C₁₂H₁₃Cl₂NO₂ (m: 1.9720 mg): C, 52.58; H, 4.78; N, 5.11. Found: C, 50.51; H, 4.72; N, 5.35.

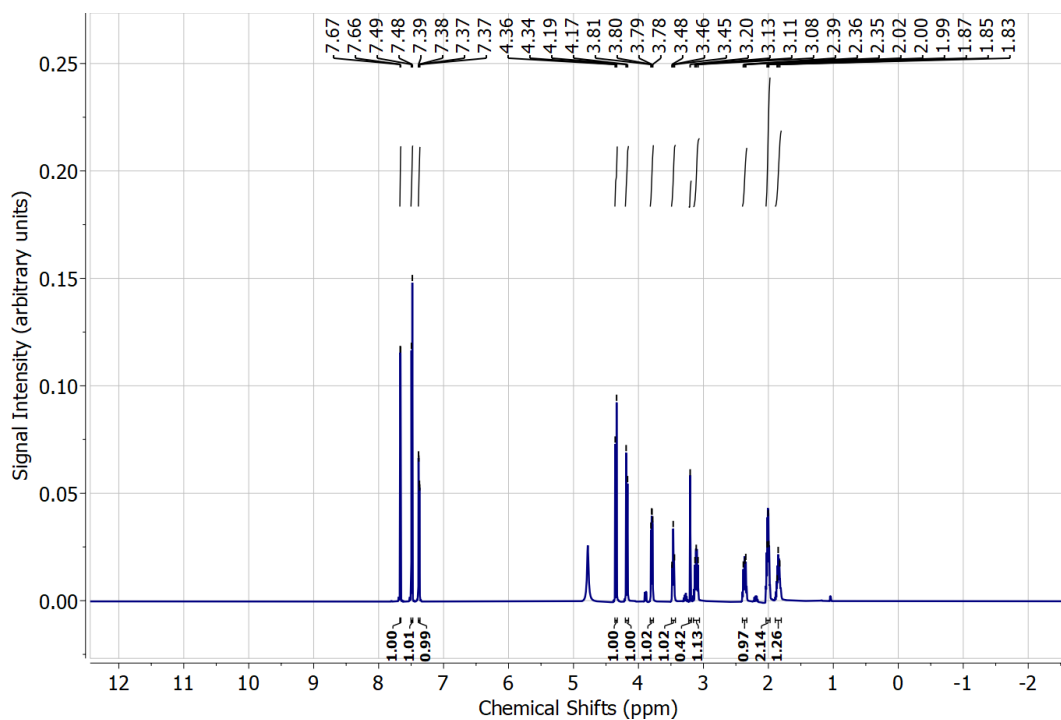


Figure S1: ^1H NMR (600 MHz) spectrum of (3,4-dichlorobenzyl)-L-proline (**2**) dissolved in MeOH-d_4 .

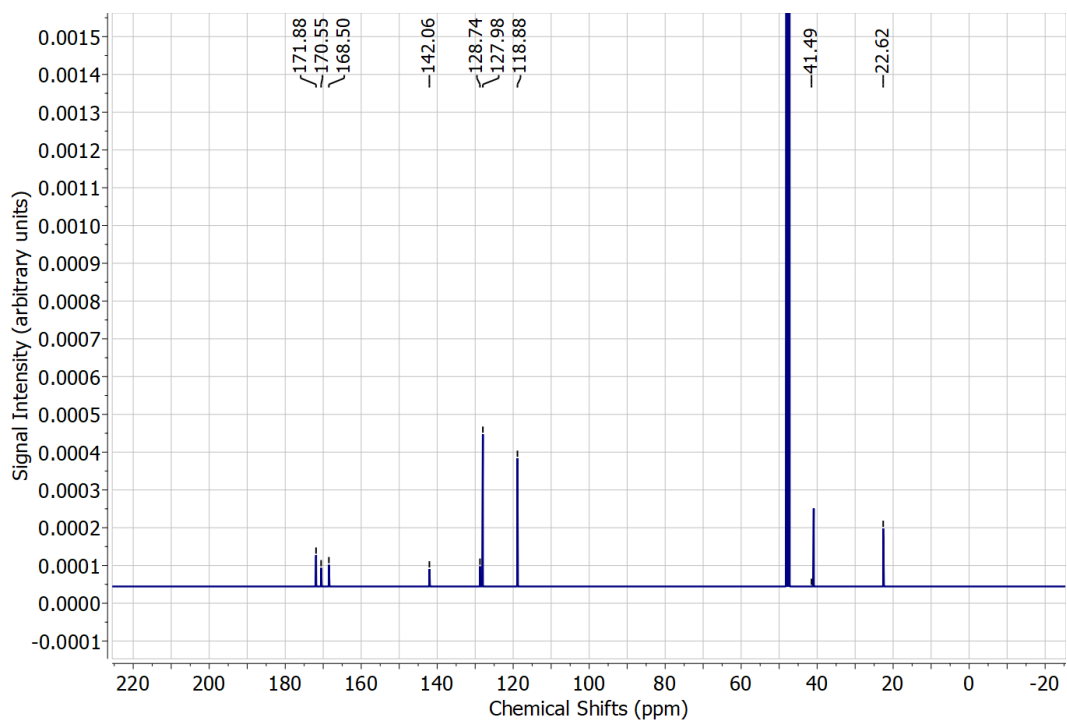


Figure S2: ^{13}C $\{^1\text{H}\}$ NMR (151 MHz) spectrum of (3,4-dichlorobenzyl)-L-proline (**2**) dissolved in MeOH-d_4 .

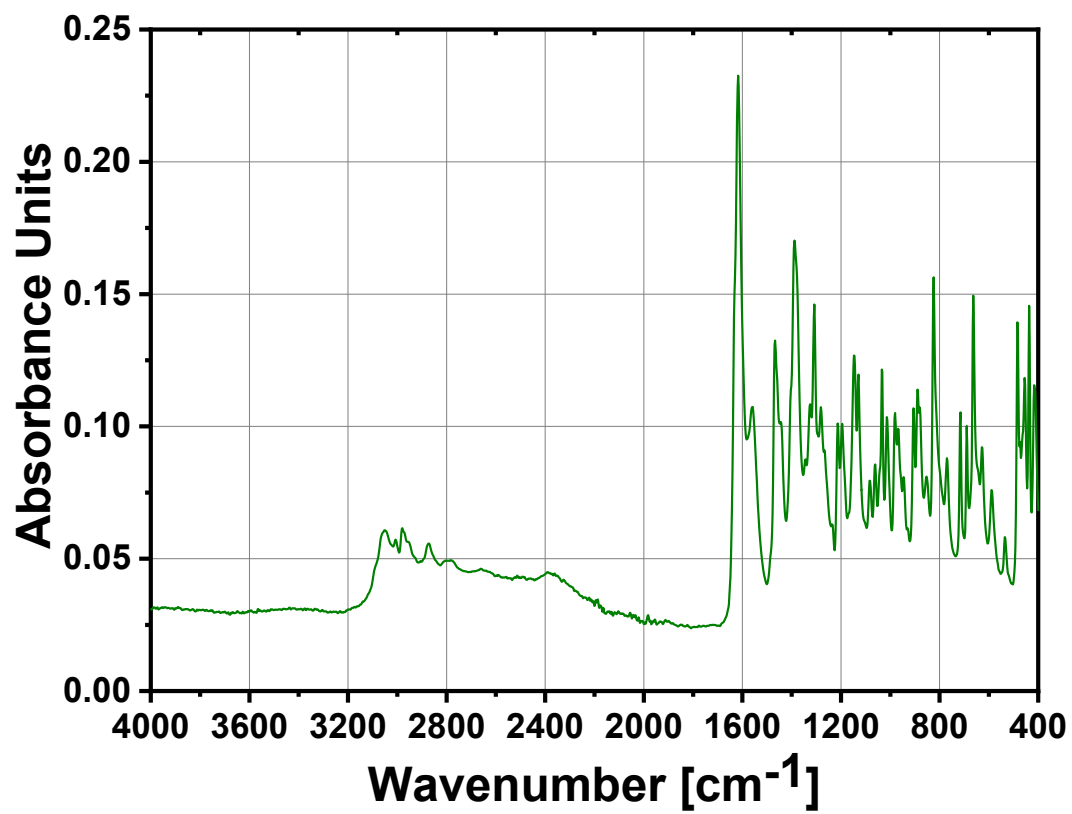


Figure S3: IR-ATR spectrum of (3,4-dichlorobenzyl)-L-proline (2).

1.2 Synthesis of *N*-(2-benzoyl-4-chlorophenyl)-1-(3,4-dichlorobenzyl)pyrrolidine-2-carboxamide (3)

Compound **2** (91.0 g, 0.33 mol, 1 equiv.) was dissolved in chlorobenzene (650 mL) and cooled to 0 °C under nitrogen protection before phosphorus pentachloride PCl_5 (68.71 g, 0.33 mol, 1 equiv.) was added slowly to the solution. The reacting mixture was stirred for 30 min at 0 °C and afterwards warmed to 23 °C while further stirring for 2 h to form the corresponding acid chloride. Then 2-amino-5-chlorobenzophenone (76.45 g, 0.33 mol, 1 equiv.) was slowly added and the reaction mixture was kept stirring at 23 °C for 2 h. This reaction was quenched by the addition of MeOH (60 mL) and further stirring for 1 h, leading to the precipitation of crude product. The precipitation was filtered and washed with chlorobenzene (120 mL) and acetone (2 * 300 mL), whereas the filtrated solution was concentrated under reduced pressure leading to further precipitation of crude product. This precipitation was filtered and washed with acetone (2 * 250 mL). Both batches of product were combined and dried *in vacuo* at 45 °C. The crude solid was afterwards washed with MeOH (300mL) for 1 min under gentle stirring, filtered and dried *in vacuo* at 45 °C.

The title compound **3** was obtained as fine white / slightly yellowish needles (128.41 g, 0.26 mol, 79%).

^1H NMR (600 MHz, METHANOL- D_4): δ = 7.73 – 7.23 (m, 11H), 4.32 – 4.18 (m, 3H), 3.54 – 3.42 (m, 1H), 2.39 – 2.22 (m, 1H), 2.13 – 2.02 (m, 1H), 1.86 – 1.72 (m, 1H), 1.52 – 1.43 (m, 1H).

^{13}C {1H} NMR (151 MHz, METHANOL- D_4): δ = 194.37, 136.57, 134.14, 133.59, 133.31, 133.03, 132.81, 132.69, 131.55, 131.10, 130.99, 130.55, 129.90, 129.66, 128.35, 125.76, 66.91, 56.50, 54.70, 28.05, 22.48.

IR (ATR): ν = 3172.20, 2951.04, 2864.40, 2732.17, 1705.04, 1660.84, 1610.42, 1535.14, 1495.99, 1463.02, 1446.54, 1386.78, 1275.51, 1254.90, 1238.42, 1209.57, 1032.36, 960.24, 880.83, 818.06, 696.15, 690.30, 665.57, 632.60 cm^{-1} .

Elemental analysis [CHN] (%) = Anal. Calcd for $\text{C}_{25}\text{H}_{21}\text{Cl}_3\text{N}_2\text{O}_2$ (m: 1.8260 mg): C, 61.56; H, 4.34; N, 5.74. Found: C, 58.31; H, 5.31; N, 4.58.

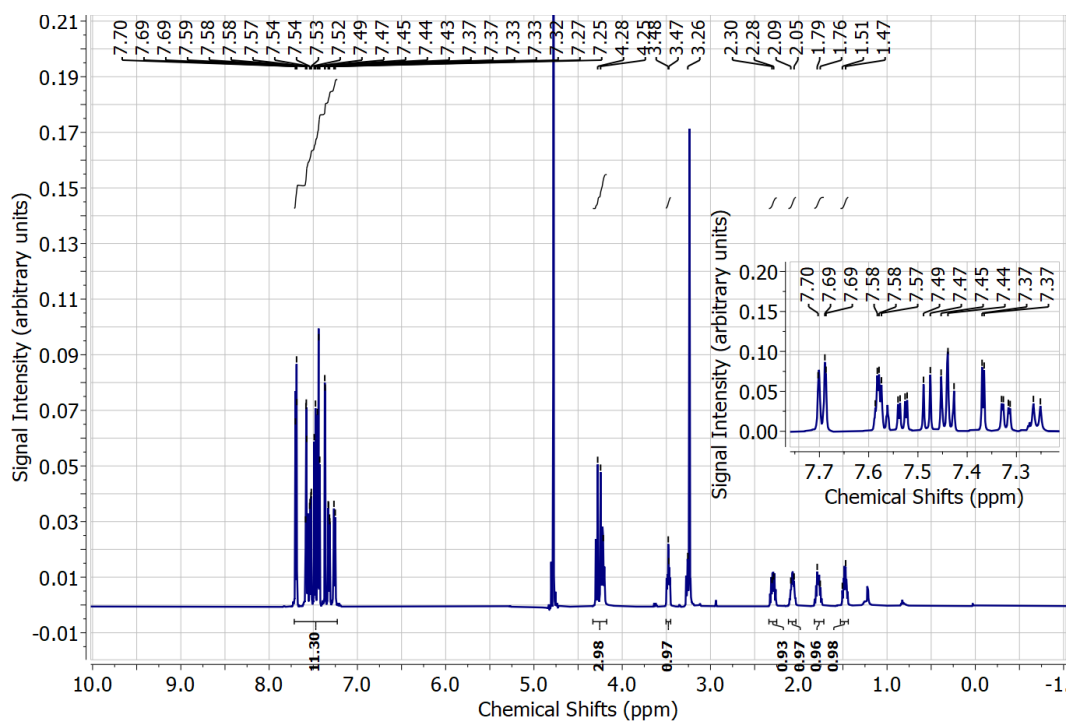


Figure S4: ^1H NMR (600 MHz) spectrum of *N*-(2-benzoyl-4-chlorophenyl)-1-(3,4-dichlorobenzyl)pyrrolidine-2-carboxamide (**3**) dissolved in MeOH-d_4 .

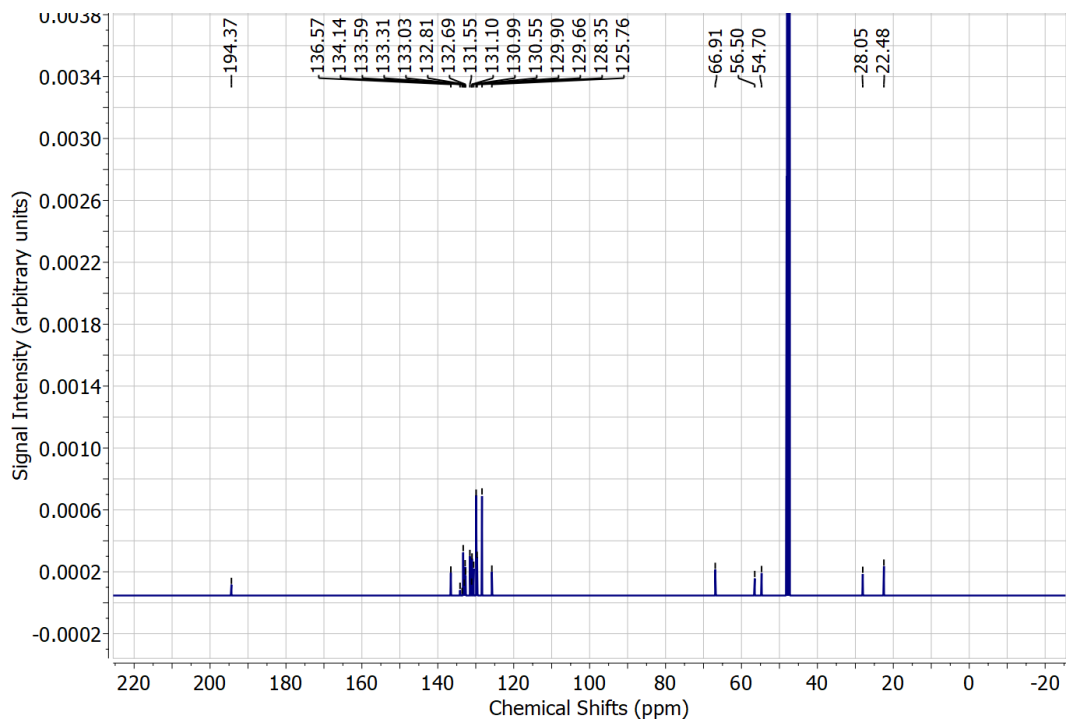


Figure S5: ^{13}C { ^1H } NMR (151 MHz) spectrum of *N*-(2-benzoyl-4-chlorophenyl)-1-(3,4-dichlorobenzyl)pyrrolidine-2-carboxamide (**3**) dissolved in MeOH-d_4 .

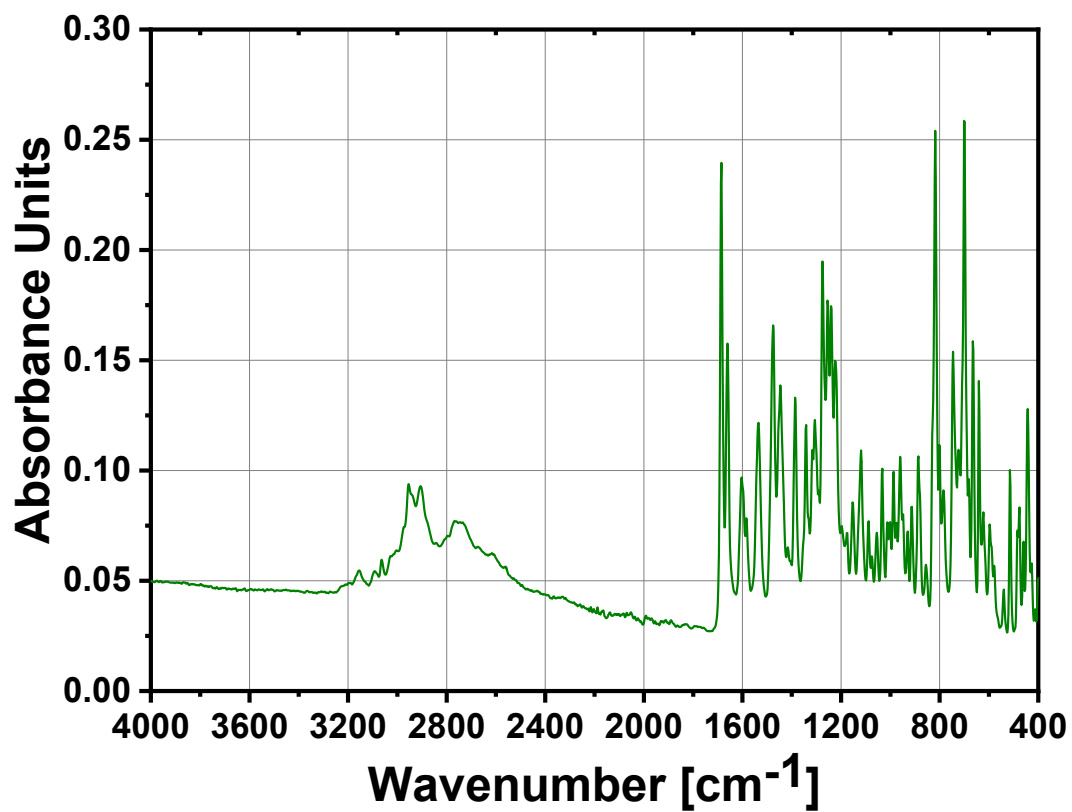


Figure S6: IR-ATR spectrum of *N*-(2-benzoyl-4-chlorophenyl)-1-(3,4-dichlorobenzyl)pyrrolidine-2-carboxamide (**3**).

1.3 Synthesis of Nickel(II)-[N-[[5-Chloro-2-[[[(S)-1-[(3,4-dichlorophenyl)methyl]-2-pyrrolidinyl-κN]carbonyl]aminokN]phenyl]phenylmethylene]-glycinato(2-)-κN, κO] -- Glycine–Ni(II) Ligand Complex (4)

At first, MeOH (1200 mL) was added to a mixture of compound **3** (128.41 g, 0.26 mol, 1 equiv.), nickel acetate tetrahydrate (129.09 g, 0.52 mol, 2 equiv.) and H-Gly-OH (40.0 g, 0.52 mol, 2 equiv.). This green suspension was stirred at 23 °C before 1,8-diazabicyclo[5.4.0]undec-7-ene DBU (175.58 mL, 1.3 mol, 5 equiv.) was slowly added. The reaction mixture was warmed to 75 °C and stirred for 24 h. Afterwards, the reaction was quenched by addition of a 6%-AcOH solution (1300 mL) and further stirring for 3 h. The crude product was filtered, washed with water (850 mL) and a water/methanol-mixture (1:1) (850 mL) and then dried *in vacuo* at 55 °C.

The title compound **4** was obtained as a red solid substance (133.45 g, 0.20 mol, 77%).

¹H NMR (600 MHz, METHANOL-D₄): δ = **8.79** (d, J = 2.1 Hz, 1H), **8.31** (dd, J = 8.2, 2.2 Hz, 1H), **7.99** (dd, J = 9.2, 1.3 Hz, 1H), **7.68 – 7.60** (m, 1H), **7.59 – 7.52** (m, 3H), **7.27** (d, J = 6.5 Hz, 1H), **7.14** (dd, J = 9.3, 2.6 Hz, 1H), **7.03** (d, J = 7.2 Hz, 1H), **6.68** (d, J = 2.6 Hz, 1H), **4.23** (d, J = 12.6 Hz, 1H), **3.56 – 3.52** (m, 1H), **3.49** (s, 1H), **3.48 – 3.36** (m, 2H), **3.34 – 3.29** (m, 1H) **2.64 – 2.53** (m, 1H), **2.51 – 2.43** (m, 1H), **2.24 – 2.12** (m, 2H).

¹³C {¹H} NMR (151 MHz, METHANOL-D₄): δ = 181.83, 179.03, 171.31, 140.45, 136.41, 133.74, 133.58, 132.90, 132.58, 131.52, 131.37, 131.12, 131.01, 129.92, 129.75, 129.34, 126.86, 126.51, 125.87, 125.60, 125.09, 70.99, 62.60, 58.29, 30.55, 23.14.

IR (ATR): ν = 3582.60, 3556.38, 3482.28, 2986.38, 2889.48, 1673.12, 1667.02, 1658.78, 1619.54, 1482.74, 1469.06, 1322.90, 1254.90, 1074.63, 1017.93, 835.23, 832.95, 717.09, 589.33, 549.09, 449.21, 429.39 cm⁻¹.

Elemental analysis [CHN] (%) = Anal. Calcd for C₂₇H₂₂Cl₃N₃NiO₃ (m: 2.2480 mg): C, 53.91; H, 3.69; N, 6.99. Found: C, 52.90; H, 4.27; N, 7.06.

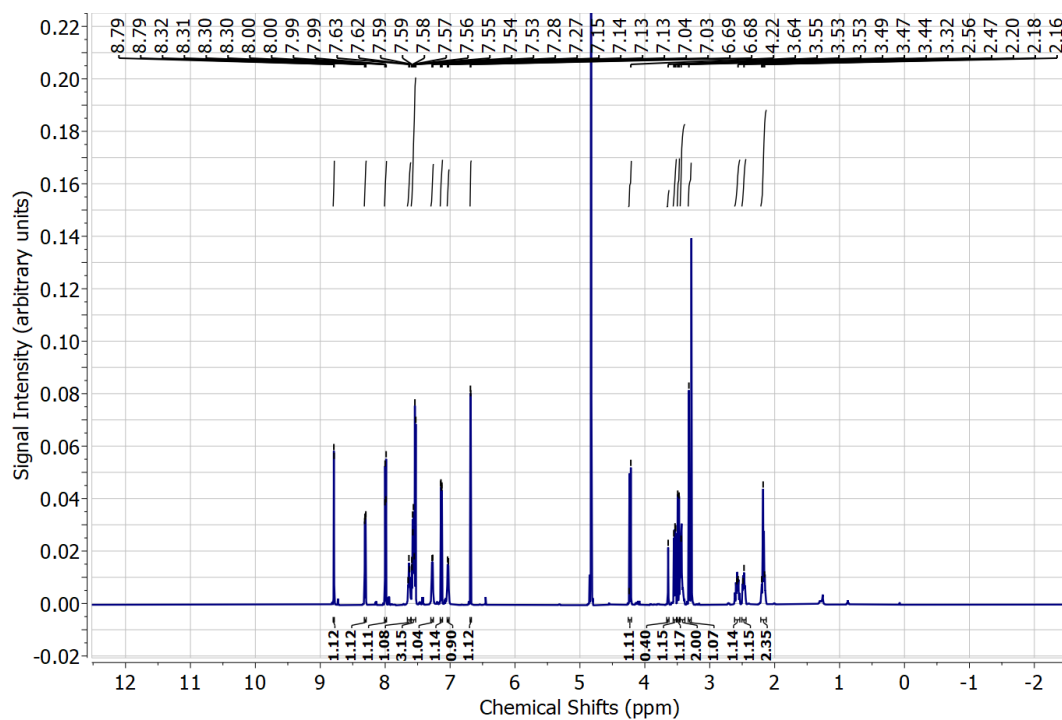


Figure S7: ^1H NMR (600 MHz) spectrum of the glycine-Ni(II) ligand complex **4** dissolved in MeOH- d_4 .

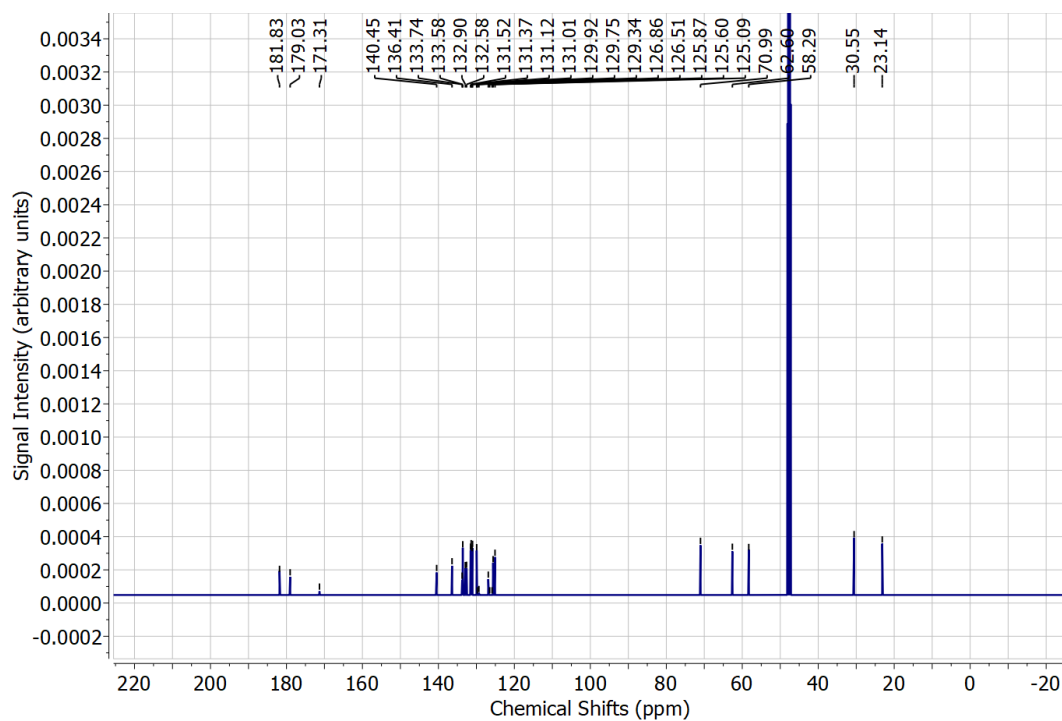


Figure S8: ^{13}C $\{^1\text{H}\}$ NMR (151 MHz) spectrum of the glycine-Ni(II) ligand complex **4** dissolved in MeOH- d_4 .

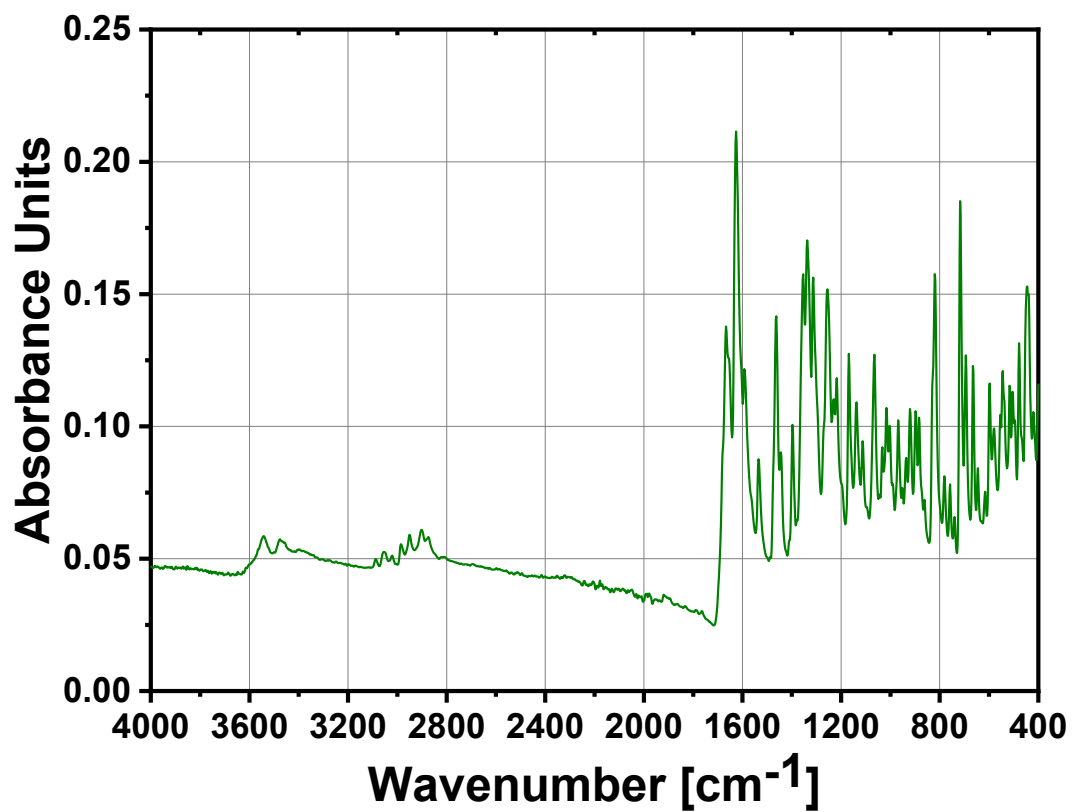


Figure S9: IR-ATR spectrum the glycine-Ni(II) ligand complex 4.

1.4 Synthesis of the CF₃-CH₂-alkylated Glycine–Ni(II) Ligand Complex 5

The glycine–Ni(II) ligand complex **4** (30.0 g, 0.049 mol, 1 equiv.) and 1,1,1-trifluoro-2-iodoethane (5.20 mL, 0.053 mol, 1.05 equiv.) were dissolved in freshly deoxygenated N,N-dimethylformamide (DMF) (300 mL) and cooled to 0 °C. Afterwards, a solution of KOH (3.0 g, 0.053 mmol, 1.05 equiv.) in freshly deoxygenated MeOH (28 mL) was slowly added under N₂ atmosphere. The reaction mixture was stirred for 3.5 h while warming up to 23 °C. For subsequent quenching, water (110 mL) was added, and the solution was further stirred for 1 h. Afterwards, water (40 mL) was added, and the solution was further stirred for 1 h. The precipitated crude product was filtered, washed with a DMF-water mixture (60 mL) and water (80 mL) and finally dried *in vacuo* at 55 °C.

The title compound **5** was obtained as a red solid substance (26.7 g, 0.039 mol, 80%).

¹H NMR (600 MHz, METHANOL-D₄): δ = 8.81 (s, 1H), 8.28 (d, J = 8.2 Hz, 1H), 8.00 (d, J = 9.4 Hz, 1H), 7.72 – 7.61 (m, 2H), 7.59 – 7.55 (m, 1H), 7.52 – 7.50 (m, 1H), 7.49 – 7.45 (m, 1H), 7.12 (d, J = 6.7 Hz, 1H), 7.00 (d, J = 7.8 Hz, 1H), 6.53 (s, 1H), 4.29 – 4.24 (m, 1H), 4.19 (d, J = 12.6 Hz, 2H), 3.61 – 3.54 (m, 1H), 3.41 – 3.36 (m, 3H), 2.68 – 2.51 (m, 2H), 2.33 – 2.25 (m, 1H), 2.23 – 2.14 (m, 2H).

¹³C {¹H} NMR (151 MHz, METHANOL-D₄): δ = 136.59, 133.15, 132.02, 131.15, 131.12, 131.01, 130.83, 130.61, 129.90, 129.83, 129.60, 129.32, 128.70, 128.41, 127.54, 126.85, 125.54, 124.18, 71.34, 67.92, 62.71, 58.38, 58.12, 54.14, 30.59, 30.51, 23.72, 22.56.

¹⁹F NMR (565 MHz, METHANOL-D₄): δ = -61.57 – -61.62 (m, 3F).

IR (ATR): ν = 3273.86, 2963.70, 2888.52, 1852.89, 1762.14, 1634.05, 1624.29, 1465.77, 1458.90, 1331.37, 1259.02, 1240.48, 1154.47, 1143.63, 1112.72, 1100.48, 831.67, 708.84, 553.68 cm⁻¹.

Elemental analysis [CHN] (%) = Anal. Calcd for C₂₉H₂₃Cl₃F₃N₃NiO₃ (m: 1.9100 mg): C, 50.96; H, 3.30; N, 6.15. Found: C, 51.83; H, 3.812; N, 6.402.

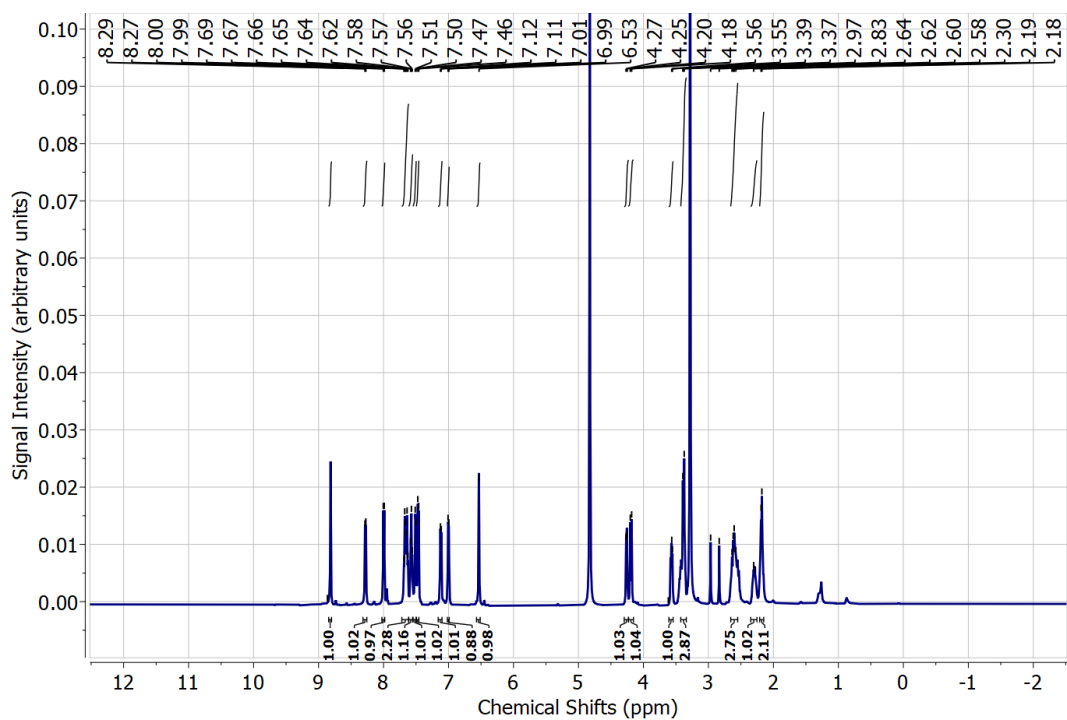


Figure S10: ^1H NMR (600 MHz) spectrum of the $\text{CF}_3\text{-CH}_2$ -alkylated Glycine-Ni(II) ligand complex **5** dissolved in MeOH-d_4 .

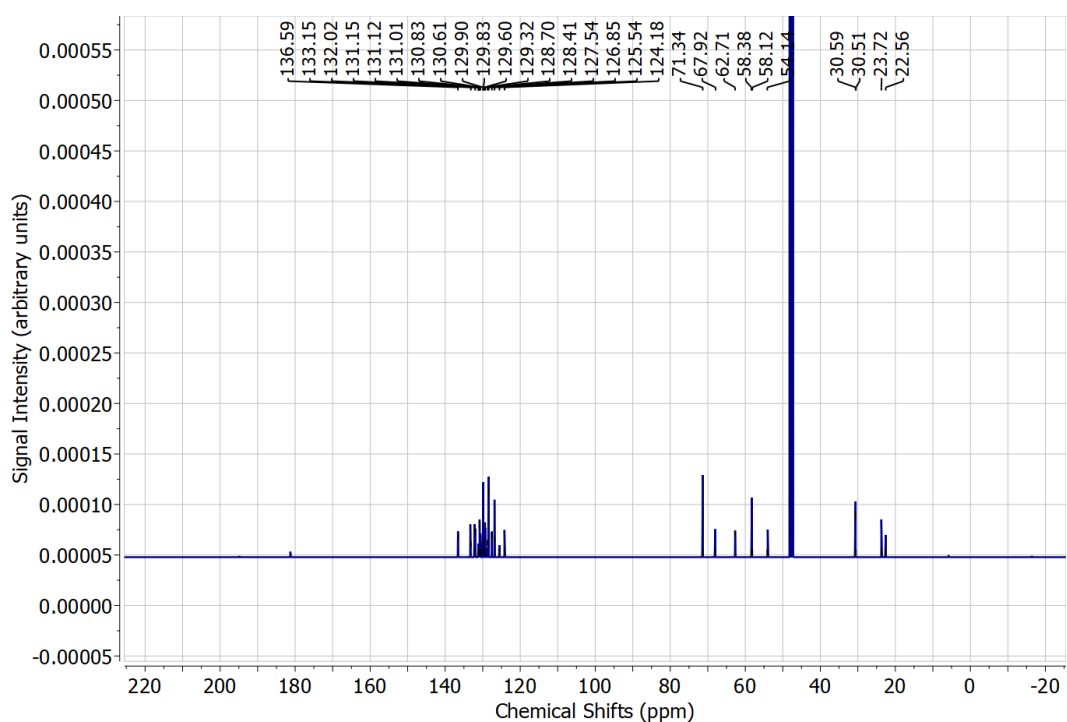


Figure S11: ^{13}C $\{^1\text{H}\}$ NMR (151 MHz) spectrum of the $\text{CF}_3\text{-CH}_2$ -alkylated Glycine-Ni(II) ligand complex **5** dissolved in MeOH-d_4 .

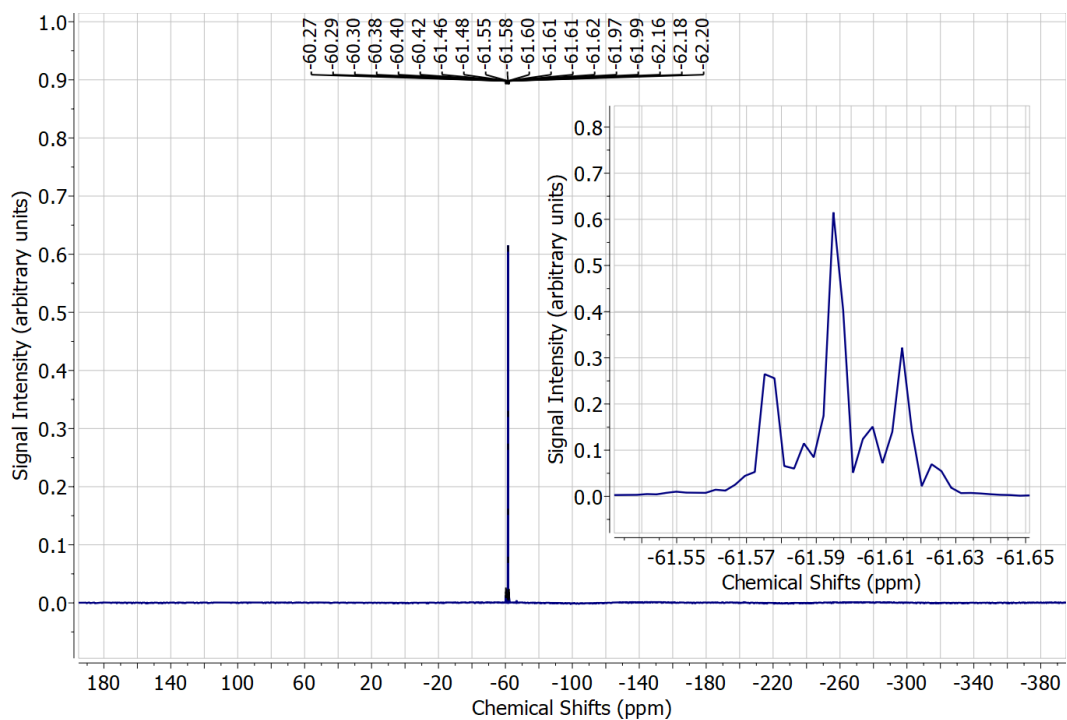


Figure S12: ^{19}F NMR (565 MHz) spectrum of the $\text{CF}_3\text{-CH}_2$ -alkylated Glycine-Ni(II) ligand complex **5** dissolved in MeOH-d_4 .

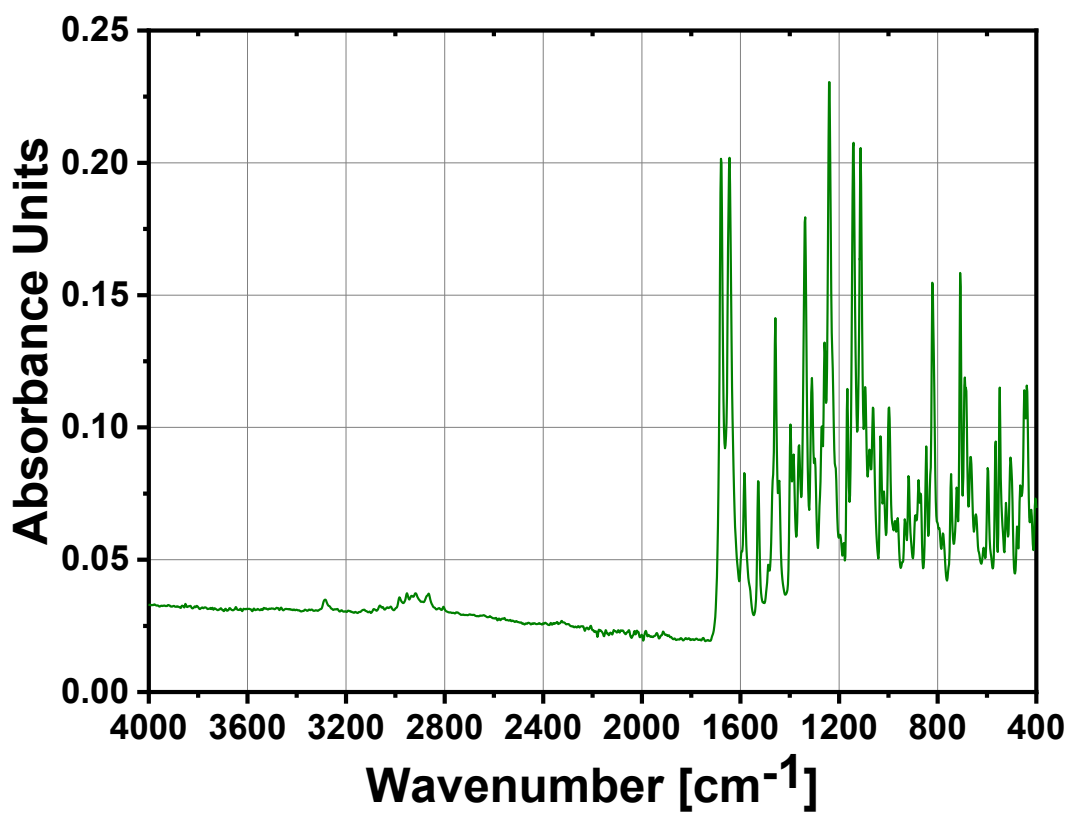


Figure S13: IR-ATR spectrum of the $\text{CF}_3\text{-CH}_2$ -alkylated Glycine-Ni(II) ligand complex **5**.

1.5 Synthesis of Fmoc-TfeGly-OH (6)

Compound **5** (26.7 g, 0.039 mol, 1 equiv.) was dissolved in dimethoxyethane (140 mL) and 3N HCl (85 mL) and heated to 60 °C while stirring for 3h. Then the mixture was filtered and washed with water (50 mL). The combined solutions were concentrated, leading to further precipitation of Ni-ligand residues. These precipitates were filtered and washed with water (25 mL) and the solutions were combined. EDTA-(Na₂) (14.51 g, 0.039 mol, 1 equiv.) in MeCN (85 mL) was added and the mixture was stirred for 2 h at 23 °C. The reaction was quenched by adjusting the pH to 8-8.5 by use of a 48%-NaOH solution. Afterwards, Na₂CO₃ (8.3 g, 0.078 mol, 2 equiv.) was supplemented and Fmoc-OSu (13.15 g, 0.039 mol, 1 equiv.) in THF (70 mL) was added slowly while the reacting mixture was stirred at 23 °C for 20 h. Then, MeCN and THF were removed from the solution under reduced pressure. The aqueous solution was washed with Et₂O (3 * 100 mL) to remove leftovers of Fmoc-OSu. Then, the pH of the solution was adjusted to 2 by using HCl_{conc.} before the aqueous phase was extracted with ethyl acetate (6 * 80 mL). The combined organic phases were dried over Na₂SO₄, filtered, concentrated, and dried *in vacuo* at 55 °C. The crude product (11.86 g) was dissolved in ethyl acetate (60 mL) and toluene (300 mL) and warmed to 75 °C for complete dissolution. Then, the solution was concentrated under reduced pressure and after further addition of toluene (100 mL) concentrated again to a total volume of approximately 200 mL. This solution was left to stand overnight at room temperature, leading to precipitation of pure Fmoc-TfeGly-OH (**6**). The amino acid was filtered, washed with ice-cold toluene (100 mL) and hexane (100 mL) and then dried *in vacuo* at 55 °C.

The title compound **6** was obtained as a white solid substance (9.18 g, 0.024 mol, 80%).

¹H NMR (600 MHz, METHANOL-D₄): δ = 7.73 (d, J = 6.6 Hz, 2H), 7.61 (d, J = 8.9 Hz, 2H), 7.33 (t, J = 7.8 Hz, 2H), 7.25 (t, J = 7.4 Hz, 2H), 4.47 (dd, J = 10.0, 3.5 Hz, 1H), 4.29 (d, J = 7.2 Hz, 2H), 4.16 (t, J = 7.1 Hz, 1H), 2.87 – 2.78 (m, 1H), 2.70 – 2.59 (m, 1H).

¹³C {¹H} NMR (151 MHz, METHANOL-D₄): δ = 171.84, 156.94, 143.86, 143.83, 141.23, 128.61, 127.90, 127.47, 127.12, 126.82, 125.29, 124.94, 119.60, 67.05, 66.89, 34.85, 34.66, 34.47, 34.28.

¹⁹F NMR (565 MHz, METHANOL-D₄): δ = 65.69 (t, J = 11.1 Hz, 3F).

IR (ATR): ν = 3317.51, 3076.28, 2926.94, 1704.70, 1551.92, 1460.96, 1392.25, 1269.33, 1249.81, 1154.47, 1120.96, 1044.19, 724.84, 618.01, 539.90 cm⁻¹.

Elemental analysis [CHN] (%) = Anal. Calcd for C₁₉H₁₆F₃NO₄ (m: 1.8930 mg): C, 60.16; H, 4.25; N, 3.69. Found: C, 60.78; H, 4.86; N, 3.69.

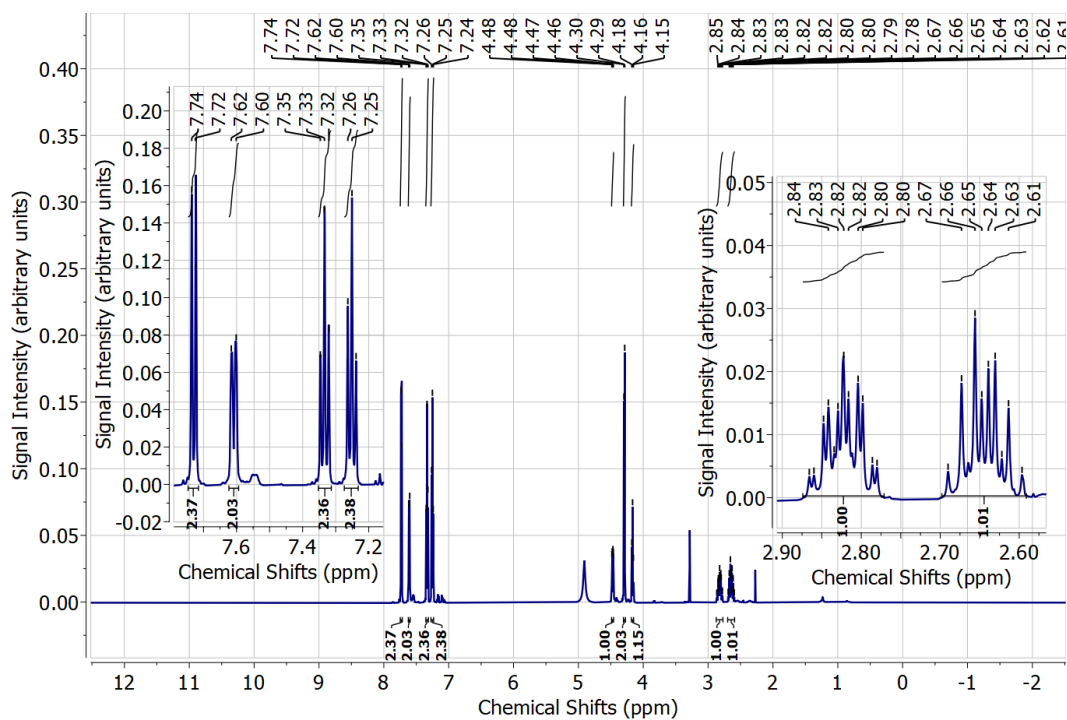


Figure S14: ^1H NMR (600 MHz) spectrum of Fmoc-TfeGly-OH (**6**) dissolved in MeOH-d_4 .

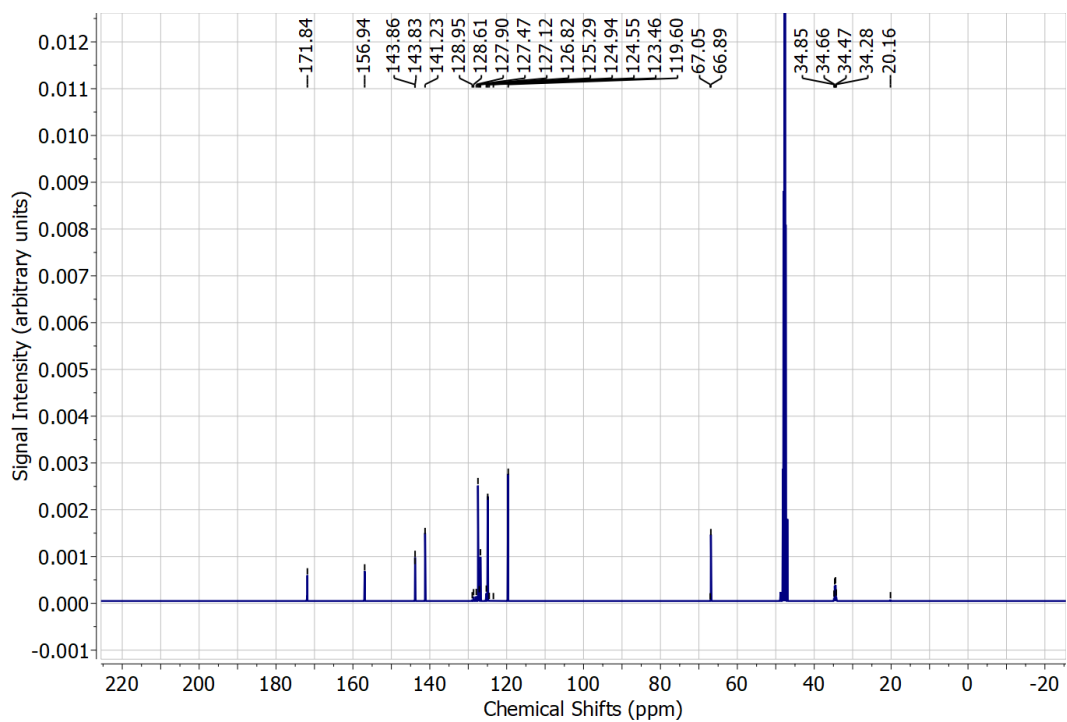


Figure S15: ^{13}C $\{^1\text{H}\}$ NMR (151 MHz) spectrum of Fmoc-TfeGly-OH (**6**) dissolved in MeOH-d_4 .

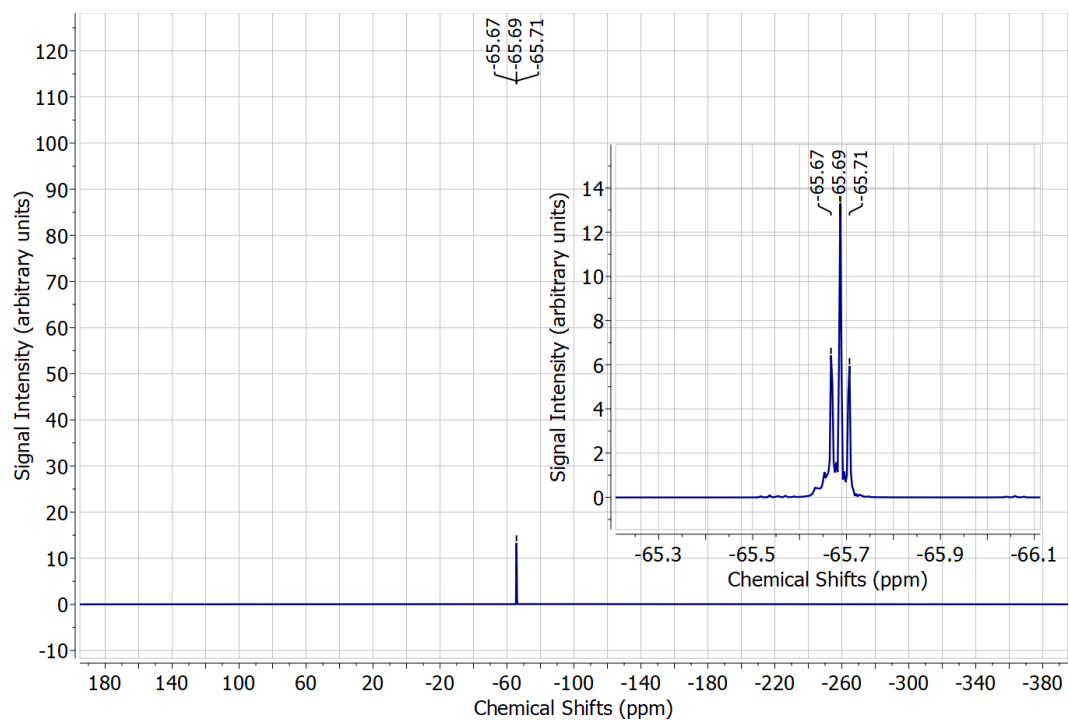


Figure S16: ^{19}F NMR (565 MHz) spectrum of Fmoc-TfeGly-OH (**6**) dissolved in MeOH-d_4 .

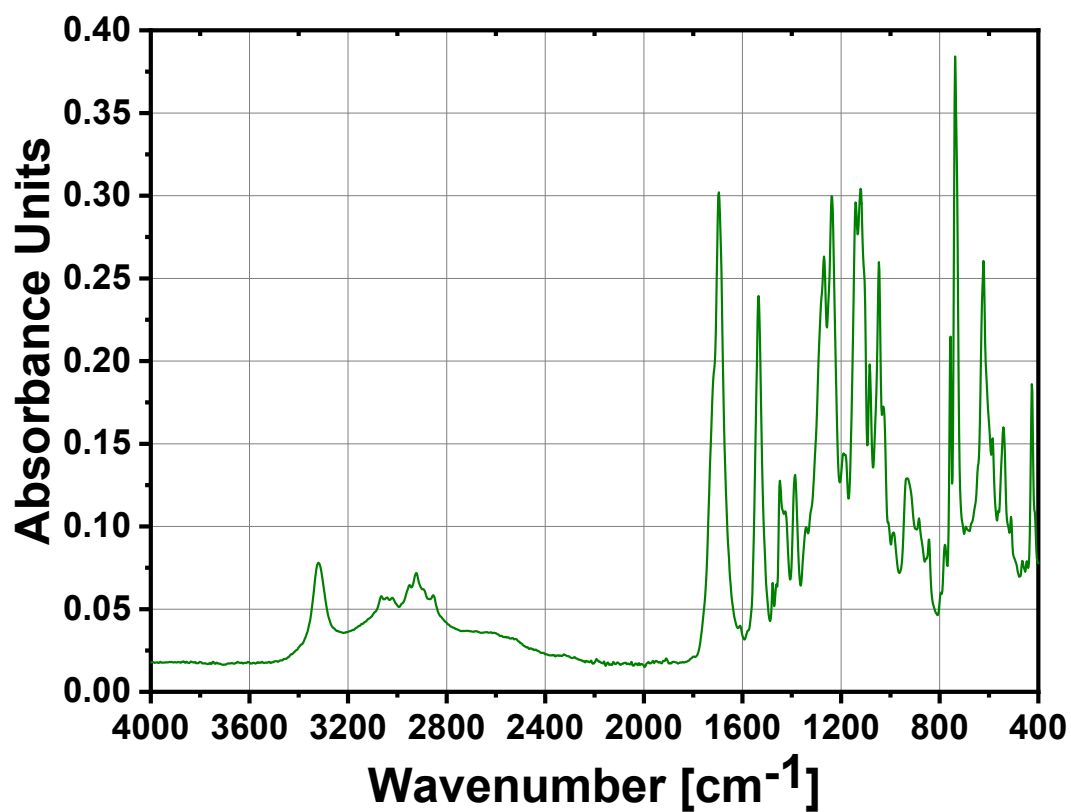
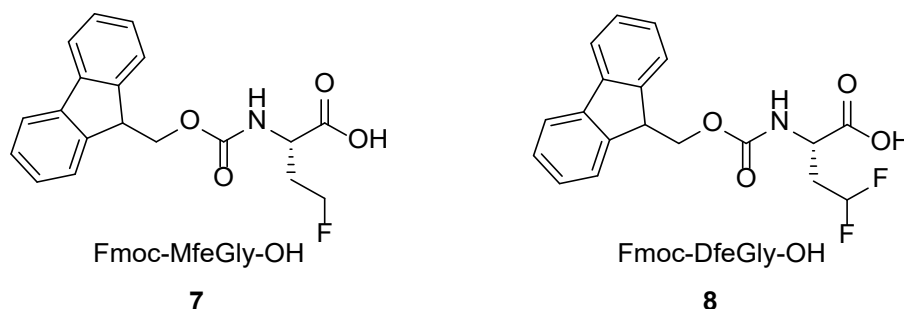


Figure S17: IR-ATR spectrum of Fmoc-TfeGly-OH (**6**).

2. Fluorinated Fmoc-protected amino acids Fmoc-MfeGly-OH (7) and Fmoc-DfeGly-OH (9)



Scheme 2: Chemical structures of Fmoc-MfeGly-OH (**7**) and Fmoc-DfeGly-OH (**8**).

The fluorinated Fmoc-protected amino acids Fmoc-MfeGly-OH (**7**) and Fmoc-DfeGly-OH (**8**) were provided by Suvrat Chowdhary & Thomas Hohmann (Freie Universität Berlin, Kokschi Group).¹¹ To validate the chemical nature and purity of these compounds, NMR and IR spectra were recorded and elemental analysis experiments proceeded.

2.1. Characterization of Fmoc-MfeGly-OH (7)

¹H NMR (600 MHz, METHANOL-D₄): δ = 7.76 (d, J = 7.6 Hz, 2H), 7.64 (t, J = 7.5 Hz, 2H), 7.35 (t, J = 7.5 Hz, 2H), 7.27 (t, J = 7.4 Hz, 2H), 4.56 – 4.40 (m, 2H), 4.37 – 4.31 (m, 2H), 4.31 – 4.25 (m, 1H), 4.19 (t, J = 7.1 Hz, 1H), 2.31 – 2.21 (m, 1H), 2.03 – 1.92 (m, 1H).

¹³C {¹H} NMR (151 MHz, METHANOL-D₄): δ = 173.98, 157.36, 143.99, 143.85, 141.27, 127.45, 126.84, 126.81, 124.93, 119.58, 80.59, 79.50, 66.66, 50.51, 32.18, 32.05.

¹⁹F NMR (565 MHz, METHANOL-D₄): δ = -222.46 – -222.83 (m, 3F)

IR (ATR): ν = 3318.16, 2968.13, 1681.65, 1537.05, 1266.21, 1211.12, 1030.30, 896.68, 760.36, 737.69, 546.06 cm⁻¹.

Elemental analysis [CHN] (%) = Anal. Calcd for C₁₉H₁₈FNO₄ (m: 1.4860 mg): C, 66.46; H, 5.28; N, 4.08. Found: C, 65.85; H, 5.926; N, 4.15.

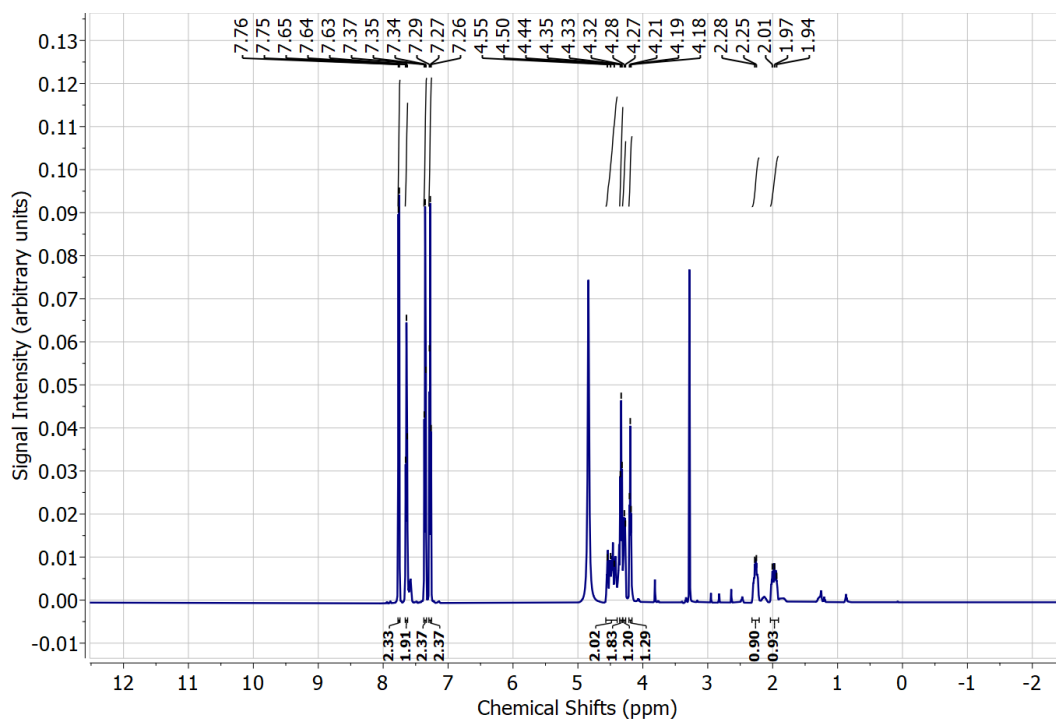


Figure S18: ^1H NMR (600 MHz) spectrum of Fmoc-MfeGly-OH (**7**) dissolved in MeOH- d_4 .

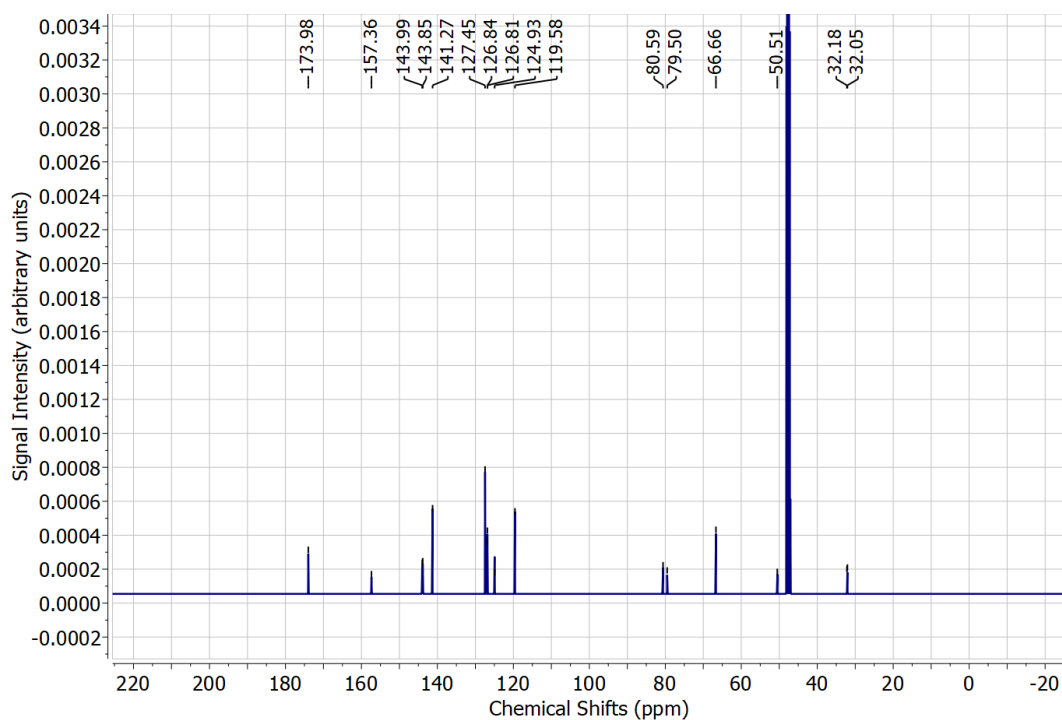


Figure S19: ^{13}C $\{^1\text{H}\}$ NMR (151 MHz) spectrum of Fmoc-MfeGly-OH (**7**) dissolved in MeOH- d_4 .

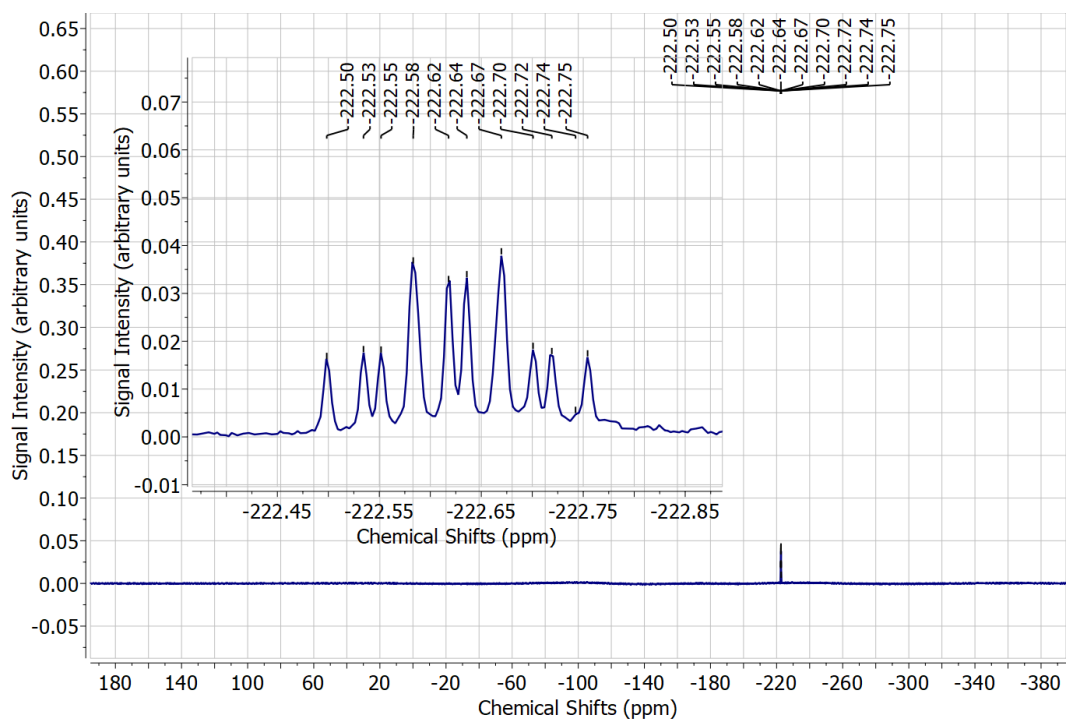


Figure S20: ^{19}F NMR (565 MHz) spectrum of Fmoc-MfeGly-OH (**7**) dissolved in MeOH-d_4 .

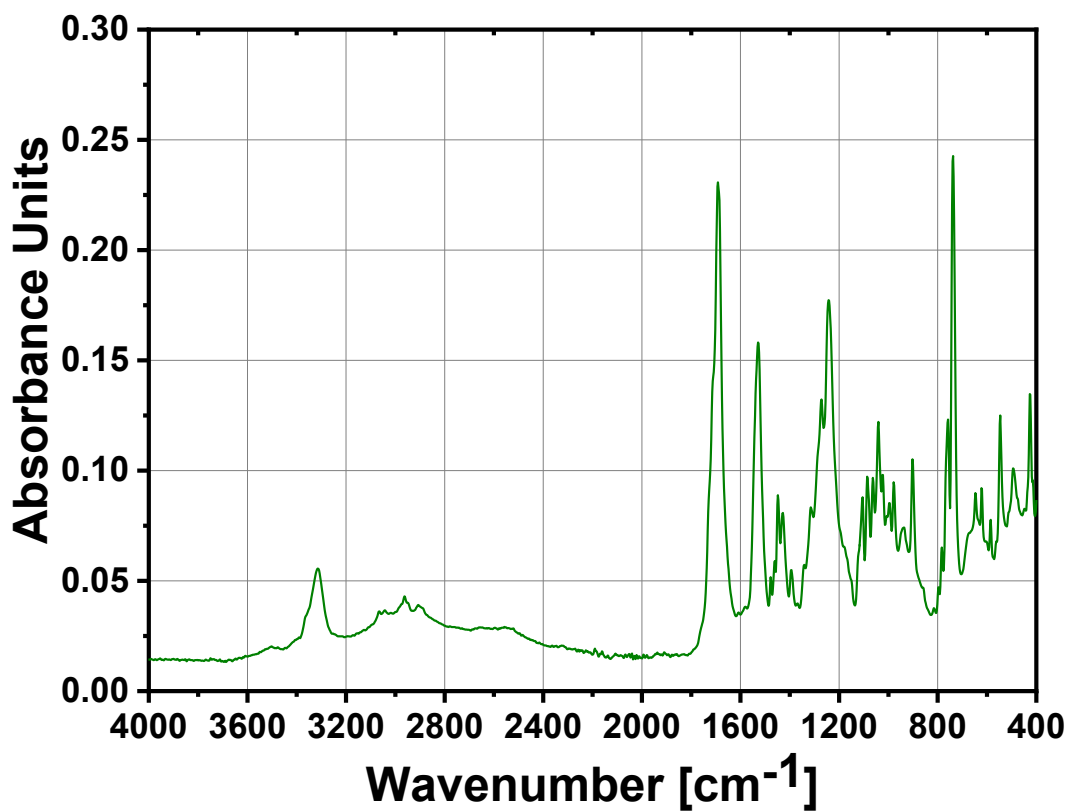


Figure S21: IR-ATR spectrum of Fmoc-MfeGly-OH (**7**).

2.2. Characterization of Fmoc-DfeGly-OH (8)

^1H NMR (600 MHz, METHANOL- D_4): δ = 7.77 (d, J = 7.6 Hz, 2H), 7.67 – 7.62 (m, 2H), 7.36 (t, J = 7.0 Hz, 2H), 7.28 (td, J = 7.4, 1.2 Hz, 2H), 6.03 – 5.81 (m, 1H), 4.41 – 4.31 (m, 2H), 4.35 – 4.27 (m, 1H), 4.20 (t, J = 6.9 Hz, 1H), 2.43 – 2.33 (m, 1H), 2.26 – 2.16 (m, 1H).

^{13}C { ^1H } NMR (151 MHz, METHANOL- D_4): δ = 13C NMR (151 MHz, METHANOL- D_4) δ 172.75, 157.13, 143.95, 143.83, 141.28, 127.46, 126.82, 124.92, 119.58, 117.30, 115.72, 66.70, 35.84, 35.69, 35.54, 24.93.

^{19}F NMR (565 MHz, METHANOL- D_4): δ = -117.45 – -119.06 (m, 3F).

IR (ATR): ν = 3314.06, 3023.44, 2898.22, 1682.88, 1548.48, 1448.60, 1423.87, 1277.57, 1216.50, 1075.20, 737.69, 531.63 cm^{-1} .

Elemental analysis [CHN] (%) = Anal. Calcd for $\text{C}_{19}\text{H}_{17}\text{F}_2\text{NO}_4$ (m: 2.1280 mg): C, 63.16; H, 4.74; N, 3.88. Found: C, 63.38; H, 5.17; N, 3.94.

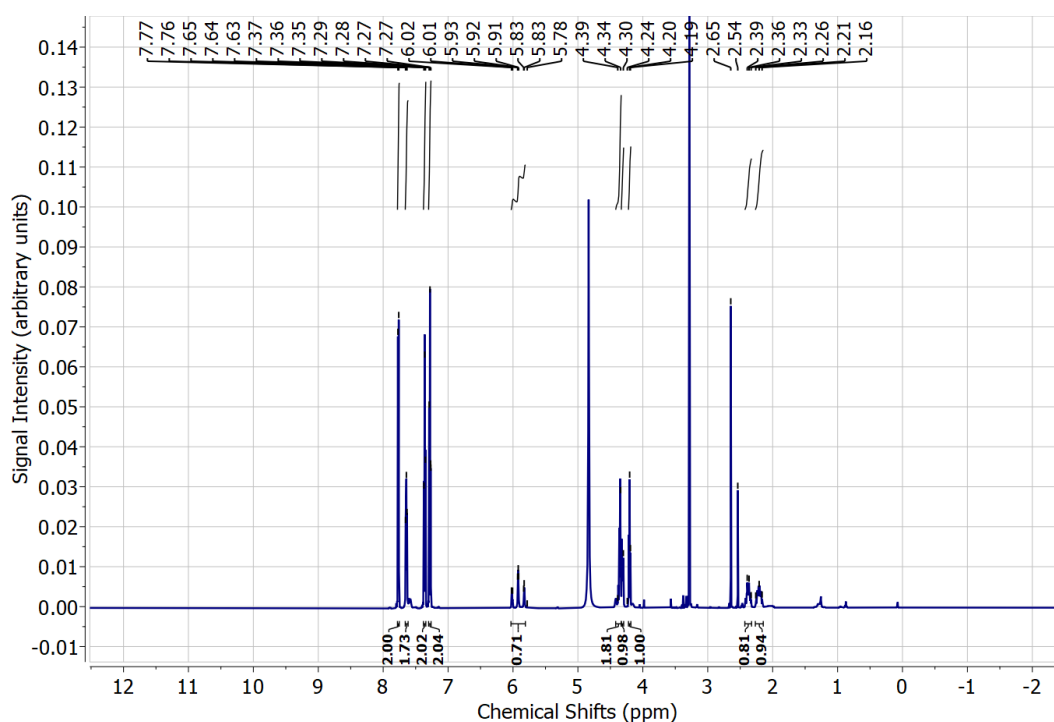


Figure S22: ^1H NMR (600 MHz) spectrum of Fmoc-DfeGly-OH (8) dissolved in $\text{MeOH-}d_4$.

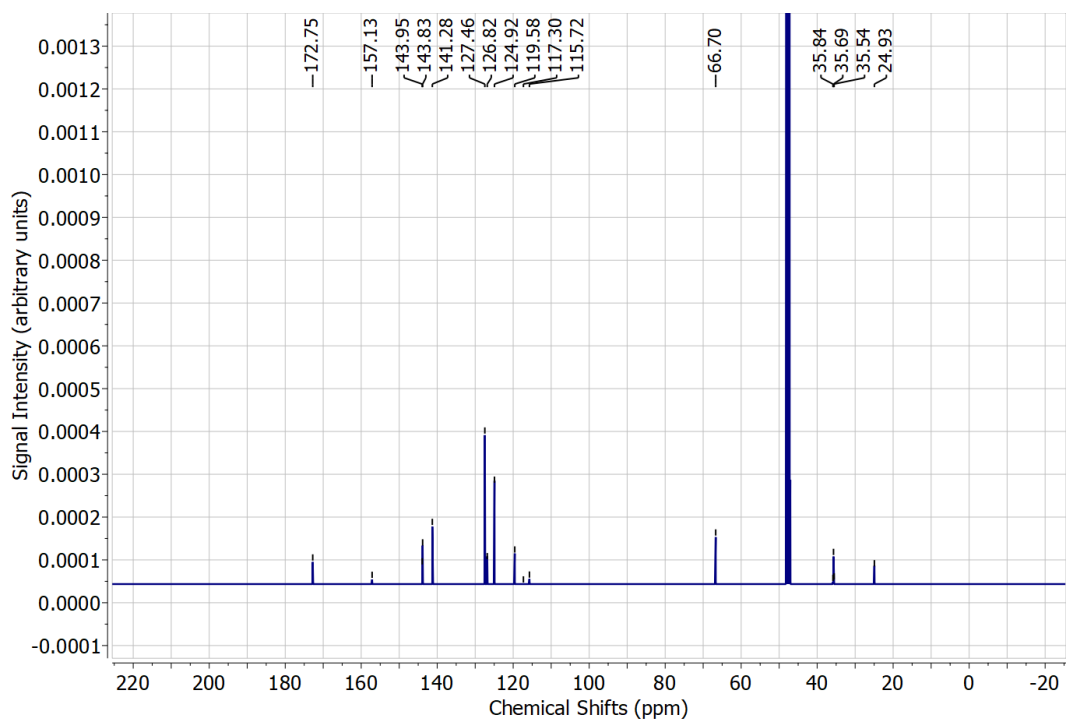


Figure S23: ^{13}C { ^1H } NMR (151 MHz) spectrum of Fmoc-DfeGly-OH (**8**) dissolved in MeOH-d_4 .

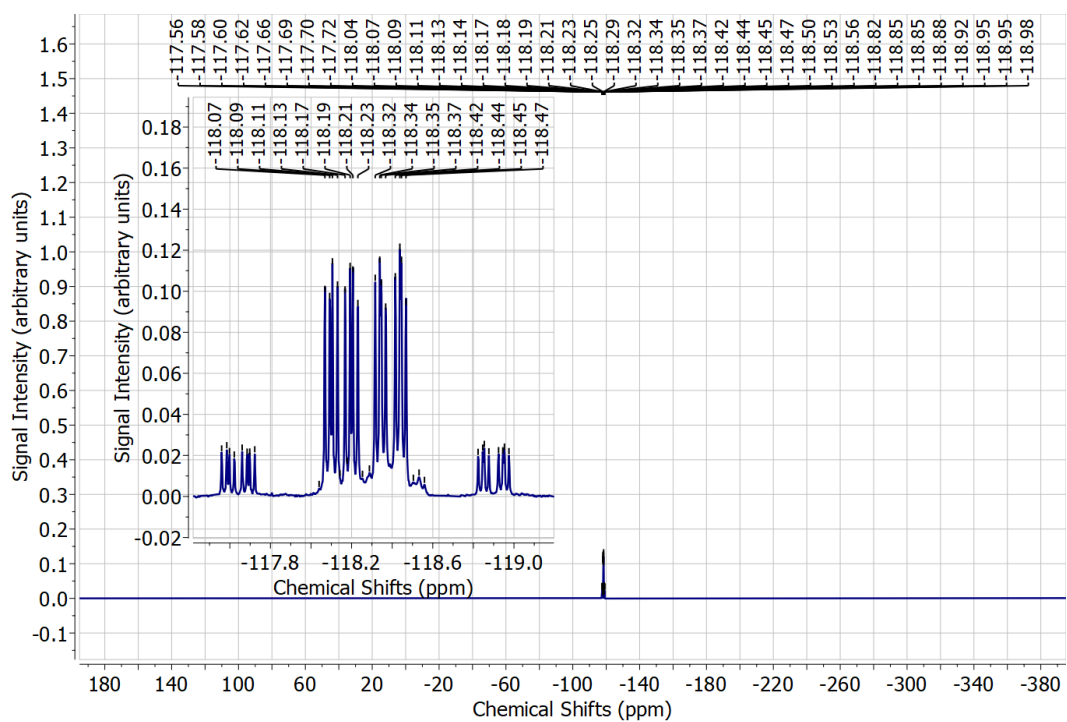


Figure S24: ^{19}F NMR (565 MHz) spectrum of Fmoc-DfeGly-OH (**8**) dissolved in MeOH-d_4 .

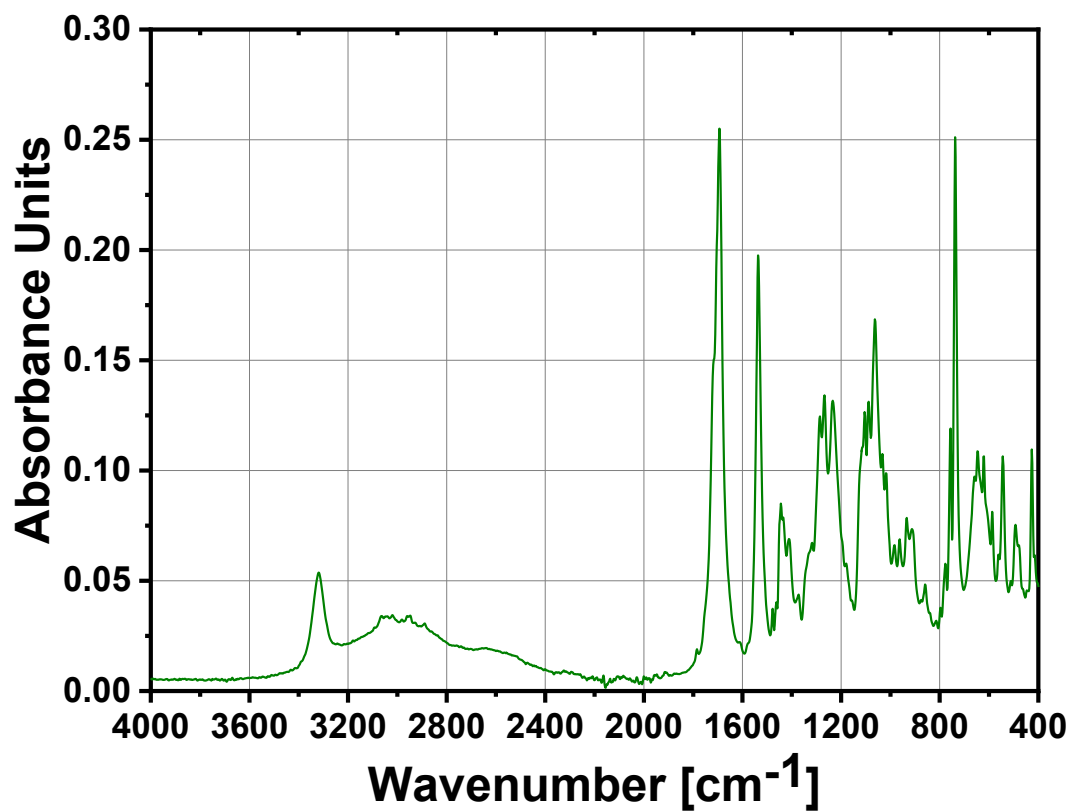


Figure S25: IR-ATR spectrum Fmoc-DfeGly-OH (8).

3. Peptide Synthesis: Selected HPLC chromatograms of crude peptides after SPPS

In this chapter, HPLC chromatograms of crude peptide samples after solid-phase peptide synthesis are presented. This is intended to give an impression about the outcome of overall peptide synthesis. All HPLC chromatograms were **directly exported** from the HPLC systems. (**VWR Chromaster 600 bar** or **Hitachi Primaide**) using EZ Chrom ELITE software (version 3.3.2, Agilent).

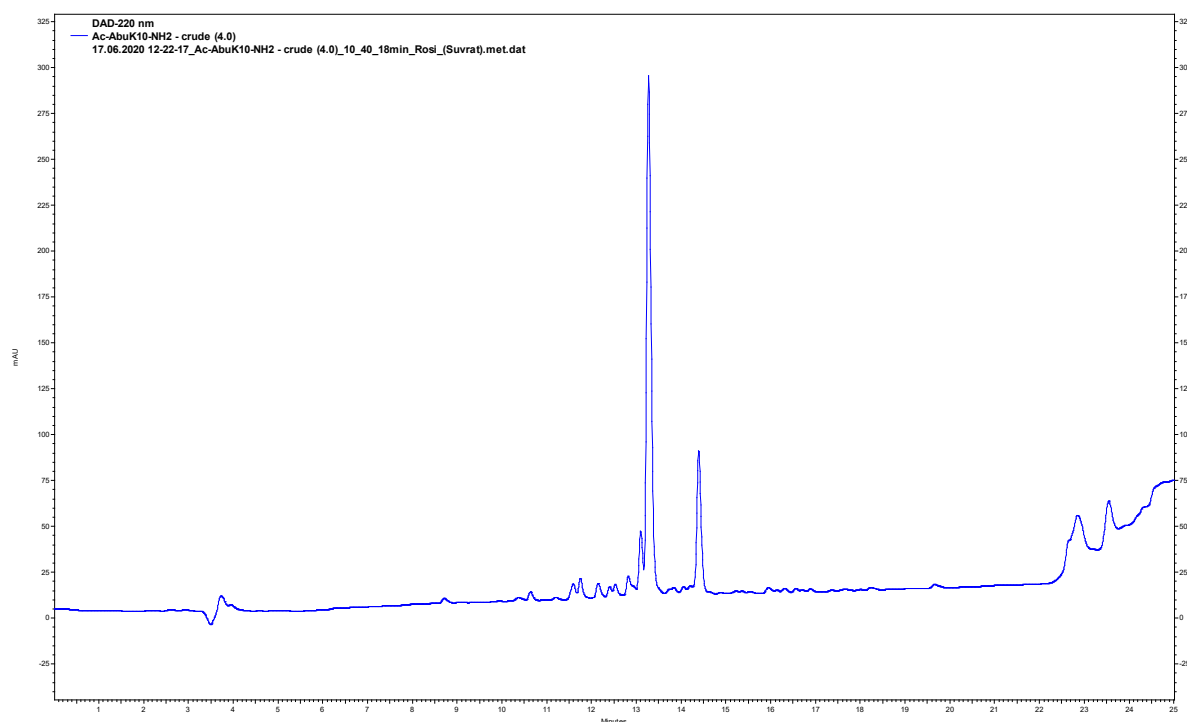


Figure S26: Crude HPLC chromatogram of peptide sequence **AbuK10** (HPLC: Chromaster 600 bar – Method: **(A)** H₂O + 0.1% TFA / **(B)** ACN + 0.1% TFA – 10% **(B)** → 40% **(B)** in 18 min. UV detection occurred at 220 nm.

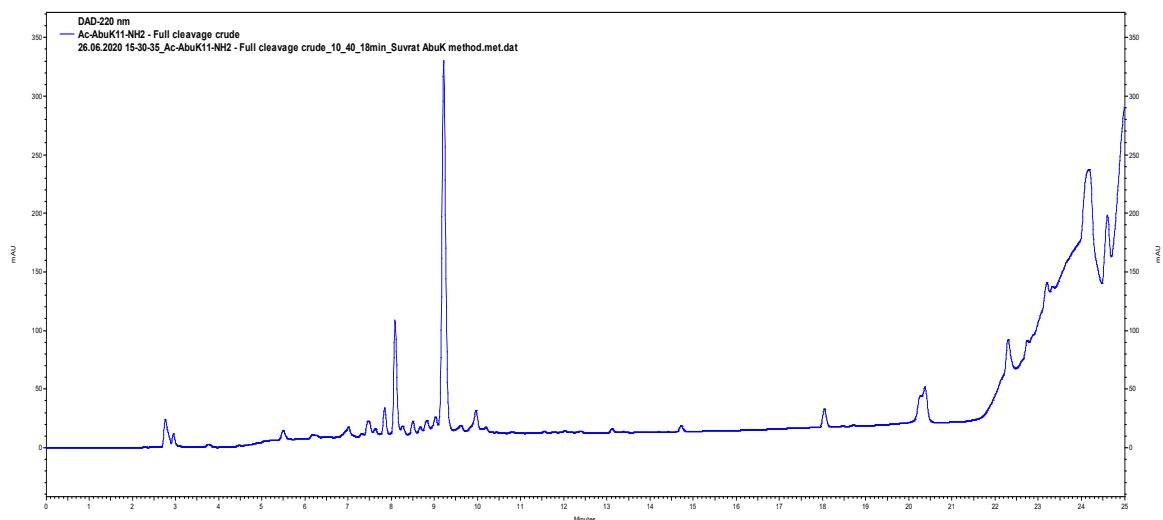


Figure S27: Crude HPLC chromatogram of peptide sequence **AbuK11** (HPLC: Hitachi Primaide – Method: **(A)** H₂O + 0.1% TFA / **(B)** ACN + 0.1% TFA – 10% **(B)** → 40% **(B)** in 18 min. UV detection occurred at 220 nm.

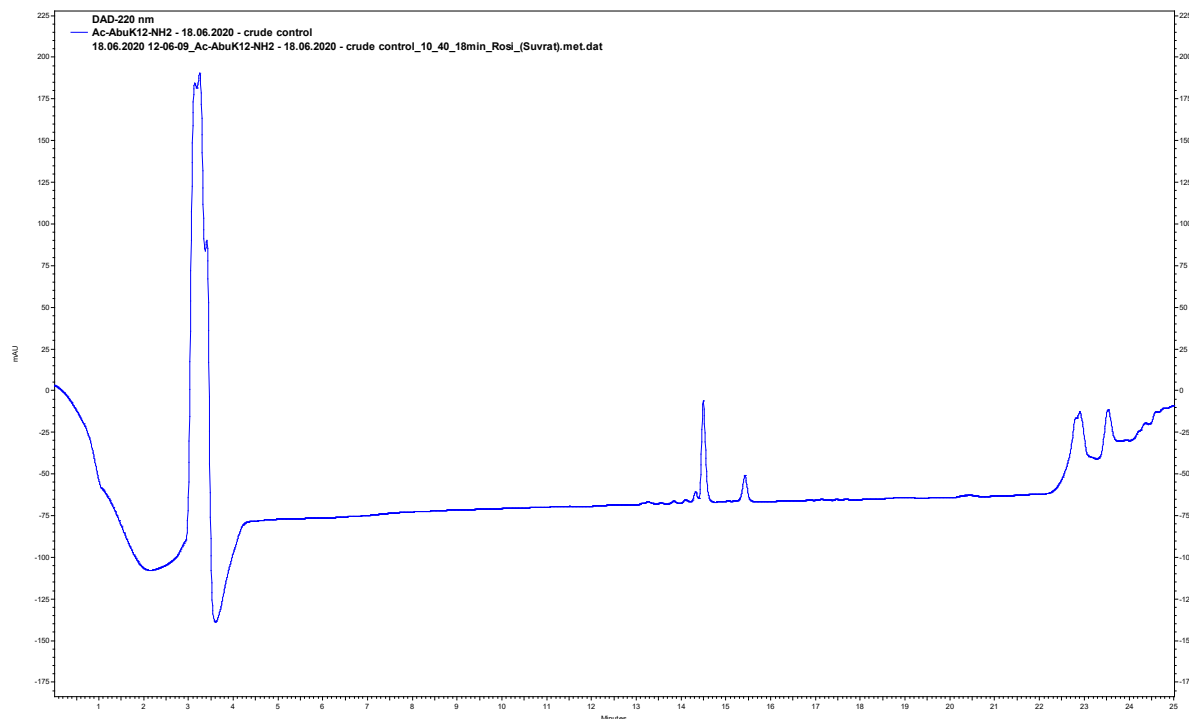


Figure S28: Crude HPLC chromatogram of peptide sequence **AbuK12** (HPLC: Chromaster 600 bar – Method: **(A)** H₂O + 0.1% TFA / **(B)** ACN + 0.1% TFA – 10% **(B)** → 40% **(B)** in 18 min. UV detection occurred at 220 nm.

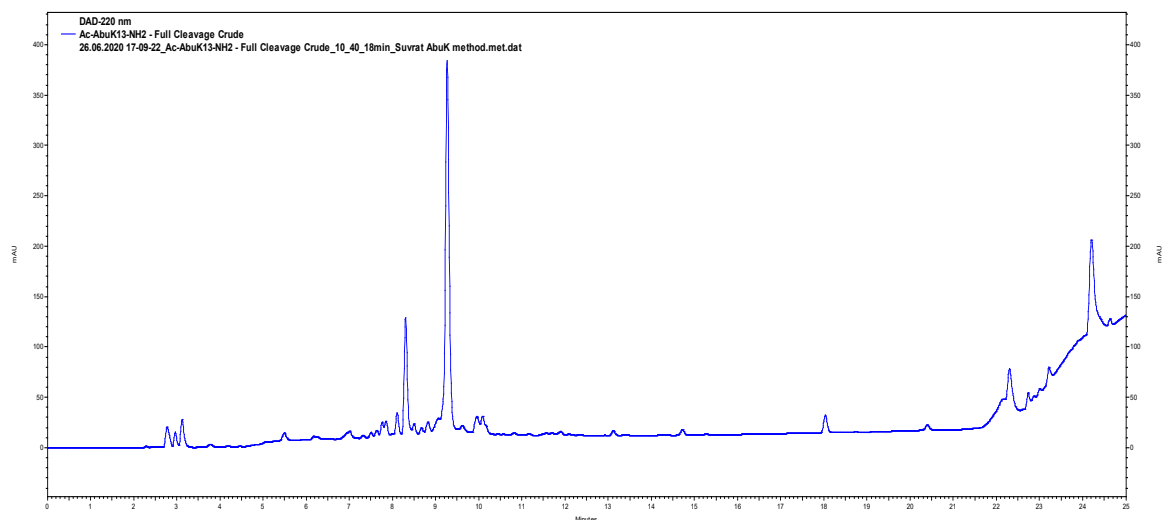


Figure S29: Crude HPLC chromatogram of peptide sequence **AbuK13** (HPLC: Hitachi Primaide – Method: **(A)** H₂O + 0.1% TFA / **(B)** ACN + 0.1% TFA – 10% **(B)** → 40% **(B)** in 18 min. UV detection occurred at 220 nm.

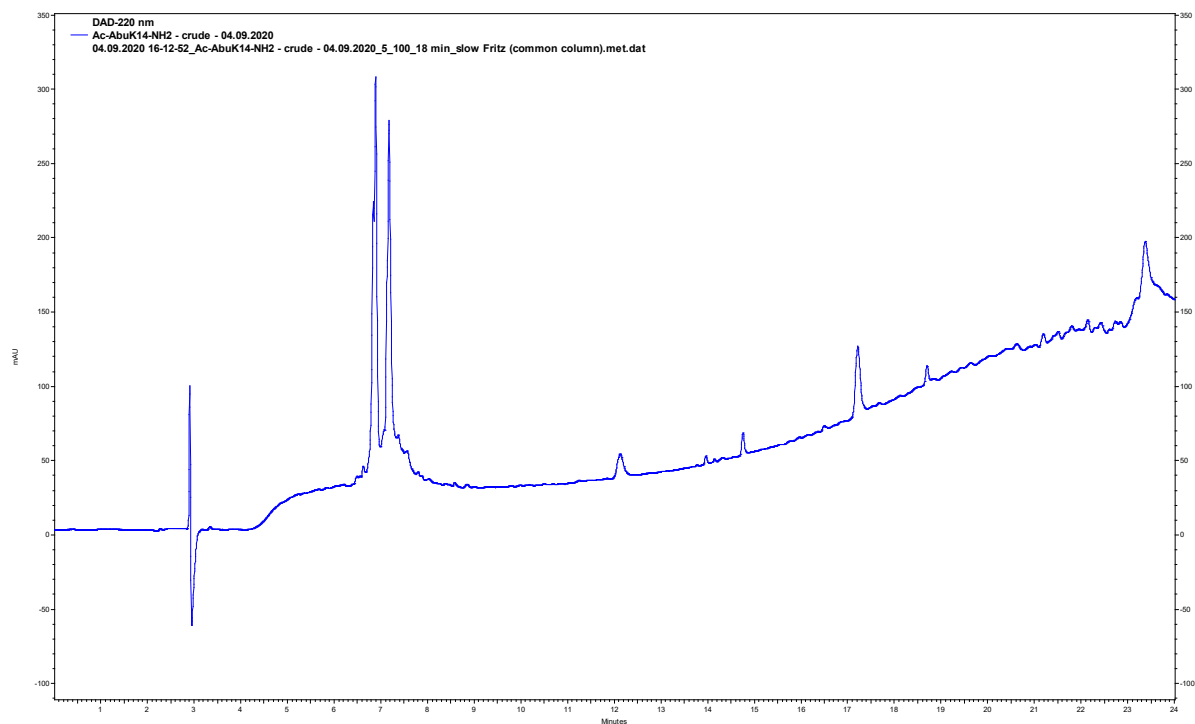


Figure S30: Crude HPLC chromatogram of peptide sequence **AbuK14** (HPLC: Chromaster 600 bar – Method: **(A)** H₂O + 0.1% TFA / **(B)** ACN + 0.1% TFA – 5% **(B)** → 100% **(B)** in 18 min. UV detection occurred at 220 nm.

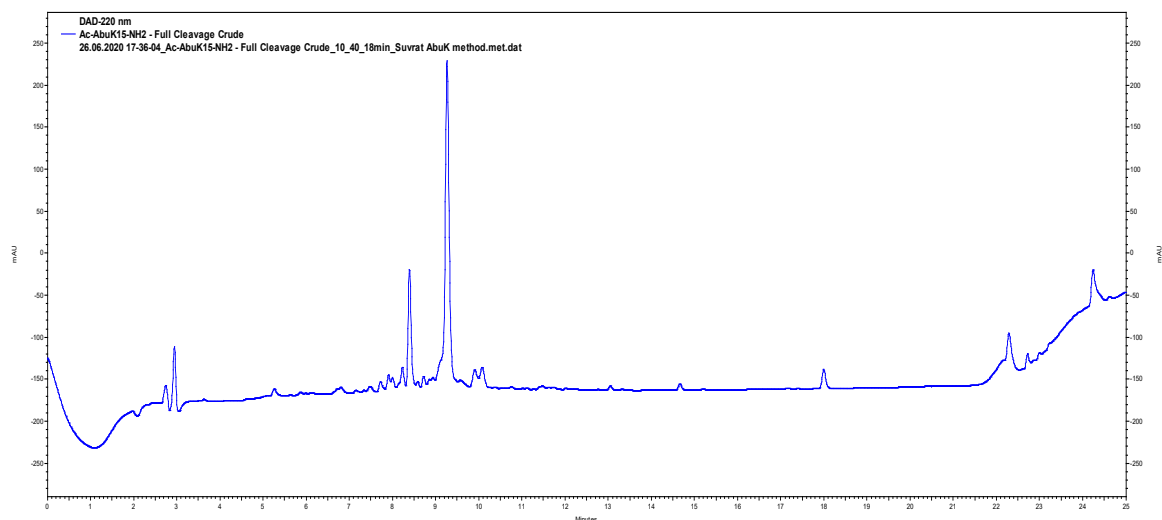


Figure S31: Crude HPLC chromatogram of peptide sequence **AbuK15** (HPLC: Hitachi Primaide – Method: **(A)** H₂O + 0.1% TFA / **(B)** ACN + 0.1% TFA – 10% **(B)** → 40% **(B)** in 18 min. UV detection occurred at 220 nm.

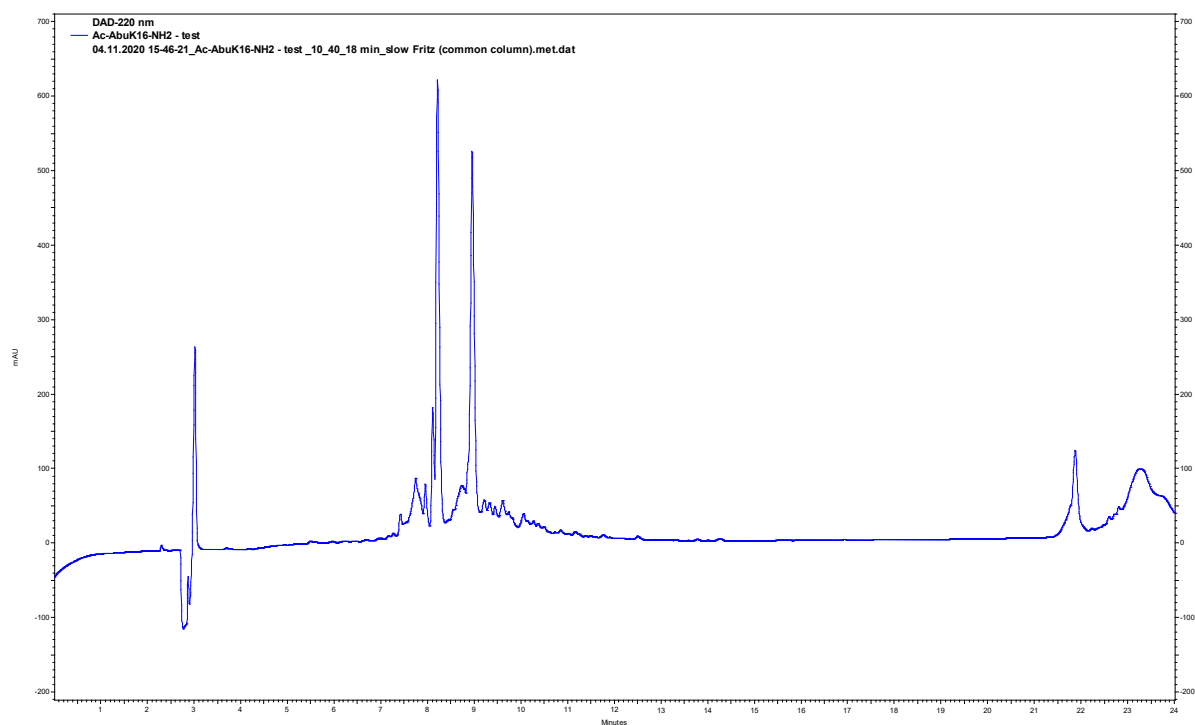


Figure S32: Crude HPLC chromatogram of peptide sequence **AbuK16** (HPLC: Chromaster 600 bar – Method: **(A)** H₂O + 0.1% TFA / **(B)** ACN + 0.1% TFA – 10% **(B)** → 40% **(B)** in 18 min. UV detection occurred at 220 nm.

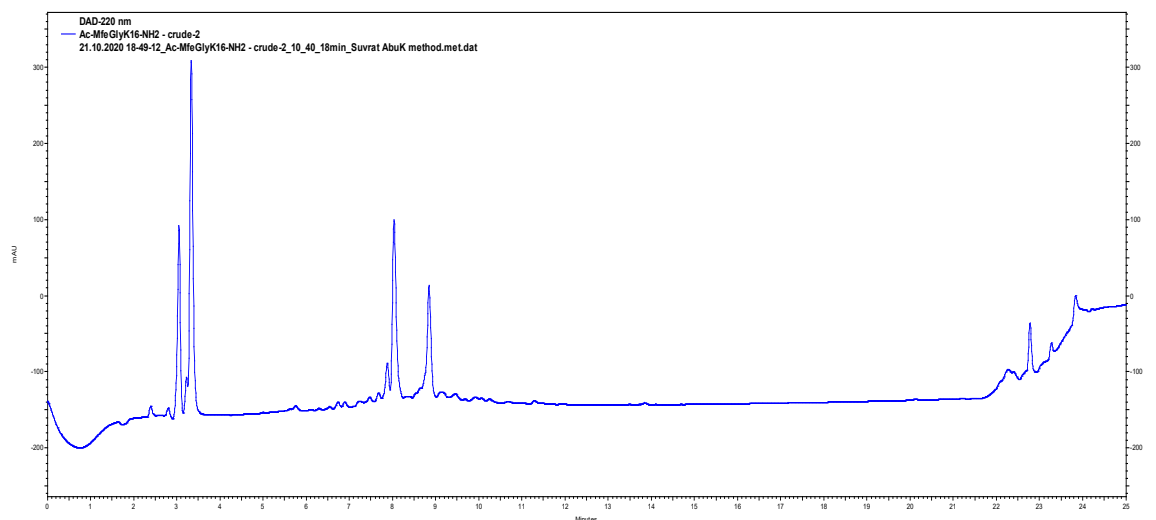


Figure S33: Crude HPLC chromatogram of peptide sequence **MfeGlyK16** (HPLC: Hitachi Primaide – Method: **(A)** H₂O + 0.1% TFA / **(B)** ACN + 0.1% TFA – 10% **(B)** → 40% **(B)** in 18 min. UV detection occurred at 220 nm.

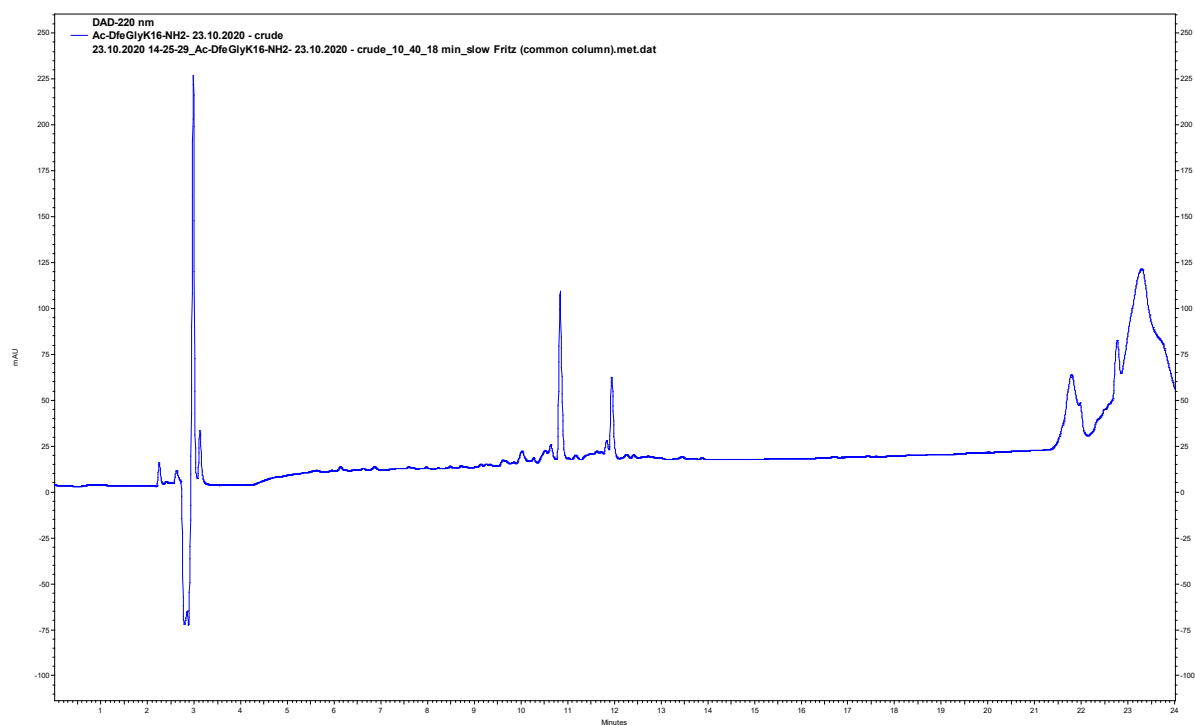


Figure S34: Crude HPLC chromatogram of peptide sequence **DfeGlyK16** (HPLC: Chromaster 600 bar – Method: **(A)** H₂O + 0.1% TFA / **(B)** ACN + 0.1% TFA – 10% **(B)** → 40% **(B)** in 18 min. UV detection occurred at 220 nm.

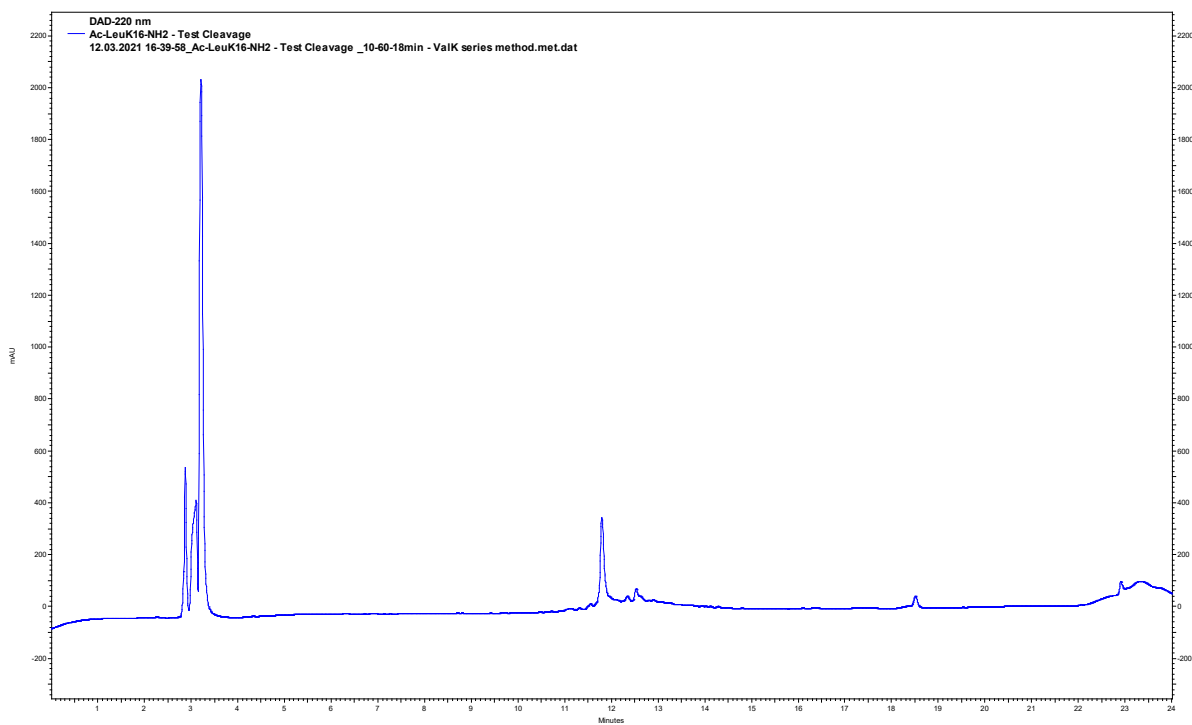


Figure S35: Crude HPLC chromatogram of peptide sequence **LeuK16** (HPLC: Chromaster 600 bar – Method: **(A)** H₂O + 0.1% TFA / **(B)** ACN + 0.1% TFA – 10% **(B)** → 60% **(B)** in 18 min. UV detection occurred at 220 nm.

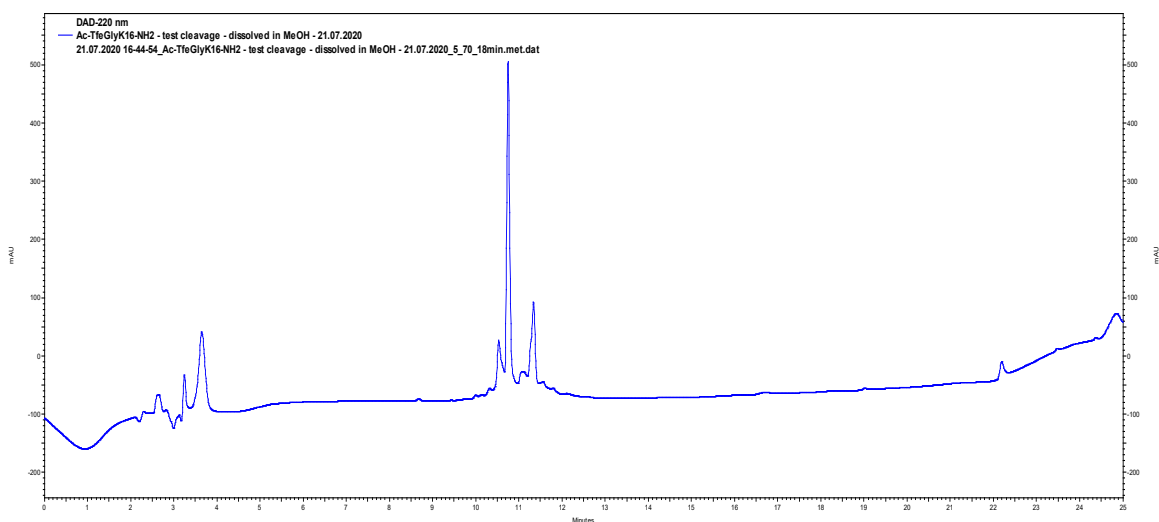


Figure S36: Crude HPLC chromatogram of peptide sequence **TfeGlyK16** (HPLC: Hitachi Primaide – Method: **(A)** H₂O + 0.1% TFA / **(B)** ACN + 0.1% TFA – 5% **(B)** → 70% **(B)** in 18 min. UV detection occurred at 220 nm.

4. Peptide Synthesis: Characterization of purified sequences

In this chapter, all peptide sequences of this research project are presented. Their purity was determined through **analytical HPLC** (DAD Detection at 220 nm) (**VWR Chromaster 600 bar** or **Hitachi Primaide**) and **high-resolution mass spectrometry (HRMS)**. All HPLC chromatograms were evaluated with the software OriginLab (OriginLab Corporation, Northampton, MA, USA). For HRMS spectra, the program MassHunter Workstation SoftwareVersion B.02.00 (Agilent Technologies, Santa Clara, CA, USA) was utilized. All HRMS spectra were compared to their **calculated isotope distribution** through MassHunter Workstation SoftwareVersion B.02.00 (Agilent Technologies, Santa Clara, CA, USA) to provide a fundamentally credible interpretation of experimental data.

<u>peptide</u>	<u>scale</u> <u>[mmol]</u>	<u>amount of purified peptide</u> <u>[mg]</u>
AbuK10	0.5	10.1
AbuK11	0.5	12.5
AbuK12	0.5	13.6
AbuK13	0.5	13.7
AbuK14	0.1	28.5
AbuK15	0.1	30.5
AbuK16	0.1	45.0
MfeGlyK16	0.1	39.1
DfeGlyK16	0.1	65.2
TfeGlyK16	0.1	78.9
LeuK16	0.1	40.3

4.1 Peptide sequence: AbuK10

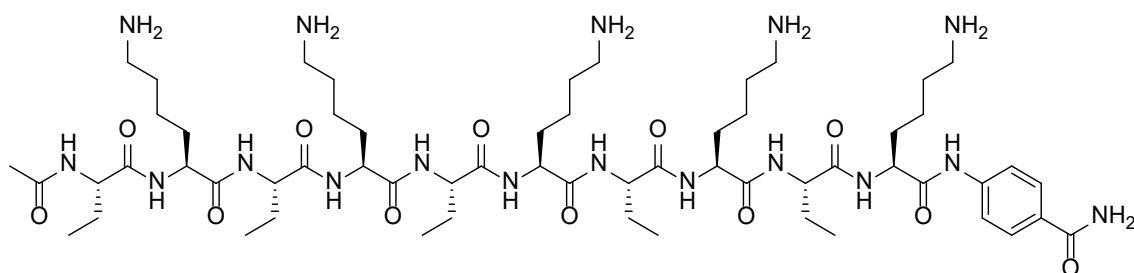


Figure S37: Chemical structure of peptide **AbuK10**.

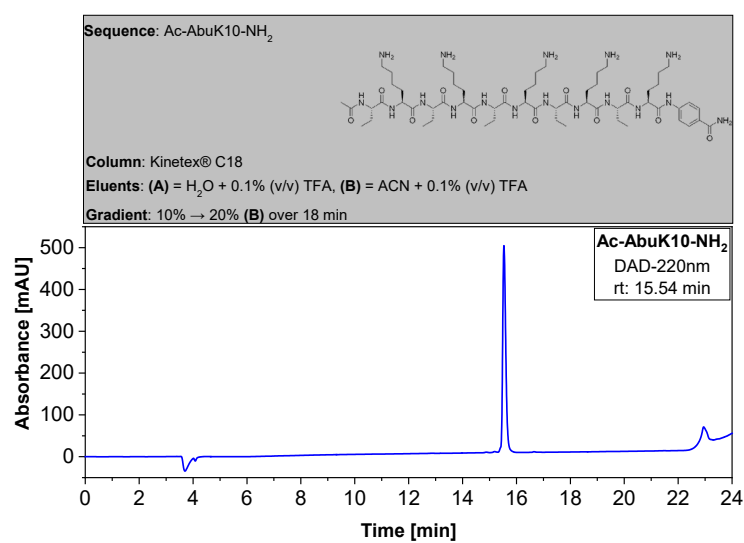


Figure S38: Analytical HPLC chromatogram of pure peptide **AbuK10**.

HPLC: VWR Chromaster 600 bar.

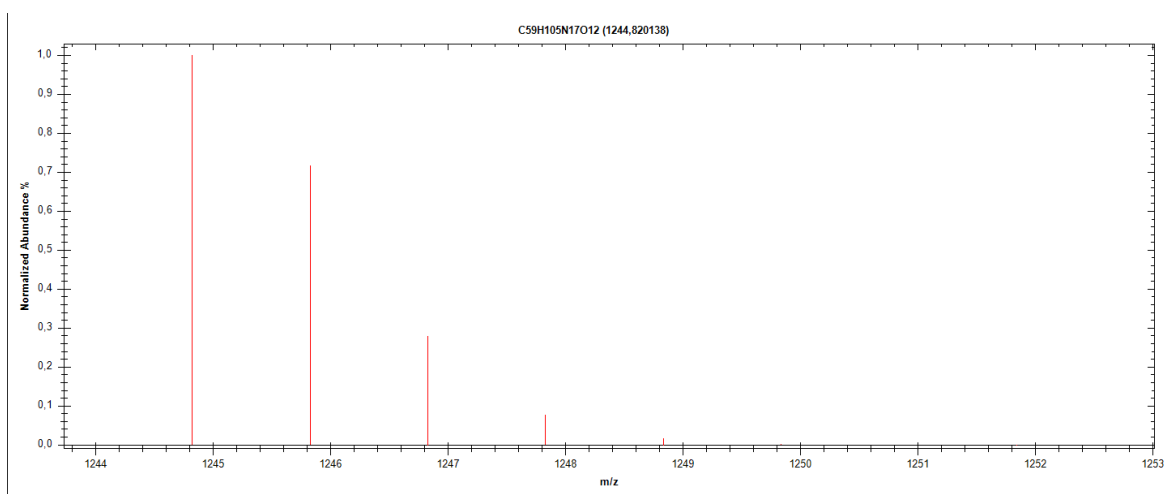


Figure S39: Calculated isotope distribution and mass intensity data for peptide **AbuK10**.

Table S1: Ion species (M+H)⁺ calculated for peptide sequence **AbuK10**.

<u>m/z</u> <u>Ion species (M+H)⁺</u>	<u>Abund</u> <u>(% largest)</u>
1244,8201	100
1245,823	71,7
1246,8257	27,81
1247,8284	7,66

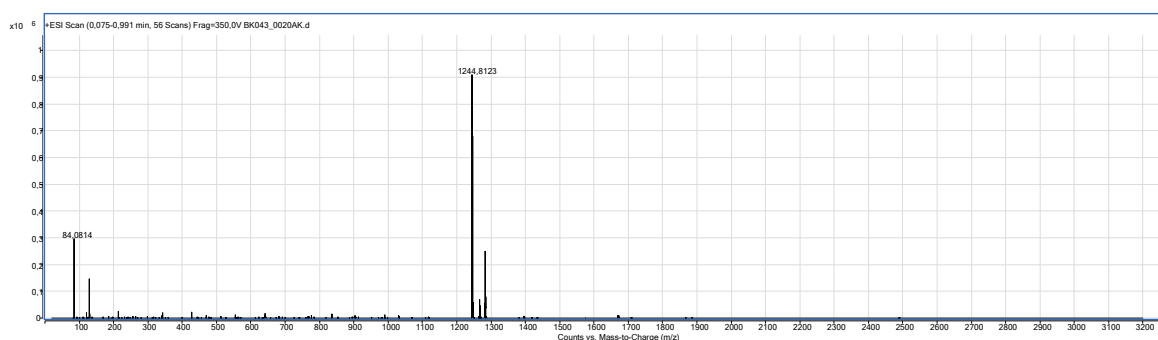


Figure S40: High resolution mass spectrometry (HRMS) spectrum of **AbuK10** in positive ionization mode (**unzoom**).

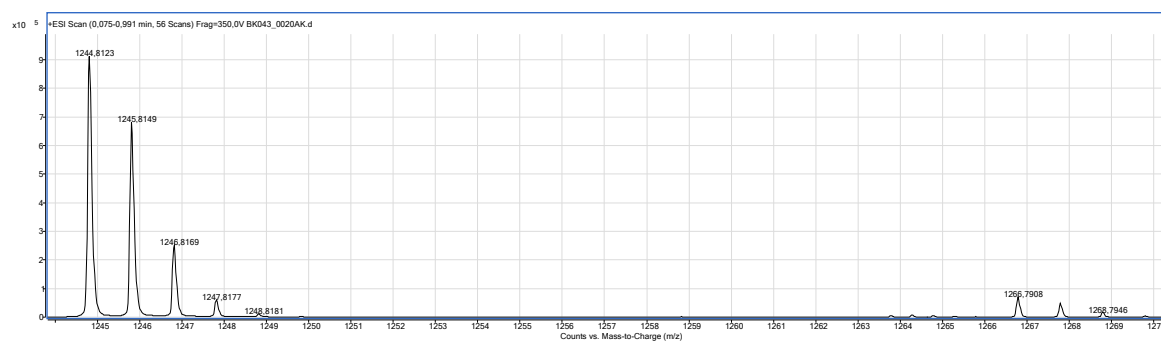


Figure S41: High resolution mass spectrometry (HRMS) spectrum of **AbuK10** in positive ionization mode (**zoom**).

Table S2: Comparison of ion species (M+H)⁺ both calc. and detected - **AbuK10**.

<u>Ion species (M+H)⁺ (calc.)</u>	<u>Ion species (M+H)⁺ (detected)</u>
1244,8201	1244,9123
1245,823	1245,9149
1246,8257	1246,9169
1247,8284	1247,9177

4.2 Peptide sequence: AbuK11

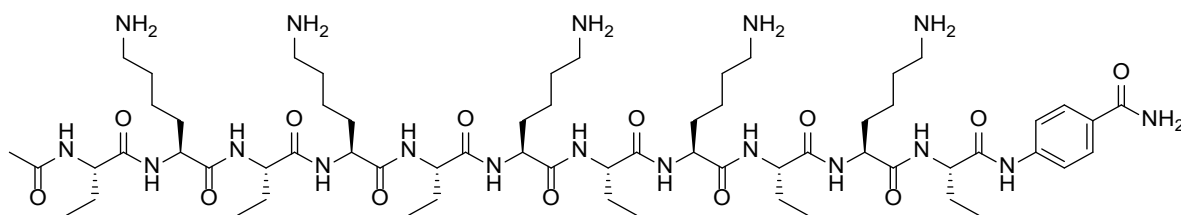


Figure S42: Chemical structure of peptide **AbuK11**.

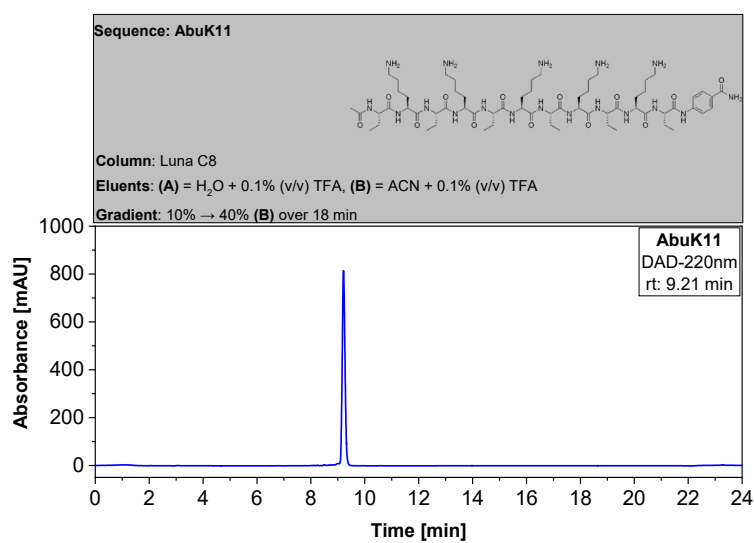


Figure S43: Analytical HPLC chromatogram of pure peptide **AbuK11**. HPLC: Hitachi Primaide.

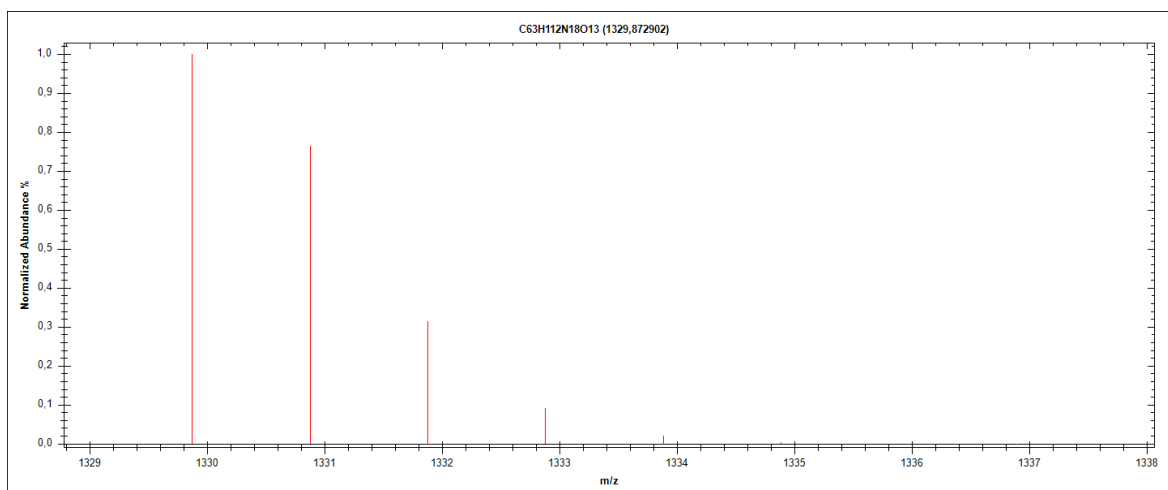


Figure S44: Calculated isotope distribution and mass intensity data for peptide **AbuK11**.

Table S3: Ion species (M+H)⁺ calculated for peptide sequence **AbuK11**.

<u>m/z</u> <u>Ion species (M+H)⁺</u>	<u>Abund</u> <u>(% largest)</u>
1329,8729	100
1330,8758	76,51
1331,8785	31,56
1332,8812	9,22

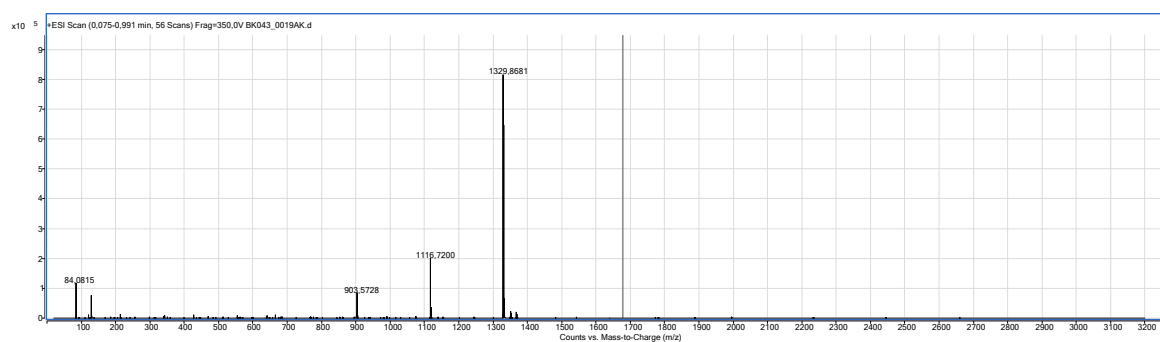


Figure 45: High resolution mass spectrometry (HRMS) spectrum of **AbuK11** in positive ionization mode (**unzoom**).

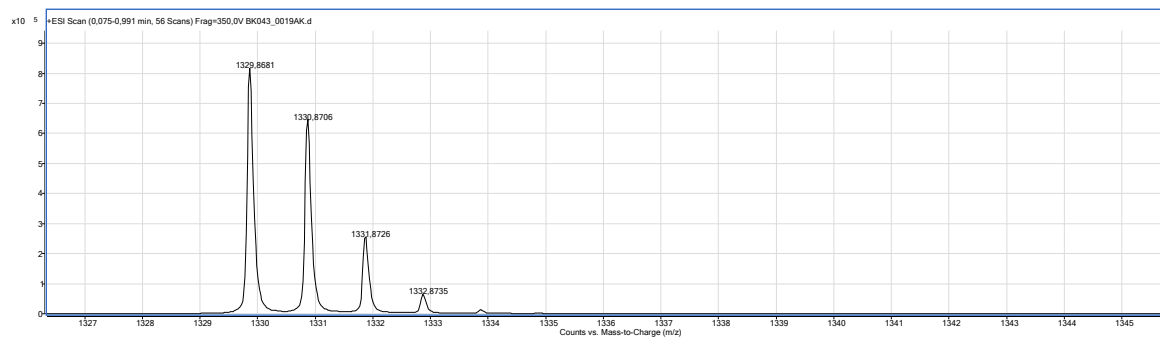


Figure S46: High resolution mass spectrometry (HRMS) spectrum of **AbuK11** in positive ionization mode (**zoom**).

Table S4: Comparison of ion species (M+H)⁺ both calc. and detected - **AbuK11**.

<u>Ion species (M+H)⁺ (calc.)</u>	<u>Ion species (M+H)⁺ (detected)</u>
1329,8729	1329,9691
1330,8758	1330,9706
1331,8785	1331,9726
1332,8812	1332,9735

4.3 Peptide sequence: AbuK12

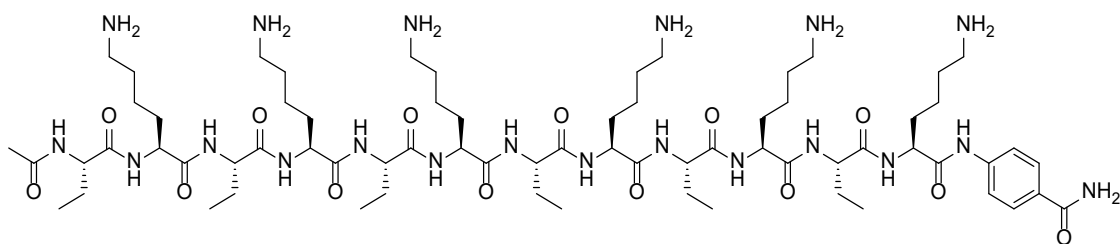


Figure S47: Chemical structure of peptide **AbuK12**.

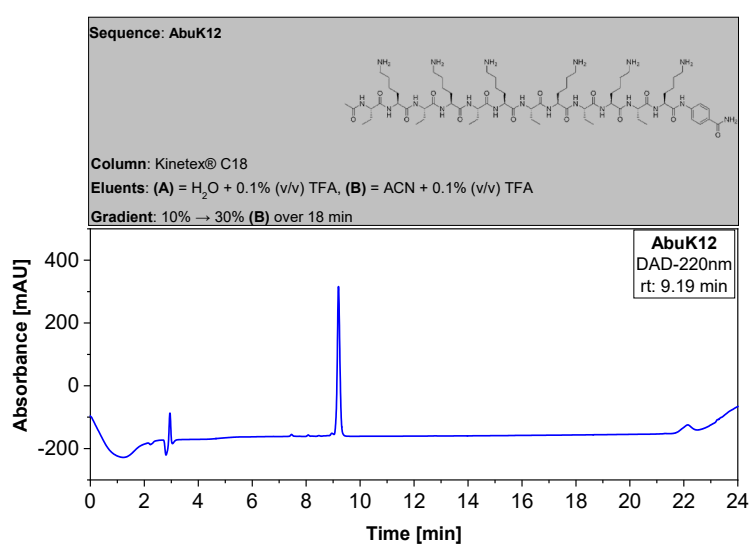


Figure S48: Analytical HPLC chromatogram of pure peptide **AbuK12**. HPLC: VWR Chromaster 600 bar.

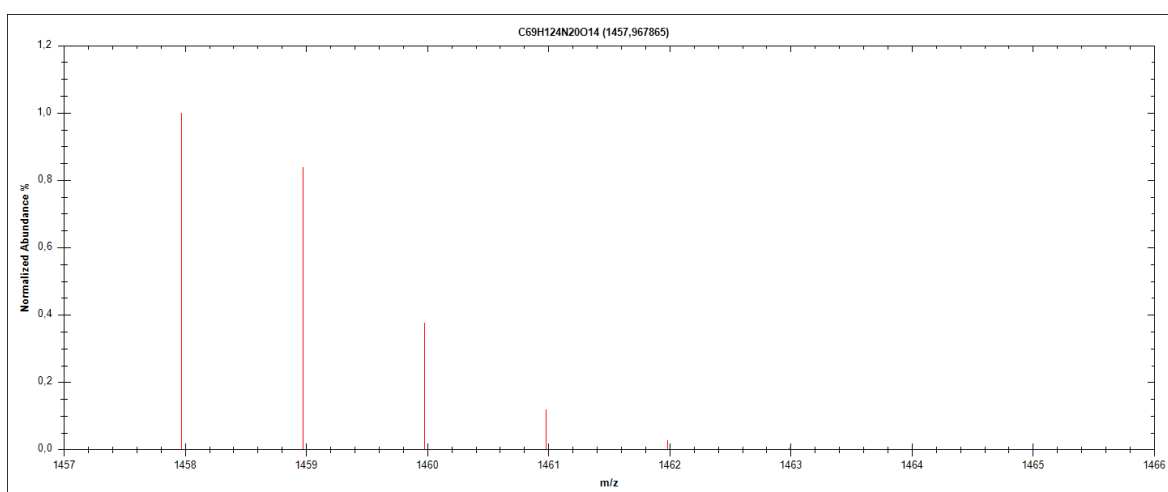


Figure S49: Calculated isotope distribution and mass intensity data for peptide **AbuK12**.

Table S5: Ion species (M+H)⁺ calculated for peptide sequence **AbuK12**.

<u>m/z</u> <u>Ion species (M+H)⁺</u>	<u>Abund</u> <u>(% largest)</u>
1457,9679	100
1458,9707	83,91
1459,9735	37,66
1460,9761	11,91

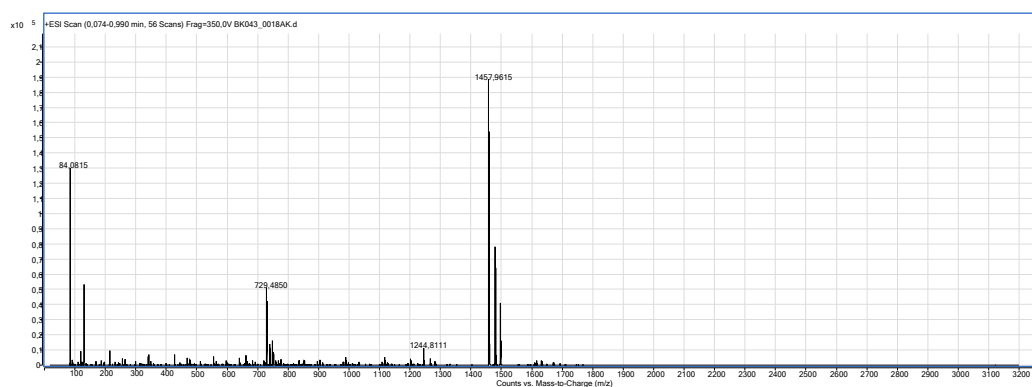


Figure S50: High resolution mass spectrometry (HRMS) spectrum of **AbuK12** in positive ionization mode (**unzoom**).

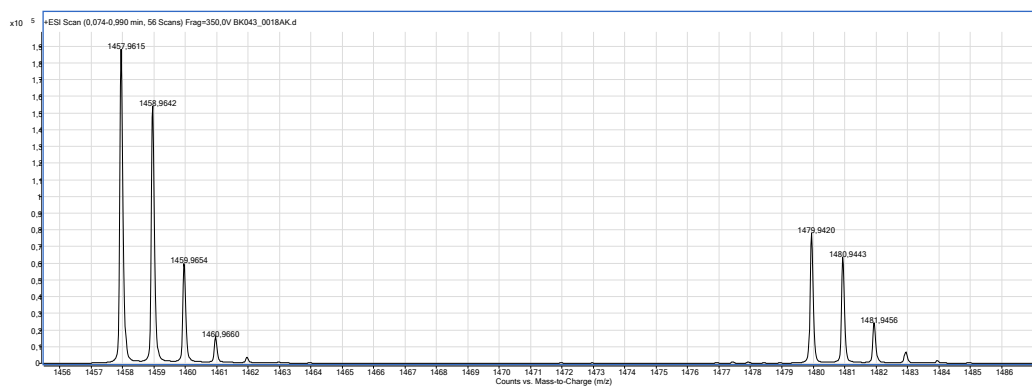


Figure S51: High resolution mass spectrometry (HRMS) spectrum of **AbuK12** in positive ionization mode (**zoom**).

Table S6: Comparison of ion species (M+H)⁺ both calc. and detected - **AbuK12**.

<u>Ion species (M+H)⁺ (calc.)</u>	<u>Ion species (M+H)⁺ (detected)</u>
1457,9679	1457,9615
1458,9707	1458,9642
1459,9735	1459,9654
1460,9761	1460,9660

4.4 Peptide sequence: AbuK13

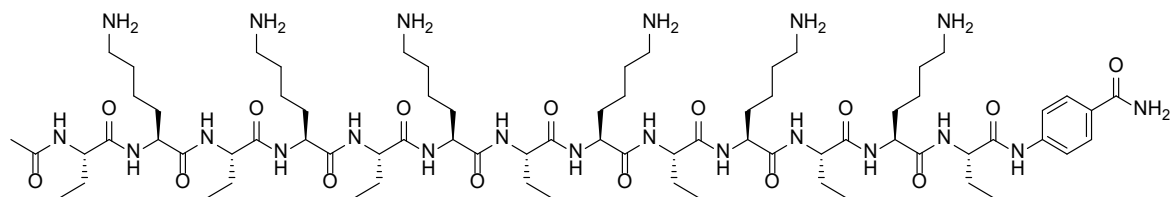


Figure S52: Chemical structure of peptide **AbuK13**.

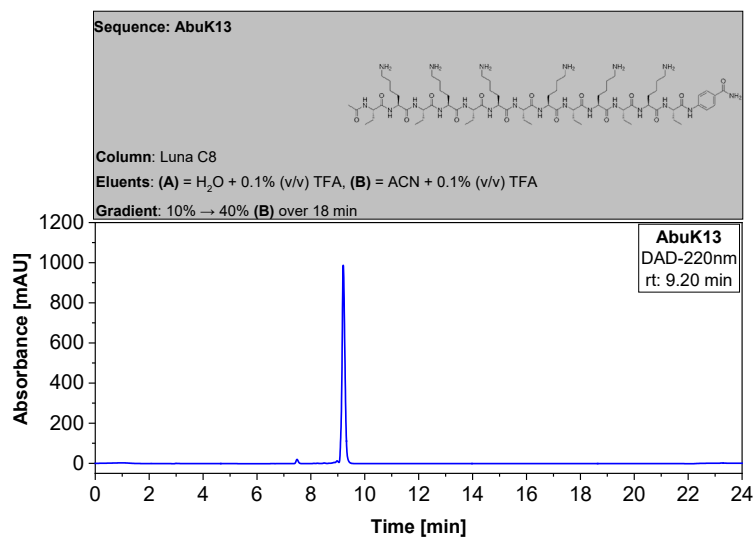


Figure S53: Analytical HPLC chromatogram of pure peptide **AbuK13**. HPLC: Hitachi Primaide.

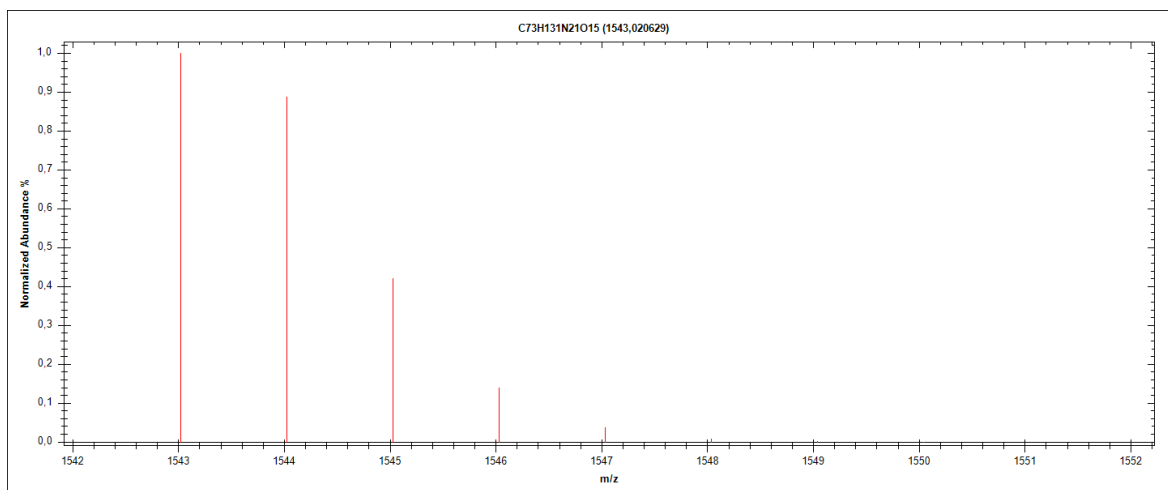


Figure S54: Calculated isotope distribution and mass intensity data for peptide **AbuK13**.

Table S7: Ion species (M+H)⁺ calculated for peptide sequence **AbuK13**.

<u>m/z</u> <u>Ion species (M+H)⁺</u>	<u>Abund</u> <u>(% largest)</u>
1543,0206	100
1544,0235	88,72
1545,0262	41,99
1546,0289	13,98

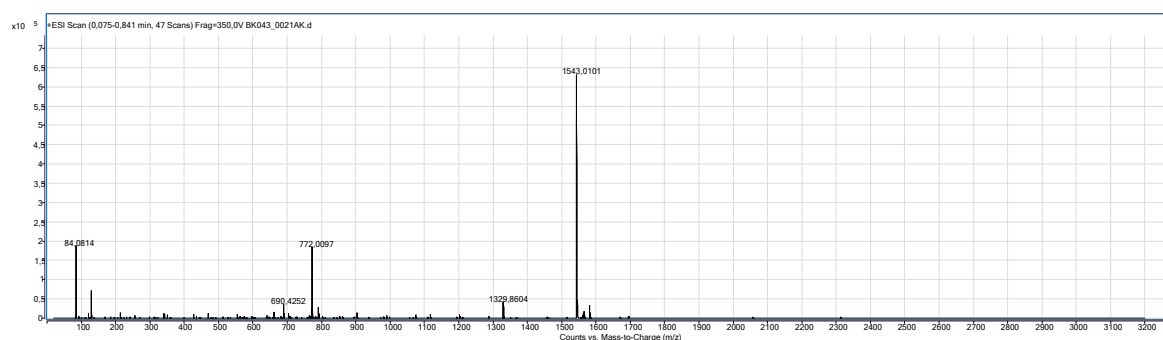


Figure S55: High resolution mass spectrometry (HRMS) spectrum of **AbuK13** in positive ionization mode (**unzoom**).

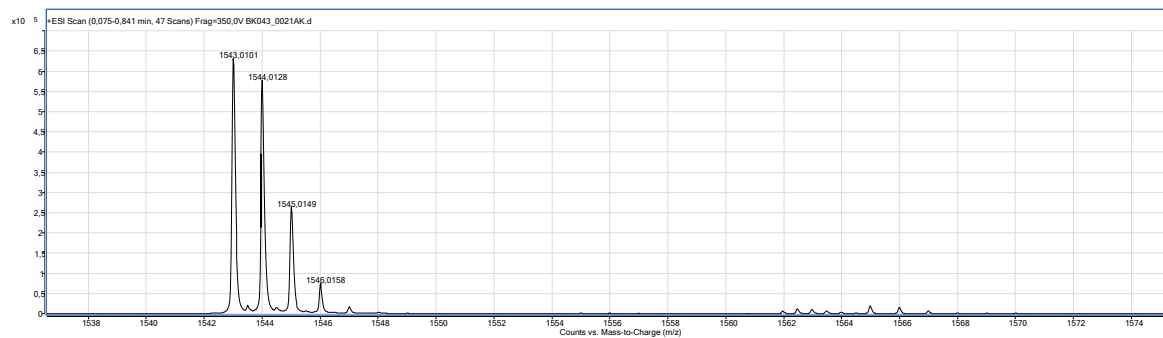


Figure S56: High resolution mass spectrometry (HRMS) spectrum of **AbuK13** in positive ionization mode (**zoom**).

Table S8: Comparison of ion species (M+H)⁺ both calc. and detected - **AbuK13**.

<u>Ion species (M+H)⁺ (calc.)</u>	<u>Ion species (M+H)⁺ (detected)</u>
1543,0206	1543,0101
1544,0235	1544,0128
1545,0262	1545,0149
1546,0289	1546,0158

4.5 Peptide sequence: AbuK14

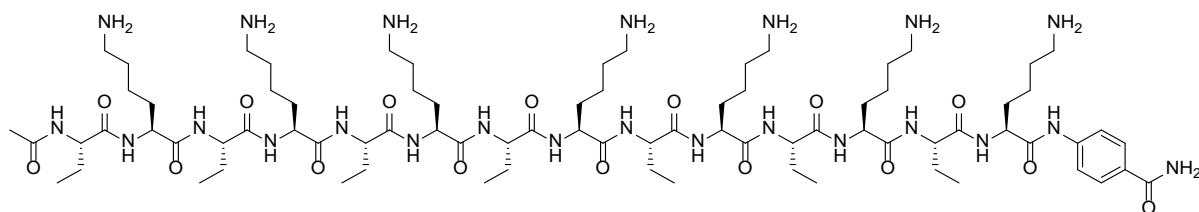


Figure S57: Chemical structure of peptide **AbuK14**.

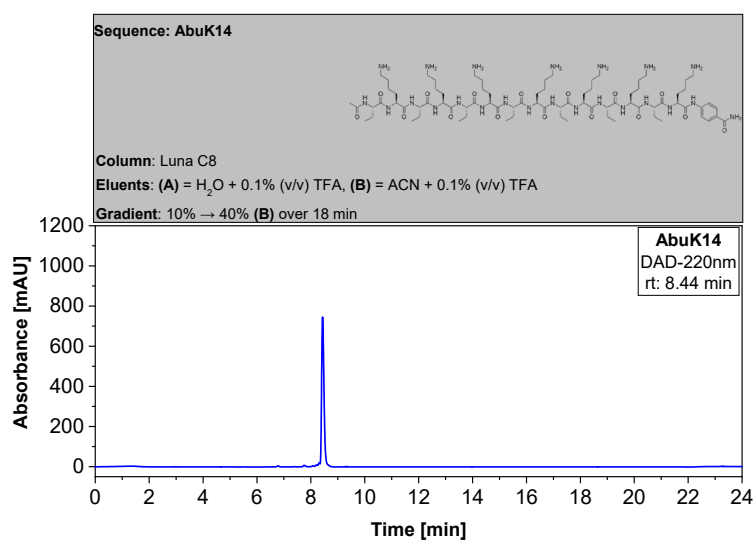


Figure S58: Analytical HPLC chromatogram of pure peptide **AbuK14**. HPLC: Hitachi Primaide

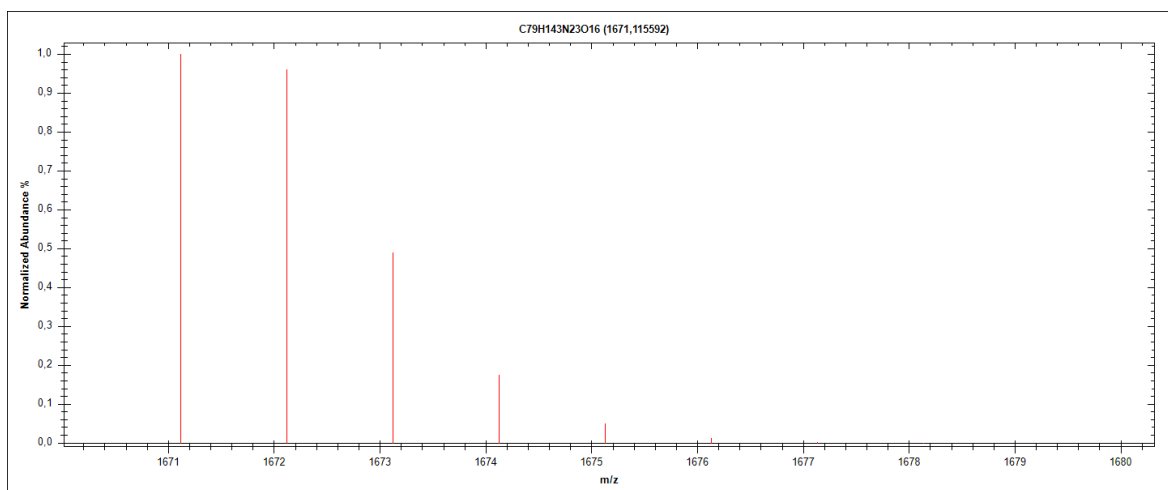


Figure S59: Calculated isotope distribution and mass intensity data for peptide **AbuK14**.

Table S9: Ion species (M+H)⁺ calculated for peptide sequence **AbuK14**.

<u>m/z</u> <u>Ion species (M+H)⁺</u>	<u>Abund</u> <u>(% largest)</u>
1671,1156	100
1672,1185	96,11
1673,1212	49
1674,1239	17,5

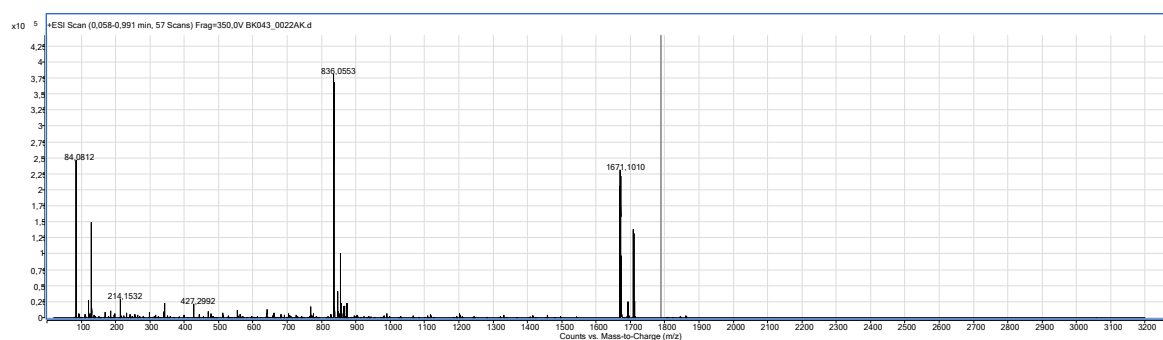


Figure S60: High resolution mass spectrometry (HRMS) spectrum of **AbuK14** in positive ionization mode (**unzoom**).

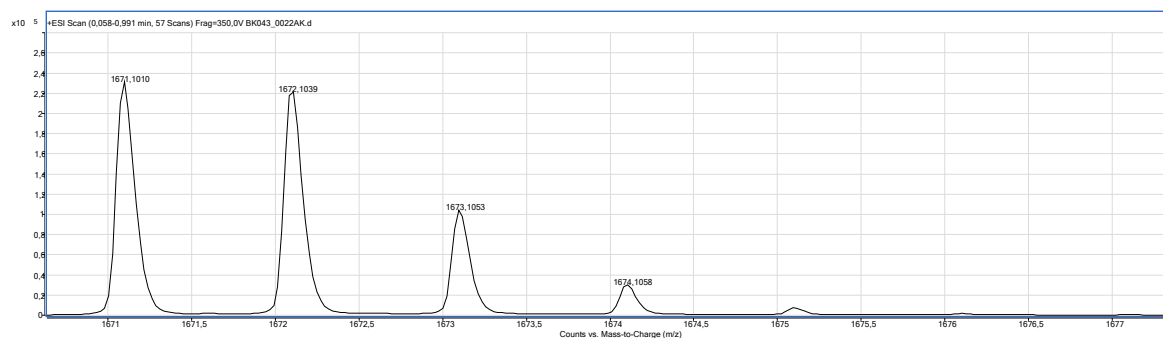


Figure S61: High resolution mass spectrometry (HRMS) spectrum of **AbuK14** in positive ionization mode (**zoom**).

Table S10: Comparison of ion species (M+H)⁺ both calc. and detected - **AbuK14**.

<u>Ion species (M+H)⁺ (calc.)</u>	<u>Ion species (M+H)⁺ (detected)</u>
1671,1156	1671,1010
1672,1185	1672,1039
1673,1212	1673,1053
1674,1239	1674,1058

4.6 Peptide sequence: AbuK15

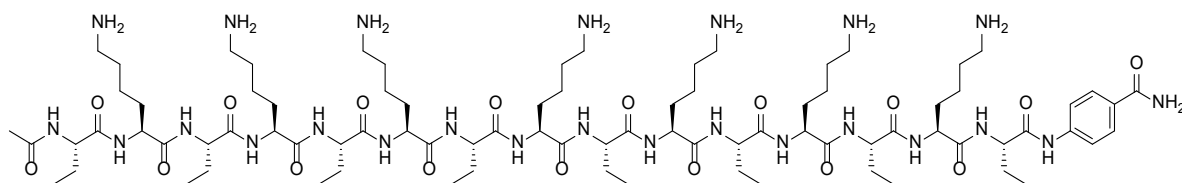


Figure S62: Chemical structure of peptide **AbuK15**.

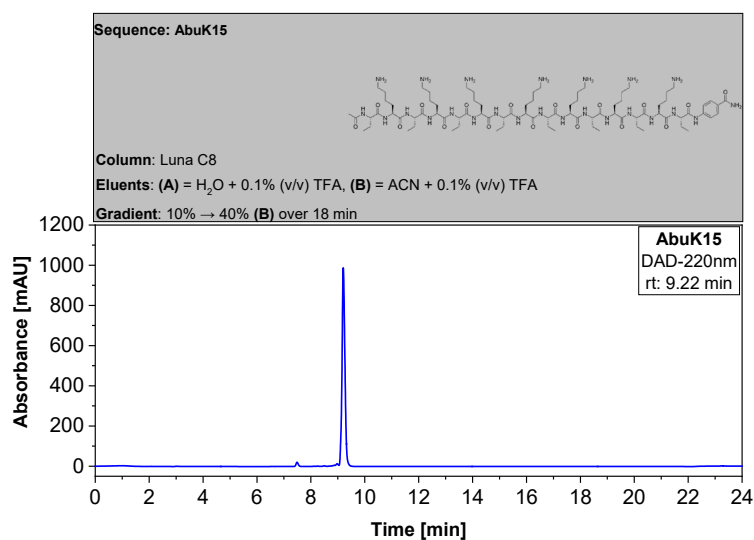


Figure S63: Analytical HPLC chromatogram of pure peptide **AbuK15**. HPLC: Hitachi Primaide

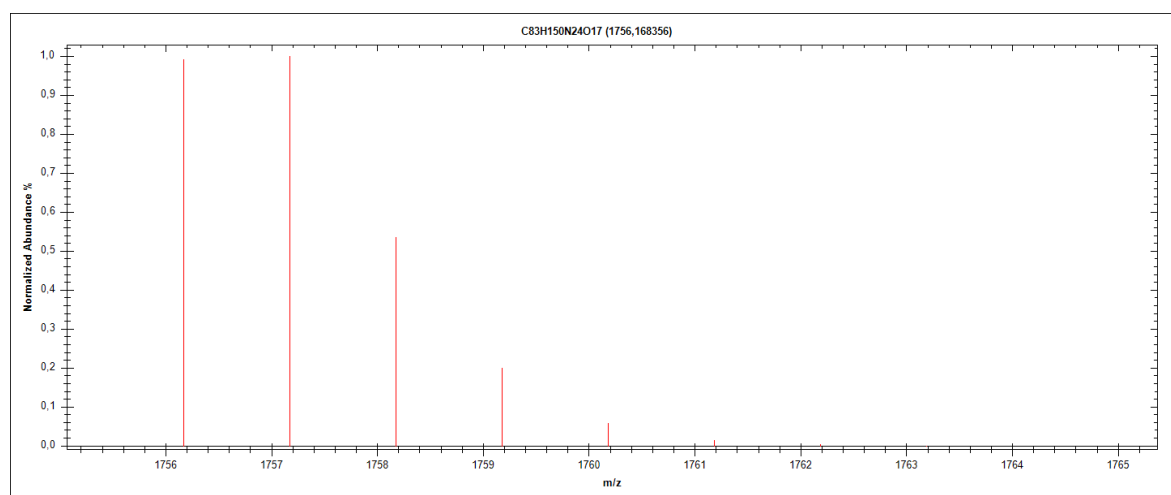


Figure S64: Calculated isotope distribution and mass intensity data for peptide **AbuK15**.

Table S11: Ion species (M+H)⁺ calculated for peptide sequence **AbuK15**.

<u>m/z</u> <u>Ion species (M+H)⁺</u>	<u>Abund</u> <u>(% largest)</u>
1756,1684	99,09
1757,1712	100
1758,1740	53,43
1759,1767	19,97

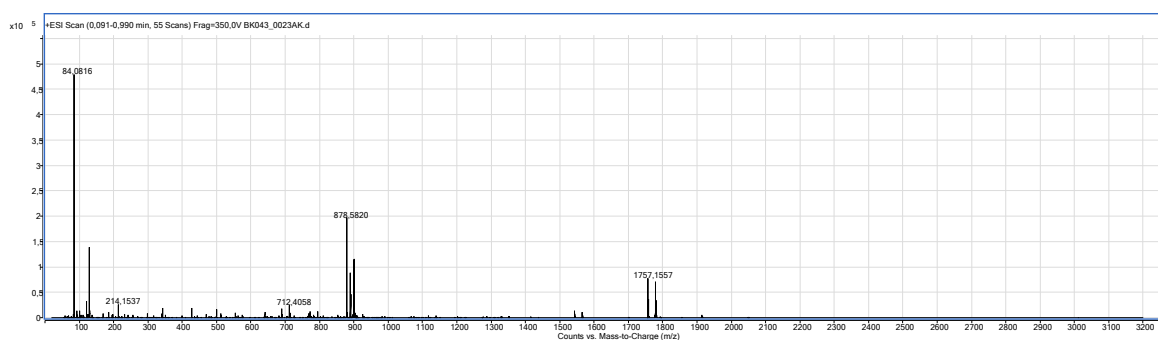


Figure S65: High resolution mass spectrometry (HRMS) spectrum of **AbuK15** in positive ionization mode (**unzoom**).

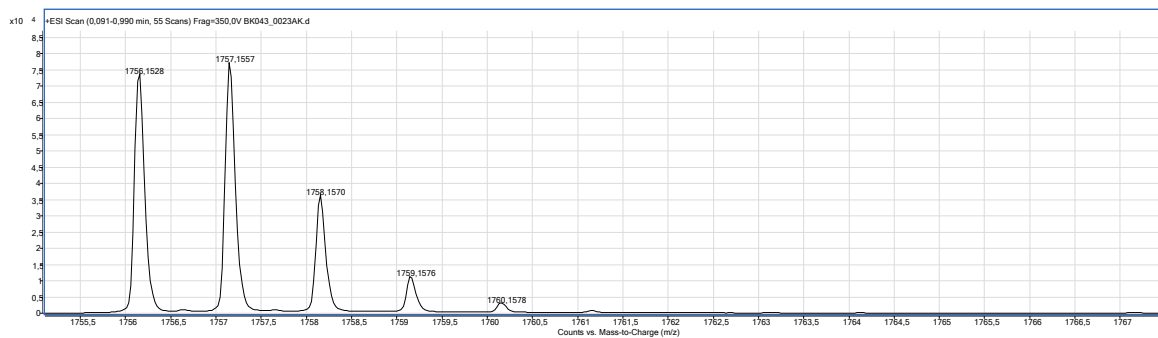


Figure S66: High resolution mass spectrometry (HRMS) spectrum of **AbuK15** in positive ionization mode (**zoom**).

Table 12: Comparison of ion species (M+H)⁺ both calc. and detected - **AbuK15**.

<u>Ion species (M+H)⁺ (calc.)</u>	<u>Ion species (M+H)⁺ (detected)</u>
1756,1684	1756,1528
1757,1712	1757,1557
1758,1740	1758,1570
1759,1767	1759,1576

4.7 Peptide sequence: AbuK16

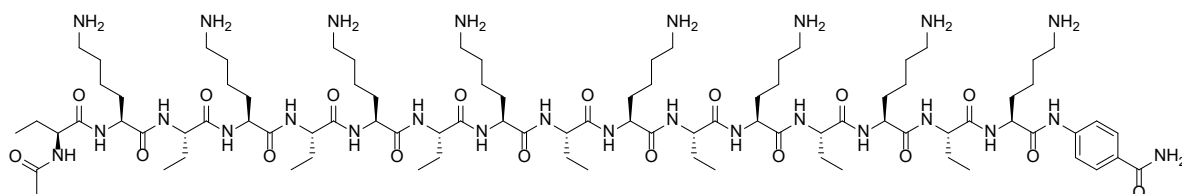


Figure S67: Chemical structure of peptide **AbuK16**.

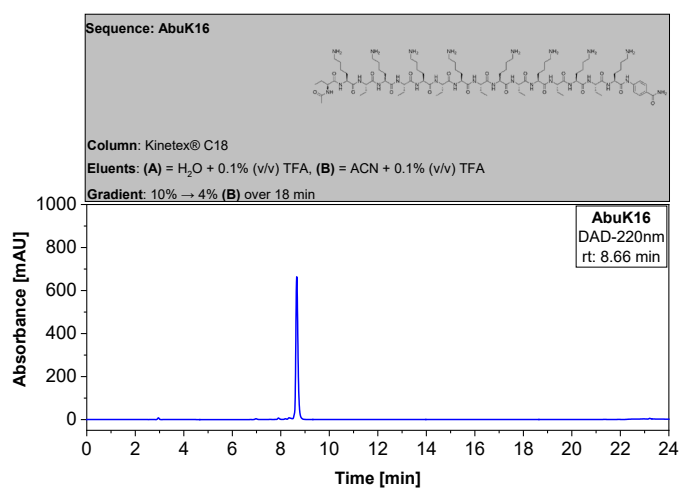


Figure S68: Analytical HPLC chromatogram of pure peptide **AbuK16**. HPLC: VWR Chromaster 600 bar.

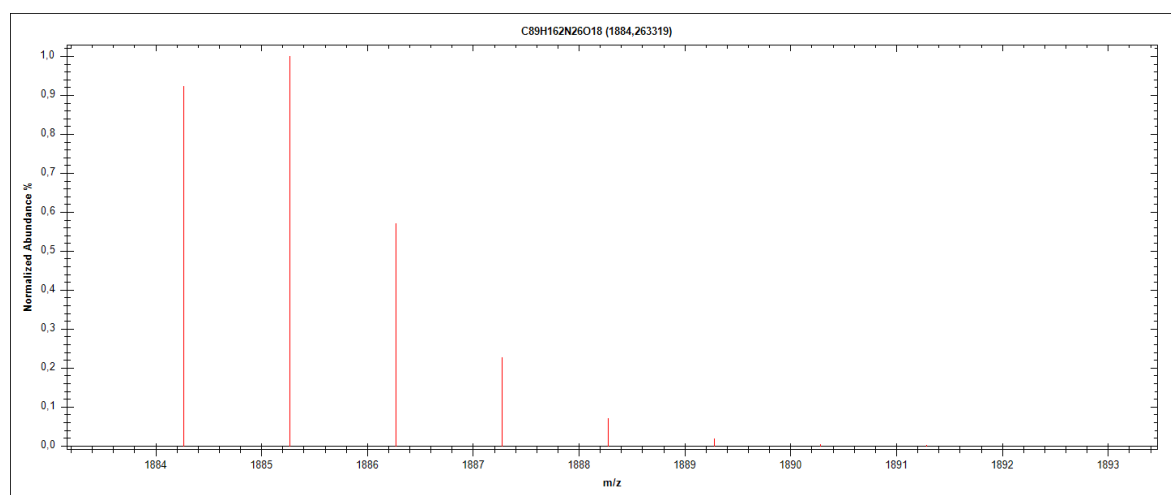


Figure S69: Calculated isotope distribution and mass intensity data for peptide **AbuK16**.

Table S13: Ion species (M+H)⁺ calculated for peptide sequence **AbuK16**.

<u>m/z</u> <u>Ion species (M+H)⁺</u>	<u>Abund</u> <u>(% largest)</u>
1884,2633	92,32
1885,2662	100
1886,2689	57,08
1887,2716	22,72

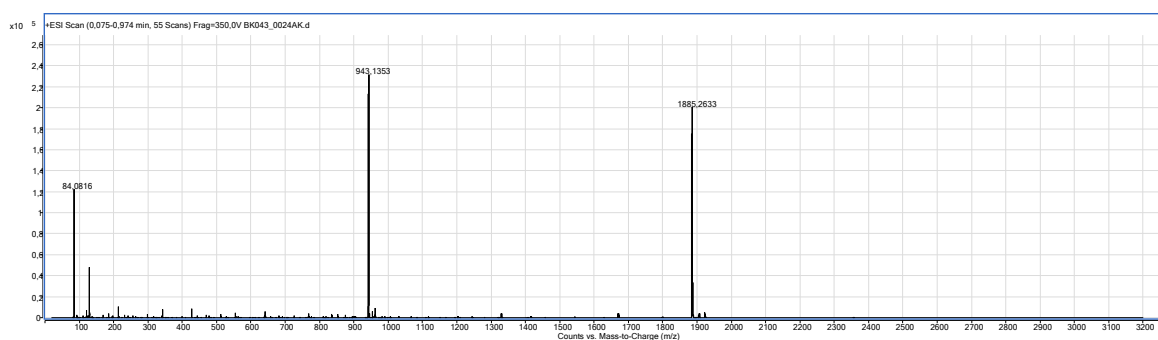


Figure S70: High resolution mass spectrometry (HRMS) spectrum of **AbuK16** in positive ionization mode (**unzoom**).

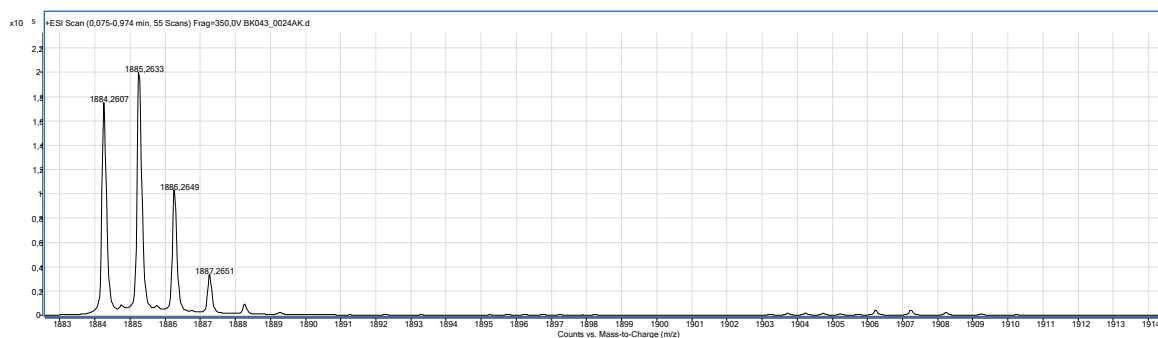


Figure S71: High resolution mass spectrometry (HRMS) spectrum of **AbuK16** in positive ionization mode (**zoom**).

Table S14: Comparison of ion species (M+H)⁺ both calc. and detected - **AbuK16**.

<u>Ion species (M+H)⁺ (calc.)</u>	<u>Ion species (M+H)⁺ (detected)</u>
1884,2633	1884,2607
1885,2662	1885,2633
1886,2689	1886,2649
1887,2716	1887,2681

4.8 Peptide sequence: MfeGlyK16

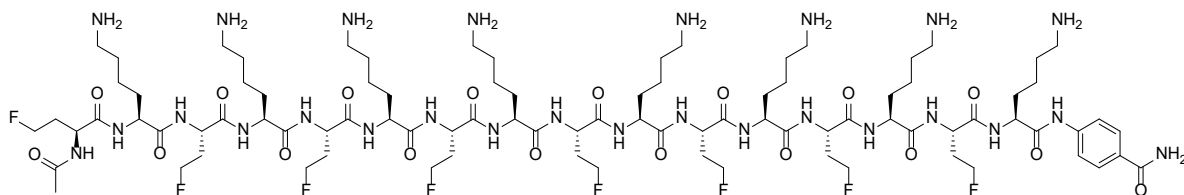


Figure S72: Chemical structure of peptide **MfeGlyK16**.

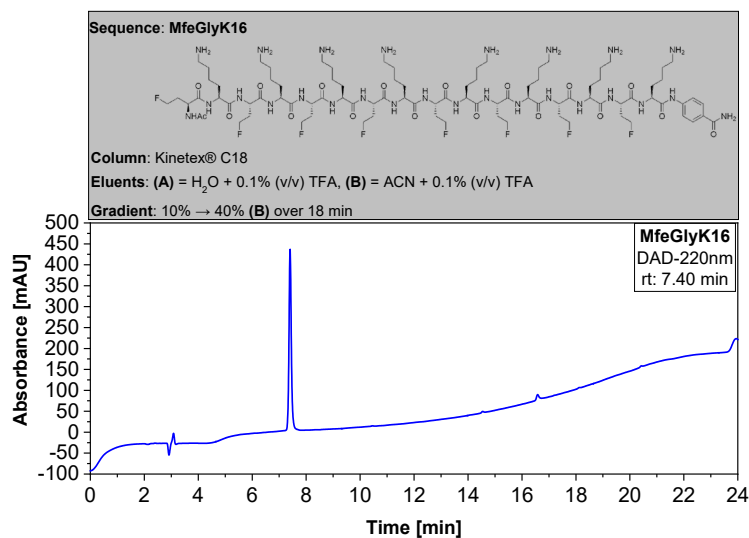


Figure S73: Analytical HPLC chromatogram of pure peptide **MfeGlyK16**. HPLC: VWR Chromaster 600 bar.

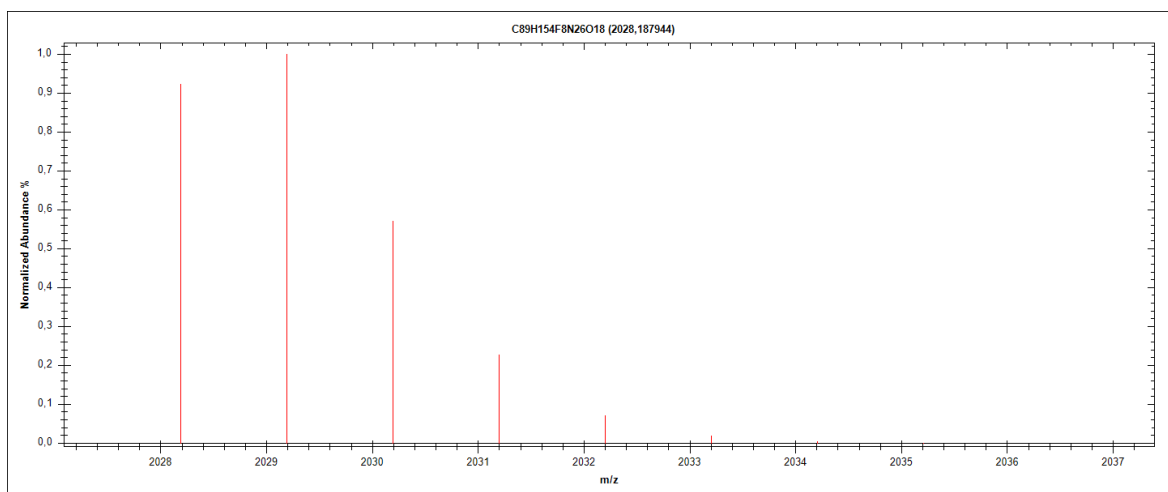


Figure S74: Calculated isotope distribution and mass intensity data for peptide **MfeGlyK16**.

Table S15: Ion species (M+H)⁺ calculated for peptide sequence **MfeGlyK16**.

<u>m/z</u> <u>Ion species (M+H)⁺</u>	<u>Abund</u> <u>(% largest)</u>
2028,1879	92,40
2029,1908	100
2030,1936	57,03
2031,1963	22,68

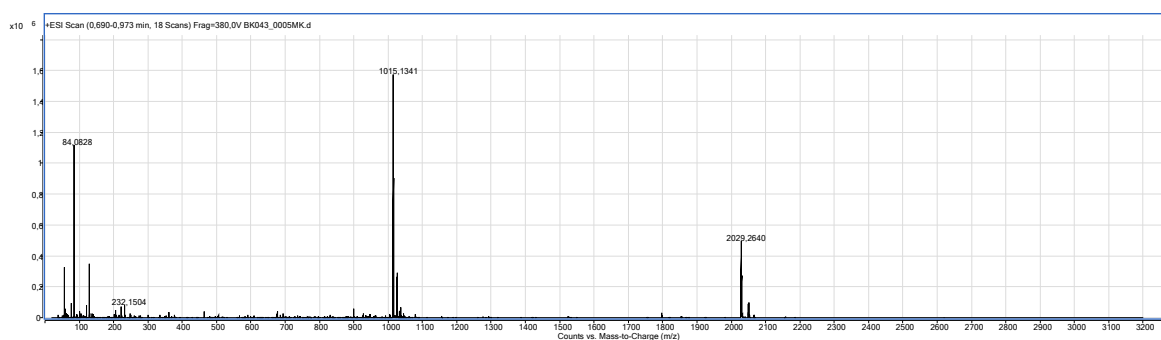


Figure S75: High resolution mass spectrometry (HRMS) spectrum of **MfeGlyK16** in positive ionization mode (**unzoom**).

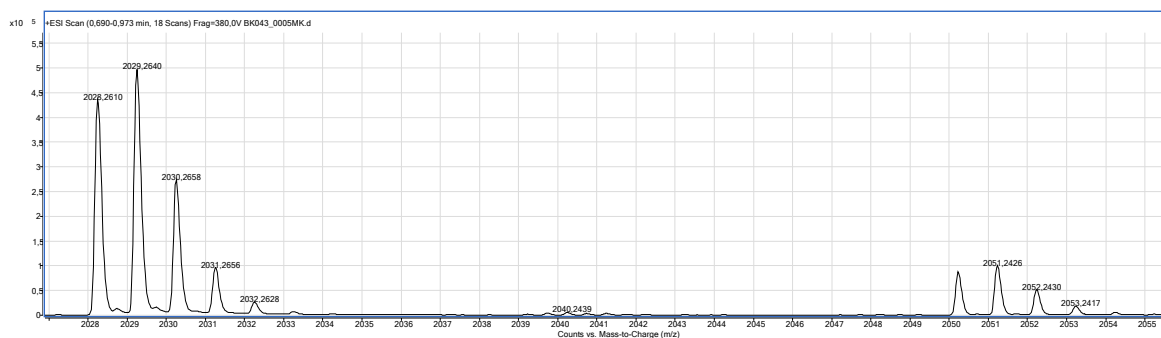


Figure S76: High resolution mass spectrometry (HRMS) spectrum of **MfeGlyK16** in positive ionization mode (**zoom**).

Table S16: Comparison of ion species (M+H)⁺ both calc. and detected - **MfeGlyK16**.

<u>Ion species (M+H)⁺ (calc.)</u>	<u>Ion species (M+H)⁺ (detected)</u>
2028,1879	2028,2610
2029,1908	2029,2640
2030,1936	2030,2658
2031,1963	2031,2656

4.9 Peptide sequence: DfeGlyK16

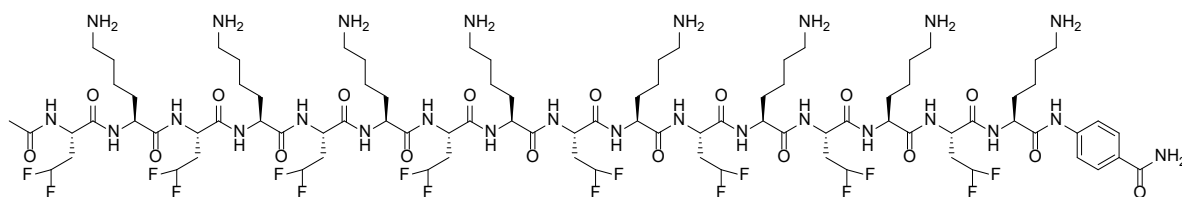


Figure S77: Chemical structure of peptide **DfeGlyK16**.

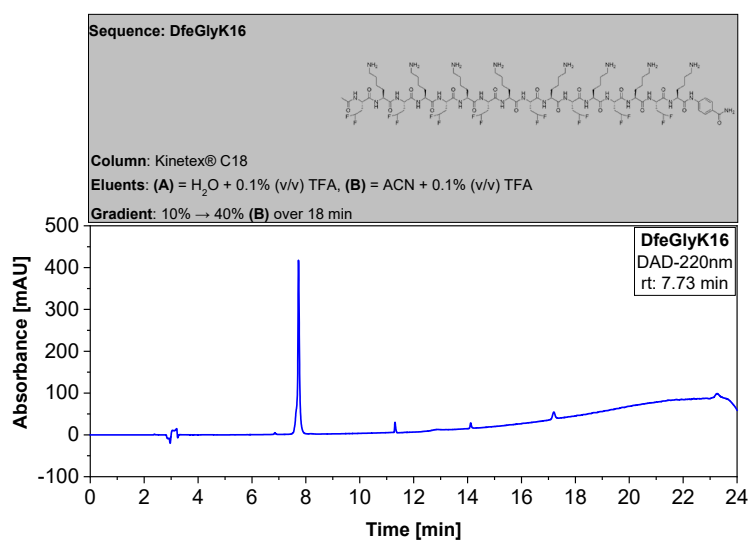


Figure S78: Analytical HPLC chromatogram of pure peptide **DfeGlyK16**. HPLC: VWR Chromaster 600 bar.

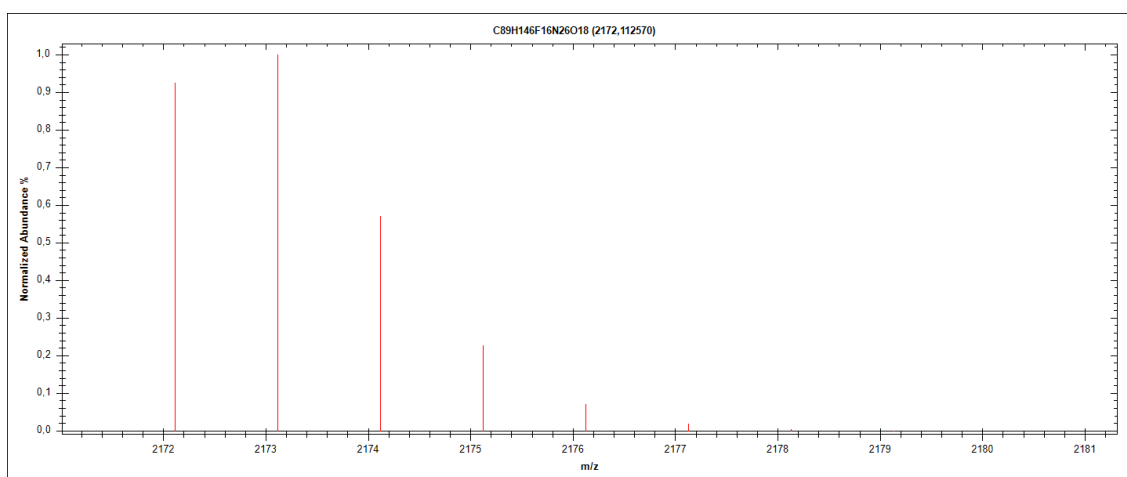


Figure S79: Calculated isotope distribution and mass intensity data for peptide **DfeGlyK16**.

Table S17: Ion species (M+H)⁺ calculated for peptide sequence **DfeGlyK16**.

<u>m/z</u> <u>Ion species (M+H)⁺</u>	<u>Abund</u> <u>(% largest)</u>
2172,1126	92,48
2173,1154	100
2174,1182	56,99
2175,1209	22,65

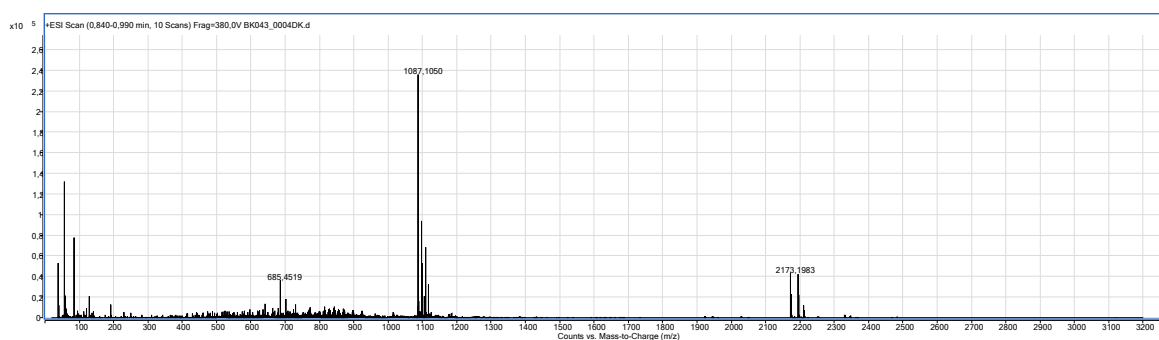


Figure S80: High resolution mass spectrometry (HRMS) spectrum of **DfeGlyK16** in positive ionization mode (**unzoom**).

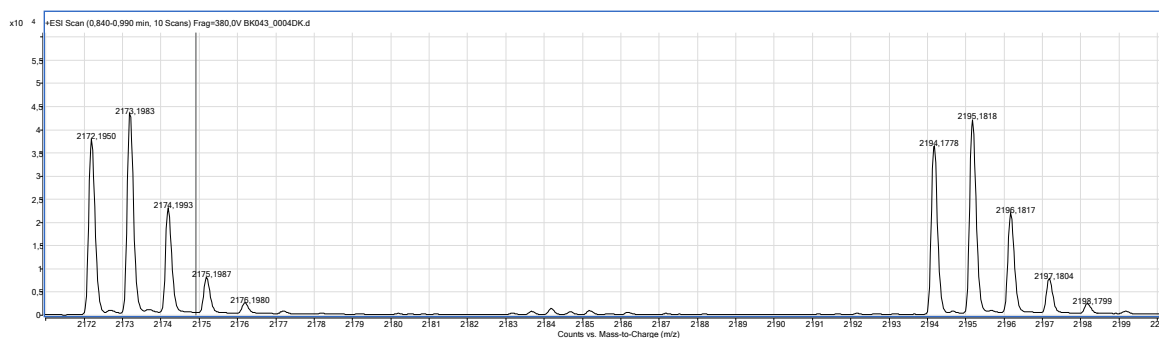


Figure S81: High resolution mass spectrometry (HRMS) spectrum of **DfeGlyK16** in positive ionization mode (**zoom**).

Table 18: Comparison of ion species (M+H)⁺ both calc. and detected – **DfeGlyK16**.

<u>Ion species (M+H)⁺ (calc.)</u>	<u>Ion species (M+H)⁺ (detected)</u>
2172,1126	2172,1950
2173,1154	2173,1983
2174,1182	2174,1993
2175,1209	2175,1987

4.10 Peptide sequence: TfeGlyK16

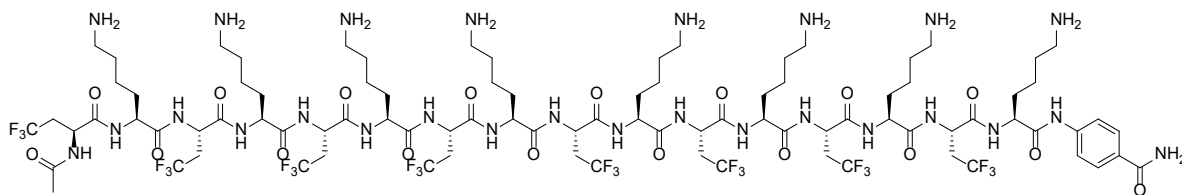


Figure S82: Chemical structure of peptide **TfeGlyK16**.

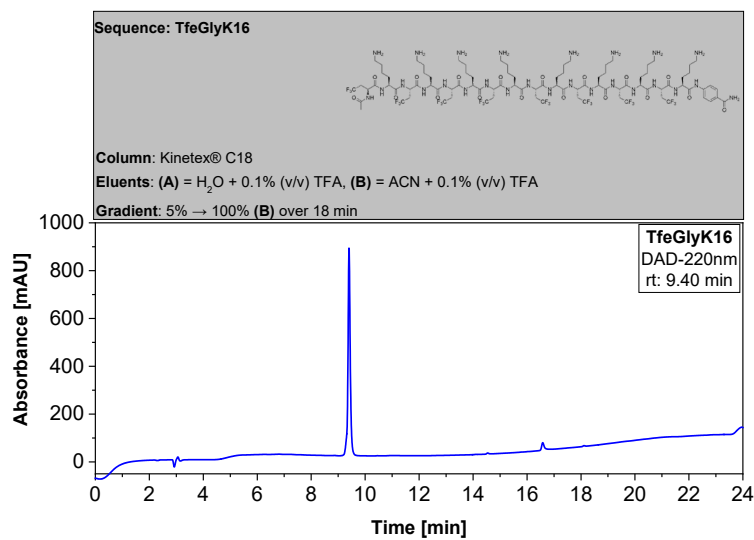


Figure S83: Analytical HPLC chromatogram of pure peptide **TfeGlyK16**. HPLC: VWR Chromaster 600 bar.

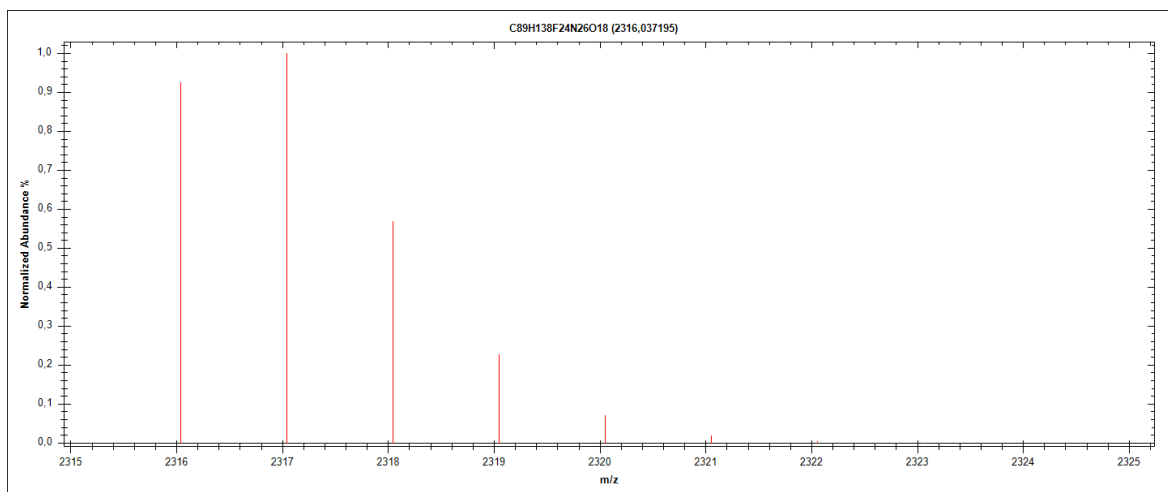


Figure S84: Calculated isotope distribution and mass intensity data for peptide **TfeGlyK16**.

Table S19: Ion species (M+H)⁺ calculated for peptide sequence **TfeGlyK16**.

<u>m/z</u> <u>Ion species (M+H)⁺</u>	<u>Abund</u> <u>(% largest)</u>
2316,0372	92,56
2317,0400	100
2318,0428	56,95
2319,0455	22,62

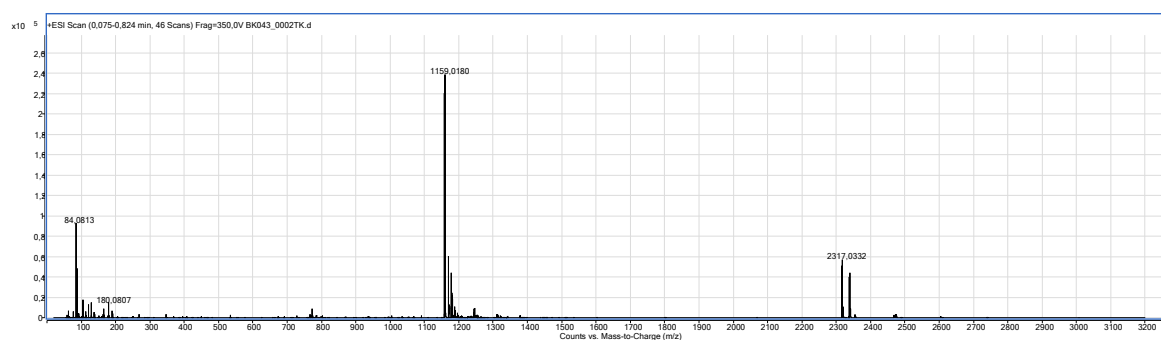


Figure S85: High resolution mass spectrometry (HRMS) spectrum of **TfeGlyK16** in positive ionization mode (**unzoom**).

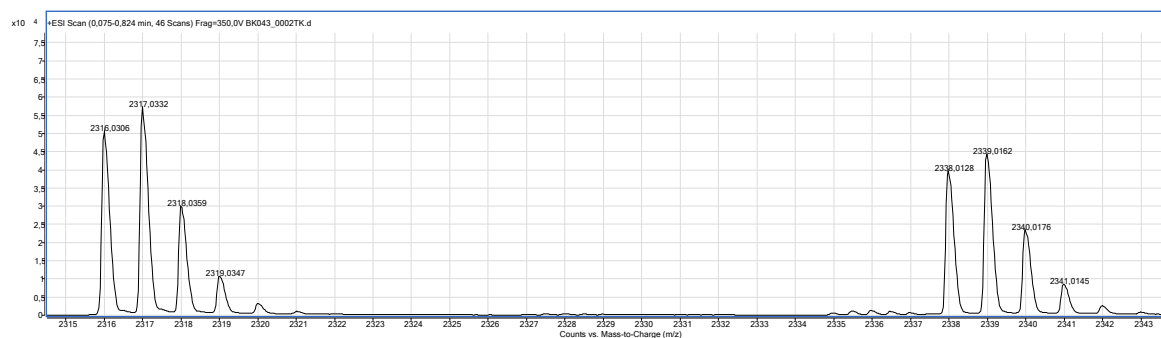


Figure S86: High resolution mass spectrometry (HRMS) spectrum of **TfeGlyK16** in positive ionization mode (**zoom**).

Table S20: Comparison of ion species (M+H)⁺ both calc. and detected – **TfeGlyK16**.

<u>Ion species (M+H)⁺ (calc.)</u>	<u>Ion species (M+H)⁺ (detected)</u>
2316,0372	2316,0306
2317,0400	2317,0332
2318,0428	2318,0359
2319,0455	2319,0347

4.11 Peptide sequence: LeuK16

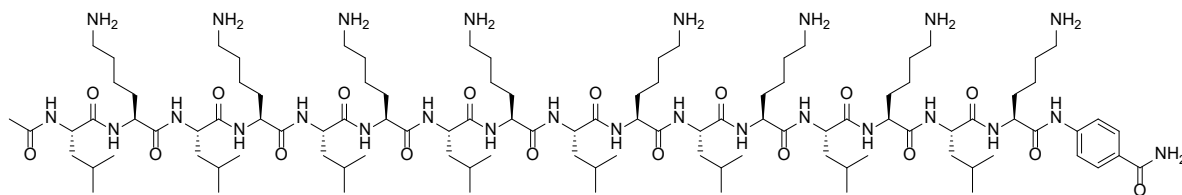


Figure S87: Chemical structure of peptide **LeuK16**.

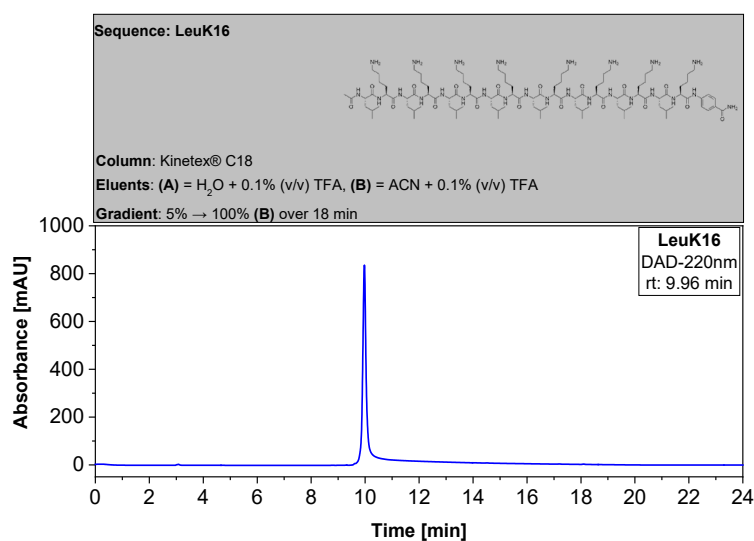


Figure S88: Analytical HPLC chromatogram of pure peptide **LeuK16**. HPLC: VWR Chromaster 600 bar.

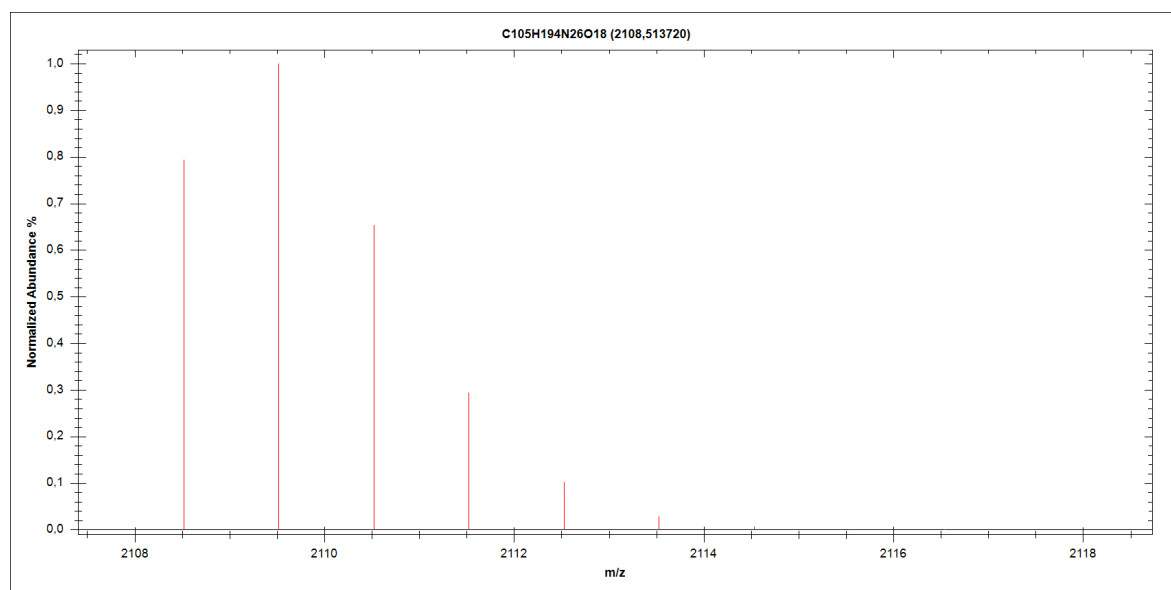


Figure S89: Calculated isotope distribution and mass intensity data for peptide **LeuK16**.

Table S21: Ion species (M+H)⁺ calculated for peptide sequence **LeuK16**.

<u>m/z</u> <u>Ion species (M+H)⁺</u>	<u>Abund</u> <u>(% largest)</u>
2108,5137	79,37
2109,5167	100
2110,5195	65.43
2111,5223	29,53

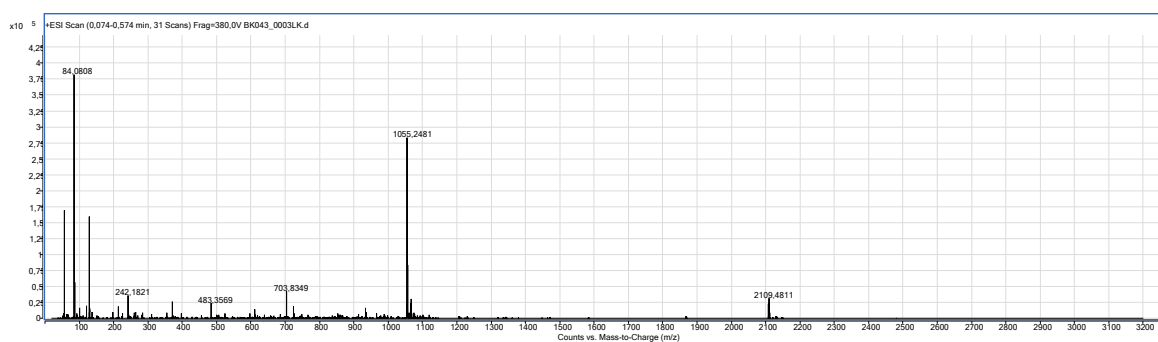


Figure S90: High resolution mass spectrometry (HRMS) spectrum of **LeuK16** in positive ionization mode (**unzoom**).

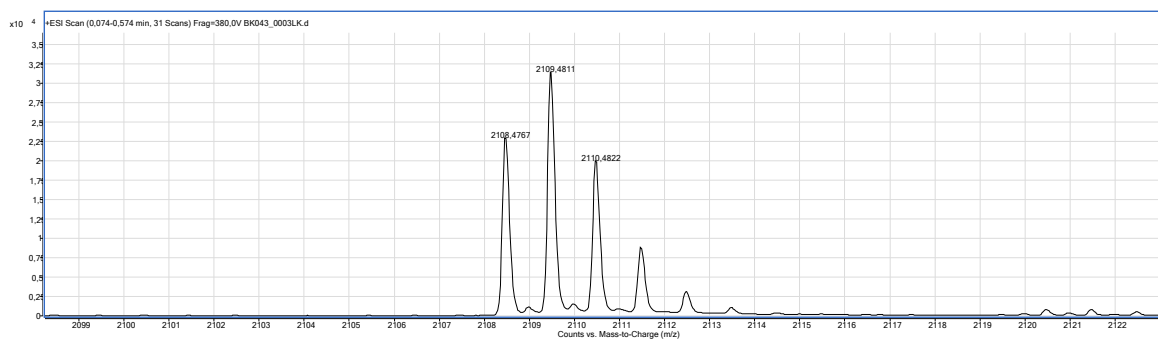


Figure S91: High resolution mass spectrometry (HRMS) spectrum of **LeuK16** in positive ionization mode (**zoom**).

Table S22: Comparison of ion species (M+H)⁺ both calc. and detected - **LeuK16**.

<u>Ion species (M+H)⁺ (calc.)</u>	<u>Ion species (M+H)⁺ (detected)</u>
2108,5137	2108,4767
2109,5167	2109,4811
2110,5195	2110,4822

5. Determination of peptide stock concentrations

To determine the concentration of each peptide stock in a reproducible and precise manner, we established a protocol for this purpose based on UV spectroscopy. Therefore, the commercially available dipeptide **H₂N-[4]Abz-Gly-OH** / *para*-aminohippuric acid (**PAH**) (Fluorochem, salt-free) was utilized as reference sample. This protocol is based on previous attempts by our group.¹²

PAH was dissolved in a 6M guanidinium hydrochloride solution, pH 7.4 and prepared in different concentrations (5 μ M, 15 μ M, 30 μ M, 50 μ M, 100 μ M, 150 μ M). A calibration curve was determined by measuring the UV absorbance (BioPhotometer plus photometer from Eppendorf, Hamburg, Germany) of each sample at 280 nm. Disposable PMMA cuvettes (Eppendorf, Hamburg, Germany) with path lengths of 10 mm were used.

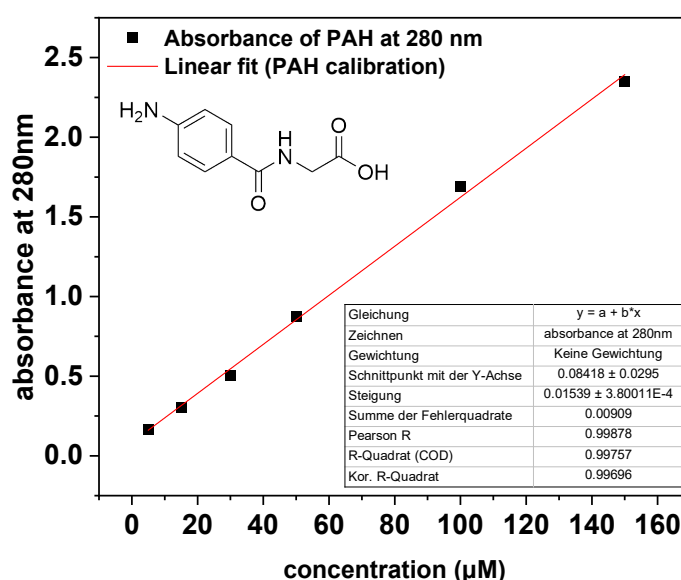


Figure S92: Calibration curve of **PAH** for the determination of peptide concentration stocks. UV absorbance was recorded at room temperature.

Then, aliquots (10 μ L) of respective peptide stocks (dissolved in HFIP) were taken and the solvent was evaporated using a gentle stream of N₂. The dried peptide film was redissolved in in a 6M guanidinium hydrochloride solution, pH 7.4 to achieve an overall peptide solution (1000 μ L) with a dilution factor (DL) of 100. UV absorbance was recorded at 280 nm and taken as mean value from three independent measurements. The concentration was calculated based on the equation $y = a + b \cdot x$ derived from a linear fit. (x = concentration in μ M)

6. CD spectroscopy: Further results

In this chapter, further CD spectra of this publication are presented and discussed.

6.1 CD Spectroscopy: AbuK10-16 – water / BTP buffer pH 9 – concentration: 2 wt%

We were surprised by the exclusive ability of **AbuK14** and **AbuK16** to undergo β -sheet formation which lacked for the truncated variants and **AbuK15**. So, we examined these peptides in only aqueous solutions (**Figure S93, a-b**), but also in buffered conditions with a more basic environment (pH 9) (**Figure S93,c-d**) to promote saturation of the positively charged lysine residues. CD spectra in water revealed the formation of PPII helices for all peptides, caused as expected by electrostatic and steric interactions of charged Lys side chains. Thus, adjustment of the buffer into more basic conditions enabled the conversion of helical structures into β -sheets for **AbuK12**, **AbuK14** and **AbuK16**, whereas **AbuK11**, **AbuK13** and **AbuK15** revealed indeterminable CD spectra. In consequence, the structural pattern given by an odd amount of amino acid residues of **AbuK11**, **AbuK13** and **AbuK15** has revealed to disrupt structure assembly in basic buffered environments, whereas we propose for **AbuK10** the truncated chain length as cause to withhold β -sheet formation.

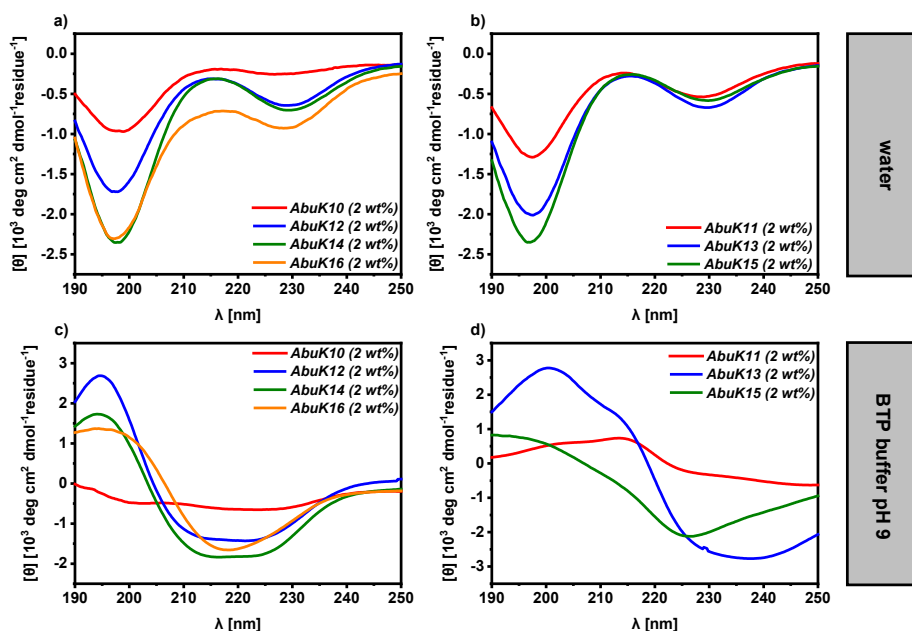


Figure S93: CD spectra of 2 wt% **AbuK10-AbuK16** in **a)** water and **b)** 50 mM Bis-tris propane + 150 mM NaCl, pH 9 recorded at 37 °C.

6.2 CD Spectroscopy: Salt effects and valency on secondary structure formation

(AbuK16, MfeGlyK16, DfeGlyK16, TfeGlyK16)

To test the stability of secondary structure formation with regards to **AbuK16**, **MfeGlyK16**, **DfeGlyK16** and **TfeGlyK16** towards several types of salts, especially with respect to mono-/divalent cationic species, CD measurements were performed with different types of buffered conditions (**Figure S94**).

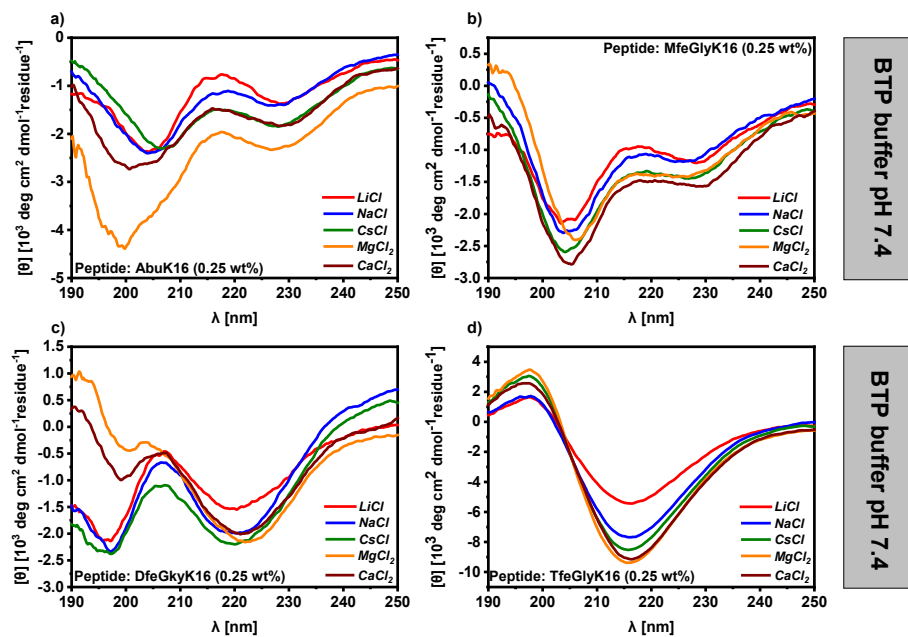


Figure S94: CD spectra of 0.25 wt% a) **AbuK16**; b) **MfeGlyK16**; c) **DfeGlyK16**; d) **TfeGlyK16** in 50 mM Bis-tris propane with 150 mM LiCl, NaCl, CsCl, MgCl₂ or CaCl₂, pH 7,4 recorded at 37 °C.

It was found that the CD signal intensity increased when rising the valency of salt as seen for LiCl compared to MgCl₂ and CaCl₂. Beside this finding, we conclude that all selected sequences were capable to undergo peptide folding despite selected cationic source.

6.3 CD Spectroscopy: Impact of non-aqueous solvents on secondary structure

formation (**AbuK16**, **MfeGlyK16**, **DfeGlyK16**, **TfeGlyK16**)

We aimed to study peptide folding of synthetic oligopeptides (**AbuK16**, **MfeGlyK16**, **DfeGlyK16**, **TfeGlyK16**) dissolved in a polar protic (MeOH), aprotic (ACN) and fluorinated (TFE) solvent. Examination of secondary structures were executed to provide an overview about the structural potentials of these novel systems (see **Figure S95**).

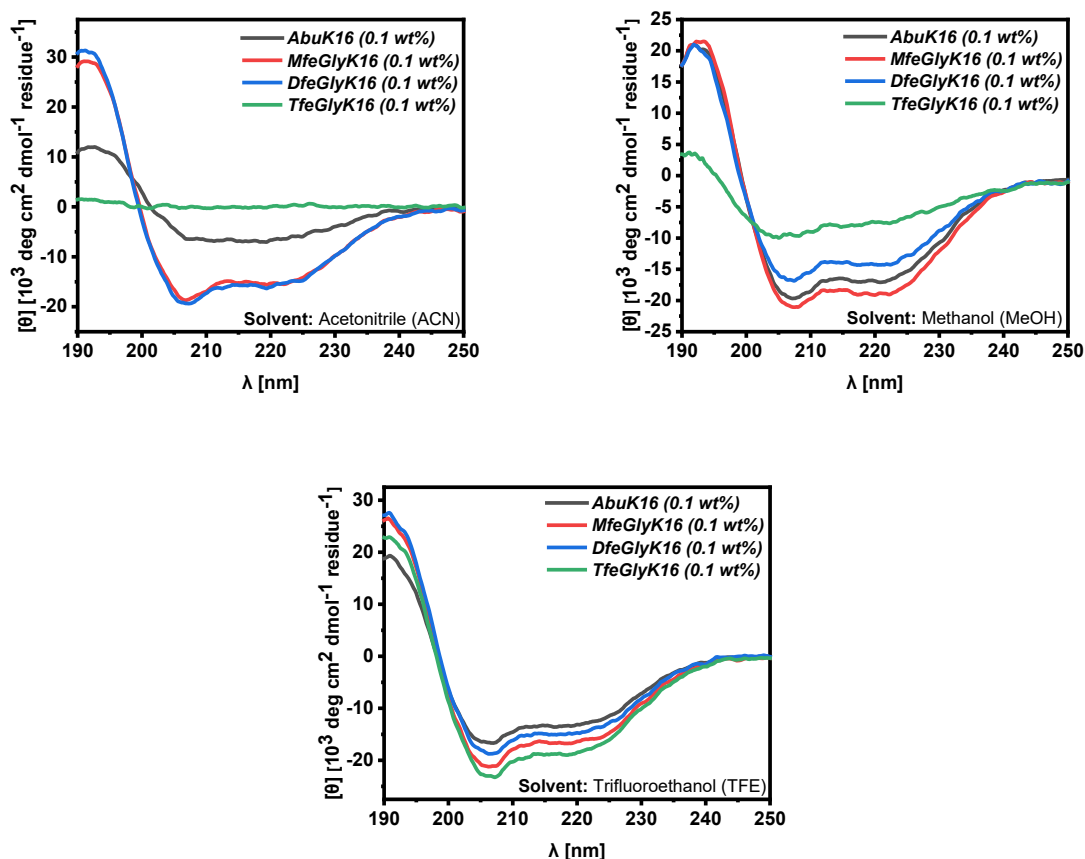


Figure S95: CD spectra of 0.1 wt% **AbuK16**; **MfeGlyK16**; **DfeGlyK16**; **TfeGlyK16** in Acetonitrile (ACN), methanol (MeOH) or 2,2,2-trifluoroethanol (TFE) recorded at 37 °C.

For most cases, the formation of α -helical structures was observed. With respect to selected solvents, these findings are in accordance with previous reports, highlighting stabilizing hydrogen bonding between the peptide-backbones and, simultaneously, weakening hydrophobic interactions as cause for helical assemblies.¹³⁻¹⁶ As PPII helices were observed for **AbuK16** and **MfeGlyK16** in aqueous buffered conditions, we propose an enhancement in peptide-peptide hydrogen bonding due to MeOH, ACN and TFE. In pure ACN, we observed precipitation of the peptide **TfeGlyK16** as represented by a lack of a defined CD spectrum. Similar results were described by Shen *et al.* by exposing an enhanced fibril growth for the β -amyloid peptide by an increased amount of ACN in water.¹⁷

7. Characterization of reference sequence LeuK16

The aliphatic oligopeptide **LeuK16** was synthesized to distinguish between hydrophobic effects and fluorine-specific interactions. Therefore, the *Leu-Lys* repeating unit was reported as a core segment to produce comparably stiff hydrogel matrices.¹⁸ We also characterized this peptide through CD spectroscopy and estimated its hydrophobic properties (RP-HPLC assay) (**Figure S96**).

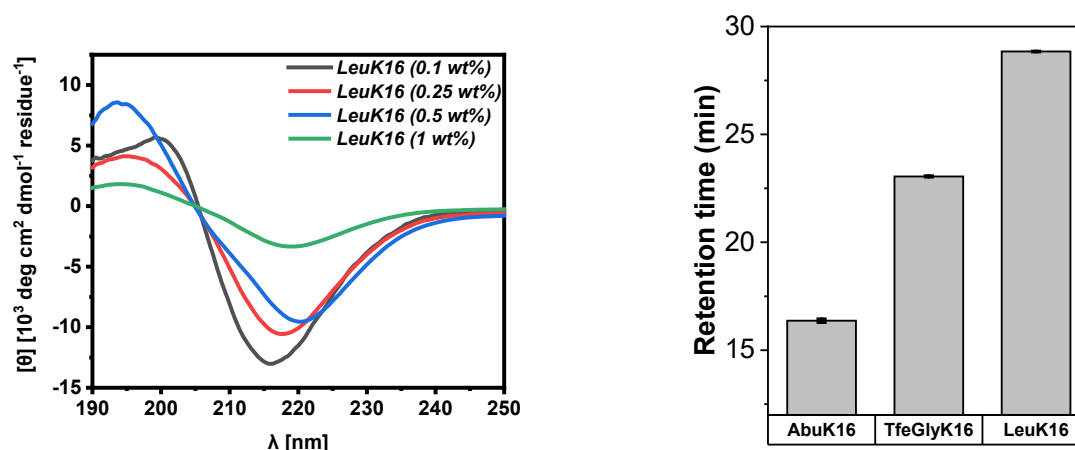


Figure S96: (left) CD spectra of 0.1- 1 wt% **LeuK16** in 50 mM Bis-tris propane + 150 mM NaCl, pH 7,4 recorded at 37 °C; (right) Estimation of hydrophobicity of **LeuK16** (28.842 ± 0.025 min) in comparison to **AbuK16** (16.368 ± 0.087 min) and **TfeGlyK16** (23.054 ± 0.031 min) [RP-HPLC assay].

The peptide **LeuK16** formed β -sheets in selected buffered system but was found to be significantly more hydrophobic than **TfeGlyK16** as determined through a RP-HPLC assay. This outcome is not surprising due to the larger size and branched pattern of the aliphatic side chain of Leu as compared to **TfeGly**.¹⁹ Obviously, the enhanced hydrophobicity in combination to the side chain of leucine led to the formation of comparably stiffer hydrogel matrices than for **TfeGlyK16** at pH 7.4.

8. Detection of amyloid-like fibrils: Congo red (CR) UV-spectroscopy

To further confirm the presence of amyloid-like fibrils, we applied congo red (CR) UV-spectroscopy to **AbuK16**, **MfeGlyK16**, **DfeGlyK16** and **TfeGlyK16**. As shown in **Figure S97**, the binding of CR to amyloid-like fibrils leads to an increase in UV intensity (550 - 450 nm) of this dye. Hence, we observed an overall increase in CR-derived UV absorbance only for **DfeGlyK16** & **TfeGlyK16** at a concentration of 0.5 wt% (pH 7.4), resembling their ability to form β -sheets at given conditions. For **AbuK16** and **MfeGlyK16**, the detected values of UV absorbance equaled to the spectra obtained for the buffer solely containing CR (black line). Consequently, an intercalation of this dye in fibrillar assemblies was not found. To disclaim any influence of the peptide's nature on determined UV signal intensity, we also measured UV spectra of these peptide only in BTP buffer. The slight increase in UV absorbance at 300 nm is derived from the C-terminal **[4]Abz** label.

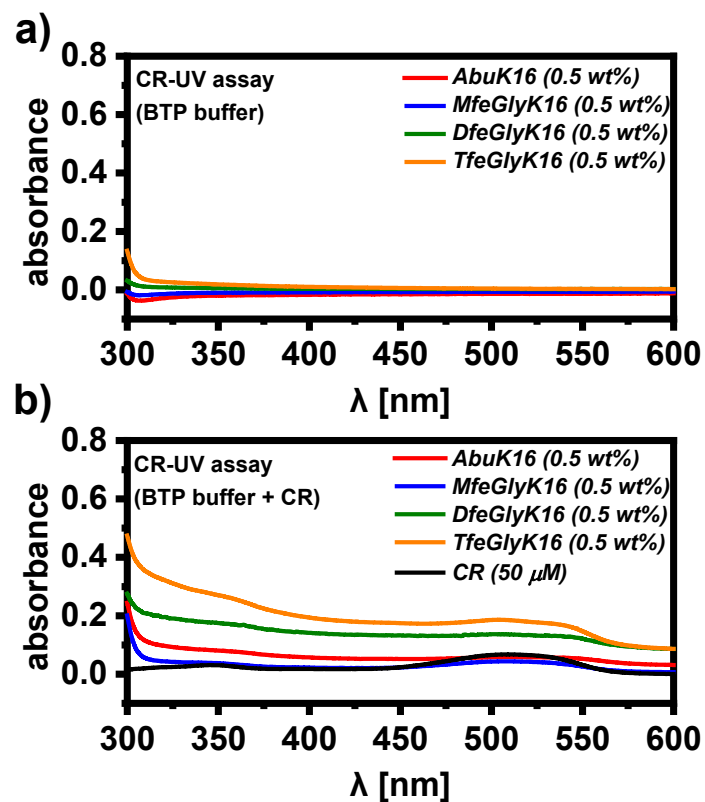


Figure S97: UV spectra (600 - 300 nm) of amphipathic peptides incubated in **a)** 50 mM bis-tris propane + 150 mM NaCl, pH 7,4 and **b)** in 50 mM bis-tris propane + 150 mM NaCl, pH 7,4 + 50 μ M CR. Additionally, a blank sample only containing buffer and congo red was recorded as reference (black line). All samples were measured after prior incubation at 37°C overnight (minimum 15 h).

9. Further cryoEM micrographs (AbuK14, AbuK16, MfeGlyK16, DfeGlyK16, TfeGlyK16)

AbuK14 – 2 wt% (10-fold dilution)

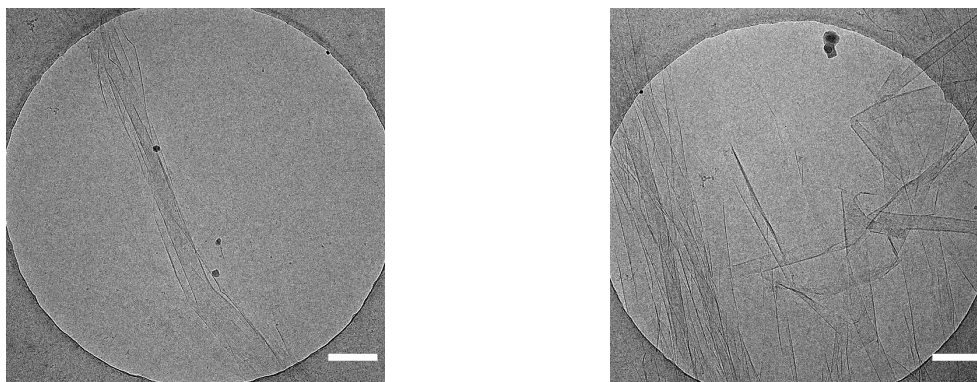


Figure S98: Cryo-EM micrographs of **AbuK14** (2 wt% (10-fold dilution)) dissolved in 50 mM Bis-tris propane + 150 mM NaCl, pH 7.4. The sample was prepared in a concentration of 2 wt% to trigger β -sheet formation and then diluted to 0.2 wt%. The scale bar denotes 200 nm each

AbuK16 - 0.25 wt% + 2 wt% (10-fold dilution)

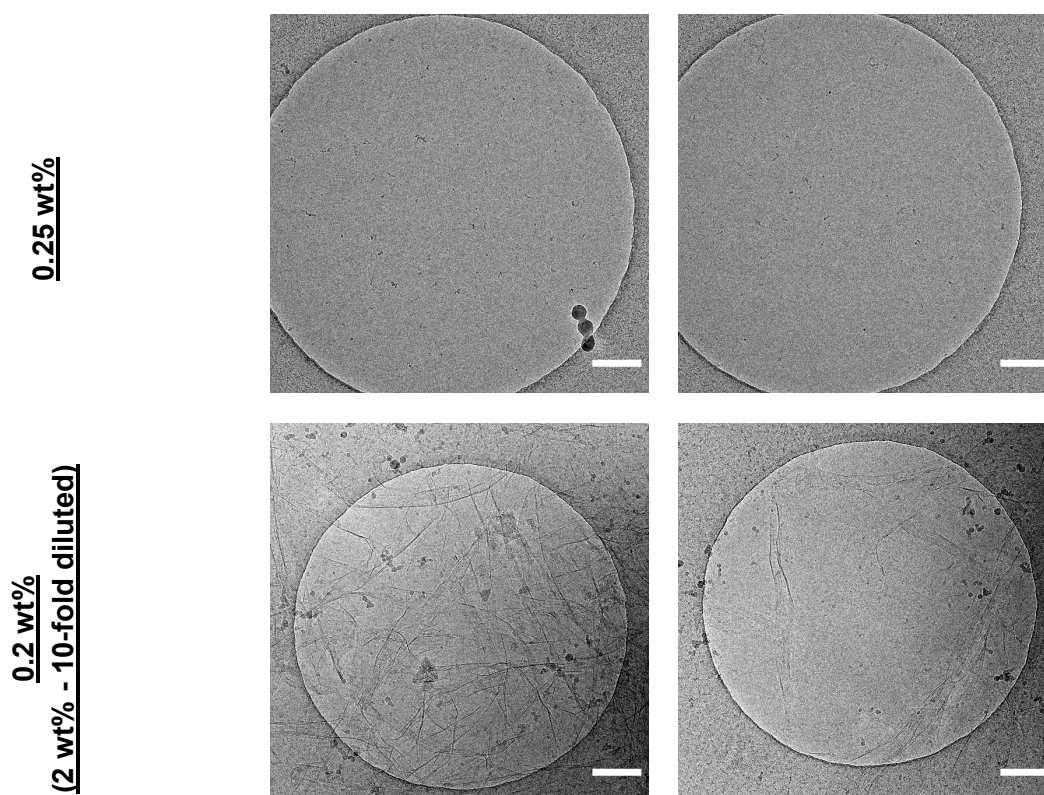


Figure S99: Cryo-EM micrographs of **AbuK16** (0.25 wt%) & (2 wt% (10-fold dilution)) dissolved in 50 mM Bis-tris propane + 150 mM NaCl, pH 7.4. The scale bar denotes 200 nm each.

MfeGlyK16 – (0.25 wt%)

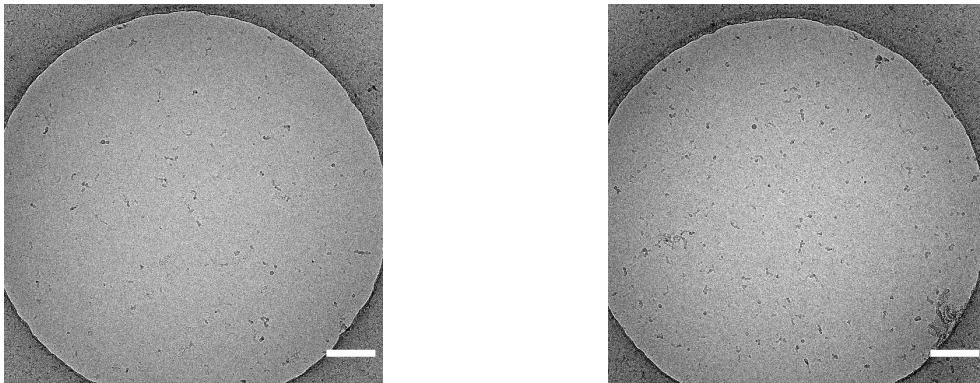


Figure S100: Cryo-EM micrographs of **MfeGlyK16** (0.25 wt%) dissolved in 50 mM Bis-tris propane + 150 mM NaCl, pH 7.4. The scale bar denotes 200 nm each.

DfeGlyK16 – (0.25 wt%)

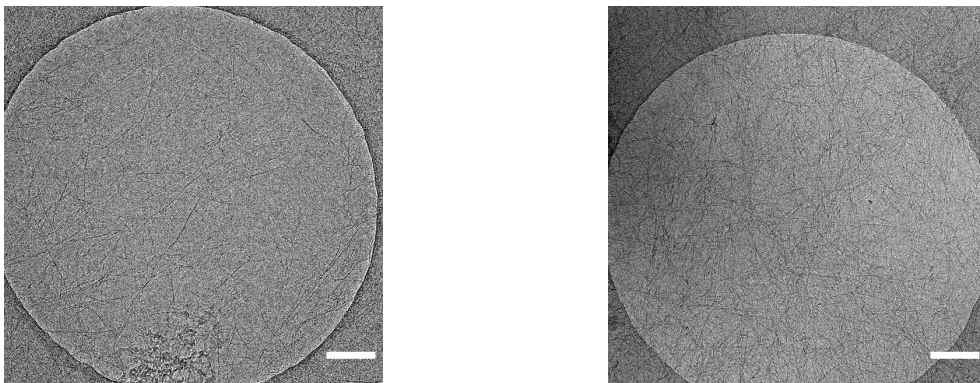


Figure S101: Cryo-EM micrographs of **DfeGlyK16** (0.25 wt%) dissolved in 50 mM Bis-tris propane + 150 mM NaCl, pH 7.4. The scale bar denotes 200 nm each.

TfeGlyK16 - 0.1 wt% + 2 wt% (10-fold dilution)

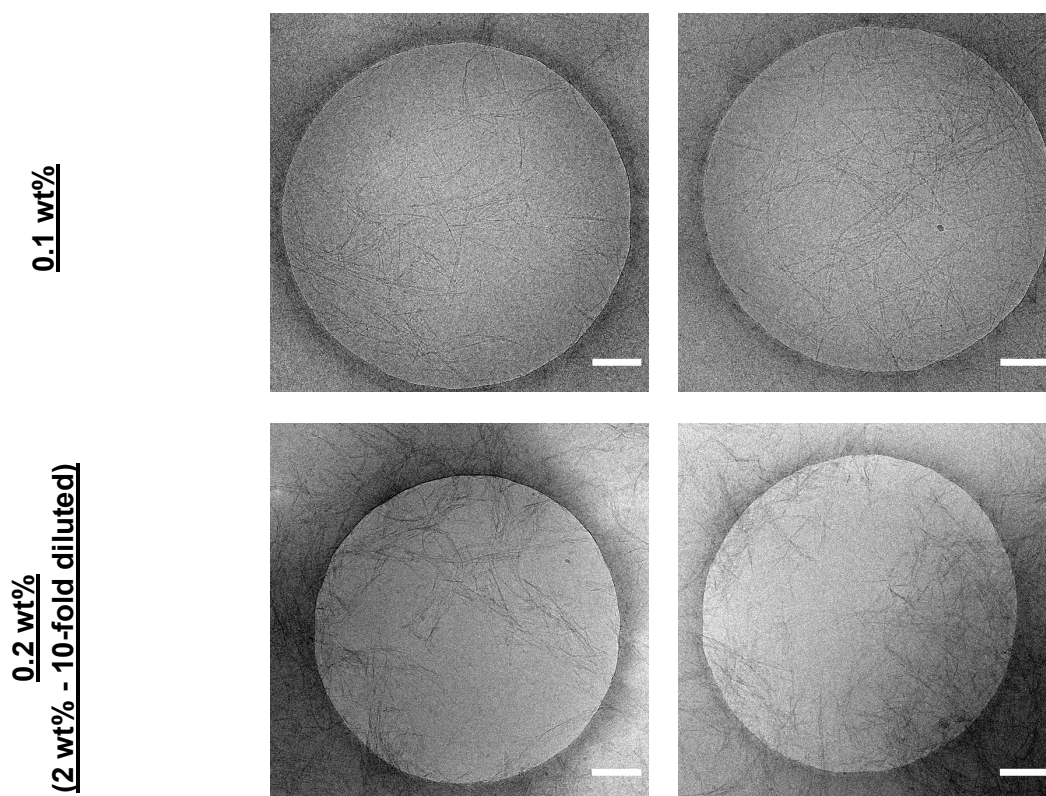


Figure S102: Cryo-EM micrographs of **TfeGlyK16** (0.1 wt%) & (2 wt% (10-fold dilution)) dissolved in 50 mM Bis-tris propane + 150 mM NaCl, pH 7.4. The scale bar denotes 200 nm each.

10. Inversion tests of peptide-based hydrogels

A protocol for the inversion test was previously reported by our group.²⁰ Peptide hydrogels composing of lyophilized samples **AbuK16**, **DfeGlyK16**, **TfeGlyK16** and **LeuK16** were dissolved in glass vial, mixed for 30 s to obtain a homogeneous mixture and incubated overnight with gentle shaking. It was avoided to implement any mechanical stress (e.g. centrifugation) in order to inhibit disruption in hydrogel formation. On the next day, sample vials were inverted for 24 h at room temperature. This was done to initially gain an idea about potential rigidity of resulting fibril matrices (**Figure S103**).

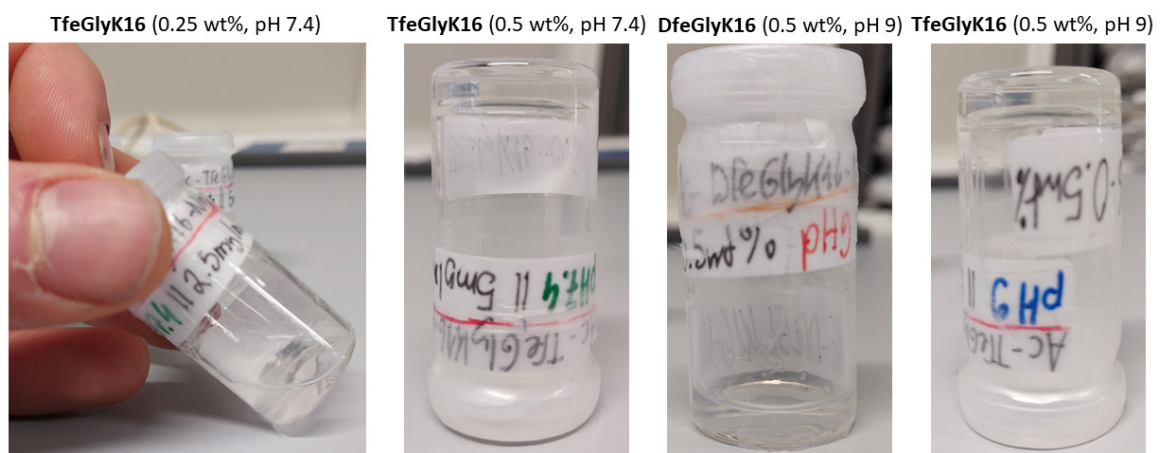


Figure S103: Selected photographs of hydrogel samples consisting of the peptide sequences **DfeGlyK16** & **TfeGlyK16**. The diameter of each glass vial was **10 mm**.

11. Rheological characterization of aliphatic oligopeptides – Further data

To determine the optimal deformation for oscillatory rheology experiments, amplitude sweeps are performed prior to each experiment. The frequency is fixed at 1 Hz and the strain γ is varied from 0.01 to 10%. The linear viscoelastic regime (LVE) is limited by the critical deformation γ^* . For $\gamma < \gamma^*$, we observe a plateau. To measure the linear response in oscillatory measurements without irreversibly breaking the three-dimensional network, the strain should be chosen such that it is smaller than γ^* . For all oscillatory measurements, γ was set to 0.1%, which is within the LVE.

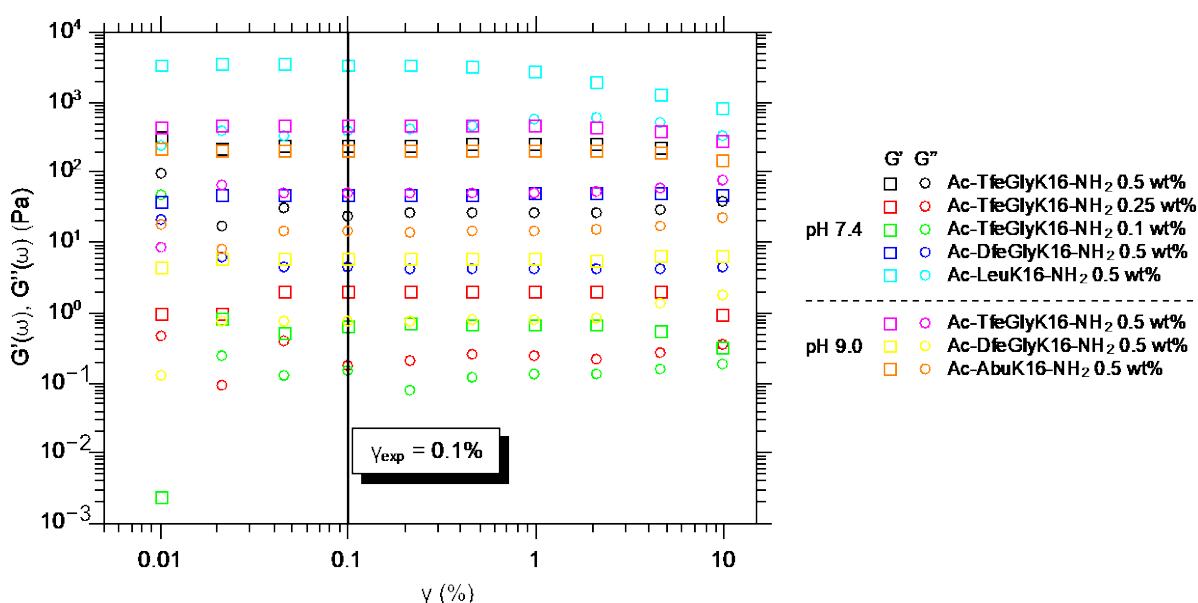


Figure S104: Amplitude sweeps for all measured samples, performed at $T = 37^\circ\text{C}$ and at constant angular frequency $\omega = 0.628$ rad/s. To stay in the linear viscoelastic regime (LVE), the strain γ for all subsequent oscillatory measurements was set to $\gamma_{exp} = 0.1\%$.

To confirm the surprising findings about the behavior of **TfeGlyK16** [Ac-TfeGlyK16-NH₂] in relation to **DfeGlyK16** [Ac-DfeGlyK16-NH₂] upon increasing the pH, the measurements were repeated with newly prepared samples. The results of the frequency sweeps are shown in **Figure S105**. The absolute values differ significantly, most likely due to small irregularities in concentration and/or time between preparation and measurement. The principle finding concerning the reversal in the trend of the plateau modulus G_0 however remains the same. For a detailed representation, we plotted the plateau modulus and mesh size as a function of the number of fluorine atoms on the peptide side chain at pH 9 (**Figure S106**).

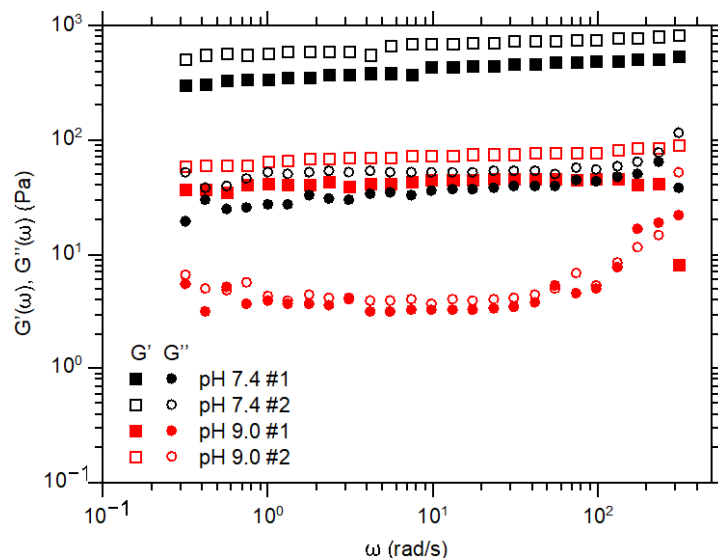


Figure S105: Repeated frequency sweeps for **TfeGlyK16** [Ac-TfeGlyK16-NH₂] at pH 7.4 and 9.0. The absolute values differ substantially, but the trends remain unchanged.

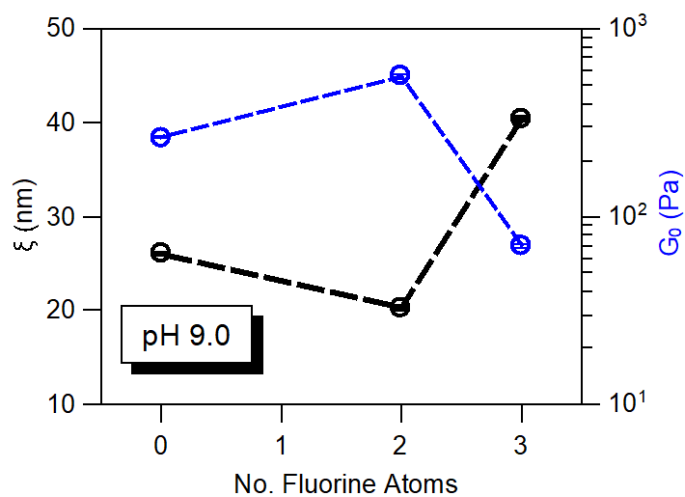


Figure S106: Plateau moduli G_0 (blue symbols) and mesh sizes ξ (black symbols) for the **GlyK16** peptides (**0-AbuK16**, **2-DfeGlyK16**, **3-TfeGlyK16**) shown as a function of the number of fluorine atoms on the side chain.

12. MD simulations of (polyfluorinated) amphipathic peptides

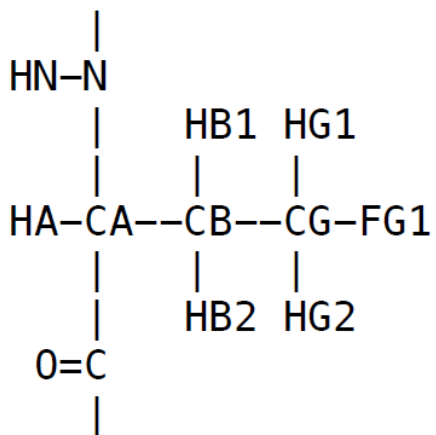
Here, we present atom names, atom types (derived from the parameter sets of CHARMM36m and CGenFF), optimized partial atomic charges, and topologies of **Abu**, **MfeGly**, **DfeGly**, and **TfeGly**. For optimization, partial charges on the protein backbone atoms (top and bottom groups) are fixed to that given in the CHARMM36m force field, to be consistent with other amino acids, and partial charges on the side chain atoms (the middle group) are varied to reproduce the QM water interaction energy.

12.1 Optimized partial charges on Abu

RESI	ABU		0.000		
GROUP					
ATOM	N	NH1	-0.47	!	
ATOM	HN	H	0.31	!	HN-N
ATOM	CA	CT1	0.07	!	
ATOM	HA	HB1	0.09	!	HB1 HG1
GROUP				!	HA-CA--CB--CG-HG3
ATOM	CB	CT2	-0.162	!	
ATOM	HB1	HA2	0.09	!	
ATOM	HB2	HA2	0.09	!	0=C
ATOM	CG	CT3	-0.288	!	
ATOM	HG1	HA3	0.09		
ATOM	HG2	HA3	0.09		
ATOM	HG3	HA3	0.09		
GROUP					
ATOM	C	C	0.51		
ATOM	O	O	-0.51		

12.2 Optimized partial charges on MfeGly

RESI	MFA		0.000	
GROUP				
ATOM	N	NH1	-0.47	!
ATOM	HN	H	0.31	!
ATOM	CA	CT1	0.07	!
ATOM	HA	HB1	0.09	!
GROUP				
ATOM	CB	CT2	-0.120	!
ATOM	HB1	HA2	0.090	!
ATOM	HB2	HA2	0.090	!
ATOM	CG	CG322	-0.063	!
ATOM	HG1	HGA6	0.111	
ATOM	HG2	HGA6	0.111	
ATOM	FG1	FGA1	-0.219	
GROUP				
ATOM	C	C	0.51	
ATOM	O	O	-0.51	



12.3 Optimized partial charges on DfeGly

RESI	DFA		0.000		
GROUP					
ATOM	N	NH1	-0.47	!	
ATOM	HN	H	0.31	!	HN-N
ATOM	CA	CT1	0.07	!	
ATOM	HA	HB1	0.09	!	
GROUP					
ATOM	CB	CT2	-0.127	!	
ATOM	HB1	HA2	0.090	!	
ATOM	HB2	HA2	0.090	!	0=C
ATOM	CG	CG312	0.228	!	
ATOM	HG1	HGA7	0.101		
ATOM	FG1	FGA2	-0.191		
ATOM	FG2	FGA2	-0.191		
GROUP					
ATOM	C	C	0.51		
ATOM	O	O	-0.51		

12.4 Optimized partial charges on TfeGly

RESI	TFA		0.000		
GROUP					
ATOM	N	NH1	-0.47	!	
ATOM	HN	H	0.31	!	HN-N
ATOM	CA	CT1	0.07	!	
ATOM	HA	HB1	0.09	!	
GROUP				!	HA-CA--CB--CG-FG3
ATOM	CB	CT2	-0.093	!	
ATOM	HB1	HA2	0.090	!	
ATOM	HB2	HA2	0.090	!	O=C
ATOM	CG	CG302	0.333	!	
ATOM	FG1	FGA3	-0.140		
ATOM	FG2	FGA3	-0.140		
ATOM	FG3	FGA3	-0.140		
GROUP					
ATOM	C	C	0.51		
ATOM	O	O	-0.51		

12.5 MD simulations – further data

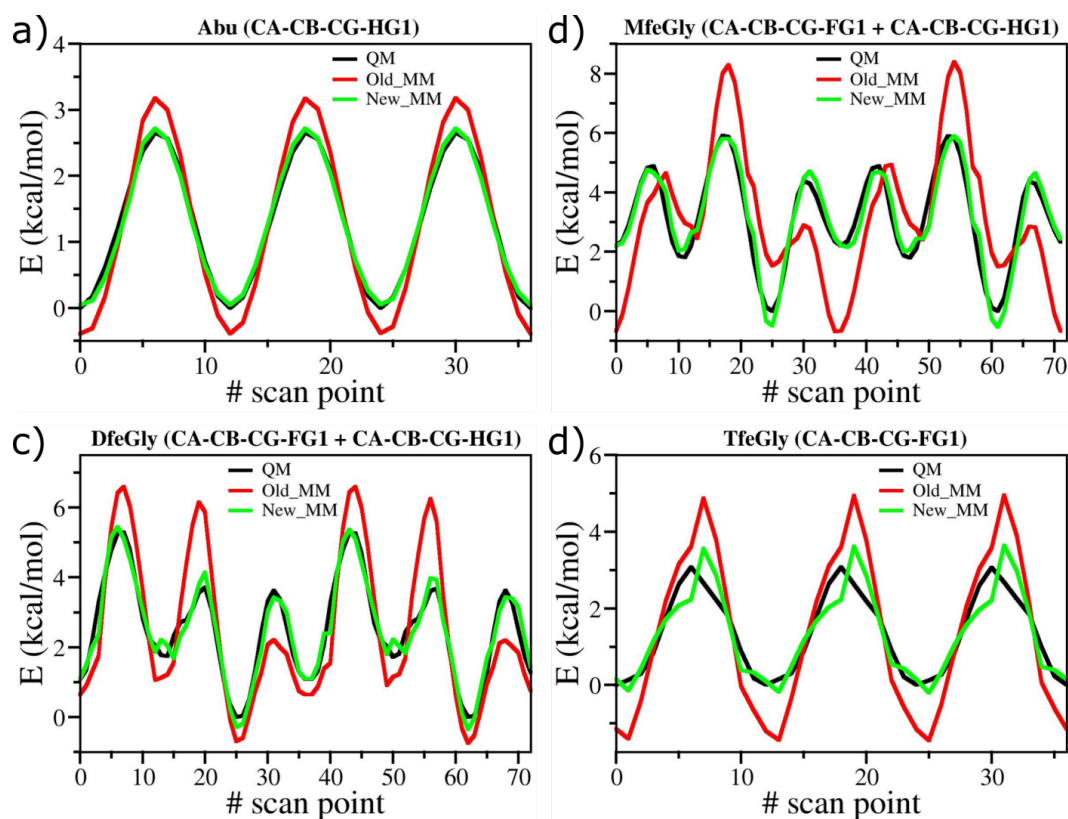


Figure S107: Optimization of dihedral angle(s) for **a) Abu**, **b) MfeGly**, **c) DfeGly**, and **d) TfeGly**. Atoms defining a dihedral angle are listed at the top of each plot. For **MfeGly**, **DfeGly**, and **TfeGly**, two dihedral angles ($C_{\alpha}-C_{\beta}-C_{\gamma}-F$ and $C_{\alpha}-C_{\beta}-C_{\gamma}-H$) are simultaneously optimized. For each dihedral angle, a total 36 QM energy scans, at intervals of 10° , are performed. Energies obtained from QM calculations are shown as black lines. Energies obtained from classical molecular mechanics using the force field parameters initially obtained from the CGenFF program are shown as red lines (Old_MM), whereas those using the optimized force field parameters are shown as green lines (New_MM). The optimized dihedral angle parameters are given in previous chapter.

Table S23: Optimized parameters for CHARMM dihedral energy function: $V_\varphi = k_\varphi [1 + \cos(n\varphi - \delta)]$.

Note that the Einstein summation convention is used.

<u>Amino Acid</u>	<u>Dihedral</u>	<u>k_φ</u>	<u>n</u>	<u>δ</u>
Abu	CA-CB-CG-HG1	0.4599	3	180.00
MfeGly	CA-CB-CG-FG1	2.1197	1	180.00
		0.1785	2	0.00
		2.6341	3	0.00
		0.3909	4	180.00
		0.2995	5	180.00
	CA-CB-CG-HG1	0.1418	1	0.00
		0.8202	2	180.00
		2.7214	3	180.00
		0.2611	5	0.00
		DfeGly	CA-CB-CG-FG1	0.3960
1.3667	3			180.00
0.3155	4			0.00
0.5123	6			0.00
CA-CB-CG-HG1	1.0158		1	0.00
	0.6083		2	0.00
	0.6043		3	0.00
	0.7729		4	0.00
0.5764	6	180.00		
TfeGly	CA-CB-CG-FG1	1.3606	3	180.00

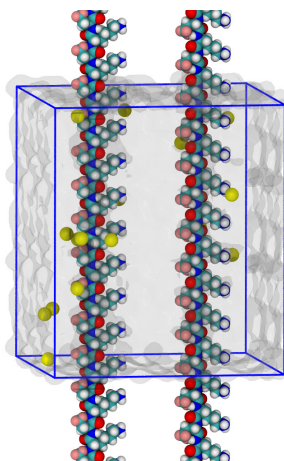


Figure S108: Simulation box (blue rectangle) containing two periodic **TfeGlyK16** strands, shown in the space-filling representation, colored according to the atom type: H (white), C (cyan), N (blue), F (pink). Cl⁻ counterions are shown as yellow spheres, whereas water is shown as semi-transparent, continuum for clarity.

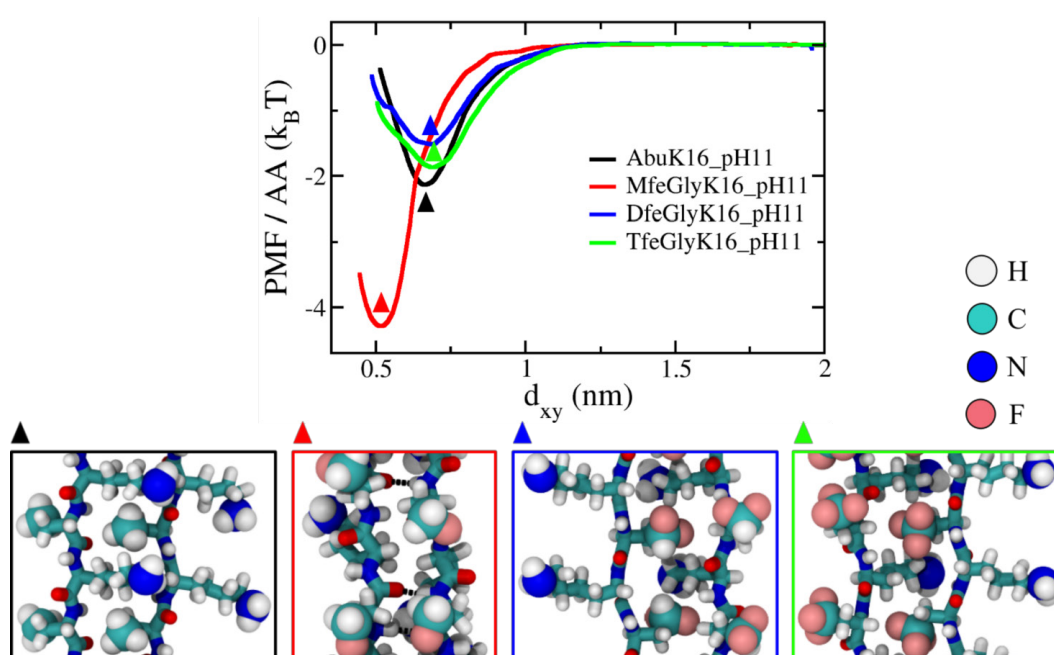


Figure S109: **a)** The potential of mean force (PMF) per amino acid (AA) as a function of inter-strand separation d_{xy} at pH11 (charge neutral Lys), depicting the free energy profile of interaction between two peptide strands for side chains with different degrees of fluorination. The free-energy minimum for each case is marked by a triangle. **b)** Structures corresponding to the free energy minimum for each case are shown in the ball-stick representation; the terminal group of each side chain is highlighted in the space-filling representation. Atom are colored as: H (white), C (cyan), N (blue), O (red), F (pink). Colors of enclosing boxes are the same as colors of the PMF profiles in **a)**. Backbone-backbone hydrogen bonds observed for **MfeGlyK16** are shown as black, dashed lines.

13. Small-angle X-ray scattering (SAXS)

Time-resolved SAXS measurements were employed to provide information on changes of the fibril cross-section dimension and shape. For this purpose, SAXS measurements of samples **AbuK16**, **MfeGlyK16**, **DfeGlyK16** and **TfeGlyK16** with peptide concentrations of 0.1, 0.5, 1 and 2 wt% were performed. The measurements were started immediately after sample preparation by mixing freeze-dried peptide powders with buffer solution. At the lowest concentration of 0.1 wt%, none of the samples display a significant SAXS intensity within 12 h. At the next higher concentration of 0.5%, the scattering intensity of **TfeGlyK16** was sufficiently high to obtain a reasonable SAXS pattern while the intensity of **DfeGlyK16** was only slightly larger than that of the buffer, and the intensities of **MfeGlyK16** and **AbuK16** were approximately the same as the buffer solution. For illustration, examples of raw SAXS data of **AbuK16**, **MfeGlyK16**, **DfeGlyK16** and **TfeGlyK16** (each at a concentration of 0.5%, measurement time of 5 min, and total incubation time of 50 min), the scattering of the buffer and the difference between raw data and buffer are provided in **figure S110** (panels in rows one and two). Much larger are the scattering intensities of the corresponding data for **DfeGlyK16** and **TfeGlyK16** at concentrations of 1 wt% and 2 wt% (see panels in rows three and four). Here, the measurement time for a data frame was set to 1 min to get insight in the kinetics of fibril formation.

The scattering contrast, defined here as the difference between the scattering length density of amyloid fibrils²¹ ($\rho_2 = 12.7 \pm 10^{10} \text{ cm}^{-2}$) and the scattering length density of buffer ($\rho_1 = 9.37 \pm 10^{10} \text{ cm}^{-2}$), is $\rho_2 - \rho_1 = 3.33 \pm 10^{10} \text{ cm}^{-2}$. This low value makes it plausible that a relatively high peptide concentration is necessary to detect the fibrils with SAXS. For the higher concentrations, reasonable signal-to-noise ratios were observed between a minimum and a maximum q -value of $q_{\min} = 0.08 \text{ nm}^{-1}$ and $q_{\max} = 4.0 \text{ nm}^{-1}$, respectively. Therefore, the SAXS data of the present study allow to obtain information in the size range of about $\pi/q_{\max} = 0.8 \text{ nm}$ to $\pi/q_{\min} = 40 \text{ nm}$.

No Guinier region²² is visible in the SAXS curves at low q -values as was expected for fibrils much longer than our upper size detection limit. Since the overall fibril length $l \gg q_{\min}^{-1}$, the SAXS form factor $P(q)$ can be factorized into a product of an axial form factor $P_a(q)$ (factors the length of the filaments) and a cross-section form factor $P_c(q)$ (factors the fiber cross-section). The model for interpretation of the SAXS pattern can be written as²³

$$I(q) = N(\rho_2 - \rho_1)^2 V^2 P_a(q) P_c(q)$$

where N is the number density of the fibrils (in fibers per cm^3) and V the volume of a fibril (in nm^3). The scattering intensities scale approximately with q^{-1} for **TfeGlyK16** and with q^{-2} for **DfeGlyK16** at low q -values (indicated as straight lines in **figure S111** and **figure S112**). These scaling behavior hints to a more circular cross-section for the fibrils of **TfeGlyK16** and a flat cross-section for **DfeGlyK16**. Therefore, we started data evaluation with the model of a circular cylinder²³ for interpretation of the scattering data of **TfeGlyK16** and an extended parallelepiped²⁴ for **DfeGlyK16**, respectively (not shown). An alternative model is a long cylinder with an elliptical cross-section. Indeed, the elliptical cylinder model was applicable for all scattering curves and provides statistically better curve fits than our first approach as indicated by lower χ -values. The axial form factor in the chosen model is

$$P_a(q) = \left[\frac{2\text{Si}(ql)}{ql} - \frac{4 \sin^2(ql/2)}{q^2 l^2} \right]$$

with the sine integral $\text{Si}(x) = \int_0^x t^{-1} \sin(t) dt$. The cross-section form factor is

$$P_c(q) = \frac{2}{\pi} \int_0^{\pi/2} \left(\frac{2J_1\left(q \sqrt{(a \sin \phi)^2 + (b \cos \phi)^2}\right)}{q \sqrt{(a \sin \phi)^2 + (b \cos \phi)^2}} \right)^2 d\phi$$

where $J_1(x)$ is the first order Bessel function, a is the major semiaxis of the elliptical cross section and b is the minor semiaxis. The fibril's cross-section area is $A = \pi a b$ and the fibril volume is $V = A l$. It should be noted that this model was employed recently by Lattanzi *et al.*²³ for interpretation of SAXS data of the fibril structure of amyloid β 42 and by Schmitt *et al.* for interpretation of the SAXS data from gelation of cellulose nanofibrils.²⁵

When employing this model, the data were represented sufficiently by the curve fits as shown in **Figure figure S111** (symbols and solid line) for **TfeGlyK16** at 0.5%. Therein a true to scale sketch of the fiber model is provided with a length of $l = 200$ nm and a cross-section with a major axis of $a = 3.7$ nm and a minor axis of $b = 0.95$ nm (see inset). For clarity, l and b were held constant at all curve fittings to avoid ambiguous results.

Next, in the time-resolved experiments of **DfeGlyK16** and **TfeGlyK16**, we found an increase in the scattering intensities and a slight change of the curve shape as a function of time. Examples for data and corresponding curve fits of measurement frames $n = 1$ (recorded ca. 120 s after sample preparation) and $n = 50$ (recorded 3000 s after sample preparation), are shown in **Figure figure S112** (symbols and solid lines, respectively). We found an increase of the major semi axis from $a = 2.7$ nm to 11.0 nm for sample **DfeGlyK16** at a concentration of 1% and from 2.9 nm to 4.4 nm at 2%. In contrast, the short semi-axis of the cross section is constant at $b = 0.85$ nm. An increase of the a -axis from 2.8 nm to 3.2 nm was determined for

sample **TfeGlyK16** at 1% and from 2.8 nm to 3.1 nm at 2%. Here, the short semi-axis of the cross section is constant at $b = 0.95$ nm. An overview on the differences of the cross-sections between data frame 1 and 50 is provided as sketch in **figure 4f** in the main paper.

In the following we tentatively try to quantify the time-dependency of the major semi axis $a(t)$, the fibril cross-section area $A(t)$, the fibril number density $N(t)$ and the weight concentration $c(t)$ with the exponential functions

$$\begin{aligned} a(t) &= a_{\infty} [1 - e^{-k_a(t-t_a)}] \\ A(t) &= A_{\infty} [1 - e^{-k_A(t-t_A)}] \\ N(t) &= N_{\infty} [1 - e^{-k_N(t-t_N)}] \\ c(t) &= c_{\infty} [1 - e^{-k_c(t-t_c)}] \end{aligned}$$

Were a_{∞} , A_{∞} , N_{∞} and c_{∞} are the parameter values extrapolated to infinite incubation times, k_a , k_A , k_N and k_c are rate constants of the parameters and t_a , t_A , t_N and t_c are delay times.

First, we applied $a(t)$ for quantification of the changes of the major semiaxis (see **figure S114**). For **DfeGlyK16** the curve fits provide $a_{\infty} = 10.5$ nm and 4.3 nm, $k_b = 1.5 \times 10^{-3} \text{ s}^{-1}$ and $2.7 \times 10^{-3} \text{ s}^{-1}$ at concentrations of 1% and 2%, respectively. For **TfeGlyK16** the fits provide $a_{\infty} = 3.1$ nm and 3.0 nm, $k_b = 12.9 \times 10^{-3} \text{ s}^{-1}$ and $12.8 \times 10^{-3} \text{ s}^{-1}$ at concentrations of 1wt% and 2wt%, respectively. The t_a were zero for all samples, indicating that fibril formation starts immediately at time of sample preparation.

The data for the cross-section area are calculated by $A(t) = \pi b a(t)$ with constant values of $b = 0.85$ nm (**DfeGlyK16**) and 0.95 nm (**TfeGlyK16**) providing A_{∞} -values of 28.1 nm² (1wt% **DfeGlyK16**), 11.6 nm² (2wt% **DfeGlyK16**), 9.4 nm² (1wt% **TfeGlyK16**) and 9.0 nm² (2wt% **TfeGlyK16**). The k_A - and t_A -values are obviously the same as the k_a - and t_a -values because b is time independent.

The fibril number density kinetics is described by N_{∞} - and k_N -values of $0.8 \times 10^{15} \text{ cm}^{-3}$ and $4.7 \times 10^{-3} \text{ s}^{-1}$ (1% **DfeGlyK16**), $N_{\infty} = 5.2 \times 10^{15} \text{ cm}^{-3}$ and $k_N = 4.7 \times 10^{-3} \text{ s}^{-1}$ (2% **DfeGlyK16**), $N_{\infty} = 4.2 \times 10^{15} \text{ cm}^{-3}$ and $k_N = 11.2 \times 10^{-3} \text{ s}^{-1}$ (1% **TfeGlyK16**) and $N_{\infty} = 7.4 \times 10^{15} \text{ cm}^{-3}$ and $k_N = 9.7 \times 10^{-3} \text{ s}^{-1}$ (2% **TfeGlyK16**). It should be noted here that the values of N_{∞} - and k_N -values must be considered as apparent values because the $N(t)$ data were calculated under the assumption of a constant fibril length of 200 nm. Since the fibrils are longer, the values for $N(t)$ are most likely too high, as $N(t)$ scales inverse with the length of the fibrils.

The data of the weight concentration of the fibrils were calculated by

$$c(t) = \rho N(t) A(t) l$$

where ρ is the density of the fibrils for which a value of 1.45 g cm^{-3} is used.²¹ The kinetics of the fibril weight concentration is described by c_∞ - and k_c -values of 6.4 mg ml^{-1} and $1.9 \times 10^{-3} \text{ s}^{-1}$ (1% **DfeGlyK16**), $c_\infty = 17.7 \text{ mg ml}^{-1}$ and $k_c = 2.0 \times 10^{-3} \text{ s}^{-1}$ (2% **DfeGlyK16**), $c_\infty = 11.3 \text{ mg ml}^{-1}$ and $k_c = 11.2 \times 10^{-3} \text{ s}^{-1}$ (1% **TfeGlyK16**) and $c_\infty = 18.9 \text{ mg ml}^{-1}$ and $k_c = 14.5 \times 10^{-3} \text{ s}^{-1}$ (2% **TfeGlyK16**). The weight concentration does in contrast to the number density not dependent on a correct value of the fibril length because for a given SAXS intensity the $N(t) \sim l^{-1}$ and $c(t) \sim l$, which means that l cancels out in determination of the weight concentration.

Of interest is a comparison of the calculated values c_∞ with the weighed-in peptide concentrations to estimate the amount of conversion of monomeric to fibrillar peptide. Conversions of 0.65% of 1.0% and 1.77% of 2.0% were found for **DfeGlyK16**. For these differences it can be assumed that 0.35% and 0.22% of the peptide are still present in form of monomer.

Conversions of 1.13% of 1.0% and 1.89% of 2.0% were found for **TfeGlyK16**. These values indicate a complete conversion of monomeric peptide to fibrils for **TfeGlyK16**. It should be noted that the uncertainty in determination of the SAXS-intensity²⁶ and therefore the concentration determination of peptides with SAXS is in the order of $\pm 10\%$.

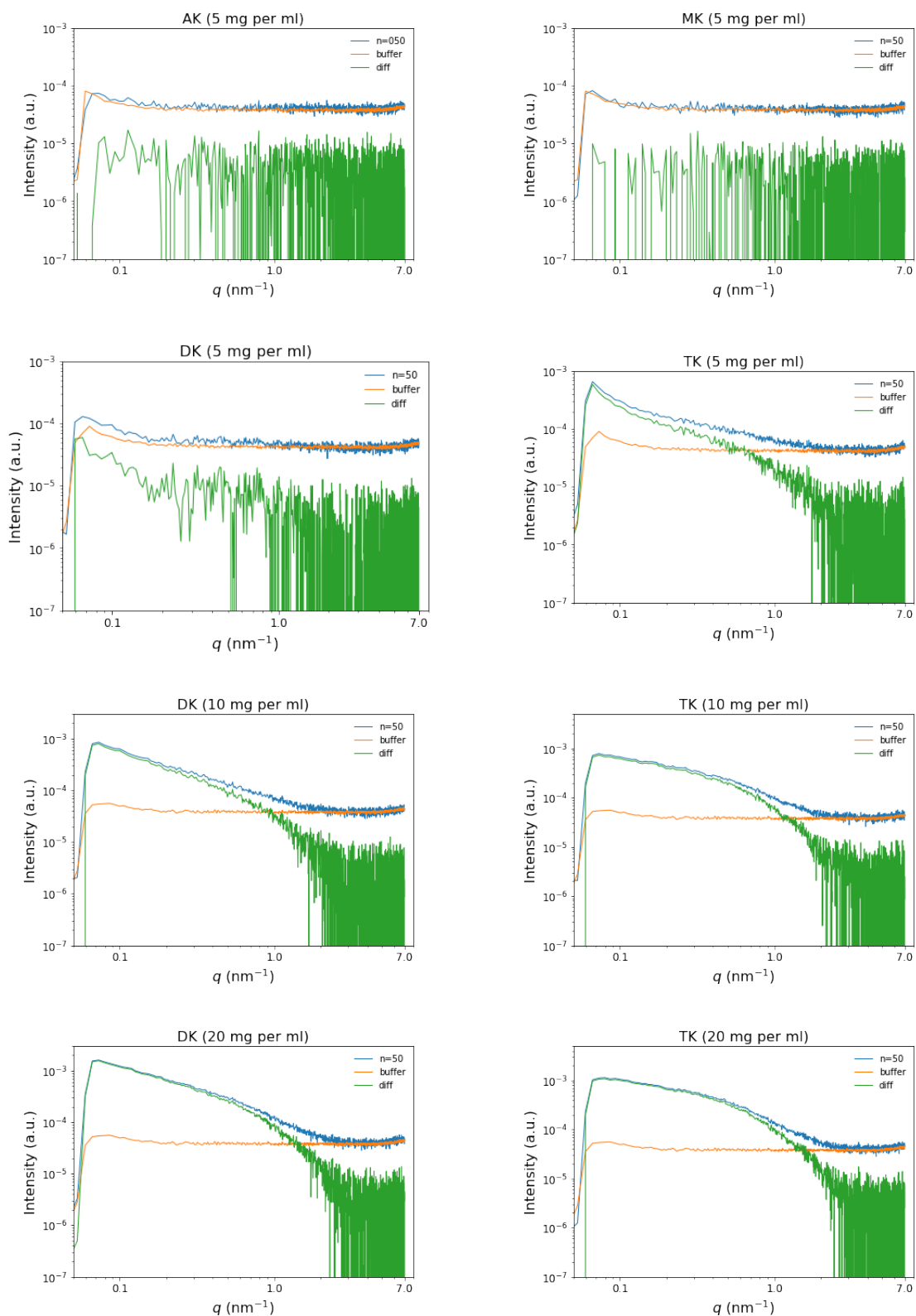


Figure S110: (First two rows) SAXS raw data of **AK (AbuK16)**, **MK (MfeGlyK16)**, **DK (DfeGlyK16)** and **TK (TfeGlyK16)** at a concentration of 5 mg per ml (0.5 wt%) (blue curves), SAXS of the buffer solution (orange) and the differences between raw data and buffer (green). (Third and fourth row) Corresponding data of **DK (DfeGlyK16)** and **TK (TfeGlyK16)** at concentration of 10 mg (1 wt%) and 20 mg (2 wt%) per ml, respectively.

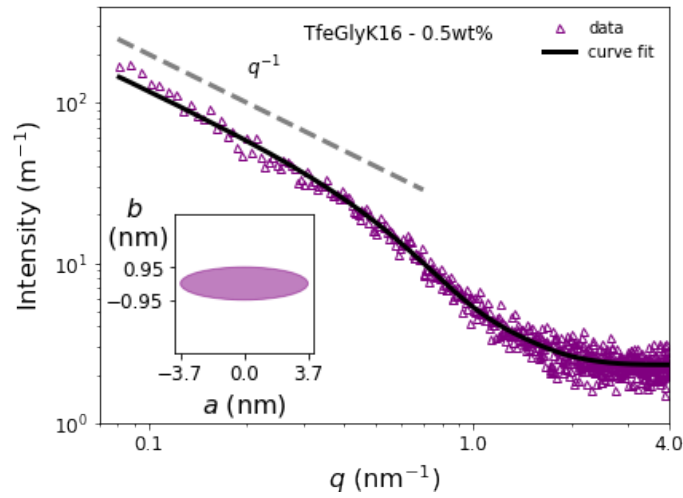


Figure S111: (top) true to scale model used for **TfeGlyK16**. (bottom) SAXS data and model curve for **TfeGlyK16** at a concentration of 0.5 wt% (symbols and line, respectively). Scaling of the intensity proportional to q^{-1} is indicated as straight line. (Inset) cross-section of the fibril.

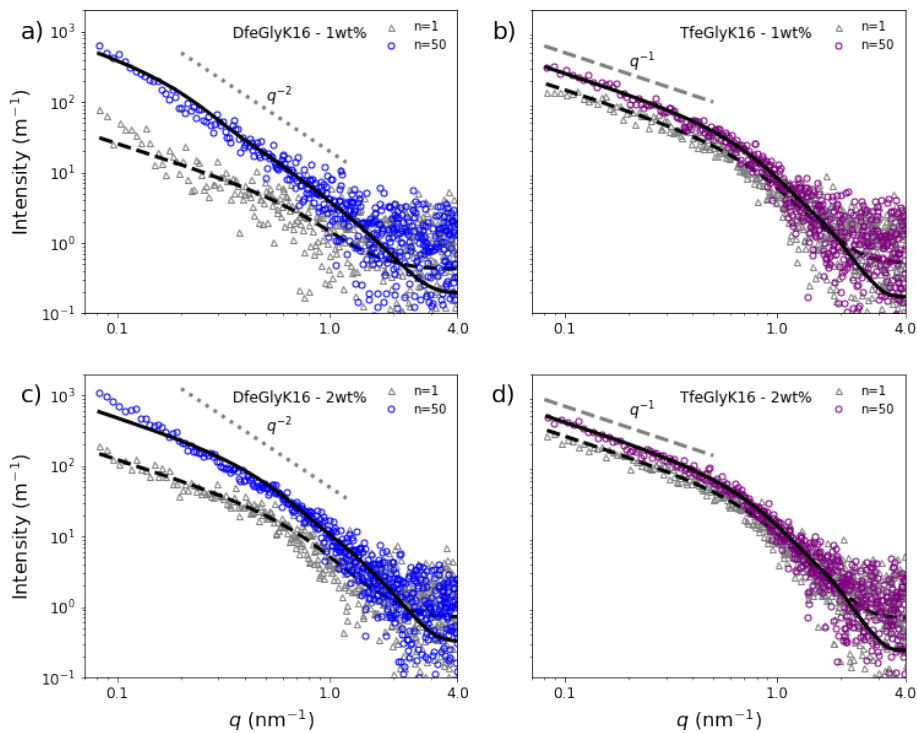


Figure S112: SAXS data and model curves for samples of **DfeGlyK16** and **TfeGlyK16** (symbols and lines, respectively). Data were from measurements directly after mixing (data frame $n=1$) and after about 3000 s ($n=50$). Scaling of the intensity proportional to q^{-2} (panel a and c) and proportional to q^{-1} (panel b and d) are indicated as straight lines.

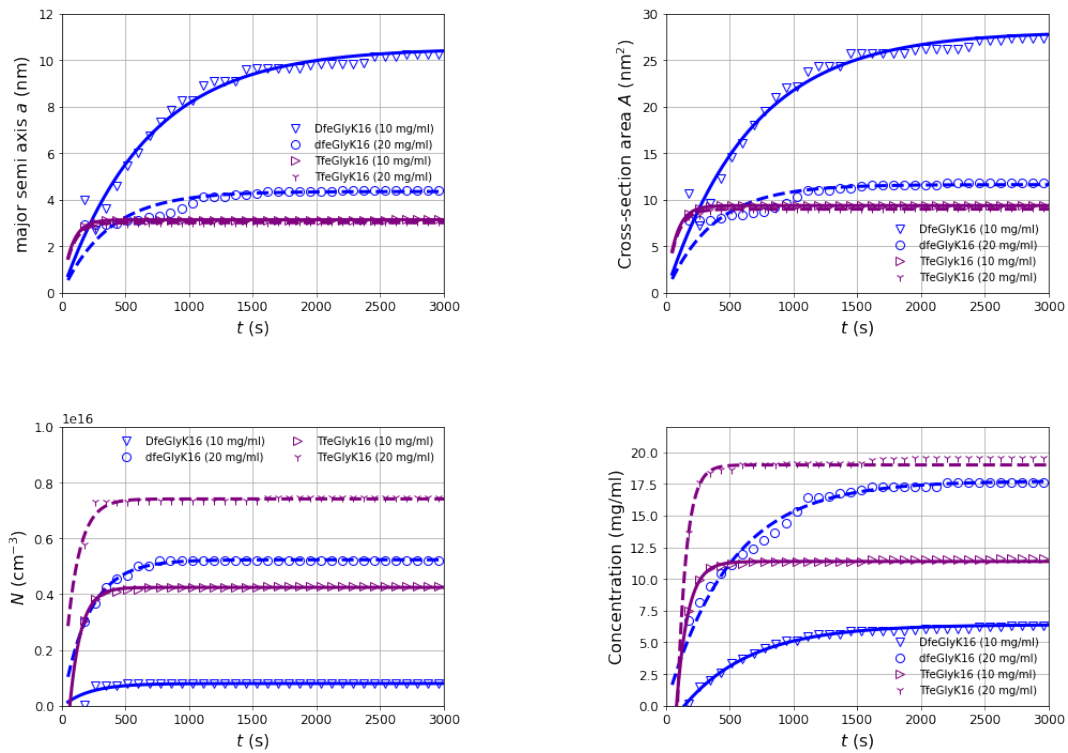


Figure S113: Kinetics of fibril formation. (top) Changes of the major semi axis and the cross-section area. (bottom) Number density and weight concentration of the fibrils.

14. References

1. V. A. Soloshonok, T. K. Ellis, H. Ueki and T. Ono, *Journal of the American Chemical Society*, 2009, **131**, 7208-7209.
2. A. E. Sorochinsky, H. Ueki, J. L. Aceña, T. K. Ellis, H. Moriwaki, T. Sato and V. A. Soloshonok, *Journal of Fluorine Chemistry*, 2013, **152**, 114-118.
3. J. Wang, M. Sánchez-Roselló, J. L. Aceña, C. del Pozo, A. E. Sorochinsky, S. Fustero, V. A. Soloshonok and H. Liu, *Chemical Reviews*, 2014, **114**, 2432-2506.
4. S. Zhou, J. Wang, X. Chen, J. L. Aceña, V. A. Soloshonok and H. Liu, 2014, **53**, 7883-7886.
5. Y. Nian, J. Wang, S. Zhou, S. Wang, H. Moriwaki, A. Kawashima, V. A. Soloshonok and H. Liu, 2015, **54**, 12918-12922.
6. T. T. Romoff, A. B. Palmer, N. Mansour, C. J. Creighton, T. Miwa, Y. Ejima, H. Moriwaki and V. A. Soloshonok, *Organic Process Research & Development*, 2017, **21**, 732-739.
7. Y. Nian, J. Wang, H. Moriwaki, V. A. Soloshonok and H. Liu, *Dalton Transactions*, 2017, **46**, 4191-4198.
8. J. Han, R. Takeda, X. Liu, H. Konno, H. Abe, T. Hiramatsu, H. Moriwaki and V. A. Soloshonok, *Molecules (Basel, Switzerland)*, 2019, **24**, 4521.
9. H. Mei, T. Hiramatsu, R. Takeda, H. Moriwaki, H. Abe, J. Han and V. A. Soloshonok, *Organic Process Research & Development*, 2019, **23**, 629-634.
10. J. Bandekar, D. J. Evans, S. Krimm, S. J. Leach, S. Lee, J. R. McQuie, E. Minasian, G. Némethy, M. S. Pottle, H. A. Scheraga, E. R. Stimson and R. W. Woody, *Int J Pept Protein Res*, 1982, **19**, 187-205.
11. J. Leppkes, T. Hohmann and B. Kocsch, *Journal of Fluorine Chemistry*, 2020, **232**, 109453.
12. M. Salwiczek, S. Samsonov, T. Vagt, E. Nyakatura, E. Fleige, J. Numata, H. Cölfen, M. T. Pisabarro and B. Kocsch, *Chemistry – A European Journal*, 2009, **15**, 7628-7636.
13. N. Hirota, K. Mizuno and Y. Goto, *Journal of molecular biology*, 1998, **275**, 365-378.
14. A. I. Arunkumar, T. K. Kumar, T. Sivaraman and C. Yu, *Int J Biol Macromol*, 1997, **21**, 299-305.
15. R. Gambaretto, L. Tonin, C. Di Bello and M. Dettin, 2008, **89**, 906-915.
16. G. D'Auria, M. Vacatello, L. Falcigno, L. Paduano, G. Mangiapia, L. Calvanese, R. Gambaretto, M. Dettin and L. Paolillo, *Journal of Peptide Science*, 2009, **15**, 210-219.
17. C. L. Shen and R. M. Murphy, *Biophysical journal*, 1995, **69**, 640-651.
18. I. M. Geisler and J. P. Schneider, *Advanced Functional Materials*, 2012, **22**, 529-537.
19. U. I. M. Gerling, M. Salwiczek, C. D. Cadicamo, H. Erdbrink, C. Czekelius, S. L. Grage, P. Wadhvani, A. S. Ulrich, M. Behrends, G. Haufe and B. Kocsch, *Chemical Science*, 2014, **5**, 819-830.
20. K. S. Hellmund, B. von Lospichl, C. Böttcher, K. Ludwig, U. Keiderling, L. Noirez, A. Weiß, D. J. Mikolajczak, M. Gradzielski and B. Kocsch, *Peptide Science*, 2021, **113**, e24201.
21. V. Lattanzi, I. Andre, U. Gasser, M. Dubackic, U. Olsson and S. Linse, *Proceedings of the National Academy of Sciences of the United States of America*, 2021, **118**.
22. A. Guinier and G. Fournet, *Small-Angle Scattering of X-Rays*, John Wiley & Sons, Inc., New York, 1955.
23. O. Glatter, *Scattering Methods and their Application in Colloid and Interface Science*, Elsevier, Amsterdam, 2018.
24. S. Chowdhary, J. Moschner, D. J. Mikolajczak, M. Becker, A. F. Thünemann, C. Kästner, D. Klemczak, A.-K. Stegemann, C. Böttcher, P. Metrangolo, R. R. Netz and B. Kocsch, *ChemBioChem*, 2020, **21**, 3544-3554.
25. J. Schmitt, V. Calabrese, M. A. da Silva, S. Lindhoud, V. Alfredsson, J. L. Scott and K. J. Edler, *Physical Chemistry Chemical Physics*, 2018, **20**, 16012-16020.

26. D. Orthaber, A. Bergmann and O. Glatter, *Journal of Applied Crystallography*, 2000, **33**, 218-225.

6.2 Fine-tuning the antimicrobial activity of β -hairpin peptides with fluorinated amino acids

S. Chowdhary, T. Pelzer, M. Saathoff, E. Quaas, J. Pendl, M. Fulde, B. Kokschi, *Pept. Sci.*, **2023**, e24306.

Submitted: 09 December 2022; **First published:** 9 March 2023

Published by Wiley Periodicals LLC., Hoboken, New Jersey, U.S.A.

The published work is available online - **DOI:** [10.1002/pep2.24306](https://doi.org/10.1002/pep2.24306).²⁴⁰

6.2.1 Individual contributions of authors

Suvrat Chowdhary (FU Berlin) conceived the overall project. Beate Kokschi and Marcus Fulde (both FU Berlin) provided guidance on peptide design and data analysis. **Suvrat Chowdhary** synthesized all amino acids and peptides. **Suvrat Chowdhary** designed and performed various experiments (SPPS, HPLC, CD, UV, FL, 6-FAM leaking, hemolysis, proteolytic digestion), analyzed and interpreted data sets, and wrote the manuscript. Tim Pelzer (FU Berlin) performed MIC, toxicity, and hemolysis studies. Mareike Saathoff (FU Berlin) performed MIC studies. Elisa Quaas (FU Berlin) performed toxicity studies. Johanna Pendl (FU Berlin) performed TEM measurements.

6.2.2 Rationale and summary of the project

In this project, the structure-activity relationships between varying degrees of aliphatic side chain fluorination and both antimicrobial activity and proteolytic stability of *de novo* designed β -hairpin AMPs were investigated. Two peptide libraries (XR14 & SAJO, in total eight sequences) bearing the *D*-Phe-[2]Abz turn motif and a diverse range of fluorinated amino acids (MfeGly, DfeGly, TfeGly, PfpGly) were studied with regards to structural folding, antimicrobial, cytotoxic and hemolytic activities, as well as enzymatic degradability (**Figure 6.5**).

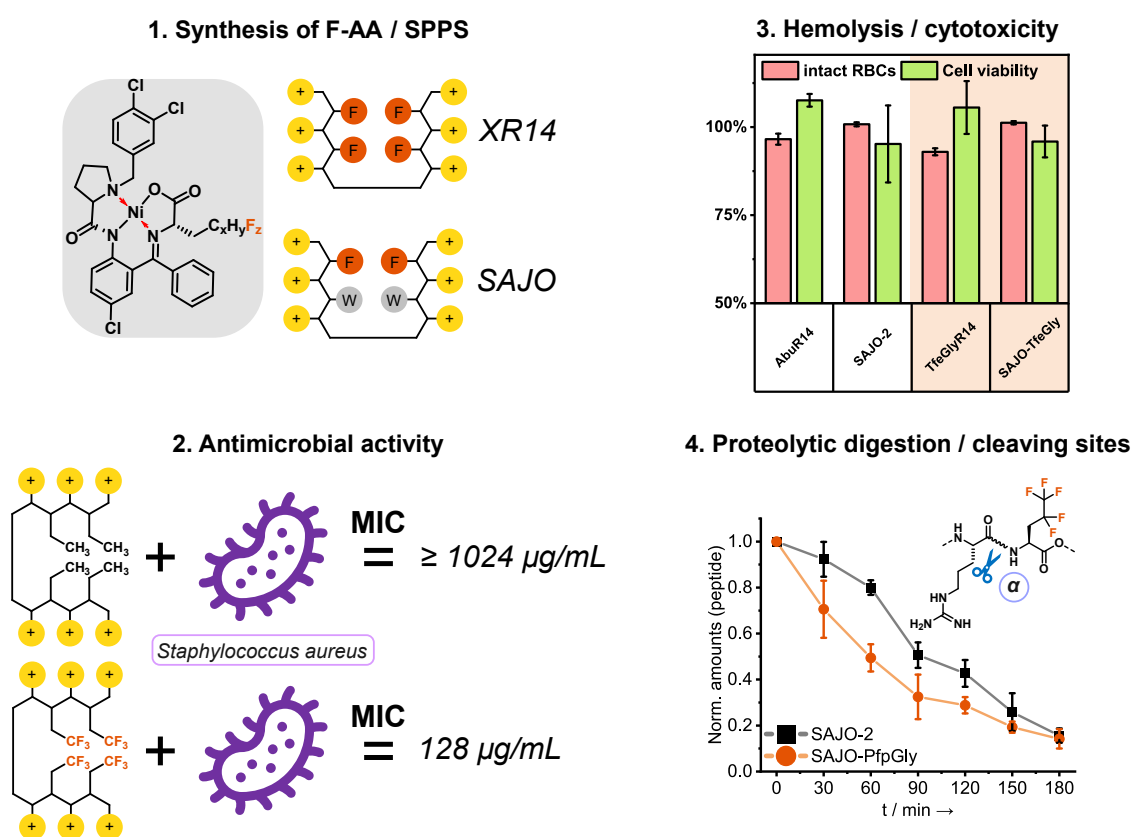


Figure 6.5 Schematic illustration of the project's working plan – “Fine-tuning the antimicrobial activity of β -hairpin peptides with fluorinated amino acids”.

In terms of the XR14 series (AbuR14, MfeGlyR14, DfeGlyR14, TfeGlyR14), the central β -turn is flanked with two amphipathic strands including the positively charged Arg and each hydrophobic amino acid. With this library, the impact of global fluorine-substitution on the AMP activity was supposed to be directly assessed. The SAJO series is based on the reported AMP SAJO-2 (Peptide “2”) by Sarojini and co-workers.⁸⁴ Site-specific incorporation of fluorinated amino acids at position 2 (Val) and 13 (Val) was intended to effectively fine-tune the intrinsic potency of this scaffold (**Figure 6.6**).

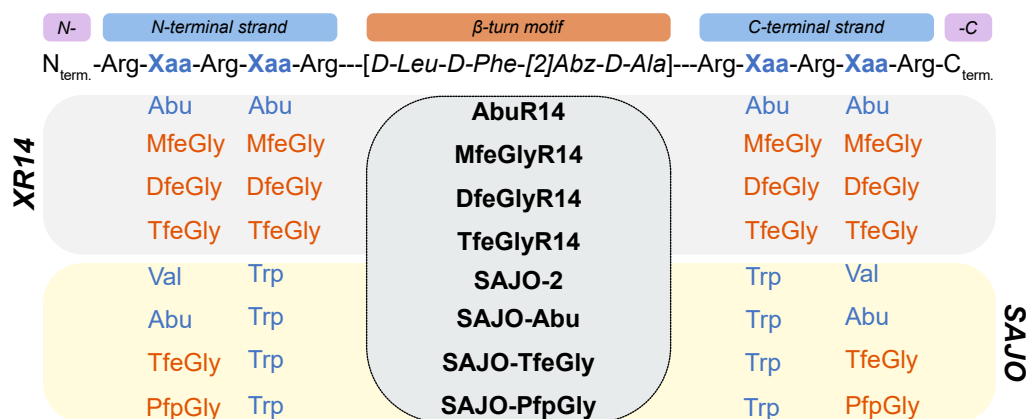


Figure 6.6 Name and sequence of amphipathic & fluorinated β -hairpins (XR14, SAJO). Adapted from Chowdhary *et al.* in a modified version (Copyright © 2023 Wiley Periodicals LLC.).²⁴⁰

Enhancements in peptide hydrophobicity through side chain fluorination were estimated by HPLC analyses (**Figure 6.7, left**). As displayed in the CD spectra, multiple incorporation of fluorinated amino acids retained β -turn formation ($\lambda_{\text{max}} = 210\text{--}215$ nm & $\lambda_{\text{min}} = 225\text{--}230$ nm) in physiological conditions (pH 7.4) (**Figure 6.7, right**). However, the co-existence of disordered peptides was detectable at 50 μM concentration (random coil, $\lambda_{\text{min}} = 200$ nm) but is diminished after increasing the peptide amount (≤ 500 μM).

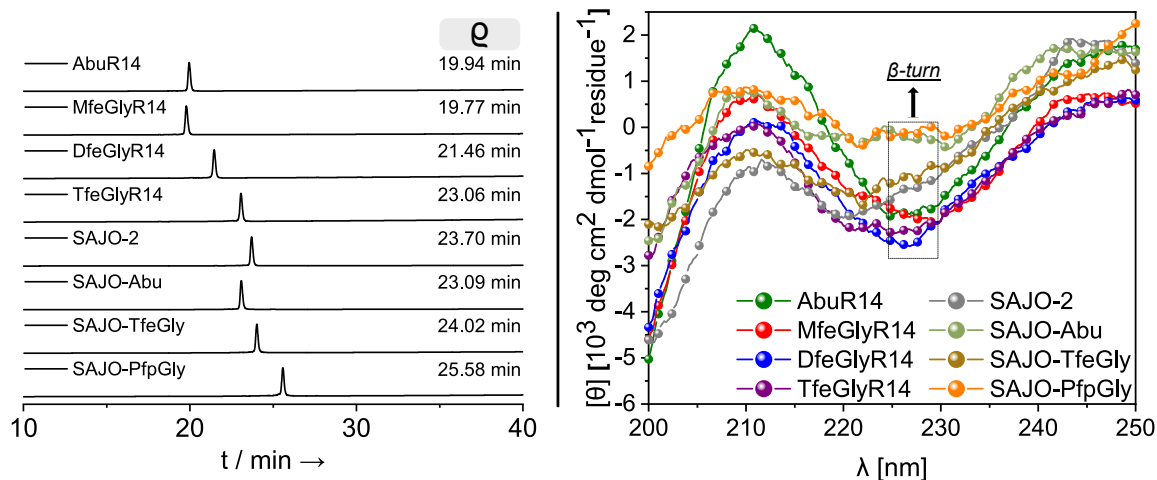


Figure 6.7 Retention times ρ of amphipathic β -hairpin peptides as experimental index of intrinsic hydrophobicity (**left**). CD spectra of amphipathic peptides AbuR14, MfeGlyR14, DfeGlyR14, TfeGlyR14, SAJO-2, SAJO-Abu, SAJO-TfeGly and SAJO-PfpGly (all at 50 μM concentration) dissolved in 10 mM phosphate buffer, pH 7.4, recorded at 37 $^{\circ}\text{C}$ (**right**). Adapted from Chowdhary *et al.* in a modified version (Copyright © 2023 Wiley Periodicals LLC.).²⁴⁰

Minimal inhibitory concentration (MIC) screenings were applied to probe the impact of growing side chain fluorination on bactericidal properties towards a panel of pathogenic strains (**Table 6.2**). Significant benefits on AMP activity were particularly found upon $-\text{CH}_3 \rightarrow -\text{CF}_3$ substitution within the XR14-series. For instance, AbuR14 was non-potent against *S. aureus* (≥ 1024 $\mu\text{g}/\text{mL}$), while the fluorinated and more hydrophobic TfeGlyR14 demonstrated notable enhancements in bactericidal activity (128 $\mu\text{g}/\text{mL}$), respectively.

In fact, up to 4-fold reduced MIC values were determined for the TfeGly-containing AMP comparing to the Abu species. Partially fluorinated amino acids (MfeGly, DfeGly), on the other hand, were found to decrease AMP efficiency. For example, substitution of Abu with MfeGly caused a significant increase in the MIC when facing *S. typhimurium* (256 → 1024 µg/mL) or *E. coli* (128 → 512 µg/mL). Considering the results from above-discussed project (**Section 6.1**), the electrostatic nature of fluorine-enhanced polarity located in an alternating H-F configuration (MfeGly, DfeGly) is hypothesized to weaken the hydrophobicity-driven disruption of bacterial membranes and, thus, AMP potency of MfeGlyR14 and DfeGlyR14.

Table 6.2 Antibacterial activities (MIC) and retention times ρ of peptides AbuR14, MfeGlyR14, DfeGlyR14, TfeGlyR14, SAJO-2, SAJO-Abu, SAJO-TfeGly and SAJO-PfpGly. Adapted from Chowdhary *et al.* in a modified version (Copyright © 2023 Wiley Periodicals LLC.).²⁴⁰

Peptide	ρ [min]	1*MIC (µg/mL)						
		<i>S.</i>	<i>E.</i>	<i>E.</i>	<i>S.</i>	<i>P.</i>	<i>K.</i>	<i>C.</i>
		<i>typhimurium</i>	<i>coli</i>	<i>faecalis</i>	<i>aureus</i>	<i>aeruginosa</i>	<i>pneumoniae</i>	<i>albicans</i>
		ATCC	ATCC	ATCC	ATCC	ATCC	ATCC	IMT
		14028	25922	29212	29213	27853	700603	9655
AbuR14	19.94	256	128	512	≥1024	≥1024	≥1024	512
MfeGlyR14	19.77	1024	512	1024	≥1024	≥1024	≥1024	1024
DfeGlyR14	21.46	128	256	1024	512	≥1024	1024	512
TfeGlyR14	23.06	128	64	128	128	1024	512	128
SAJO-2	23.70	16	8	64	64	64	32	32
SAJO-Abu	23.09	32	16	256	64	128	64	32
SAJO-TfeGly	24.02	32	8	64	64	64	64	32
SAJO-PfpGly	25.59	16	4	32	16	64	16	32

MIC values obtained for the SAJO-series, harboring two membrane-active Trp residues, were significantly lower than found for the XR14 series.²⁴¹ The reference SAJO-2 (Trp, Val) and SAJO-TfeGly (Trp, TfeGly) possessed similar AMP activities, which harmonizes with their similar hydrophobicity estimated *via* HPLC while the less hydrophobic SAJO-Abu revealed higher MICs. Most interestingly, the pentafluoroalkyl-equipped peptide

SAJO-PfpGly owned the highest activity (up to 4-fold) towards two Gram-positive microbes (*S. aureus*, 16 µg/mL / *E. faecalis*, 32 µg/mL) as well as the Gram-negative *E. coli* (4 µg/mL).

Adverse effects like cytotoxicity or hemolytic activity were barely detected for both XR14 and SAJO-peptides up to concentrations of 250-254 µg/mL. In fact, only SAJO-PfpGly showed slightly cytotoxic properties towards the human epithelial cells A549 at elevated concentrations. Furthermore, TEM experiments with *E. coli* samples found SAJO-PfpGly to exert a lytic and disruptive effect towards the bacterial cell wall with fatal consequences for the microbe (bacteria death) (**Figure 6.8**).

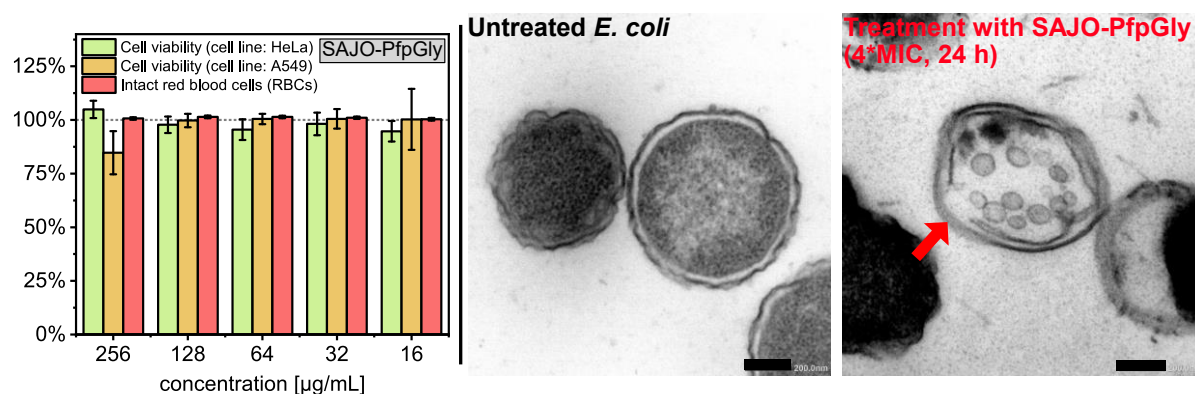


Figure 6.8 Evaluation of peptide-induced hemolysis (incubation with 1% RBCs solution) and cytotoxicity (incubation with HeLa and A549 cells) for the most potent AMP SAJO-PfpGly among this project (**left**). TEM micrographs of untreated *E. coli* samples (Scale bar: 200 nm) and after treatment with SAJO-PfpGly for 24 h (4*MIC) (Scale bar: 200 nm). Presumably, membrane pore formation (indicated by a red arrow) caused bacteria lysis and death (**right**). Adapted from Chowdhary *et al.* in a modified version (Copyright © 2023 Wiley Periodicals LLC.).²⁴⁰

The final approach towards this work was the HPLC-based real-time monitoring on AMP degradation *via* digestive endopeptidases. Upon incubation with the serine protease β -trypsin, peptide digestion was confirmed for all substrates (XR14 and SAJO series) despite the degree of side chain fluorination (**Figure 6.9a**). Moreover, introducing fluorine-containing amino acids in higher proportions maintained peptide degradability but generated new proteolytic cleaving sites. MS-assisted identification of digestion products by α -chymotrypsin proved the pentafluoro-alkylated residue of SAJO-PfpGly to act as a susceptible P1' residue. Interestingly, hydrolysis of the P1-P1' amide bond did not occur with Val (SAJO-2) as P1' residue (**Figure 6.9b**). As described in earlier reports by Schellenberger *et al.*, a higher degree of hydrophobicity and side chain volume as given for PfpGly is proposed to promote enzyme-substrate recognition *via* beneficial P1'-S1' interactions.^{227, 228} Similarly, the depicted digestion products of AbuR14 and TfeGlyR14 validate an increase in cleaving sites when TfeGly instead of Abu is set as hydrophobic

residue. In fact, herein discussed findings support prior assumptions on fluorine-induced P1'-S1' interactions described by Asante *et al.* and Huhmann *et al.* (**Section 4**).^{236, 237}

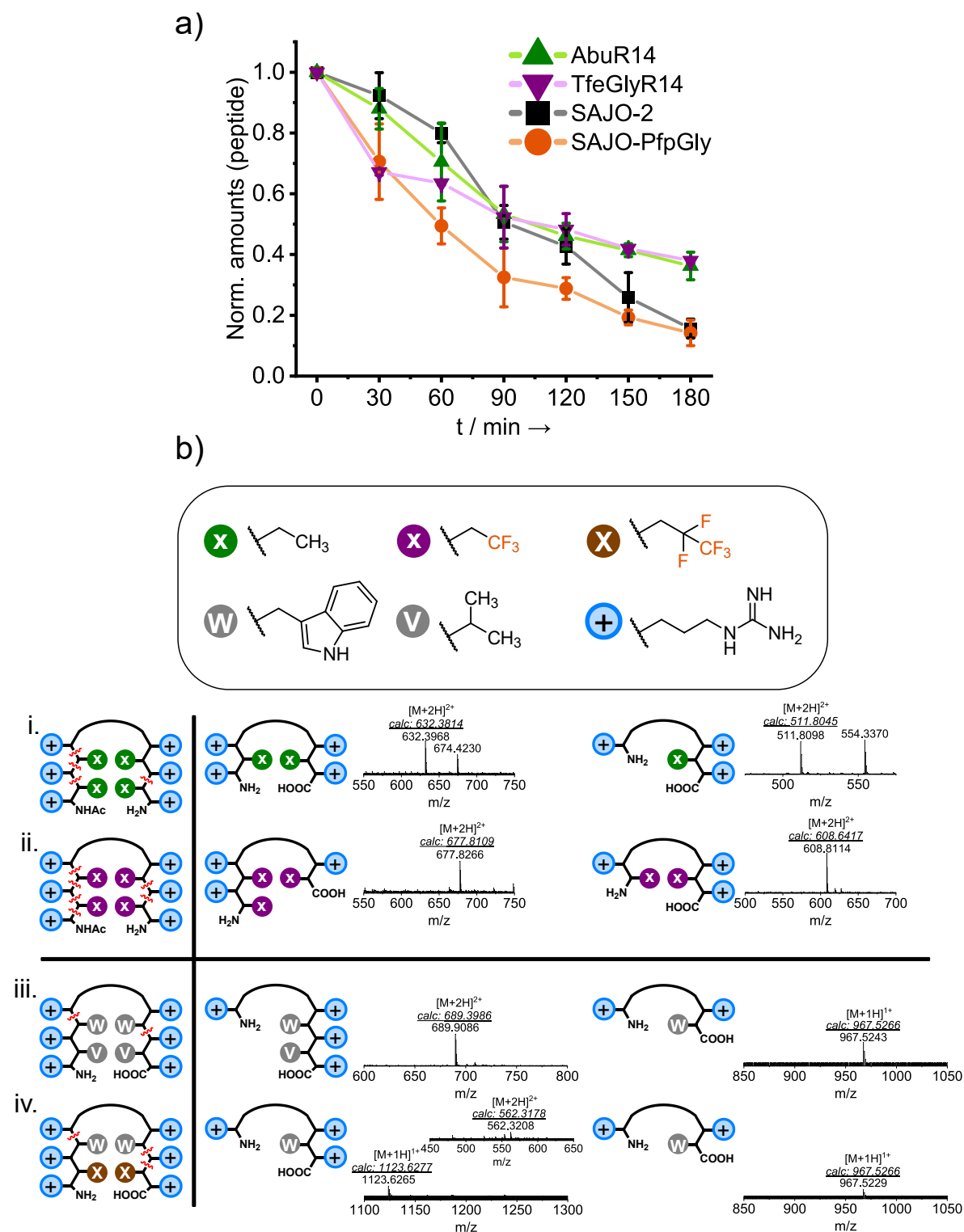


Figure 6.9 a) Digestion profiles of AbuR14, TfeGlyR14, SAJO-2 and SAJO-PfpGly (all 100 μM) with β -trypsin (0.075 μM) dissolved in 10 mM phosphate buffer, pH 7.4, 30 $^{\circ}\text{C}$ over a period of 3 h. **b)** Digestion products from i. AbuR14, ii. TfeGlyR14, iii. SAJO-2 and iv. SAJO-PfpGly during incubation with α -chymotrypsin. Adapted from Chowdhary *et al.* in a modified version (Copyright \textcopyright 2023 Wiley Periodicals LLC.).²⁴⁰

In summary, this work provides novel insights into the link between side chain fluorination and both antimicrobial activity and proteolytic stability. By establishing two

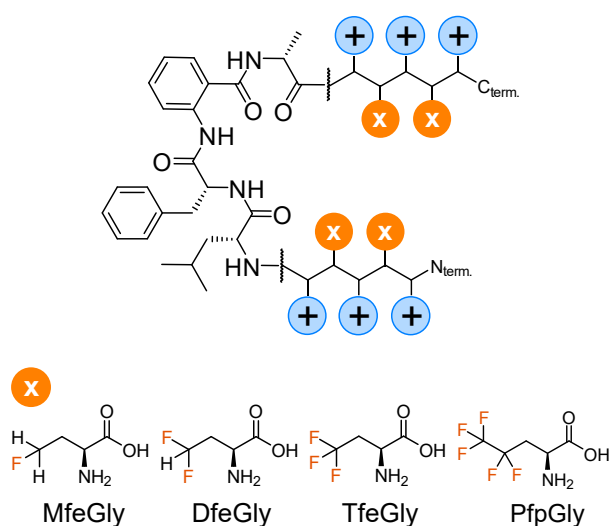
libraries of polyfluorinated β -hairpin AMPs, a synergy between antimicrobial activity and fluorination-enhanced peptide hydrophobicity was experimentally determined. Notably, emergences on blood-cell hemolysis or cytotoxicity upon fluorine-substitution were foremost omitted. Furthermore, as otherwise expected for the implementation of D- or β -amino acids, introducing fluorinated amino acids in varying proportions and amounts of this element retained peptide proteolysis by α -chymotrypsin and β -trypsin. Thus, herein described AMP activities and non-toxic / non-hemolytic properties of the most potent agent SAJO-PfpGly in this work may contribute to the future development of antibiotic peptides for therapeutical applications.²⁴⁰

6.2.3 Publication and supplementary information

Fine-tuning the antimicrobial activity of β -hairpin peptides with fluorinated amino acids

S. Chowdhary, T. Pelzer, M. Saathoff, E. Quaas, J. Pendl, M. Fulde, B. Kokschi,
Pept. Sci., **2023**, e24306.

Fluorinated Antimicrobial Peptides





DOI: 10.1002/pep2.24306.

Creative Commons license: [CC BY-NC-ND 4.0](https://creativecommons.org/licenses/by-nc-nd/4.0/)

ARTICLE

Fine-tuning the antimicrobial activity of β -hairpin peptides with fluorinated amino acids

Suvrat Chowdhary¹  | Tim Pelzer¹ | Mareike Saathoff² | Elisa Quaas³ | Johanna Pendl⁴ | Marcus Fulde^{2,5} | Beate Kokschi¹ 

¹Institute of Chemistry and Biochemistry, Freie Universität Berlin, Berlin, Germany

²Institute of Microbiology and Epizootics, Centre of Infection Medicine, Freie Universität Berlin, Berlin, Germany

³Institute of Chemistry and Biochemistry, Core Facility SupraFAB, Freie Universität Berlin, Berlin, Germany

⁴Institute of Veterinary Anatomy, Freie Universität Berlin, Berlin, Germany

⁵Veterinary Centre for Resistance Research (TZR), Freie Universität Berlin, Berlin, Germany

Correspondence

Beate Kokschi, Institute of Chemistry and Biochemistry, Freie Universität Berlin, Arnimallee 20, 14195 Berlin, Germany. Email: beate.kokschi@fu-berlin.de

Funding information

Deutsche Forschungsgemeinschaft, Grant/Award Number: CRC-1349"Fluorine-SpecificInteractions"/387284271

Abstract

Antimicrobial peptides (AMPs) possess bactericidal activity against a variety of pathogens depending on an overall balance of positively charged and hydrophobic residues. Selective fluorination of peptides serves to fine-tune the intrinsic hydrophobicity and that could improve AMP bioactivity without affecting the sequence length. Only a few studies have focused on the impact of this unique element on antimicrobial potency and came to somewhat contractionary results. Moreover, the influence of fluorinated amino acids on peptide proteolysis is yet not fully understood. In this work, we tackle the link between side chain fluorination and both antimicrobial activity and proteolytic stability for two series of amphiphilic β -hairpin peptides. In particular, a synergy between antimicrobial activity and peptide hydrophobicity was determined. All peptides were found to be barely hemolytic and non-toxic. Most surprisingly, the fluorinated peptides were susceptible to enzymatic degradation. Hence, the distinctive properties of these polyfluorinated AMPs will serve for the future design of peptide-based drugs.

KEYWORDS

antimicrobial peptides, fluorinated antibiotics, fluorinated biomaterials, peptide digestion, polyfluorinated oligopeptides

1 | INTRODUCTION

Peptides can adopt a multitude of biologically active conformations. In particular, the β -turn motif is one of these biomolecules' most common structural features and provides a nearly 180° reverse turn.^[1-4] The β -hairpin structure, whose structural hallmark comprises two antiparallel β -strands connected by a central β -turn, is an especially interesting scaffold.^[5] It is found in a wide range of naturally occurring antimicrobial peptides (AMPs) and formed by amphiphilic sequences.^[6-9] In general, cationic amino acids mediate electrostatic attractions to the negatively charged bacterial membrane surface and the hydrophobic residues penetrate and disorganize the lipid tail region. This mode of action causes

the disruption of the physical membrane integrity and, ultimately, cell death.^[10,11]

The design of new & synthetic AMPs is of paramount interest since the emerging resistance of pathogenic microbes toward current antibiotics is a rapidly growing threat to global healthcare management.^[8,12] To overcome this limitation, the incorporation of fluorine into peptide-based antibiotics may suit as a promising approach. This element was mainly neglected in biochemical evolution^[13] but often serves as a powerful tool in medicinal chemistry for enhancing a drug's intrinsic potency and membrane permeability.^[14] The replacement of a single carbon-bonded hydrogen with a fluorine atom causes only minimal steric perturbations. However, the hydrophobic

This is an open access article under the terms of the [Creative Commons Attribution-NonCommercial-NoDerivs](https://creativecommons.org/licenses/by-nc-nd/4.0/) License, which permits use and distribution in any medium, provided the original work is properly cited, the use is non-commercial and no modifications or adaptations are made.

© 2023 The Authors. *Peptide Science* published by Wiley Periodicals LLC.

nature and polarity of an artificial amino acid are significantly affected by the number of fluorine substituents.^[15] In fact, only a few reports focusing on the selective fluorination of AMPs are available to date. In 2006, Giménez et al. described trifluoromethylated amino acids to enhance the antibacterial efficiency of cationic oligopeptides toward a few Gram-negative and Gram-positive bacterial strains.^[16] Notably, the perfluorinated amino acid L-5,5,5,5',5',5'-hexafluoro-leucine (HfLeu) has been extensively studied in synthetic AMPs. When incorporated into *Pexiganan*, a 22-amino acid peptide-based drug, antibiotic potencies were retained and peptide-induced hemolysis was omitted up to a concentration of 250 µg/mL.^[17] However, HfLeu-containing variants of the β-hairpin peptide *Protegrin-1* showed weaker antimicrobial activities against a diverse range of pathogenic bacteria and increased rates of hemolysis than the native AMP.^[18] Meng et al. introduced a library of HfLeu-containing *Buforin-2* and *Magainin-2* mutants and reported comprehensive improvements in antimicrobial activity but partially increased hemolysis.^[19] Further studies by Setty et al. focused on fluorine-substituted phenylalanine derivatives in AMPs and determined an overall loss in antibiotic strength upon fluorination.^[20] Summarizing these case studies, the outcome of fluorination regarding AMP potencies is controversially discussed. Similarly, divergent conclusions about the impact of fluorinated amino acids on the proteolytic stability of peptides are reported.^[21] Thus, the current state of the art in this field of research requires further systematic studies for elucidating the promising potentials of fluorinated amino acids as engineering tools in future drug development.^[22]

Our approach here was to introduce artificial amino acids with distinctive degrees of side chain fluorination into two series of amphiphilic β-hairpin peptides. We characterized their folding pattern, membrane-disrupting properties, antimicrobial, cytotoxic, and hemolytic activities. A main highlight of this report is constituted by the data set on peptide proteolysis. We provide experimental evidence that the fluorinated β-strands of each AMP are enzymatically degradable regardless of the proportions and chemical nature of the particular fluorinated side chain.

2 | EXPERIMENTAL SECTION

2.1 | General methods

¹H-, ¹³C- and ¹⁹F-NMR spectra (see Data S1) were recorded by using a JEOL ECX 400 (JEOL, Tokyo, Japan), a JEOL ECP 500 (JEOL, Tokyo, Japan) or a Bruker AVANCE III 700 (700 MHz, BRUKER, Billerica, MA, USA). Chemical shifts δ are reported in ppm with MeOH-d₄ as the internal standard. HRMS were determined on an Agilent 6220 ESI-TOF MS instrument (Agilent Technologies, Santa Clara, CA, USA). All chemicals were purchased from commercial sources (Merck, Sigma-Aldrich, VWR, Fluorochem), used without further purification, and treated according to their material safety data sheet. Chemical experiments and sample preparations were performed in ventilated fume hoods if required. All experiments were executed at settled safety precautions on laboratory safety (Freie Universität Berlin). Peptide

stock concentrations were determined via UV spectroscopy (see Data S1, Figures S33 and S34).

2.2 | Synthesis of fluorinated amino acids

The fluorinated amino acid **TfeGly** was synthesized according to protocols published by our group.^[23] The synthesis of **MfeGly** and **DfeGly** is described in the Data S1 including NMR spectra of respective amino acids. **PfpGly** was provided by Thomas Hohmann (Freie Universität Berlin) (see Data S1, Schemes S1 and S2 & Figures S1–S9).^[24]

2.3 | Synthesis and purification of peptides

All peptides were synthesized with a microwave-equipped Liberty Blue™ peptide synthesizer (CEM, Matthews, NC, USA). Detailed protocols are listed in the Data S1 (Tables S1 and S2).

All peptides were cleaved from the resin by treatment with a mixture of TFA/TIPS/H₂O (90/5/5). The crude batches were purified on a low-pressure and semi-preparative RP-HPLC system (Knauer GmbH, Berlin, Germany) with H₂O + 0.1% TFA and ACN + 0.1% TFA as HPLC solvents. Analytical HPLC was performed either on a Chromaster 600 bar DAD-system (VWR/Hitachi, Darmstadt, Germany) or a Hitachi Primaide™ DAD-system (VWR/Hitachi, Darmstadt, Germany) with both H₂O + 0.1% TFA and ACN + 0.1% TFA as HPLC solvents. All essential data (HPLC chromatograms and HRMS spectra) can be found in the Data S1 (Table S3 & Figures S10–S32).

2.4 | Sample preparation—Exchange of TFA salts

Peptide samples (about 15 mg each) were dissolved in 5 mM HCl solution (5 mL) and stirred for 1 min at rt before lyophilization. This step was repeated thrice. To remove potential leftovers of HCl, the peptide samples were subsequently dissolved in MilliQ-water (10 mL) and stirred for 1 min before lyophilization.

2.5 | CD spectroscopy

Circular dichroism experiments were performed using a Jasco J-810 spectropolarimeter using Quartz Suprasil® cuvettes (Hellma). CD spectra were recorded at 37°C from 190 to 250 nm at 0.2 nm intervals, 1 nm bandwidth, 4 s response time, and a scan speed of 100 nm min⁻¹. Baselines were subtracted from experimental data. Further experimental data can be found in the Data S1 (Figures S35 and S36).

2.6 | Carboxyfluorescein [6-FAM] leakage assay

Concentrated stocks (each 10 mg/mL) of 1-palmitoyl-2-oleoyl-sn-glycero-3-phosphocholine (POPC) and 1-palmitoyl-2-oleoyl-sn-glycero-3-[phospho-rac-(1-glycerol)] (POPG) were prepared by dissolving the

compounds in CHCl_3 . Aliquots from both stocks were mixed and CHCl_3 was evaporated. The lipid film was dried in vacuo overnight and then dissolved in 50 mM 6-carboxyfluorescein (6-FAM) in 10 mM phosphate buffer, pH 7.4. The suspension was first treated with 10 freeze-thaw cycles, then ultrasonicated at rt for 30 min, and finally rest for 1 h at rt. Untrapped 6-FAM was removed by gel filtration on PD-10 desalting columns packed with Sephadex G-25. For each sample, 25 μL of peptide solution in serial dilutions were slowly added to 25 μL of liposome solution. The final lipid concentrations were: 5 mM POPG/POPG (1:1, each 2.5 mM) or 5 mM POPC. The mixed samples were incubated for 30 min at 30°C before each measurement. 6-FAM leakage was detected by measuring the fluorescence intensity ($\lambda_{\text{ex}} = 493 \text{ nm}$ / $\lambda_{\text{em}} = 517 \text{ nm}$) with an Infinite M Nano⁺ plate reader (Tecan Deutschland GmbH, Crailsheim, Germany). 100% dye release was achieved through the addition of 5% (v/v) Triton X-100 in buffer. A negative control was constituted by measuring the FL emission of the liposome solution only containing buffer. All measurements were done in triplicates. EC_{50} values were calculated by dose-response fitting (see Data S1). Further experimental data (6-FAM leakage monitored in the case of 100% POPC) can be found in the Data S1 (Figure S37).

2.7 | Hemolytic assay

For both procedures, an approval code was not needed according to the principles of the ethical committee of our institute (Freie Universität Berlin). Further experimental data (snapshots of the treated RBC solutions) can be found in the Data S1 (Figures S42 and S43).

2.7.1 | Procedure A (XR14-series)

Purification of the erythrocytes from hRBCs containing 10% citrate phosphate dextrose was accomplished according to a published protocol by our group.^[25] In general, 1 mL pure hRBC solution was diluted with PBS buffer to a concentration of 2% hRBCs (v/v). For sample preparation, 100 μL of peptide solution in PBS buffer in serial dilutions (two-fold concentration) was added to 100 μL 2% hRBC solution. These samples were incubated at 37°C for 45 min. A [1:1] mixture of 2% (v/v) Triton X-100 and 2% hRBC solution served as a positive control and a [1:1] mixture of 2% hRBC solution with sole buffer as a negative control. After incubation, the samples were centrifuged, and the UV absorbance of the supernatants was measured at 540 nm to determine the extent of peptide-induced blood-cell hemolysis. All measurements were done in triplicates. Erythrocytes were purchased from DRK Blutspendendienst Nord-Ost Berlin.

2.7.2 | Procedure B (SAJO-series)

Purification of the erythrocytes from 8 mL whole pigs' blood was accomplished according to a published protocol by our group.^[25] In general, 1 mL pure RBC solution was diluted with PBS buffer to a concentration of 2% RBCs (v/v). The lyophilized peptides were dissolved

in PBS buffer in serial dilutions starting from a concentration of 512 $\mu\text{g}/\text{mL}$ (two-fold concentration). In a 96-well plate, 100 μL of peptide solution in PBS buffer were prepared before adding 100 μL of the 2% RBC solution. Further samples were prepared that contained only 1% RBCs in PBS buffer for serving as a negative control. Two positive controls were prepared by [1:1] mixtures of 0.2% (v/v) & 2% (v/v) Triton X-100 and 2% RBC solution. Then, the well plate was incubated at 37°C for 45 min without agitation. After that, the well plate was centrifuged and 100 μL of the supernatant was removed and added to a new 96-well plate. UV absorbance of the supernatants was measured at 540 nm to determine the extent of peptide-induced blood-cell hemolysis. All measurements were done in triplicates and **TfeGlyR14** was set as an internal control for the comparability of both approaches. The porcine blood used in this study is a surplus and was generated during clinical training (Freie Universität Berlin).

2.8 | Proteolytic digestion assay

For real-time monitoring of enzymatic digestion, peptides **AbuR14**, **TfeGlyR14**, **SAJO-2**, **SAJO-TfeGly**, and **SAJO-PfpGly** were dissolved in 10 mM phosphate buffer, pH 7.4 (125 μL) at a two-fold concentration of 200 μM and gently mixed to obtain a homogeneous mixture. After that, 125 μL of β -trypsin (0.015 μM , dissolved in 10 mM phosphate buffer, pH 7.4) was added and the samples were gently mixed for 5 s. The final reaction mixture comprised 100 μM peptide and 0.0075 μM enzyme, respectively. All samples were incubated at 30°C over a period of 3 h. Aliquots of 40 μL were taken at fixed time points and quenched with 40 μL of a solution of 5% TFA in a [1:1] water-methanol mixture containing 100 μM Ac-[2]Abz-Gly-OH as reference. Peptide degradation was monitored by HPLC analysis, and the remaining amounts of substrates were calculated by comparison to the reference signal. All experiments were performed in triplicates.

For the detection of peptide fragments derived from peptide proteolysis, all peptide samples were dissolved in 10 mM phosphate buffer, pH 7.4 (170 μL , 1 mM peptide concentration), and gently mixed to obtain a homogeneous solution. Then, 35 μL of either α -chymotrypsin or β -trypsin (both 20 μM concentration stocks in 10 mM phosphate buffer, pH 7.4) were added and the samples were gently mixed for 5 s. After that, the samples were incubated at 30°C over a period of 6 h. Aliquots of 25 μL were taken at fixed time points and quenched with 50 μL of a solution of 1% TFA in water containing 75 μM Ac-[2]Abz-Gly-OH as reference & 50 μL MeOH. Peptide degradation was monitored by HPLC analysis. For determining the digestion profile of each AMP, all detected peptide fragments were isolated and identified through HRMS analysis. All experiments were performed in triplicates.

Further experimental data can be found in the Data S1 (Tables S4 and S5 & Figures S38–S41).

2.9 | Antimicrobial susceptibility testing

Minimum inhibitory concentrations (MIC) assays were performed according to Clinical and Laboratory Standards Institute (CLSI)

recommendations in cation-adjusted Mueller-Hinton broth (Mueller-Hinton II) broth in flat-bottomed, 96-well plates (Corning, Wiesbaden, Germany) with an inoculum of 10⁵ bacteria/well. Bacteria colonies were grown on blood agar or LB agar plates overnight at 37°C, accordingly. For antimicrobial testing, these colonies were resuspended in MHII and the optical density at 600 nm was measured. The bacterial suspension was diluted right before the experiment to achieve 2 × 10⁶ CFU/mL. From a 2.5 mg/mL peptide stock solution, a starting concentration of 2048 µg/mL was prepared. Peptide concentrations from 1024 µg/mL to 0.5 µg/mL were achieved by serial dilutions. To the wells containing 50 µL of peptide in PBS/MHII, 50 µL of bacterial suspension was added. Wells containing only MHII and bacterial suspension in MHII were prepared as a negative and positive control, respectively. The OD at 460 and 600 nm was measured at *t*₀ right after inoculation and after 24 h of incubation at 37°C. The resulting MIC was detected and determined as the peptide concentration where no bacterial growth could be observed after incubation.

2.10 | Cytotoxicity tests for the determination of cell viability

All cell experiments were performed according to German genetic engineering laws and German biosafety guidelines in the laboratory (safety level 1). In the case of both procedures, HeLa and A549 cells were obtained from Leibniz-Institut DSMZ—Deutsche Sammlung von Mikroorganismen und Zellkulturen GmbH.

2.10.1 | Procedure A (XR14-series)

Cell viability was determined using a CCK-8 Kit (Sigma-Aldrich). HeLa cells were cultured in DMEM and A549 in RPMI medium supplemented with 10% (v/v) FBS, 100 U/mL penicillin, and 100 µg/mL streptomycin. All cells were seeded in a 96-well plate at a density of 5 × 10⁴ cells/mL in 90 µL DMEM/RPMI medium per well overnight at 37°C and 5% CO₂. 10 µL of peptide sample dissolved in PBS buffer were added in serial dilutions including positive (1% SDS) and negative controls (only buffer and medium) and incubated for 24 h at 37°C and 5% CO₂. For further background subtraction, wells containing only the peptide sample were used. After 24 h incubation, the CCK8 solution was added (10 µL per well) and the UV absorbance (450 nm/650 nm) was measured after about 3 h incubation. The cell viability was calculated by setting the “non-treated” control to 100% and the “non-cell” control to 0% after subtracting the background signal. For both cell lines, the experiment was performed in 3 biological replicas each containing three internal replicas.

2.10.2 | Procedure B (SAJO-series)

Cytotoxicity assays were performed using a CytoTox-ONE™ Homogenous Membrane Integrity Assay (Promega). DMEM/F-12 supplemented

with 10% v/v FBS was used for culturing the cells which were seeded at 25% confluency in 96-well well plates. These well plates were incubated at 37°C and 5% CO₂ until reaching approximately 85–90% confluency. The medium was exchanged for medium containing the AMPs in concentrations ranging from 256 µg/mL to 16 µg/mL and incubated for another 24 h. The well plates were brought to rt and 50 µL medium was removed from each well. 1 µL “Lysis Solution” was added to the wells prepared as a positive control. Subsequently, 50 µL of CytoTox-ONE™ reagent was added to each well. The well plate was shaken for 30 s and left to incubate at rt for 10 min. After incubation, 25 µL of “Stop Solution” was added. The well plate was shaken for another 10 s before the fluorescence intensity ($\lambda_{\text{ex}} = 560 \text{ nm}/\lambda_{\text{em}} = 590 \text{ nm}$) was measured. For both cell lines, the experiment was performed in 3 biological replicas each containing three internal replicas. TfeGlyR14 was set as an internal control for the comparability of both approaches.

2.11 | Transmission electron microscopy (TEM)

E. coli (ATCC 25922) was grown in LB medium overnight and diluted to achieve an OD of 0.4 at 600 nm for all samples. To the bacterial suspension, the polyfluorinated peptide SAJO-PfpGly in PBS buffer was added to obtain bacteria/AMP mixtures containing either 2*MIC or 4*MIC. The samples were incubated at 37°C for 24 h. Additionally, control samples containing only bacteria were prepared as a negative control. Upon incubation, the samples were centrifuged at 4000 rpm for 5 min. The medium was discarded, and the pellet was resuspended in PBS buffer to remove any residual medium. After centrifuging once more and discarding the PBS wash solution, the bacterial pellets were fixed in Karnovsky fixative (7.5% glutaraldehyde, 3% paraformaldehyde) for 24 h at 5°C. Samples were washed with 0.1 M cacodylate buffer, incubated in 1% osmium tetroxide for 2 h, and washed again with cacodylate buffer. After that, the samples were dehydrated in increasing concentrations of ethanol and embedded in a mixture of epoxy resin, DDSA softener, MNA hardener, and BDMA catalyst. The resin was polymerized for 48 h at 50°C. Ultrathin sections (about 80 nm) were mounted on nickel grids and analyzed using a transmission electron microscope (TEM, JOEL, JEM-1400 Flash). TEM data can be found in the Data S1 (Figures S44 and S45).

2.12 | Thioflavin T (ThT) fluorescence spectroscopy

This experiment was performed according to a published protocol by our group.^[23] All samples were dissolved in 10 mM phosphate buffer supplemented with 20 µM Thioflavin T (ThT) (pH 7.4) and incubated for 24 h at 37°C. ThT fluorescence (FL) intensity ($\lambda_{\text{ex}} = 420 \text{ nm}$, $\lambda_{\text{em}} = 485 \text{ nm}$) was measured with an Infinite® M Nano⁺ plate reader (Tecan Deutschland GmbH, Crailsheim, Germany). FL values were normalized to a negative control solely containing buffer and ThT (set as FL_{int} = 1.0). The experimental data can be found in the Data S1 (Figure S46).

3 | RESULTS AND DISCUSSION

3.1 | Rational design of amphipathic peptides

We utilized the *D*-Phe-[2]Abz motif recently reported by Sarojini and co-workers.^[26–28] It is a peptidomimetic β -turn including the sterically inflexible 2-aminobenzoic acid [2]Abz. This β -amino acid has been found, for instance, in the cytotoxic cyclic tetrapeptide *Asperterrestide* A, a secondary metabolite derived from *Aspergillus terreus*.^[29,30] The turn segment consists of a linear tetrapeptide sequence $[(D\text{-Leu})^i\text{-}(D\text{-Phe})^{i+1}\text{-}([2]\text{Abz})^{i+2}\text{-}(D\text{-Ala})^{i+3}]$.^[27,30] As shown in the reported crystal structure^[27] (Figure 1), the planar β -turn is stabilized by three main hydrogen bonds: (a) N–H of residue *i* with C=O of residue *i* + 3 (2.90 Å); (b) N–H of residue *i* with C=O of residue *i* + 2 (2.94 Å) and (c) an intramolecular H-bond in residue *i* + 2 (2.64 Å).^[27]

Follow-up studies by the Sarojini research group focused on the introduction of the *D*-Phe-[2]Abz motif into acyclic and cyclic AMPs.^[26,31] We decorated this β -turn unit with two Arg-rich amphipathic strands on each terminus and varied the degree of fluorination on the hydrophobic positions by iterative incorporation of either **Abu** (**AbuR14**), **MfeGly** (**MfeGlyR14**), **DfeGly** (**DfeGlyR14**) or **TfeGly** (**TfeGlyR14**) (**XR14**-series, see Table 1); the termini were capped to avoid intermolecular electrostatic repulsion. Thus, the **XR14**-series served as a systematic library for studying the beneficial effects of increasing fluorine content on AMP activity.

Besides the **XR14**-series, the peptide **SAJO-2** developed by the Sarojini research group (named peptide “2” in their work) was chosen as a reference peptide.^[26,31] Contrary to the above-described variants, this sequence possesses both terminal charges as well as a tryptophan zipper-like motif.^[32,33] Herein, investigations on the **SAJO**-scaffold aimed to fine-tune the biological activity of the control sequence with varying hydrophobicity on site-specific positions. In particular, both valine residues located at positions 2 and 13 were replaced with **Abu** (**SAJO-Abu**) or **TfeGly** (**SAJO-TfeGly**) as hydrophobic moieties. The incorporation of the pentafluoro-alkylated **PfpGly** (**SAJO-PfpGly**) constitutes, to the best of our knowledge, the first reported study of this artificial amino acid into a bioactive peptide next to its recent implementation in the β -trypsin inhibitor BPTI.^[24,34]

3.2 | Secondary structure and hydrophobicity of amphiphilic peptides

The peptide **SAJO-2** is reported to exist as a mixture of conformers in physiological conditions. Cameron et al. suggested major amounts of disordered structures according to a random coil ($\lambda_{\min} = 198$ nm) and a minor content of an ordered β -sheet pattern.^[26] Typically, the presence of type II β -turn structures can be confirmed by CD spectroscopy due to a characteristic maximum at $\lambda_{\max} = 210\text{--}215$ nm and negative band around $\lambda_{\min} = 225\text{--}230$ nm.^[35,36] We recorded CD spectra for all peptides dissolved in phosphate buffer (pH 7.4) at either 50 μM or 500 μM concentration (Figure 2). All peptides adopted a β -turn structure indicating no significant structural

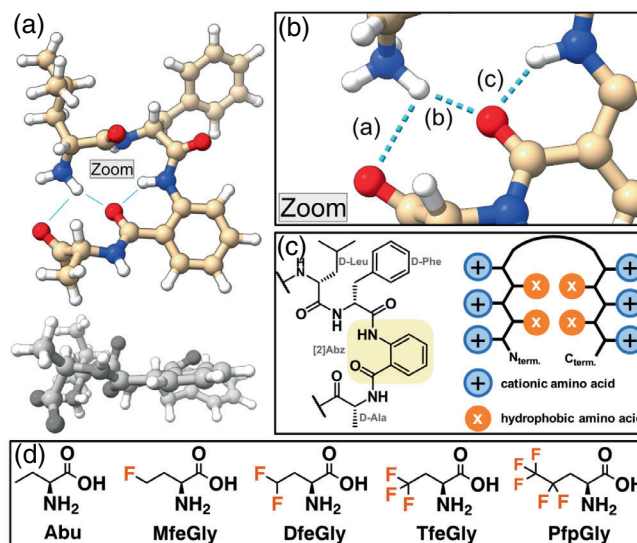


FIGURE 1 (a) Crystal structure of the linear tetrapeptide H-(D-Leu)-(D-Phe)-([2]Abz)-(D-Ala)-OH displayed from both a front view and top view (colored in gray). (b) Zoom-in view of the crystal structure with three main hydrogen bonds [(a)–(c)] maintaining this sequence in a turn-like structure (PDB Code: 6ANM). (c) Chemical structure of the *D*-Phe-[2]Abz β -turn and schematic illustration of the peptide motif (**XR14/SAJO**). [2]Abz is highlighted in yellow. (d) Chemical structures of the hydrophobic amino acids **Abu**, **MfeGly**, **DfeGly**, **TfeGly**, and **PfpGly**.

TABLE 1 Nomenclature of peptides (**XR14**-series, **SAJO**-series) and their sequences.

Peptide	Sequence
AbuR14	Ac-R- Abu -R- Abu -R-[l-f-[2]Abz-a]-R- Abu -R- Abu -R-NH ₂
MfeGlyR14	Ac-R- MfeGly -R- MfeGly -R-[l-f-[2]Abz-a]-R- MfeGly -R- MfeGly -R-NH ₂
DfeGlyR14	Ac-R- DfeGly -R- DfeGly -R-[l-f-[2]Abz-a]-R- DfeGly -R- DfeGly -R-NH ₂
TfeGlyR14	Ac-R- TfeGly -R- TfeGly -R-[l-f-[2]Abz-a]-R- TfeGly -R- TfeGly -R-NH ₂
SAJO-2	H-R-Val-R-Trp-R-[l-f-[2]Abz-a]-R-Trp-R-Val-R-OH
SAJO-Abu	H-R- Abu -R-Trp-R-[l-f-[2]Abz-a]-R-Trp-R- Abu -R-OH
SAJO-TfeGly	H-R- TfeGly -R-Trp-R-[l-f-[2]Abz-a]-R-Trp-R- TfeGly -R-OH
SAJO-PfpGly	H-R- PfpGly -R-Trp-R-[l-f-[2]Abz-a]-R-Trp-R- PfpGly -R-OH

Note: Substituted amino acids and [2]Abz are three-letter coded. Also, D-amino acids are defined by lowercase letters. Fluorinated amino acids are orange-colored.

perturbations due to side chain fluorination. Whereas a minimum at about $\lambda_{\min} = 200$ nm confirms the coexistence of random coils at 50 μM concentration, a further increase in peptide concentration

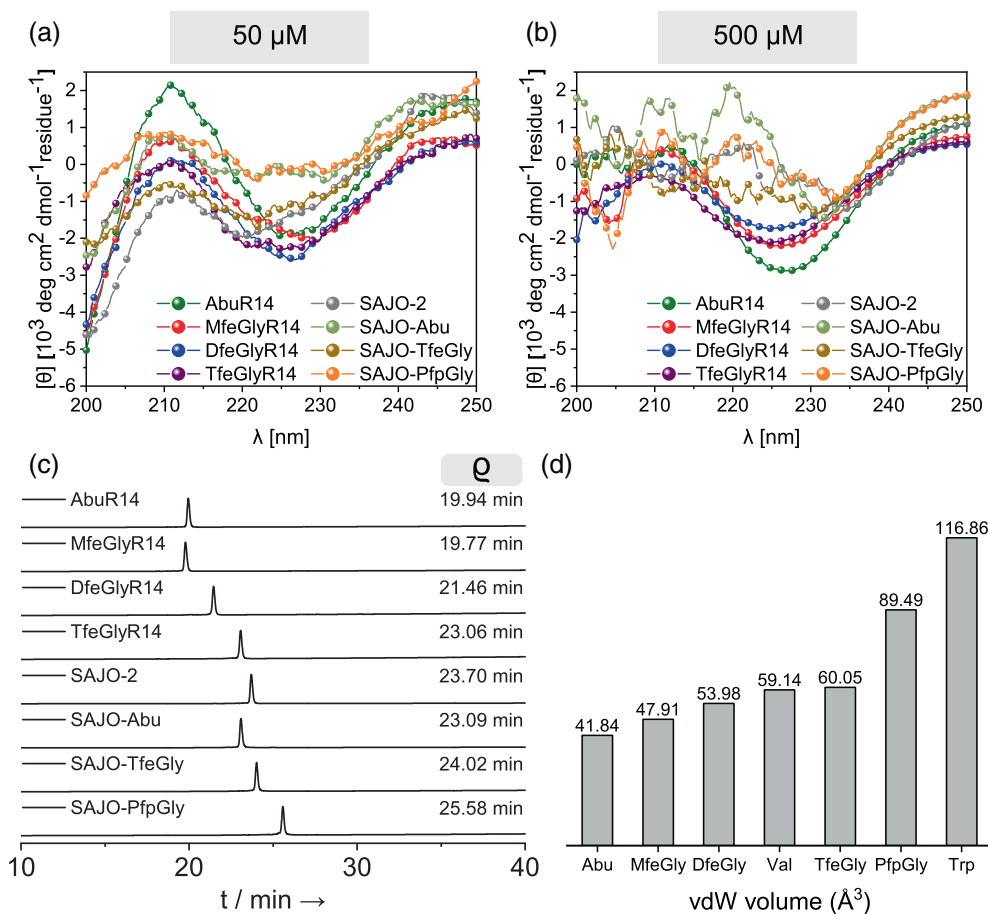


FIGURE 2 CD spectra of amphipathic peptides at (a) 50 μM and (b) 500 μM concentration dissolved in 10 mM phosphate buffer, pH 7.4, recorded at 37°C; (c) Intrinsic hydrophobicity of amphipathic peptides estimated through a RP-HPLC-based assay: The retention time ρ served as a dimension of non-polar character—HPLC conditions: CAPCELL PAK C18 MG—H₂O + 0.1% TFA/ACN + 0.1% TFA/gradient: 5% → 70% ACN + 0.1% TFA over 40 min. (d) Calculated vdW volumes of hydrophobic amino acid side chains.

(500 μM) diminishes this course of absorption. This indicates a concentration-dependency of β -turn formation. Higher peptide concentrations led to indeterminate CD spectra for all SAJO-derivatives. This circumstance can be explained by the proximity of four aromatic amino acids within the sequences, which can produce overlapping contributions in absorption and likely result in high proportions of scattering in the CD spectra.

A RP-HPLC-based assay served to determine the hydrophobicity of each peptide in this work (Figure 2c). In addition, the van der Waals volume of each amino acid residue was calculated according to Zhao et al. (Figure 2d).^[37] The trends of enhanced lipophilic properties through fluorination determined for the XR14- and SAJO-series are in accordance with prior reports on the amino acid series Abu, MfeGly, DfeGly, and TfeGly.^[38] Increasing the fluorine content on a particular residue enhances its spatial demand as well. Monofluorination of the hydrophobic side chains (MfeGlyR14, $\rho = 19.77$ min) retains the degree of hydrophobicity compared to AbuR14 ($\rho = 19.94$ min). Further growth in fluorine content (DfeGlyR14, TfeGlyR14) enhances the intrinsic hydrophobicity significantly ($\rho = 21.46$ and 23.06 min). With regards to the SAJO-series, we determined the substitution of valine

with TfeGly to generate a peptide (SAJO-TfeGly, $\rho = 24.02$ min) with equal hydrophobicity and residual vdW volume as SAJO-2 ($\rho = 23.70$ min). SAJO-Abu ($\rho = 23.09$ min), as expected, possesses comparably less hydrophobic properties. The highest degree of hydrophobicity was found for SAJO-PfpGly ($\rho = 25.58$ min) which owns the by far most hydrophobic and largest side chain among the library of fluorinated amino acids.^[24]

3.3 | XR14-series: Evaluation of membrane-disrupting, antimicrobial, hemolytic and cytotoxic properties

We selected a 6-carboxyfluorescein (6-FAM) based leakage assay to initially probe the lytic activity of the XR14-series.^[39] When this dye is encapsulated in liposomes its fluorescence (FL) is self-quenched by intermolecular interactions. Peptide-induced disruption of the liposomes leads to a release of the dye and, therefore, can be assessed directly from the observed increase in FL intensity.^[40] The artificial liposomes were prepared in equal amounts of 1-palmitoyl-2-oleoylsn-

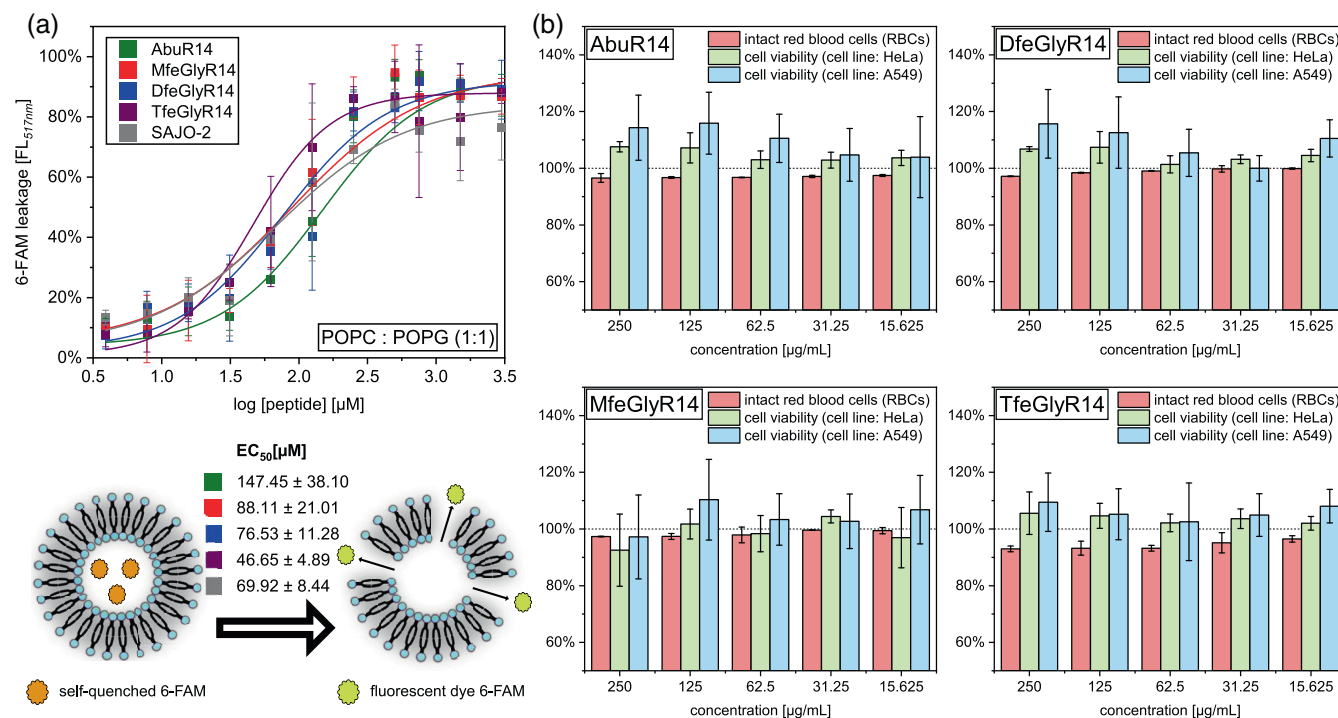


FIGURE 3 (a) Membrane permeabilization of amphipathic peptides detected via 6-FAM leaking. The dye was encapsulated in 5 mM liposome solution containing a phospholipid mixture of POPC:POPG [1:1] and its release upon the addition of peptides samples in serial dilutions after 30 min incubation (30°C) was monitored via fluorescence (FL) spectroscopy ($\lambda_{\text{ex}} = 493 \text{ nm}/\lambda_{\text{em}} = 517 \text{ nm}$). FL values were normalized to 100% dye release determined by adding 5% (v/v) Triton X-100 to the liposome solution as positive control. Dose–response curves were fitted with data sets derived from three separate experiments. The error bars show the standard deviation; (b) evaluation of peptide-induced hemolysis (incubation with 1% RBC solution) and cytotoxicity (incubation with HeLa and A549 cells) for peptides **AbuR14**, **MfeGlyR14**, **DfeGlyR14**, and **TfeGlyR14**.

glycero-3-phosphocholine (POPC) and 1-palmitoyl-2-oleoyl-sn-glycero-3-phospho-(1'-rac-glycerol) (POPG). As shown in Figure 3a, the treatment of POPC:POPG liposomes with the XR14-peptides above a threshold concentration enhances real-time detected FL intensity. Peptide-induced membrane disrupting activity was determined by calculation of EC_{50} values. **AbuR14** possesses the weakest activity ($\text{EC}_{50} = 148 \pm 39 \mu\text{M}$) in this series and replacement with **MfeGlyR14** reduces the EC_{50} to about 41% ($88 \pm 21 \mu\text{M}$). **DfeGlyR14** ($\text{EC}_{50} = 77 \pm 12 \mu\text{M}$) revealed comparably minor changes in EC_{50} , but for **TfeGlyR14** ($\text{EC}_{50} = 47 \pm 5 \mu\text{M}$) a 3-fold optimization of membrane activity than for **AbuR14** was determined. Interestingly, this peptide possesses superior membrane activity than the reference peptide **SAJO-2** ($\text{EC}_{50} = 70 \pm 9 \mu\text{M}$). Subsequently, we checked if the multiple incorporation of hydrophobic and fluorine-containing amino acids may cause adverse effects on cell cytotoxicity and hemolysis. As shown in Figure 3b, hemolysis assays with red blood cells (RBCs) and cytotoxicity tests with two cell lines (HeLa, A549) were performed. We were pleased to determine a lack of potent hemolytic activity for all peptides up to a concentration of 250 $\mu\text{g}/\text{mL}$. Further measurements revealed peptide-induced hemolysis for the most fluorinated variant **TfeGlyR14** at minimum concentrations of 1000 $\mu\text{g}/\text{mL}$ (500 $\mu\text{g}/\text{mL}$ for **SAJO-2**), which is in accordance with prior observed trends of fluorine-containing AMPs (see Data S1, Figure S42).^[19,41] Furthermore, all peptides exhibited near to zero cytotoxicity up to

250 $\mu\text{g}/\text{mL}$ concentration toward both cell lines. Thus, the overall proportion of fluorine in the AMPs was pivotal in the ability to permeabilize artificial phospholipid membranes without affecting the blood or human cells.

The bacterial cell envelope, however, is a complex multilayered network. The typical classification of bacterial species—Gram-positive or Gram-negative—is based on the composition of their cell walls. Gram-negative bacteria are surrounded by a thin peptidoglycan cell wall, which itself is surrounded by an outer membrane containing a variety of lipopolysaccharides. Gram-positive bacteria lack an outer membrane but are surrounded by several layers of crosslinked peptidoglycans decorated with negatively charged (lipo)teichoic acids in a thicker matrix than found in Gram-negatives.^[42] Consequently, the action mechanism of AMPs differs from the present bacterial surface. In the case of Gram-positive bacteria, an AMP must surpass the peptidoglycan barrier first before disrupting the cytoplasmic membrane. When facing Gram-negative bacteria, on the other hand, a two-step process comprising the perturbation of the outer and cytoplasmic membrane takes place.^[43,44]

Therefore, minimal inhibitory concentration (MIC) screenings for the XR14-series were performed against a variety of Gram-negative (*S. typhimurium*, *E. coli*, *P. aeruginosa*, *K. pneumoniae*) and Gram-positive (*E. faecalis*, *S. aureus*) bacteria species, but also a fungal pathogen (*C. albicans*). The MIC values are listed in Table 2 and reveal side

chain fluorination to hold a significant impact on the activity toward each pathogen but in varying magnitudes, leading to both decreased and enhanced antibiotic properties. The most fluorinated variant **TfeGlyR14** was found to be the most active AMP among the **XR14**-series but the benefits upon $-\text{CH}_3 \rightarrow -\text{CF}_3$ substitution differed. For example, we determined only a 2-fold increased potency of the fluorinated AMP when facing *S. typhimurium* (128 $\mu\text{g}/\text{mL}$) or *E. coli* (64 $\mu\text{g}/\text{mL}$). In terms of *S. aureus*, however, **AbuR14** was non-potent (≥ 1024 $\mu\text{g}/\text{mL}$) but **TfeGlyR14** was strongly active (128 $\mu\text{g}/\text{mL}$), respectively. Similar results on fluorination-enhanced potencies in the case of *S. aureus* were observed as well by the Marsh laboratory.^[17,18] These findings confirm the antimicrobial activity of this scaffold to be fine-tuned via implementation of trifluoromethylated residues (**TfeGly**) instead of a methyl group.

In terms of partially fluorinated residues, **MfeGlyR14** owns a 2- to 4-fold decreased activity than **AbuR14**, contrary to the results obtained through 6-FAM leaking assays. An interesting data set was obtained for **DfeGlyR14**: This peptide was found to be either superiorly (*S. typhimurium*, *S. aureus*) equally (*C. albicans*, *P. aeruginosa*) or less potent (*E. coli*, *E. faecalis*) than the non-fluorinated **AbuR14**. Due to its enhanced hydrophobic properties, a generous increase in antimicrobial activity for **DfeGlyR14** in comparison to **AbuR14** and **MfeGlyR14** was otherwise forecasted. We assume this circumstance to originate from fluorine-induced changes in side chain polarity. As discussed before, hydrophobicity-driven perturbations of cytosolic membranes by AMPs demand previous electrostatic attractions onto microbial cell

surfaces.^[45,46] Here, the polar character located in partially fluorinated side chains could act as a diametrical driving force against lipophilic accumulation. This interplay between fluorine-induced hydrophobicity and polarity was recently demonstrated by the Kocsch laboratory to alter supramolecular self-assembly and bioactivity.^[23,34,47] For supporting this hypothesis, the retention times of the **XR14**-peptides were plotted against recently reported water interaction energies ΔE_{int} for **Abu**, **MfeGly**, **DfeGly**, and **TfeGly** as an estimate of fluorine-induced polarity (Figure 4, left).^[23] An increase in ΔE_{int} , as given for **MfeGly**, leads to reduced hydrophobicity and, simultaneously, higher MIC values. Also, **DfeGly** possesses a much higher polarity in the side chain than **Abu** and **TfeGly**. An increasing degree of fluorination, therefore, does not automatically result in improved AMP activity. In fact, a similar trend exemplified for the antibiotic strength and ΔE_{int} indicates the impact of fluorination on antibiotic potency to be notably dependent on the side chain pattern in relation to a coaction of fluorine-enhanced polarity and hydrophobicity (see Figure 4, right).

The fungal pathogen *C. albicans* is part of the mucous flora and its yeast membrane is surrounded by a cell wall mainly composed of chitin, β -glucan, and mannoproteins.^[48] As illustrated in Figure 4, the antifungal properties of the **XR14**-series toward the pathogenic yeast follow an analogous trend of potency as determined for the bacterial species.

At last, we found all **XR14**-peptides to be non or less active toward the Gram-negative *P. aeruginosa*. We consider this circumstance to be caused by the missing Trp residues, typically present as a

TABLE 2 Antibacterial activities of peptides **AbuR14**, **MfeGlyR14**, **DfeGlyR14**, and **TfeGlyR14**.

Peptide	1*MIC [$\mu\text{g}/\text{mL}$]						
	<i>S. typhimurium</i> ATCC 14028	<i>E. coli</i> ATCC 25922	<i>E. faecalis</i> ATCC 29212	<i>S. aureus</i> ATCC 29213	<i>P. aeruginosa</i> ATCC 27853	<i>K. pneumoniae</i> ATCC 700603	<i>C. albicans</i> IMT 9655
AbuR14	256	128	512	≥ 1024	≥ 1024	≥ 1024	512
MfeGlyR14	1024	512	1024	≥ 1024	≥ 1024	≥ 1024	1024
DfeGlyR14	128	256	1024	512	≥ 1024	1024	512
TfeGlyR14	128	64	128	128	1024	512	128

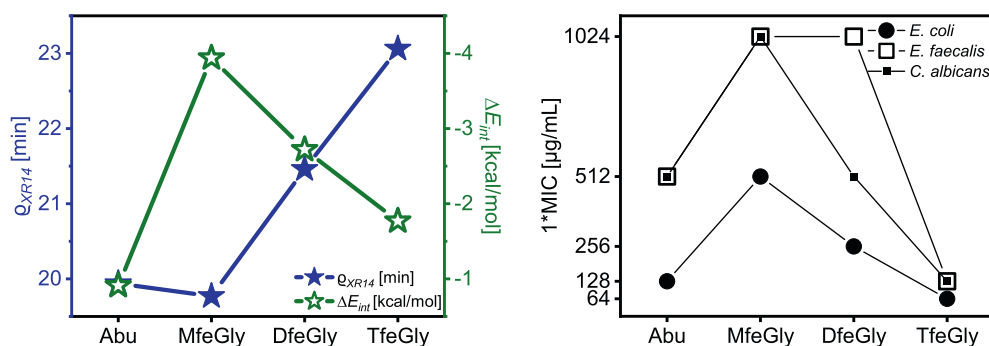


FIGURE 4 Retention times Q of **AbuR14**, **MfeGlyR14**, **DfeGlyR14**, and **TfeGlyR14** plotted against the water interaction energies ΔE_{int} calculated for **Abu**, **MfeGly**, **DfeGly**, and **TfeGly** (left). MIC values of *E. coli* (Gram-negative), *E. faecalis* (Gram-positive) and *C. albicans* (yeast fungus) plotted for each hydrophobic amino acid (**Abu**, **MfeGly**, **DfeGly**, **TfeGly**) in the **XR14**-series (right).

hydrophobic moiety in a multitude of AMPs.^[49] As reported by Shan et al., Trp-containing AMPs were particularly found to depolarize the outer and inner membrane of the bacterial cells, explaining the strong activity of tryptophane toward this bacterial species.^[50]

3.4 | SAJO-series: Evaluation of antimicrobial, hemolytic, and cytotoxic properties

The reference **SAJO-2** is reported to possess a broad spectrum of antimicrobial activity. Experimental data obtained through transmission electron microscopy (TEM) suggested this AMP to cause bacterial death by membrane lysis.^[26] MIC data of the **SAJO**-peptides (see Table 3) revealed an overall superiority in antimicrobial efficiency toward the **XR14**-series. This overall trend underlines the contribution of Trp residues to enhance membrane-disruptive properties.^[50–52]

SAJO-2 was effective against all tested organisms in concentrations ranging from 8–64 µg/mL. Similar MIC values were determined for **SAJO-TfeGly**, harmonizing with both analogous non-polar properties estimated via RP-HPLC. A loss in hydrophobicity, as probed for **SAJO-Abu**, caused a 4-fold enhanced MIC of 256 µg/mL for *E. faecalis* compared to **SAJO-2**. With regards to antifungal activities, the substitution of the hydrophobic residues led to retained MICs for *C. albicans*, very different from observations on the **XR14**-series. These results could hint at alterations in the mode of action when comparing the decrease in MIC for **AbuR14** → **TfeGlyR14**.

Most interesting MIC data were obtained for the pentafluoroalkyl-equipped peptide **SAJO-PfpGly**, which performed much better than **SAJO-TfeGly**. This polyfluorinated AMP shows the highest activity (up to 4-fold) toward all Gram-positive microbes (*S. aureus*, 16 µg/mL/*E. faecalis*, 32 µg/mL) tested in this work, as well as the Gram-negative *E. coli* (4 µg/mL). Thus, our experimental data validates the enhancement of intrinsic hydrophobicity to strengthen antimicrobial properties.

Furthermore, transmission electron microscopy (TEM) served to gain insights into the mode of action for **SAJO-PfpGly**. Incubation of *E. coli* with this AMP after 24 h was found to cause membrane pore formation, exposing a lytic and disruptive effect toward the bacterial cell wall (see Data S1, Figures S44 and S45). As illustrated in Figure 5, all **SAJO**-derivatives were tested regarding their blood cell-disrupting and cytotoxic properties. Due to the utilization of different experimental protocols (see Section 2), we set the above-discussed peptide **TfeGlyR14** as an internal control. All peptides were found in this case to be neither hemolytic nor cytotoxic. Moreover, we obtained similar

results for **TfeGlyR14** which confirmed previous studies. The only exception was found for **SAJO-PfpGly** with slightly toxic properties on the A549 cell line at the highest concentration (256 µg/mL); reducing the peptide amount, however, obviated cell cytotoxicity.

3.5 | Enzymatic degradation of (polyfluorinated) peptides

Lastly, we raised the question about the enzymatic degradability of these AMPs due to the varying degrees of side chain fluorination. The

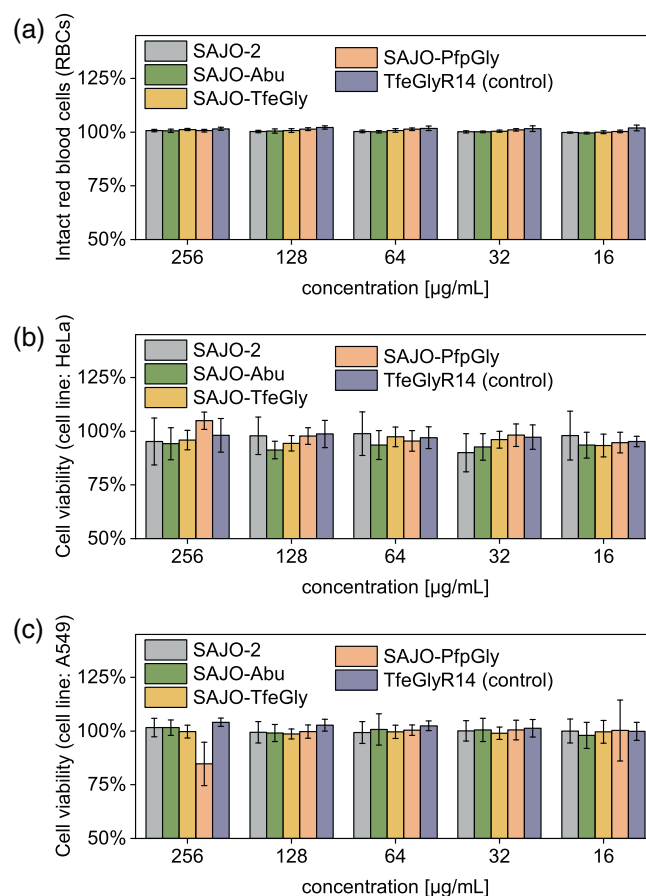


FIGURE 5 (a) Evaluation of peptide-induced hemolysis (incubation with 1% RBC solution) and cytotoxicity (incubation with (b) HeLa and (c) A549 cells) for peptides **SAJO-2**, **SAJO-Abu**, **SAJO-TfeGly**, **SAJO-PfpGly**, and **TfeGlyR14** as an internal control.

TABLE 3 Antibacterial activities of peptides **SAJO-2**, **SAJO-Abu**, **SAJO-TfeGly**, and **SAJO-PfpGly**.

Peptide	1*MIC [µg/mL]						
	<i>S. typhimurium</i> ATCC 14028	<i>E. coli</i> ATCC 25922	<i>E. faecalis</i> ATCC 29212	<i>S. aureus</i> ATCC 29213	<i>P. aeruginosa</i> ATCC 27853	<i>K. pneumoniae</i> ATCC 700603	<i>C. albicans</i> IMT 9655
SAJO-2	16	8	64	64	64	32	32
SAJO-Abu	32	16	256	64	128	64	32
SAJO-TfeGly	32	8	64	64	64	64	32
SAJO-PfpGly	16	4	32	16	64	16	32

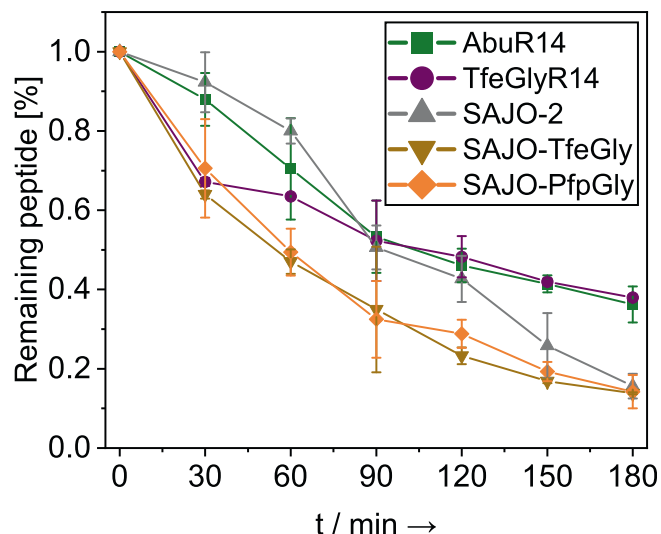


FIGURE 6 Digestion profiles of amphipathic peptides **AbuR14**, **TfeGlyR14**, **SAJO-2**, **SAJO-TfeGly**, and **SAJO-PfpGly** (all 100 μ M) with β -trypsin (0.0075 μ M) dissolved in 10 mM phosphate buffer, pH 7.4 and incubated at 30°C.

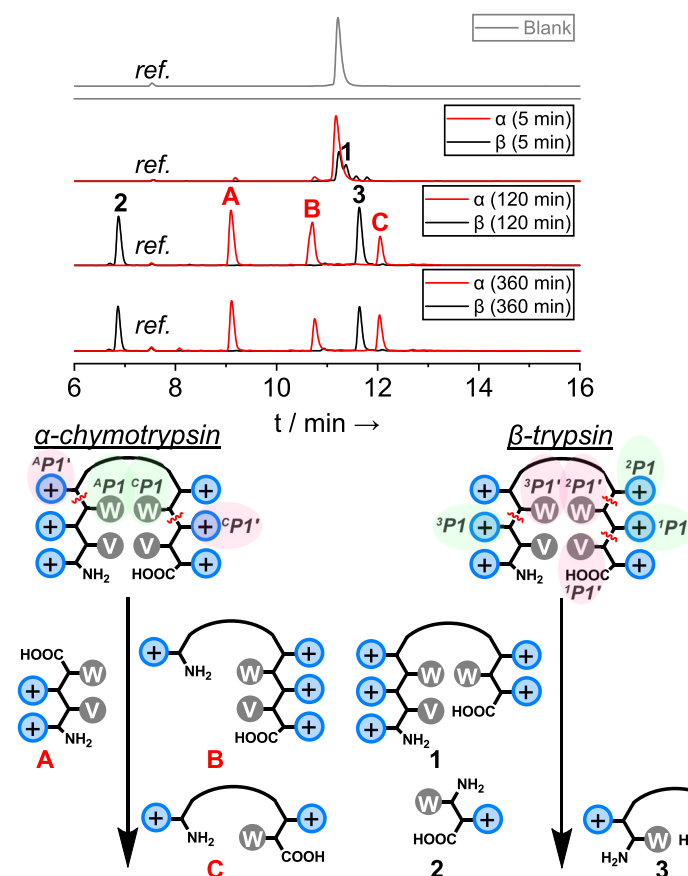
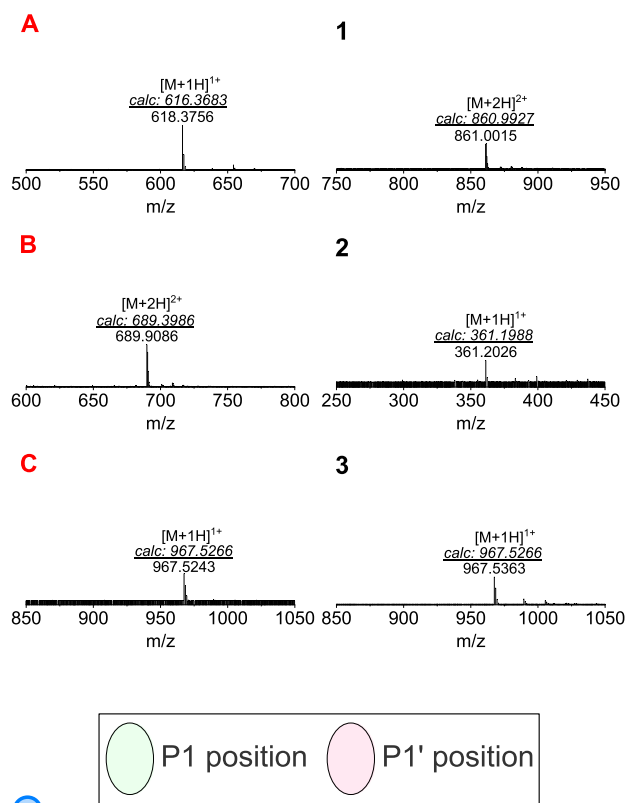


FIGURE 7 Real-time monitoring of proteolytic digestion at 5, 120 and 360 min (HPLC, DAD-280 nm) and MS-based detection and determination of peptide fragments of **SAJO-2** (1 mM stock concentration) during incubation with either α -chymotrypsin (α) or β -trypsin (β) (both 20 μ M stock concentration) at 30°C. The dipeptide Ac-[2]Abz-Gly-OH was used as reference signal. The black arrows indicate the proteolysis of **SAJO-2** into the illustrated digestion fragments. Arginine residues are illustrated as blue-colored positive charges (+). Trp and Val are described with one letter abbreviations. Cleaving sites are illustrated with squiggly lines (red-colored) and defined according to *Schechter and Berger* nomenclature. Measurements were performed in triplicates.

incorporation of non-natural α -amino acid in high proportions is frequently used to alter or even eliminate primary cleaving sites, thus increasing the proteolytic stability of peptides.^[53] For example, D-amino acid substitution is well-known to protect from proteolysis by altered stereochemistry properties that prohibit sufficient enzyme-substrate binding.^[54,55] Therefore, the *D*-Phe-[2]Abz turn unit was predicted to remain persistent under enzymatic conditions.

The introduction of fluorine is extensively applied in medicinal chemistry to improve the metabolic stability of drugs.^[14,56] In the context of side chain fluorinated amino acids, however, a wide range of reports with different outcomes exists. Both cases, namely the enhanced stabilities of fluorinated peptides against proteolysis as well as rapid digestion rates due to beneficial enzyme-substrate interactions, were described.^[21,22] Various studies including our efforts identified several aspects for which fluorinated amino acids can contribute to either favored or disfavored interactions like steric bulk,^[19,57] proximity to the predominant cleavage site^[58,59] or electrostatic perturbations^[60] by a polarized side chain within an enzyme's active site.

We tested the proteolytic stability of these peptides toward the serine protease β -trypsin. This enzyme exhibits a strong S1 specificity



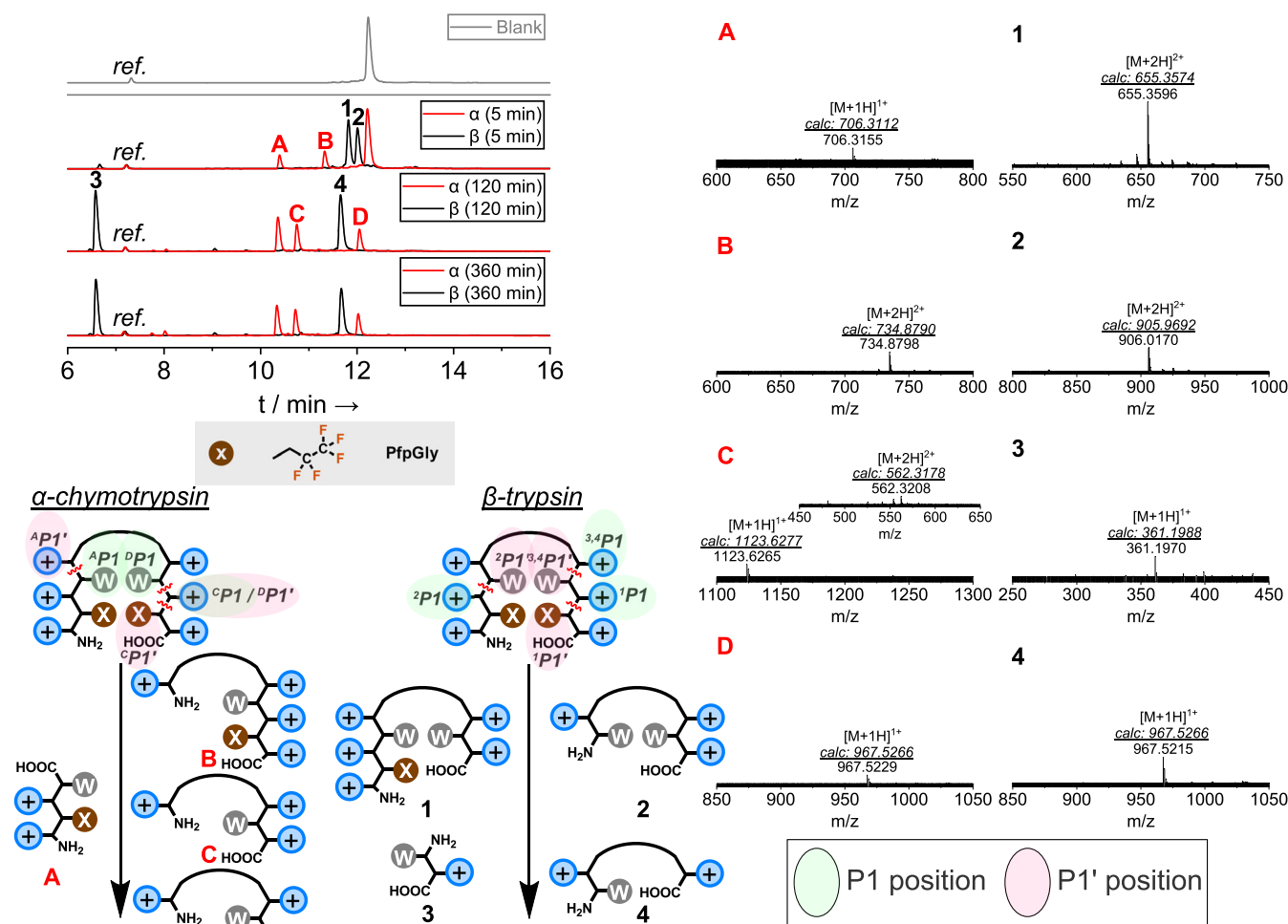


FIGURE 8 Real-time monitoring of proteolytic digestion at 5, 120 and 360 min (HPLC, DAD-280 nm) and MS-based detection and determination of peptide fragments of **SAJO-PfpGly** (1 mM stock concentration) during incubation with either α -chymotrypsin (α) or β -trypsin (β) (both 20 μ M stock concentration) at 30°C. The dipeptide Ac-[2]Abz-Gly-OH was used as reference signal. The black arrows indicate the proteolysis of **SAJO-PfpGly** into the illustrated digestion fragments. Arginine residues are illustrated as blue-colored positive charges (+). Trp is described with one letter abbreviations. Cleaving sites are illustrated with squiggly lines (red-colored) and defined according to *Schechter and Berger* nomenclature. Measurements were performed in triplicates.

(according to *Schechter and Berger* nomenclature)^[61] for Arg and Lys residues (P1 position) so that the herein-described AMPs bear multiple cleaving sites due to their amphiphilicity. In this experiment, **AbuR14**, **TfeGlyR14**, **SAJO-2**, **SAJO-TfeGly**, and **SAJO-PfpGly** were incubated at 30°C after the addition of the enzyme and their degradation profile was monitored by HPLC-analysis over a period of 3 h (Figure 6).

In fact, all peptides were found to be enzymatically degradable despite the degree of fluorination. Ultimately, the variant **SAJO-PfpGly** bearing two pentafluoroalkyl-chains was accepted as a suitable substrate by the serine protease. Real-time monitoring of peptide degradation revealed the **SAJO**-derivatives to remain in significantly lower amounts (13–15%) than **AbuR14** and **TfeGlyR14** (36–37%) after 3 h incubation. We presume this circumstance to be caused by terminal modifications of the **XR14**-derived AMPs, particularly C-terminal amidation and N-terminal acetylation. Both modifications are described to facilitate proteolytic resistance.^[62] For example, Nguyen et al. reported

greater protease stabilities of Trp- and Arg-rich peptides when both N- and C-terminal charges were capped.^[63]

Excited by this unique finding, we were engaged to determine if the presence of fluorinated amino acids also influences enzyme-substrate recognition resembled by changes in cleavage sites. For this purpose, we enhanced the concentration of the peptides (stock: 1 mM) and enzymes (stock: 20 μ M) to enable fragment detection via RP-HPLC and HRMS analysis (Figure 7 (**SAJO-2**) and Figure 8 (**SAJO-PfpGly**)). Firstly, we probed peptide digestion by the serine protease α -chymotrypsin which predominantly cleaves the amide bonds of aromatic P1 amino acids (Phe, Tyr, Trp). Also, secondary hydrolysis of bonds formed by asparagine, glutamine, methionine, glycine, histidine, and positively charged residues were reported to originate from favored P1'-S1' interactions.^[64–66] It was not surprising to observe the N-terminal aliphatic strand to be foremost cleaved (Trp: P1/Arg: P1') for both **SAJO-2** and **SAJO-PfpGly**. Interestingly, further proteolysis of digestion product "B" differed significantly for both peptides.

In the case of **SAJO-2**, this fragment remained stable during the experiment and enzyme hydrolysis was only found for the C-terminal strand between Trp (P1) and the centrally located Arg (P1') (formation of fragment “C” of **SAJO-2**) (Figure 7). In contrast, product “B” was completely consumed when both valine residues were substituted with **PfpGly** (Figure 8). We detected the release of the dipeptide fragment “PfpGly-Arg” from the C-terminal strand (formation of fragment “C” of **SAJO-PfpGly**), as well as the fragmentation up to the proteolytically stable β -turn core flanked with two Arg residues and one remaining Trp (P1) (formation of fragment “D”). It is most noteworthy that the enzyme-assisted release of the dipeptide fragment “PfpGly-Arg” confirms the fluorinated amino acid to act as a P1'-substrate for α -chymotrypsin. This finding is in accordance with earlier reports by our laboratory describing favorable side chain interactions between a few fluororous amino acids with the S1'-binding site of this serine protease.^[67,68] The branched amino acid valine (**SAJO-2**) may be unsuited as a P1'-substrate and, therefore, prevents further proteolysis. Furthermore, we examined a similar digestion profile for **SAJO-TfeGly** (see Data S1, Figure S38). Based on these results and in synergy with previous studies by Schellenberger et al., we consider the enhancement of side chain volume and fluorine-induced hydrophobicity to unleash peptide proteolysis in the case of **SAJO-PfpGly**.^[65]

When probing peptide degradation through β -trypsin, similar digestion profiles for **SAJO-2** and **SAJO-PfpGly** were again determined. The centrally located Arg residue on the C-terminal amphipathic strand acts as P1 residue leading to the formation of digestion product “1” for both peptides. This is validated by the detected cleavage of the terminal dipeptide-fragments “Val-Arg” and “PfpGly-Arg”. The P1' hydrophobic residues (Val, **PfpGly**), consequently, were accommodated within the S1' subsite. This can be explained by a broad S1' specificity of β -trypsin for aliphatic residues at P1', whereas the S2' site was reported to prefer positively charged P2' residues.^[69] In consequence, the enzyme favorably cleaves between Arg-X-Arg bonds (P1-P1'-P2', X = hydrophobic residue). Therefore, it seems that the pentafluoroalkyl-side chain of **PfpGly** neglects any interferences with the enzyme's binding pocket. After 6 h of incubation, the β -turn motif flanked with an “Arg-Trp” strand and one opposing Arg residue was found as the remaining digestion product as well as the released dipeptide fragment “Trp-Arg”. The remaining Trp residue is located at the N-terminal strand, but at the C-terminus in the case of α -chymotrypsin, which explains the slight difference in retention times depicted by HPLC analysis.

To get deeper insights into the impact of side chain fluorination on protease cleaving sites, the digestion profiles of **AbuR14**, **MfeGlyR14**, **DfeGlyR14**, and **TfeGlyR14** with both serine proteases were determined as well. All digestion profiles are placed in the Data S1 and the main cleaving sites are presented in Figure 9 for simplicity.

In the context of α -chymotrypsin, the determination of digestion products derived from the solely aliphatic strands became rather sophisticated (see *HPLC chromatograms in the Data S1, Figures S39–S41*). The lack of aromatic P1 amino acids, thus, evolved a non-specific cleavage pattern in which the hydrophobic moieties act as both P1 & P1' residues. Increasing the degree of fluorination (**DfeGly**, **TfeGly**) leads to the

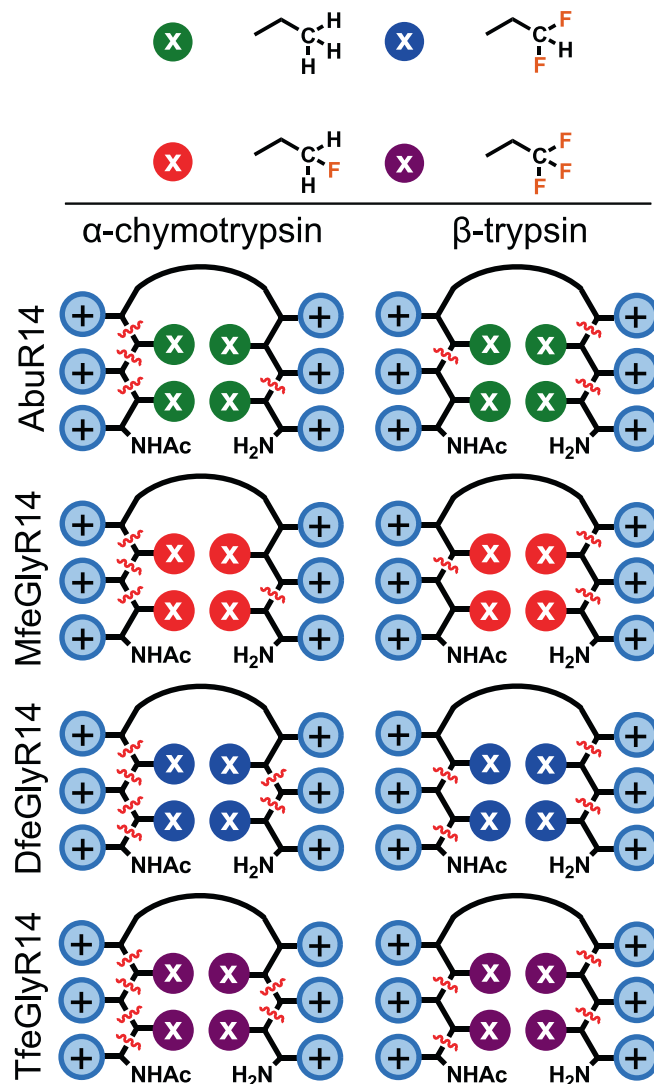


FIGURE 9 Cleavage positions observed in the enzymatic digestion of **AbuR14**, **MfeGlyR14**, **DfeGlyR14**, and **TfeGlyR14** with α -chymotrypsin and β -trypsin. Detailed digestion profiles of each peptide can be found in the Data S1. Cleaving sites are illustrated with squiggly lines (red-colored).

emergence of an Arg (P1)–fluorinated residue (P1') cleaving site on the N-terminal strand as confirmed by HPLC chromatograms & HRMS spectra. These findings further appoint higher degrees of aliphatic side chain fluorination, as present for **DfeGlyR14** and **TfeGlyR14**, to contribute to substrate recognition and peptide degradability. Similar results have been described in prior studies by Asante et al.^[67] A detailed discussion on the digestion profile of the N-terminal strands is provided in the Data S1.

On the C-terminal strand, we consider all hydrophobic residues to act as P1' residues in correlation to the centrally located Arg residue (P1). Again, the incorporation of **DfeGly** and **TfeGly** emerges a further cleaving site in which these amino acids serve as additional P1 residues. An increase in intrinsic hydrophobicity and spatial demand, consequently, acts as leverage for favored P1-S1 interactions in terms of α -chymotrypsin.

When selecting β -trypsin as an enzyme we obtained, as described for the SAJO-derivatives, comparable digestion plots. A slight difference was constituted for DfeGlyR14 and TfeGlyR14 since both substrates possess a further cleavage site between the acetylated Arg (P1) and respective hydrophobic moiety (P1') on the N-terminal strand. Similarly, an increase in fluorination exhibits an enhanced hydrophobic character and, thus, attracts the fluorinated residue into the S1' subsite of β -trypsin.

In summary, we explored and quantified a retainment of enzymatic degradability (when using α -chymotrypsin and β -trypsin) for both amphipathic motifs despite the degree of side chain fluorination. Experimentally described fluorine-triggered changes on the main cleavage sites suggest favored interactions of these non-natural derivatives with both proteases. This interesting and rarely described phenomenon^[21] is going to be further pursued in future work.

4 | CONCLUSION

In this work, we elucidated the impact of side chain fluorination on the antimicrobial activity and proteolytic stability for two series of amphipathic β -hairpin peptides. The incorporation of a wide range of unnatural & aliphatic building blocks with distinctive degrees of fluorination retained secondary structure formation and functioned as an approach to strengthen peptide hydrophobicity. MIC screenings revealed a correlation between fluorine-enhanced hydrophobicity and superior AMP activities. In this manner, the peptide SAJO-PfpGly equipped with two pentafluoro-alkylated residues was identified as the most potent AMP within this work. Simultaneously, our results may indicate a decrease in AMP activity by fluorine-induced polarity originating from the partially fluorinated side chains of MfeGly and DfeGly. All peptides presented in this work revealed zero or low values of blood cell hemolysis and cytotoxicity, which opens the door for potential therapeutical applications. Most interestingly, the implementation of fluorinated amino acids has been proven in this context to preserve peptide degradability while causing notable changes in enzyme-substrate recognition. This is supported by the identification of diverse cleaving sites for the fluorinated substrates. Our data set confirms fluorinated amino acids even with a large fluoroalkyl side chain (PfpGly) to be tolerated as substrates by α -chymotrypsin and β -trypsin; a finding that could be useful for the de novo design of artificial but enzyme-degradable peptide biomaterials. Herein described biological properties of the polyfluorinated β -hairpins highlight the tremendous opportunities which tailor-made fluorinated amino acids offer as a toolbox in modern peptide engineering to develop next-generation peptide-based antimicrobial drugs.

AUTHOR CONTRIBUTIONS

Beate Kokschi, Marcus Fulde, and Suvrat Chowdhary conceived the overall project. Beate Kokschi and Marcus Fulde provided guidance on data analysis and interpretation. Suvrat Chowdhary synthesized fluorinated amino acids and peptides, designed, and performed experiments (HPLC, CD, 6-FAM leaking, hemolysis, peptide digestion), analyzed

and interpreted data sets, and wrote the manuscript. Tim Pelzer performed MIC, toxicity, and hemolysis studies. Mareike Saathoff performed MIC studies. Elisa Quaas performed toxicity studies. Johanna Pendl performed TEM measurements.

ACKNOWLEDGMENTS

S.C. and B.K. gratefully acknowledge financial support by the Deutsche Forschungsgemeinschaft (DFG) through the collaborative research center CRC-1349 "Fluorine-Specific Interactions" project no. 387284271. We thank Dr. Anil Kumar Sahoo and Prof. Dr. Roland R. Netz for fruitful scientific discussions. We would like to acknowledge the assistance of the Core Facility BioSupraMol supported by the DFG. We thank Tiemo tom Dieck for experimental help and Pascal-Kolja Hass for TEM expertise. Finally, we thank Thomas Hohmann & Michael Dyrks for providing the fluorinated amino acid PfpGly. Open Access funding enabled and organized by Projekt DEAL.

CONFLICT OF INTEREST STATEMENT

Beate Kokschi serves as an Advisory Board member of Peptide Science and was excluded from the peer-review process and all editorial decisions related to the publication of this article. The authors declare no conflict of interest.

DATA AVAILABILITY STATEMENT

The data that support the findings of this study are available from the corresponding author (Prof. Dr. Beate Kokschi) upon reasonable request.

ORCID

Suvrat Chowdhary  <https://orcid.org/0000-0001-8669-4362>

Beate Kokschi  <https://orcid.org/0000-0002-9747-0740>

REFERENCES

- [1] R. B. Dyer, S. J. Maness, E. S. Peterson, S. Franzen, R. M. Fesinmeyer, N. H. Andersen, *Biochemistry* **2004**, 43(36), 11560.
- [2] L. Wang, N. Wang, W. Zhang, X. Cheng, Z. Yan, G. Shao, X. Wang, R. Wang, C. Fu, *Signal Transduct. Target. Ther.* **2022**, 7(1), 48.
- [3] A. G. de Brevern, *Sci. Rep.* **2016**, 6(1), 33191.
- [4] E. G. Hutchinson, J. M. Thornton, *Protein Sci.* **1994**, 3(12), 2207.
- [5] S. Fischer, M. Lamping, M. Gold, Y. Röttger, D. Brödje, R. Dodel, R. Frantz, M. A. Mraheil, T. Chakraborty, A. Geyer, *Bioorg. Med. Chem.* **2017**, 25(2), 603.
- [6] S.-n. Nishimura, K. Nishida, M. Tanaka, *Chem. Commun.* **2022**, 58(4), 505.
- [7] G. Wang, X. Li, Z. Wang, *Nucleic Acids Res.* **2016**, 44(D1), D1087.
- [8] Y. Huan, Q. Kong, H. Mou, H. Yi, *Front. Microbiol.* **2020**, 11(2559), 1-21.
- [9] J.-P. S. Powers, R. E. W. Hancock, *Peptides* **2003**, 24(11), 1681.
- [10] R. Kundu, *ChemMedChem* **2020**, 15(20), 1887.
- [11] J. A. Killian, G. von Heijne, *Trends Biochem. Sci.* **2000**, 25(9), 429.
- [12] K. Lewis, *Nat. Rev. Drug Discov.* **2013**, 12(5), 371.
- [13] N. Budisa, V. Kubyschkin, D. Schulze-Makuch, *Life* **2014**, 4(3), 374.
- [14] E. P. Gillis, K. J. Eastman, M. D. Hill, D. J. Donnelly, N. A. Meanwell, *J. Med. Chem.* **2015**, 58(21), 8315.
- [15] M. Salwiczek, E. K. Nyakatura, U. I. M. Gerling, S. Ye, B. Kokschi, *Chem. Soc. Rev.* **2012**, 41(6), 2135.

- [16] D. Giménez, C. Andreu, M. I. d. Olmo, T. Varea, D. Diaz, G. Asensio, *Bioorg. Med. Chem.* **2006**, *14*(20), 6971.
- [17] L. M. Gottler, H. Y. Lee, C. E. Shelburne, A. Ramamoorthy, E. N. Marsh, *ChemBioChem* **2008**, *9*(3), 370.
- [18] L. M. Gottler, R. de la Salud Bea, C. E. Shelburne, A. Ramamoorthy, E. N. G. Marsh, *Biochemistry* **2008**, *47*(35), 9243.
- [19] H. Meng, K. Kumar, *J. Am. Chem. Soc.* **2007**, *129*(50), 15615.
- [20] S. C. Setty, S. Horam, M. Pasupuleti, W. Haq, *Int. J. Pept. Res. Ther.* **2017**, *23*(2), 213.
- [21] S. Huhmann, B. Kokschi, *Eur. J. Org. Chem.* **2018**, 2018(27–28), 3667.
- [22] Z. Lai, X. Yuan, H. Chen, Y. Zhu, N. Dong, A. Shan, *Biotechnol. Adv.* **2022**, *59*, 107962.
- [23] S. Chowdhary, R. F. Schmidt, A. K. Sahoo, T. tom Dieck, T. Hohmann, B. Schade, K. Brademann-Jock, A. F. Thünemann, R. R. Netz, M. Grzdzinski, B. Kokschi, *Nanoscale* **2022**, *14*(28), 10176.
- [24] T. Hohmann, M. Dyrks, S. Chowdhary, M. Weber, D. Nguyen, J. Moschner, B. Kokschi, *J. Org. Chem.* **2022**, *87*(16), 10592.
- [25] C. K. Thota, A. A. Berger, B. Harms, M. Seidel, C. Böttcher, H. von Berlepsch, C. Xie, R. Süßmuth, C. Roth, B. Kokschi, *Pept. Sci.* **2020**, *112*(1), e24130.
- [26] A. J. Cameron, K. G. Varnava, P. J. B. Edwards, E. Harjes, V. Sarojini, *J. Pept. Sci.* **2018**, *24*(8–9), e3094.
- [27] A. J. Cameron, C. J. Squire, P. J. B. Edwards, E. Harjes, V. Sarojini, *Chem. Asian J.* **2017**, *12*(24), 3195.
- [28] A. J. Cameron, P. J. B. Edwards, E. Harjes, V. Sarojini, *J. Med. Chem.* **2017**, *60*(23), 9565.
- [29] F. He, J. Bao, X. Y. Zhang, Z. C. Tu, Y. M. Shi, S. H. Qi, *J. Nat. Prod.* **2013**, *76*(6), 1182.
- [30] S. S. Kale, G. Priya, A. S. Kotmale, R. L. Gawade, V. G. Puranik, P. R. Rajamohanam, G. J. Sanjayan, *Chem. Commun.* **2013**, *49*(22), 2222.
- [31] K. G. Varnava, P. J. B. Edwards, A. J. Cameron, E. Harjes, V. Sarojini, *J. Pept. Sci.* **2020**, *27*, e3291.
- [32] T. Podewin, M. S. Rampp, I. Turkanovic, K. L. Karaghiosoff, W. Zinth, A. Hoffmann-Röder, *Chem. Commun.* **2015**, *51*(19), 4001.
- [33] A. G. Cochran, N. J. Skelton, M. A. Starovasnik, *Proc. Natl. Acad. Sci. U. S. A.* **2001**, *98*(10), 5578.
- [34] J. Leppkes, N. Dimos, B. Loll, T. Hohmann, M. Dyrks, A. Wieseke, B. G. Keller, B. Kokschi, *RSC Chem. Biol.* **2022**, *3*(6), 773.
- [35] T. L. Gururaja, S. Narasimhamurthy, D. G. Payan, D. C. Anderson, *Chem. Biol.* **2000**, *7*(7), 515.
- [36] S. Brahm, J. Brahm, *J. Mol. Biol.* **1980**, *138*(2), 149.
- [37] Y. H. Zhao, M. H. Abraham, A. M. Zissimos, *J. Org. Chem.* **2003**, *68*(19), 7368.
- [38] U. I. M. Gerling, M. Salwiczek, C. D. Cadicamo, H. Erdbrink, C. Czekelius, S. L. Grage, P. Wadhvani, A. S. Ulrich, M. Behrends, G. Haufe, B. Kokschi, *Chem. Sci.* **2014**, *5*(2), 819.
- [39] T. Vagt, O. Zschörnig, D. Huster, B. Kokschi, *ChemPhysChem* **2006**, *7*(6), 1361.
- [40] J. N. Weinstein, R. Blumenthal, R. D. Klausner, *Methods Enzymol.* **1986**, *128*, 657.
- [41] B. C. Buer, E. N. G. Marsh, *Protein Sci.* **2012**, *21*(4), 453.
- [42] T. J. Silhavy, D. Kahne, S. Walker, *Cold Spring Harbor Perspect. Biol.* **2010**, *2*(5), a000414.
- [43] H. Nikaïdo, *Microbiol. Mol. Biol. Rev.* **2003**, *67*(4), 593.
- [44] F. P. Tally, M. F. DeBruin, *J. Antimicrob. Chemother.* **2000**, *46*(4), 523.
- [45] N. Malanovic, K. Lohner, *Biochim. Biophys. Acta (BBA) Biomembr.* **2016**, *1858*(5), 936.
- [46] J. Li, J.-J. Koh, S. Liu, R. Lakshminarayanan, C. S. Verma, R. W. Beuerman, *Front. Neurosci.* **2017**, *11*, 1–18.
- [47] S. Chowdhary, J. Moschner, D. J. Mikolajczak, M. Becker, A. F. Thünemann, C. Kästner, D. Klemczak, A.-K. Stegemann, C. Böttcher, P. Metrangolo, R. R. Netz, B. Kokschi, *ChemBioChem* **2020**, *21*(24), 3544.
- [48] R. Garcia-Rubio, H. C. de Oliveira, J. Rivera, N. Trevijano-Contador, *Front. Microbiol.* **2020**, *10*, 1–13.
- [49] S. Clark, T. A. Jowitt, L. K. Harris, C. G. Knight, C. B. Dobson, *Commun. Biol.* **2021**, *4*(1), 605.
- [50] X. Zhu, Z. Ma, J. Wang, S. Chou, A. Shan, *PLoS One* **2014**, *9*(12), e114605.
- [51] H. Khandelia, Y. N. Kaznessis, *J. Phys. Chem. B* **2007**, *111*(1), 242.
- [52] X. Bi, C. Wang, W. Dong, W. Zhu, D. Shang, *J. Antibiot.* **2014**, *67*(5), 361.
- [53] Z. Feng, B. Xu, *Biomol. Concepts* **2016**, *7*(3), 179.
- [54] Y. P. Di, Q. Lin, C. Chen, R. C. Montelaro, Y. Doi, B. Deslouches, *Sci. Adv.* **2020**, *6*(18), eaay6817.
- [55] T. Manabe, K. Kawasaki, *Sci. Rep.* **2017**, *7*(1), 43384.
- [56] I. Ojima, *J. Org. Chem.* **2013**, *78*(13), 6358.
- [57] H. Meng, S. T. Krishnaji, M. Beinborn, K. Kumar, *J. Med. Chem.* **2008**, *51*(22), 7303.
- [58] V. Asante, J. Mortier, H. Schlüter, B. Kokschi, *Bioorg. Med. Chem.* **2013**, *21*(12), 3542.
- [59] S. Huhmann, A. K. Stegemann, K. Folmert, D. Klemczak, J. Moschner, M. Kube, B. Kokschi, *Beilstein J. Org. Chem.* **2017**, *13*, 2869.
- [60] B. Kokschi, N. Sewald, H.-J. Hofmann, K. Burger, H.-D. Jakubke, *J. Pept. Sci.* **1997**, *3*(3), 157.
- [61] I. Schechter, A. Berger, *Biochem. Biophys. Res. Commun.* **1968**, *32*(5), 898.
- [62] D. Li, Y. Yang, R. Li, L. Huang, Z. Wang, Q. Deng, S. Dong, *J. Pept. Sci.* **2021**, *27*(9), e3337.
- [63] L. T. Nguyen, J. K. Chau, N. A. Perry, L. de Boer, S. A. J. Zaat, H. J. Vogel, *PLoS One* **2010**, *5*(9), e12684.
- [64] R. L. Hill, in *Advances in Protein Chemistry*, Vol. 20 (Eds: C. B. Anfinsen, M. L. Anson, J. T. Edsall, F. M. Richards), Academic Press, **1965**, p. 37. Cambridge, Massachusetts.
- [65] V. Schellenberger, U. Schellenberger, Y. V. Mitin, H. D. Jakubke, *Eur. J. Biochem.* **1990**, *187*(1), 163.
- [66] L. Hedstrom, *Chem. Rev.* **2002**, *102*(12), 4501.
- [67] V. Asante, J. Mortier, G. Wolber, B. Kokschi, *Amino Acids* **2014**, *46*(12), 2733.
- [68] S. Huhmann, E. K. Nyakatura, H. Erdbrink, U. I. M. Gerling, C. Czekelius, B. Kokschi, *J. Fluorine Chem.* **2015**, *175*, 32.
- [69] T. Kurth, S. Grahn, M. Thormann, D. Ullmann, H.-J. Hofmann, H.-D. Jakubke, L. Hedstrom, *Biochemistry* **1998**, *37*(33), 11434.

SUPPORTING INFORMATION

Additional supporting information can be found online in the Supporting Information section at the end of this article.

How to cite this article: S. Chowdhary, T. Pelzer, M. Saathoff, E. Quaas, J. Pendl, M. Fulde, B. Kokschi, *Pept. Sci.* **2023**, e24306. <https://doi.org/10.1002/pep2.24306>

Fine-tuning the Antimicrobial Activity of β -Hairpin Peptides with Fluorinated Amino Acids

Suvrat Chowdhary^[a], Tim Pelzer^[a], Mareike Saathoff^[b], Elisa Quaas^[c], Johanna Pendl^[d], Marcus Fulde^[b,e] and Beate Koksch*^[a]

[a] S. Chowdhary, T. Pelzer, Prof. Dr. B. Koksch
Institute of Chemistry and Biochemistry
Freie Universität Berlin
Arnimallee 20, 14195 Berlin (Germany)
E-mail: beate.koksch@fu-berlin.de

[b] M. Saathoff, Prof. Dr. M. Fulde
Institute of Microbiology and Epizootics, Centre of Infection Medicine
Freie Universität Berlin
Robert-von-Ostertag-Straße 7, 14163 Berlin (Germany)

[c] E. Quaas
Institute of Chemistry and Biochemistry
Core Facility *SupraFAB*
Freie Universität Berlin
Altensteinstr. 23a, 14195 Berlin (Germany)

[d] Prof. Dr. J. Pendl
Institute of Veterinary Anatomy,
Freie Universität Berlin
Koserstr. 20, 14195 Berlin (Germany)

[e] Prof. Dr. M. Fulde
Veterinary Centre for Resistance Research (TZR),
Freie Universität Berlin,
Robert-von-Ostertag-Straße 8, 14163 Berlin (Germany)

*** Corresponding author:**

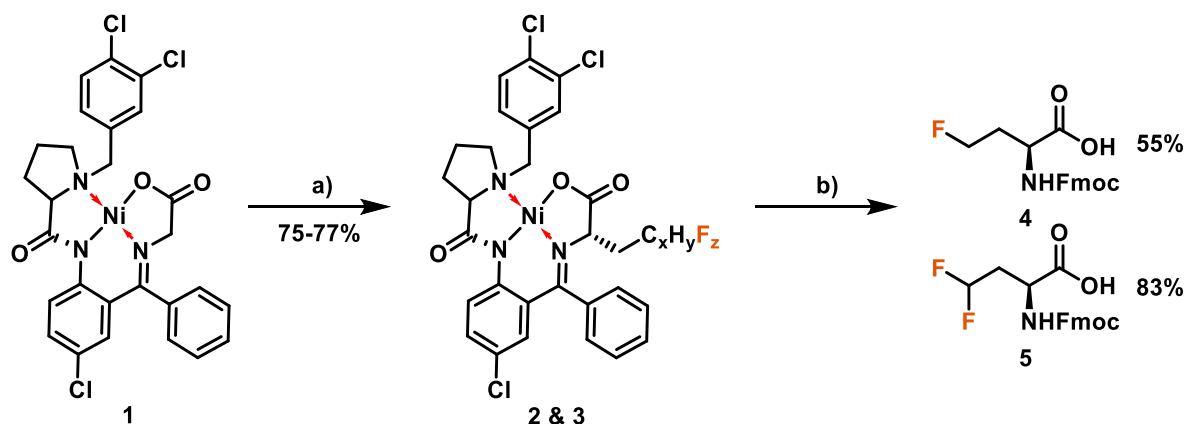
Prof. Dr. Beate Koksch; beate.koksch@fu-berlin.de; Phone: +49 30 838 55344

SUPPORTING INFORMATION

Content

1. Synthesis of fluorinated amino acids MfeGly & DfeGly.....	3
1.1 Synthesis of the CH ₂ F-CH ₂ -/CHF ₂ -alkylated Glycine–Ni(II) Ligand Complex 2 & 3.....	4
1.1 Synthesis of Fmoc-MfeGly-OH (4) & Fmoc-DfeGly-OH (5)	8
2. Synthesis of Ac-[2]Abz-Gly-OH (6)	12
3. Characterization of Fmoc-PfpGly-OH (8)	14
4. Synthesis and purification of peptides.....	16
4.1 AbuR14.....	20
4.2 MfeGlyR14	21
4.3 DfeGlyR14.....	22
4.4 TfeGlyR14.....	23
4.5 SAJO-2	24
4.6 SAJO-Abu	25
4.7 SAJO-TfeGly.....	26
4.8 SAJO-PfpGly	27
4.9 AbuR20.....	28
4.10 TfeGlyR20.....	29
4.11 H-Gly-[D-Phe-[2]Abz]-Gly-OH	30
5. Determination of peptide stock concentrations	31
6. UV and FL spectroscopy	32
7. CD spectroscopy – further data (XR14-series) & information	33
8. 6-FAM leakage assay - Dose-response fitting & 100% POPC leakage.....	35
9. Peptide digestion assay – further data & information.....	37
10. Hemolytic activity assay – further data & information.....	43
11. Transmission electron microscopy (TEM) – SAJO-PfpGly	45
12. Thioflavin T (ThT) fluorescence spectroscopy	47
13. References.....	48

1. Synthesis of fluorinated amino acids MfeGly & DfeGly



- a) 1-fluoro-2-iodoethane / 1,1-difluoro-2-iodoethane, KOH/MeOH, DMF, 0°C, 3.5 h.
b) **1.** 3N HCl, DME, 60°C, 3h. **2.** EDTA-(Na₂), MeCN, 23 °C, 2 h.
3. Fmoc-OSu, Na₂CO₃, THF/H₂O, 23°C, 20 h.

Scheme S1: Synthetic strategy to obtaining fluorinated amino acids Fmoc-MfeGly-OH (**4**) and Fmoc-DfeGly-OH (**5**).

The fluorinated amino acids Fmoc-MfeGly-OH (**4**) and Fmoc-DfeGly-OH (**5**) were obtained through a five-step synthetic strategy based on the stereoselective alkylation of a chiral Ni-ligand **1** introduced by Soloshonok *et al.*. A standard protocol for the synthesis of **1** can be found in literature.¹ The alkylation of **1** and subsequent release and Fmoc-protection of amino acids are based on an optimized strategy developed by Hohmann *et al.* for the gram-scale synthesis of a wide range of aliphatic fluorinated derivatives. The gram-scale synthesis of Fmoc-TfeGly-OH was accomplished according to Chowdhary *et al.*² The amino acid Fmoc-PfpGly-OH was provided by Thomas Hohmann and was synthesized to analog protocols accordingly.³

1.1 Synthesis of the CH₂F-CH₂-/CHF₂-alkylated Glycine–Ni(II) Ligand

Complex 2 & 3

The chiral Ni ligand (20.00 g, 33.3 mmol, 1.00 equiv.) and 1-fluoro-2-iodoethane (8.68 g, 5.85 mL, 49.9 mmol, 1.50 equiv.) / 1,1-difluoro-2-iodoethane (9.57 g, 4.39 mL, 49.9 mmol, 1.50 equiv.) were dissolved in dried and freshly degassed dimethylformamide (200 mL) under inert conditions. The reaction mixture was cooled down to 0 °C. Potassium hydroxide (1.96 g, 34.9 mmol, 1.05 equiv.) was dissolved in dried and freshly degassed MeOH (18 mL) and added dropwise to the reaction mixture. The mixture was stirred for 3 h at 0 °C for the synthesis of the mono- and difluorinated compounds. Water (64 mL) was added and stirred for 1 h at room temperature. Subsequently, water (36 mL) was again added, and stirred for 1 h at room temperature. The reaction mixture was filtered and washed with a mixture of dimethylformamide/water (2:1, 36 mL) and water (40 mL). Finally, the purified compounds were dried *in vacuo* at 55 °C.

The title compounds **2** and **3** were obtained as red coloured solid (**2**, 16.24 g, 25.1 mmol, 75%) or purple coloured solid (**3**, 17.08 g, 25.7 mmol, 77%).

CH₂F-CH₂-alkylated Glycine–Ni(II) Ligand Complex 2

¹H NMR (600 MHz, METHANOL-D₄) δ = 8.81 (d, J = 2.1 Hz, 1H), 8.26 – 8.24 (m, 1H), 7.97 (d, J = 9.3 Hz, 1H), 7.66 – 7.62 (m, 1H), 7.59 (t, J = 7.6 Hz, 1H), 7.52 (t, J = 6.5 Hz, 1H), 7.47 (d, J = 8.3 Hz, 1H), 7.43 (d, J = 7.5 Hz, 1H), 7.10 (dd, J = 9.3, 2.6 Hz, 1H), 7.02 (dt, J = 7.7 Hz, 1H), 6.54 (d, J = 2.6 Hz, 1H), 4.91 – 4.82 (m, 1H), 4.81 – 4.71 (m, 1H) 4.18 (d, J = 12.6 Hz, 1H), 4.04 (dd, J = 3.7 Hz, 1H), 3.58 – 3.50 (m, 2H), 3.39 – 3.34 (m, 2H), 2.66 – 2.57 (m, 2H), 2.24 – 2.13 (m, 2H), 2.10 – 2.01 (m, 1H) ppm.

¹³C {¹H} NMR (151 MHz, METHANOL-D₄): δ = 181.29, 180.13, 171.28, 140.61, 136.61, 133.31, 133.00, 132.73, 131.89, 131.73, 131.10, 130.80, 130.23, 129.24, 129.14, 127.79, 127.62, 127.02, 125.53, 124.22, 80.20, 79.10, 71.36, 67.49, 62.57, 58.27, 34.88, 30.59, 23.03 ppm.

¹⁹F NMR (565 MHz, METHANOL-D₄): δ = -218.30 – -218.58 (m, 3F) ppm.

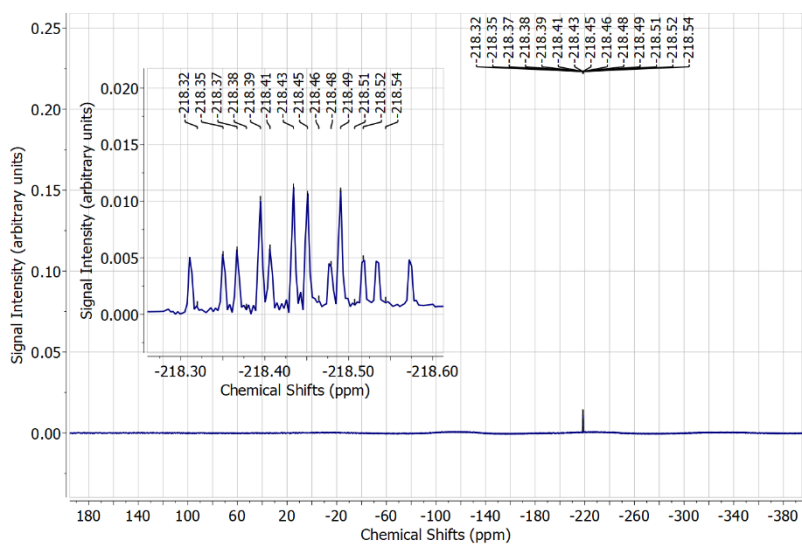
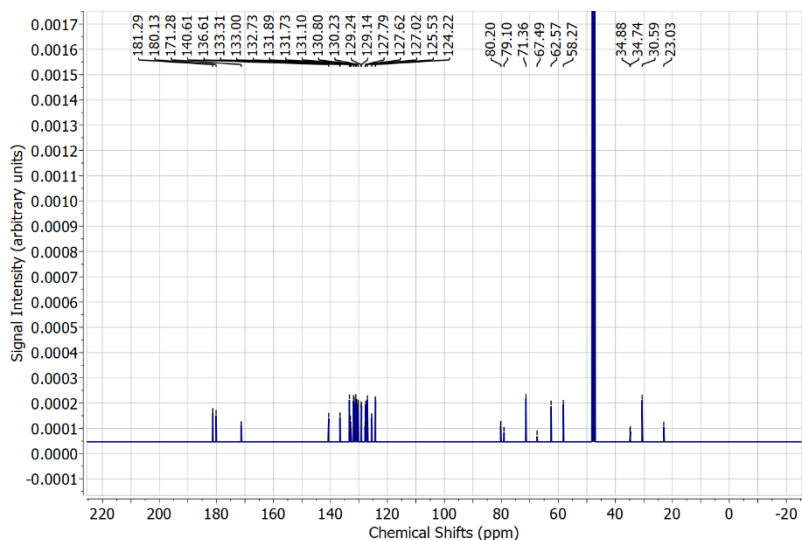
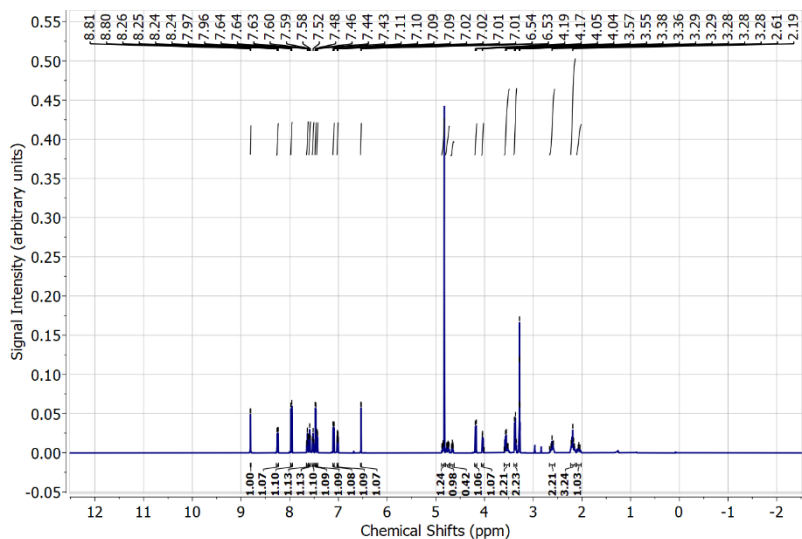


Figure S1: ^1H NMR (600 MHz), ^{13}C { ^1H } NMR (151 MHz) and ^{19}F NMR (565 MHz) spectrum of the $\text{CH}_2\text{F}-\text{CH}_2$ -alkylated Glycine-Ni(II) Ligand Complex **2**.

CHF₂-CH₂-alkylated Glycine-Ni(II) Ligand Complex 3

¹H NMR (600 MHz, METHANOL-D₄) δ = 8.79 (d, J = 2.1 Hz, 1H), 8.27 (dd, J = 8.2 Hz, 1H), 7.98 – 7.94 (m, 1H), 7.60-7.41 (m, 2H), 7.55 – 7.50 (m, 2H), 7.48 – 7.44 (m, 2H), 7.11 (dd, J = 11.9 Hz, 1H), 7.04 (d, J = 1.5 Hz, 1H), 6.54 (d, J = 2.6 Hz, 1H), 4.18 (d, J = 12.5 Hz, 1H), 4.09 – 4.03 (m, 1H), 3.70 – 3.48 (dd, J = 13.7, 4.7 Hz, 2H), 3.41 – 3.33 (m, 2H), 2.66 – 2.56 (m, 2H), 2.42 (td, $2J$ = 9.6 Hz, $3J$ = 6.2 Hz, 1H), 2.26 – 2.08 (m, 3H) ppm.

¹³C {¹H} NMR (151 MHz, METHANOL-D₄): δ = 181.30, 179.35, 171.94, 140.76, 136.58, 133.29, 133.17, 132.86, 132.74, 131.95, 131.91, 131.12, 130.83, 130.40, 129.85, 129.37, 129.24, 128.42, 127.56, 126.97, 125.55, 124.27, 114.95, 71.28, 62.55, 58.31, 30.55, 30.50, 23.14.

¹⁹F NMR (565 MHz, METHANOL-D₄): δ = -155.45 – -117.53 (m, 3F) ppm.

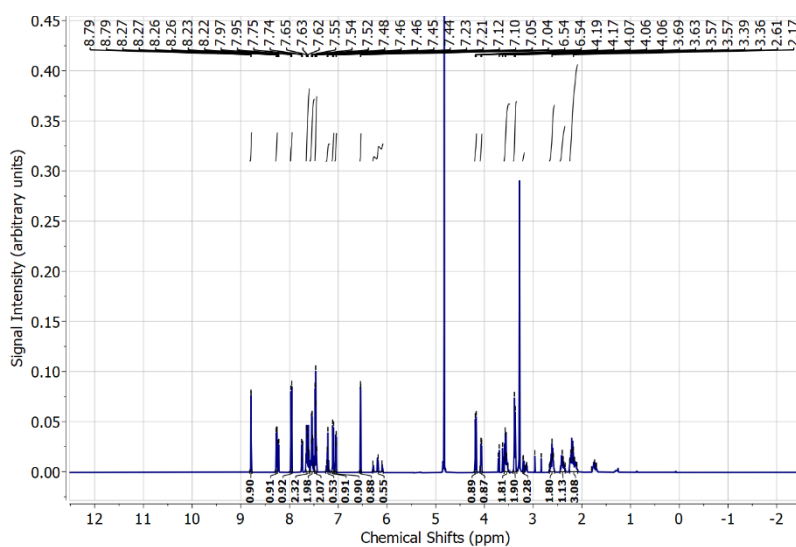


Figure S2: ¹H NMR (600 MHz) spectrum of the CHF₂-CH₂-alkylated Glycine-Ni(II) Ligand Complex 3.

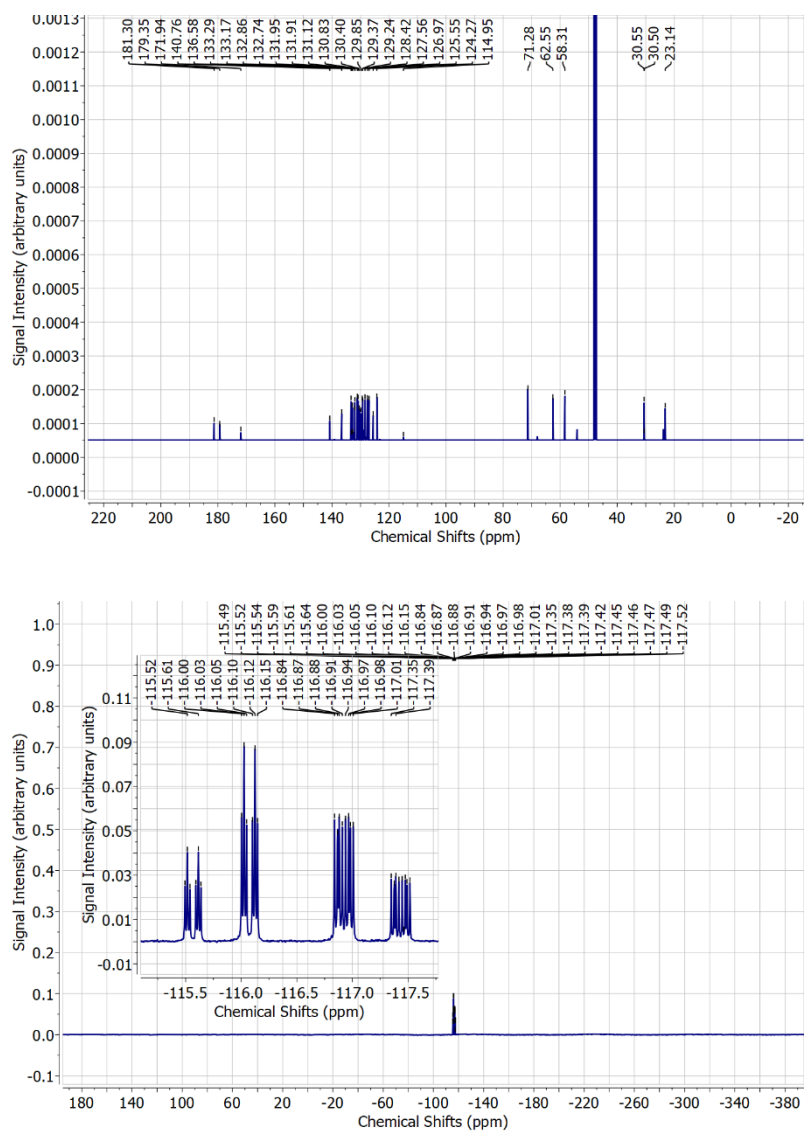


Figure S3: ¹³C {¹H} NMR (151 MHz) and ¹⁹F NMR (565 MHz) spectrum of the CHF₂-CH₂-alkylated Glycine-Ni(II) Ligand Complex 3.

1.1 Synthesis of Fmoc-MfeGly-OH (4) & Fmoc-DfeGly-OH (5)

Compound **2** / **3** (15 g, 0.023 mol [**2**] / 0,022 mol [**3**], 1 equiv.) was dissolved in dimethoxyethane (110 mL) and 3N HCl (66.5 mL) and heated to 60 °C while stirring for 3h. Then the mixture was filtered and washed with water (30 mL). The combined solutions were concentrated, leading to further precipitation of Ni-ligand residues. These precipitates were filtered and washed with water (25 mL) and the solutions were combined. EDTA-(Na₂) (8.56 g, 0.023 mol, 1 equiv.) in MeCN (55 mL) was added and the mixture was stirred for 2 h at 23 °C. The reaction was quenched by adjusting the pH to 8-8.5 by use of a 48%-NaOH solution. Afterwards, Na₂CO₃ (4.9 g, 0.046 mol, 2 equiv.) was supplemented and Fmoc-OSu (7.75 g, 0.023 mol, 1 equiv.) in acetone (45 mL) was added slowly while the reacting mixture was stirred at 23 °C for 20 h. Then, MeCN and acetone were removed from the solution under reduced pressure. The aqueous solution was washed with Et₂O (3 * 30 mL) to remove leftovers of Fmoc-OSu. Then, the pH of the solution was adjusted to 2 by using HCl_{conc.} before the aqueous phase was extracted with ethyl acetate (6 * 50 mL). The combined organic phases were dried over Na₂SO₄, filtered, concentrated, and dried *in vacuo* at 55 °C. The crude product (about 8.5 g) was dissolved in ethyl acetate (30 mL) and toluene (150 mL) and warmed to 75 °C for complete dissolution. Then, the solution was concentrated under reduced pressure and after further addition of toluene (75 mL) concentrated again to a total volume of approximately 100 mL. This solution was left to stand overnight at room temperature, leading to precipitation of pure Fmoc-protected amino acids MfeGly (**4**) and DfeGly (**5**). The amino acid was filtered, washed with ice-cold toluene (100 mL) and hexane (100 mL). Fmoc-MfeGly-OH (**4**) was washed additionally with ice-cold DCM (20 mL) to remove impurities. Both products were afterwards dried *in vacuo* at 55 °C.

The title compounds **4** and **5** were both obtained as white solid substances (4.34 g, 0.0126 mol, 55% [**4**] and 6.59 g, 0.0182 mol, 83% [**5**]).

Fmoc-MfeGly-OH (4)

¹H NMR (600 MHz, METHANOL-D₄): δ = 7.76 (d, J = 7.6 Hz, 2H), 7.64 (t, J = 7.5 Hz, 2H), 7.35 (t, J = 7.5 Hz, 2H), 7.27 (t, J = 7.4 Hz, 2H), 4.56 – 4.40 (m, 2H), 4.37 – 4.31 (m, 2H), 4.31 – 4.25 (m, 1H), 4.19 (t, J = 7.1 Hz, 1H), 2.31 – 2.21 (m, 1H), 2.03 – 1.92 (m, 1H).

¹³C {¹H} NMR (151 MHz, METHANOL-D₄): δ = 173.98, 157.36, 143.99, 143.85, 141.27, 127.45, 126.84, 126.81, 124.93, 119.58, 80.59, 79.50, 66.66, 50.51, 32.18, 32.05.

¹⁹F NMR (565 MHz, METHANOL-D₄): δ = -222.46 – -222.83 (m, 3F)

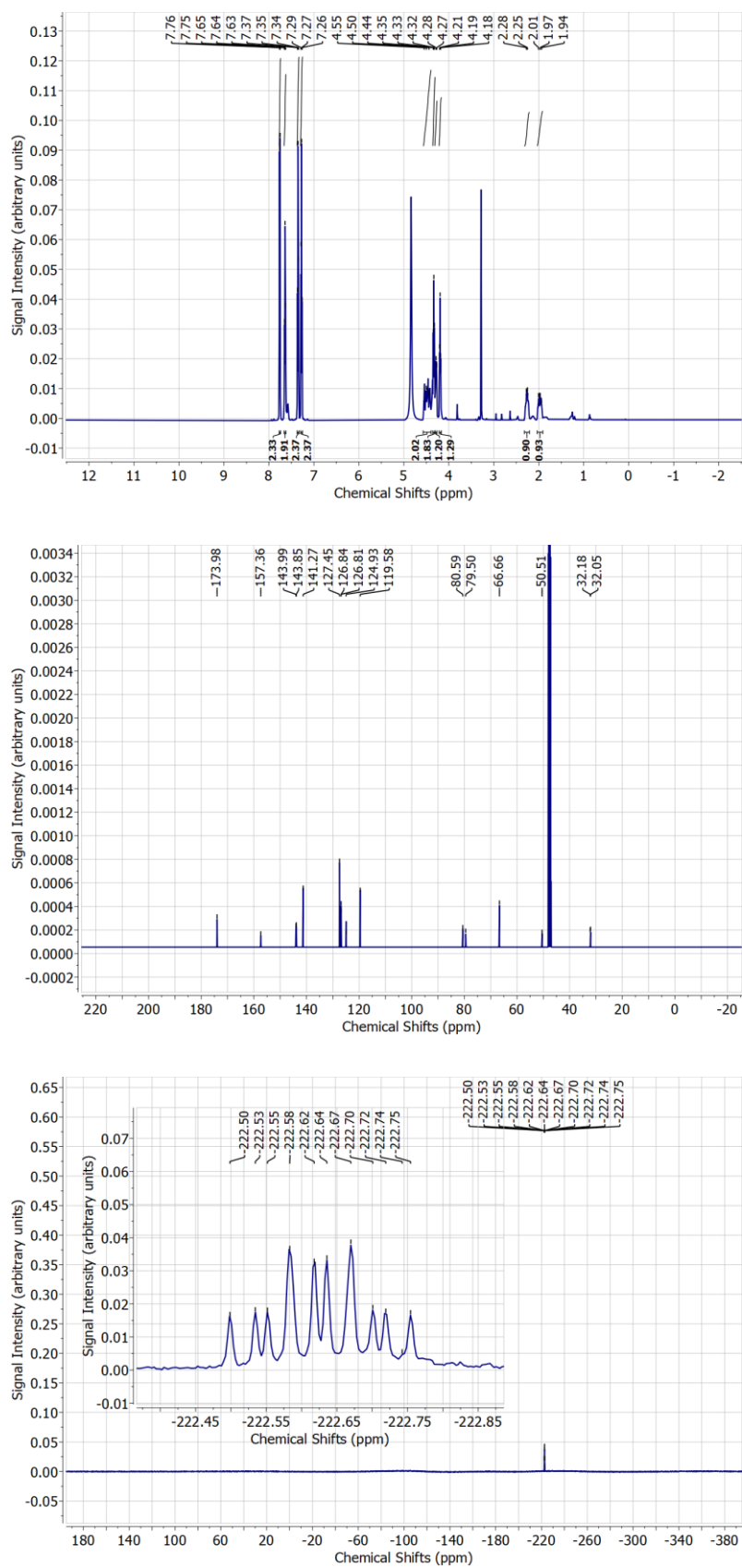


Figure S4: ^1H NMR (600 MHz), ^{13}C { ^1H } NMR (151 MHz) and ^{19}F NMR (565 MHz) spectrum of Fmoc-MfeGly-OH (**4**).

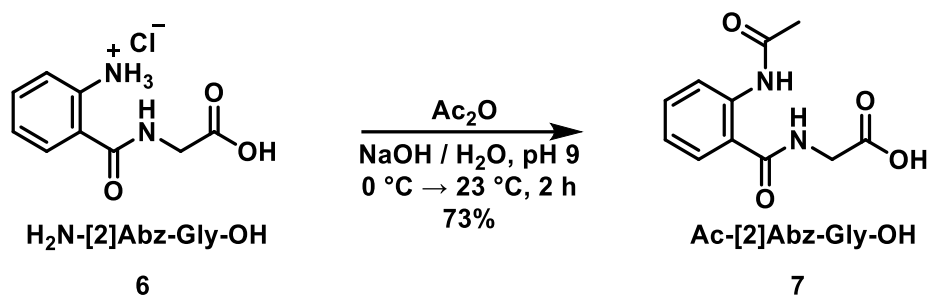
Fmoc-DfeGly-OH (5)

¹H NMR (600 MHz, METHANOL-D₄): δ = 7.77 (d, J = 7.6 Hz, 2H), 7.67 – 7.62 (m, 2H), 7.36 (t, J = 7.0 Hz, 2H), 7.28 (td, J = 7.4, 1.2 Hz, 2H), 6.03 – 5.81 (m, 1H), 4.41 – 4.31 (m, 2H), 4.35 – 4.27 (m, 1H), 4.20 (t, J = 6.9 Hz, 1H), 2.43 – 2.33 (m, 1H), 2.26 – 2.16 (m, 1H).

¹³C {¹H} NMR (151 MHz, METHANOL-D₄): δ = 172.75, 157.13, 143.95, 143.83, 141.28, 127.46, 126.82, 124.92, 119.58, 117.30, 115.72, 66.70, 35.84, 35.69, 35.54, 24.93.

¹⁹F NMR (565 MHz, METHANOL-D₄): δ = -117.45 – -119.06 (m, 3F).

2. Synthesis of Ac-[2]Abz-Gly-OH (6)



Scheme S2: Synthesis of Ac-[2]Abz-Gly-OH (**7**) by acetylation of H₂N-[2]Abz-Gly-OH * HCl (**6**).

As shown in **Scheme S2**, The synthesis of Ac-[2]Abz-Gly-OH (**7**) comprises a single-step synthetic strategy by treating the commercially available H₂N-[2]Abz-Gly-OH * HCl (**6**) with a standard acetylation-protocol.

H₂N-[4]Abz-Gly-OH * HCl (250 mg, 1.083 mmol, 1 equiv.) was dissolved in MilliQ-H₂O (3 mL). Then, the pH was adjusted to 9 with a 1M NaOH solution. The mixture was cooled to 0 °C and freshly distilled acetic anhydride (0.20 mL, 5.14 mmol, 2 equiv.) was added slowly. The pH was again adjusted to 9 and the reacting mixture was stirred for 2 h while warming to 23 °C. Thereupon HCl_{conc.} Was added slowly until a pH of 2 was reached. The reaction mixture was extracted with ethyl acetate (5 × 5 mL). The organic layers were combined, dried over Na₂SO₄, filtered, concentrated, and dried *in vacuo*.

The title compound **7** was obtained as a yellow powder (186.7 mg, 0.79 mol, 73%).

¹H NMR (600 MHz, METHANOL-D₄): δ = 8.92 (d, *J* = 9.4 Hz, 1H), 8.29 (dd, *J* = 7.9, 1.5 Hz, 1H), 8.09 (d, *J* = 9.0 Hz, 1H), 7.81 - 7.77 (m, 1H), 4.70 (s, 2H), 2.77 (s, 3H).

¹³C {¹H} NMR (151 MHz, METHANOL-D₄): δ = 172.50, 170.87, 170.50, 138.56, 132.30, 128.24, 124.00, 123.18, 122.06, 41.47, 23.92.

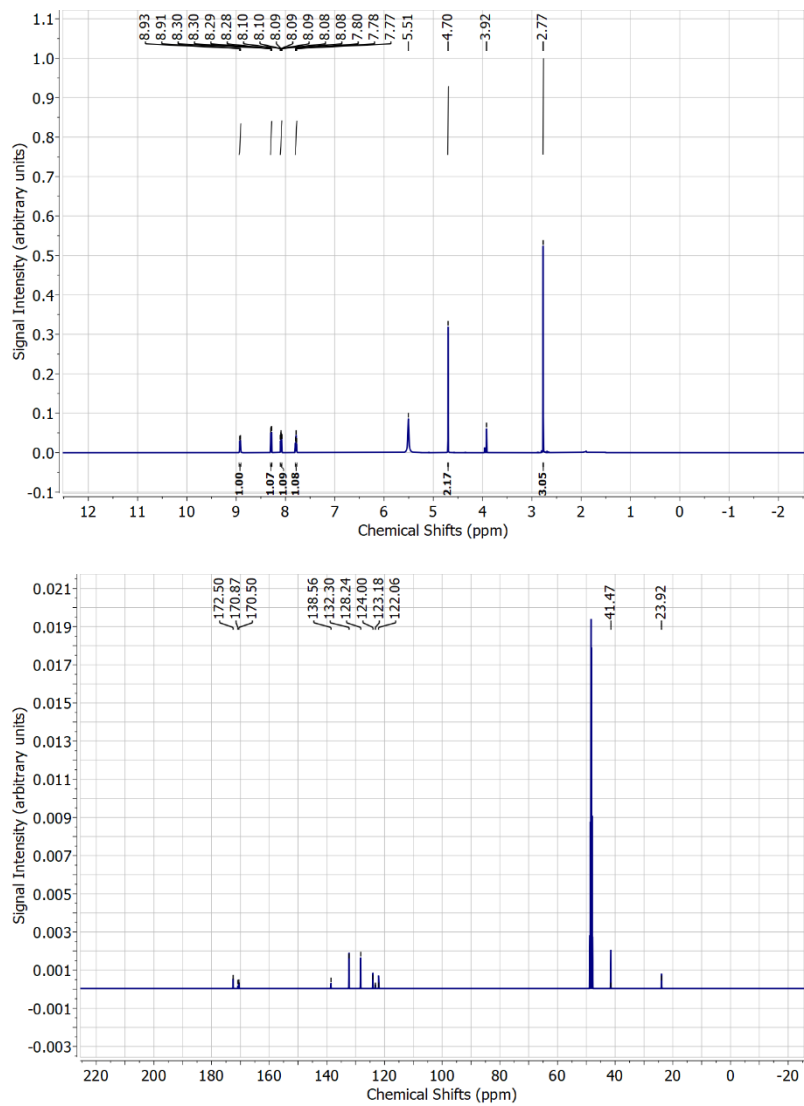


Figure S6: ^1H NMR (600 MHz) and ^{13}C { ^1H } NMR (151 MHz) spectrum of Ac-[2]Abz-Gly-OH (**7**).

3. Characterization of Fmoc-PfpGly-OH (8)

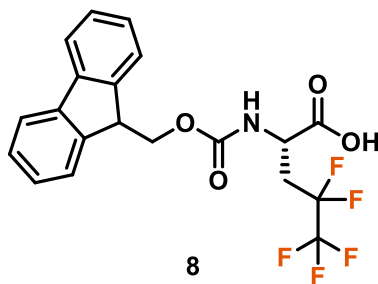


Figure S7: Chemical structure of Fmoc-PfpGly-OH (**8**).

^1H NMR (600 MHz, METHANOL- D_4): δ = 8.41 (d, J = 7.6 Hz, 2H), 8.28 (d, J = 7.6 Hz, 2H), 8.00 (t, J = 7.5 Hz, 2H), 7.92 (t, J = 7.5 Hz, 2H), 5.18 (d, J = 9.9 Hz, 1H), 4.97 (d, J = 7.1 Hz, 1H), 4.84 (d, J = 7.1 Hz, 1H), 3.48 – 3.37 (m, 1H), 3.32 – 3.21 (m, 1H).

^{13}C { ^1H } NMR (151 MHz, METHANOL- D_4): δ = 172.60, 157.47, 144.45, 141.86, 128.14, 127.44, 125.62, 120.12, 67.57, 32.13, 25.75.

^{19}F NMR (565 MHz, METHANOL- D_4): δ = -86.67 (s), -118.21 (ddd, J = 267.3, 26.1, 8.5 Hz).

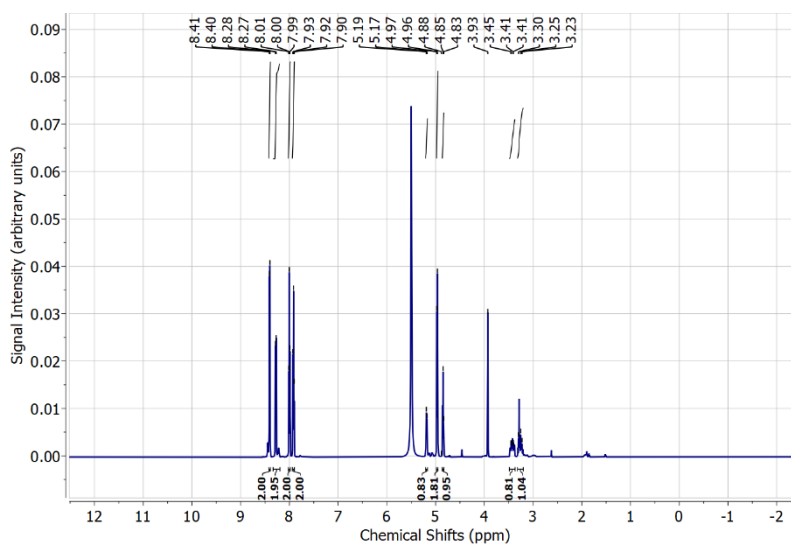


Figure S8: ^1H NMR (600 MHz) and ^{13}C { ^1H } NMR (151 MHz) spectrum of Fmoc-PfpGly-OH (**8**).

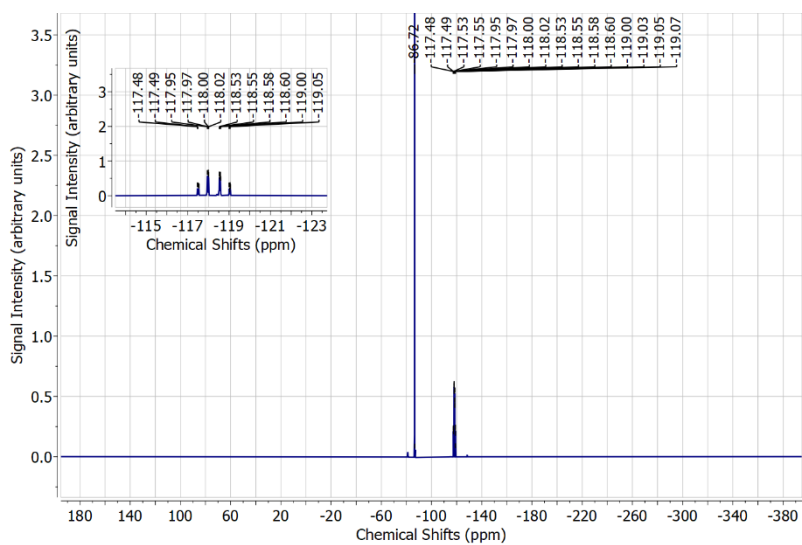
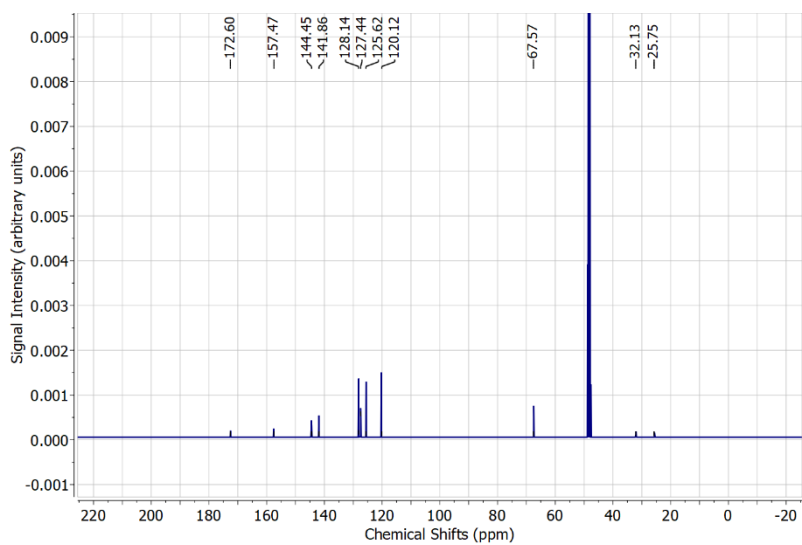


Figure S9: ^{13}C { ^1H } NMR (151 MHz) and ^{19}F NMR (565 MHz) spectrum of Fmoc-PfpGly-OH (**8**).

4. Synthesis and purification of peptides

Peptide synthesis was performed with a Liberty Blue automated microwave-assisted peptide synthesizer (CEM Corporation, Mathews, NC, USA) by a Fmoc-based SPPS approach. **AbuR14**, **AbuR20**, **MfeGlyR14**, **DfeGlyR14**, **TfeGlyR14** and **TfeGlyR20** were synthesized as C-terminal amides on a Rink Amide ProTide Resin (LL) resin (0.19-0.20 mmol/g resin substitution) on a 0.1 mmol scale. **SAJO-2**, **SAJO-Abu**, **SAJO-TfeGly** and **SAJO-PfpGly** were synthesized as C-terminal acids on a Cl-MPA ProTide LL resin (0.18-0.22 mmol/g resin substitution) on a 0.1 mmol scale. Fmoc deprotection was carried out with 10 wt% piperazine in EtOH/NMP (1/9, v/v). All amino acids were coupled with Oxyma/DIC as activators. Amino acids D-Leu, D-Phe, [2]Abz, D-Ala and Arg were coupled through a “single-coupling” approach. The non-canonical amino acids Abu, MfeGly, DfeGly, TfeGly and PfpGly were introduced with a “special coupling” cycle reported by Leppkes *et al.*⁴ It uses elongated microwave heating time, reduced equivalents of the amino acid (1.5 eq.) employed and additional washing steps between Fmoc deprotection and coupling step. For subsequent capping of N-terminal amino groups with acetic anhydride, a solution of Ac₂O (10 % (v/v) and DIPEA (10 % (v/v) in DMF (6 mL) was added in three batches manually and the reaction was then shaken for 3 * 10 min. For peptide cleavage, the dried resin was treated with 20 mL of TFA/water/TIPS (90/5/5, v/v) for 3 h at room temperature. Afterwards, the resin was washed thrice with TFA and CH₂Cl₂. Organic solvent was removed, and the peptides were dissolved in water & lyophilized overnight before purification by preparative HPLC. Precipitation of peptides in Et₂O was omitted in all cases. General conditions for HPLC purification and SPPS are listed in **table S1** and **S2**. Crude amounts of about **210-250 mg** (0.1 mmol scale SPPS) were generally obtained after SPPS and HPLC purification led to an isolation of about **22-28 mg** pure peptide.

Table S1: Gradient methods used for analytical HPLC. Solvent: **(A)** H₂O + 0.1% TFA / **(B)** ACN + 0.1% TFA

Time [min]	Solvent (A) [%]	Solvent (B) [%]
0	90	10
18	30	70
20	0	100
23	0	100
24	90	10
27	90	10

Table S2: Cycles for automated microwave assisted SPPS with a 0.1 mmol scale on Liberty Blue peptide synthesizer. All reagents were dissolved in DMF, if not otherwise stated.

	<u>Process step</u>	<u>Reagents</u>			<u>Reaction conditions</u>		
		Name	Conc. [M]	Volume [mL]	Temp [°C]	Power [W]	Time [s]
Loading / Single coupling	Loading (Cl-MPA ProTide)	DIPEA	1	2	80	75	60
		KI	0.125	5	90	20	540
	+	Fmoc-AA	0.2	2			
	Washing	DMF	-	4	25	-	5
		Piperazine	10 wt%		75	155	15
	[1] Deprotection	HOBt	0.1	4 ⁽¹⁾	90	30	60
		DMF	-	4	25	-	5
	[2] Washing (4*)	DMF	-	4	25	-	5
	[3] AA coupling	Fmoc-AA	0.2	2.5	75	217	15
		DIC	1	1			
Oxyma		1	0.5	90	43	225	
DIPEA		0.1					
[4] Washing	DMF	-	4	25	-	5	
Special coupling	[1] Deprotection	Piperazine	10 wt%		75	155	15
		HOBt	0.1	4 ⁽¹⁾	90	30	60
	[2] Washing (4* - 9 cycles)	DMF	-	4	25	-	5
	[3] AA coupling	Fmoc-(F)AA	0.05	2.5	75	217	15
		DIC	1	1			
		Oxyma	1	0.5	90	43	585
		DIPEA	0.1				
[4] Washing (4*)	DMF	-	4	25	-	5	

⁽¹⁾ EtOH/NMP, 1/9, v/v

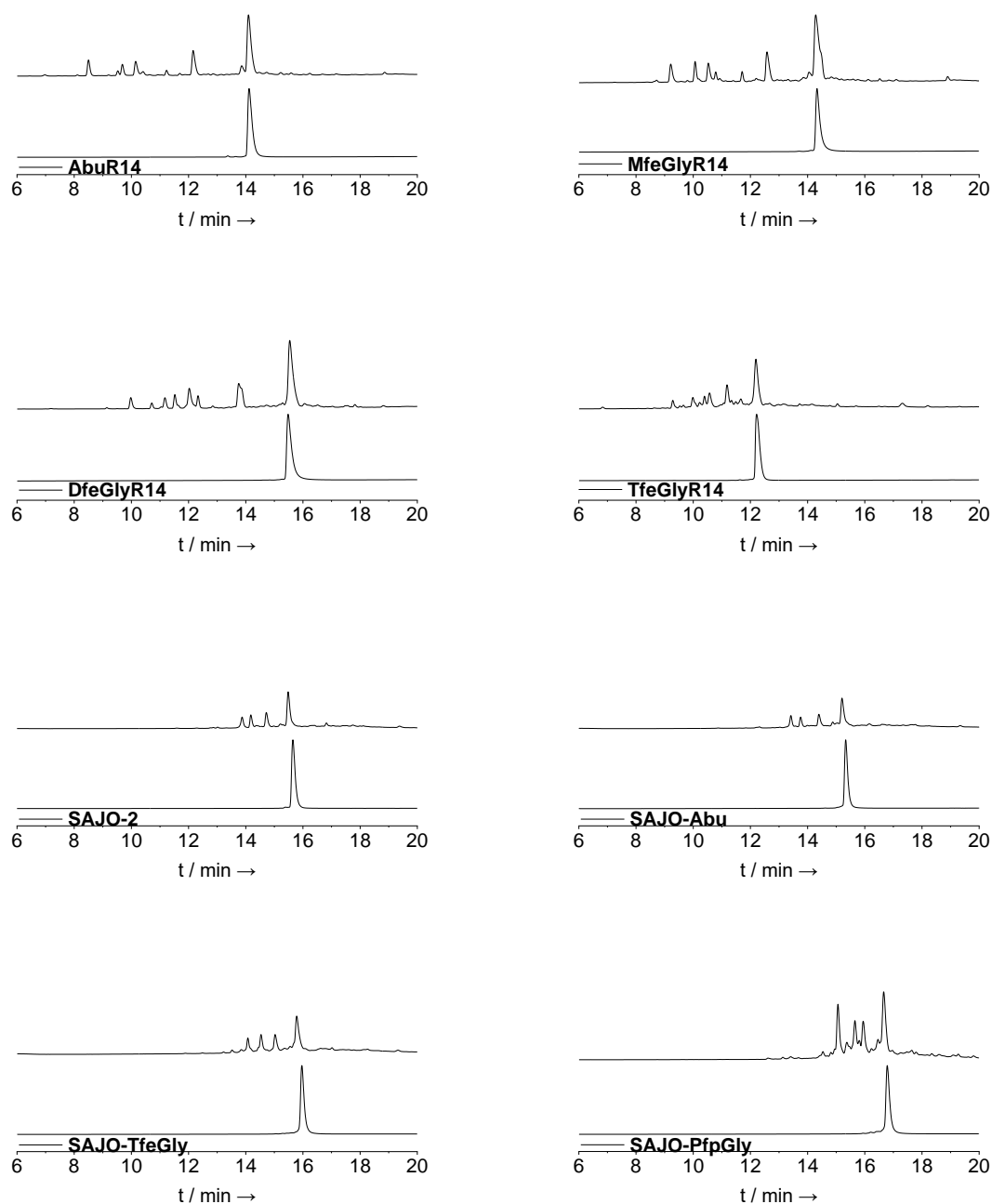


Figure S10: Crude and pure chromatograms of amphipathic peptides. HPLC conditions for **AbuR14**, **MfeGlyR14**, **DfeGlyR14** = (A) H₂O + 0.1% TFA / (B) ACN + 0.1% TFA / gradient: 10% (B) → 40% (B) over 18 min. HPLC conditions for **TfeGlyR14** = (A) H₂O + 0.1% TFA / (B) ACN + 0.1% TFA / gradient: 10% (B) → 70% (B) over 18 min. HPLC conditions for **SAJO-2**, **SAJO-Abu**, **SAJO-TfeGly** and **SAJO-PfpGly** = (A) H₂O + 0.1% TFA / (B) ACN + 0.1% TFA / gradient: 10% (B) → 60% (B) over 18 min.

Table S3: Nomenclature of peptides and their sequences. Substituted amino acids and [2]Abz are three-letter coded. Also, D-amino acids are defined by lower case letters.

Peptide	Sequence
AbuR14	Ac-R- <i>Abu</i> -R- <i>Abu</i> -R-[l-f-[2]Abz-a]-R- <i>Abu</i> -R- <i>Abu</i> -R-NH ₂
MfeGlyR14	Ac-R- <i>MfeGly</i> -R- <i>MfeGly</i> -R-[l-f-[2]Abz-a]-R- <i>MfeGly</i> -R- <i>MfeGly</i> -R-NH ₂
DfeGlyR14	Ac-R- <i>DfeGly</i> -R- <i>DfeGly</i> -R-[l-f-[2]Abz-a]-R- <i>DfeGly</i> -R- <i>DfeGly</i> -R-NH ₂
TfeGlyR14	Ac-R- <i>TfeGly</i> -R- <i>TfeGly</i> -R-[l-f-[2]Abz-a]-R- <i>TfeGly</i> -R- <i>TfeGly</i> -R-NH ₂
SAJO-2	H-R- <i>Val</i> -R- <i>Trp</i> -R-[l-f-[2]Abz-a]-R- <i>Trp</i> -R- <i>Val</i> -R-OH
SAJO-Abu	H-R- <i>Abu</i> -R- <i>Trp</i> -R-[l-f-[2]Abz-a]-R- <i>Trp</i> -R- <i>Abu</i> -R-OH
SAJO-TfeGly	H-R- <i>TfeGly</i> -R- <i>Trp</i> -R-[l-f-[2]Abz-a]-R- <i>Trp</i> -R- <i>TfeGly</i> -R-OH
SAJO-PfpGly	H-R- <i>PfpGly</i> -R- <i>Trp</i> -R-[l-f-[2]Abz-a]-R- <i>Trp</i> -R- <i>PfpGly</i> -R-OH

4.1 AbuR14

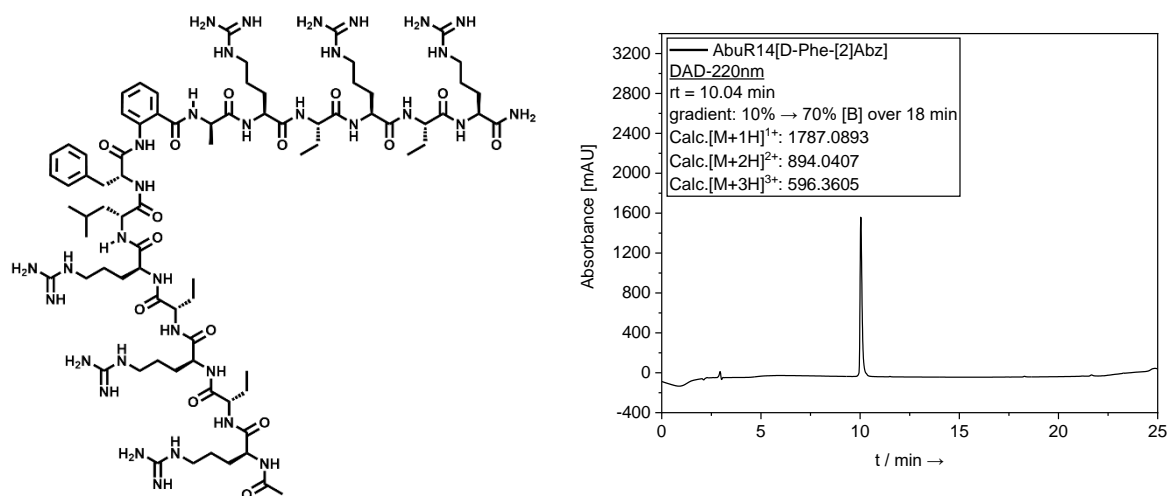


Figure S11: Chemical structure of peptide **AbuR14**. The purity of this peptide after synthesis and isolation was determined through analytical HPLC with DAD detection at 220 nm. HPLC: Hitachi Primaide with Kinetex® C18 RP-column / solvent: **(A)** H₂O + 0.1% TFA / **(B)** ACN + 0.1% TFA / gradient: 10% (B) → 70% (B) over 18 min.

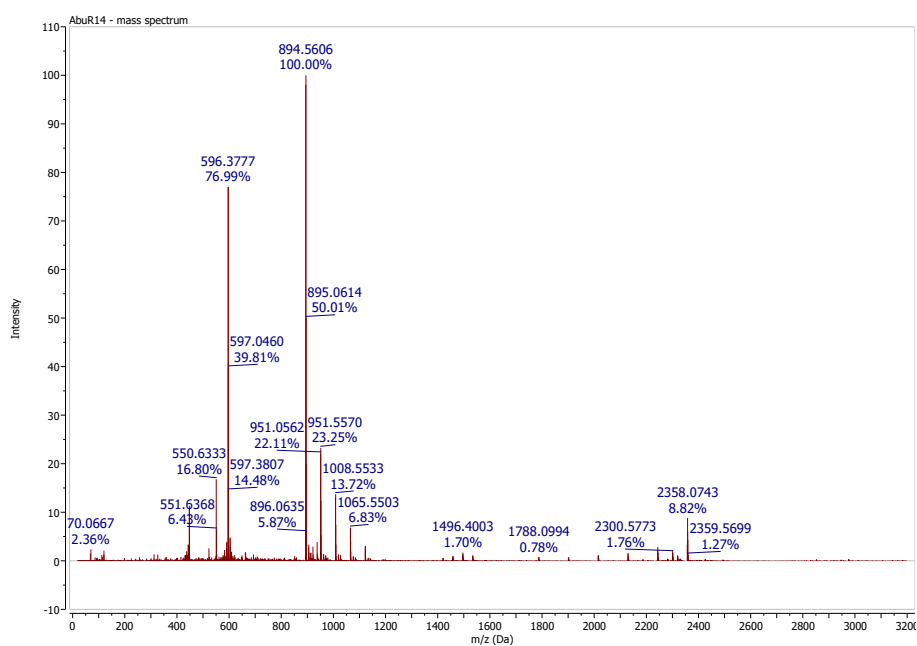


Figure S12: High resolution mass spectrometry (HRMS) spectrum of the purified peptide **AbuR14** in positive ionization mode (20-3200 m/z [Da]). Calculated ion species (M+H)⁺ for this peptide are listed in respective HPLC chromatogram.

4.2 MfeGlyR14

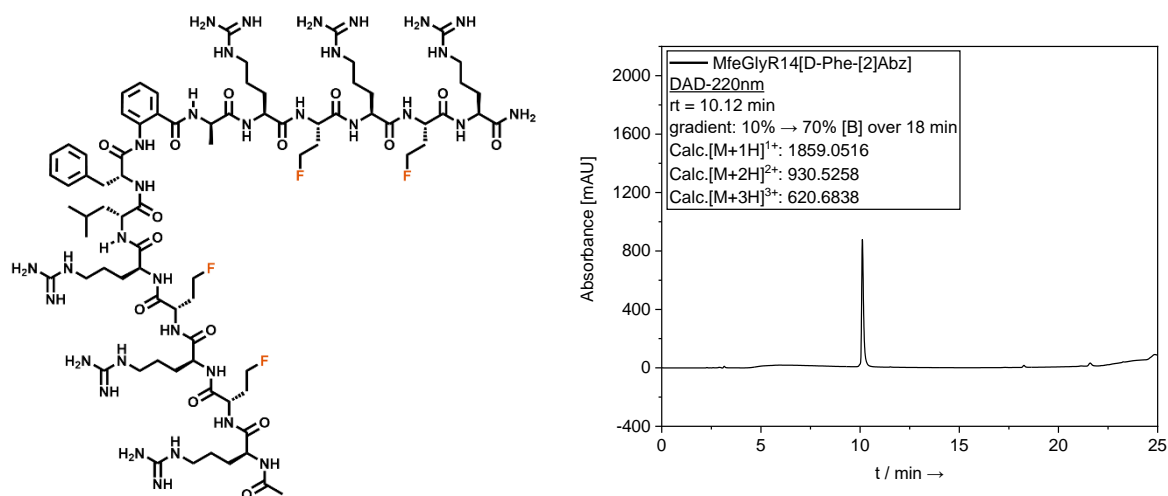


Figure S13: Chemical structure of peptide **MfeGlyR14**. The purity of this peptide after synthesis and isolation was determined through analytical HPLC with DAD detection at 220 nm. HPLC: Hitachi Primaide with Kinetex® C18 RP-column / solvent: **(A)** H₂O + 0.1% TFA / **(B)** ACN + 0.1% TFA / gradient: 10% (B) → 70% (B) over 18 min.

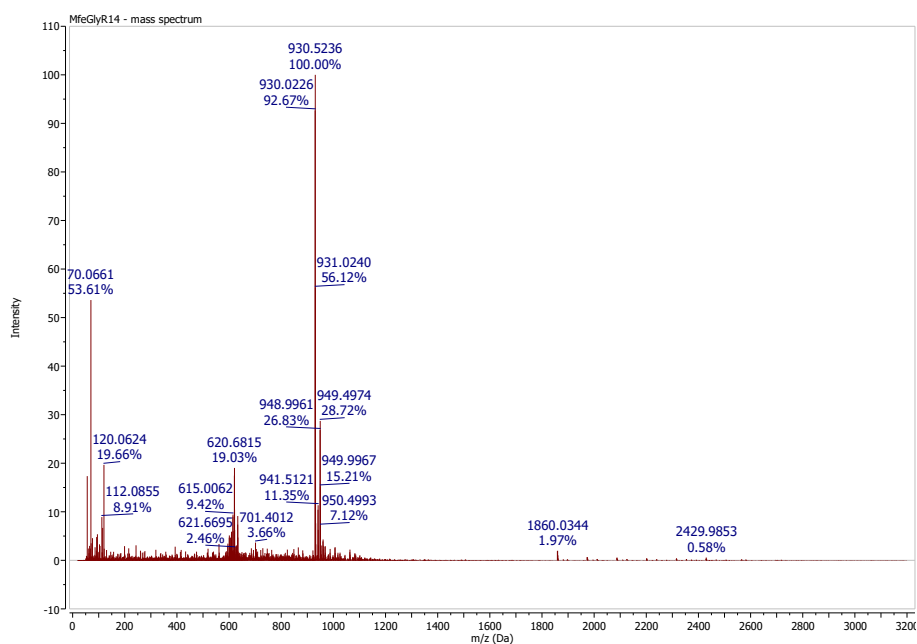


Figure S14: High resolution mass spectrometry (HRMS) spectrum of the purified peptide **MfeGlyR14** in positive ionization mode (20-3200 m/z [Da]). Calculated ion species (M+H)⁺ for this peptide are listed in respective HPLC chromatogram.

4.3 DfeGlyR14

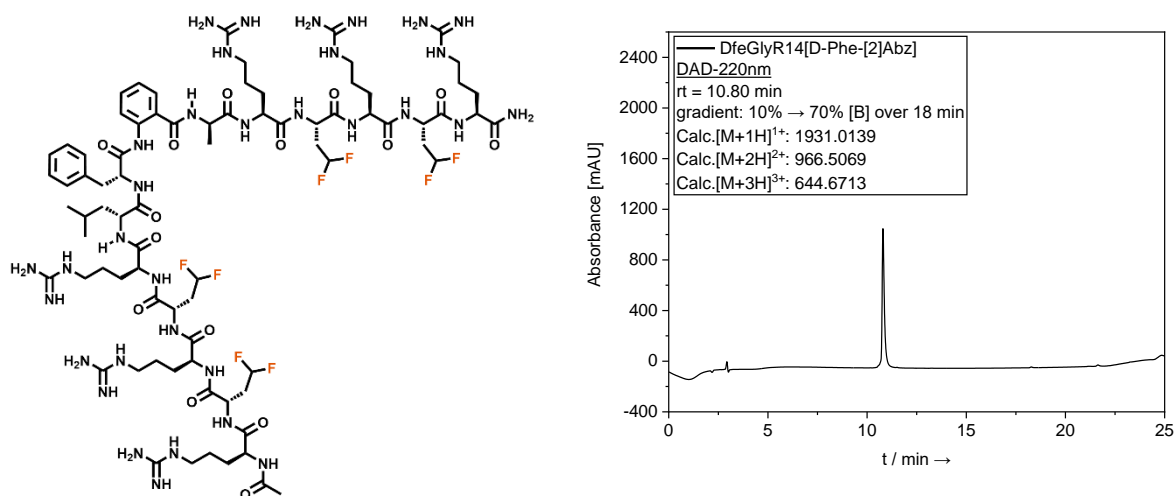


Figure S15: Chemical structure of peptide **DfeGlyR14**. The purity of this peptide after synthesis and isolation was determined through analytical HPLC with DAD detection at 220 nm. HPLC: Hitachi Primaide with Kinetex® C18 RP-column / solvent: **(A)** H₂O + 0.1% TFA / **(B)** ACN + 0.1% TFA / gradient: 10% **(B)** → 70% **(B)** over 18 min.

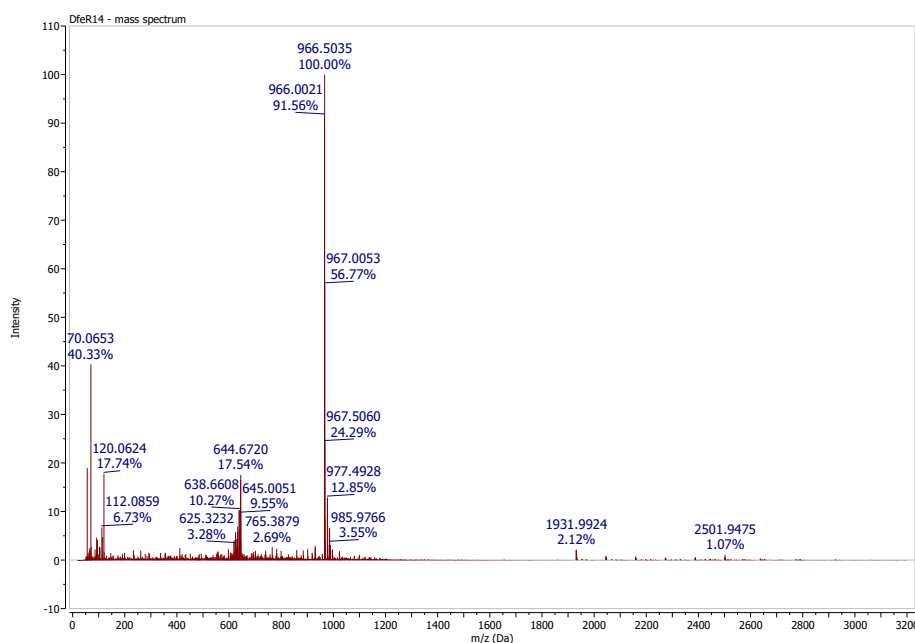


Figure S16: High resolution mass spectrometry (HRMS) spectrum of the purified peptide **DfeGlyR14** in positive ionization mode (20-3200 m/z [Da]). Calculated ion species (M+H)⁺ for this peptide are listed in respective HPLC chromatogram.

4.4 TfeGlyR14

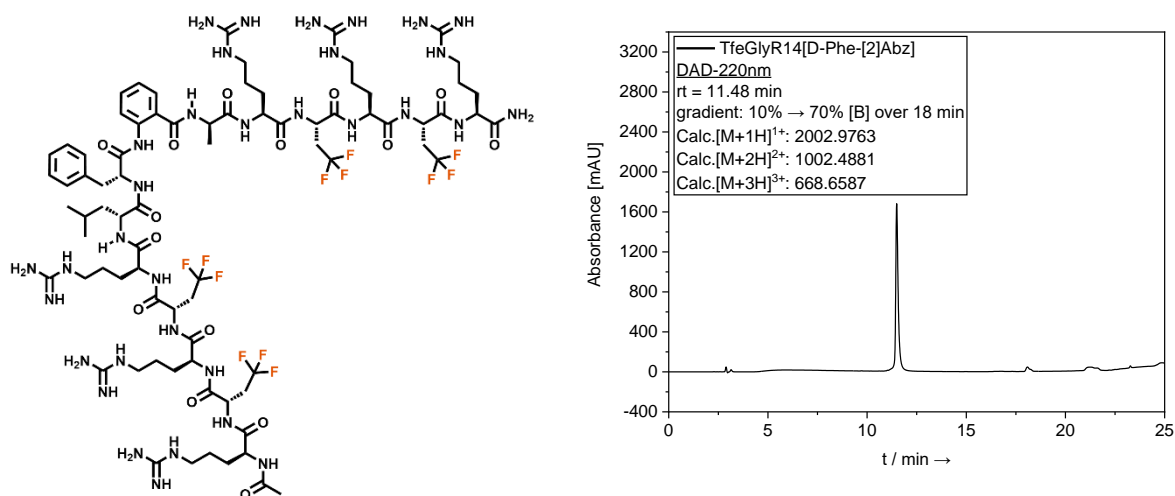


Figure S17: Chemical structure of peptide **TfeGlyR14**. The purity of this peptide after synthesis and isolation was determined through analytical HPLC with DAD detection at 220 nm. HPLC: Hitachi Primaide with Kinetex® C18 RP-column / solvent: **(A)** H₂O + 0.1% TFA / **(B)** ACN + 0.1% TFA / gradient: 10% (B) → 70% (B) over 18 min.

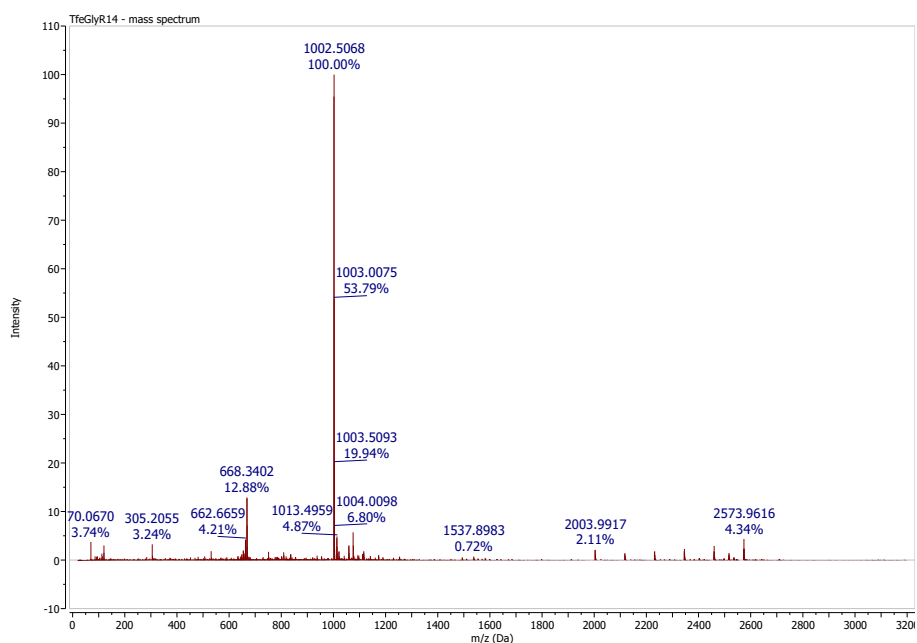


Figure S18: High resolution mass spectrometry (HRMS) spectrum of the purified peptide **TfeGlyR14** in positive ionization mode (20-3200 m/z [Da]). Calculated ion species (M+H)⁺ for this peptide are listed in respective HPLC chromatogram.

4.5 SAJO-2

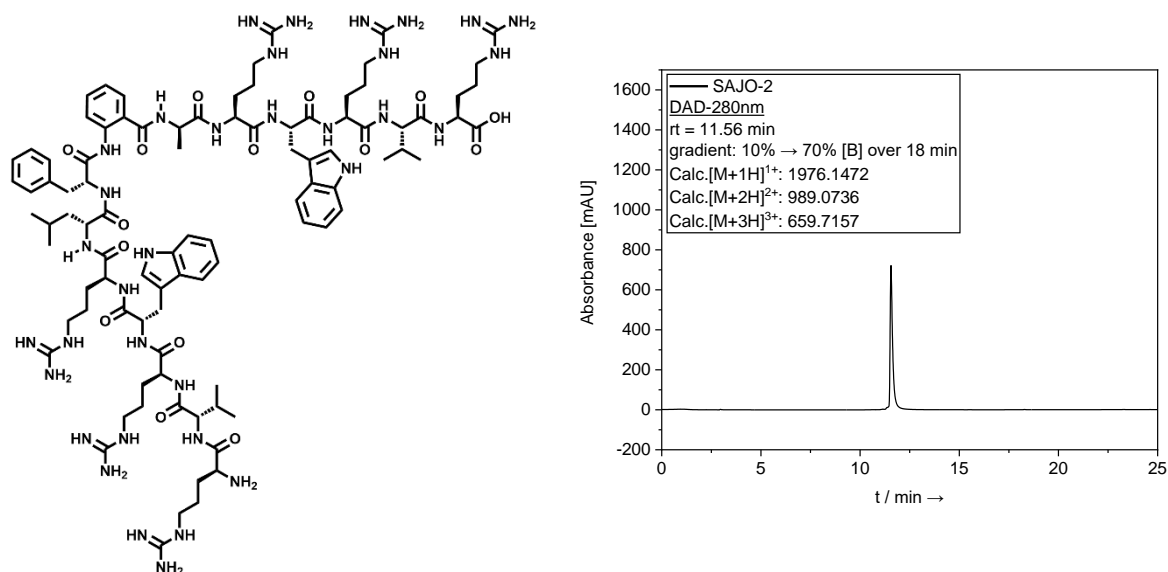


Figure S19: Chemical structure of peptide **SAJO-2**. The purity of this peptide after synthesis and isolation was determined through analytical HPLC with DAD detection at 280 nm. HPLC: Hitachi Primaide with Kinetex® C18 RP-column / solvent: **(A)** H₂O + 0.1% TFA / **(B)** ACN + 0.1% TFA / gradient: 10% (B) → 70% (B) over 18 min.

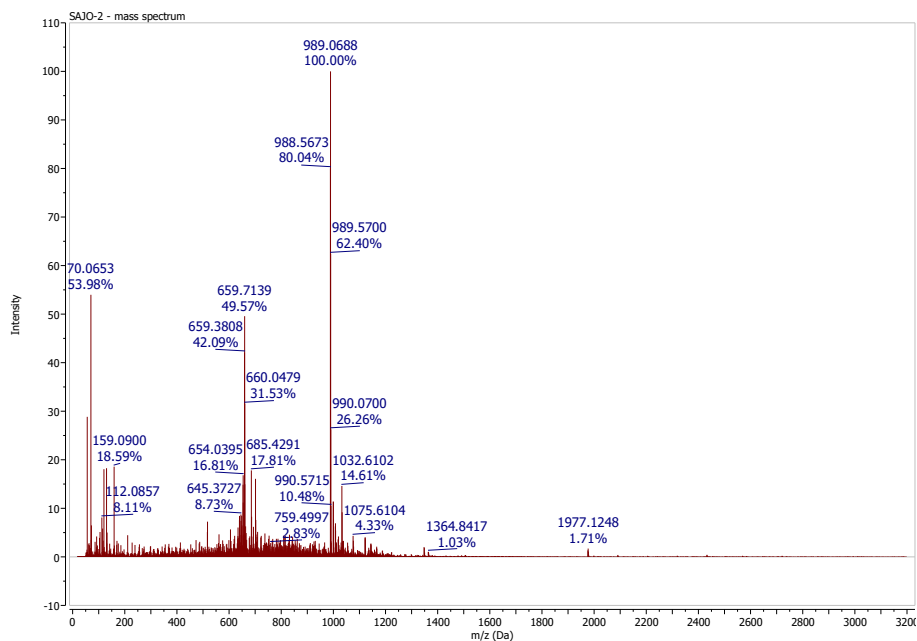


Figure S20: High resolution mass spectrometry (HRMS) spectrum of the purified peptide **SAJO-2** in positive ionization mode (20-3200 m/z [Da]). Calculated ion species (M+H)⁺ for this peptide are listed in respective HPLC chromatogram.

4.6 SAJO-Abu

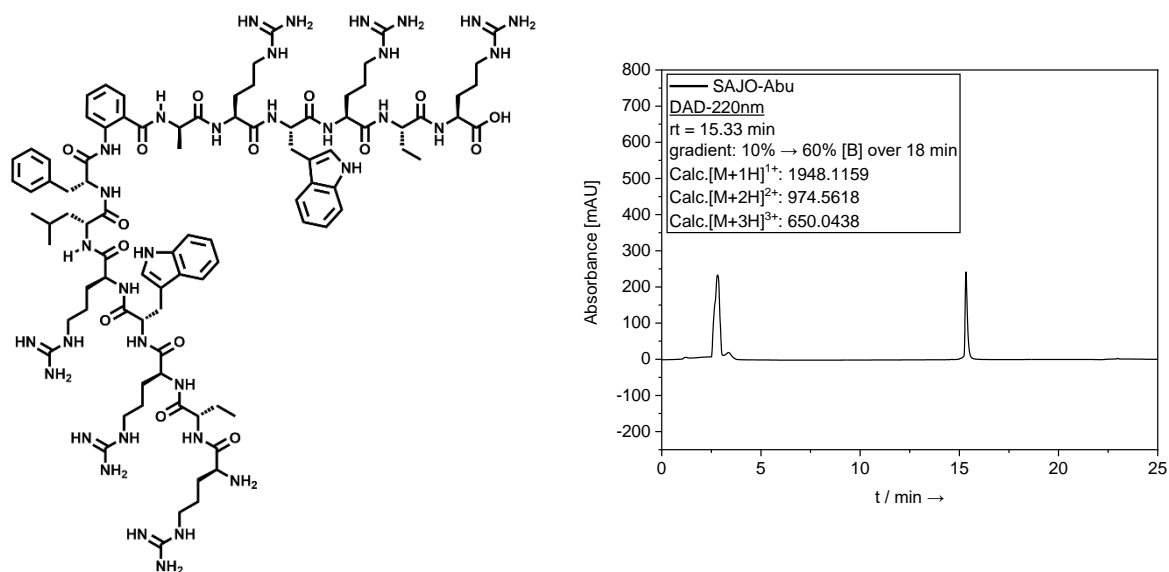


Figure S21: Chemical structure of peptide **SAJO-Abu**. The purity of this peptide after synthesis and isolation was determined through analytical HPLC with DAD detection at 220 nm. HPLC: Hitachi Primaide with Kinetex® C18 RP-column / solvent: **(A)** H₂O + 0.1% TFA / **(B)** ACN + 0.1% TFA / gradient: 10% (B) → 60% (B) over 18 min.

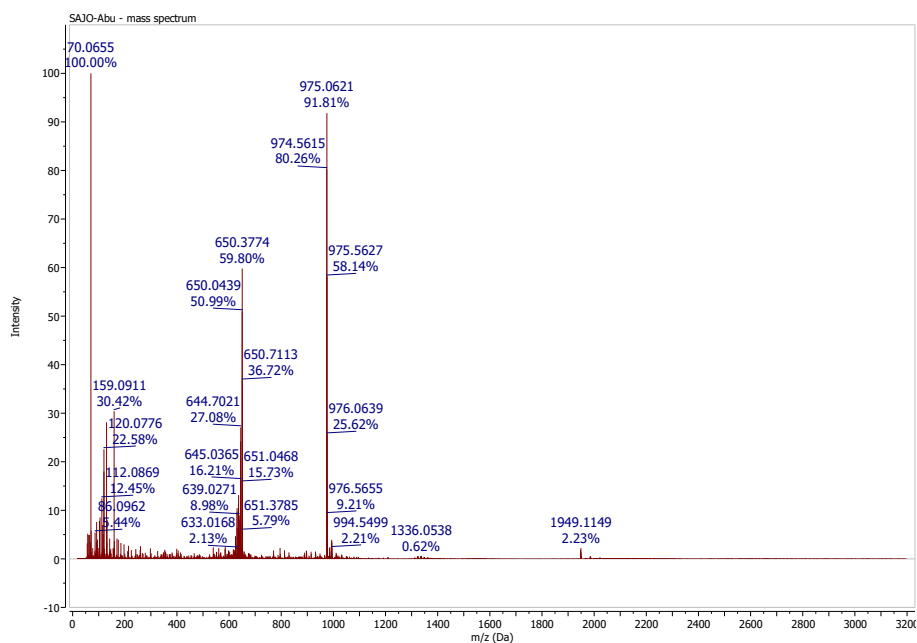


Figure S22: High resolution mass spectrometry (HRMS) spectrum of the purified peptide **SAJO-2** in positive ionization mode (20-3200 m/z [Da]). Calculated ion species (M+H)⁺ for this peptide are listed in respective HPLC chromatogram.

4.7 SAJO-TfeGly

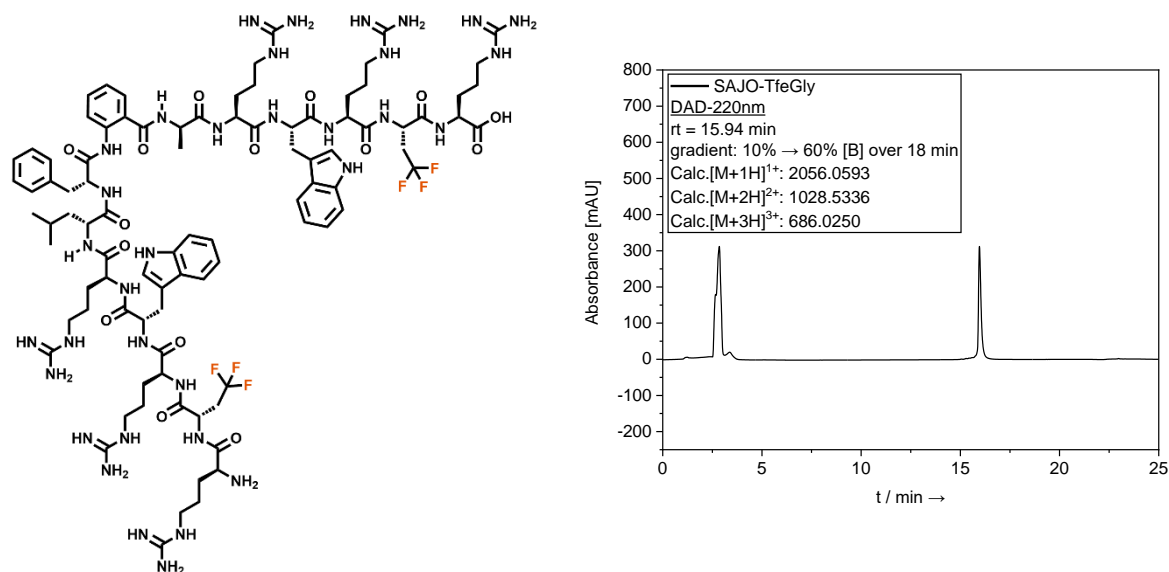


Figure S23: Chemical structure of peptide **SAJO-TfeGly**. The purity of this peptide after synthesis and isolation was determined through analytical HPLC with DAD detection at 220 nm. HPLC: Hitachi Primaide with Kinetex® C18 RP-column / solvent: **(A)** H₂O + 0.1% TFA / **(B)** ACN + 0.1% TFA / gradient: 10% (B) → 60% (B) over 18 min.

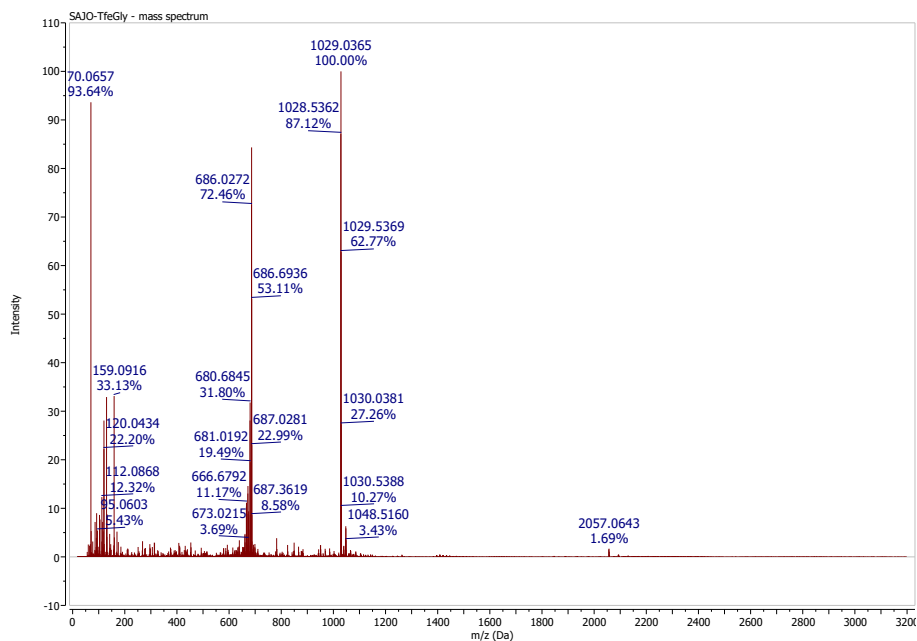


Figure S24: High resolution mass spectrometry (HRMS) spectrum of the purified peptide **SAJO-TfeGly** in positive ionization mode (20-3200 m/z [Da]). Calculated ion species (M+H)⁺ for this peptide are listed in respective HPLC chromatogram.

4.8 SAJO-PfpGly

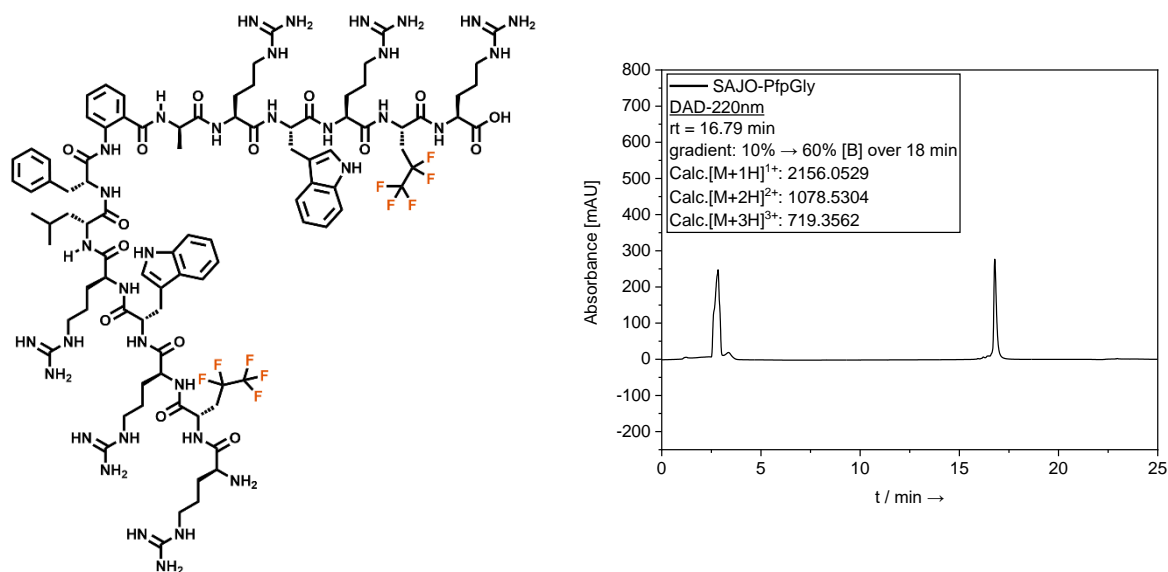


Figure S25: Chemical structure of peptide **SAJO-PfpGly**. The purity of this peptide after synthesis and isolation was determined through analytical HPLC with DAD detection at 220 nm. HPLC: Hitachi Primaide with Kinetex® C18 RP-column / solvent: **(A)** H₂O + 0.1% TFA / **(B)** ACN + 0.1% TFA / gradient: 10% (B) → 60% (B) over 18 min.

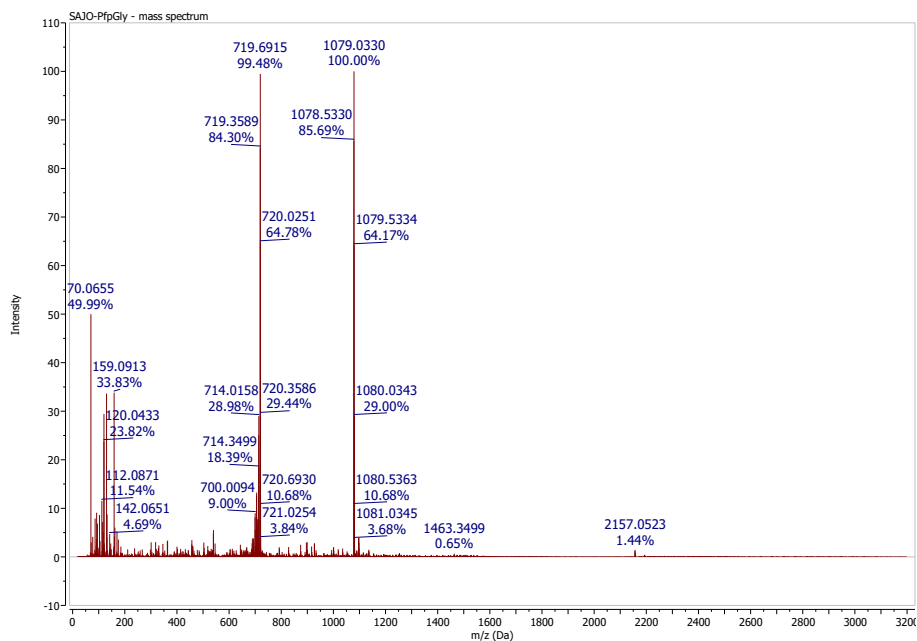


Figure S26: High resolution mass spectrometry (HRMS) spectrum of the purified peptide **SAJO-PfpGly** in positive ionization mode (20-3200 m/z [Da]). Calculated ion species (M+H)ⁿ⁺ for this peptide are listed in respective HPLC chromatogram.

4.9 AbuR20

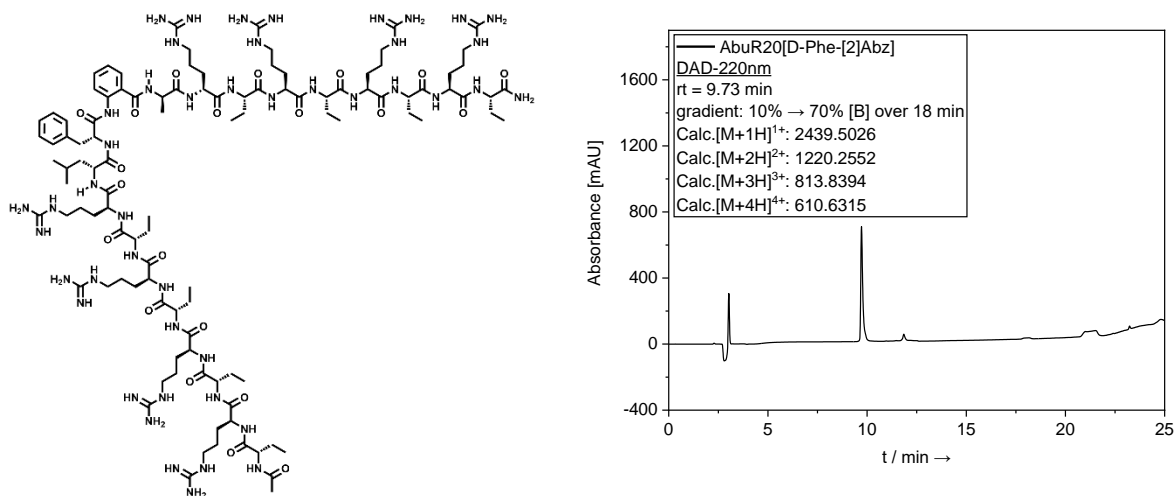


Figure S27: Chemical structure of peptide **AbuR20**. The purity of peptide samples after synthesis and isolation was determined through analytical HPLC with DAD detection at 220 nm. HPLC: Hitachi Primaide with Kinetex® C18 RP-column / solvent: **(A)** H₂O + 0.1% TFA / **(B)** ACN + 0.1% TFA / gradient: 10% (B) → 70% (B) over 18 min.

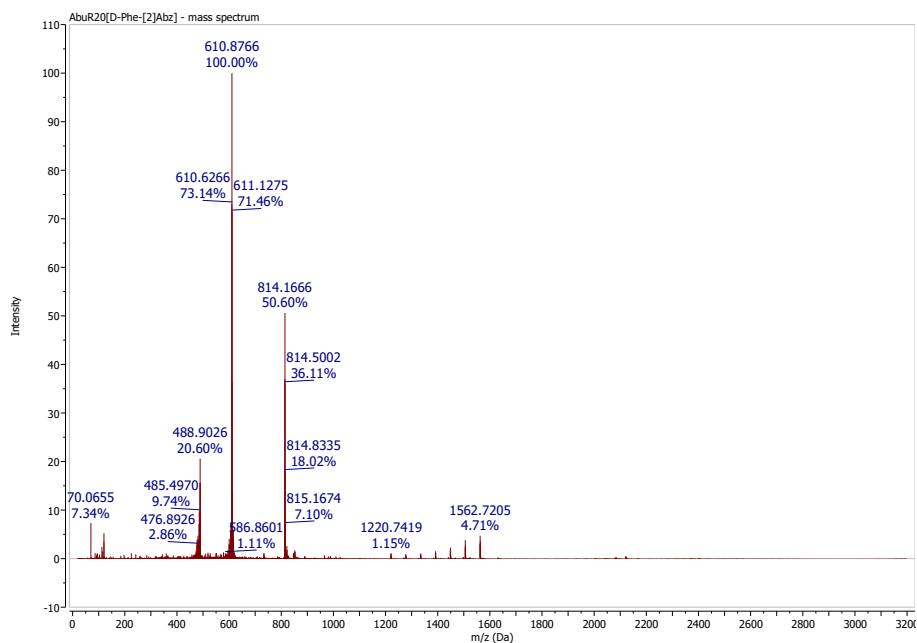


Figure S28: High resolution mass spectrometry (HRMS) spectrum of the purified peptide **AbuR20** in positive ionization mode (20-3200 m/z [Da]). Calculated ion species $(M+H)^+$ for this peptide are listed in respective HPLC chromatogram.

4.10 TfeGlyR20

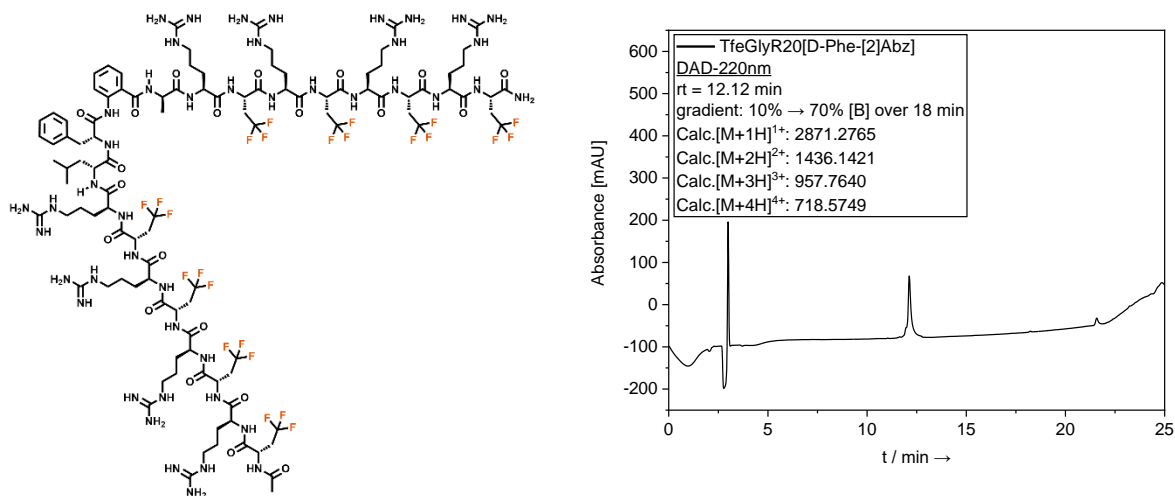


Figure S29: Chemical structure of peptide **TfeGlyR20**. The purity of peptide samples after synthesis and isolation was determined through analytical HPLC with DAD detection at 220 nm. HPLC: Hitachi Primaide with Kinetex® C18 RP-column / solvent: **(A)** H₂O + 0.1% TFA / **(B)** ACN + 0.1% TFA / gradient: 10% (B) → 70% (B) over 18 min.

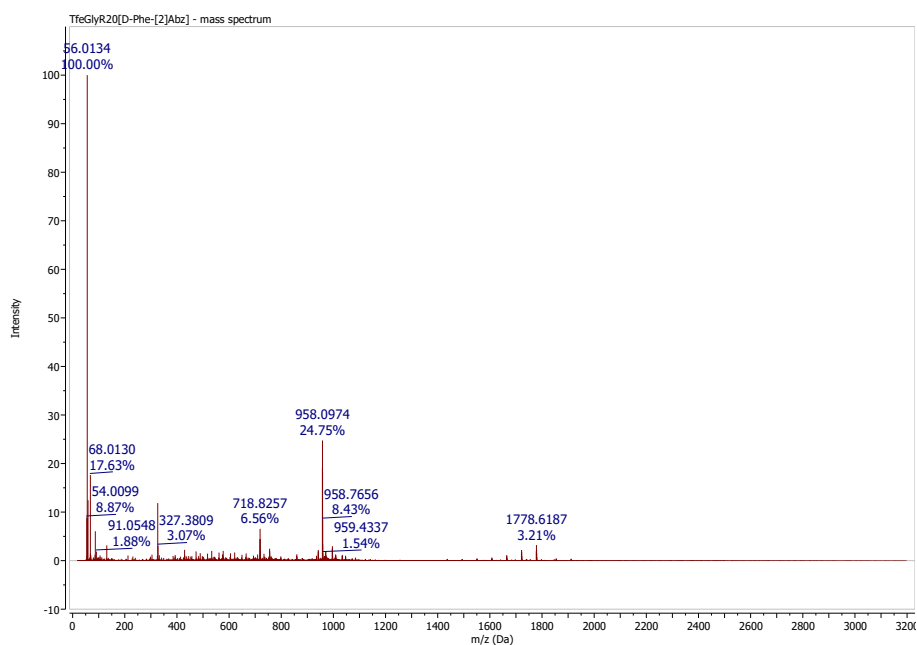


Figure S30: High resolution mass spectrometry (HRMS) spectrum of the purified peptide **TfeGlyR20** in positive ionization mode (20-3200 m/z [Da]). Calculated ion species (M+H)⁺ for this peptide are listed in respective HPLC chromatogram.

4.11 H-Gly-[D-Phe-[2]Abz]-Gly-OH

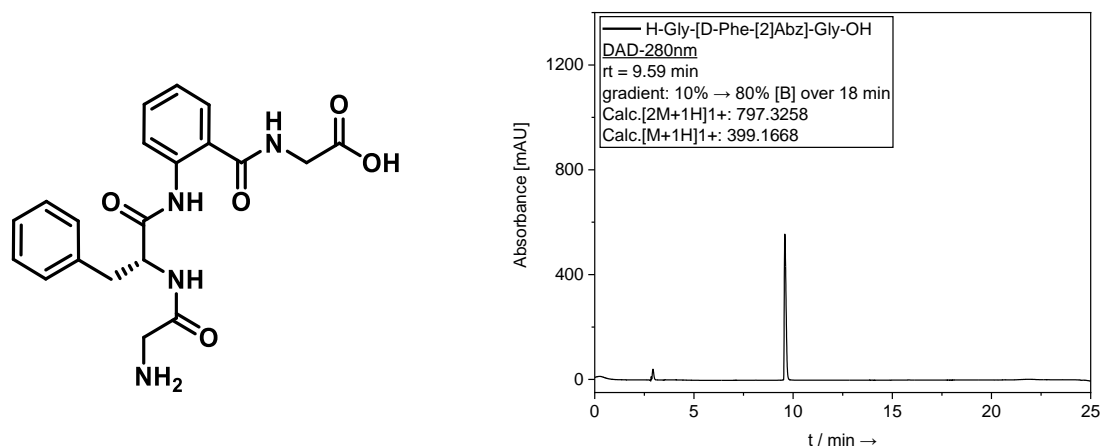


Figure S31: Chemical structure of peptide H-Gly-[D-Phe-[2]Abz]-Gly-OH. The purity of peptide samples after synthesis and isolation was determined through analytical HPLC with DAD detection at 280 nm. HPLC: Hitachi Primaide with Kinetex® C18 RP-column / solvent: **(A)** H₂O + 0.1% TFA / **(B)** ACN + 0.1% TFA / gradient: 10% (B) → 80% (B) over 18 min.

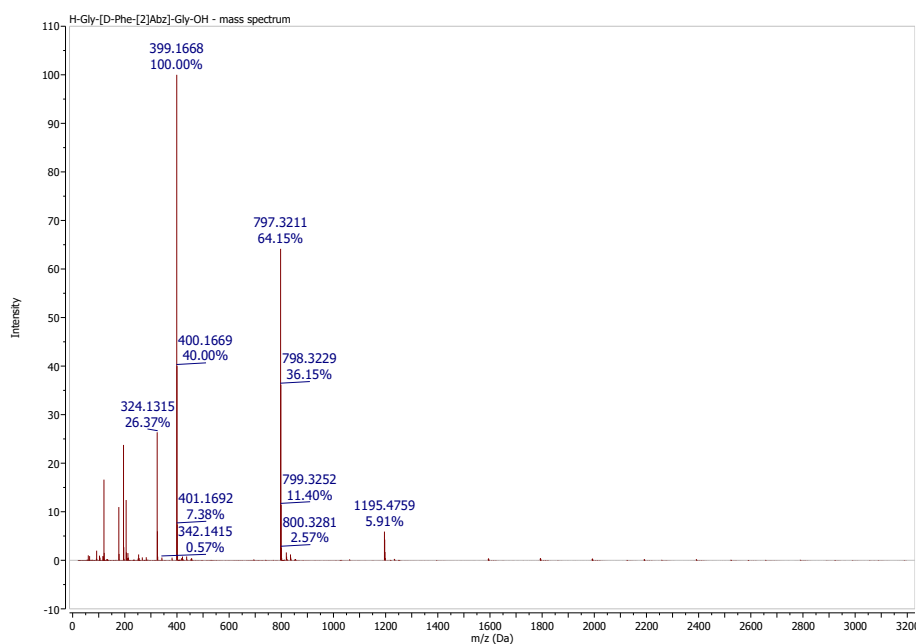


Figure S32: High resolution mass spectrometry (HRMS) spectrum of the purified peptide H-Gly-[D-Phe-[2]Abz]-Gly-OH in positive ionization mode (20-3200 m/z [Da]). Calculated ion species (M+H)⁺ for this peptide are listed in respective HPLC chromatogram.

5. Determination of peptide stock concentrations

For UV-based determination of peptide stock concentration, we synthesized the tetrapeptide H-Gly-[D-Phe-[2]Abz]-Gly-OH comprising the σ -framework based β -turn segment. Substitution of the D-amino acid derivatives from leucine and alanine (original β -turn core) with glycine simplified peptide synthesis and purification significantly. Desalted samples of this peptide were dissolved in a 6M guanidinium hydrochloride solution, pH 7.4, and prepared in different concentrations. A calibration curve was determined by measuring the UV absorbance (BioPhotometer plus photometer from Eppendorf, Hamburg, Germany) of each sample at 280 nm. Disposable PMMA cuvettes (Eppendorf, Hamburg, Germany) with path lengths of 10 mm were used. Then, aliquots (10 μ L) of respective peptide stocks (dissolved in HFIP) were taken and the solvent was evaporated using a gentle stream of N₂. The dried peptide film was redissolved in a 6M guanidinium hydrochloride solution, pH 7.4 to achieve an overall peptide solution (1000 μ L) with a dilution factor (DL) of 100. UV absorbance was recorded at 280 nm and taken as the mean value from three independent measurements. The concentration was calculated based on the equation $y = a + b \cdot x$ derived from a linear fit. (x = concentration in μ M). For **SAJO**-derived sequences, the presence of tryptophan residue was count in according to Pace *et al.*⁵

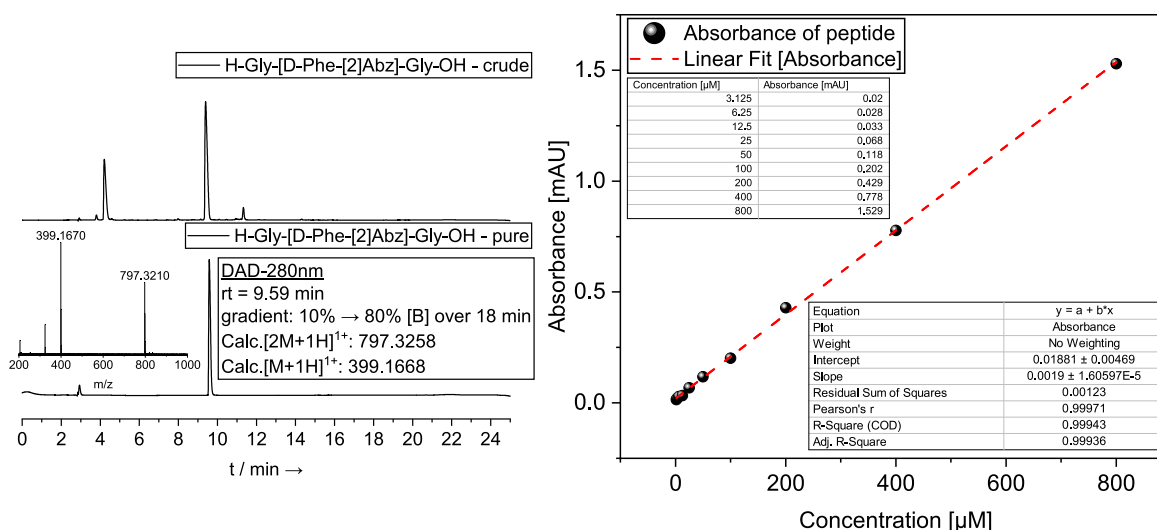


Figure S33: Chemical structure of reference H-Gly-[D-Phe-[2]Abz]-Gly-OH with HPLC chromatogram (crude peptide after SPPS vs. pure peptide after HPLC purification) & HRMS spectra. A UV-Vis-based calibration curve of this sequence was recorded for the determination of peptide concentration stocks. UV absorbance was recorded at room temperature.

6. UV and FL spectroscopy

For UV (250-600 nm) and FL measurements ($\lambda_{\text{ex}} = 270$ nm), an Infinite® M Nano+ plate reader (Tecan Deutschland GmbH, Crailsheim, Germany) was utilized. In **figure S34**, selected spectra at 50 μM , 250 μM and 500 μM concentration are presented. Chemical denaturation of the hairpin structure was tested by dissolving the peptide either in 3M or 6M guanidine hydrochloride (GndHCl) in water, pH 7.4. As a result, a notable increase in FL intensity was observed for **SAJO-2** (**figure S34a**) and **SAJO-Abu** (**figure S34b**) upon GndHCl addition, whereas the spectra of **SAJO-TfeGly** and **SAJO-PfpGly** retained their course of FL spectra and intensity. One explanation for this finding could be the decrease in hairpin content upon denaturation for the non-fluorinated variants. In turn, this would lead to a higher distance of oppositely located Trp residues by diminishing aromatic FL quenching. On the other hand, the FL spectra of **AbuR14** and **TfeGlyR14** in pure water and in 6M GndHCl solution revealed a similar pattern and values of FL intensity.

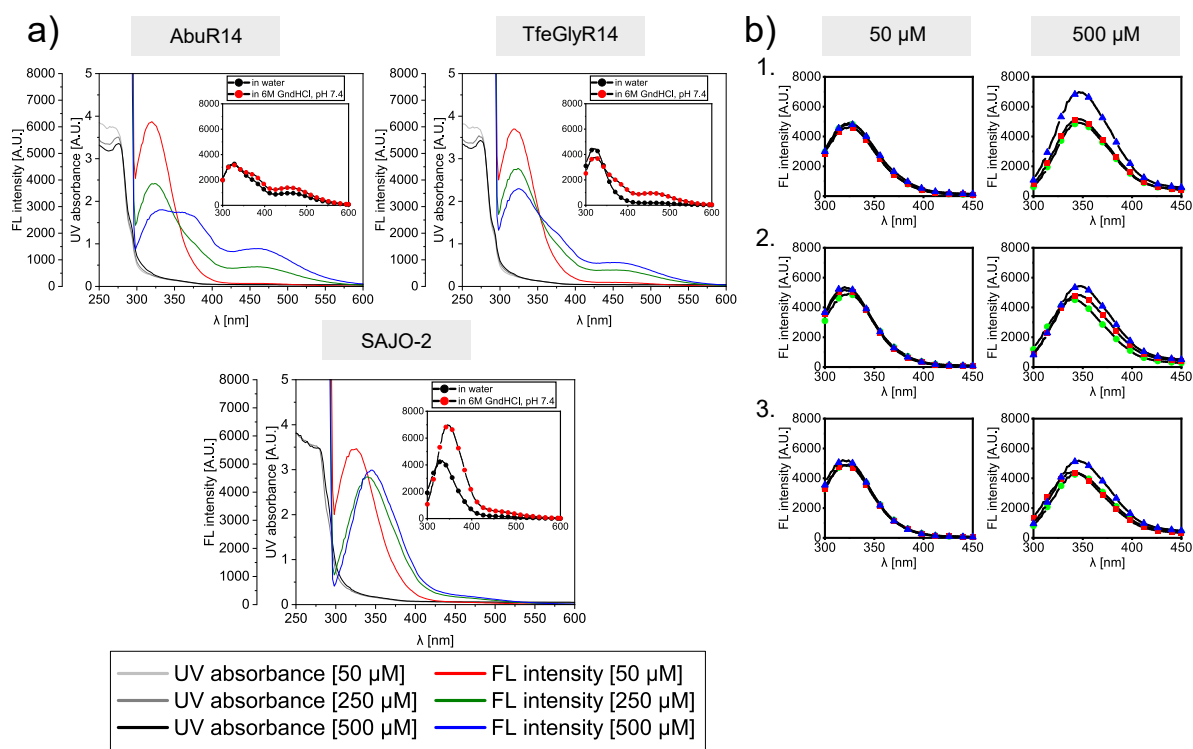


Figure S34: **a)** UV & FL spectra ($\lambda_{\text{ex}} = 270$ nm) of **AbuR14**, **TfeGlyR14** and **SAJO-2** at different concentrations dissolved in 10 mM phosphate buffer, pH 7.4 and measured at 24 °C. Peptide denaturation was probed at 500 μM dissolved in 6M GndHCl in water, pH 7.4., (red circles) and solely water (black circles) as negative control. **b)** FL spectra of **1. SAJO-Abu**, **2. SAJO-TfeGly** and **3. SAJO-PfpGly** at 50 μM (left) and 500 μM (right) dissolved in pure water (green circles). Peptide denaturation was tested with 3M (red squares) or 6M GndHCl in water, pH 7.4, (blue triangles) at 24 °C.

7. CD spectroscopy – further data (XR14-series) & information

The ellipticity θ_{obs} was normalized for concentration c [mol L⁻¹], number of residues n and path length l (0.1 cm) using equation (1):

$$[\theta] = \frac{\theta_{obs}}{10^4 * l * c * n} \quad (1)$$

Measured ellipticity θ_{obs} is given in mdeg and molar ellipticity per residue $[\theta]$ in 10³ deg cm² dmol⁻¹ residue⁻¹.

Further CD studies focused on the impact of concentration, pH and membrane-like environments using SDS as suitable mimicry.

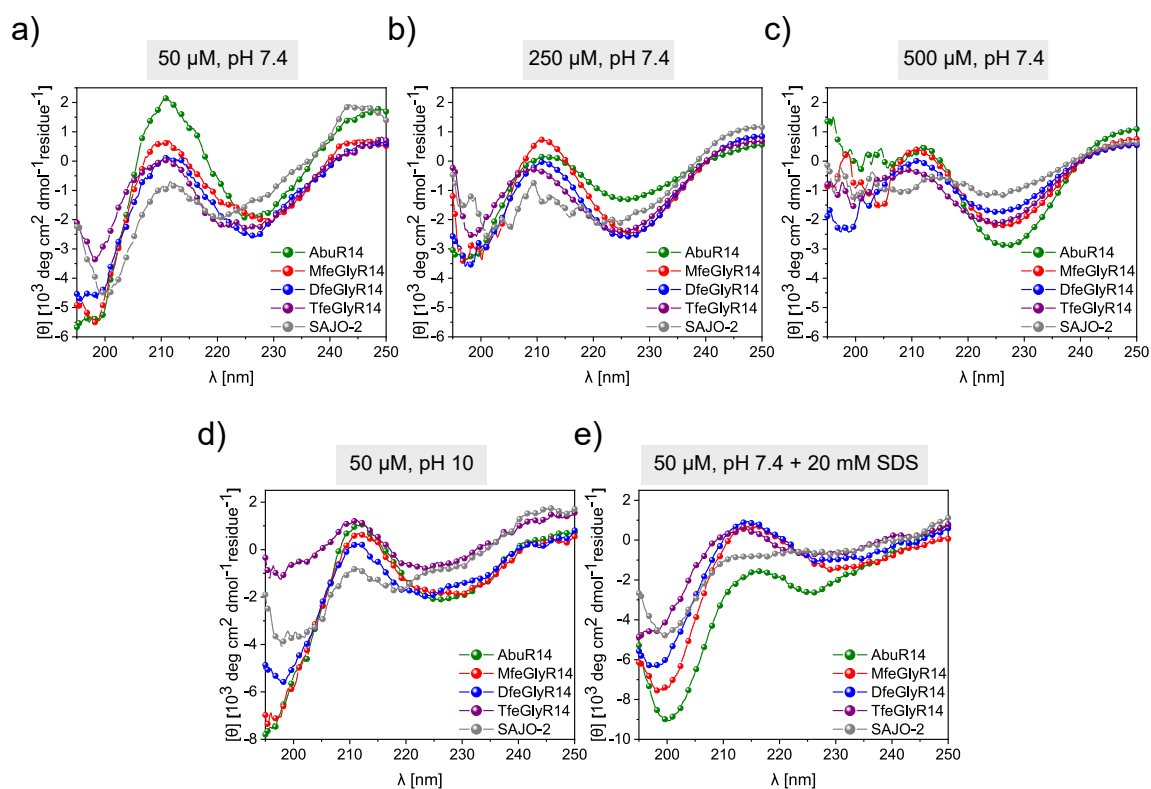


Figure S35: CD Spectra of peptides **AbuR14**, **MfeGlyR14**, **DfeGlyR14**, **TfeGlyR14** and **SAJO-2** at following conditions: **a)** 50 μ M peptide concentration dissolved in 10 mM phosphate buffer, pH 7.4, recorded at 37 $^{\circ}$ C; **b)** 250 μ M peptide concentration dissolved in 10 mM phosphate buffer, pH 7.4, recorded at 37 $^{\circ}$ C; **c)** 500 μ M peptide concentration dissolved in 10 mM phosphate buffer, pH 7.4, recorded at 37 $^{\circ}$ C; **d)** 50 μ M peptide concentration dissolved in 10 mM glycine-NaOH buffer, pH 10, recorded at 37 $^{\circ}$ C; **e)** 50 μ M peptide concentration dissolved in 10 mM phosphate buffer + 20 mM SDS, pH 7.4, recorded at 37 $^{\circ}$ C.

As depicted in **figure S35** for the **XR14**-series and **SAJO-2**, neither a basic pH (typically encouraging secondary structure formation of cationic amphipathic peptides by neutralizing the positively charged residues [Arg]) nor an artificial membrane environment facilitated the formation a type II β -turn structure exclusively, as a main proportion of random coils ($\lambda_{\min} = 198$ nm) were present in these cases. Only an increase in peptide concentration up to 0.5 mM diminished the CD pattern of a disordered structure emphasizing a concentration-dependent β -hairpin formation.

We also tested the elongation of the peptide chain-length to encourage the formation of the β -hairpin structure. As depicted in **figure S36**, respective peptides **AbuR20** and **TfeGlyR20** revealed an analog folding pattern by means of the truncated variants. Also here, a mixture of unordered structures (random coil) and an ordered peptide folding (β -turn) were found at 50 μ M concentration, for which the overall proportion of latter secondary structure raised with an increase in amount of peptide.

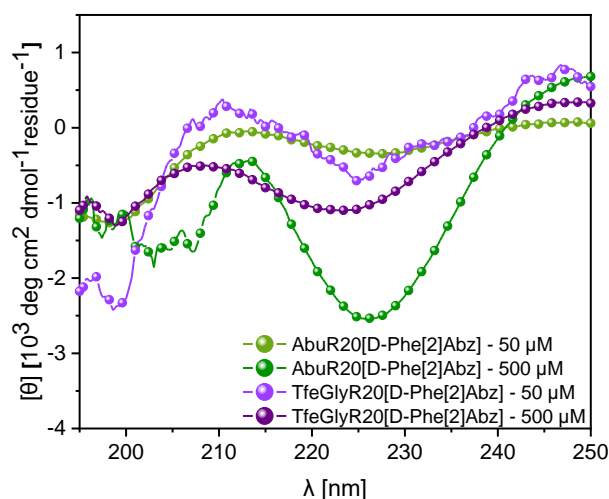


Figure S36: CD Spectra of peptides **AbuR20** and **TfeGlyR20** (50 μ M + 500 μ M concentration) dissolved in 10 mM phosphate buffer, pH 7.4, recorded at 37 $^{\circ}$ C.

However, both peptides highly tend to aggregate under physiological conditions, probably due to their extended amphipathic strands. Therefore, these sequences were excluded from further experiments.

8. 6-FAM leakage assay - Dose-response fitting & 100% POPC leakage

Fluorescence intensity data derived from the dye 6-FAM during membrane permeabilization of the peptides **AbuR14**, **MfeGlyR14**, **DfeGlyR14**, **TfeGlyR14** and **SAJO-2** served for calculation of EC_{50} through sigmoidal dose-response curves. Therefore, the efficiency of 6-FAM leakage at ($\lambda_{ex} = 493$ nm, $\lambda_{em} = 517$ nm) in [%] was calculated with respect to the negative control FL_0 (FL intensity measured for liposome solution solely dissolved in buffer after 30 min incubation, 30 °C) and positive control FL_{100} (FL intensity measured for liposome solution dissolved in 5% (v/v) Triton X-100 in buffer after 30 min incubation, 30 °C) using equation (2):

$$[\%] = \frac{FL_{obs} - FL_0}{FL_{100} - FL_0} * 100\% \quad (2)$$

Calculated efficiencies in [%] were plotted against the logarithmic peptide concentration (0.0305175781 μ M, 0.0610351563 μ M, 0.1220703125 μ M, 0.244140625 μ M, 0.48828125 μ M, 0.9765625 μ M, 1.953125 μ M, 3.90625 μ M, 7.8125 μ M, 15.625 μ M, 31.25 μ M, 62.5 μ M, 125 μ M, 250 μ M, 500 μ M, 750 μ M, 1500 μ M, 3000 μ M) using OriginPro 2020b (OriginLab Corporation, Northampton, MA, USA) according to equation (3):

$$y = A1 + \frac{A2 - A1}{1 + 10^{(LOGx0-x)p}} * 100\% \quad (3)$$

Dose-response fitting was executed by means of the bottom asymptote A1, the top asymptote A2 and the hill slope $p > 0$. EC_{50} values were calculated as average of three independent measurements

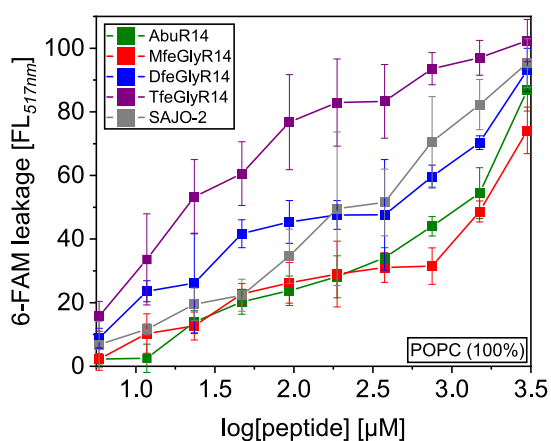


Figure S37: Membrane permeabilization of amphipathic peptides detected *via* 6-FAM leaking. The dye was encapsulated in 5 mM liposome solution containing solely POPC and its release induced by the peptide as a function of concentration after 30 min incubation (30°C) was monitored *via* fluorescence (FL) spectroscopy ($\lambda_{ex} = 493$ nm / $\lambda_{em} = 517$ nm). FL values were normalized to 100% dye release determined by adding (5% (v/v) Triton X-100 to the liposome solution as positive control.

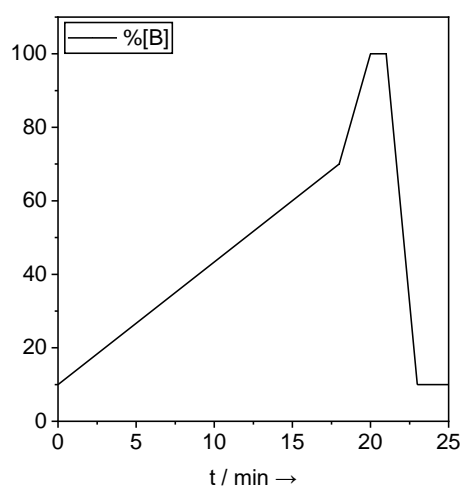
As shown in **figure S37**, we also tried to determine EC_{50} values for analog values of peptide concentration upon the leaking of solely POPC-containing liposomes. However, the obtained trends of efficiencies [%] did were not appropriate for sigmoidal fitting. We explain the divergences in membrane disruption due to an equal proportion of net charges by the zwitterionic POPC and a lack of the negatively charged POPG. This absence of charges alters the nature of electrostatic recognition between liposomes and amphipathic peptides tremendously. Besides, our data set for 100% POPC-based liposomes show a consistent analogy to the hydrophobicity trend depicted through our RP-HPLC assay for the fluorinated **XR14**-derived peptides and underline a direct coherence between membrane-disrupting properties and fluorine-induced hydrophobicity (**MfeGlyR14** \leq **AbuR14** < **DfeGlyR14** < **TfeGlyR14**).

9. Peptide digestion assay – further data & information

In **table S3**, the general conditions of the HPLC gradients used for the peptide digestion assay are listed. In **figure S38** the digestion profile of **SAJO-TfeGly** is presented. A detailed overview of the digestion profile of the **XR14**-derived peptides **AbuR14**, **MfeGlyR14**, **DfeGlyR14** and **TfeGlyR14** with identified peptide fragments and corresponding mass spectra / HPLC chromatograms is introduced (**table S4** & **figure S39-41**) and discussed as well.

Table S4: HPLC gradient (digestion plot).

Time [min]	%[A]	%[B]	Flor Rate [mL/min]
0.0	90	10	1.00
18.0	30	70	1.00
20.0	0	100	1.00
21.0	0	100	1.00
23.0	90	10	1.00
25.0	90	10	1.00



Enzyme stock concentrations were determined by measuring the UV absorbance (BioPhotometer plus photometer) of these solutions at 280 nm in triplicates with PMMA cuvettes (both Eppendorf, Hamburg, Germany) with path lengths of 10 mm. According to Lambert–Beer law, the concentration of α -chymotrypsin or β -trypsin with extinction coefficients ϵ calculated according to Pace *et al.* were determined using equation (4,5):⁵

$$[M_{\alpha\text{-chymotrypsin}}] = \frac{\text{Absorbance}[a. u.]}{50.585 M * cm^{-1}} \quad [M_{\beta\text{-trypsin}}] = \frac{\text{Absorbance}[a. u.]}{37.650 M * cm^{-1}} \quad (4,5)$$

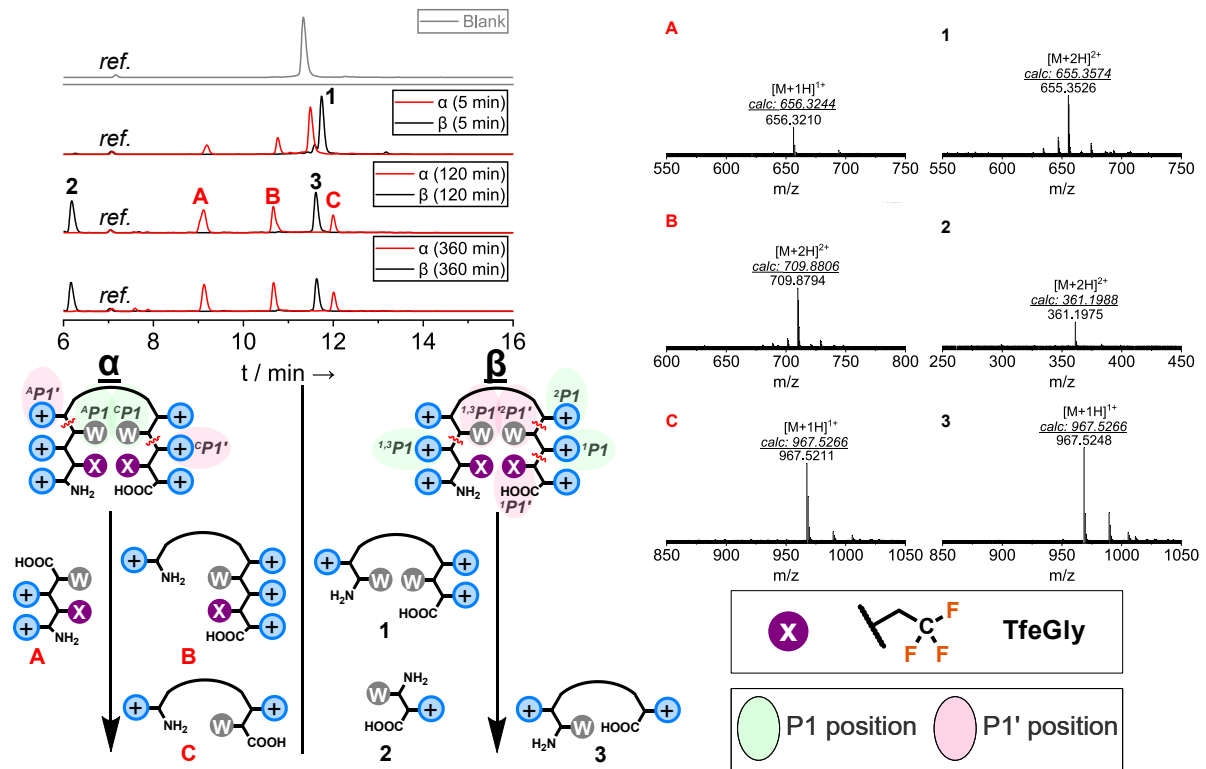


Figure S38: Real-time monitoring of proteolytic digestion at 5, 120 and 360 min (HPLC, DAD-280nm) and MS-based (ESI-ToF) detection and determination of peptide fragments of **SAJO-TfeGly** at 1 mM stock concentration during incubation with either α -chymotrypsin or β -trypsin (both 20 μ M stock concentration) at 30 °C. The dipeptide Ac-[2]Abz-Gly-OH was used as reference signal. Cleaving sites are illustrated with squiggly lines (red-colored) and defined according to Schechter and Berger nomenclature. Measurements were performed in triplicates. Arginine residues are illustrated as blue-colored positive charges (+). Colors of hydrophobic side chains are the same as introduced in the main paper.

As illustrated in **figure S38**, **SAJO-TfeGly** follows an analog digestion profile as **SAJO-2** for both digesting enzymes. Taking similar properties in hydrophobicity and spatial demand into account, this finding was rather unsurprising. The suitability of **PfpGly (SAJO-PfpGly)** as C-terminal P1' residue is, consequently, suggested to be rather facilitated by an enhanced size of the unbranched side chain and hydrophobicity due to perfluorination.

We also calculated the proportions of HPLC signals during peptide proteolysis (α -chymotrypsin) for **SAJO-2**, **SAJO-TfeGly** and **SAJO-PfpGly**. The normalized values are presented in **table S5**. Interestingly, we determined similar values of peptide-fragment amounts after 6 h incubation. Furthermore, the fluorinated variants were remaining in significantly lower amounts than the non-fluorinated **SAJO-2** after 5 min incubation, which may suggest favored accommodation of the fluorinated side chains in the enzyme's active site as discussed in the main paper.

Table S5: Normalized amounts of remaining peptide during peptide digestion of **SAJO-2**, **SAJO-TfeGly** and **SAJO-PfpGly** by α -chymotrypsin (**figure 7 + S38**). Calculated values refer only to the HPLC signal of each respective peptide-(fragments) for simplicity. Errors are derived from the standard deviation (n=3).

Peptide	Time [min]	Substrate [%]	Peptide-fragments [%]			
			(A)	(B)	(C)	(D)
SAJO-2	5	91.5 \pm 2.2	3.2 \pm 0.9	5.4 \pm 1.3	-	-
	120	-	40.4 \pm 0.1	38.1 \pm 2.0	21.6 \pm 2.0	-
	360	-	40.6 \pm 0.1	29.0 \pm 0.3	30.4 \pm 0.5	-
SAJO-TfeGly	5	67.0 \pm 1.1	12.7 \pm 0.3	20.3 \pm 1.0	-	-
	120	-	39.7 \pm 0.3	37.8 \pm 0.4	22.5 \pm 0.4	-
	360	-	38.0 \pm 0.2	37.2 \pm 0.2	24.8 \pm 0.3	-
SAJO-PfpGly	5	72.6 \pm 2.6	11.6 \pm 2.1	15.8 \pm 0.5	-	-
	120	-	38.6 \pm 0.4	-	30.2 \pm 0.1	31.2 \pm 0.5
	360	-	36.5 \pm 0.6	-	31.45 \pm 0.2	32.0 \pm 0.7

In **figure S39**, the digestion profiles for the **XR14**-series are presented. As discussed in the main paper, we found alterations in cleaving sites (proteolysis through α -chymotrypsin) on the N-terminal amphipathic strand for **DfeGlyR14** (digestion product **15**) & **TfeGlyR14** (digestion product **21**); for both cases, the hydrophobic amino acids act as P1' residue. Firstly, we considered a change in digestion by a deficit of a fluorinated residue (P1) – centrally located Arg (P1') cleaving site [N-terminal strand, found for **AbuR14** (digestion product **1**) and **MfeGlyR14** (digestion product **7**)] and, simultaneously, the emergence of an Arg (P1) – fluorinated residue (P1') cleaving site. Further analysis of digested fragments, however, exposed the formation of similar products for both higher fluorinated peptides in comparably lower proportions (see **figure S40**).

The exclusive emergence of a cleavage pattern for digestion products **15** & **21** for the higher fluorinated derivatives may correlate, as discussed before, to beneficial effects in enzyme-substrate recognition due to an increase in side chain volume and hydrophobicity. Similar conclusions are considered for changes in proteolysis of the C-terminal strands. It is most noteworthy, that **TfeGly** does occupy a P1' position within the digestion profile of **TfeGlyR14** but not in **SAJO-TfeGly** (**figure S39 & 40**). This may correlate, as mentioned in the main paper with regards to **figure 6**, to structural alterations between both β -hairpin libraries (terminal modifications, presence of Trp). The digestion profiles obtained for β -trypsin are discussed in the main paper.

We also tested the stability of peptide-fragments derived from proteolysis after 6 h incubation and the results are presented in **figure S41**.

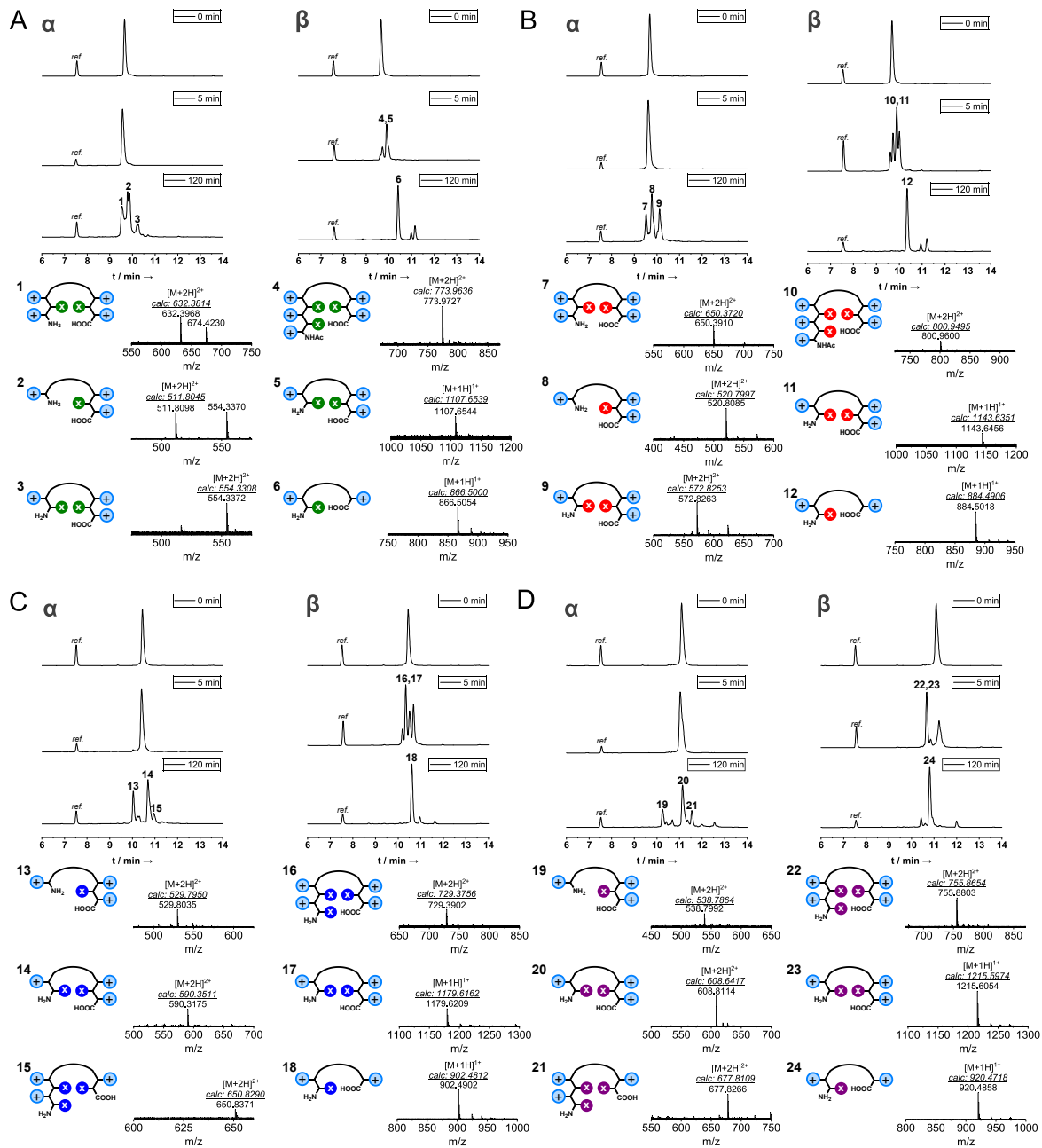


Figure S39: Real-time monitoring of proteolytic digestion at 5 and 120 min (HPLC, DAD-280nm) and MS-based (ESI-ToF) detection and determination of peptide fragments of (A) *AbuR14*, (B) *MfeGlyR14*, (C) *DfeGlyR14* and (D) *TfeGlyR14* (all at 1 mM stock concentration) during incubation with either α -chymotrypsin [left, (α)] or β -trypsin [right (β)] (both 20 μ M stock concentration) at 30 $^{\circ}$ C. The dipeptide **Ac-[2]Abz-Gly-OH** was used as reference signal. Measurements were performed in triplicates. Arginine residues are illustrated as blue-colored positive charges (+). Colors of hydrophobic side chains are the same as introduced in the main paper.

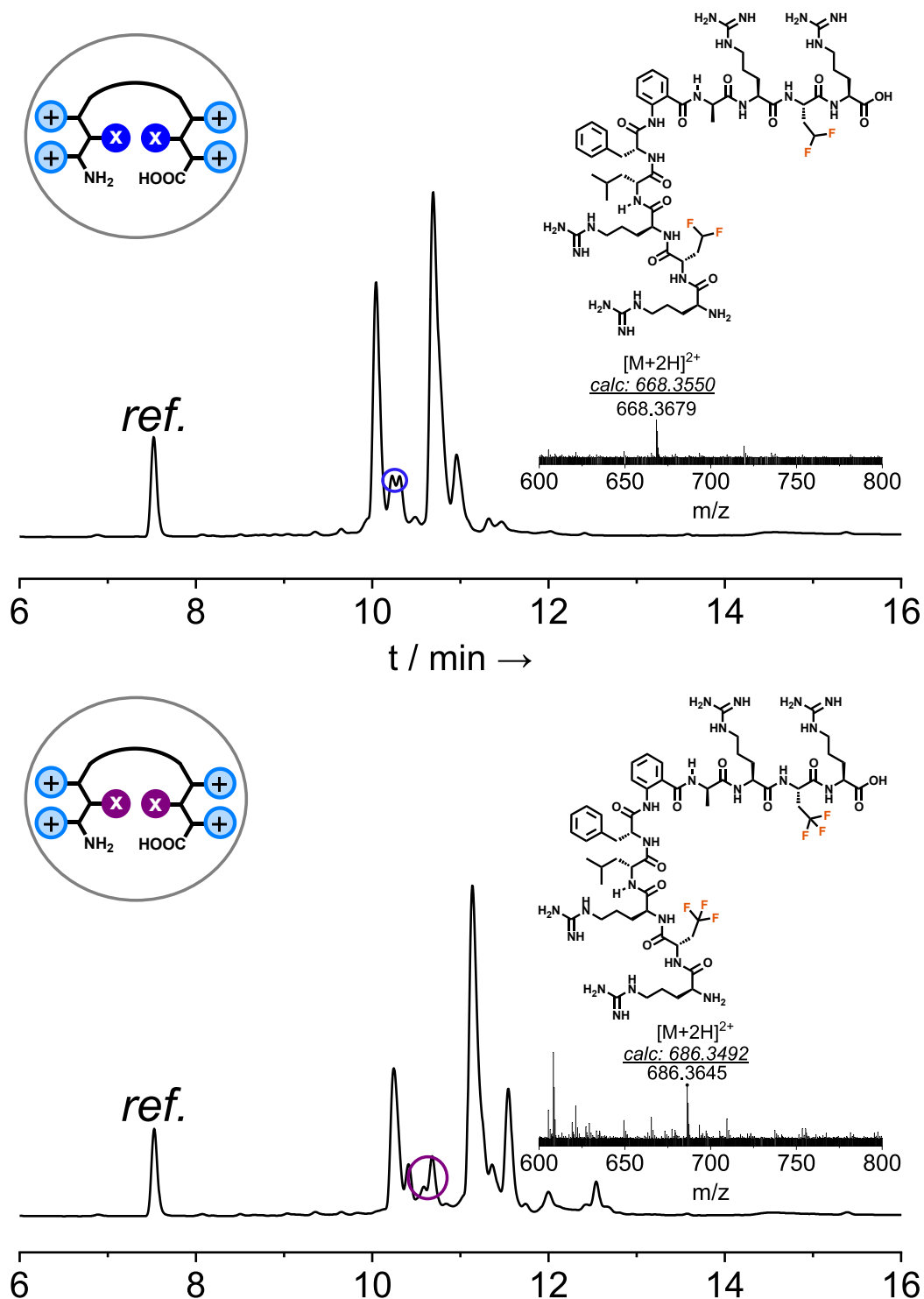


Figure S40: Real-time monitoring of proteolytic digestion at 120 min (HPLC, DAD-280nm) and MS-based (ESI-ToF) detection and determination of peptide fragments of **DfeGlyR14**, (top) and **TfeGlyR14** (bottom) (both 1 mM stock concentration) during incubation with α -chymotrypsin (20 μ M stock concentration) at 30 $^{\circ}$ C. Isolated HPLC signals for subsequent HRMS-analysis are marked in colored ellipses. The dipeptide Ac-[2]Abz-Gly-OH was used as reference signal. Measurements were performed in triplicates. Arginine residues are illustrated as blue-colored positive charges (+). Colors of hydrophobic side chains are the same as introduced in the main paper.

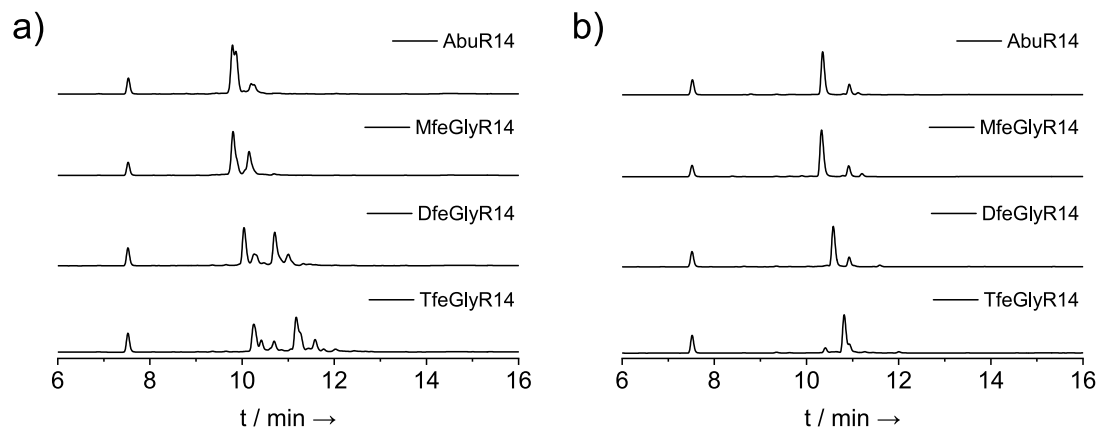


Figure S41: Real-time monitoring of proteolytic digestion at 360 min (HPLC, DAD-280nm) and MS-based (ESI-ToF) detection and determination of peptide fragments of **AbuR14**, **MfeGlyR14**, **DfeGlyR14** and **TfeGlyR14** (all at 1 mM stock concentration) during incubation with either α -chymotrypsin [left, (a)] or β -trypsin [right (b)] (both 20 μ M stock concentration) at 30 °C. The dipeptide **Ac-[2]Abz-Gly-OH** was used as reference signal. Measurements were performed in triplicates.

It is immediately apparent that the HPLC chromatograms after 6 h do not differ significantly from the profiles obtained after 2 h, except for **AbuR14** and **MfeGlyR14** in the case of α -chymotrypsin (**figure S41a**). Here, we discovered the HPLC signal of digestion products **1** & **7** to be vanished, resembling further digestion of these peptide-fragments. For example, further cleavage of a N-terminal Abu-Lys or MfeGly-Lys dipeptide would lead to the formation of digestion product **2** & **8**.

10. Hemolytic activity assay – further data & information

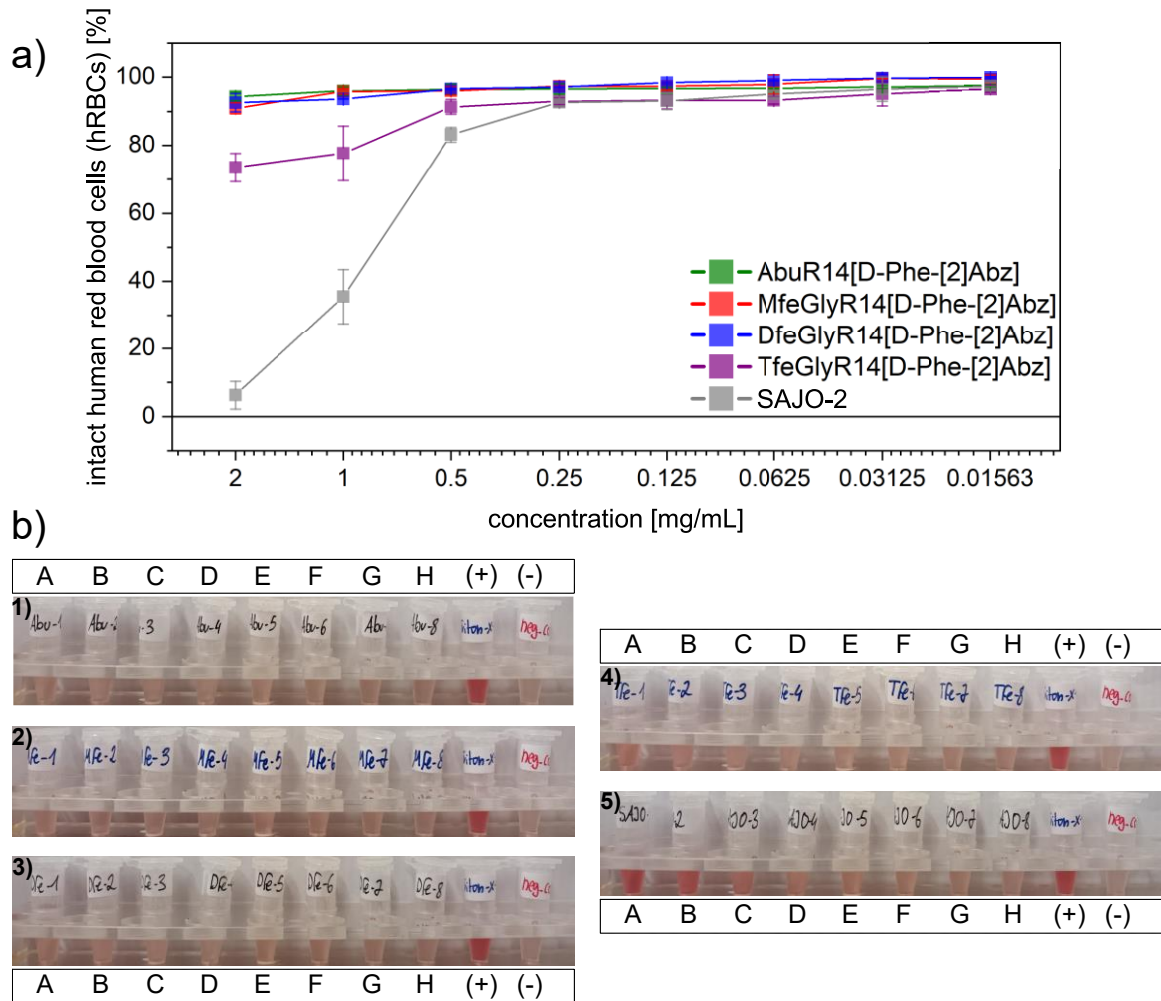


Figure S42: a) Comparison of the hemolytic activity of **AbuR14**, **MfeGlyR14**, **DfeGlyR14**, **TfeGlyR14** and **SAJO-2** as internal control against hRBCs. The standard deviation from three independent experiments is plotted. b) Snapshots of hRBCs-samples incubated with **1) AbuR14**, **2) MfeGlyR14**, **3) DfeGlyR14**, **4) TfeGlyR14** and **5) SAJO-2**. The concentration of samples were A = 2 mg/mL, B = 1 mg/mL, C = 0.5 mg/mL, D = 0.25 mg/mL, E = 0.125 mg/mL, F = 0.0625 mg/mL, G = 0.03125 mg/mL and H = 0.01563 mg/mL. The blood cells were centrifuged before, so that a transparent solution corresponds to zero/low hemolysis and, accordingly, a red-colored solution (due to the release of hemoglobin) to high blood-disrupting properties. This is present, for example, in the case of the positive control (+) [(–) = negative control].

For both experimental approaches, the absorbance measured at 540 nm (A_{exp}) was used for calculation of hemolytic activity through equation (6)

$$[\%_{hemolysis}] = \frac{A_{exp} - A_{PBS}}{A_{100\%} - A_{PBS}} \times 100 \quad (6)$$

With A_{PBS} : negative control, $A_{100\%}$: positive control

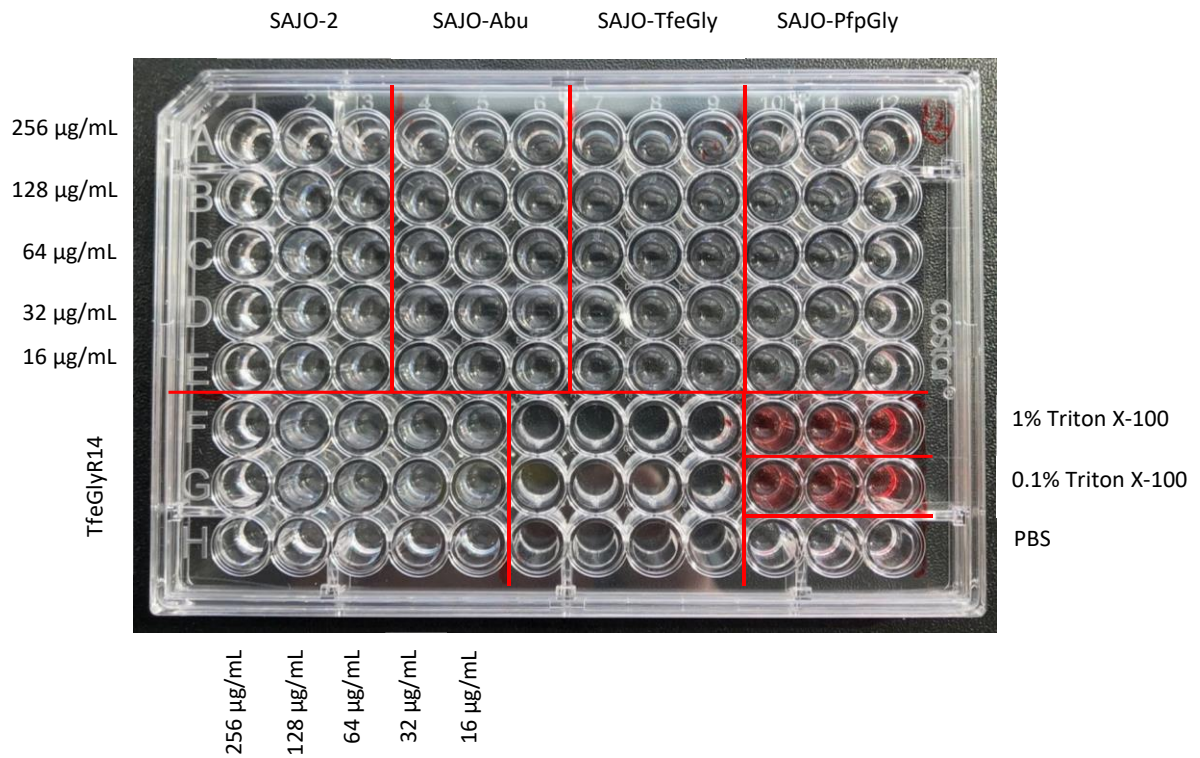


Figure S43: Snapshot of buffered supernatants after 45 min incubation of RBC samples with all Trp-containing peptides and **TfeGlyR14** as internal control and subsequent separation of blood cells through centrifugation. All supernatants (except the positive control) were found to be transparent, resembling zero to low rates of hemolysis.

11. Transmission electron microscopy (TEM) – SAJO-PfpGly

Transmission electron microscopy was performed for *E. coli* ATCC 25922 both upon treatment with **SAJO-PfpGly** at different concentrations (2*MIC / 4*MIC); untreated samples served as negative control. The images obtained from the negative control are shown in **Figure S44** and after treatment with **SAJO-PfpGly** for 24 h in **Figure S45**.

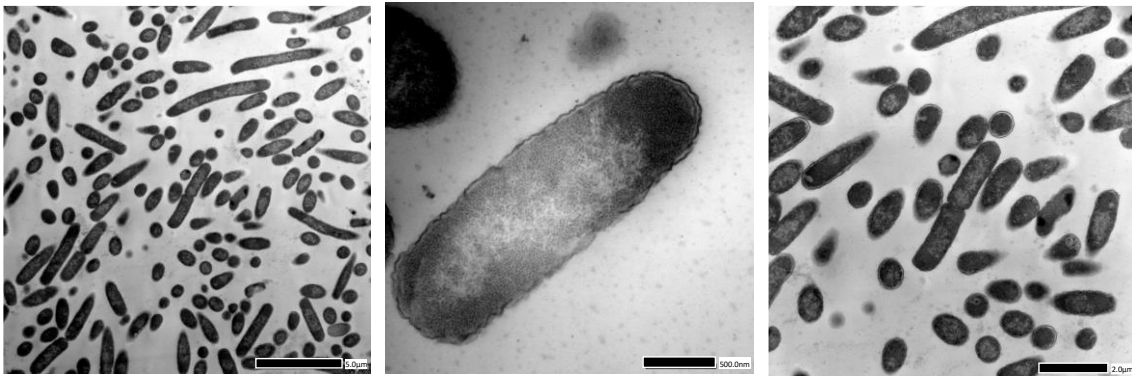


Figure S44: Negative control samples of untreated *E. coli* ATCC 25922 as obtained by TEM.

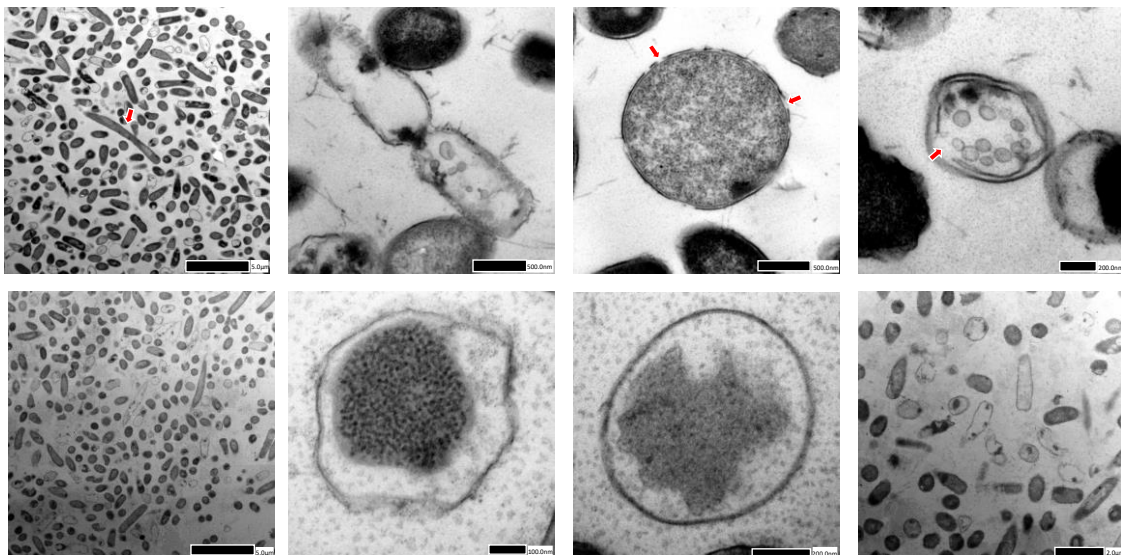


Figure S45: TEM images for **SAJO-PfpGly** treated samples of *E. coli* ATCC 25922 after 24 h of incubation at 37 °C. Top: 2*MIC, bottom: 4*MIC.

In case of untreated *E. coli* samples, cells remained mostly intact. Upon treatment with the polyfluorinated AMP for 24 h, disruptions of both the outer and the cell membrane are clearly

visible (indicated by red arrows). Samples treated at 4*MIC were overall much more affected than those treated at 2*MIC, respectively. Both concentrations led to similar results and the AMP seems to effect membrane stability as pores are formed / observed in both the inner and outer membrane. Overall, treatment of *E. coli* with **SAJO-PfpGly** finally results in leakage of the cellular material causing bacterial death.

12. Thioflavin T (ThT) fluorescence spectroscopy

As an initial test for probing the formation of amyloid-like β -sheet assemblies, thioflavin T (ThT) fluorescence spectroscopy was performed for **AbuR14**, **MfeGlyR14**, **DfeGlyR14**, **TfeGlyR14**, **SAJO-2**, **SAJO-Abu**, **SAJO-TfeGly** and **SAJO-PfpGly** (peptide concentration: 1mg /mL) (**Figure S46**).

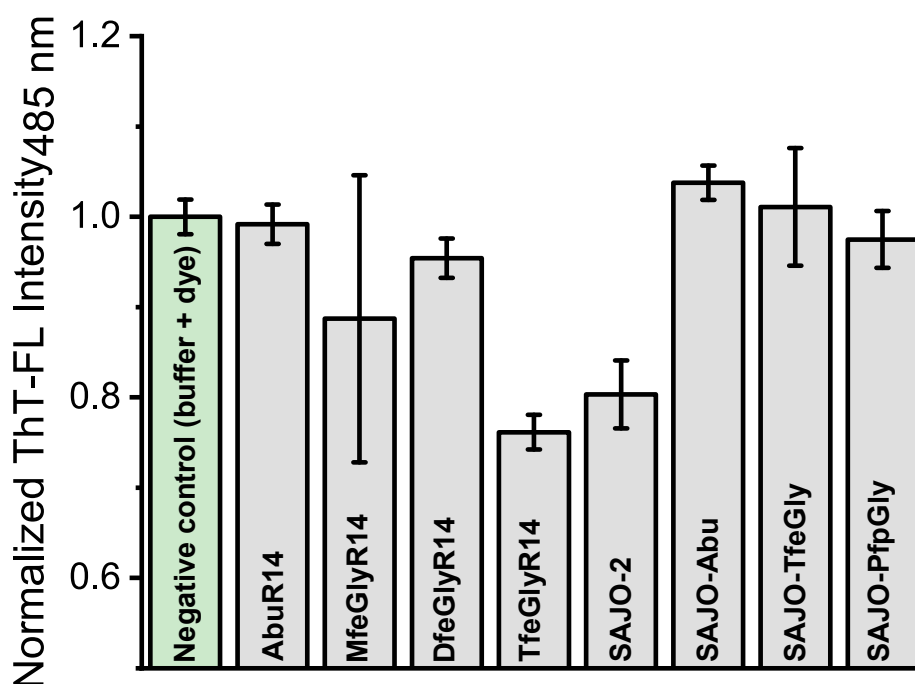


Figure S46: Thioflavin T based fluorescence assays ($\lambda_{\text{ex}} = 420 \text{ nm}$, $\lambda_{\text{em}} = 485 \text{ nm}$) for the detection of supramolecular β -sheet assembly. All peptides (1 mg/mL) were incubated for 24 h at 37 °C in 10 mM phosphate buffer containing 20 μM ThT dye, pH 7.4. FL values were normalized to a negative control (buffer + ThT) which was set as 1.0.

The dye ThT gives a strong fluorescence upon binding to supramolecular β -sheet structures caused by rotational immobilization.⁶ In brief, incubation (24 h) of the peptides in buffered solution supplemented with ThT did not lead to an increase in fluorescence intensity when comparing to the negative control (buffer + ThT). In consequence, the β -hairpin peptides discussed in this work were not found to form high-order supramolecular assemblies.

13. References

1. Romoff, T. T.; Palmer, A. B.; Mansour, N.; Creighton, C. J.; Miwa, T.; Ejima, Y.; Moriwaki, H.; Soloshonok, V. A., Scale-up Synthesis of (R)- and (S)-N-(2-Benzoyl-4-chlorophenyl)-1-(3,4-dichlorobenzyl)pyrrolidine-2-carboxamide Hydrochloride, A Versatile Reagent for the Preparation of Tailor-Made α - and β -Amino Acids in an Enantiomerically Pure Form. *Organic Process Research & Development* **2017**, *21* (5), 732-739.
2. Chowdhary, S.; Schmidt, R. F.; Sahoo, A. K.; tom Dieck, T.; Hohmann, T.; Schade, B.; Brademann-Jock, K.; Thünemann, A. F.; Netz, R. R.; Gradzielski, M.; Kokschi, B., Rational design of amphiphilic fluorinated peptides: evaluation of self-assembly properties and hydrogel formation. *Nanoscale* **2022**, *14* (28), 10176-10189.
3. Hohmann, T.; Dyrks, M.; Chowdhary, S.; Weber, M.; Nguyen, D.; Moschner, J.; Kokschi, B., Gram-Scale Asymmetric Synthesis of Fluorinated Amino Acids Using a Chiral Nickel(II) Complex. *The Journal of Organic Chemistry* **2022**.
4. Leppkes, J.; Dimos, N.; Loll, B.; Hohmann, T.; Dyrks, M.; Wieseke, A. R.; Keller, B. G.; Kokschi, B., Fluorine-induced polarity increases inhibitory activity of BPTI towards chymotrypsin. *RSC Chemical Biology* **2022**.
5. Pace, C. N.; Vajdos, F.; Fee, L.; Grimsley, G.; Gray, T., How to measure and predict the molar absorption coefficient of a protein. *Protein Science* **1995**, *4* (11), 2411-2423.
6. Chowdhary, S.; Moschner, J.; Mikolajczak, D. J.; Becker, M.; Thünemann, A. F.; Kästner, C.; Klemczak, D.; Stegemann, A.-K.; Böttcher, C.; Metrangolo, P.; Netz, R. R.; Kokschi, B., The Impact of Halogenated Phenylalanine Derivatives on NFGAIL Amyloid Formation. *ChemBioChem* **2020**, *21* (24), 3544-3554.

6.3 Introducing Aliphatic Fluoropeptides: Perspectives on Folding Properties, Membrane Partition and Proteolytic Stability

T. Hohmann[†], S. Chowdhary[†], K. Ataka, J. Er, G. H. Dreyhsig, J. Heberle, B. Kokschi, *Eur. J.*, **2023**, e202203860.

[†] *Authors contributed equally*

Submitted: 09 December 2022; **First published:** 01 February 2023

Published by Wiley-VCH GmbH, Weinheim, Germany.

The published work is available online - **DOI:** 10.1002/chem.202203860.²⁴²

6.3.1 Individual contributions of authors

Thomas Hohmann and **Suvrat Chowdhary** (both FU Berlin) developed the overall project and synthesized fluorinated amino acids and (fluoro)peptides. In brief, Thomas Hohmann synthesized and purified the peptides Abu₁₀GY(K)₃, MfeGly₁₀GY(K)₃, DfeGly₁₀GY(K)₃, Abu₁₃GY(K)₄, MfeGly₁₃GY(K)₃, DfeGly₁₃GY(K)₄, Abu₁₅GY(K)₄, MfeGly₁₅GY(K)₃ and DfeGly₁₅GY(K)₄. **Suvrat Chowdhary** synthesized and purified the peptides TfeGly₁₀GY(K)₃, TfeGly₁₃GY(K)₄, TfeGly₁₅GY(K)₄, Abu₄[4]Abz, MfeGly₄[4]Abz, DfeGly₄[4]Abz and TfeGly₄[4]Abz. Thomas Hohmann and **Suvrat Chowdhary** prepared and wrote the manuscript. Beate Kokschi (FU Berlin) provided guidance on data analysis and interpretation. Thomas Hohmann performed CD studies on above-mentioned peptides and the determination of hydrophobicity (log *P*). **Suvrat Chowdhary** performed CD studies on above-mentioned peptides, membrane leaking assays (6-FAM) and proteolytic digestion assays with proteinase k & elastase. Kenichi Ataka (FU Berlin) performed SEIRAS studies and wrote the manuscript. Jasmin Er (FU Berlin) assisted Thomas Hohmann in SPPS and log *P* determination. Gesa Heather Dreyhsig assisted **Suvrat Chowdhary** in SPPS and proteolytic digestion assays. Joachim Heberle provided expertise and feedback.

6.3.2 Rationale and summary of the project

Depending on their side chain pattern and overall content, the application of fluorinated amino acids in peptide engineering serves as a powerful approach to direct hydrophobicity, secondary structure formation and self-assembly. Despite numerous milestones of research in peptide science during the last decades, however, synthetic fluoropeptides consisting exclusively of fluorinated amino acids have not been described yet. Their first generation, as introduced in this work, comprises a 10-mer ($X_{10}GY(K)_3$), 13-mer ($X_{13}GY(K)_4$) or 15-mer ($X_{15}GY(K)_4$) homopeptide sequence based on the iterative incorporation of either Abu, MfeGly, DfeGly or TfeGly. A Tyr residue was set for UV-based concentration determination and a solubility tag with three or four Lys residues for an appropriate solubility in physiological conditions. A main highlight is constituted by the first-ever experiments on the enzymatic degradability of solely fluorinated peptides ($X_4[4]Abz$) via HPLC/MS-based digestion studies (**Figure 6.10**).

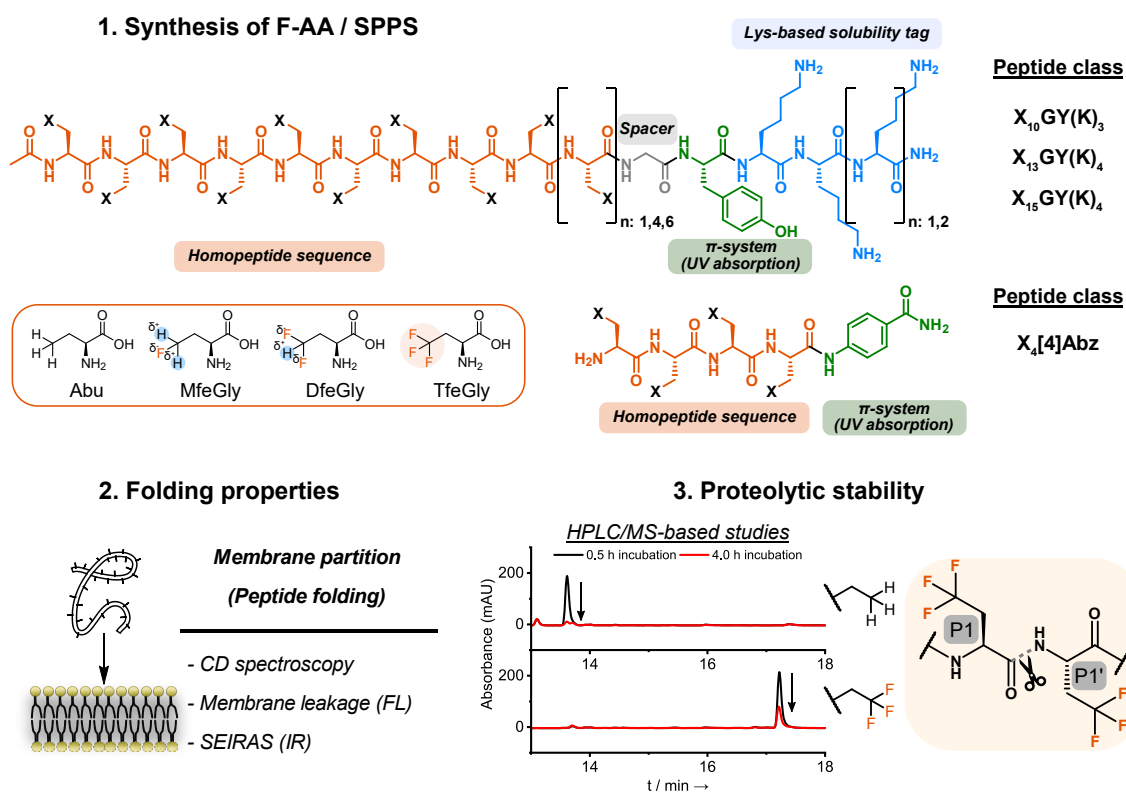


Figure 6.10 Schematic illustration of the project's working plan – "Introducing Aliphatic Fluoropeptides: Perspectives on Folding Properties, Membrane Partition and Proteolytic Stability".

CD spectroscopic investigations were accomplished in physiological buffer supplemented with a wide range of SDS concentrations. Significant alterations on β -strand to α -helix transition in membrane-mimicking environments were found (**Figure 6.11**). Focusing on the 13-meric sequence length, $Abu_{13}GY(K)_4$ exhibits the highest degree on α -helix

formation, whereas mono- (MfeGly₁₃GY(K)₄) and difluorination (DfeGly₁₃GY(K)₄) tend to weaken α -helical folding. In fact, higher amounts of SDS were required for adopting an α -helical conformation as well as significantly lower values of normalized molar ellipticity θ at $\lambda_{\min} = 208$ and $\lambda_{\min} = 222$ nm were measured. Thus, log P determination on the X₁₃GY(K)₄ series revealed a loss in hydrophobicity by Abu (log P : 3.03) \rightarrow MfeGly (log P : 1.89) / DfeGly (log P : 2.79) substitution. In case of TfeGly₁₃GY(K)₄ (log P : 3.79), however, an unusual formation of PPII-like helices ($\lambda_{\min} = 196$ nm & $\lambda_{\max} = 220$ nm) was observed. Higher amounts of SDS led to increased θ values which hints an enhanced stabilization of this folding pattern.

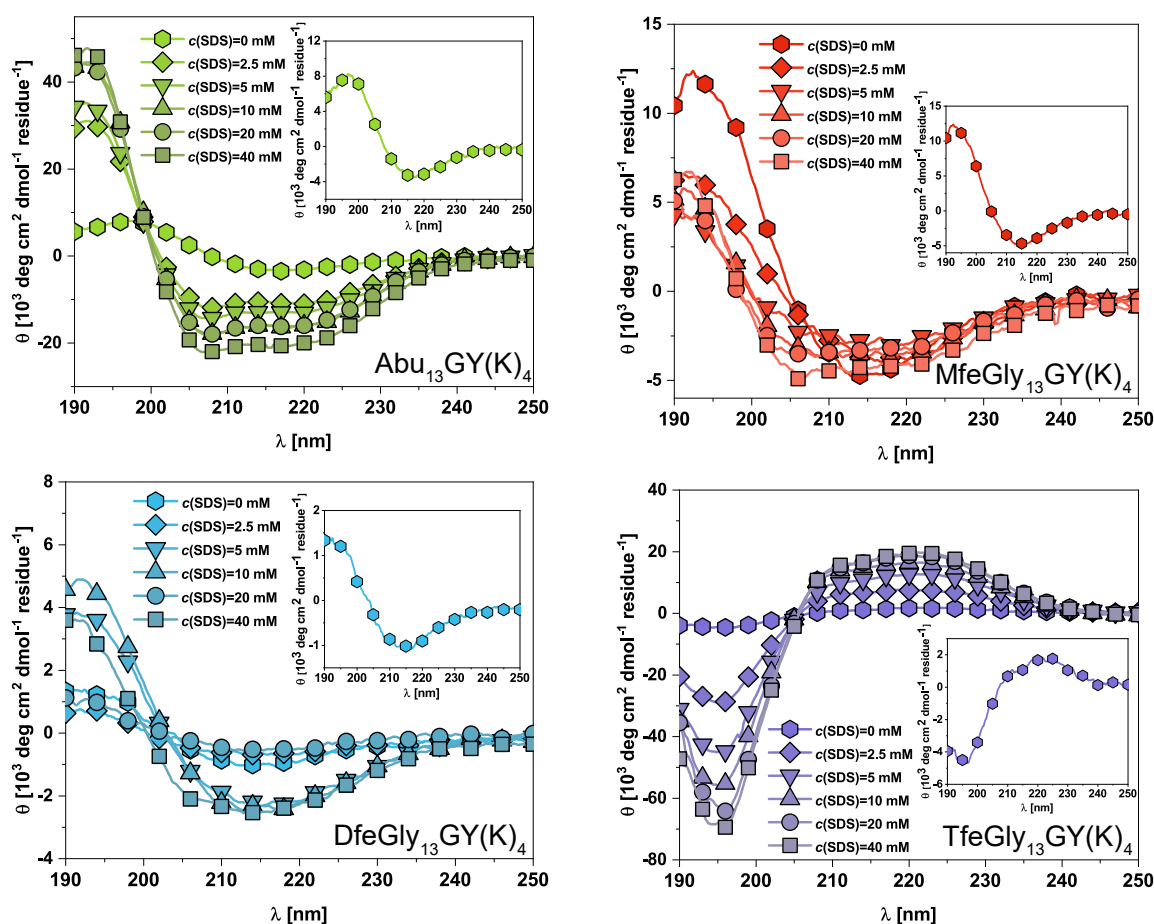


Figure 6.11 CD spectra of (fluoro)peptides (25 μ M) in 10 mM sodium phosphate buffer, pH 7.4 supplemented with varying amounts of SDS (2.5, 5, 10, 20, 40 mM). The insets show the zoomed-in spectra at solely buffered solutions. All spectra were recorded at 20 $^{\circ}$ C. Adapted from Hohmann & Chowdhary *et al.* in a modified version (Copyright \copyright 2023 John Wiley & Sons, Ltd).²⁴²

The insertion and (re)folding of the X₁₃GY(K)₄ fluoro-peptides in POPC:POPG unilamellar vesicles were studied by a combination of CD spectroscopy, surface-enhanced infrared absorption spectroscopy (SEIRAS), as well as FL-based leaking assays that identified lipid partitioning as a prolonged process, with a FL saturation after approximately 10 h. SEIRAS was applied after mixing (Au)-solid-supported POPC:POPG-bilayers with dissolved

peptides samples. Herein obtained IR spectra (**Figure 6.12**) recorded at different time points reveal the amide I and II vibrational modes of the peptide backbone at around $\sim 1650\text{ cm}^{-1}$ and $\sim 1550\text{ cm}^{-1}$ to increase with time, indicating a greater partitioning of the peptides on the casted lipid bilayer (max. 10 h).

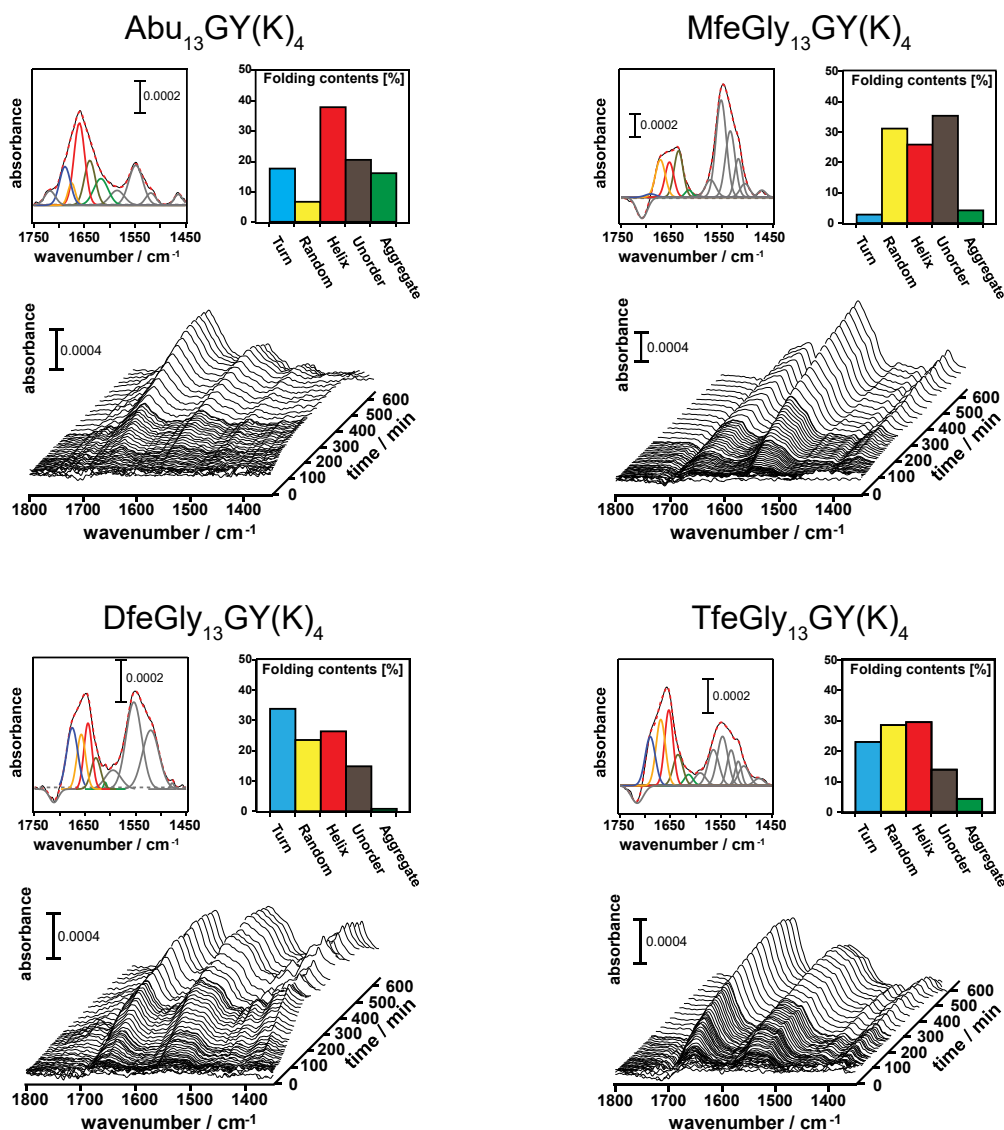


Figure 6.12 *In-situ* SEIRA spectra of the adsorption process on POPG/POPC lipid bilayers with peak fittings of the amide bands for determining average contents of the secondary structure components of Abu₁₃GY(K)₄, MfeGly₁₃GY(K)₄, DfeGly₁₃GY(K)₄, and TfeGly₁₃GY(K)₄. Adapted from Hohmann & Chowdhary *et al.* in a modified version (Copyright © 2023 John Wiley & Sons, Ltd).²⁴²

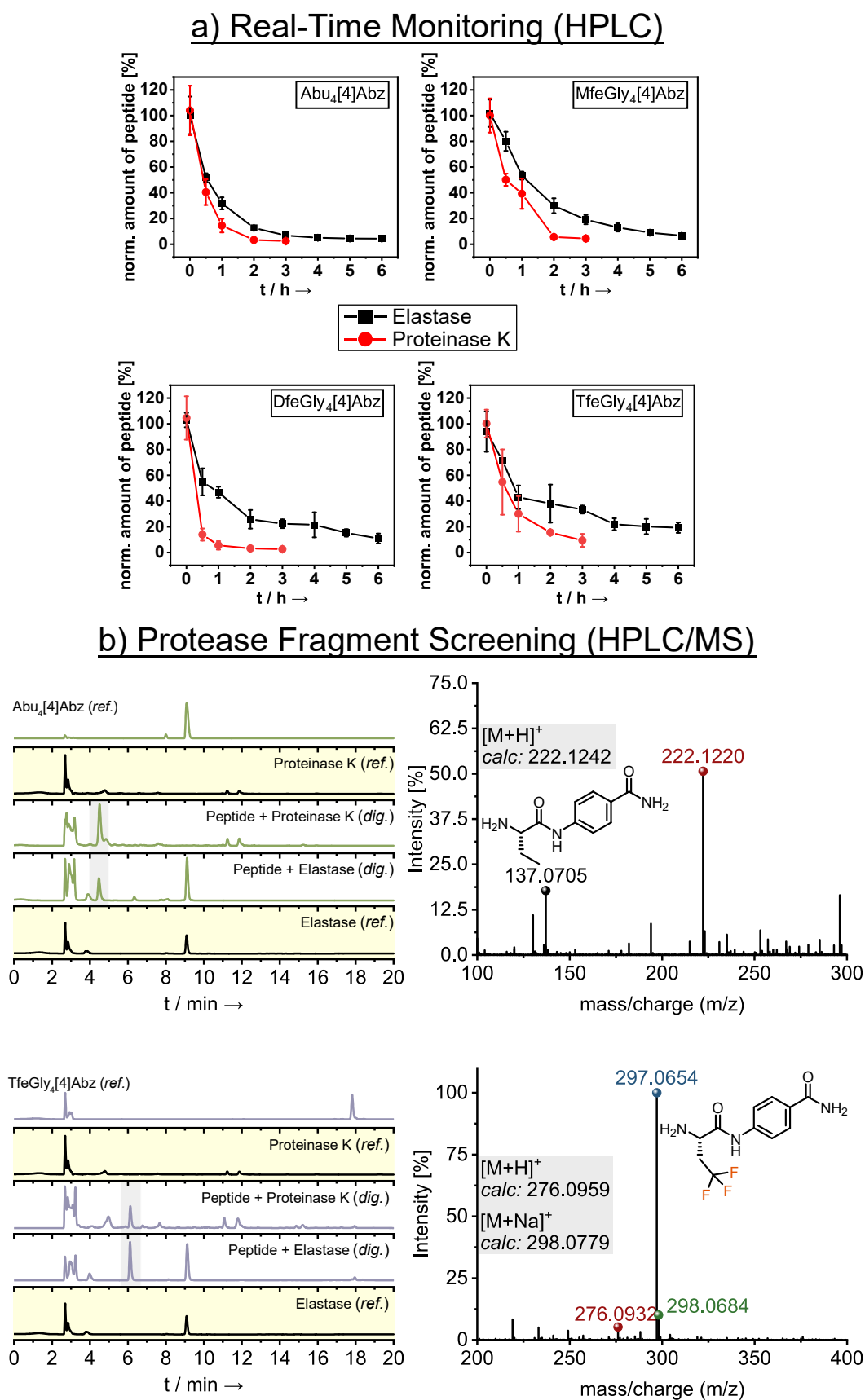
Peak fitting of the amide I band was accomplished to predict the statistical contribution on individual secondary structure components. For Abu₁₃GYK₄, the predominant component is a helical structure (about 40%). In the case of both MfeGly₁₃GY(K)₄ and DfeGly₁₃GY(K)₄, the helical fraction decreases significantly (26% for MfeGly₁₃GY(K)₄ and DfeGly₁₃GY(K)₄) which is in accordance with prior CD data. The structural evaluation of

TfeGly₁₃GY(K)₄ shows the proportion of bend/turn structures to decrease (from 34 to 23 %) while the helical structure increases (26 to 30 %).

The enzymatic degradability of fluoropeptides was investigated with the serine proteases elastase & proteinase K and the 4-meric [X]₄Abz series as substrates. Truncation of the homopeptide scaffold and exclusion of the GYK_{3/4} sequence aimed to prevent peptide aggregation upon enzymatic hydrolysis of the solubility tag. DMSO [25%, v/v] was further added to the reaction mixture to ensure substrate-solubility. At first, real-time monitoring of peptide proteolysis by HPLC analyses of quenched aliquots confirmed digestibility for all sequences (**Figure 6.13a**). Notably, the most fluorinated variant TfeGly₄[4]Abz remained in up to 4-fold higher amounts after 6 h incubation with elastase ($19.3 \pm 4.0\%$)_[TfeGly] and 3 h incubation with proteinase k ($9.3 \pm 5.0\%$)_[TfeGly] than the non-fluorinated Abu₄[4]Abz [$4.3 \pm 0.1\%$]_[Abu] and ($2.5 \pm 0.1\%$)_[Abu].

Second, HPLC/MS-assisted investigations on peptide proteolysis were executed for the identification of hydrolyzed peptide fragments (**Figure 6.13b**). In brief, the Abz-labeled amino acids Abu-Abz, MfeGly-Abz, DfeGly-Abz and TfeGly-Abz were identified as main digestion products during peptide degradation by both enzymes, respectively. Their origin is constituted by a predominant cleaving site according to H₂N-Faa^{P3}-Faa^{P2}-Faa^{P1}-Faa^{P1'}-[4]Abz^{P2'}-NH₂. Thus, the released fragments occupied the P1' & P2' position, so that the fluorinated amino acids are supposed to function as both P1 & P1' residues, accordingly.

In summary, this work describes the first study on the folding properties, membrane partition and proteolytic stability of peptide sequences consisting of fluorinated amino acids in main proportions. In particular, the degree of side chain fluorination was found to dictate the folding propensity in hydrophobic environments while maintaining enzyme-catalyzed hydrolysis of the peptides' amide bonds. The rational design presented in this work could play an intriguing role in the development of novel & fluorinated peptide-based biomaterials.²⁴²

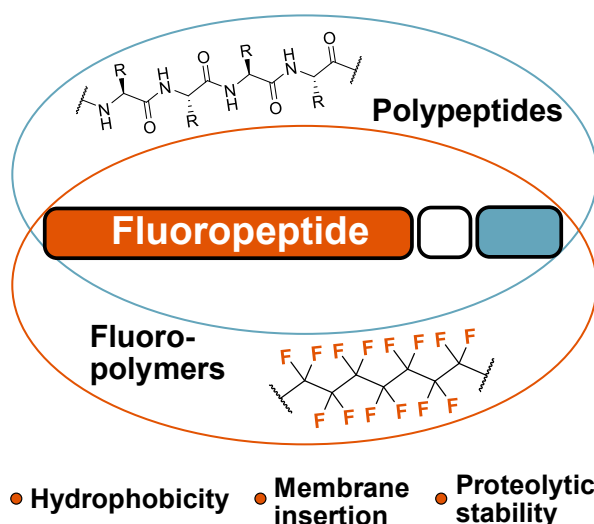


6.3.3 Publication and supplementary information

Introducing Aliphatic Fluoropeptides: Perspectives on Folding Properties, Membrane Partition and Proteolytic Stability

T. Hohmann[†], S. Chowdhary[†], K. Ataka, J. Er, G. H. Dreyhsig, J. Heberle, B. Kocsch, *Chem. Eur. J.*, **2023**, e202203860.

[†] Authors contributed equally



DOI: 10.1002/chem.202203860

Creative Commons license: [CC BY-NC-ND 4.0](https://creativecommons.org/licenses/by-nc-nd/4.0/)

Introducing Aliphatic Fluoropeptides: Perspectives on Folding Properties, Membrane Partition and Proteolytic Stability

Thomas Hohmann^{+, [a]} Suvrat Chowdhary^{+, [a]} Kenichi Ataka,^[b] Jasmin Er,^[a]
Gesa Heather Dreyhsig,^[a] Joachim Heberle,^[b] and Beate Koksch^{*[a]}

Abstract: A de novo designed class of peptide-based fluoropolymers composed of fluorinated aliphatic amino acids as main components is reported. Structural characterization provided insights into fluorine-induced alterations on β -strand to α -helix transition upon an increase in SDS content and revealed the unique formation of PPII structures for trifluorinated fluoropeptides. A combination of circular dichroism, fluorescence-based leaking assays and surface enhanced infrared absorption spectroscopy served to examine the insertion and folding processes into unilamellar

vesicles. While partitioning into lipid bilayers, the degree of fluorination conducts a decrease in α -helical content. Furthermore, this study comprises a report on the proteolytic stability of peptides exclusively built up by fluorinated amino acids and proved all sequences to be enzymatically degradable despite the degree of fluorination. Herein presented fluoropeptides as well as the distinctive properties of these artificial and polyfluorinated foldamers with enzyme-degradable features will play a crucial role in the future development of fluorinated peptide-based biomaterials.

Introduction

The introduction of fluorine into bioactive compounds as well as the utilization of fluorocarbon-based polymers attract growing interest in biochemical and pharmaceutical research.^[1] Several reports have shown that selective fluorination often can enhance hydrophobic properties and biological activity.^[2] It is not surprising that, presently, about 20–25% of commercially available pharmaceuticals do contain fluorinated residues, and perfluorocarbons (PFCs) are widely studied as fluorous tags in the context of gene, protein, and peptide delivery in vitro and in vivo.^[3] In general, PFCs are both hydrophobic and lipophobic which ensures superior membrane permeability as well as a promising potential for mediating drug delivery and cell internalization for pharmaceutical applications.^[4] For example, conjugation or co-assembly of fluoroalkanes with cargo

peptides and proteins was reported to significantly enhance intracellular uptake.^[5] A notable drawback of perfluorinated compounds, however, comprises their biological inertness prohibiting biodegradation by digestive enzymes, microbes, and metabolic processes. As a result, PFCs have shown to be very persistent in the environment and can undergo bioaccumulation and biomagnification.^[6] Consequently, the development of biodegradable fluoropolymers is of paramount importance to design next-generation biomaterials.^[3b]

Incorporation of fluorinated amino acids into peptide & proteins has gained significant relevance in biosciences as it imparts unique biophysical features, like an enhancement in thermal and chemical stability or modulation of folding properties.^[7] Depending on the degree of fluorination and side chain pattern, these synthetic building blocks can be used to fine-tune peptide secondary structure formation and bioactivity.^[8] Replacing a hydrophobic amino acid with its fluorinated counterpart was reported to facilitate peptide self-assembly in membrane environments, mimicking the properties of fluoroalkyl tags discussed before. For example, Godbout et al. reported a fluorinated 21-residue peptide and showed that fluorous interactions, derived from six residues of (2S)-4,4,4-trifluoroethylglycine (TfeGly), drive the assembly into helical superstructures. These biomaterials functioned for the generation of artificial ion channels in lipid bilayers.^[9] Furthermore, Naarmann et al. and Bilgiçer et al. described the incorporation of hexafluoroisoleucine (up to seven residues) into a coiled-coil motif to efficiently drive the formation of defined helical bundles in lipid bilayers and SDS micelles.^[10] Finally, fluorine can be a powerful tool to study the interaction of membrane-active peptides with lipids using ¹⁹F NMR and has an essential significance for in vivo ¹⁹F magnetic resonance imaging.^[11]

[a] T. Hohmann,⁺ S. Chowdhary,⁺ J. Er, G. H. Dreyhsig, Prof. Dr. B. Koksch
Institute of Chemistry and Biochemistry
Freie Universität Berlin
Arnimallee 20, 14195 Berlin (Germany)
E-mail: beate.koksch@fu-berlin.de

[b] Dr. K. Ataka, Prof. Dr. J. Heberle
Department of Physics
Freie Universität Berlin
Arnimallee 14, 14195 Berlin (Germany)

[⁺] Authors contributed equally.

Supporting information for this article is available on the WWW under <https://doi.org/10.1002/chem.202203860>

© 2023 The Authors. Chemistry - A European Journal published by Wiley-VCH GmbH. This is an open access article under the terms of the Creative Commons Attribution Non-Commercial NoDerivs License, which permits use and distribution in any medium, provided the original work is properly cited, the use is non-commercial and no modifications or adaptations are made.

The Kocsch laboratory has recently established the access to a variety of aliphatic fluorinated amino acids in gram scale, enabling the fabrication of synthetic peptides consisting of multiple of these building blocks.^[12] One of our recent works demonstrated the impact of fluorine-specific interactions to be controlled by the degree of side chain fluorination as well as the overall proportion of fluorinated building blocks.^[13] Our ultimate goal, therefore, is the systematic de novo design of peptide-based fluoropolymers with distinct fluorine-driven folding & assembly properties while the peptide scaffold is predestined to maintain biodegradability and biocompatibility.

In this study, we introduce the first generation of fluorine-rich peptide oligomers with diverse chain lengths and degrees of side chain fluorination by the consecutive coupling of either 2-aminobutyric acid **1a** or its fluorinated analogs (2S)-4-monofluoroethylglycine (MfeGly) **1b**, (2S)-4,4-difluoroethylglycine (DfeGly) **1c** or (2S)-4,4,4-trifluoroethylglycine (TfeGly) **1d**. These fluoropeptides were studied with respect to a wide range of biophysical parameters such as hydrophobicity, secondary structure formation, but also the allocation and conformation within interfacial layers of artificial membranes using a combination of CD spectroscopy, 6-FAM leaking assays and surface enhance infrared absorption spectroscopy (SEIRAS)^[14]. Furthermore, we present investigations on the proteolytic stability of these fluoropeptides with an exceptional fluorine content (up to 28.5%). To our own surprise, obtained experimental data revealed these fluoropeptides to be enzymatically degradable, regardless of the degree of side chain fluorination. Hence, this data set provides insights into an unexplored class of foldamers constituted at the multidisciplinary interface of peptide science and fluorine chemistry.

Results and Discussion

Peptide design & synthesis

With the aim of systematically studying the impact of fluorination degree of the single building blocks on the overall hydrophobicity, folding and proteolytic stability, the corresponding sequences were constructed from amino acids with different amounts of fluorine. For this purpose, we used 2-aminobutyric acid **1a** and its fluorinated analogs MfeGly **1b**, DfeGly **1c**, and TfeGly **1d** (Figure 1a).

A solubility tag consisting of three or four lysine residues was introduced at the C-terminus of each peptide to facilitate solubility in physiological conditions. The concentration determinations by UV absorbance were achieved by the incorporation of a tyrosine residue. Finally, we included a glycine residue to separate the fluoropeptide sequence from the solubility tag. The N-terminus of the peptides was acetylated. In addition to the degree of fluorination, we examined the influence of the length of the fluoropeptide fragment on above-discussed properties of the respective peptides. Three different lengths, 10, 13, and 15, were selected for this purpose, with three lysine residues (as solubility tag) added to the decamers and four lysines attached to the longer sequences 13

and 15. Hence, a total of twelve peptides was to be synthesized: $X_{10}GY(K)_3$ ($X=A$, Abu **2a**; M, MfeGly **2b**; D, DfeGly **2c**; T, TfeGly **2d**), $X_{13}KY(K)_4$ ($X=A$, Abu **3a**; M, MfeGly **3b**; D, DfeGly **3c**; T, TfeGly **3d**), and $X_{15}GY(K)_4$ ($X=A$, Abu **4a**; M, MfeGly **4b**; D, DfeGly **4c**; T, TfeGly **4d**) (Figure 1a). All peptides studied in this work were synthesized using microwave-assisted solid-phase peptide synthesis (SPPS). By using optimized coupling conditions recently published by Leppkes et al.,^[15] all fluorinated amino acids could be incorporated with using only 1.5 equivalents of fluorinated species. *N,N'*-Diisopropylcarbodiimide (DIC) and ethyl cyanohydroxyiminoacetate (oxyma) were used as the coupling reagents (Figure 1b). After full cleavage from the resin, the peptides were purified by RP-HPLC (Figure 1c).

Looking at the yields of the peptides, it quickly emerges that the trifluorinated sequences are by far the most difficult to synthesize (Figure 1d). The yields of TfeGly₁₀GY(K)₃ **2d** and TfeGly₁₃GY(K)₄ **3d** are among the lowest in the series. TfeGly₁₅GY(K)₄ **4d** was only synthesized in traces and could not be isolated. The highest yield was achieved with the non-fluorinated decamer Abu₁₀GY(K)₃ **2a**. In general, longer homooligopeptide sequences are, as expected, more difficult to generate, which can be explained by the increased tendency to aggregate.^[16] Therefore, structural investigations were carried out with eleven isolated peptides.

Hydrophobicity of fluoropeptides

Since PFCs can be used as efficient tools to facilitate the uptake by cell membranes, we were especially eager to study the properties of fluoropeptides not only in aqueous but also in lipophilic environments. We assumed that hydrophobicity of the corresponding peptide sequences should be a driving force behind the interactions with membrane models. To quantify the corresponding individual lipophilicity values for each peptide studied in this work, we adapted an HPLC-based assay that was used to estimate the log *P* values of small organic molecules. A library of tri-, tetra- and pentameric peptides with known log *P* values was used to determine the unknown log *P* values for the peptides of interest using their retention times on a reversed-phase C18 column (Supporting Information). In Figure 2, the corresponding data are presented. The comparison to the hydrophobicity of the Fmoc-protected amino acids (Supporting Information, Figure S33), which were previously determined and published in our group, shows that the log *P* values of $X_{10}GY(K)_3$ peptides ($X=$ Abu **2a**, MfeGly **2b**, DfeGly **2c**, TfeGly **2d**) have the same tendencies.

Monofluorination lowers the hydrophobicity compared to the non-fluorinated variant while the di-, and trifluorination increase the log *P* values. The elevation of polarity by monofluorination was expected and has already been discussed extensively in the literature.^[8] This finding can be readily explained by the fluorine-induced dipole moment within the aliphatic side chain. Furthermore, it is characteristic how considerably the trifluorination increases the hydrophobicity of the peptide: the log *P* of the five residues shorter TfeGly₁₀GY(K)₃ **2d** peptide (3.16) is nearly the same as the value of the

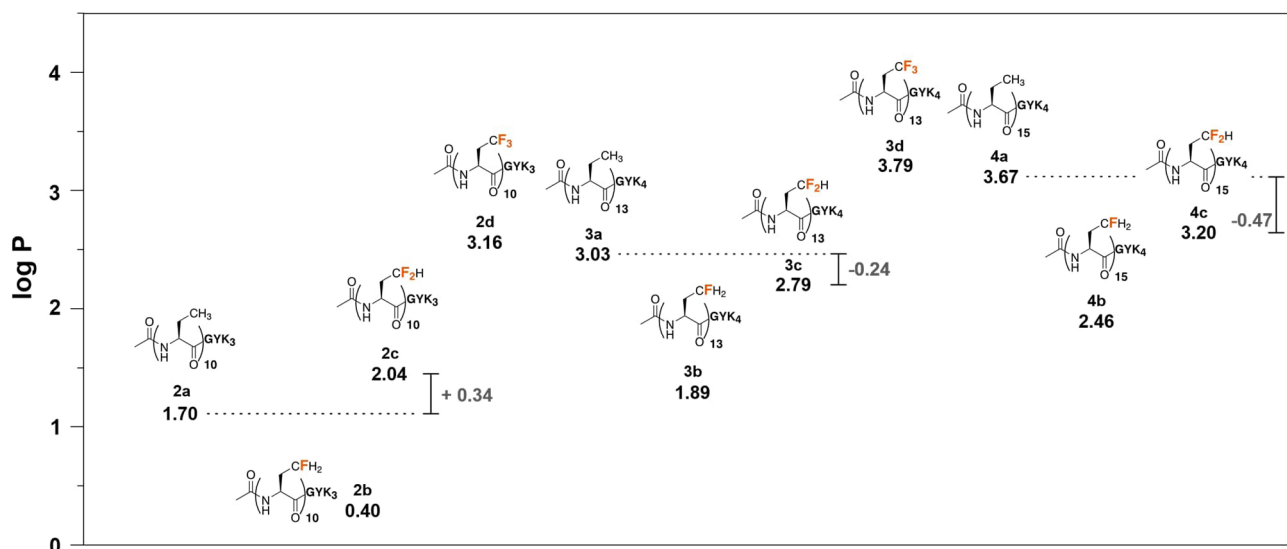


Figure 2. Determined log P values of the fluorinated peptides. The relative increase in polarity of the difluorinated peptides with respect to the nonfluorinated analogues was highlighted.

the α -helix in the case of Abu₁₅GY(K)₄ **4 a**, an SDS concentration of 2.5 mM was already sufficient. Similar transition was observed for the mono- and difluorinated peptides. An important distinction, compared to the non-fluorinated compounds, is both the stronger influence of the length of the corresponding fluoropeptide sequence, and the minimal amount of SDS required for the stabilization of the α -helix. This trend can be described very well in the case of DfeGly peptides. DfeGly₁₀GY(K)₃ **2 c** peptide forms a β -strand structure in water. With increasing amount of SDS, the signal diminishes significantly indicating an unordered structure and peptide precipitation at high SDS concentrations.

In the case of DfeGly₁₃GY(K)₄ **3 c** and DfeGly₁₅GY(K)₄ **4 c**, a β -strand to α -helix transition was observed as well. Nevertheless, especially for DfeGly₁₃GY(K)₄ **3 c**, a concentration of 40 mM was required to see a distinct band in the 208 nm region. Analogous conclusions can be drawn for the monofluorinated peptides. A longer sequence or higher SDS amount is needed for the stabilization of the α -helical conformation in a SDS environment. For DfeGly₁₅GY(K)₄ **4 c** and apart from one exception for DfeGly₁₃GY(K)₄ **3 c**, an isodichroic point near 200 nm could be detected indicating a two-state transition. Dual wavelength parametric test supports a two-state model, with larger deviations in the slope of the θ_{208} vs. θ_{222} correlation seen in the case of DfeGly₁₃GY(K)₄ **3 c** (Supporting Information, Figures S38, 39). This was not observed in the case of MfeGly peptides, suggesting a more complex composition of multiple conformations, besides α -helix and β -strand structures.

At this point, it should be mentioned that despite the Lys-tag, the solubility of the peptides in the aqueous medium was severely limited. Therefore, the CD studies described in this work were performed at concentrations between 25 and 50 μ M. Apart from DfeGly₁₀GY(K)₃ **2 c**, no peptide precipitation was observed upon increasing the SDS concentration.

Subsequently, we wanted to use the obtained log P values to explain the tendency to form α -helical structure in the presence of SDS micelles for Abu, MfeGly and DfeGly peptides. The Figure S34 shows the normalized molar ellipticity at 208 nm of the corresponding peptides at different SDS concentrations, which is characteristic for the transition from a β -strand structure to an α -helix. The presented trends show that four of the peptides with the highest log P values also exhibit the strongest α -helical structure formation. An exception is Abu₁₀GY(K)₃ **2 a**, which, despite its comparatively low hydrophobicity, displays a strong tendency to α -helix formation in the presence of SDS. In addition to hydrophobicity, the length of the peptides seems to be a crucial factor for the stabilization of the α -helical structure in a membrane environment. The X₁₀GY(K)₃ **2 a-d** and X₁₃GY(K)₄ **3 a-d** peptides of mono and difluorinated amino acids exhibit the lowest helical content in the vicinity of micelles. In conclusion, mono- and difluorination tend to disrupt the α -helix formation in a hydrophobic environment, which is somewhat consistent with the increase in polarity relative to the non-fluorinated sequences.

Quite unexpectedly, the trifluorinated peptides revealed a completely different picture. Neither an α -helix nor a β -strand conformation could be identified. For TfeGly₁₀GYK₃ **2 d**, a minimum at 214 nm was observed, which is significantly blue shifted from a minimum at 218 nm that corresponds to a β -strand structure. Additionally, a band at 198 nm was not observed making a β -strand conformation highly unlikely. The CD spectrum of TfeGly₁₃GY(K)₄ **3 d** shows a minimum at 196 nm and a broad positive band in the 220 nm region. Since the later CD spectrum is somewhat more distinct, we will start our discussion with the structural properties of TfeGly₁₃GY(K)₄ **3 d**.

Both bands are signatures of a polyproline type II (PPII) helix.^[18] Poly(L-prolines), their derivatives, poly(L-lysine) and comparable peptides are known to adapt a PPII conformation^[19], an extended left-handed helix (3.1 Å per

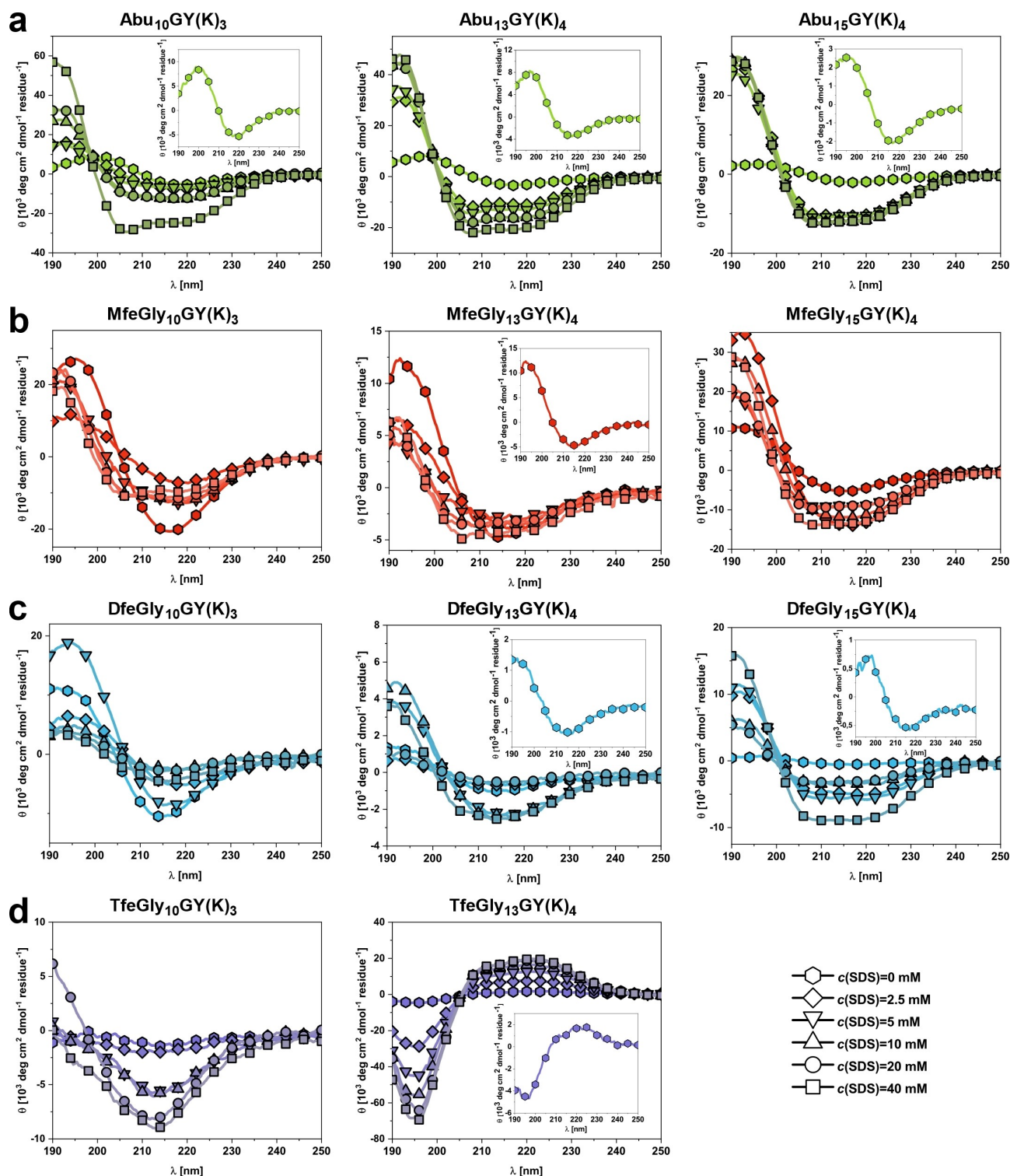


Figure 3. CD spectra of (fluorinated) peptides (25 μM) in aqueous solution (phosphate buffer, 10 mM, pH = 7.4) and in the presence of SDS (2.5, 5, 10, 20, 40 mM); a. CD spectra of Abu oligomers; b. CD spectra of MfeGly oligomers; c. CD spectra of DfeGly oligomers; d. CD spectra of TfeGly oligomers. The insets show the zoomed-in spectra at a SDS concentration of 0 mM.

residue) and defined by backbone dihedral angles ϕ , ψ of -75° and $+145^\circ$ (CD spectrum: minimum at 206 nm; maximum at 225 nm).

In the case of TfeGly₁₃GY(K)₄ **3d**, the intensity of both bands increases drastically with the amount of SDS indicating a stabilization of a PPII helix in a hydrophobic environment (additional discussion corresponding the PPII structure is placed

in the Supporting Information). This was rather surprising, since the hydrogen bond network between backbone and water molecules is generally considered to be the greatest stabilizing factor for the PPII conformation.^[18a,d,20] Nevertheless, the Budisa research group could already demonstrate based on their work on octahydroindole-2-carboxylic acid oligomers that a PPII conformation can also be formed in a transmembrane environment.^[21] In this context, it should be mentioned that these are highly rigid structures which are locked in a PPII conformation. Flexible peptides, analogous to TfeGly oligomers, that can form a PPII helix in a membrane environment are, to the best of our knowledge, unknown. In addition to the backbone solvation, other factors, such as side chain-side chain interactions or side chain conformational entropy, were discussed as possible ways to stabilize a PPII conformation.^[18a,22] Particularly in the case of poly(L-lysine) peptides, the repulsion between positive charges of the corresponding side chains was discussed as an important factor for the formation of a PPII structure forcing the peptide chain into an extended conformation.^[22–23] Similar considerations could also apply to TfeGly oligomers. Recently, we reported a structural study discussing an alternating peptide structure consisting of TfeGly and lysine residues. Molecular dynamics simulations showed that the most stable structural state of CF₃ groups decline spatial proximity to each other.^[13] Here we observe something comparable: In contrast to Abu, MfeGly, and DfeGly oligomers, an α -helical structure is not formed in the presence of SDS. In case of TfeGly-derived fluoropeptides, the CF₃ residues with *i, i + 4* spacing turn out to be unfavorable and, thus adopt an extended PPII conformation. Furthermore, an isodichroic point near 206 nm was detected. Additionally, an excellent correlation with a constant slope was observed for the wavelengths at 196 and 221 nm (Supporting Information, Figure S40). Both factors highly support a two-state transition model for the TfeGly₁₃GY(K)₄ **3 d** peptide in the presence of SDS. It should be mentioned that in the case of TfeGly₁₃GY(K)₄ **3 d**, the band at 220 nm appears very broad compared to poly(L-lysine). This might be due to the influence of tyrosine on the one hand, but on the other hand it could also involve secondary solvent effects. Kubyskin et al. showed in their work that especially the positive band of the PPII conformation can be very strongly influenced by the environment.^[24]

To get a better insight into the structural properties of TfeGly₁₀GY(K)₃ **2 d**, we explored the influence of multiple solvents with varying polarity on its structure (Supporting Information, Figure S41). Octan-1-ol simulates an strong hydrophobic environment. Consistent with the results of TfeGly₁₃GY(K)₄ **3 d**, TfeGly₁₀GY(K)₃ **2 d** adopts a PPII conformation as well. Moreover, it seems that the TfeGly₁₀GY(K)₃ **2 d** peptide adopts a PPII conformation in membrane-like environment while in a more polar environment at least one further conformation may be present. In hexafluoroisopropanol (HFIP), representing a fluorous-polar solvent, the CD spectrum showed a minimum below 200 nm, but a positive band at a wavelength above 210 nm was absent. This finding could be indicative of a higher random coil fraction^[25]. Consequently, experimental data confirms the PPII structure in the case of TfeGly oligomers more

likely to be supported by a hydrophobic environment. Subsequently, the structure of TfeGly₁₀GY(K)₃ **2 d** in phosphate buffer was examined more closely (Supporting Information, Figure S42). At a 25 mM concentration, the spectrum is reminiscent of a random coil structure. The spectrum at 50 mM showed a minimum at 214 nm, as mentioned earlier. The inset in Supporting Information shows divergence in the CD spectra of TfeGly₁₀GY(K)₃ **2 d** at 25 μ M and at 50 μ M in phosphate buffer. The corresponding spectrum resembles a β -strand type CD spectra.^[20a,26] In general, PPII helix is mostly in a multi-conformational equilibrium with β -strand, β -turn and unordered structures, which can be explained by the great similarities in the corresponding backbone dihedral angles.^[18d] Therefore, it seems only consistent and completes the picture that TfeGly₁₀GY(K)₃ **2 d** forms multiple conformations, like β -strand, besides the PPII helix. Furthermore, the comparison between TfeGly₁₀GY(K)₃ **2 d** and TfeGly₁₃GY(K)₄ **3 d** shows that the longer peptide seems to be better accommodated in a more hydrophobic environment. If TfeGly₁₀GY(K)₃ **2 d** shows a PPII helix in a strictly hydrophobic medium, as a consequence, it intercalates less strongly with the micelles in the presence of SDS, resulting in a CD spectrum with a higher β -strand fraction.

Structural studies in presence of POPC/POPG

To further deepen our insights into the structural properties of fluoropeptides, especially focusing on their interactions with biomembrane models, CD measurements were carried out in the presence of unilamellar vesicles. The corresponding liposomes were composed of 1-palmitoyl-2-oleoyl-glycero-3-phosphocholine (POPC) and 1-palmitoyl-2-oleoyl-sn-glycero-3-(phosphor-rac-(1-glycerol)) (POPG) lipids (1:1 ratio). Negatively charged POPG was used to facilitate the peptide-liposome interactions. Figure 4a summarizes the CD spectra of all eleven peptides in the presence of POPC/POPG. It must be noted that the measurements were made at a much smaller liposome/peptide ratio of 150:1 compared to the studies with SDS (SDS/peptide = 1600:1, for 40 mM SDS concentration). CD measurements at higher liposome concentrations and at wavelengths below 200 nm were not possible due to the absorbance properties of the liposome suspension. Overall, it can be stated that almost identical trends, compared to the SDS studies, were observed. Again, the most pronounced α -helical structures were formed by Abu₁₃GY(K)₄ **3 a**, Abu₁₅GY(K)₄ **4 a** and DfeGly₁₅GY(K)₄ **4 c**. For other difluorinated peptides and especially for the monofluorinated analogs, CD spectra with higher β -strand content were detected. In synergy to prior data, the length of the peptides and their hydrophobicity are the two decisive factors for the formation of a helical structure in a hydrophobic environment, with monofluorination reducing the stability of that conformation. Both TfeGly peptides adopt a different structure under these conditions. A maxima at wavelengths above 210 nm could be observed indicating the formation of PPII structures. Interestingly, in the case of liposomes, TfeGly₁₀GY(K)₃ **2 d** adopts this conformation as well. In a time-dependent manner, comparable to the SDS CD

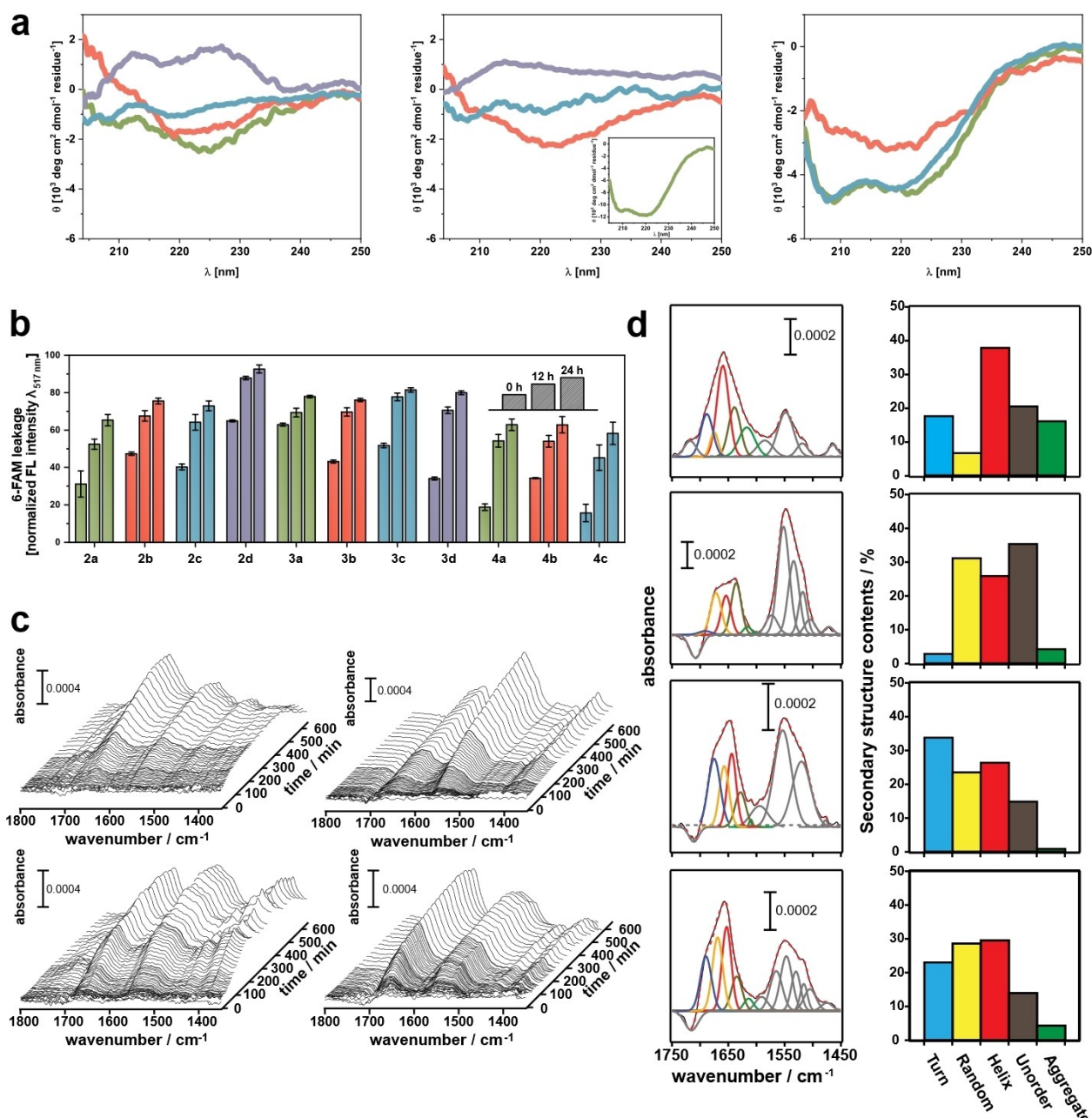


Figure 4. a. Circular dichroism spectra of fluorinated peptides (25 μM) in the presence of POPC:POPG = 1 : 1 (liposome:peptide = 150 : 1) in phosphate buffer (10 mM, pH = 7.4) [left: $X_{10}\text{GY}(K)_3$ / center: $X_{13}\text{GY}(K)_4$ / right: $X_{15}\text{GY}(K)_4$]; b. Monitored leakage of the 6-FAM dye (ratio: 1 : 100 peptide:lipid); c. In-situ SEIRA spectra of the adsorption process of $X_{13}\text{GY}(K)_4$ **3 a–d** peptides on the POPG/POPC lipid bilayer; d. Peak fittings of the amide band of the fluorinated peptides adsorbed on the lipid (left) and contents of the secondary structure components (right) of $\text{Abu}_{13}\text{GY}(K)_4$ **3 a** (first row), $\text{MfeGly}_{13}\text{GY}(K)_4$ **3 b** (second row), $\text{DfeGly}_{13}\text{GY}(K)_4$ **3 c** (third row), and $\text{TfeGly}_{13}\text{GY}(K)_4$ (fourth row).

spectra, a minimum at 214 nm is formed and the maximum disappears (Supporting Information, Figure S44). This contradicts the hypothesis that a PPII conformation occurs almost exclusively in a hydrophobic environment as $\text{TfeGly}_{10}\text{GY}(K)_3$ **2 d** seems rather to exhibit several conformations (PPII, β -strand) in the presence of micelles as well as in the presence of liposomes. For $\text{TfeGly}_{13}\text{GY}(K)_4$ **3 d** peptide, no time-dependent structural changes were observed.

The disruptive interactions of fluoropeptides with liposome vesicles was studied by a fluorescence-based leakage assay using 6-carboxyfluorescein (6-FAM) as a fluorescence dye. For all eleven peptides an increase in fluorescence could be observed due to an intrusion of peptides into the membrane bilayer (Figure 4b). What was already indicated by CD data was also demonstrated by the leakage assay: the penetration of fluoropeptides into the liposomes is a slow process, with fluorescence saturation occurring after approximately 10 h. To

study the structure formation in the course of peptide-membrane interactions, we subsequently carried out infrared spectroscopy experiments.

Surface enhance infrared absorption spectroscopy (SEIRAS)

Since conventional FTIR spectroscopy is not sufficiently sensitive to detect the peptide oligomers at the given concentration, we employed Surface-Enhanced Absorption Spectroscopy (SEIRAS).^[27] For this purpose, large unilamellar vesicles (LUV) of POPC/POPG (1:1) were casted over the SEIRA active gold film surface to form a solid-supported lipid bilayer. The lipid-modified SEIRA chip was submitted to a PBS buffer and the peptides were subsequently added. The sample SEIRA spectra were simultaneously measured to observe adsorption/folding process of the polypeptides on the solid-supported lipid bilayer.^[27] For these studies, the X13 K peptides were selected, since here, both all degrees of fluorination were present and the structural diversity within the series was the most pronounced.

Figure 4c shows SEIRA spectra of each peptide. Three-dimensional presentation of these spectra provides overviews on the adsorption process of the peptides. As the peptides were added, two marker bands appeared at around ~ 1650 and ~ 1550 cm^{-1} and increased with time. These bands are assigned to amide I and II vibrational modes of the peptide backbone. Increase of these bands indicates a greater partitioning of peptides on the supported lipid bilayer with time. What was already indicated by CD measurements and fluorescence leakage assay was confirmed by SEIRA measurements: the increasing rate of the amide bands for each peptide is relatively slow, with saturation intensity being reached after 200 to 600 minutes depending on the degree of fluorination. SEIRA spectra at the saturation coverage of each adsorbed peptide illustrated that the spectral features of each peptide are very different to each other (Figure 4d). In the non-fluorinated peptide, Abu₁₃GY(K)₄ **3a**, amide I and II appear as broad and symmetrical features peaking at 1659 and 1549 cm^{-1} , respectively. These peak positions are typical of α -helical structure of long-chain peptides or proteins, suggesting that the lipid adsorbed Abu₁₃GY(K)₄ **3a** is present as an α -helix. On the other hand, amide bands of the fluorinated peptides **3b-d** show characteristic asymmetrical features different from those of Abu₁₃GY(K)₄ **3a**. This is consistent with the obtained CD data (see above), which showed different conformational compositions depending on the degree of fluorination.

Peak fitting of the amide I band was carried out and the integrated peak areas were used to quantify the individual secondary structure components. Details of the peak fittings are described in the Supporting Information, section 3.6. We limited the analysis to five representative structures, namely 'Turn/Bend', 'Random', 'Helix', 'Unordered', and ' β -aggregate/sheet'. Since distinction between β -sheet and β -aggregate is difficult due to overlap of absorption region, the contribution from β -sheet structure is included in ' β -aggregate' structures. The component bands appear in the range of 1675–1695 cm^{-1}

(Turn), 1660–1675 cm^{-1} (Random), 1660–1645 cm^{-1} (helix), 1630–1645 cm^{-1} (Unordered), 1610–1630 cm^{-1} (Aggregate), respectively (Figure 4d). For non-fluorinated Abu₁₃GY(K)₄ **3a** peptide, the predominant component is a helical structure, which occupies about 40% of the conformational space. This is in agreement with our CD measurements, which showed that Abu oligomers have the highest tendency of all investigated peptides to form α -helical structures. In the case of both MfeGly₁₃GY(K)₄ **3b** and DfeGly₁₃GY(K)₄ **3c**, the helical fraction decreases significantly (26% for MfeGly₁₃GY(K)₄ **3b** and DfeGly₁₃GY(K)₄ **3c**). Something similar was also shown by the CD spectra, which indicated a more complex conformational composition with a lower α -helical content in a hydrophobic environment. If the TfeGly₁₃GY(K)₄ **3d** is compared with DfeGly₁₃GY(K)₄ **3c**, it can be observed that the proportion of bend/turn structures decreases (from 34 to 23%) and slightly increases in the case of the helical structure (26 to 30%). As discussed in detail in the previous sections, no alpha helix was observed during CD experiments with trifluorinated peptides. Unfortunately, the discrimination of different helical structures by IR spectroscopy is difficult. Therefore, we interpret the observed higher content of helical structure, compared to the monofluorinated and difluorinated peptides, as presence of an extended helical conformation.

Truncated fluoro-peptides: folding, membrane partition and proteolysis

As discussed before, PFCs hardly degrade under environmental conditions and are often characterized as persistent. Therefore, we raised the question about the proteolytic stability of the fluoro-peptides. Preliminary studies showed that fluoro-peptides with solely fluorinated residues about $n \geq 6$ are insoluble in aqueous conditions. To accomplish efficient proteolysis studies, a sufficient solubility of starting material is required. The GYK_{3/4} tag in above-discussed library would immediately be degraded by the protease and, thus, cannot serve for elucidation of the fluoro-peptides' degradability. We, therefore, established a small new library of truncated fluoro-peptides (X₄[4]Abz; with X = Abu (Abu₄[4]Abz) **5a**, MfeGly (MfeGly₄[4]Abz) **5b**, DfeGly (DfeGly₄[4]Abz) **5c** & TfeGly (TfeGly₄[4]Abz) **5d**) which are soluble in given conditions of the peptide digestion assay. On the C-terminus, *para*-aminobenzoic acid [4]Abz was attached for determination of peptide stock concentrations.^[28] Acetylation of the N-terminus was omitted to provide a somewhat net charge on this hydrophobic scaffold (Figure 5).

At first, we aimed to explore whether previously described observations on fluorine-directed peptide folding in lipid environments can be also complied to truncated derivatives. CD experiments were done in physiological conditions at 100 μM peptide concentration and varying amounts of SDS (10 mM, 20 mM, 40 mM) as discussed before (Figure 6a). We observed for the labeled tetrapeptides Abu₄[4]Abz **5a** and DfeGly₄[4]Abz **5c** a global minimum at 198–200 nm and a shallow minimum at 218 nm. This CD pattern can be interpreted as a mixture of disordered peptide ($\lambda_{\text{min}} = 198$ nm) and

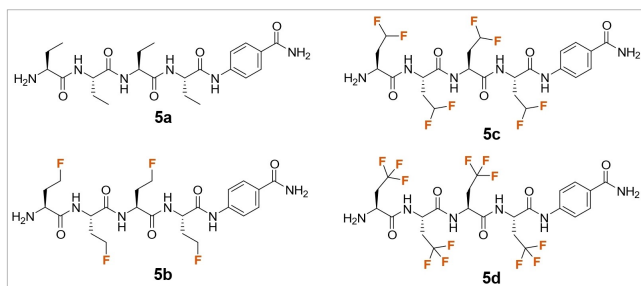


Figure 5. Chemical structures of labeled fluoropeptides ($X_4[4]Abz$ series).

minor amounts of β -strand-like conformations ($\lambda_{\min} = 218$ nm). This evaluation is in accordance with prior work by Schweitzer-Stenner and co-workers.^[29] The latter minimum was not observed for the MfeGly-derived tetrapeptide, indicating a major presence of random coils. The general absence of β -sheet to α -helix transitions as described for the $X_{10}GY(K)_3$, $X_{13}GY(K)_4$ and $X_{15}GY(K)_4$ series can be explained by the short sequence length of the $[X]_4[4]Abz$ series and, consequently, a lack of the typical backbone $i \rightarrow i-4$ hydrogen bonding pattern as indispensable criterion for α -helical structures.

For TfeGly₄[4]Abz **5d**, however, we determined the typical course of adsorption for β -strands due to the negative band between 218–220 nm and positive band between 195–200 nm. Upon addition of SDS (10 mM–20 mM) the β -strand content increases significantly as observed in the wavelength shift for the negative band to around 215 nm and increased ellipticity at 195 nm. These results are in good agreement with prior reports by Barnham and co-workers about SDS-generated stabilization of A β -derived β -sheet conformers.^[30] It is most noteworthy that higher amounts of SDS (40 mM) lead to a further shift of the global minimum to about 210 nm, indicating a coexistence of different folding patterns. As discussed before for TfeGly₁₀GY(K)₃ **3d** and TfeGly₁₃GY(K)₄ **4d**, this data set would corroborate our considerations about a multiconformational equilibrium in membrane-like environments. Consequently, the observed blue-shift in the CD spectra can be assigned to a growing content of extended PPII-like conformations caused by side chain – side chain interactions. As reported by Rausch et al., a rising degree of structured peptides through SDS addition can correspond to β -strand driven intercalation into lipid bilayers.^[31] In a similar manner, 6-FAM leaking assays with POPC:POPG liposomes revealed all $X_4[4]Abz$ peptides to disrupt artificial lipid bilayers but with superior potency for TfeGly₄[4]Abz **5d** after 24 h (about 67%) in comparison to **5a–c** (about 35%) (Figure 6b).

Finally, we studied whether these fluoropeptides can be degraded through digestive enzymes. The incorporation of non-natural amino acids in high proportion is a well-known strategy to alter or even eliminate peptide proteolysis.^[32] In the context of side chain fluorinated amino acids, a wide range of studies exist with diverse outcomes of such modifications. Moreover, the enzymatic degradation of peptides consisting mainly of fluorinated amino acids has not been studied yet.^[33]

In this work, we probed the stability of these fluoropeptides towards peptide digestion by the serine proteases elastase and proteinase k. Both endoproteases possess a particular specificity to cleave the amide bonds of aliphatic amino acids at the P1 position.^[34] All $X_4[4]Abz$ peptides were dissolved in physiological buffer supplemented with 25% DMSO and, after addition of enzyme, the amount of degradation was determined via HPLC analysis. Quite unexpectedly, we observed peptide degradation for all fluoropeptides upon incubation with both enzymes (see Figure 6c (left) and Supporting Information, Figure S49). After 6 h incubation after addition of elastase (Figure 6c (right), black line), we found major proportions of all labeled tetrapeptides to be digested. Remaining amounts of Abu₄[4]Abz **5a** ($4.3 \pm 0.1\%$), MfeGly₄[4]Abz **5b** ($6.6 \pm 1.1\%$), DfeGly₄[4]Abz **5c** ($10.9 \pm 3.8\%$) and TfeGly₄[4]Abz ($19.3 \pm 4.0\%$) **5d** appoint a synergy between the growing degree of fluorination and enhanced proteolytic stability with up to 4.4-fold improved rates upon CH₃ (Abu) to CF₃ (TfeGly) substitution. Nevertheless, these astonishing results display an overall accommodation of the fluoropeptides within the enzymes active site. Real-time monitoring of peptide digestion by proteinase k (Figure 6c (right), red line) validated the enzymatic degradability properties of all fluoropeptides. After 3 h of incubation, TfeGly₄[4]Abz **5d** was mainly degraded by the enzyme but remained in about 3.7-fold increased amounts ($9.3 \pm 5.0\%$) than the Abu-derived tetrapeptide ($2.5 \pm 0.1\%$). Further comparison with leftovers detected for MfeGly₄[4]Abz **5b** ($4.4 \pm 2.2\%$) and DfeGly₄[4]Abz **5c** ($2.6 \pm 0.3\%$) after 3 h highlights the scope of substrate acceptance of both enzymes regardless to the fluorinated side chain pattern. Furthermore, we were engaged to determine predominant cleaving sites via HPLC/MS-assisted analysis (experimental data and discussion are provided in the Supporting Information, Figure S51–S54). It is most noteworthy that the [4]Abz-labeled amino acids Abu, MfeGly, DfeGly or TfeGly were found as remaining digestion fragments for both serine proteases. This confirms a main P1-P1' scissile bond in which the fluorinated amino acids act as both P1 and P1' residues, thereby proving susceptibility towards enzymatic degradation in terms of elastase or proteinase K.^[35]

Prior studies from our laboratory^[33a], but also the research groups of Jakubke^[36], Kumar^[37] and Marsh^[38] came to somewhat contradictory outcomes about the proteolytic stability of peptides when incorporating one or a few fluorinated amino acids. In this study, we investigated the enzymatic degradability of fluoropeptides containing exclusively fluorinated aliphatic amino acids. Experimental evidence obtained in this work let us conclude that these fluoropeptides can be rather considered as biodegradable fluoropolymers than synthetic & persistent PFC-mimicries.

Conclusion

In this work, we present the first series of artificial fluoropeptides ever reported. Depending on the sequence-length and degree of side chain fluorination, we found notable differences in peptide secondary structure formation under membrane-

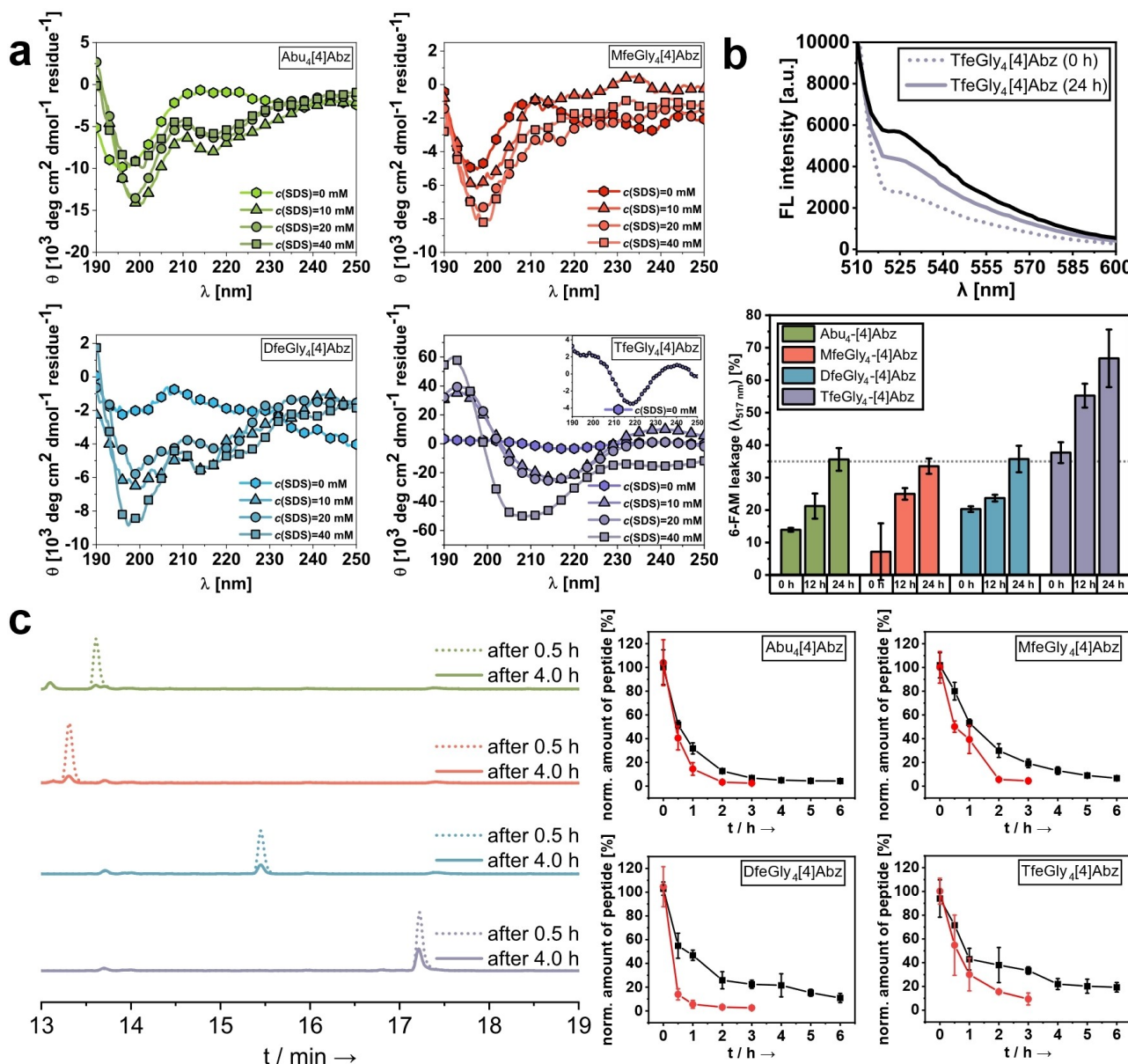


Figure 6. a. CD spectra of truncated fluoropeptides (100 μM) in aqueous solution (phosphate buffer, 10 mM, pH = 7.4) and in the presence of SDS (10, 20, 40 mM). b. Monitored increase in FL intensity resulting from dye-release in case of TfeGly₄[4]Abz 5d (100 μM) during incubation [at the start of experiment (dashed line) and after 24 h incubation (solid line)] in POPC:POPG liposome solution (liposome:peptide = 50:1). The FL intensity derived from the positive control [5% (v/v) Triton X-100 in buffer] is illustrated as black line (top). Also, calculated percentages of 6-FAM dye leakage (X_4 [4]Abz series, liposome:peptide = 50:1) reveal superior membrane-disrupting properties upon CH₃ to CF₃ substitution (5d). Lower degrees of dye leaking resembled by average FL values of about 35% were found similarly for 5a, 5b and 5c and are marked as grey-colored dotted line (bottom). c. Real-time monitoring of peptide proteolysis for 5a–5d by the serine protease elastase depicted after 0.5 h (dashed line) and 4 h (solid line) incubation (colors are the same as presented in a. and b.) via HPLC analysis (Supporting Information, Table S20) (left). Normalized amounts of remaining tetrapeptides (230 μM) determined during enzymatic degradation by elastase (0.91 μM , black line) and proteinase k (0.0091 μM , red line) (right).

mimicking environments. A wide range of experimental techniques ranging from CD spectroscopy to SEIRAS, and FL-based leaking assays served to elucidate the intercalation of these fluoropeptides into lipid bilayers and resulting folding patterns. In general, a β -sheet to α -helix transition was observed in most cases series. For the TfeGly-containing fluoropeptides, however, experimental data indicates a unique fluorine-driven formation of PPII structures. Monitoring the partition into POPC:POPG lipid bilayers exposed alterations in

structural compositions, like a decrease in α -helical content in response to the total degree of fluorination. Moreover, proteolysis studies of truncated fluoropeptides exclusively built up from fluorinated amino acids revealed an overall degradability. This study lays the foundation for the development of de novo designed foldamers with fluorine-directed folding and membrane-disrupting properties by maintaining biodegradability. We consider this class of peptide-based fluorooligomers to serve as initial templates in the future design of fluorinated

biomaterials as, for example, fluorous tags for biomolecule or drug delivery. Ongoing work focusses on the biocompatibility of these fluoropeptides and will provide further insights into potential biomedical applications.

Experimental Section

General methods: HRMS were determined on an Agilent 6220 ESI-TOF MS instrument (Agilent Technologies, Santa Clara, CA, USA). For analysis, the MassHunter Workstation Software Version B.02.00 (Agilent Technologies, Santa Clara, CA, USA) was used. All chemicals were purchased from commercial sources (Merck, Sigma-Aldrich, VWR, Fluorochem) and used without further purification. The fluorinated amino acids MfeGly, DfeGly and TfeGly were synthesised according to literature.^[12b]

Synthesis and purification of peptides: All fluoropeptides ($X_{10}GY(K)_3$, $X_{13}GY(K)_4$ and $X_{15}GY(K)_4$ series) were synthesized with a microwave-equipped Liberty Blue™ peptide synthesizer (CEM, Matthews, NC, USA). A Rink Amide ProTide™ resin (CEM, Matthews, NC, USA) was utilized and the synthesis was performed either in 0.05 mmol or 0.1 mmol scale using Oxyma/DIC as activating reagents. Detailed coupling protocols are listed in the Supporting Information. Acetylation was done manually in three batches using acetic anhydride (10% v/v) and DIPEA (10% v/v) in DMF (6 mL). The labeled tetrapeptides $X_4[4]Abz$ were synthesized through standard manual SPPS.

All peptides were cleaved from the resin by treatment with TFA/TIPS/H₂O (90/5/5) [1 mL cleavage cocktail per 50 mg resin] for three hours using sonication at room temperature. Then the resins were washed with TFA and DCM, and excess of solvents were removed by evaporation. Peptides were dried by lyophilization before purification with preparative reversed phase HPLC. Purification of synthesized peptides was performed on a Knauer low-pressure HPLC system (Knauer GmbH, Berlin, Germany) sold by VWR (Darmstadt, Germany), comprising a LaPrep Sigma preparative pump (LP1200), a ternary low-pressure gradient, a dynamic mixing chamber, a 6-port-3-channel injection valve with an automated preparative 10 mL sample loop, a LaPrep Sigma standard 1-channel-UV-detector (LP3101), a flow cell with 0.5 mm thickness and a 16-port LaPrep Sigma fractionation valve (LP2016). A Kinetex RPC18 endcapped (5 μM, 100 Å, 250 × 21.2 mm, Phenomenex®, USA) HPLC-column was used. A Security Guard™ PREP Cartridge Holder Kit (21.20 mm, ID, Phenomenex®, USA) served as pre-column. As eluents water and ACN, both containing 0.1% (v/v) TFA were applied. HPLC runs were performed with a flow rate of 15.0 mL/min, UV-detection occurred at 220 nm for respective peptides. Data analysis occurred with an EZChrom Elite-Software (Version 3.3.2 SP2, Agilent). After separation, the purity of the collected fractions was determined by analytical HPLC. Analytical HPLC was carried out on a Chromaster 600 bar DAD-System with CSM software or a Hitachi Primaide™ UV-HPLC system (both from VWR/Hitachi, Darmstadt, Germany). A Kinetex® RP-C18 (5 μM, 100 Å, 250 × 4.6 mm, Phenomenex®, USA) column and a SecurityGuard™ Cartridge Kit equipped with a C18 cartridge (4 × 3.0 mm, Phenomenex®, USA) as pre-column was used. Otherwise, a Luna® RP-C8 (5 μM, 100 Å, 150 × 3 mm, Phenomenex®, USA) column was used. As eluents water and ACN, both containing 0.1% (v/v) TFA were applied. A flow rate of 1 mL/min was used and UV-detection occurred at 220 nm or 280 nm for respective peptides. Data analysis was done with EZ Chrom ELITE software (version 3.3.2, Agilent). The resulting pure peptides (> 95%) were obtained after lyophilization of the collected fractions. All essential data for the quantification of

purified peptides (HPLC chromatograms, HRMS spectra) can be found in the Supporting Information.

CD spectroscopy: Circular dichroism experiments were performed using a Jasco J-810 spectropolarimeter fitted with a recirculating chiller. Data were recorded using 0.1 mm or 0.2 mm Quartz Suprasil® cuvettes (Hellma) equipped with a stopper. Spectra were recorded at 37 °C from 190 to 250 nm at 0.2 nm intervals, 1 nm bandwidth, 4 s response time and a scan speed of 100 nm min⁻¹. Baselines were recorded and were subtracted from the data. Each reported CD value represents the average of minimum three measurements.

Lyophilization: To lyophilize the synthesized peptides a laboratory freeze dryer ALPHA 1–2 LD (Christ Gefriertrocknungsanlagen GmbH, Osterode am Harz, Germany) was used.

Preparation of large unilamellar vesicles (LUV): POPC and POPG were each dissolved in chloroform (1 mL). From these stock solutions, POPC and POPG (1:1) were suspended in phosphate buffer (10 mM, pH=7.4) at a concentration of 3.75 mM. The suspension was submitted to ten freeze and thaw cycles. Subsequently, large unilamellar vesicles (LUVs) were prepared by extrusion across a polycarbonate Nuclepore™ track-etched membrane (0.1 μm pore size, Whatman International Ltd., Kent, United Kingdom) using an Avanti extruder (Avanti Polar Lipids, Birmingham, AL, USA).

6-Carboxyfluorescein [6-FAM] leakage assay: At first, stocks of 1-palmitoyl-2-oleoyl-sn-glycero-3-phosphocholine (POPC) and 1-palmitoyl-2-oleoyl-sn-glycero-3-[phospho-rac-(1-glycerol)] (POPG) were prepared by dissolving the compounds in CHCl₃ in a concentration of 10 mg/mL. Aliquots were taken from both stocks and CHCl₃ was evaporated. The amount of aliquots corresponded to a liposome solution of POPC/POPG (1:1, each 5 mM [1 mL]). The lipid film was dried *in vacuo* overnight and then dissolved in 50 mM 6-carboxyfluorescein (6-FAM) in 10 mM phosphate buffer, pH 7.4. The pH of this solution was adjusted to pH 7.4 with a 1 N NaOH solution before addition to the lipid film. The suspension was submitted to ten freeze–thaw cycles and then rest for 1 h at rt for equilibration. Untrapped dye was removed by gel filtration on PD-10 desalting columns containing Sephadex G-25. To prepare peptide/lipids sample, aliquots were taken from respective peptide stocks in HFIP and dried under a gentle stream of nitrogen. Then, dried peptide films were dissolved in 25 μL buffer and mixed for 5–10 seconds to obtain a homogeneous mixture. Subsequently, 25 μL of liposome solution were added and the solution was gently mixed for 5 seconds. The final concentrations were: 50 μM ($X_{10}GY(K)_3$ - $X_{13}GY(K)_4$ - $X_{15}GY(K)_4$ series) or 100 μM peptide ($X_4[4]Abz$) + 5 mM POPC:POPG (1:1, each 2.5 mM). The leakage of 6-FAM was detected by measuring the fluorescence intensity at 37 °C and an excitation wavelength of 493 nm; fluorescence emission was recorded at 517 nm. 100% dye release was achieved from the liposomes with the addition of 5% (v/v) Triton X-100 in buffer. A negative control was constituted by measuring FL emission of the liposome solution only containing buffer. All samples were transferred on BRAND® microplates (size: 96 wells, color: black; Sigma-Aldrich), sealed to prevent evaporation and placed in an Infinite M Nano+ plate reader (Tecan Deutschland GmbH, Crailsheim, Germany). Fluorescence intensity was followed over 24 h after sample preparation and a fluorescence scan was measured every 30 min.

Estimation of log P values: The estimation of log P values was carried out according a HPLC-based protocol adapted from the O'Hagan working group. A library of short peptides with known log P values was synthesized and analyzed by HPLC. The corresponding retention times were measured using a reversed-phase C18 column. Subsequently, the correlation between known log P values and

retention times was fitted. The obtained linear function was used to estimate the log P values of fluoropeptides from the corresponding measured retention times. A detailed description of the protocol can be found in the Supporting Information.

Peptide digestion assay: For all enzymes, following buffer mixture was used: 50 mM bis-tris propane + 20 mM CaCl₂, pH 8 [75%] + DMSO [25%]. All samples were dissolved in buffer (400 μL) and then were gently mixed to obtain a homogeneous solution. Afterwards, 40 μL of an enzyme-solution in buffer (elastase: 10 μM / proteinase k: 0.1 μM) were added and the samples were again gently mixed for 5 seconds. The concentration of each enzyme was adjusted before to obtain well-detectable digestion kinetics. The final concentrations were: 230 μM X₄[4]Abz peptide + 0.91 μM elastase or 0.0091 μM proteinase k. All samples were incubated at 30 °C over a period of 3–6 h. Aliquots of 15 μL were taken at fixed time points and quenched with 90 μL of a solution of 30% AcOH in water containing 130 μM Ac-[4]Abz-Gly-OH as reference. Afterwards, peptide degradation was monitored by HPLC analysis. In all cases, the peaks corresponding to each peptide sample (full-length peptides) and the reference sample were integrated and used to determine the amount of substrate still present in solution. The content of starting material after 5 min was termed as absolute amount for simplicity. For the detection of peptide fragments derived from proteolysis, all samples were prepared accordingly and incubated at 30 °C over a period of 24 h. Afterwards, aliquots of the reaction mixture were monitored by HPLC analysis. To identify the cleaving site of each peptide, each HPLC signal from a digestion fragment cleaved from the full-length peptide was isolated and analyzed by ESI-ToF mass analysis on an Agilent 6220 ESI-ToF-MS spectrometer (Agilent Technologies, Santa Clara, CA, USA).

Surface enhanced infrared absorption spectroscopy (SEIRAS): The required amount of a 1:1 volume ratio of 1-palmitoyl-2-oleoyl-glycero-3-phosphocholine (POPC) and 1-palmitoyl-2-oleoyl-sn-glycero-3-phospho-1'-rac-glycerol (POPG) (Avanti Polar Lipids, Alabama, USA) dissolved in chloroform was placed in a septum capped glass tube and dried under a gentle flow of argon. The dried lipid was resuspended in 10 mM phosphate buffer (pH 6.0). The suspension was freeze-thawed at least 5 times, followed by extrusion with a 100 nm filter to form Large Unilamellar Vesicles (LUV) of POPC/POPG. Then, ~1.2 mg/ml of lipid LUV was casted over the surface of Au film substrate to form a solid-supported lipid layer by spontaneous vesicle fusion. After incubation in the lipid containing solution for overnight (> 12 h), the Au film surface was thoroughly rinsed with Milli-Q water and the buffer solution to remove excess amount of the lipid accumulated over the solid supported lipid bilayer. SEIRAS experiments were conducted as described before.^[39] Briefly, Attenuated Total Reflection (ATR) optical configuration was employed with a micro-grooved silicon chip crystal as internal reflection element (IRE, from IRUBIS GmbH, München, Germany). A SEIRA active gold film was formed on reflection surface of IRE by chemical deposition. A background spectrum was taken on the gold surface with presence of the solid supported POPC/POPG bilayer in 200 μL of 10 mM phosphate buffer solution with pH = 7.4 prior to the sample measurement. Then, 200 μL of the peptide samples dissolved in same buffer was added to the solution and sample IR spectra were subsequently measured to monitor the adsorption process on the lipid surface. Final concentration of each peptide during the adsorption measurement was kept ~25 μg/ml. Baseline of the obtained spectra were corrected at the position of 1800 cm⁻¹, where no absorption from the band relate to the samples occur, to become zero.

Author contributions

T.H. and S.C. developed the overall project, provided fluorinated amino acids, synthesized & purified all fluoropeptides and wrote the manuscript. B.K. provided guidance on data analysis and interpretation. T.H. performed CD studies, structural studies with POPC/POPG liposomes and determination of hydrophobicity. S.C. performed CD studies, leaking & peptide digestion assays. K.A. performed SEIRAS studies and wrote the manuscript. J.E. assisted T.H. in synthesis and analysis. G.H.D. assisted S.C. in synthesis and digestion assays. J.H. provided expertise and feedback.

Acknowledgements

The authors gratefully acknowledge financial support by the Deutsche Forschungsgemeinschaft (DFG) through the collaborative research center CRC-1349 "Fluorine-Specific Interactions" project no. 387284271. T.H. thanks the Studienstiftung des deutschen Volkes for financial support. We thank Dr. Stephan Block, Dr. Katharina G. Hugentobler and Dr. Stephanie Wedepohl for scientific discussions and expertise. We thank Balu and Honey for continuous encouragement and support. We would like to acknowledge the assistance of the Core Facility *BioSupraMol* supported by the DFG. Open Access funding enabled and organized by Projekt DEAL.

Conflicts of interest

There are no conflicts to declare.

Data Availability Statement

The data that support the findings of this study are available in the supplementary material of this article.

Keywords: fluorinated biomaterials · fluoropeptides · fluorour amino acids · foldamers · membrane disruption

- [1] a) I. Ojima, *J. Org. Chem.* **2013**, *78*, 6358–6383; b) J. M. Wolfe, C. M. Fadzen, R. L. Holden, M. Yao, G. J. Hanson, B. L. Pentelute, *Angew. Chem. Int. Ed.* **2018**, *57*, 4756–4759; c) E. N. G. Marsh, B. C. Buer, A. Ramamoorthy, *Mol. Biosyst.* **2009**, *5*, 1143–1147.
- [2] a) M. P. Krafft, *Adv. Drug Delivery Rev.* **2001**, *47*, 209–228; b) H.-J. Böhm, D. Banner, S. Bendels, M. Kansy, B. Kuhn, K. Müller, U. Obst-Sander, M. Stahl, *ChemBioChem* **2004**, *5*, 637–643.
- [3] a) J. Han, A. M. Remete, L. S. Dobson, L. Kiss, K. Izawa, H. Moriwaki, V. A. Soloshonok, D. O'Hagan, *J. Fluorine Chem.* **2020**, *239*, 109639; b) J. Lv, Y. Cheng, *Chem. Soc. Rev.* **2021**, *50*, 5435–5467.
- [4] T. Song, Y. Gao, M. Song, J. Qian, H. Zhang, J. Zhou, Y. Ding, *Med. Drug Discovery* **2022**, *14*, 100123.
- [5] a) Z. Zhang, W. Shen, J. Ling, Y. Yan, J. Hu, Y. Cheng, *Nat. Commun.* **2018**, *9*, 1377; b) G. Rong, C. Wang, L. Chen, Y. Yan, Y. Cheng, *Sci. Adv.* **2020**, *6*, eaaz1774.
- [6] a) T. Stahl, D. Mattern, H. Brunn, *Environ. Sci. Europe* **2011**, *23*, 38; b) V. Ochoa-Herrera, J. A. Field, A. Luna-Velasco, R. Sierra-Alvarez, *Environ. Sci. Process. Impacts* **2016**, *18*, 1236–1246.

- [7] C. Jäckel, M. Salwiczek, B. Koksich, *Angew. Chem. Int. Ed.* **2006**, *45*, 4198–4203.
- [8] A. A. Berger, J.-S. Völler, N. Budisa, B. Koksich, *Acc. Chem. Res.* **2017**, *50*, 2093–2103.
- [9] a) R. Godbout, S. Légaré, M. Auger, C. Carpentier, F. Otis, M. Auger, P. Lagüe, N. Voyer, *PLoS One* **2016**, *11*, e0166587–e0166587; b) M. Auger, T. Lefèvre, F. Otis, N. Voyer, M. Auger, *Pept. Sci.* **2019**, *111*, e24051.
- [10] a) B. Bilgiçer, K. Kumar, *Proc. Natl. Acad. Sci. USA* **2004**, *101*, 15324–15329; b) N. Naarmann, B. Bilgiçer, H. Meng, K. Kumar, C. Steinem, *Angew. Chem. Int. Ed.* **2006**, *45*, 2588–2591.
- [11] a) B. Meng, S. L. Grage, O. Babii, M. Takamiya, N. MacKinnon, T. Schober, I. Hutskalov, O. Nassar, S. Afonin, S. Koniev, I. V. Komarov, J. G. Korvink, U. Strähle, A. S. Ulrich, *Small* **2022**, e2107308; b) S. E. Kirberger, S. D. Maltseva, J. C. Manulik, S. A. Einstein, B. P. Weegman, M. Garwood, W. C. K. Pomerantz, *Angew. Chem. Int. Ed. Engl.* **2017**, *56*, 6440–6444; c) P. Wadhvani, P. Tremouilhac, E. Strandberg, S. Afonin, S. Grage, M. Ieronimo, M. Berditsch, A. S. Ulrich, in *Current Fluoroorganic Chemistry*, Vol. 949, American Chemical Society, **2007**, pp. 431–446.
- [12] a) J. Leppkes, T. Hohmann, B. Koksich, *J. Fluorine Chem.* **2020**, *232*, 109453; b) T. Hohmann, M. Dyrks, S. Chowdhary, M. Weber, D. Nguyen, J. Moschner, B. Koksich, *J. Org. Chem.* **2022**, *87*, 10592–10604.
- [13] S. Chowdhary, R. F. Schmidt, A. K. Sahoo, T. tom Dieck, T. Hohmann, B. Schade, K. Brademann-Jock, A. F. Thünemann, R. R. Netz, M. Gradzielski, B. Koksich, *Nanoscale* **2022**, *14*, 10176–10189.
- [14] K. Ataka, T. Kottke, J. Heberle, *Angew. Chem. Int. Ed.* **2010**, *49*, 5416–5424.
- [15] J. Leppkes, N. Dimos, B. Loll, T. Hohmann, M. Dyrks, A. Wieseke, B. G. Keller, B. Koksich, *RSC Chem. Biol.* **2022**, *3*, 773–782.
- [16] M. Paradis-Bas, J. Tulla-Puche, F. Albericio, *Chem. Soc. Rev.* **2016**, *45*, 631–654.
- [17] P. Wallimann, R. J. Kennedy, J. S. Miller, W. Shalongo, D. S. Kemp, *J. Am. Chem. Soc.* **2003**, *125*, 1203–1220.
- [18] a) A. A. Adzhubei, M. J. E. Sternberg, A. A. Makarov, *J. Mol. Biol.* **2013**, *425*, 2100–2132; b) Z. Shi, K. Chen, Z. Liu, N. R. Kallenbach, *Chem. Rev.* **2006**, *106*, 1877–1897; c) Z. Shi, R. W. Woody, N. R. Kallenbach, in *Advances in Protein Chemistry*, Vol. 62, Academic Press, **2002**, pp. 163–240; d) B. Bochicchio, A. M. Tamburro, *Chirality* **2002**, *14*, 782–792.
- [19] P. M. Cowan, S. McGavin, *Nature* **1955**, *176*, 501–503.
- [20] a) F. Eker, K. Griebenow, R. Schweitzer-Stenner, *J. Am. Chem. Soc.* **2003**, *125*, 8178–8185; b) Z. Liu, K. Chen, A. Ng, Z. Shi, R. W. Woody, N. R. Kallenbach, *J. Am. Chem. Soc.* **2004**, *126*, 15141–15150.
- [21] V. Kubyshkin, S. L. Grage, J. Bürck, A. S. Ulrich, N. Budisa, *J. Phys. Chem. Lett.* **2018**, *9*, 2170–2174.
- [22] A. L. Rucker, T. P. Creamer, *Protein Sci.* **2002**, *11*, 980–985.
- [23] A. I. Arunkumar, T. K. S. Kumar, C. Yu, *Biochim. Biophys. Acta (BBA) – Protein Structure and Molecular Enzymology* **1997**, *1338*, 69–76.
- [24] V. Kubyshkin, J. Bürck, O. Babii, N. Budisa, A. S. Ulrich, *Phys. Chem. Chem. Phys.* **2021**, *23*, 26931–26939.
- [25] J. L. S. Lopes, A. J. Miles, L. Whitmore, B. A. Wallace, *Protein Sci.* **2014**, *23*, 1765–1772.
- [26] Z. Shi, C. A. Olson, D. Rose George, L. Baldwin Robert, R. Kallenbach Neville, *Proc. Nat. Acad. Sci.* **2002**, *99*, 9190–9195.
- [27] K. Ataka, J. Drauschke, V. Stulberg, B. Koksich, J. Heberle, *Biochim. Biophys. Acta Biomembr.* **2022**, *1864*, 183873.
- [28] K. Pagel, K. Seeger, B. Seiwert, A. Villa, A. E. Mark, S. Berger, B. Koksich, *Org. Biomol. Chem.* **2005**, *3*, 1189–1194.
- [29] a) T. J. Measey, R. Schweitzer-Stenner, *J. Am. Chem. Soc.* **2006**, *128*, 13324–13325; b) R. Schweitzer-Stenner, T. Measey, A. Hagarman, F. Eker, K. Griebenow, *Biochemistry* **2006**, *45*, 2810–2819.
- [30] D. J. Tew, S. P. Bottomley, D. P. Smith, G. D. Ciccotosto, J. Babon, M. G. Hinds, C. L. Masters, R. Cappai, K. J. Barnham, *Biophys. J.* **2008**, *94*, 2752–2766.
- [31] J. M. Rausch, J. R. Marks, R. Rathinakumar, W. C. Wimley, *Biochemistry* **2007**, *46*, 12124–12139.
- [32] Z. Lai, X. Yuan, H. Chen, Y. Zhu, N. Dong, A. Shan, *Biotechnol. Adv.* **2022**, *59*, 107962.
- [33] a) S. Huhmann, B. Koksich, *Eur. J. Org. Chem.* **2018**, *2018*, 3667–3679; b) R. Smits, B. Koksich, *Curr. Top. Med. Chem.* **2006**, *6*, 1483–1498.
- [34] L. Hedstrom, *Chem. Rev.* **2002**, *102*, 4501–4524.
- [35] a) I. Schechter, A. Berger, *Biochem. Biophys. Res. Commun.* **1967**, *27*, 157–162; b) I. Schechter, A. Berger, *Biochem. Biophys. Res. Commun.* **1968**, *32*, 898–902.
- [36] B. Koksich, N. Sewald, H.-J. Hofmann, K. Burger, H.-D. Jakubke, *J. Peptide Sci.* **1997**, *3*, 157–167.
- [37] H. Meng, K. Kumar, *J. Am. Chem. Soc.* **2007**, *129*, 15615–15622.
- [38] L. M. Gottler, R. de la Salud Bea, C. E. Shelburne, A. Ramamoorthy, E. N. G. Marsh, *Biochemistry* **2008**, *47*, 9243–9250.
- [39] a) N. J. Harris, E. Reading, K. Ataka, L. Grzegorzewski, K. Charalambous, X. Liu, R. Schlesinger, J. Heberle, P. J. Booth, *Sci. Rep.* **2017**, *7*, 8021; b) A. Baumann, S. Kerruth, J. Fitter, G. Büldt, J. Heberle, R. Schlesinger, K. Ataka, *PLoS One* **2016**, *11*, e0151051; c) K. Ataka, S. T. Stripp, J. Heberle, *Biochim. Biophys. Acta Biomembr.* **2013**, *1828*, 2283–2293.

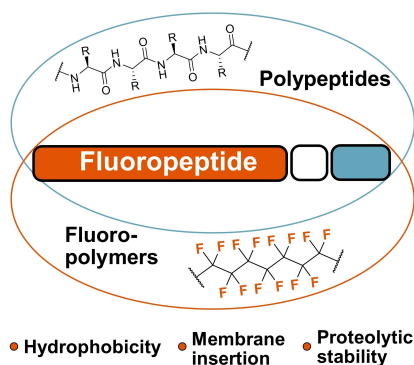
Manuscript received: December 9, 2022

Accepted manuscript online: February 1, 2023

Version of record online: ■■■, ■■■

RESEARCH ARTICLE

Peptide-based fluorooligomers bearing fluorinated amino acids as main components are reported. Fluorine-induced alterations on the intrinsic hydrophobicity, β -strand to α -helix transitions in membrane-mimicking environments and proteolytic digestion are discussed



T. Hohmann, S. Chowdhary, Dr. K. Ataka, J. Er, G. H. Dreyhsig, Prof. Dr. J. Heberle, Prof. Dr. B. Kocsch*

1 – 14

Introducing Aliphatic Fluoropeptides: Perspectives on Folding Properties, Membrane Partition and Proteolytic Stability



Chemistry–A European Journal

Supporting Information

Introducing Aliphatic Fluoropeptides: Perspectives on Folding Properties, Membrane Partition and Proteolytic Stability

Thomas Hohmann, Suvrat Chowdhary, Kenichi Ataka, Jasmin Er, Gesa Heather Dreyhsig,
Joachim Heberle, and Beate Kocsch*

Content

1. Synthesis of fluorinated amino acids.....	1
2. Solid-phase peptide synthesis (SPPS) – synthesis and purification	2
2.1 Microwave-assisted solid-phase peptide synthesis.....	2
2.2 Manual solid-phase peptide synthesis	4
2.3 Preparative & analytical HPLC	6
2.4 Peptide synthesis: HPLC chromatograms and HRMS spectra	8
2.4.1 Abu ₁₀ GY(K) ₃ 2a	9
2.4.2 MfeGly ₁₀ GY(K) ₃ 2b	10
2.4.3 DfeGly ₁₀ GY(K) ₃ 2c.....	11
2.4.4 TfeGly ₁₀ GY(K) ₃ 2d.....	12
2.4.5 Abu ₁₃ GY(K) ₄ 3a	13
2.4.6 MfeGly ₁₃ GY(K) ₄ 3b	14
2.4.7. DfeGly ₁₃ GY(K) ₄ 3c.....	15
2.4.8 TfeGly ₁₃ GY(K) ₄ 3d.....	16
2.4.9 Abu ₁₅ GY(K) ₄ 4a	17
2.4.10 MfeGly ₁₅ GY(K) ₄ 4b	18
2.4.11 DfeGly ₁₅ GY(K) ₄ 4c.....	19
2.4.12 Abu ₄ [4]Abz 5a	20
2.4.13 MfeGly ₄ [4]Abz 5b.....	21
2.4.14 DfeGly ₄ [4]Abz 5c.....	22
2.4.15 TfeGly ₄ [4]Abz 5d	23
3. Circular Dichroism and SEIRAS Infrared Spectroscopy – further data	24
3.1 Fundamentals: Hydrophobicity Studies.....	24
3.2 Parametric dual wavelength two-state test	25
3.1.1 Abu ₁₀ GY(K) ₃ 2a	25
3.1.2 Abu ₁₃ GY(K) ₄ 3a	25
3.1.3 Abu ₁₅ GY(K) ₄ 4a	26
3.1.4 DfeGly ₁₃ GY(K) ₄ 3c.....	26
3.1.5 DfeGly ₁₅ GY(K) ₄ 4c.....	27
3.1.6 TfeGly ₁₃ GY(K) ₄ 3d.....	27
3.3 TfeGly ₁₀ GY(K) ₃ 2d.....	28
3.4 Poly(L-lysine).....	28
3.5 Time-dependent measurements in the presence of POPC/POPG	30
3.6 Additional SEIRAS Spectra	31
4. Estimation of log P values by HPLC.....	34
5. 6-FAM leaking assay – further data	38
6. Peptide digestion assay	39
7. References.....	44

1. Synthesis of fluorinated amino acids

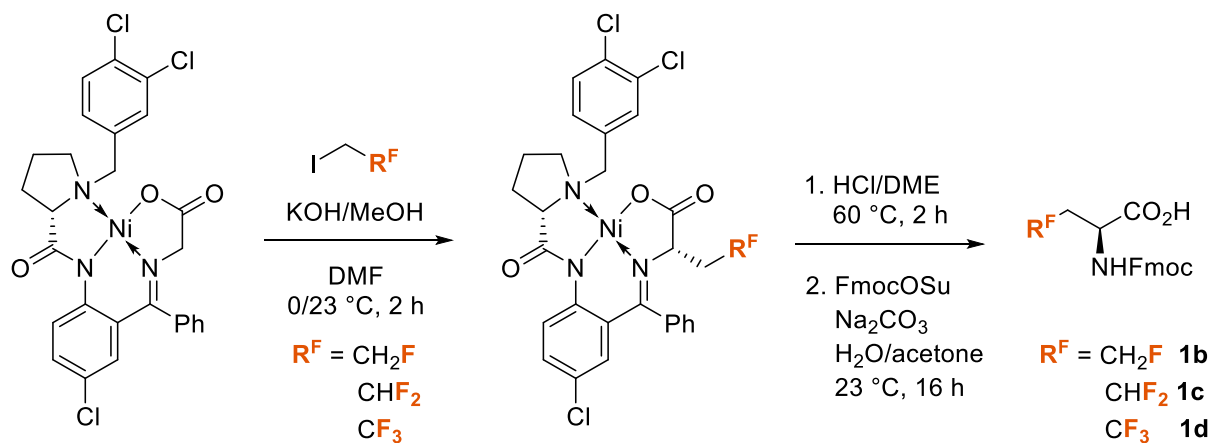


Figure S1: Synthesis of Fmoc-protected fluorinated amino acids (Fmoc-MfeGly **1b**, Fmoc-DfeGly **1c**, Fmoc-TfeGly **1d**) using a chiral Ni(II) complex.

The compounds **1b-d** were synthesized according to the procedures described by Hohmann *et al.*^[1] and Han *et al.*^[2]

2. Solid-phase peptide synthesis (SPPS) – synthesis and purification

2.1 Microwave-assisted solid-phase peptide synthesis

Peptide synthesis ($X_{10}GY(K)_3$, $X_{13}GY(K)_4$ and $X_{15}GY(K)_4$ series) was performed with a Liberty Blue automated microwave-assisted peptide synthesizer (CEM Corporation, Mathews, NC, USA) in an Fmoc-based SPPS approach. All peptides were synthesized as C-terminal amides on a Rink Amide ProTide Resin (LL) resin (0.19-0.20 mmol/g resin substitution) in a 0.05 mmol scale. General conditions for Fmoc deprotection & amino acid coupling are listed in **table S1**. Fmoc deprotection was carried out with 10 wt% piperazine in EtOH/NMP (1/9, v/v). All amino acids were coupled with Oxyma/DIC as activators. The proteogenic amino acids glycine, tyrosine and lysine were coupled through a “single-coupling” approach. The non-canonical amino acids Abu, MfeGly, DfeGly and TfeGly were introduced with a “special coupling” cycle established by Leppkes *et al.*^[3] It used elongated microwave heating time, reduced equivalents of the amino acid employed and additional washing steps between Fmoc deprotection and coupling step. For subsequent capping of N-terminal amino groups with acetic anhydride, a solution of Ac₂O (10 % (v/v) and DIPEA (10 % (v/v) in DMF (6 mL) was added in three batches manually and the reaction was then shaken for 3 * 10 min. For peptide cleavage, the dried resin was treated with 20 mL of TFA/water/TIPS (90/5/5, v/v) for 3 h at room temperature. Afterwards, the resin was washed thrice with TFA and CH₂Cl₂. Organic solvent was removed in vacuo and the peptides were precipitated in ice-cold Et₂O and centrifuged. The precipitate was washed thrice more with Et₂O and centrifuged. The supernatant was discarded, dissolved in water and lyophilized overnight before purification through preparative HPLC.

Table S1: Cycles for automated microwave-assisted SPPS with a 0.05 mmol scale on Liberty Blue peptide synthesizer. All reagents were dissolved in DMF, if not otherwise stated.

	<u>Process step</u>	<u>Reagents</u>			<u>Reaction conditions</u>		
		Name	Conc. [M]	Volume [mL]	Temp [°C]	Power [W]	Time [s]
Loading / Single coupling	[1] Deprotection	Piperazine	10 wt%	2 ^[1]	75	155	15
		HOBt	0.1		90	30	60
	[2] Washing (4*)	DMF	-	2	25	-	5
	[3] AA coupling	Fmoc-AA-OH	0.2	1.25	75	217	15
		DIC	1	0.5			
Oxyma		1	0.25	90	43	225	
DIPEA	0.1						
[4] Washing	DMF	-	2	25	-	5	
Special coupling	[1] Deprotection	Piperazine	10 wt%	2 ^[1]	75	155	15
		HOBt	0.1		90	30	60
	[2] Washing (4* - 9 cycles)	DMF	-	2	25	-	5
	[3] AA coupling	Fmoc-(F)AA- OH	0.05	1.25	75	217	15
		DIC	1	0.5			
Oxyma		1	0.25	90	43	585	
DIPEA	0.1						
[4] Washing (4*)	DMF	-	2	25	-	5	
^[1] EtOH/NMP, 1/9, v/v							

2.2 Manual solid-phase peptide synthesis

The peptides Abu₄[4]Abz **5a**, MfeGly₄[4]Abz **5b**, DfeGly₄[4]Abz **5c** and TfeGly₄[4]Abz **5d** were synthesized using standard Fmoc-chemistry at room temperature in a 0.1 mmol scale. A NovaSyn®TGR resin (0.21 mmol / resin substitution) was chosen to obtain C-terminal peptide amides. Fmoc deprotection was carried out with a 20% piperidin in DMF. All amino acids were coupled with HATU/DIPEA as activators. Fmoc-[4]Abz-OH was loaded on the resin with 5 equivalents and double coupling. The non-canonical amino acids Abu, MfeGly, DfeGly and TfeGly were introduced through single coupling with only 1.5 equivalents of amino acid. Before each step (deprotection and coupling) the resin was washed with DMF and DCM. The N-terminal amine was kept free to provide solubility of these hydrophobic sequences. For peptide cleavage, the dried resin was treated with 10 mL of TFA/water/TIPS (95/2.5/2.5, v/v) for 3 h at room temperature. Afterwards, the resin was washed thrice with TFA and CH₂Cl₂. Afterwards, the crude product was dissolved in water and lyophilized overnight.

Standard conditions of manual SPPS are listed in **table S2**. HPLC chromatograms obtained from crude & pure peptide during synthesis are presented in **figure S2**.

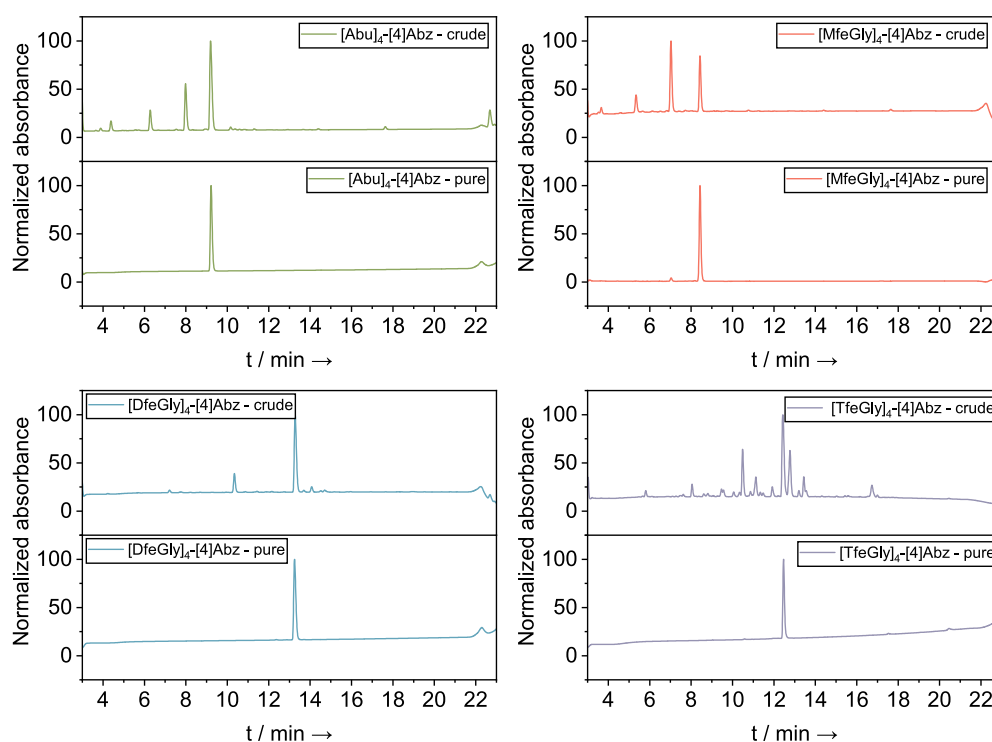


Figure S2: HPLC chromatograms of crude and pure peptides. H₂O + 0.1% TFA (A) and ACN + 0.1% TFA (B) served as eluents. The HPLC gradients were 10 → 40% (B) in 18 min for Abu₄[4]Abz, MfeGly₄[4]Abz and DfeGly₄[4]Abz and 10 → 70% (B) in 18 min for TfeGly₄[4]Abz.

Table S2: Process steps for manual SPPS. All reagents were dissolved in DMF.

Process step		Reagent	Reaction time
	[1] Swelling	5.0 mL DMF	2 * 30 min
	[2] Loading	5 eq. Fmoc-[4]Abz-OH, 5 eq. HATU and 10 eq. DIPEA in 4.0 mL DMF	2 * 60 min
	[3] Washing	5.0 mL DMF 5.0 mL DCM	3 * 1 min 3 * 1 min
Coupling cycle	[4] Deprotection	2.0 mL 20% piperidine in DMF	3 * 10 min
	[5] Washing	5.0 mL DMF 5.0 mL DCM	3 * 1 min 3 * 1 min
	[6] Coupling	1.5 eq. Fmoc-(F)AA-OH, 1.5 eq. HATU and 3 eq. DIPEA in 2.0 mL DMF	1 * 60 min
	[7] Washing	5.0 mL DMF 5.0 mL DCM	3 * 1 min 3 * 1 min

2.3 Preparative & analytical HPLC

LaPrep Σ HPLC system (preparative HPLC)

Purification of the synthesized peptides was performed on a LaPrep Σ HPLC system (VWR International GmbH, Darmstadt, Germany), comprising a LaPrep Σ LP 1200 preparative solvent pump with 100 mL titanium pump head, a ternary low-pressure gradient, a dynamic mixing chamber, a 6-port-3-channel injection valve with an automated preparative 10 mL sample loop, a LaPrep Σ LP 3101 1-channel UV-detector, a LaPrep Σ semi-preparative flow cell with 0.5 mm path length and a LaPrep Σ LP2016 17-port/1-channel fractionation valve. A Kinetex[®] C18 RP-HPLC column with TMS endcapping (5 μ m, 100 Å, 250 \times 21.2 mm, Phenomenex[®], Torrance, CA, USA) was used. A SecurityGuard[™] PREP Cartridge Holder Kit (21.20 mm ID, Ea, Phenomenex[®], Torrance, CA, USA) holding a C18 cartridge (15 \times 21.2mm, Phenomenex[®], Torrance, CA, USA) served as pre-column. As eluents deionized water and ACN, both containing 0.1% (v/v) TFA were applied. HPLC runs were performed according to the methods given in Table SX. Data analysis occurred with an EZChrom *Elite* software (Version 3.3.2 SP2, Agilent Technologies, Santa Clara, CA, USA).

Chromaster HPLC system (analytical HPLC)

The VWR-Hitachi Chromaster HPLC 600 bar system (VWR International GmbH, Darmstadt, Germany) works with a low-pressure gradient, and comprises a 5160 pump with a 6-channel solvent degasser, an organizer, a 5260 autosampler with a 100 μ L sample loop, a 5310 column oven and a 5430 diode array detector with a standard flow cell (10 mm optical path length). A Kinetex[®] C18 column (5 μ m, 100 Å, 250 \times 4.6 mm, Phenomenex[®], Torrance, CA, USA), was used. A SecurityGuard[™] Cartridge Kit (Ea, Phenomenex[®], Torrance, CA, USA) with a C18 SecurityGuard[™] cartridge (4 \times 3.0 mm, Phenomenex[®], Torrance, CA, USA) served as pre-column. Deionized water and ACN, both containing 0.1% (v/v) TFA, served as eluents. The flow rate was adjusted to 1 mL/min and the column was heated to 24°C. UV-detection of the peptides occurred at 220 nm or 280 nm while running a linear gradient of ACN + 0.1% (v/v) TFA. Data analysis was performed with EZChrom *Elite* software (version 3.3.2, Agilent Technologies, Santa Clara, CA, USA).

LaChrom ELITE® HPLC system (analytical HPLC)

Analytical HPLC was carried out on a LaChrom ELITE®-HPLC-System from VWR-Hitachi (VWR International GmbH, Darmstadt, Germany). The system contains an organizer, two HPLC pumps (L-2130) with solvent degaser, an autosampler (L-2200) with a 100 µL sample loop, a diode array flow detector (L-2455), and a high-pressure gradient mixer. A Kinetex® C18 column (5 µm, 100 Å, 250 × 4.6 mm, Phenomenex®, Torrance, CA, USA) was used. A SecurityGuard™ Cartridge Kit (Ea, Phenomenex®, Torrance, CA, USA) holding a C8 or C18 SecurityGuard™ cartridge (4 × 3.0 mm, Phenomenex®, Torrance, CA, USA), respectively, served as pre-column. A flow rate of 1.0 mL/min was applied with deionized water and ACN, both containing 0.1% (v/v) TFA, as eluents. The used gradient methods are shown in Table 7.4, and the UV-detection occurred at 220 or 280 nm. Data analysis was performed with EZChrom *Elite* software (version 3.3.2, Agilent Technologies, Santa Clara, CA, USA).

2.4 Peptide synthesis: HPLC chromatograms and HRMS spectra

Table S3: Overview of fluoro-peptides studied in this work.

Peptide sequence	X	Compound number
X₁₀ GY(K) ₃	Abu	2a
	MfeGly	2b
	DfeGly	2c
	TfeGly	2d
X₁₃ GY(K) ₄	Abu	3a
	MfeGly	3b
	DfeGly	3c
	TfeGly	3d
X₁₅ GY(K) ₄	Abu	4a
	MfeGly	4b
	DfeGly	4c
X₄ [4]Abz	Abu	5a
	MfeGly	5b
	DfeGly	5c
	TfeGly	5d

2.4.1 Abu₁₀GY(K)₃ 2a

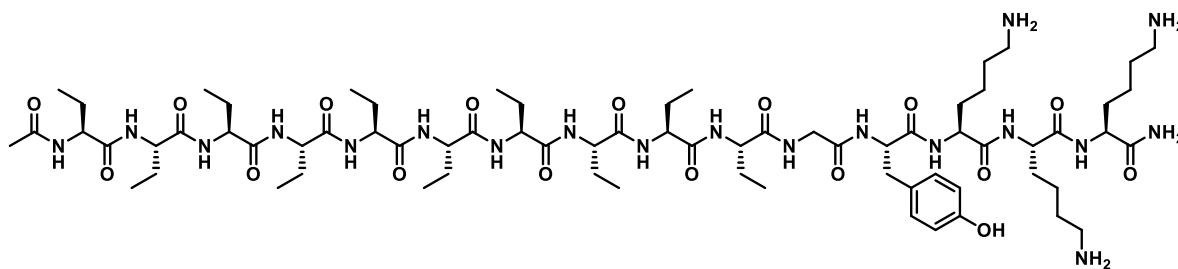


Figure S3: Chemical structure of Abu₁₀GY(K)₃.

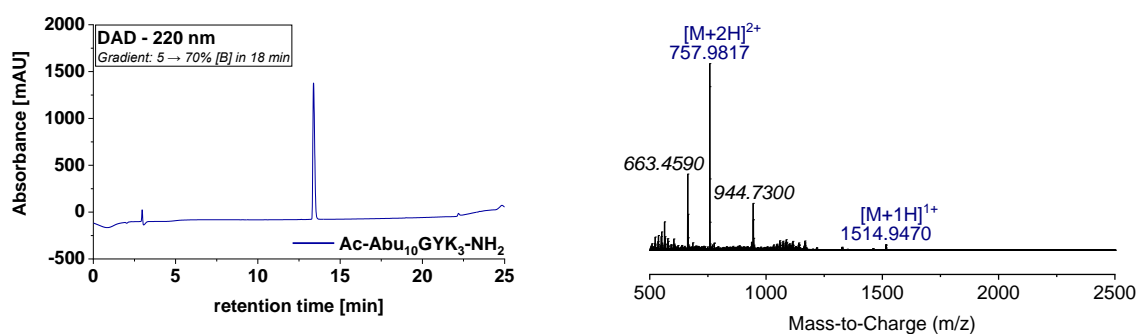


Figure S4: HPLC chromatogram (left) and HRMS spectrum (right) of purified peptide Abu₁₀GY(K)₃.

Table S4: Ion species (positive mode) calculated and observed for peptide Abu₁₀GY(K)₃.

Ion species	Mass (calc.)	Mass (obs.)
[M+H] ⁺	1514.9422	1514.7700
[M+2H] ²⁺	757.9750	757.9817

2.4.2 MfeGly₁₀GY(K)₃ 2b

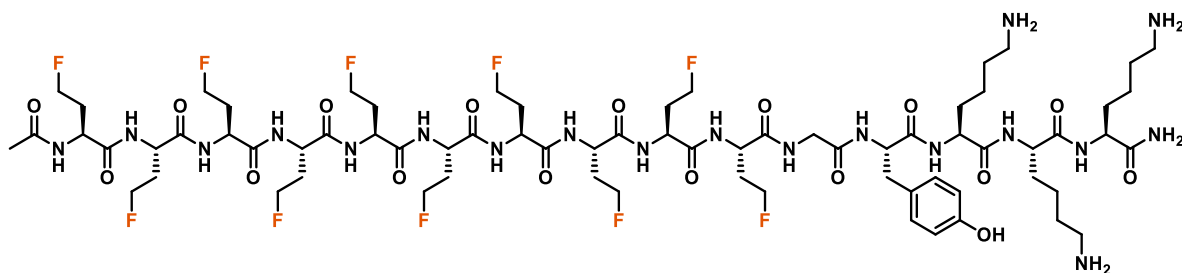


Figure S5: Chemical structure of MfeGly₁₀GY(K)₃.

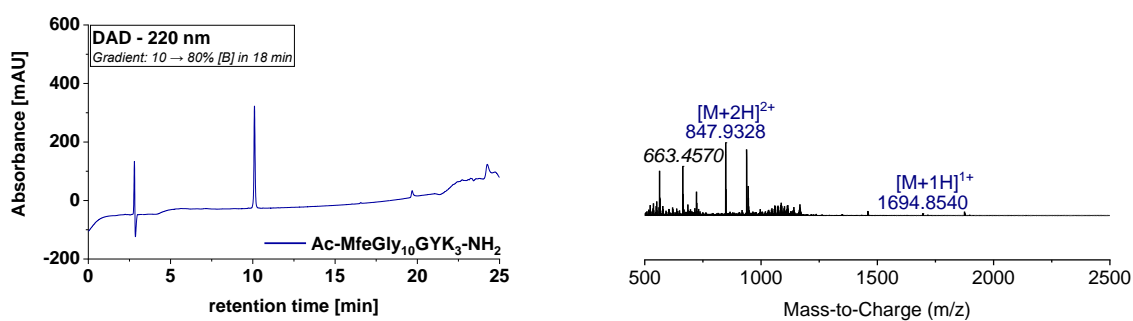


Figure S6: HPC chromatogram (left) and HRMS spectrum (right) of purified peptide MfeGly₁₀GY(K)₃.

Table S5: Ion species (positive mode) calculated and observed for peptide MfeGly₁₀GY(K)₃.

Ion species	Mass (calc.)	Mass (obs.)
[M+H] ⁺	1694.8480	1694.8540
[M+2H] ²⁺	847.9279	847.9328

2.4.3 DfeGly₁₀GY(K)₃ 2c

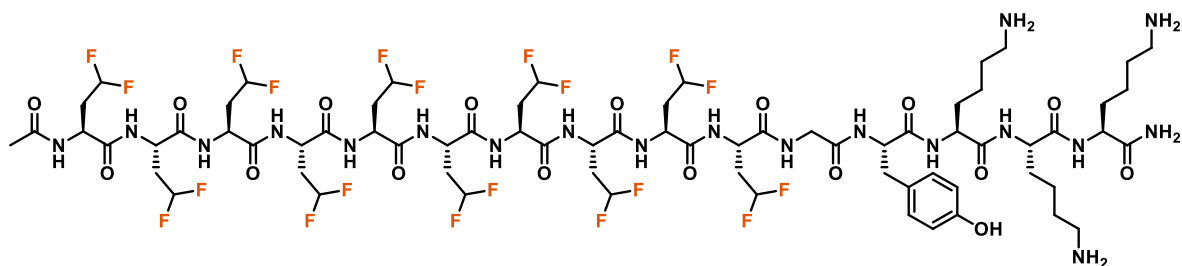


Figure S7: Chemical structure of DfeGly₁₀GY(K)₃.

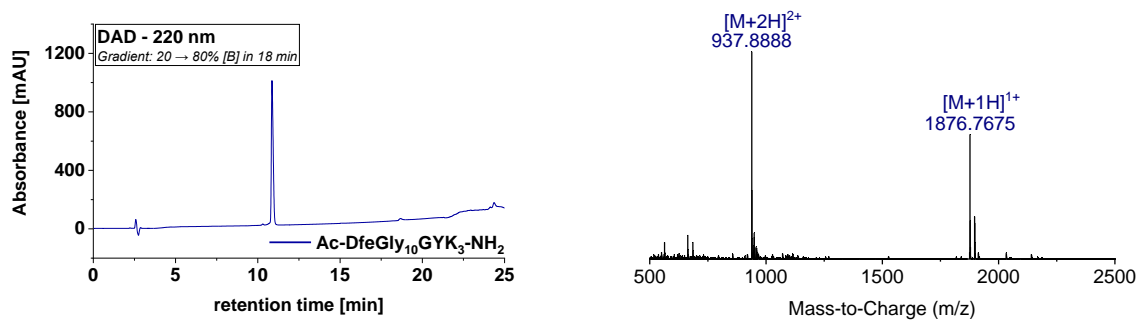


Figure S8: HPC chromatogram (left) and HRMS spectrum (right) of purified peptide DfeGly₁₀GY(K)₃.

Table S6: Ion species (positive mode) calculated and observed for peptide DfeGly₁₀GY(K)₃.

Ion species	Mass (calc.)	Mass (obs.)
[M+H] ⁺	1874.7538	1874.7675
[M+2H] ²⁺	937.8808	937.8888

2.4.4 TfeGly₁₀GY(K)₃ 2d

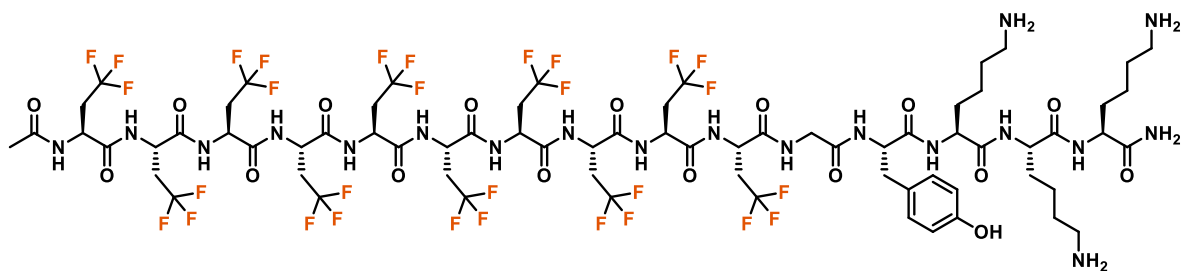


Figure S9: Chemical structure of TfeGly₁₀GY(K)₃.

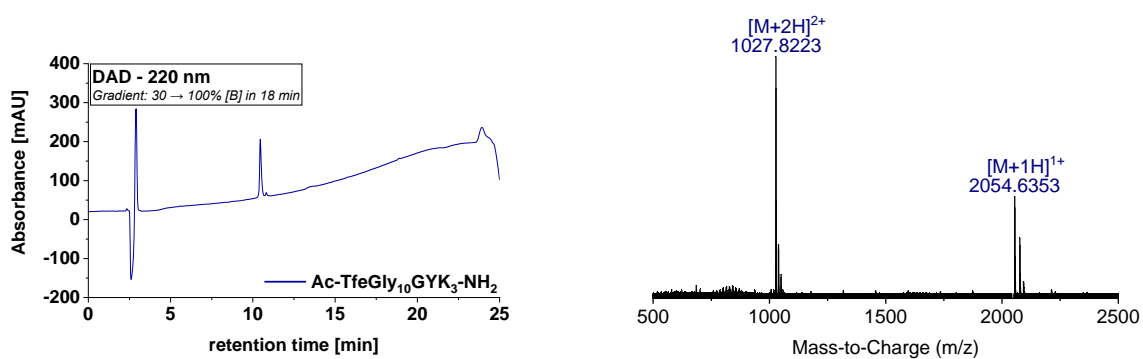


Figure S10: HPC chromatogram (left) and HRMS spectrum (right) of purified peptide TfeGly₁₀GY(K)₃.

Table S7: Ion species (positive mode) calculated and observed for peptide TfeGly₁₀GY(K)₃.

Ion species	Mass (calc.)	Mass (obs.)
[M+H] ⁺	2054.6596	2054.6353
[M+2H] ²⁺	1027.8337	1027.8223

2.4.5 Abu₁₃GY(K)₄ 3a

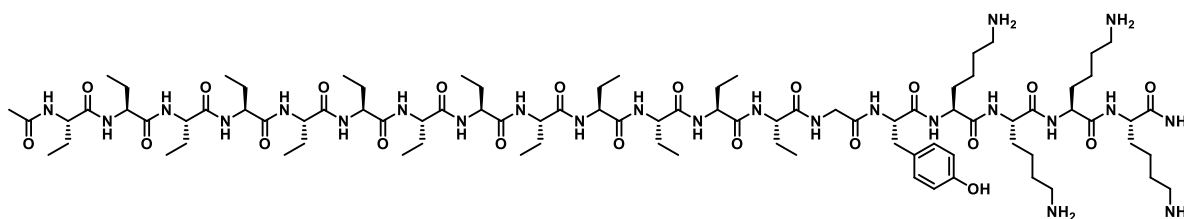


Figure S11: Chemical structure of Abu₁₃GY(K)₄.

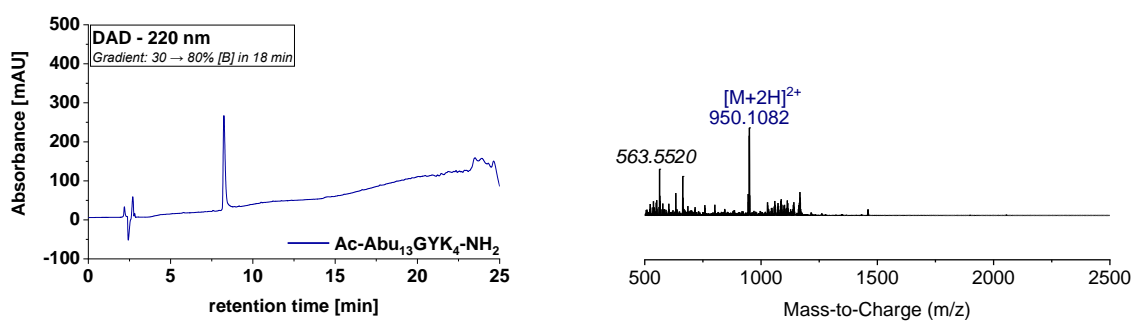


Figure S12: HPC chromatogram (left) and HRMS spectrum (right) of purified peptide Abu₁₃GY(K)₄.

Table S8: Ion species (positive mode) calculated and observed for peptide Abu₁₃GY(K)₄.

Ion species	Mass (calc.)	Mass (obs.)
[M+H] ⁺	1898.1876	-
[M+2H] ²⁺	950.0977	950.1082

2.4.6 MfeGly₁₃GY(K)₄ 3b

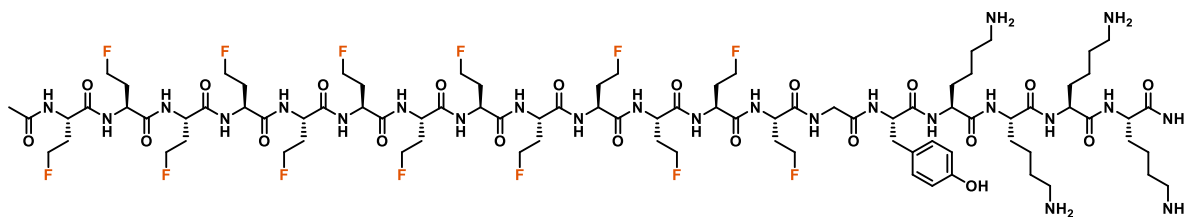


Figure S13: Chemical structure of MfeGly₁₃GY(K)₄.

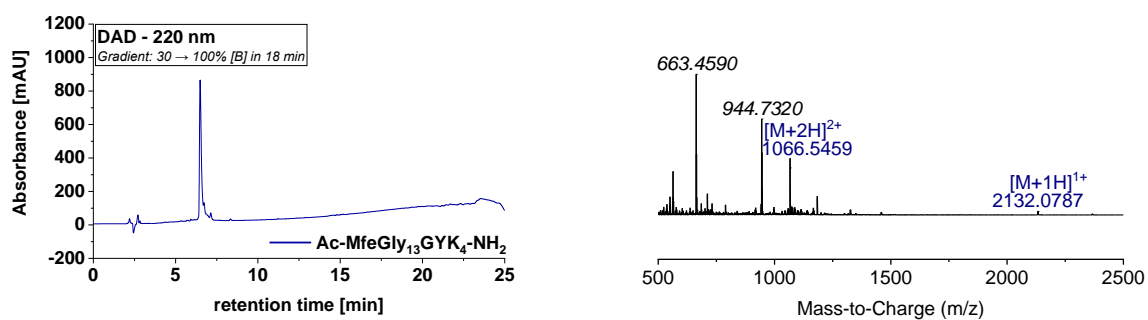


Figure S14: HPC chromatogram (left) and HRMS spectrum (right) of purified peptide MfeGly₁₃GY(K)₄.

Table S9: Ion species (positive mode) calculated and observed for peptide MfeGly₁₃GY(K)₄.

Ion species	Mass (calc.)	Mass (obs.)
[M+H] ⁺	2132.0652	2132.0787
[M+2H] ²⁺	1067.5404	1067.5459

2.4.7. DfeGly₁₃GY(K)₄ 3c

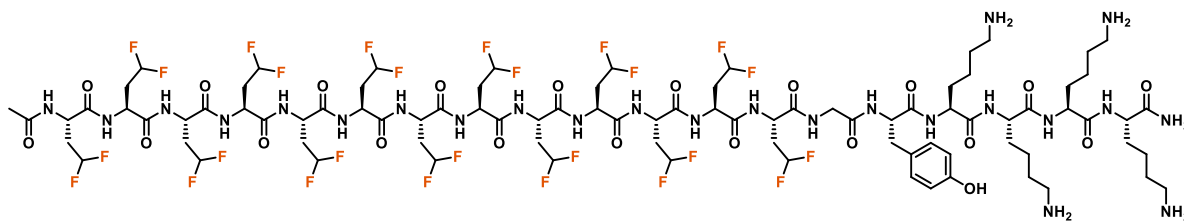


Figure S15: Chemical structure of DfeGly₁₃GY(K)₄.

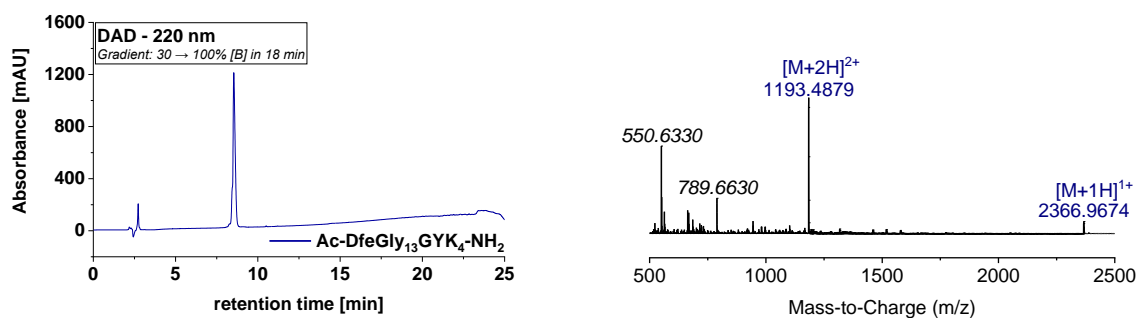


Figure S16: HPC chromatogram (left) and HRMS spectrum (right) of purified peptide DfeGly₁₃GY(K)₄.

Table S10: Ion species (positive mode) calculated and observed for peptide DfeGly₁₃GY(K)₄.

Ion species	Mass (calc.)	Mass (obs.)
[M+H] ⁺	2365.9505	2365.9674
[M+2H] ²⁺	1183.4791	1183.4879

2.4.8 TfeGly₁₃GY(K)₄ 3d

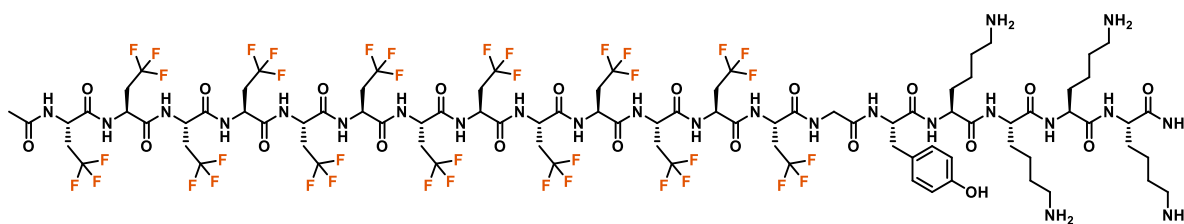


Figure S17: Chemical structure of TfeGly₁₃GY(K)₄.

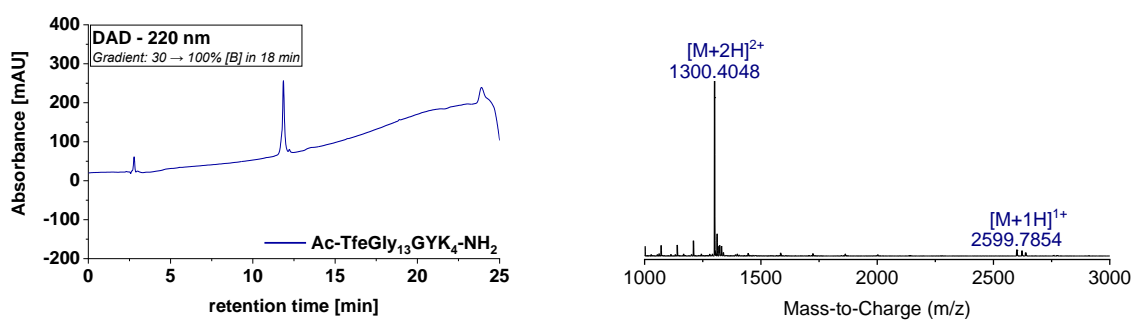


Figure S18: HPC chromatogram (left) and HRMS spectrum (right) of purified peptide TfeGly₁₃GY(K)₄.

Table S11: Ion species (positive mode) calculated and observed for peptide TfeGly₁₃GY(K)₄.

Ion species	Mass (calc.)	Mass (obs.)
[M+H] ⁺	2599.8280	2599.7854
[M+2H] ²⁺	1300.4179	1300.4048

2.4.9 Abu₁₅GY(K)₄ 4a

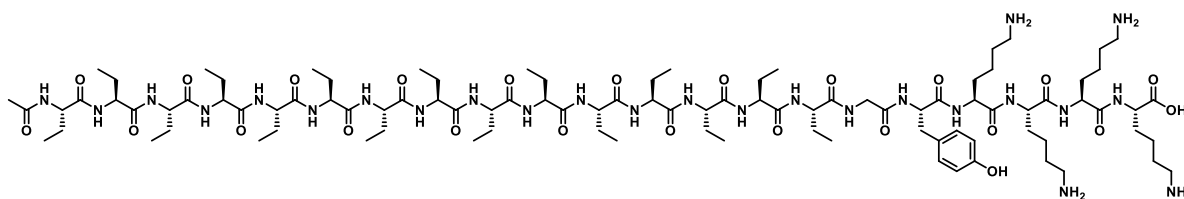


Figure S19: Chemical structure of Abu₁₅GY(K)₄.

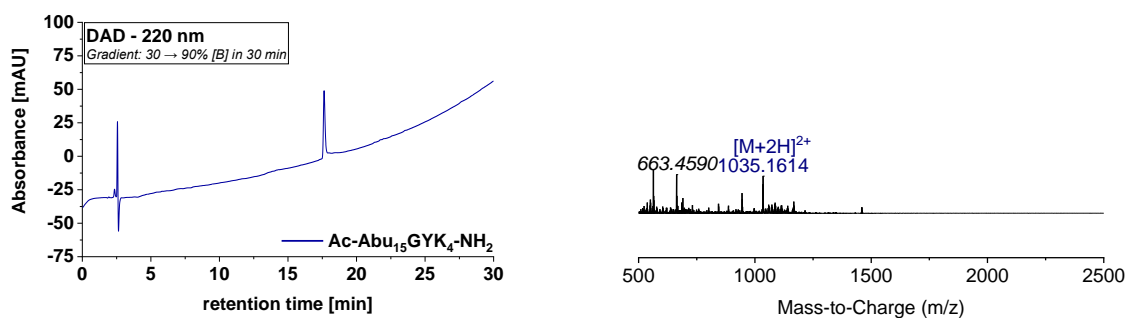


Figure S20: HPC chromatogram (left) and HRMS spectrum (right) of purified peptide Abu₁₅GY(K)₄.

Table S12: Ion species (positive mode) calculated and observed for peptide Abu₁₅GY(K)₄.

Ion species	Mass (calc.)	Mass (obs.)
(M+H) ⁺	2069.2850	-
(M+2H) ²⁺	1.035.1464	1035.1614

2.4.10 MfeGly₁₅GY(K)₄ 4b

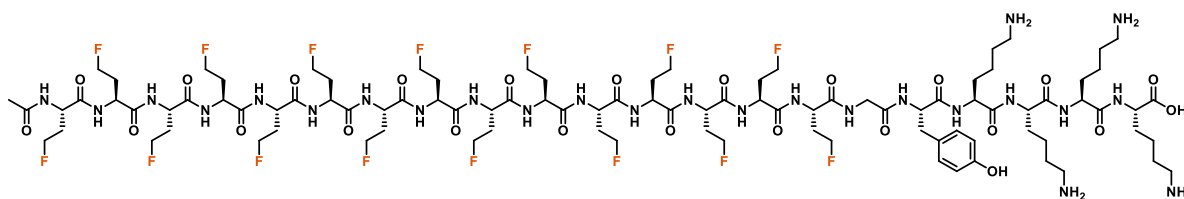


Figure S21: Chemical structure of MfeGly₁₅GY(K)₄.

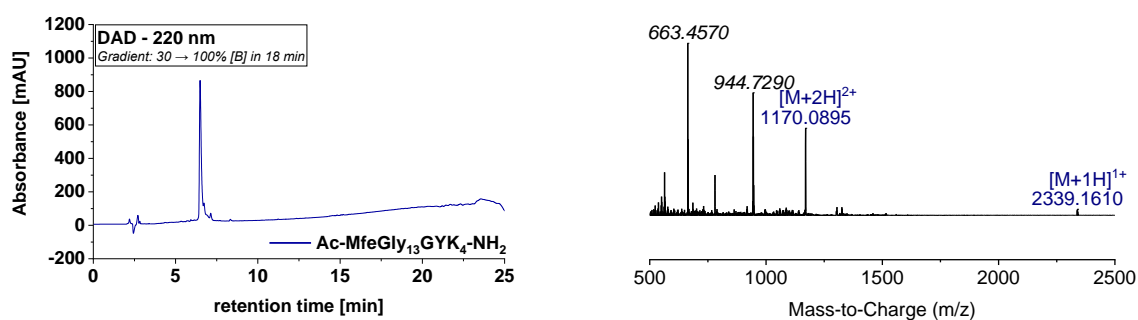


Figure S22: HPC chromatogram (left) and HRMS spectrum (right) of purified peptide MfeGly₁₅GY(K)₄.

Table S13: Ion species (positive mode) calculated and observed for peptide MfeGly₁₅GY(K)₄.

Ion species	Mass (calc.)	Mass (obs.)
(M+H) ⁺	2339.1437	2339.1610
(M+2H) ²⁺	1170.0757	1170.0895

2.4.11 DfeGly₁₅GY(K)₄ 4c

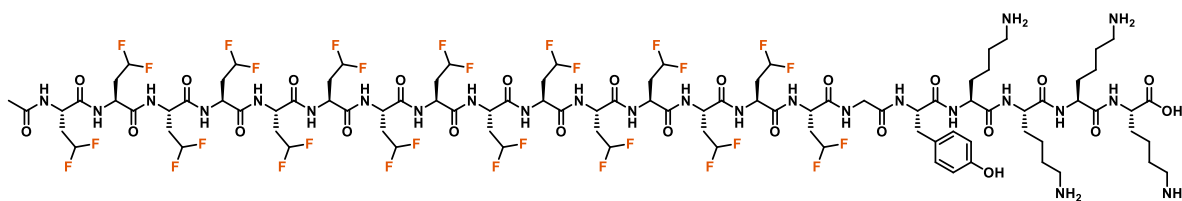


Figure S23: Chemical structure of DfeGly₁₅GY(K)₄.

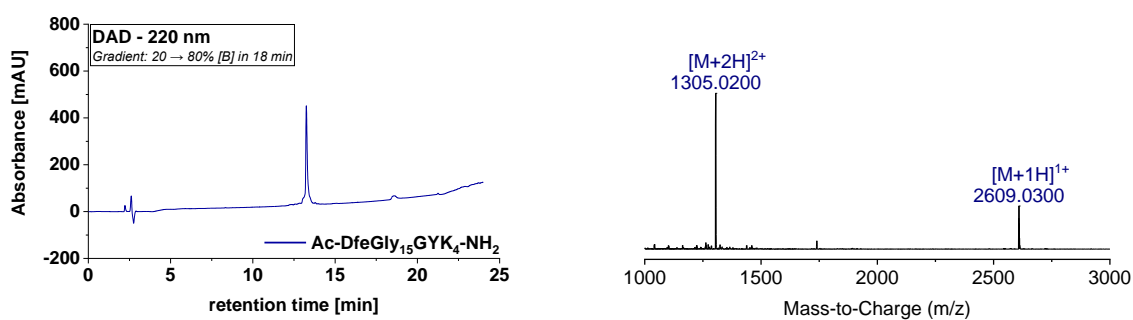


Figure S24: HPC chromatogram (left) and HRMS spectrum (right) of purified peptide DfeGly₁₅GY(K)₄.

Table S14: Ion species (positive mode) calculated and observed for peptide MfeGly₁₅GY(K)₄.

Ion species	Mass (calc.)	Mass (obs.)
(M+H) ⁺	2609.0024	2609.0300
(M+2H) ²⁺	1305.0051	1205.0200

2.4.12 Abu₄[4]Abz 5a

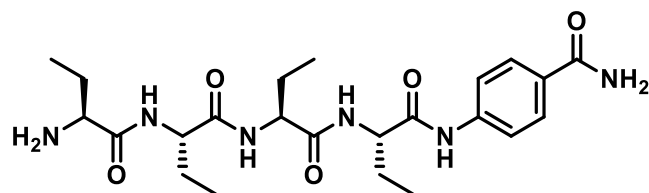


Figure S25: Chemical structure of [Abu]₄-[4]Abz.

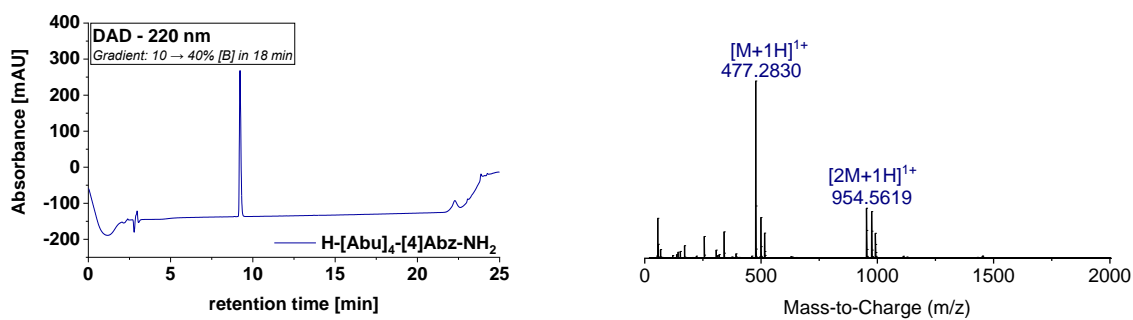


Figure S26: HPC chromatogram (left) and HRMS spectrum (right) of purified peptide [Abu]₄-[4]Abz.

Table S15: Ion species (positive mode) calculated and observed for peptide [Abu]₄-[4]Abz.

Ion species	Mass (calc.)	Mass (obs.)
(M+H) ⁺	477.2825	477.2830
(2M+H) ⁺	954.5650	954.5619

2.4.13 MfeGly₄[4]Abz 5b

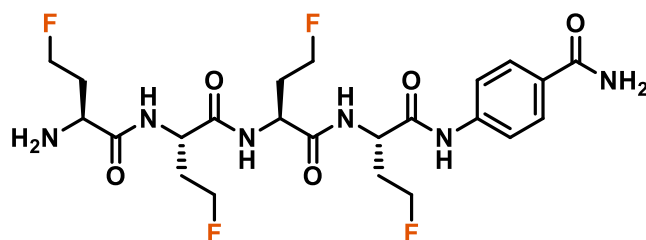


Figure S27: Chemical structure of [MfeGly]₄-[4]Abz.

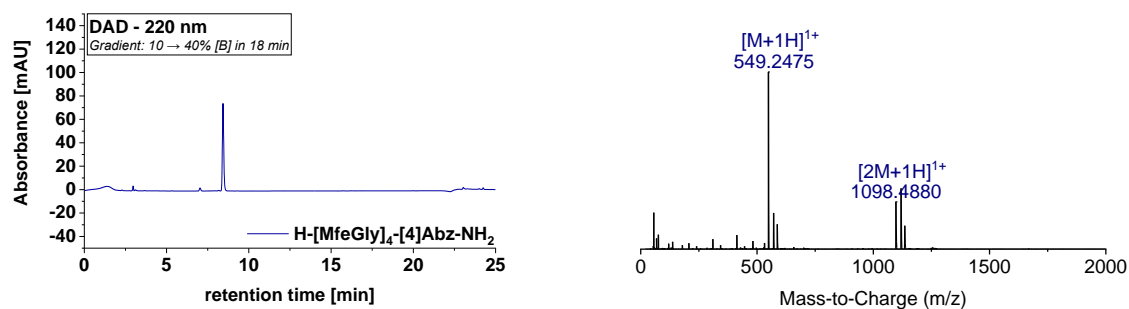


Figure S28: HPC chromatogram (left) and HRMS spectrum (right) of purified peptide [MfeGly]₄-[4]Abz.

Table S16: Ion species (positive mode) calculated and observed for peptide [MfeGly]₄-[4]Abz.

Ion species	Mass (calc.)	Mass (obs.)
(M+H) ⁺	548.2448	549.2475
(M+2H) ²⁺	1098.4896	1098.4880

2.4.14 DfeGly₄[4]Abz 5c

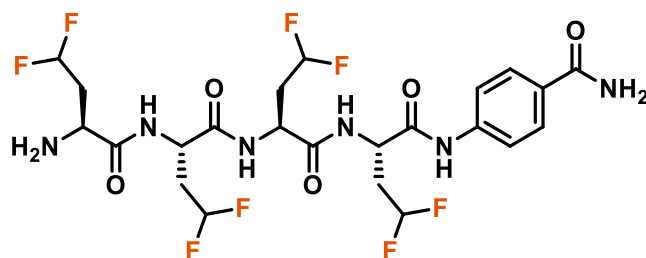


Figure S29: Chemical structure of [DfeGly]₄-[4]Abz.

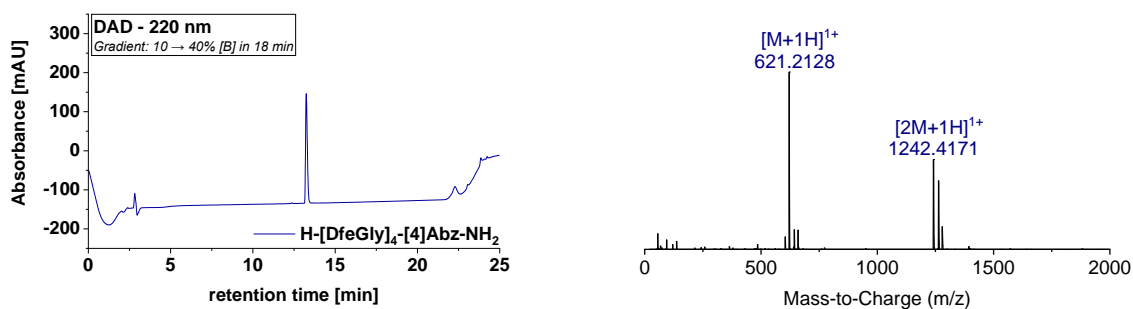


Figure S30: HPC chromatogram (left) and HRMS spectrum (right) of purified peptide [DfeGly]₄-[4]Abz.

Table S17: Ion species (positive mode) calculated and observed for peptide [DfeGly]₄-[4]Abz.

Ion species	Mass (calc.)	Mass (obs.)
(M+H) ⁺	621.2071	621.2128
(M+2H) ²⁺	1242.4142	1242.4171

2.4.15 TfeGly₄[4]Abz 5d

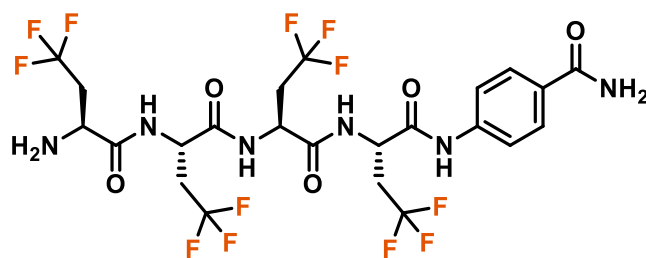


Figure S31: Chemical structure of [TfeGly]₄-[4]Abz.

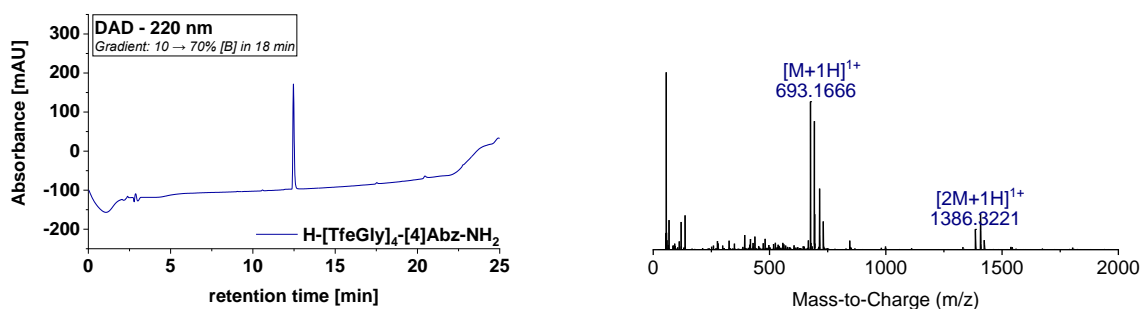


Figure S32: HPC chromatogram (left) and HRMS spectrum (right) of purified peptide [TfeGly]₄-[4]Abz.

Table S18: Ion species (positive mode) calculated and observed for peptide [TfeGly]₄-[4]Abz.

Ion species	Mass (calc.)	Mass (obs.)
(M+H) ⁺	693.1694	693.1694
(M+2H) ²⁺	1386.3388	1386.3221

3. Circular Dichroism and SEIRAS Infrared Spectroscopy – further data

3.1 Fundamentals: Hydrophobicity Studies

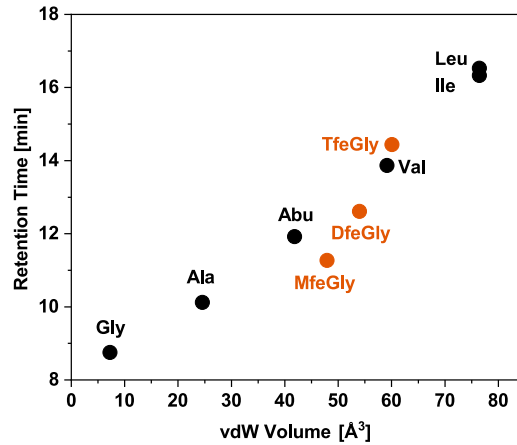


Figure S33: Retention times of amino acids plotted against the vdW volume of the side chains.

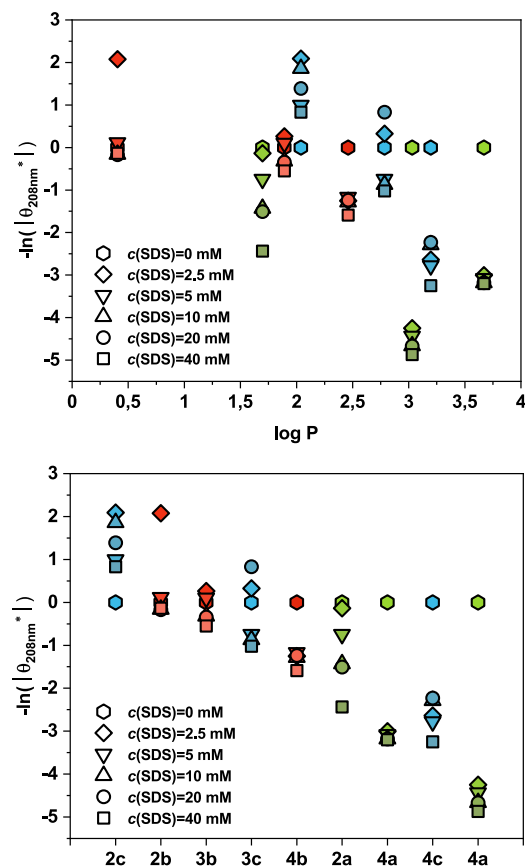


Figure S34: Normalized molar ellipticity (θ_{208nm}^*) plotted against the corresponding $\log P$ values (**top**) or ordered by increasing intensity (**bottom**). (θ_{208nm}^*)^{*} = θ_{208nm} (at specific SDS concentration) / θ_{208nm} (at SDS concentration of 0 mM).

3.2 Parametric dual wavelength two-state test

3.1.1 Abu₁₀GY(K)₃ 2a

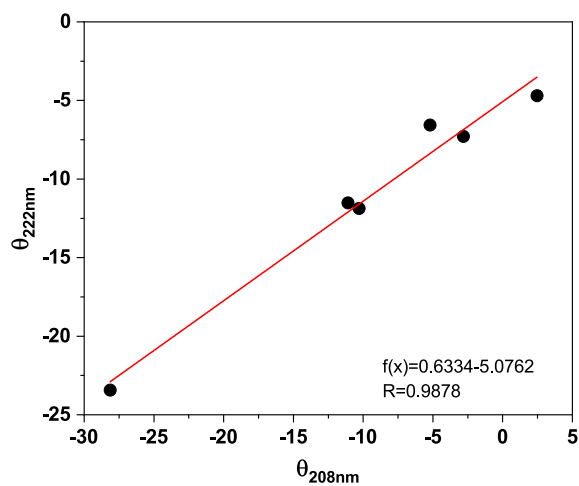


Figure S35: Dual wavelengths plot of θ_{208} vs θ_{222} for **2a** over the SDS concentrations of 0, 2.5, 5, 10, 20, 40 mM.

3.1.2 Abu₁₃GY(K)₄ 3a

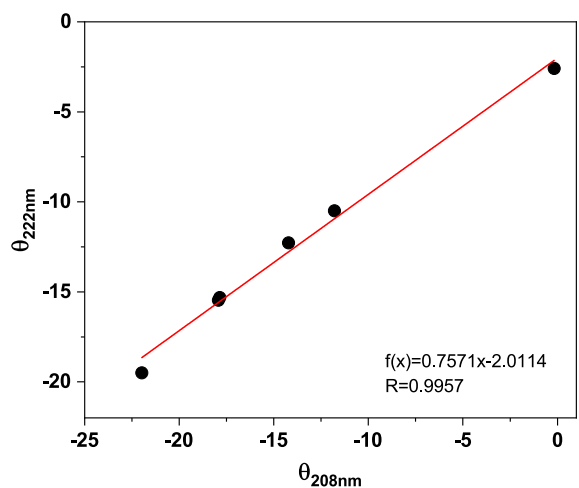


Figure S36: Dual wavelengths plot of θ_{208} vs θ_{222} for **3a** over the SDS concentrations of 0, 2.5, 5, 10, 20, 40 mM.

3.1.3 Abu₁₅GY(K)₄ 4a

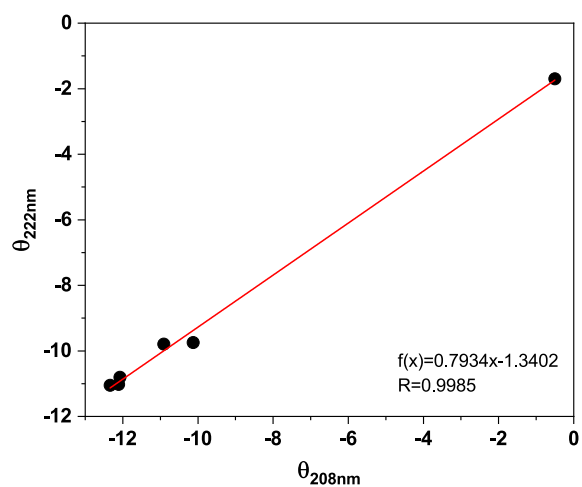


Figure S37: Dual wavelengths plot of θ_{208} vs θ_{222} for **4a** over the SDS concentrations of 0, 2.5, 5, 10, 20, 40 mM.

3.1.4 DfeGly₁₃GY(K)₄ 3c

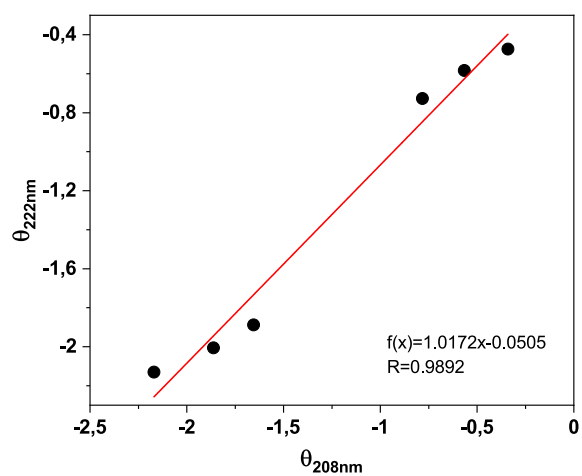


Figure S38: Dual wavelengths plot of θ_{208} vs θ_{222} for **3c** over the SDS concentrations of 0, 2.5, 5, 10, 20, 40 mM.

3.1.5 DfeGly₁₅GY(K)₄ 4c

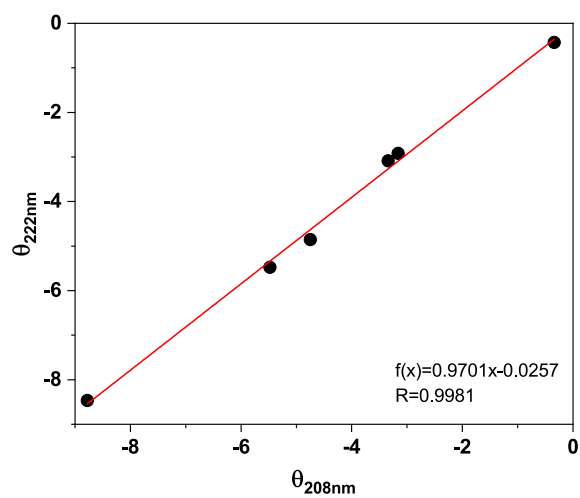


Figure S39: Dual wavelengths plot of θ_{208} vs θ_{222} for **4c** over the SDS concentrations of 0, 2.5, 5, 10, 20, 40 mM.

3.1.6 TfeGly₁₃GY(K)₄ 3d

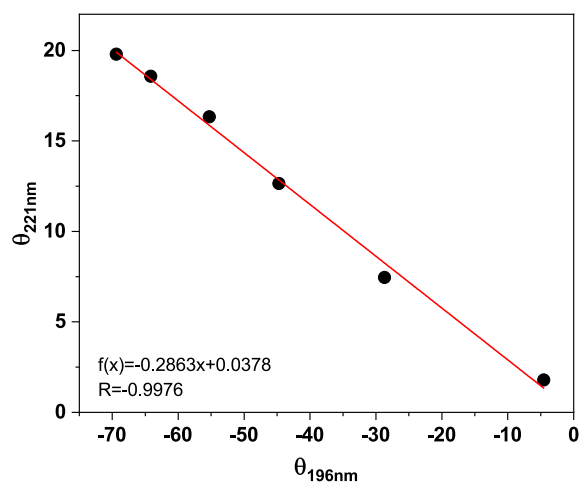


Figure S40: Dual wavelengths plot of θ_{196} vs θ_{221} for **3d** over the SDS concentrations of 0, 2.5, 5, 10, 20, 40 mM.

3.3 TfeGly₁₀GY(K)₃ 2d

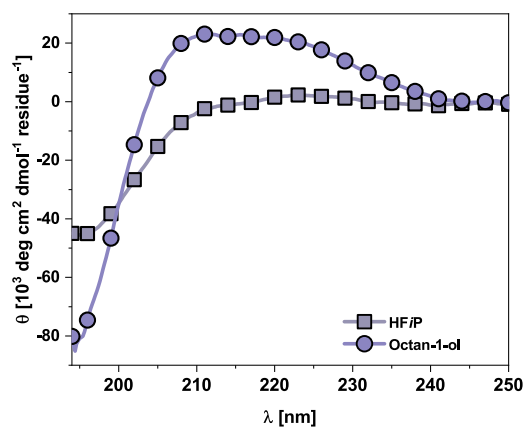


Figure S41: CD spectrum of **2d** (25 μM) in HFIP and octan-1-ol.

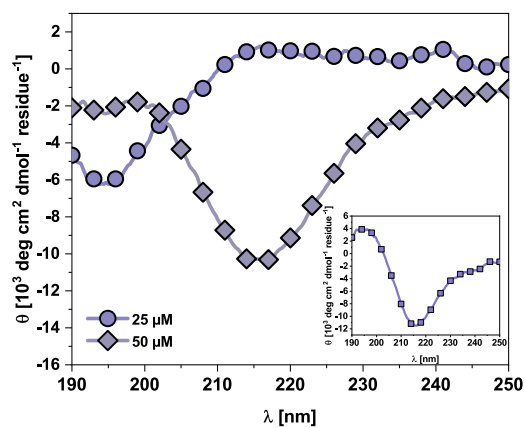


Figure S42: CD spectrum of **2d** at different concentrations (25 μM/50 μM) phosphate buffer (10 mM, pH = 7.4). Inlet shows the corresponding difference spectrum

3.4 Poly(L-lysine)

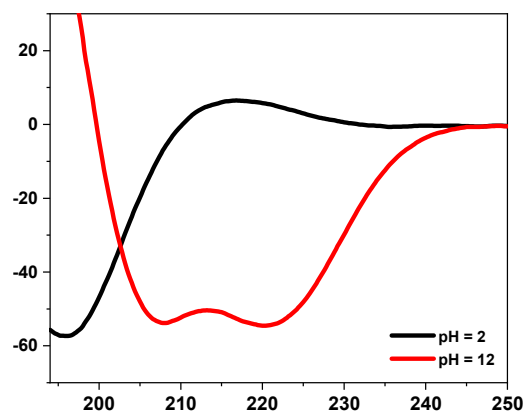


Figure S43: CD spectrum of poly(L-lysine) at different pH values (pH = 2/12).

For a period of time, it was assumed that this structure could only be formed by this type of peptides. However, this changed when Tiffany and Krimm published a work showing that poly(L-lysine) and poly(L-glutamic acid) peptides can also adopt a PPII conformation (minimum at 198 nm; maximum at 218 nm).^[4] The observed blue shift compared to the poly(L proline) peptides can be explained by the difference between secondary and tertiary amides.^[5] This assumption was questioned by Mattice who showed that short dipeptides can also produce similar CD spectra.^[6] Since at that time it was considered unlikely that such short peptides could adopt a distinct conformation, these results were used to refute the statement made by Tiffany and Krimm. As it was assumed that a minimum at 195 nm is characteristic of a random coil, a claim still made to this day, the structures of poly(L-lysine) and poly(L-glutamic acid) were described as unordered. Yet, there is now a substantial amount of work supporting Tiffany and Krimm's hypothesis. Thus, the working groups of Schweitzer-Stenner^[7], Kallenbach^[8], and others^[9] showed that even short model peptides are capable to adopt a PPII conformation. Meanwhile, it can even be assumed that in the unfolded state proteins, certain stretches are not present as random coils, but in fact in an extended PPII conformation.^[10] The CD spectrum of TfeGly₁₃GY(K)₄ **3d** is in a great agreement with the literature spectra of poly(L-lysine), poly(L-glutamic acid), and other PPII helix forming peptides.

3.5 Time-dependent measurements in the presence of POPC/POPG

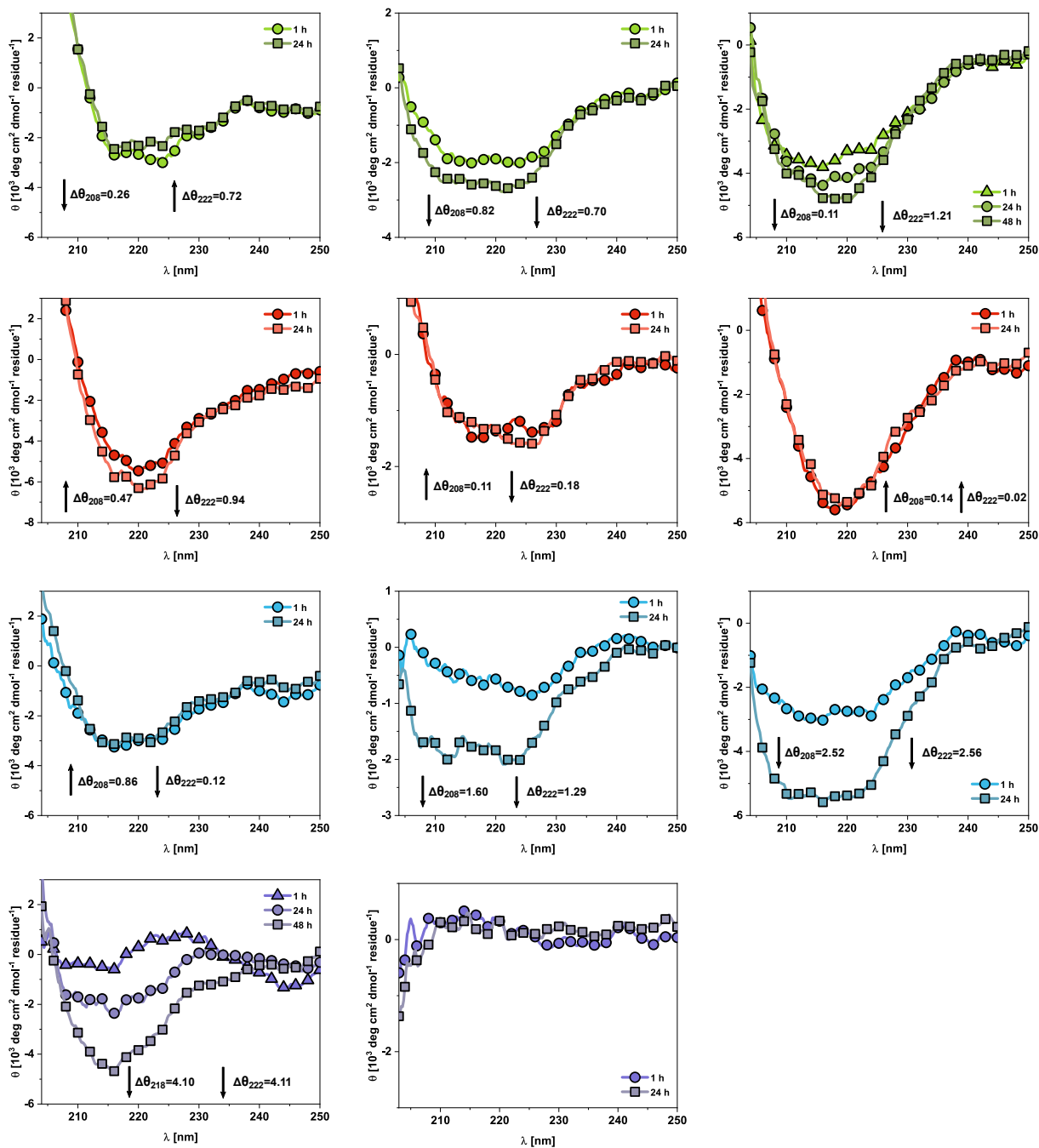


Figure S44: CD spectra of (from left to right) Abu₁₀GY(K)₃ **2a**, Abu₁₃GY(K)₄ **3a**, and Abu₁₅GY(K)₄ **4a** (first row), MfeGly₁₀GY(K)₃ **2b**, MfeGly₁₃GY(K)₄ **3b**, and MfeGly₁₅GY(K)₄ **4b** (Second row), DfeGly₁₀GY(K)₃ **2c**, DfeGly₁₃GY(K)₄ **3c**, and DfeGly₁₅GY(K)₄ **4c** (third row), TfeGly₁₀GY(K)₃ **2d** and TfeGly₁₃GY(K)₄ **3d** (fourth row) in phosphate buffer (10 mM, pH = 7.4) in the presence of POPC/POPG = 1:1 after 1 h and 24 h (peptide concentration: 50 μM).

3.6 Additional SEIRAS Spectra

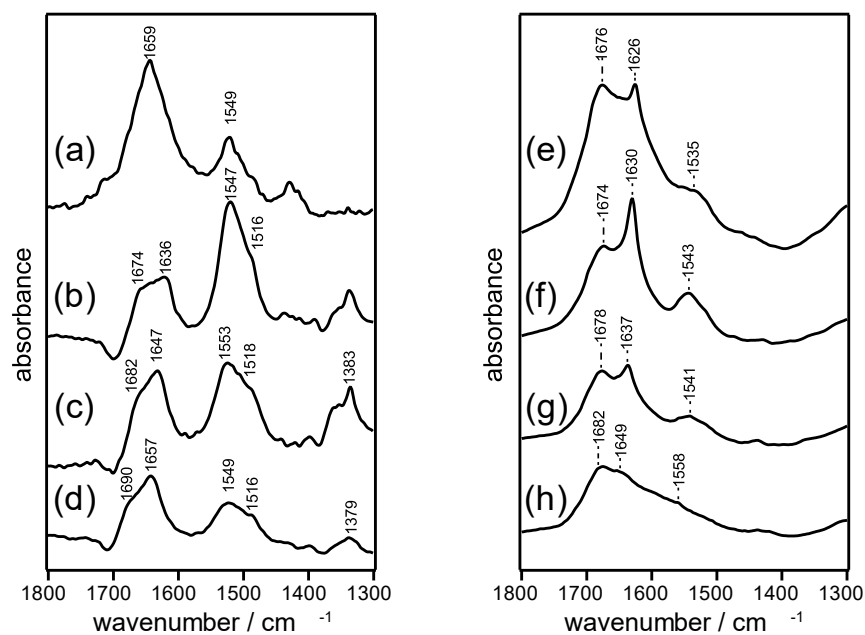


Figure S45: SEIRA spectra of the peptides adsorbed on the lipid (a) Abu₁₃GY(K)₄ **3a**, (b) MfeGly₁₃GY(K)₄ **3b**, (c) DfeGly₁₃GY(K)₄ **3c**, (d) TfeGly₁₃GY(K)₄ **3d** and ATR-IR spectra of the peptides without lipid (e) Abu₁₃GY(K)₄ **3a**, (f) MfeGly₁₃GY(K)₄ **3b**, (g) DfeGly₁₃GY(K)₄ **3c**, (h) TfeGly₁₃GY(K)₄ **3d**.

As a control for the spectra of the peptides adsorbed on the lipid bilayer, IR spectra of corresponding peptides in the absence of the lipid bilayer are shown in **Figure S45e-h**. Spectra of the samples were taken at standard ATR conditions by evaporating the water solvent. Amide I bands of each peptide show characteristic double peaks at 1672-1680 cm⁻¹ and at 1630-1649 cm⁻¹. The lower band around 1620-1640 cm⁻¹ is particularly a marker band for the degree of intra- or intermolecular hydrogen bond interactions of the corresponding peptide backbones. A lower peak position of this band indicates stronger hydrogen bond interactions in the aggregate. With the increasing degree of fluorination, the corresponding band shifts to higher wavenumbers indicating weaker hydrogen bond interactions for high fluorinated peptides. Especially the spectra of DfeGly₁₃GY(K)₄ **3c** and TfeGly₁₃GY(K)₄ **3d** show an up-shifted band at 1637 and 1649 cm⁻¹, respectively. These peak positions are no longer assigned to a typical aggregate but rather close to a plain random structure of the peptides. These results suggest that the fluorination of the Abu₁₃GY(K)₄ **3a** side chain suppress the hydrogen bond interactions of the peptide backbones and prevent the formation of aggregated structures. Interestingly, these data draw a similar picture as already seen in the structural studies of trifluorinated oligomers. Similar to PPII formation, the CF₃ groups appear to be spaced farther apart, inhibiting aggregation processes.

The frequency range between 1700-1600 cm^{-1} represents vibrational bands of the amide C=O stretching modes of the polypeptide. A broad feature of this band is a result of overlapping of different secondary structure components rise from different degree of hydrogen bonding strength among the amides.

To identify the contributions of individual secondary structure elements, a peak fitting had been carried out over the amide I band. Fitting was restricted to following five different secondary component in order to avoid overestimation of the fine structures, namely: **(1) β -turn/bend structures** appearing in the range between 1670 and 1685 cm^{-1} indicative of weak hydrogen bonding due to disruption of intra/inter-hydrogen bond network among the peptide backbone (shown as blue), **(2) random structure** appearing between 1670-1660 cm^{-1} indicative of weak hydrogen bonding among the peptide backbone (shown as yellow), **(3) α -helical structures** appearing between 1645 and 1660 cm^{-1} (shown as red), **(4) unordered and strongly hydrogen-bonded amide structures** appearing between 1635 and 1645 cm^{-1} (shown as dark gray), **(5) β -aggregates/sheets** appearing 1610 and 1635 cm^{-1} indicative of a formation of strong hydrogen bonds.^[11]

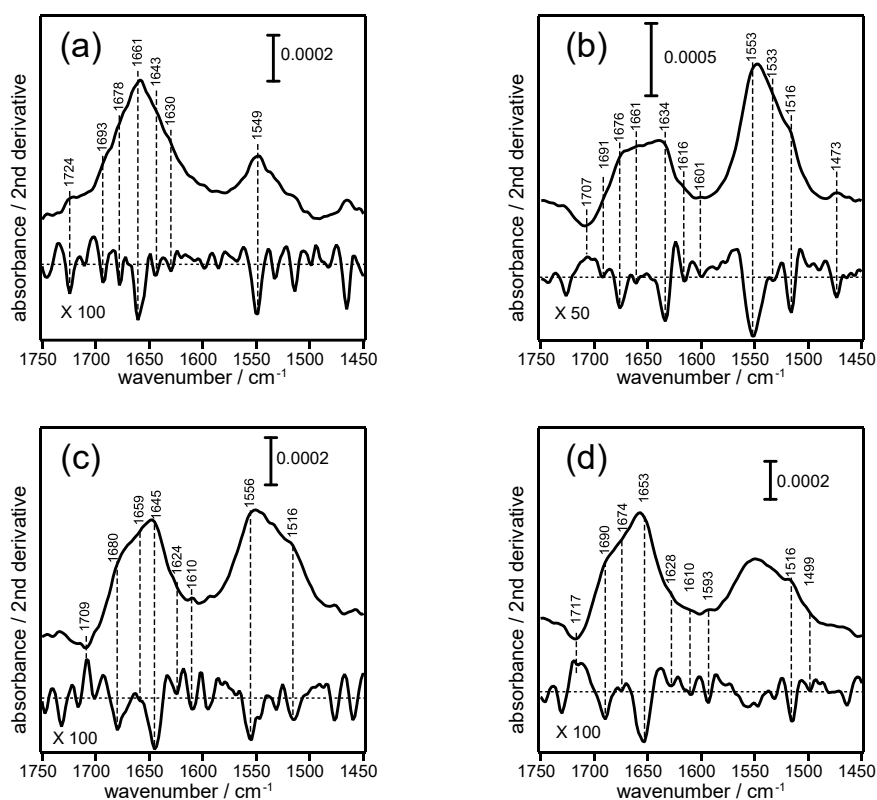


Figure S46. SEIRA spectra (**top**) and the second derivative (**bottom**) spectra of **(a)** Abu₁₃GY(K)₄ **3a**, **(b)** MfeGly₁₃GY(K)₄ **3b**, **(c)** DfeGly₁₃GY(K)₄ **3c**, and **(d)** TfeGly₁₃GY(K)₄ **3d**.

It should be noted that distinction between β -aggregate and β -sheet is difficult to make by IR spectrum because they appear in same spectral range. Therefore, we included the contribution from β -sheet structures as part of the components under **(1)** and **(5)**.

As first step, we exploited the second derivative method to estimate initial peak position of each component. **Figure S46** shows the result of the second derivative of each polypeptide. In the second derivative spectra, inflexion points in the amide I band are observed as negative peaks. We employed these negative peaks as the starting peak positions for the estimation of each component.

After setting the initial peak position, we proceed to the peak fitting of the observed amide I band to elucidate contribution of each component. During this estimation process, we applied following constraints:

- 1)** The peak position of each component can change within the range of $\pm 2 \text{ cm}^{-1}$ during the fitting. The range of the position shift was defined by the spectral resolution of obtained spectra (4 cm^{-1})
- 2)** The numbers of peaks are fixed to five components.
- 3)** The peak width of each component does not exceed more than 20 cm^{-1} to avoid overly broad peak shapes overlapping with the baseline.
- 4)** All peaks are Gaussian.

Results of the fittings are shown in **Figure 4d** in main text.

4. Estimation of log P values by HPLC

The log P values were estimated using a HPLC-based assay that was adapted from the O'Hagan group, which used this method to determine the lipophilicity of small fluorinated organic compounds.^[12] We transferred this method to the field of peptide chemistry.

To estimate the hydrophobicity of fluorinated peptides **2-4**, a library of short peptides with known log P values was synthesized.^[13] To ensure that the influence of both chain length and charges was considered, peptides of different lengths (tri-, tetra- and pentamers), with an amide or carboxylic acid functionalities at the C-terminus and blocked or unblocked N-terminal ends were synthesized. Subsequently, the retention times of these peptides were determined in triplicates using a reversed-phase C18 column. A gradient consisting of acetonitrile and water both with 0.1% TFA was used (MeCN:H₂O (0.1% TFA) = 5:95 to 70:30, flow rate 1.0 mL/min). The peptides were injected at a concentration of 0.1 mM. The correlation between the retention time and the log P values was fitted using a linear function. The latter was then used to calculate the corresponding unknown log P values from the measured retention times. **Table S18** summarizes the peptide library and shows the determined retention times of the short peptides.

Table S19: Determined log k values for the reference peptides. Capacity factor $k=(R_t - [\text{dead time of the column}]) / [\text{dead time of the column}]$. Dead time of the column is the time period required for a solvent to pass through a column.

Entry	Peptides	log P ⁴	R _{t1} [min]	R _{t2} [min]	R _{t3} [min]	Average R _t [min]	Capacity factor k	log k
1	Ac-FPIIV-NH2	1,61	29,52	29,48	29,49	29,50	9,171	0,962
2	Ac-WIG-NH2	0,62	22,58	22,6	22,62	22,60	6,793	0,832
3	H-WLLV-OH	0,23	27,36	27,35	27,35	27,35	8,432	0,926
4	Ac-IAV-NH2	-0,21	17,96	17,96	17,96	17,96	5,193	0,715
5	Ac-YPINV-NH2	-0,42	21,85	21,83	21,83	21,84	6,530	0,815
6	H-IVVVI-OH	-0,89	22,95	22,97	22,86	22,93	6,906	0,839
7	H-IIIIIG-OH	-0,97	22,42	22,42	22,43	22,42	6,732	0,828
8	H-SLAIV-OH	-1,94	20,91	20,92	20,93	20,92	6,214	0,793
9	H-SLI-OH	-1,99	18,62	18,61	18,6	18,61	5,417	0,734
10	H-FVG-OH	-2,33	13,83	13,82	13,82	13,82	3,767	0,576

To obtain the linear regression function, the determined log k values were plotted against the known log P values (**Figure S47**).

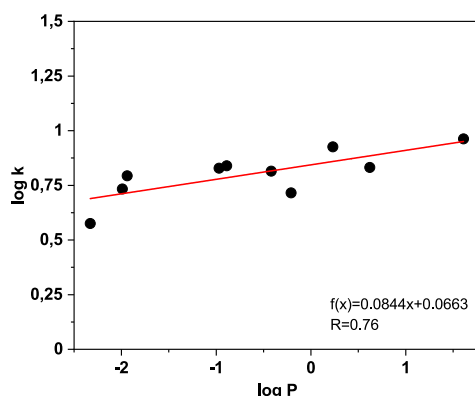


Figure S47: Log P values plotted against log k values and the corresponding linear fit function.

The obtained linear function was used to calculate the unknown log P values of fluorinated peptides **2-4** (**Table S19**). Same conditions as described above were used to determine the corresponding retention times.

Table S20: Log P values of fluorinated peptides **2-4** were estimated from determined log k values.

Peptides	R _{t1} [min]	R _{t2} [min]	R _{t3} [min]	Average R _t [min]	Capacity factor k	log k	log P
Abu ₁₀ GY(K) ₃ 2a	29,14	29,13	29,09	29,12	9,041	0,956	1,70
MfeGly ₁₀ GY(K) ₃ 2b	24,41	24,44	24,44	24,43	7,424	0,871	0,40
DfeGly ₁₀ GY(K) ₃ 2c	30,54	30,54	30,52	30,53	9,529	0,979	2,04
TfeGly ₁₀ GY(K) ₃ 2d	35,7	35,66	35,66	35,67	11,301	1,053	3,16
Abu ₁₃ GY(K) ₄ 3a	35,06	35,06	35,03	35,05	11,086	1,045	3,03
MfeGly ₁₃ GY(K) ₄ 3b	29,77	29,99	29,98	29,91	9,315	0,969	1,89
DfeGly ₁₃ GY(K) ₄ 3c	33,83	33,89	33,87	33,86	10,677	1,028	2,79
TfeGly ₁₃ GY(K) ₄ 3d	39,12	38,92	38,94	38,99	12,446	1,095	3,79
Abu ₁₅ GY(K) ₄ 4a	38,37	38,34	38,33	38,35	12,223	1,087	3,67
MfeGly ₁₅ GY(K) ₄ 4b	32,41	32,36	32,33	32,37	10,161	1,007	2,46
DfeGly ₁₅ GY(K) ₄ 4c	35,91	35,88	35,82	35,87	11,369	1,056	3,20

To verify that the hydrophobicity of fluorinated peptides **2-4** was correctly estimated, classical octan-1-ol/water partitioning experiments were carried with the Abu₁₀GY(K)₃ **2a** peptide. Other

peptides precipitated during the experiments, making it impossible to determine the log P values using this method.

To determine the log P value of Abu₁₀GY(K)₃ **2a** by partitioning experiments, according to Hill,⁵ the peptide **2a** (0.5 mg) was dissolved in 10 mL octan-1-ol saturated phosphate buffer (10 mM, pH=7.4). Starting from this stock solution, four mixtures were prepared in HPLC sample vials:

- (1) stock solution 1 mL
- (2) octan-1-ol:stock=20 μ L:1 mL
- (3) octan-1-ol:stock=200 μ L:1 mL
- (4) octan-1-ol:stock=1 mL:500 μ L

The vials were gently shaken for 90 min at 25 °C. Subsequently, the mixtures were analyzed by RP-HPLC. As stated by Hill, the aqueous phase can be analyzed directly from the HPLC vials as the injection needle can pass through the octan-1-ol phase without being contaminated by it.^[14] The corresponding chromatograms are shown in **Figure S48**.

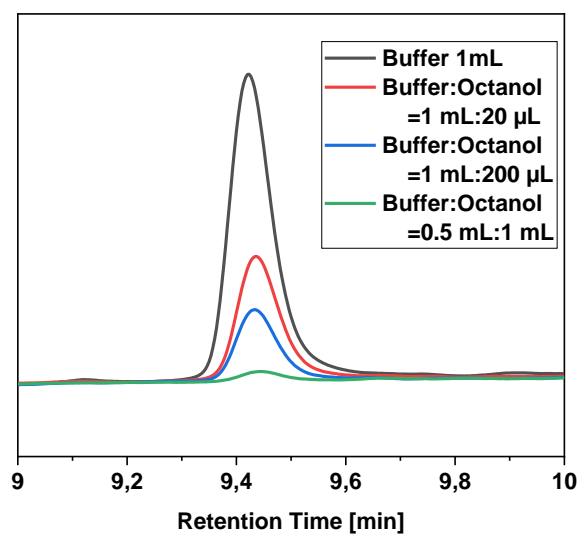


Figure S48: HPLC chromatograms of corresponding samples (1), (2), (3), and (4).

By integrating the peak area, the log P value can be calculated using the following equation:

$$\log P = \log \left(\frac{A_1 A_F V_W}{A_F V_O} \right) \quad (\text{eq. 1})$$

A_1 : peak area of the stock solution (sample (1))

A_F : peak area of the samples (2-4)

V_O : volume of the octan-1-ol phase

V_W : volume of the aqueous phase

For Abu₁₀GY(K)₃ **2a** a log P value of 1.56±0.30 was determined, which is in an excellent agreement with the estimated log P value that was determined using the HPLC-based assay.

5. 6-FAM leaking assay – further data

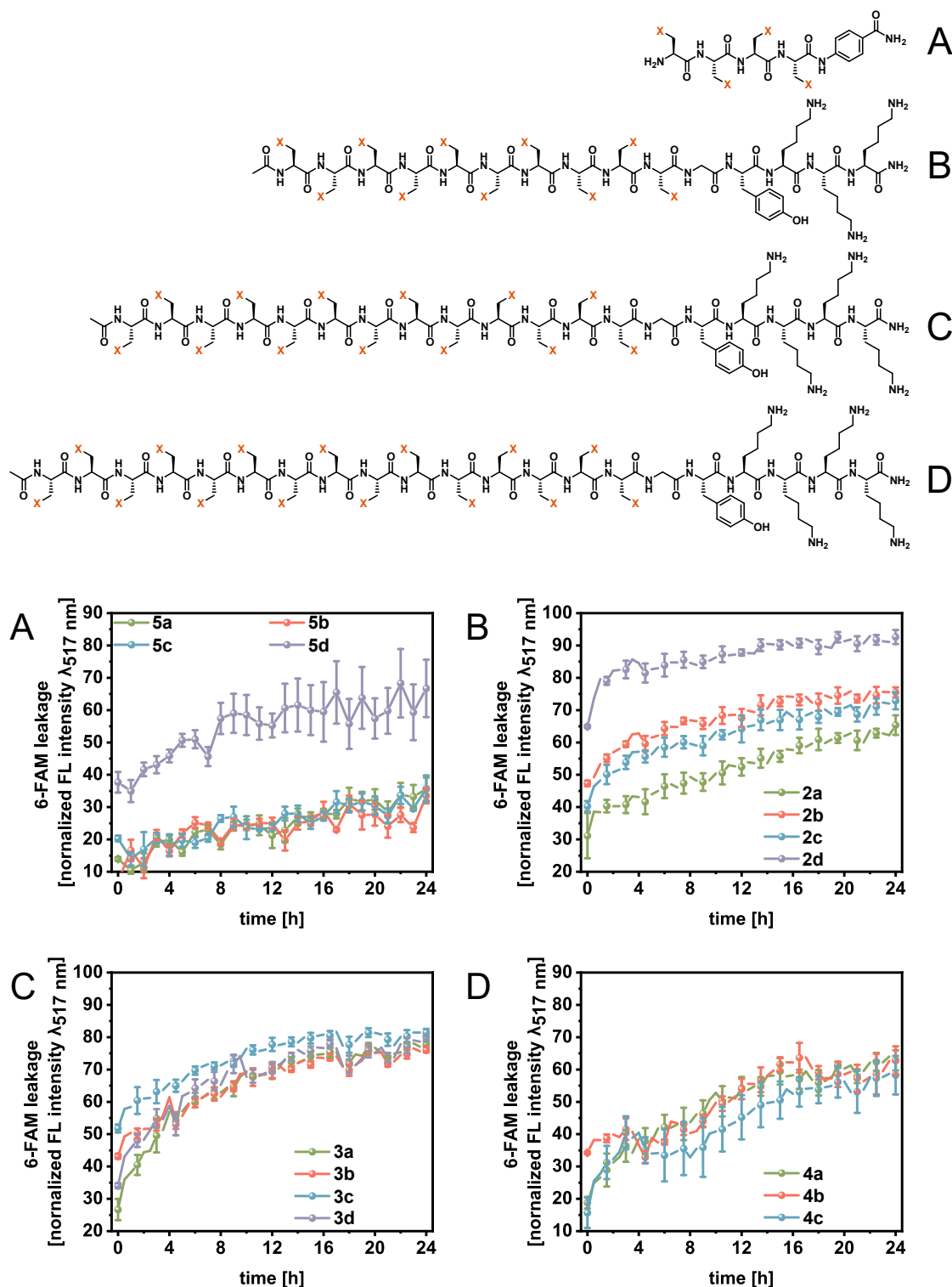


Figure S49: Real-time monitoring of peptide-caused 6-FAM leaking: The dye was encapsulated in 5 mM liposome solution (POPC:POPC [1:1]) and its release upon incubation (37 °C, 24 h) with homooligopeptides $[X]_4[4]Abz$ (A, 100 μ M), $X_{10}GY(K)_3$ (B, 50 μ M), $X_{13}GY(K)_4$ (C, 50 μ M) and $X_{15}GY(K)_4$ (D, 50 μ M) was detected *via* fluorescence spectroscopy ($\lambda_{ex}=493$ nm/ $\lambda_{em}=517$ nm). FL values were normalized to 100% dye release (5% (v/v) Triton X-100 in buffer).

6. Peptide digestion assay

The proteolytic digestion studies of peptides were monitored through a Hitachi Primaide™ UV-HPLC system (VWR/Hitachi, Darmstadt, Germany). A Kinetex® RP-C18 (5 μM, 100 Å, 250 x 4.6 mm, Phenomenex®, USA) column and a SecurityGuard™ Cartridge Kit equipped with a C18 cartridge (4 x 3.0mm, Phenomenex®, USA)) as pre-column was used. As eluents water and ACN, both containing 0.1% (v/v) TFA were applied. A flow rate of 1 mL/min was used and UV-detection occurred at 280 nm for respective peptides. Data analysis was done with EZ Chrom ELITE software (version 3.3.2, Agilent). The calculation of remaining peptide amount was done with OriginPro 2020b (OriginLab Corporation, Northampton, MA, USA).

Table S21: Analytical HPLC conditions for peptide digestion assay (real-time monitoring).

Time (min)	Eluent (A)	Eluent (B)	Flow (mL/min)
0.0	95.0	5.0	1.0
5.0	95.0	5.0	1.0
20.0	50.0	50.0	1.0
22.0	0.0	100.0	1.0
24.0	0.0	100.0	1.0
26.0	95.0	5.0	1.0
30.0	95.0	5.0	1.0

Due to the highly hydrophobic nature of the truncated homopeptides **5a-5d**, negative controls of these peptides were initially probed to determine the impact of peptide aggregation during the experiment. Here, the peptides (0.23 mM) were dissolved in 50 mM BTP + 20 mM CaCl₂; pH 8 **without enzyme (!)** and incubated for 24 h at 30 °C as described in the main paper. Aliquots (15 μL) were diluted with 30% AcOH + 0.13 mM reference (90 μL) and the remaining content of soluble peptide was determined through HPLC analysis (all at DAD-280 nm) (see **Figure S50**). We detected partial aggregation these peptides while the amount of soluble peptide decreases with time. Obviously, the effect of aggregation enhances with increasing hydrophobicity of the fluorinated amino acids. (MfeGly < Abu < DfeGly < TfeGly). However, the loss in soluble peptide is rather neglectable with respect to the digestion profiles shown for elastase after 6 h and for proteinase k after 3 h in the main paper.

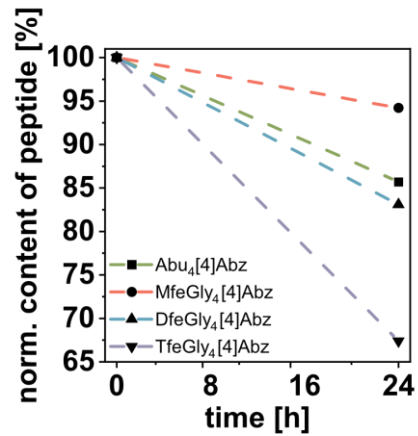
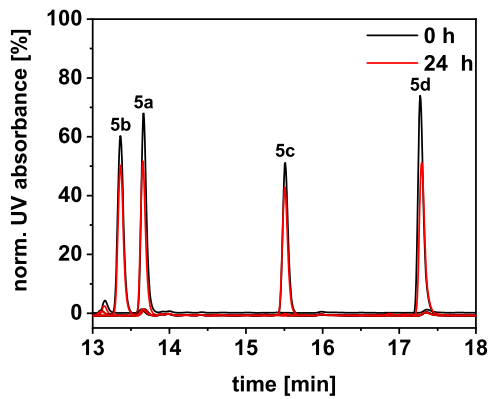


Figure S50: HPLC chromatograms (negative controls) of fluoropeptides Abu₄[4]Abz **5a**, MfeGly₄[4]Abz **5b**, DfeGly₄[4]Abz **5c** and TfeGly₄[4]Abz **5d** after incubation according to the standard digestion protocol after 0 h and 24 h (left). Schematic representation of normalized peptide content over a time period of 24 hours (right).

In **Figure S51**, HPLC chromatograms (all at DAD-280 nm) derived from the peptide digestion assays are illustrated. Peptide amounts decreased significantly faster than for the negative controls validating the degradation of substrates through both serine proteases elastase + proteinase k.

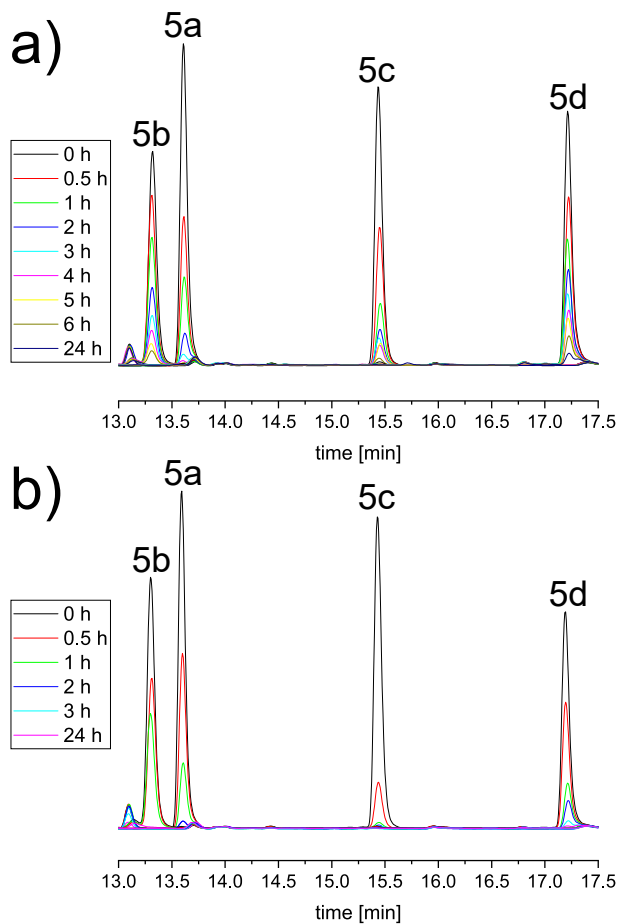


Figure S51: Real-time monitoring on the proteolytic digestion profile of fluoropeptides Abu₄[4]Abz **5a**, MfeGly₄[4]Abz **5b**, DfeGly₄[4]Abz **5c** and TfeGly₄[4]Abz **5d** (each 230 μM) in **a)** elastase (0.91 μM) or **b)** proteinase K (0.0091 μM) dissolved in 50 mM Bis-tris propane + 20 mM CaCl₂ (pH 8) [75%] + DMSO [25%] and incubation at 30 °C.

For identification of digestion products derived from Abu₄[4]Abz **5a**, MfeGly₄[4]Abz **5b**, DfeGly₄[4]Abz **5c** and TfeGly₄[4]Abz **5d**, non-quenched aliquots were taken from the reaction mixture and screened through HPLC analysis (all at DAD-280 nm) after 24 h incubation to ensure complete proteolysis of the substrate. For each peptide, **one particular digestion fragment** cleaved from the full-length peptide was identified *via* HPLC (highlighted in grey color in the chromatograms) and, subsequently, analyzed by ESI–ToF mass analysis on an Agilent 6220 ESI–ToF–MS spectrometer (Agilent Technologies, Santa Clara, CA, USA). The HPLC conditions are listed in **table 22** and the HPLC & MS spectra in **Figure 51-54**. Comparison of given analytical data on enzymatic digestion to the full-length peptides reference HPLC chromatograms [“**Peptide (ref.)**”, each top chromatogram in **Figure 51-54**] before addition of the enzymatic solution confirmed complete consumption of the substrate. Further reference HPLC chromatograms [“**Proteinase K (ref.)**” and “**Elastase (ref.)**”, highlighted in yellow] of the buffered enzyme stock solutions were recorded to differ between the HPLC signals of formed digestion products [“**Peptide + Proteinase K (dig.)**” and “**Peptide + Elastase (dig.)**”] and enzyme-related autolysis.

Table S22: Analytical HPLC conditions for peptide digestion assay (fragment-identification).

Time (min)	Eluent (A)	Eluent (B)	Flow (mL/min)
0.0	90.0	10.0	1.0
18.0	60.0	40.0	1.0
20.0	0	100.0	1.0
22.0	0	100.0	1.0
23.0	90.0	10.0	1.0
25.0	90.0	10.0	1.0

It becomes apparent that detection and identification of the Abz-labeled fragments Abu[4]Abz, MfeGly[4]Abz, DfeGly[4]Abz and TfeGly[4]Abz validates the existence of a predominant cleaving site for the fluoropeptides. For both digestive enzymes, two consecutive amino acids “Abu-Abu”, “MfeGly-MfeGly”, “DfeGly-DfeGly” and “TfeGly-TfeGly” serve as P1-P1’ residues (according to *Schechter & Berger* nomenclature) bearing the hydrolyzed amide bond.^[15] A proposed model on enzyme-substrate recognition is illustrated in **Figure 55**.

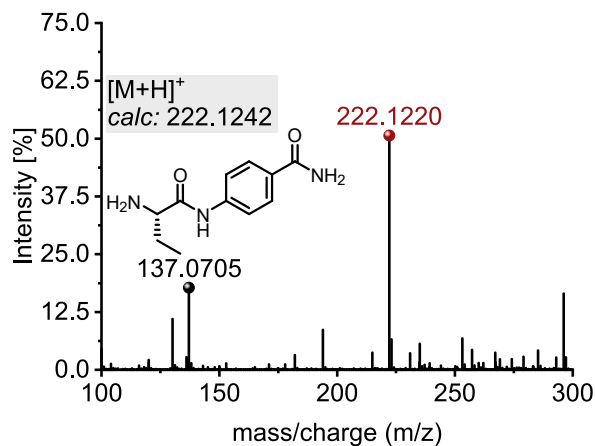
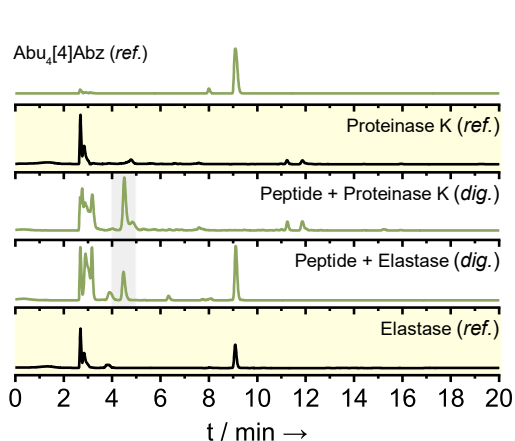


Figure S51: Digestion-fragment analysis on the proteolytic digestion profile of Abu₄[4]Abz **5a** (230 μM) in elastase (0.91 μM) and proteinase K (0.0091 μM) dissolved in 50 mM Bis-tris propane + 20 mM CaCl₂ (pH 8) [75%] + DMSO [25%] after 24 h incubation at 30 °C. The Abz-labeled compound Abu[4]Abz (HPLC signal is highlighted in grey) was determined as main digestion product *via* HRMS.

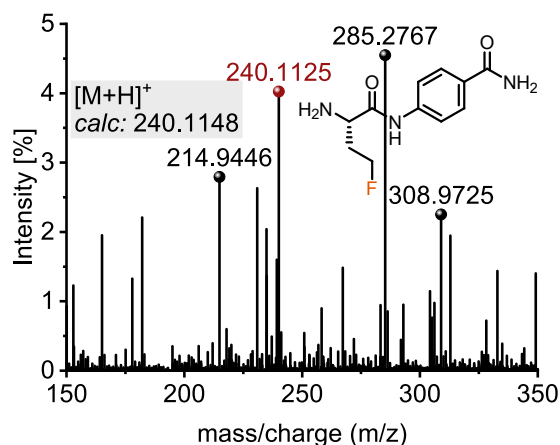
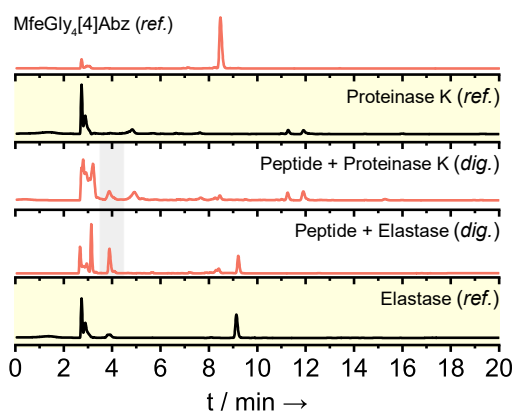


Figure S52: Digestion-fragment analysis on the proteolytic digestion profile of MfeGly₄[4]Abz **5b** (230 μM) in elastase (0.91 μM) and proteinase K (0.0091 μM) dissolved in 50 mM Bis-tris propane + 20 mM CaCl₂ (pH 8) [75%] + DMSO [25%] after 24 h incubation at 30 °C. The Abz-labeled compound MfeGly[4]Abz (HPLC signal is highlighted in grey) was determined as main digestion product *via* HRMS.

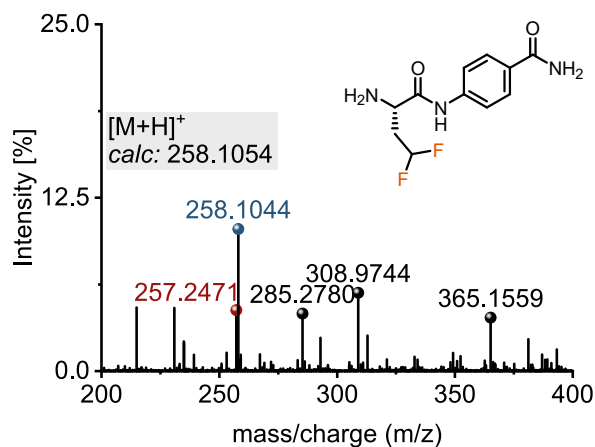
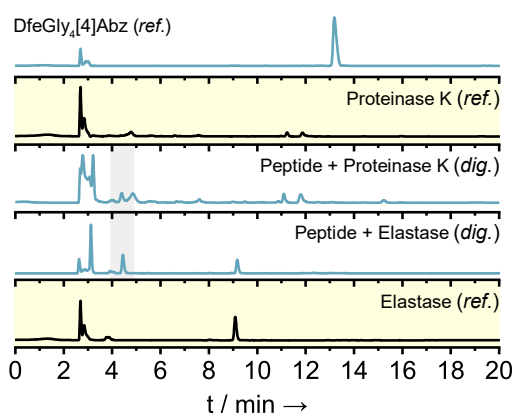


Figure S53: Digestion-fragment analysis on the proteolytic digestion profile of DfeGly₄[4]Abz **5c** (230 μM) in elastase (0.91 μM) and proteinase K (0.0091 μM) dissolved in 50 mM Bis-tris propane + 20 mM CaCl₂ (pH 8) [75%] + DMSO [25%] after 24 h incubation at 30 °C. The Abz-labeled compound DfeGly[4]Abz (HPLC signal is highlighted in grey) was determined as main digestion product *via* HRMS.

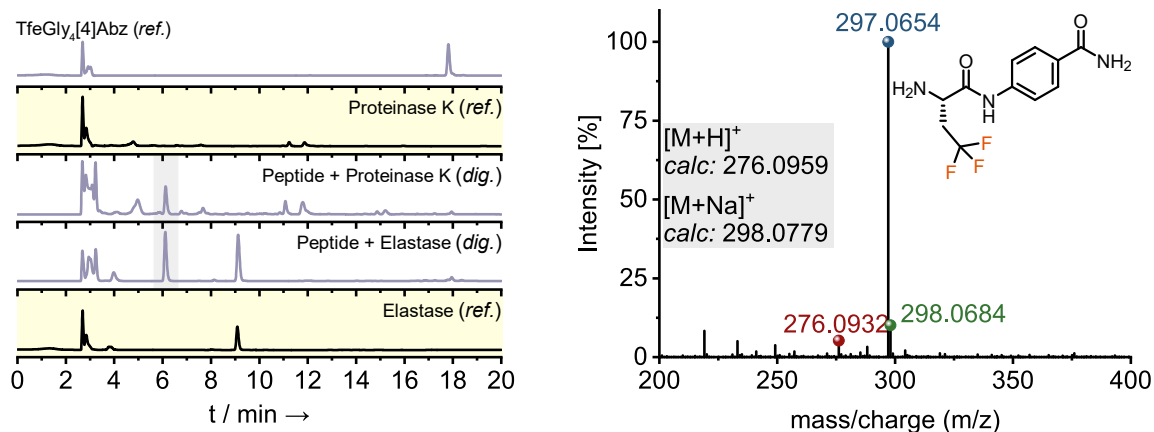


Figure S54: Digestion-fragment analysis on the proteolytic digestion profile of TfeGly₄[4]Abz **5d** (230 μM) in elastase (0.91 μM) and proteinase K (0.0091 μM) dissolved in 50 mM Bis-tris propane + 20 mM CaCl₂ (pH 8) [75%] + DMSO [25%] after 24 h incubation at 30 °C. The Abz-labeled compound TfeGly₄[4]Abz (HPLC signal is highlighted in grey) was determined as main digestion product *via* HRMS.

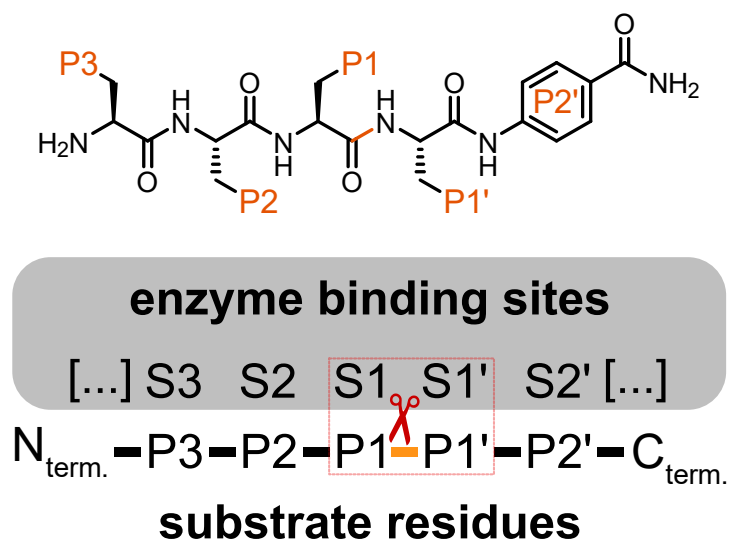


Figure S55: Simplified model of enzyme-substrate interaction despite the side chains' fluorine-content according to Schechter & Berger nomenclature.^[15]

7. References

- [1] T. Hohmann, M. Dyrks, S. Chowdhary, M. Weber, D. Nguyen, J. Moschner, B. Kokschi, *The Journal of Organic Chemistry* **2022**, *87*, 10592-10604.
- [2] J. Han, R. Takeda, X. Liu, H. Konno, H. Abe, T. Hiramatsu, H. Moriwaki, V. A. Soloshonok, *Molecules (Basel, Switzerland)* **2019**, *24*, 4521.
- [3] J. Leppkes, N. Dimos, B. Loll, T. Hohmann, M. Dyrks, A. R. Wieseke, B. G. Keller, B. Kokschi, *RSC Chemical Biology* **2022**.
- [4] M. L. Tiffany, S. Krimm, *Biopolymers* **1968**, *6*, 1379-1382.
- [5] R. W. Woody, *Journal of the American Chemical Society* **2009**, *131*, 8234-8245.
- [6] W. L. Mattice, *Biopolymers* **1974**, *13*, 169-183.
- [7] aF. Eker, X. Cao, L. Nafie, R. Schweitzer-Stenner, *Journal of the American Chemical Society* **2002**, *124*, 14330-14341; bF. Eker, K. Griebenow, R. Schweitzer-Stenner, *Journal of the American Chemical Society* **2003**, *125*, 8178-8185; cR. Schweitzer-Stenner, F. Eker, K. Griebenow, X. Cao, L. A. Nafie, *Journal of the American Chemical Society* **2004**, *126*, 2768-2776; dR. Schweitzer-Stenner, T. Measey, L. Kakalis, F. Jordan, S. Pizzanelli, C. Forte, K. Griebenow, *Biochemistry* **2007**, *46*, 1587-1596.
- [8] aZ. Shi, C. A. Olson, D. Rose George, L. Baldwin Robert, R. Kallenbach Neville, *Proceedings of the National Academy of Sciences* **2002**, *99*, 9190-9195; bZ. Liu, K. Chen, A. Ng, Z. Shi, R. W. Woody, N. R. Kallenbach, *Journal of the American Chemical Society* **2004**, *126*, 15141-15150.
- [9] aM. A. Kelly, B. W. Chellgren, A. L. Rucker, J. M. Troutman, M. G. Fried, A.-F. Miller, T. P. Creamer, *Biochemistry* **2001**, *40*, 14376-14383; bA. L. Rucker, T. P. Creamer, *Protein science : a publication of the Protein Society* **2002**, *11*, 980-985; cA. L. Rucker, C. T. Pager, M. N. Campbell, J. E. Qualls, T. P. Creamer, *Proteins: Structure, Function, and Bioinformatics* **2003**, *53*, 68-75; dE. A. Bienkiewicz, A. Y. Moon Woody, R. W. Woody, *Journal of Molecular Biology* **2000**, *297*, 119-133; eA. K. Pandey, K. M. Thomas, C. R. Forbes, N. J. Zondlo, *Biochemistry* **2014**, *53*, 5307-5314.
- [10] Z. Shi, R. W. Woody, N. R. Kallenbach, in *Advances in Protein Chemistry, Vol. 62*, Academic Press, **2002**, pp. 163-240.
- [11] A. Barth, *Biochim Biophys Acta* **2007**, *1767*, 1073-1101.
- [12] A. Rodil, S. Bosisio, M. S. Ayoub, L. Quinn, D. B. Cordes, A. M. Z. Slawin, C. D. Murphy, J. Michel, D. O'Hagan, *Chemical Science* **2018**, *9*, 3023-3028.
- [13] aM. Akamatsu, Y. Yoshida, H. Nakamura, M. Asao, H. Iwamura, T. Fujita, *Quantitative Structure-Activity Relationships* **1989**, *8*, 195-203; bM. Akamatsu, S.-I. Okutani, K. Nakao, N. J. Hong, T. Fujita, *Quantitative Structure-Activity Relationships* **1990**, *9*, 189-194; cM. Akamatsu, T. Fujita, *Journal of Pharmaceutical Sciences* **1992**, *81*, 164-174.
- [14] K. Valkó, in *Handbook of Analytical Separations, Vol. 1* (Ed.: K. Valkó), Elsevier Science B.V., **2000**, pp. 535-583.
- [15] I. Schechter, A. Berger, *Biochemical and Biophysical Research Communications* **1967**, *27*, 157-162.

7 Cooperation projects & unpublished work

In this chapter, unpublished data derived from ongoing research about the biodegradability (**Section 7.1**) and biocompatibility (**Section 7.2**) of polyfluorinated & amphiphilic SAPs (**Section 6.1**) will be discussed. **Section 7.1** contains figures which are part of a recently submitted manuscript entitled “*Biodegradation of amphipathic fluorinated peptides reveals a new bacterial defluorinating activity and a new source of natural organofluorine compounds.*” written by Mohd Faheem Khan, **Suvrat Chowdhary**, Beate Koksich and Cormac D. Murphy (Submission: 14 February 2023).

7.1 Biodegradation of fluorinated amphipathic peptides and amino acids (with Prof. Dr. Cormac D. Murphy, University College Dublin)

At first, recent results on the enzymatic digestion of amphipathic peptides AbuK16, MfeGlyK16, DfeGlyK16 and TfeGlyK16 (**Section 6.1**) are discussed. Three serine proteases (β -trypsin, elastase, proteinase K) and one cysteine protease (bromelain) were selected; the catalytic mechanisms of serine and cysteine peptidases are very similar and discussed in-depth in **Section 4**. Amino acid and peptide synthesis, CD spectroscopic measurements and HPLC-based experiments on the enzymatic degradation were applied and evaluated by **Suvrat Chowdhary** (Freie Universität Berlin). All experiments on the microbial degradation of fluorinated peptides and amino acids were performed by Dr. Mohd Faheem Khan under the supervision of Prof. Dr. Cormac D. Murphy (University College Dublin, Ireland).

Initially, buffered conditions were established in which the amphipathic SAPs are rather present as monomeric units than β -sheet-based fibrillary structures. When dissolved in 50 mM BTP buffer supplemented with 20 mM CaCl_2 , AbuK16 and MfeGlyK16 adopted a PPII-like conformation. For DfeGlyK16, a random coil conformation was observed which confirmed the formation of soluble & monomeric / disordered structures as well.²⁴³ The CD spectrum of TfeGlyK16 has two local minima at 220 and 204 nm (**Figure 7.1a**). An analog CD pattern obtained from the amphipathic peptide Ac-(AAKA)₄-NH₂ was reported by Schweitzer-Stenner and co-workers and was interpreted as a multi-state folding conformation including PPIIs, β -strands, and α -helix-like structures.²⁴⁴ Afterwards, RP-HPLC based real-time monitoring of enzyme-catalyzed peptide proteolysis was employed with above-mentioned endopeptidases. The digestion plots are presented in **Figure 7.1b**.

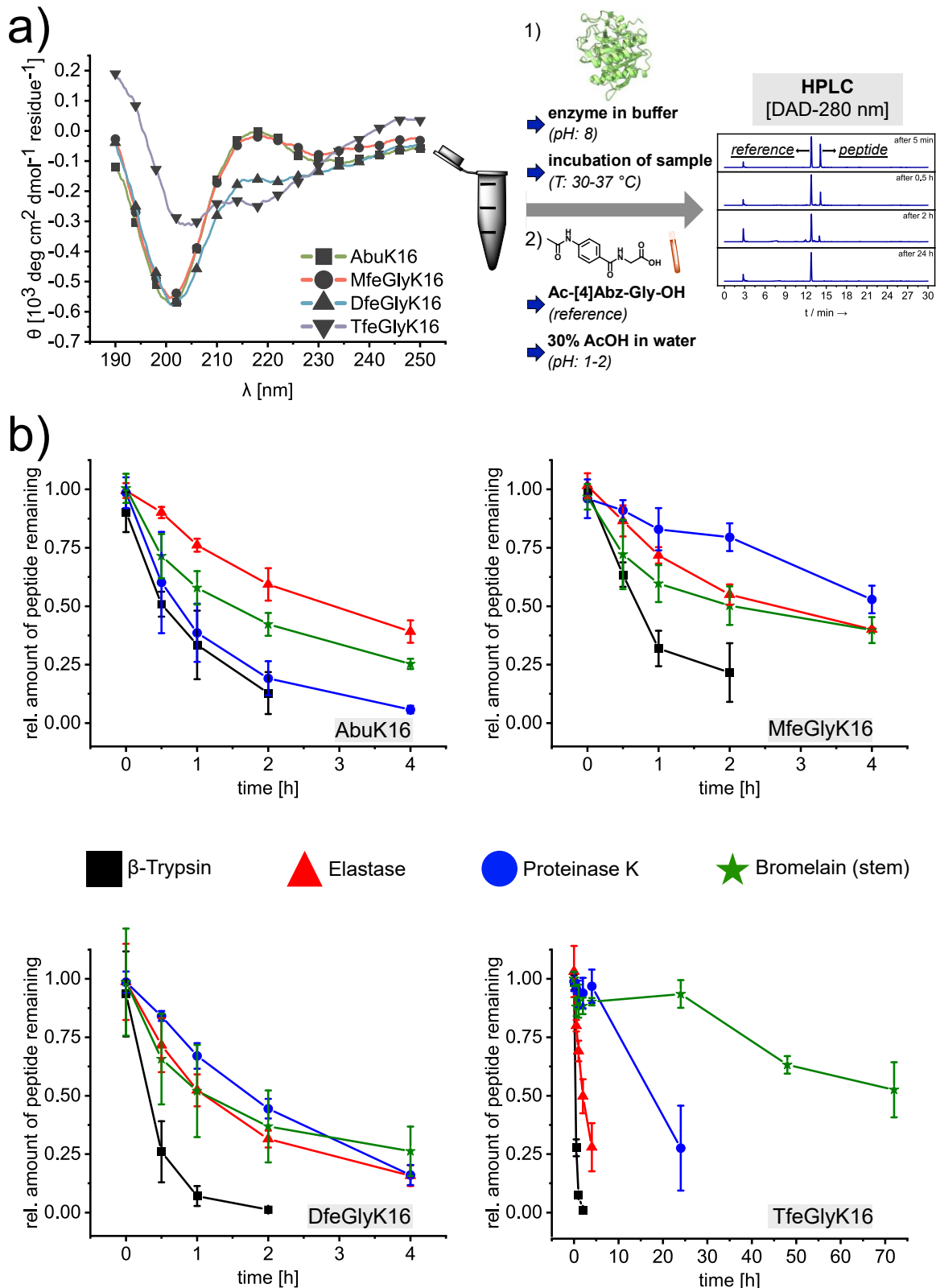


Figure 7.1 a) CD spectra of amphipathic peptides AbuK16, MfeGlyK16, DfeGlyK16 and TfeGlyK16 (all 0.5 mM) in 50 mM Bis-tris propane + 20 mM CaCl₂, pH 8.0, recorded at 37 °C (**left**). General workflow of the RP-HPLC based peptide digestion assay – non-gelating conditions (50 mM Bis-tris propane + 20 mM CaCl₂, pH 8.0) were required to enable HPLC-based monitoring of substrate digestion (**right**). **b)** Proteolytic digestion plots of amphipathic peptides AbuK16, MfeGlyK16, DfeGlyK16 and TfeGlyK16 (500 μ M stock) obtained for β -trypsin (0.075 μ M stock), elastase (0.45 μ M stock), proteinase k (0.075 μ M stock) and bromelain (stem, 4.5 μ M stock) in analog conditions. Values were normalized to the amount of specific peptide detected after 5 min of incubation. All digestion profiles represent the average of minimum three independent measurements. Errors are derived from the standard deviation.

In case of β -trypsin, a decrease in proteolytic resistance was observed when, surprisingly, a higher degree of fluorination was present. After 2 h, both peptides DfeGlyK16 [$1 \pm 0.5\%$] and TfeGlyK16 [$1 + 0.6\%$] were mostly digested, whereas higher amounts of peptide were detected for AbuK16 [$13 \pm 9\%$] and MfeGlyK16 [$22 \pm 13\%$]. Similar results were obtained for elastase after 4 h of incubation and, thus, lower amounts of DfeGlyK16 [$16 \pm 4\%$] and TfeGlyK16 [$28 \pm 10\%$] than for AbuK16 [$40 \pm 5\%$] and MfeGlyK16 [$40 \pm 0.6\%$] were detected.

These conclusions can, however, not be generalized since proteinase k and bromelain reveal different trends in their digestion plots. After 4 h of incubation, the digestion plots of proteinase k revealed a higher proteolytic stability of MfeGlyK16 [$53 \pm 6\%$] compared to $6 \pm 2\%$ and $16 \pm 4\%$ which were determined for AbuK16 and DfeGlyK16. Moreover, TfeGlyK16 [$97 \pm 7\%$] remained stable towards proteinase k for 4 h, whereas significantly lower amounts [$28 \pm 19\%$] upon proteolysis were detectable after 24 h. For the cysteine protease bromelain, TfeGlyK16 was found to be comparably persistent over several days. Whereas AbuK16 [$6 \pm 0.7\%$], MfeGlyK16 [$20 \pm 3\%$] and DfeGlyK16 [$7 \pm 3\%$] were mainly digested within 4 h, $93 \pm 6\%$ of remaining TfeGlyK16 were still present after 24 h. Even after 3 days of incubation, this peptide was found in noticeable amounts [$52 \pm 11\%$], indicating considerable stabilization of this peptide motif towards degradation by this cysteine protease.

Thus, the fluorinated SAPs are broadly susceptible to proteolytic digestion, but the degree of degradation depended on the enzyme employed and the extent of fluorination. However, a more detailed investigation of the peptides' degradation was warranted owing to the lack of enzymes in the biosphere that have evolved to specifically cleave the carbon-fluorine bond (see **Section 3.3**). Further studies on the biodegradation of these fluorinated peptides by microorganisms became indispensably important, since both the production and application of such materials is accompanied by their environmental exposure and that may have significant impacts on wild-life and human health as controversially discussed for some PFASs as ubiquitous pollutants and health hazards.¹⁷⁸ In the present work, a soil microbial (SM) consortium cultivated from Irish soil was employed by Dr. Mohd Faheem Khan and Prof. Dr. Cormac D. Murphy (University College Dublin, Ireland) since they own a broad range of proteases and other enzymes that might contribute to the biotransformation of the polyfluorinated substrates. In first biodegradation studies, this consortium was initially cultivated in tryptic soy broth (TSB)

for 24 h before the peptides MfeGlyK16, DfeGlyK16 and TfeGlyK16 were added into the media culture, and the incubation continued for 48 h (**Figure 7.2a**).

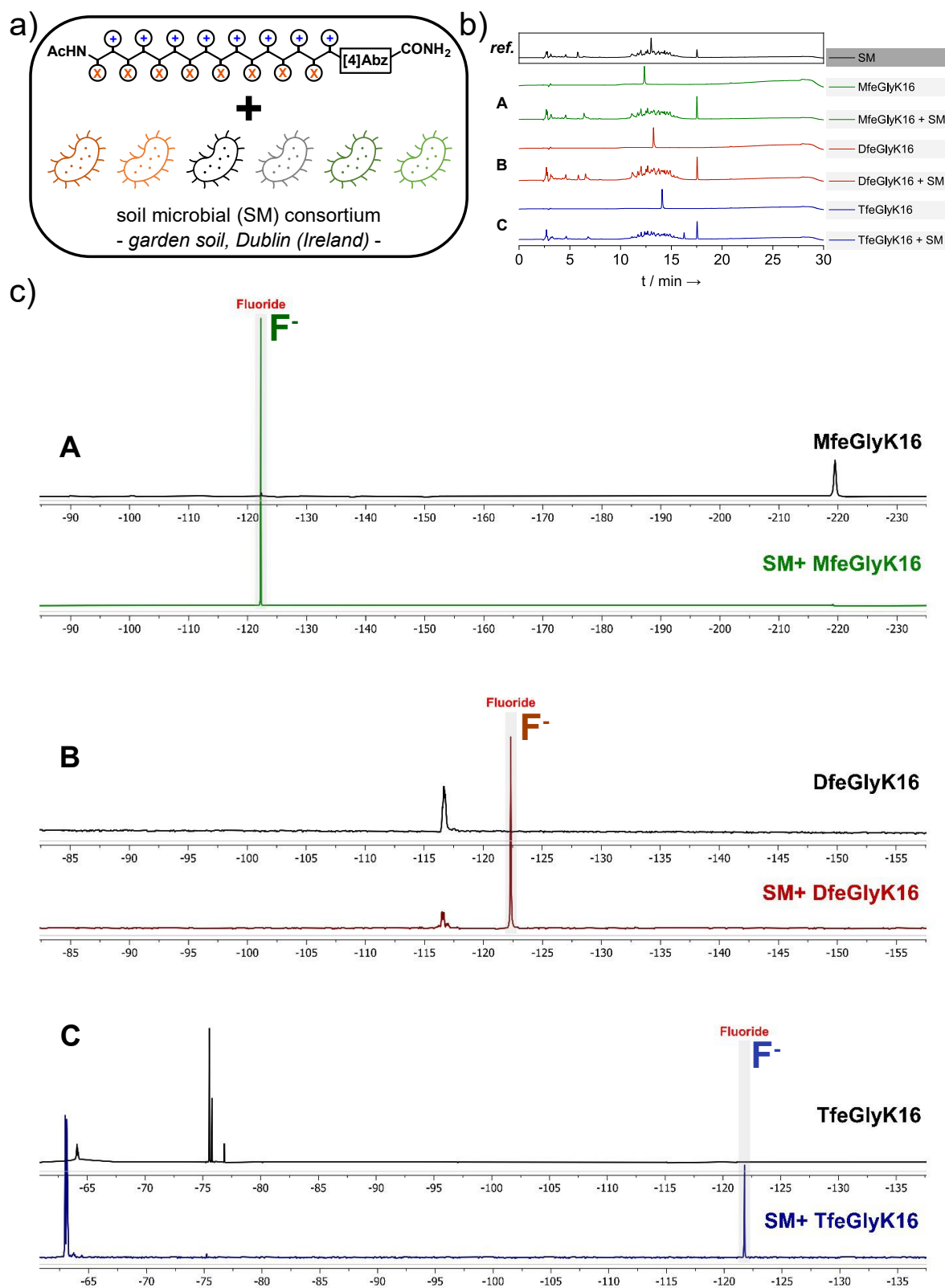
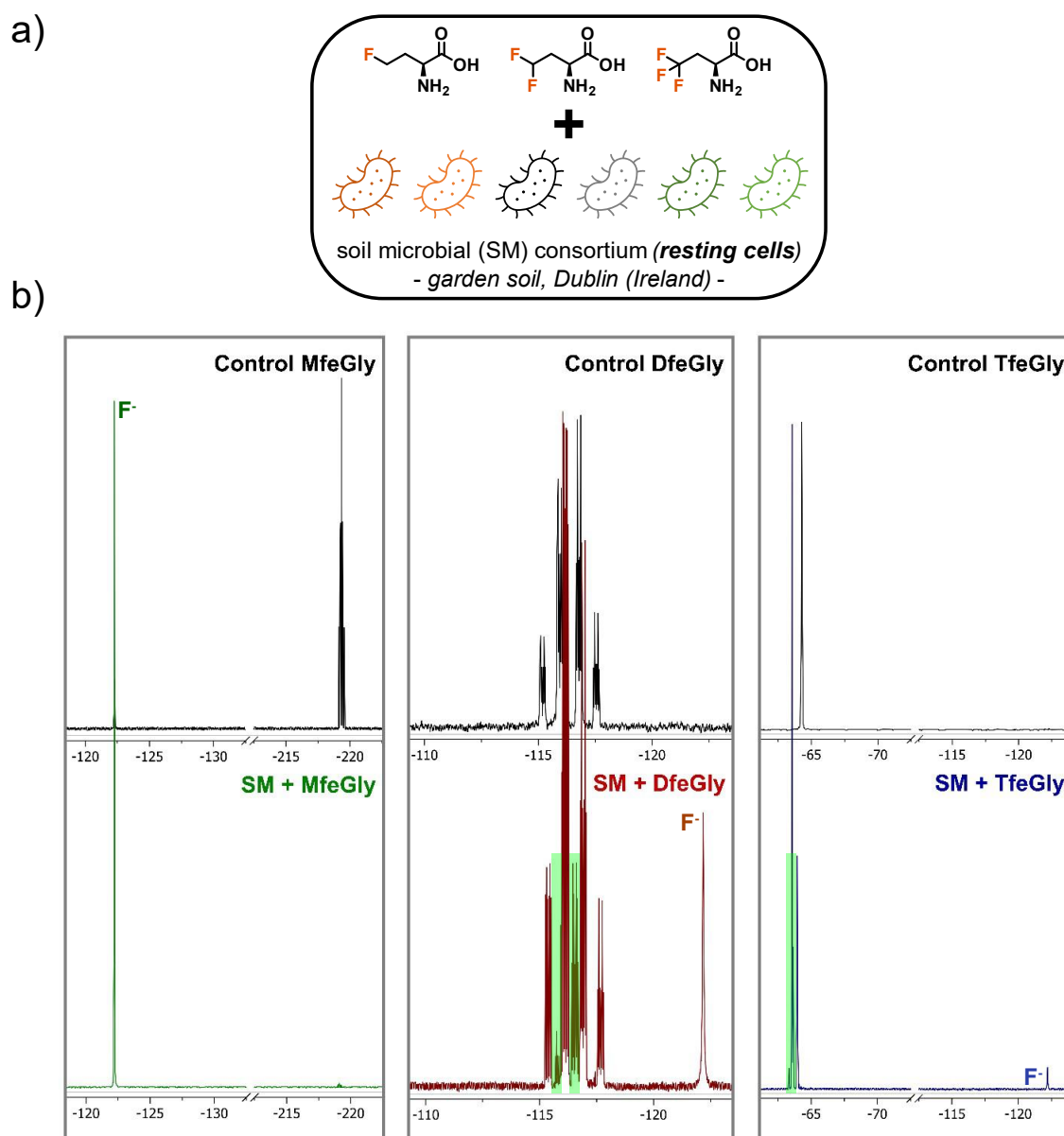


Figure 7.2 a) Schematic illustration of the experimental setup. **b)** HPLC chromatograms (DAD-220 nm) and **c)** ¹⁹F NMR spectra of "A" – MfeGlyK16, "B" – DfeGlyK16 and "C" – TfeGlyK16 as sole peptide and after incubation with soil microbes (SM). The HPLC experiments were accomplished by **Suvrat Chowdhary**. Biodegradation experiments were accomplished by Dr. Mohd Faheem Khan and Prof. Dr. Cormac D. Murphy.

HPLC analysis of the culture supernatants displayed a loss of the substrates' HPLCs signal, thereby confirming peptide hydrolysis (**Figure 7.2b**). Most noteworthy, ^{19}F NMR spectra revealed the release of fluoride ions (δ : -122 – -123 ppm) which indicated the individual amino acids to be metabolized by the SM consortium (**Figure 7.2c**).

To investigate if further degradation of the different fluorinated side chains takes place, the fluorinated amino acids MfeGly, DfeGly and TfeGly were incubated with resting cells of the soil bacteria and the products were monitored by ^{19}F NMR after 48 h incubation (**Figure 7.3a**). In brief, a resting cell suspension in this experiment comprises the bacteria consortium suspended in non-growth medium (HEPES buffer) instead of TSB so that cell mitosis is absent or much decreased (interphase).²⁴⁵



Therefore, the fluorinated amino acids added to the soil microbial consortium served as sole carbon and energy source required for bacteria growth. Comparison of the relative resonance intensities in the ^{19}F NMR spectra suggested the occurrence of bacteria-induced amino acid defluorination but its extent to be decreased by a higher degree of fluorine-substitution (MfeGly > DfeGly > TfeGly). In fact, the NMR spectrum with MfeGly as substrate confirmed its complete degradation by the bacteria, whereas the emergence of additional NMR signals in the spectra of DfeGly (δ : -117 ppm) and TfeGly (δ : -64 ppm) indicate the intermediate formation of biotransformed fluorometabolites (**Figure 7.3b**). Next, cell free extracts (in HEPES buffer) of the microbial consortium (CF SM) were prepared by harvesting the cells cultivated in TSB media, followed by their suspension in HEPES buffer (as for the resting cells) and subsequent membrane lysis *via* sonication. In consequence, the cell free extracts served as multi-enzyme solution *in vitro* (**Figure 7.4**). This experiment was suggested to determine if the microbial degradation originates from an enzyme-catalyzed defluorination apart from a full cell system. Additionally, an enrichment culture was established on agar plates with the fluorinated amino acid MfeGly as sole carbon source and best substrate for defluorination as applied for the resting cells. This approach enables the efficient enrichment and selection of microorganisms that succeeded in microbial growth by metabolizing this substrate. One grown strain (strain B) was depicted from the agar plates, then cultivated in TSB media before resuspension in buffer, cell lysis and separation of its cell free extract (CF Strain B, in HEPES buffer). To investigate the enzyme-catalyzed defluorination of MfeGly, this amino acid was incubated with both cell free extracts for 6 h and subsequent analysis by GC-MS was applied after the remaining substrate and metabolites in the culture extracts were derivatized by silylation. TIC chromatograms displaying both approaches on enzymatic degradation reveal the formation of one main digestion product from MfeGly [$m/z_{\text{GC-MS}}$ = calc.: 265.13 / found: 265.1 (silylated)] which was identified as homoserine [$m/z_{\text{GC-MS}}$ = calc.: 335.17 / found: 335.1 (silylated)]. These results emphasized the presence of an enzyme in the SM extract and, particularly, in the isolated strain B with a similar mechanism than the known *fluoroacetate dehalogenase* that is capable to cleave a carbon-fluoride bond, the strongest carbon-halogen bond in nature, *via* nucleophilic substitution.¹⁷³ Therefore, a further control experiment on the microbial degradation of MfeGly through strain B was settled including the fluoroacetate-degrading microbe *P. fluorescens* DSM 8341 and fluoroacetate as control substrate.¹⁷⁶

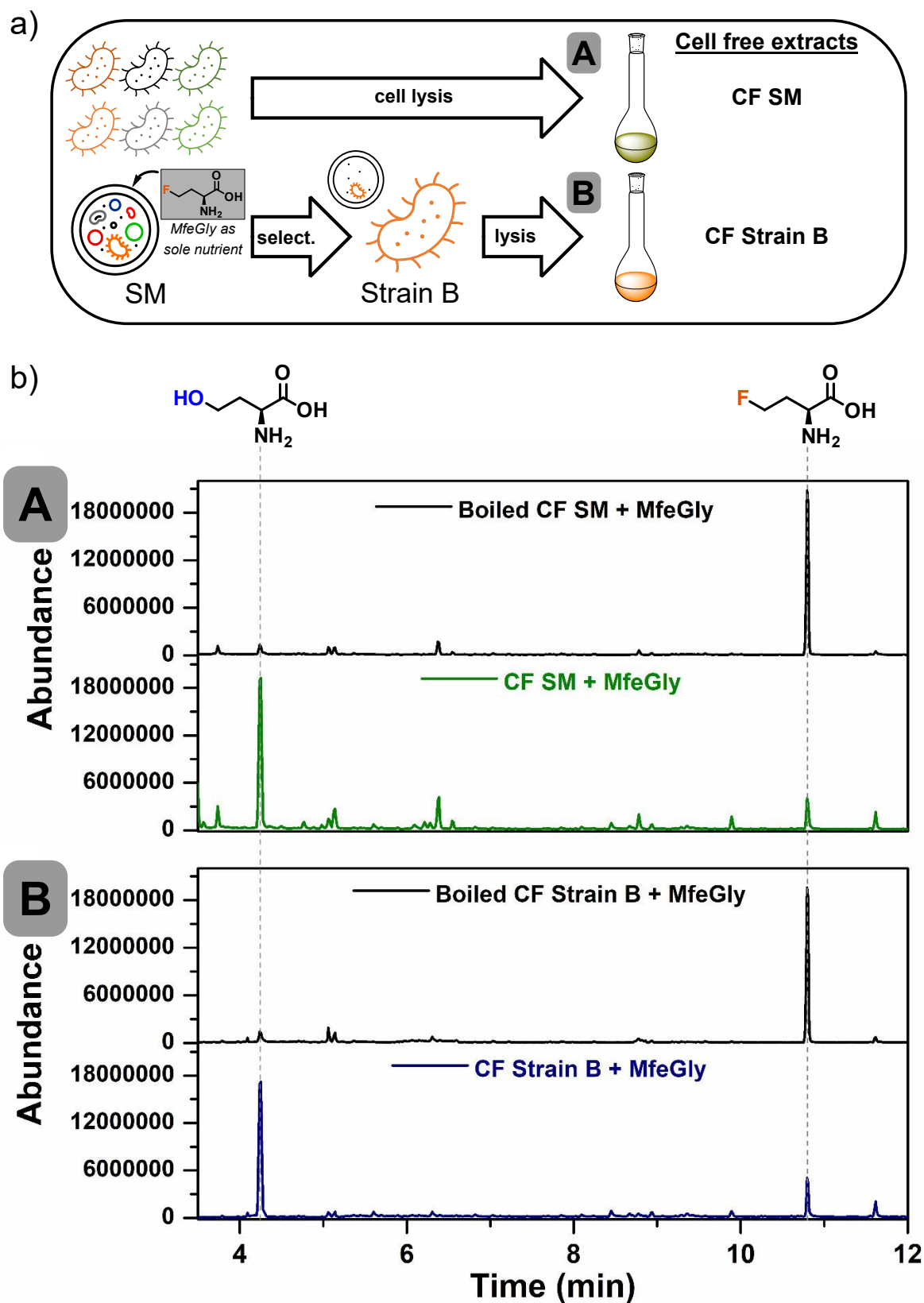


Figure 7.4 Schematic illustration of the experimental setup. Two different approaches [“A”: Cell free extract of the total SM / “B”: Cell free extract of isolated strain B] were applied to study enzyme-catalyzed C-F bond cleavage. **b)** TIC chromatograms (measured and analyzed by Dr. Mohd Faheem Khan and Prof. Dr. Cormac D. Murphy) of silylated CF extracts from SM (“A”) and strain B (“B”) after incubation with MfeGly (6 h) leading to the formation of homoserine. Further experiments with boiled extracts are included as control experiments.

Fluoride ion release was measured using a colorimetric assay (**Section 8.7**) that is based on an UV-detectable fluoride-binding reaction of lanthanum-alizarin complexes.²⁴⁶ As demonstrated in **Figure 7.5**, both bacterial strains were found to hydrolyze the C-F bond of MfeGly as well as fluoroacetate.

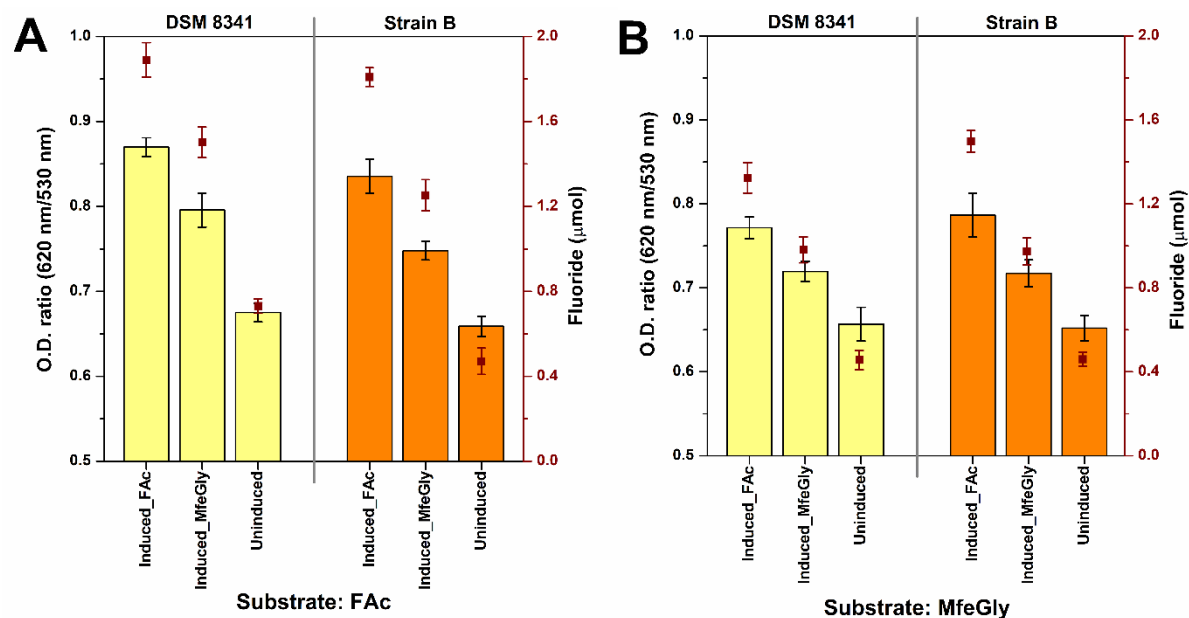


Figure 7.5 Colorimetric detection of fluoride ion release after microbial degradation through *P. fluorescens* DSM 8341 and strain B with “A” fluoroacetate (FAC) and “B” MfeGly for 6 h. The bacteria were cultivated in TSB media either with (induced) and without (uninduced) added substrates to promote defluorinating activity.

In summary, this data set appoints a novel defluorinating activity derived from an Irish soil bacterium with key similarities on substrate conversion to other known *fluoroacetate dehalogenases*.

7.2 Cytotoxicity and hemolytic activity of AbuK16, MfeGlyK16, DfeGlyK16 and TfeGlyK16 (unpublished work)

In this chapter, first results on the biocompatibility of the (fluorinated) SAPs (**Section 6.1**) are presented. These are part of ongoing studies and have therefore remained unpublished to date. The hemolytic activity assays were performed by **Suvrat Chowdhary** (Freie Universität Berlin) and the cell viability tests were executed by Elisa Quaas (Freie Universität Berlin). For examination of cell cytotoxicity, AbuK16, MfeGlyK16, DfeGlyK16 and TfeGlyK16 were probed towards the cervical carcinoma line HeLa and the murine tissue fibroblasts line L9S9 *via* Cell Counting Kit 8 (CCK-8) cell viability experiments (**Figure 7.6**). This colorimetric assay is based on the yellow-colored tetrazolium salt WST-8 which is reduced by cellular dehydrogenases yielding an orange-colored formazan dye. The activity of dehydrogenases in cells is determined by measuring the UV absorbance of formazan at 450 nm and depends on the overall amount of living cells in the culture media.²⁴⁷

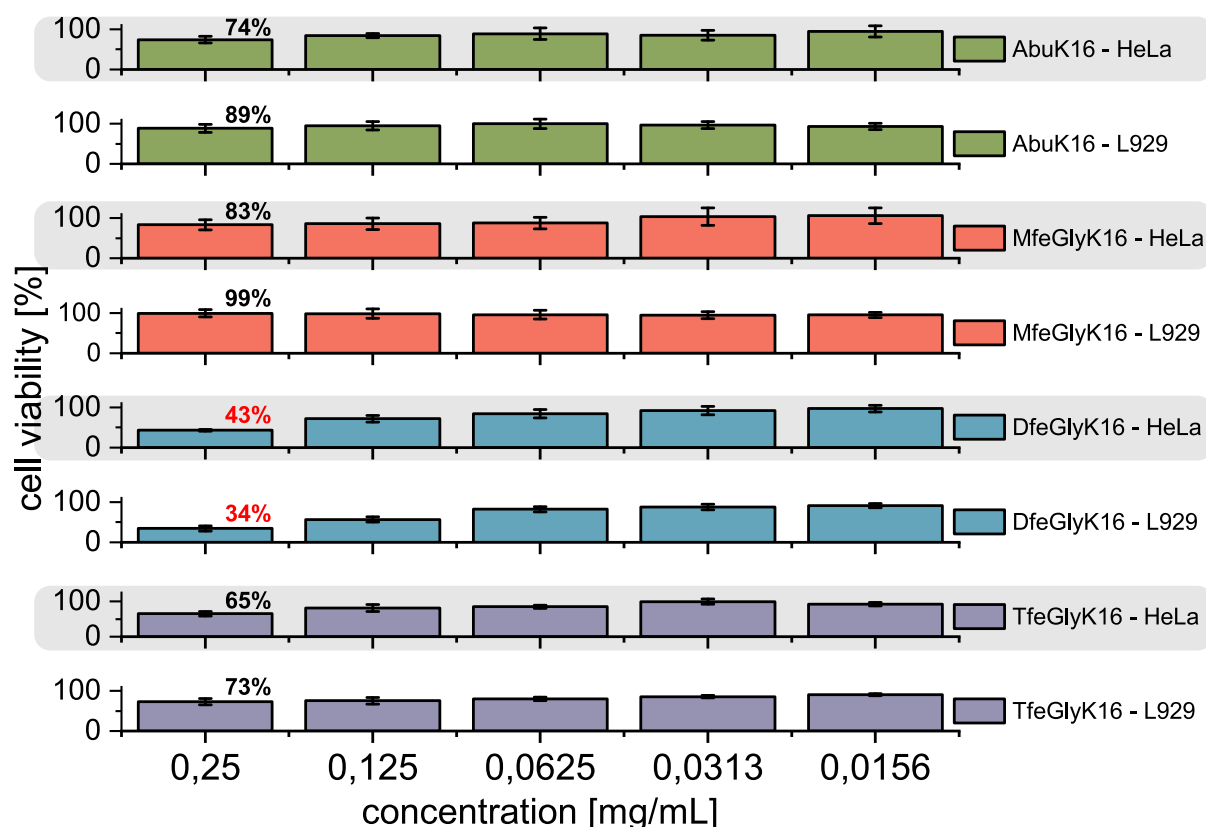


Figure 7.6 Viability profiles of seeded HeLa and L929 cells incubated with AbuK16, MfeGlyK16, DfeGlyK16 and TfeGlyK16 for 24 h. Each peptide was prepared in a stock solution (2.5 mg/mL) and diluted to following concentrations: 0.25 mg/mL, 0.125 mg/mL, 0.0625 mg/mL, 0.0313 mg/mL & 0.0156 mg/mL. Error bars were calculated from triplicate determinations.

After incubation with the substrates for 24 h, similar trends on survival ratios were found for both cell lines. High survival ratios (> 80%) were found for all substrates up to a concentration of 0.0625 mg/mL. At the highest concentration (0.25 mg/mL) probed in this assay, enhanced values on cell viability were found for MfeGlyK16 [$^{HeLa}(83.49 \pm 12.87)\%$ + $^{L9S9}(99.12 \pm 9.31)\%$] than AbuK16 [$^{HeLa}(73.74 \pm 8.25)\%$ + $^{L9S9}(88.64 \pm 10.35)\%$]. Similar findings on non-cytotoxic properties of peptide hydrogels equipped with monofluorinated side chains were reported by Lin and co-workers.²⁴⁸ DfeGlyK16 was found to be the most toxic peptide in this study since a significant loss on cell viability [$^{HeLa}(42.94 \pm 1.81)\%$ + $^{L9S9}(34.37 \pm 6.71)\%$] was determined. Surprisingly, (-CF₃)-substitution reversed this trend and exposes significantly lower effects on cell death for TfeGlyK16 [$^{HeLa}(64.68 \pm 6.09)\%$ + $^{L9S9}(73.47 \pm 7.65)\%$] than DfeGlyK16.

Earlier reports state higher rates of hemolysis by cationic peptides upon multiple incorporation of fluorinated amino acids.^{217, 218} In this work, the hemolytic activities against human red blood cells (hRBCs) were estimated *via* UV-Vis-based detection of hemoglobin release after incubation with various concentrations of AbuK16 and its fluorinated analogs (**Figure 7.7**).

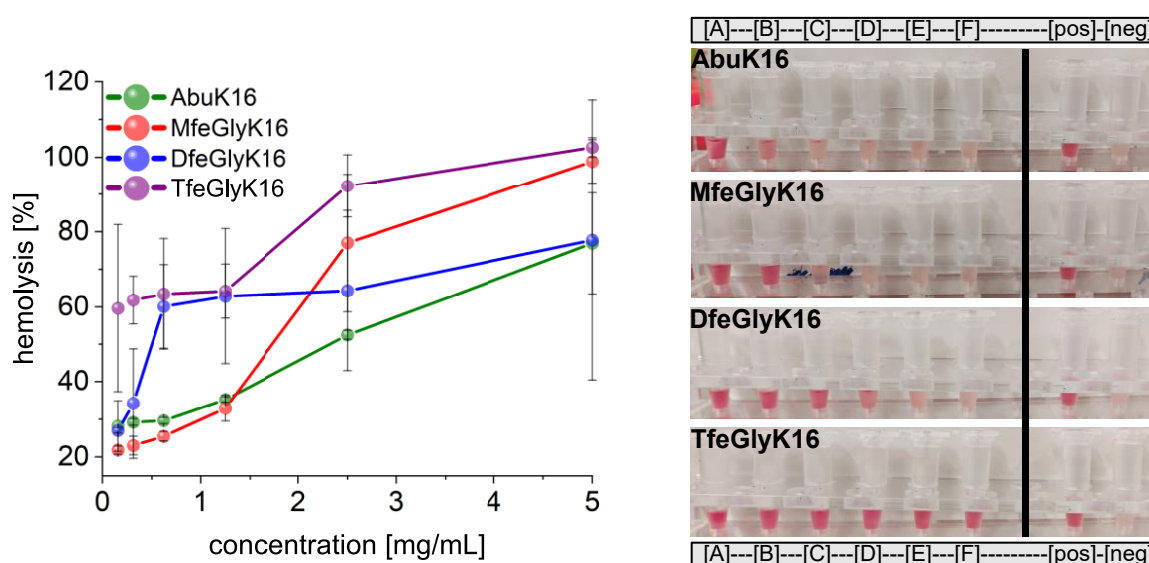


Figure 7.7 Evaluating the hemolytic activity (1% hRBC solution in PBS, pH 7.4) of (polyfluorinated) amphipathic peptides (**left**). Snapshots of hRBCs-samples after incubation at peptide concentrations **A** = 5 mg/mL, **B** = 2.5 mg/mL, **C** = 1.25 mg/mL, **D** = 0.625 mg/mL, **E** = 0.3125 mg/mL, **F** = 0.15625 mg/mL. Blood cells were centrifuged before, so that high blood-disrupting properties are visible by red-colored solutions (due to the release of hemoglobin) (**right**).

As illustrated in **Figure 7.7**, the degree of side chain fluorination has a tremendous impact on peptide-induced hemolysis. At a concentration of 0.03125 mg/mL (**Figure 7.7, sample E**) high populations of blood cells were disrupted upon incubation with TfeGlyK16

[^{Hem}(61.82 ± 6.38)%]. AbuK16 [^{Hem}(29.21 ± 0.85)%] was less hemolytic than DfeGlyK16 [^{Hem}(34.19 ± 14.56)%] but more than MfeGlyK16 [^{Hem}(21.89 ± 1.11)%]. This trend remained consistent up to 4-fold higher concentrations of 1.25 mg/mL (540 - 664 μM), thereby highlighting a synergy of peptide-induced hemolysis with altered degrees of intrinsic hydrophobicity upon side chain fluorination according to the trend “MfeGly < Abu < DfeGly < TfeGly”.

8 Experimental section

8.1 Overview of experimental & theoretical procedures (Section 6)

An overview of the experimental and theoretical techniques described in **Section 6 (published work)** is provided in **Table 8.1**. Detailed protocols for each method are provided in the experimental section of respective paper and supporting information.

Table 8.1 Summary of experimental / theoretical methods (published work - **Section 6**).

Method	<i>Nanoscale</i> (2022) ²³⁸	<i>Pept. Sci.</i> (2023) ²⁴⁰	<i>Chem. Eur. J</i> (2023) ²⁴²
Analytical / (semi)-preparative RP-HPLC	✓	✓	✓
Antimicrobial susceptibility testing		✓	
Carboxyfluorescein [6-FAM] leakage assay		✓	✓
CD spectroscopy	✓	✓	✓
Congo red (CR) UV assay for fibril detection	✓		
Cryogenic electron microscopy (cryo-EM)	✓		
Cytotoxicity tests (cell viability)		✓	
Elemental analysis	✓		
Equilibrium MD simulations	✓		
Estimation of peptide hydrophobicity (RP-HPLC)	✓	✓	✓
Exchange of TFA-salts	✓	✓	
FL spectroscopy	✓	✓	✓
Fluorinated amino acids – synthesis & purification	✓	✓	
Hemolytic assay (with red blood cells)		✓	
High-resolution mass spectrometry (HRMS)	✓	✓	✓
IR spectroscopy	✓		✓
Lyophilization	✓	✓	✓
NMR spectroscopy (¹ H, ¹³ C, ¹⁹ F)	✓	✓	
Oscillatory shear rheology	✓		
Peptide stock preparation (+ UV spectroscopy)	✓	✓	✓
Preparation of large unilamellar vesicles (LUV, CD)			✓
Proteolytic / peptide digestion assay (RP-HPLC / HRMS)		✓	✓
QM calculations (optimized structures, ΔE_{int} , ESP)	✓		
Small-angle-X-ray scattering (SAXS)	✓		
Surface enhanced IR absorption spectroscopy (SEIRAS)			✓
Solid-phase peptide synthesis (SPPS)	✓	✓	✓
Transmission electron microscopy (TEM)		✓	
Thioflavin T (ThT) FL assay for fibril detection	✓	✓	
Umbrella sampling simulations	✓		
UV-Vis spectroscopy	✓	✓	✓

8.2 General experimental conditions (Section 7.1-2)

In the following chapters (**Section 8.2-9**) all experimental procedures will be discussed which were not part of the published work (see **Section 6 & 8.1**).

All chemicals & materials described in **Section 7.1-2** were purchased from commercial sources and utilized as recommended by their material safety data sheet. Sample preparation was performed in laboratory fume hoods if needed. The Fmoc-protected amino acids were prepared according to Chowdhary *et al.* and Hohmann *et al.*^{202,238} After synthesis of MfeGly, DfeGly and TfeGly their purity was checked by recording ¹H and ¹⁹F NMR spectra using a Jeol ECZ600 or Jeol ECX400 NMR spectrometer. The amphipathic peptides AbuK16, MfeGlyK16, DfeGlyK16 and TfeGlyK16 were synthesized *via* SPPS. All experiments were executed in accordance with safety precautions on laboratory safety (Freie Universität Berlin). The experiments on microbial degradation were executed by Dr. Mohd Faheem Khan under the supervision of Prof. Dr. Cormac D. Murphy according to the safety precautions on laboratory safety of the University College Dublin. Toxicity tests (CCK-8) were executed by Elisa Quaas (Freie Universität Berlin) and conducted according to German genetic engineering laws and German biosafety guidelines in the laboratory (safety level 1). If not otherwise stated, the remaining experiments (F-AA synthesis, SPPS, CD spectroscopy, peptide digestion studies, hemolytic assay) were all applied and evaluated by **Suvrat Chowdhary**.

8.3 Preparation of MfeGly, DfeGly and TfeGly (Section 7.1)

These experiments were performed by **Suvrat Chowdhary**. Fmoc-protected amino acid MfeGly (500 mg, 1.45 mmol, 1 equiv.), DfeGly (500 mg, 1.38 mmol, 1 equiv.) or TfeGly (500 mg, 1.33 mmol, 1 equiv.) were dissolved in a [1:1] DCM/acetone mixture [10 mL] containing 2% piperidine for Fmoc-deprotection and stirred for 2 h. After that, the solution was evaporated, and the crude leftover dried *in vacuo*. The crude product was subsequently dissolved in MilliQ water [10 mL] and washed with EtOAc (3*5 mL) and CHCl₃ (3*5 mL). Upon that ion-exchange beads (Dowex 50WX8, 200-400 mesh, 3.5 g) were added to the aqueous phase and the reaction mixture was stirred slowly for 2 h. Then, the resin was filtered and washed with MilliQ water. The L-amino acid were eluted from the resin with a 1M NH₃ solution [20 mL] and dried by lyophilization.

The title compounds H-MfeGly-OH (93.9 mg, 0.77 mmol, 53%), H-DfeGly-OH (129.7 mg, 0.93 mmol, 67%) and H-TfeGly-OH (183.4 mg, 1.16 mmol, 87%) were obtained as white powders.

¹H-NMR / ¹⁹F-NMR spectroscopy

H-MfeGly-OH (C₄H₈FNO₂)

¹H NMR (600 MHz, D₂O) δ = 4.60 – 4.46 (m, 2H), 3.75 (s, 1H), 2.27 – 2.05 (m, 2H) ppm.

¹⁹F NMR (565 MHz, D₂O) δ = -219.04 – -219.41 (m, 1F) ppm.

H-DfeGly-OH (C₄H₇F₂NO₂)

¹H NMR (600 MHz, D₂O) δ = 6.06 – 5.89 (m, 1H), 3.95 – 3.69 (m, 1H), 2.51 – 2.20 (m, 2H) ppm.

¹⁹F NMR (565 MHz, D₂O) δ = -115.18 – -117.83 (m, 2F) ppm.

H-TfeGly-OH (C₄H₆F₃NO₂)

¹H NMR (600 MHz, D₂O) δ = 3.76 – 3.48 (m, 1H), 2.79 – 2.59 (m, 1H), 2.53 – 2.26 (m, 1H) ppm.

¹⁹F NMR (565 MHz, D₂O) δ = -63.51 – -63.60 (m, 3F) ppm.

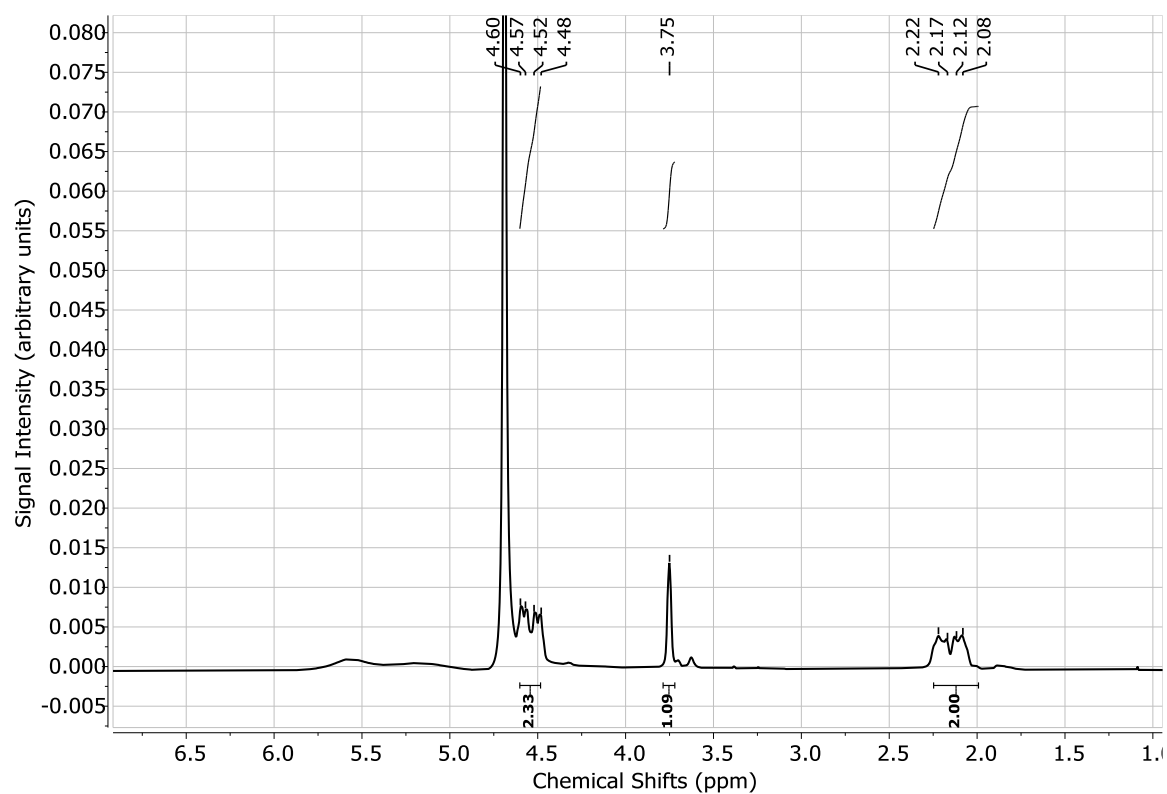


Figure 8.1 $^1\text{H-NMR}$ (600 MHz) spectrum of H-MfeGly-OH.

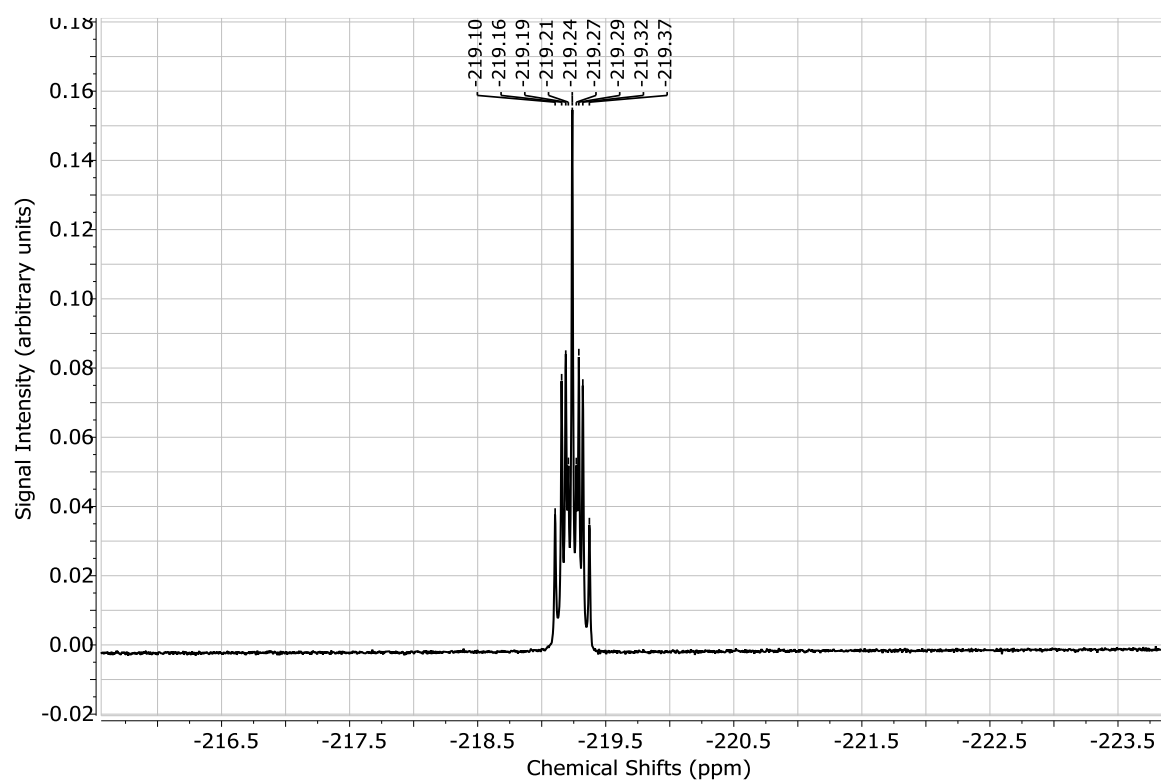


Figure 8.2 $^{19}\text{F-NMR}$ (565 MHz) spectrum of H-MfeGly-OH.

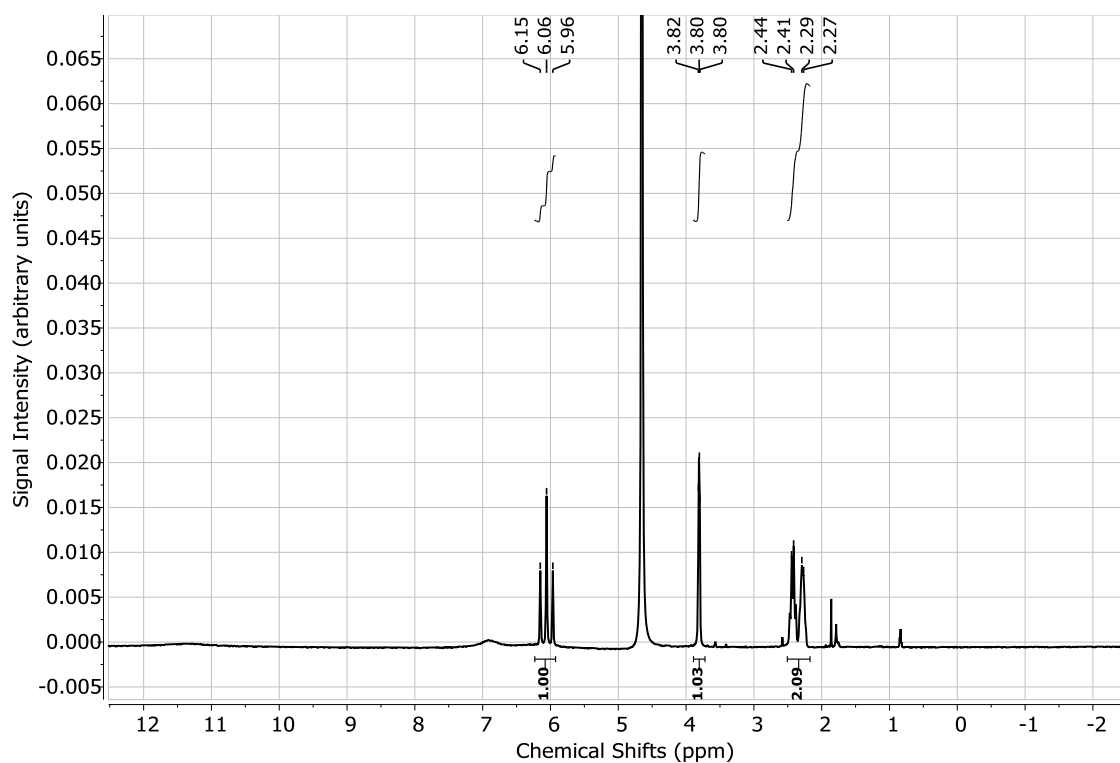


Figure 8.3 $^1\text{H-NMR}$ (600 MHz) spectrum of H-DfeGly-OH.

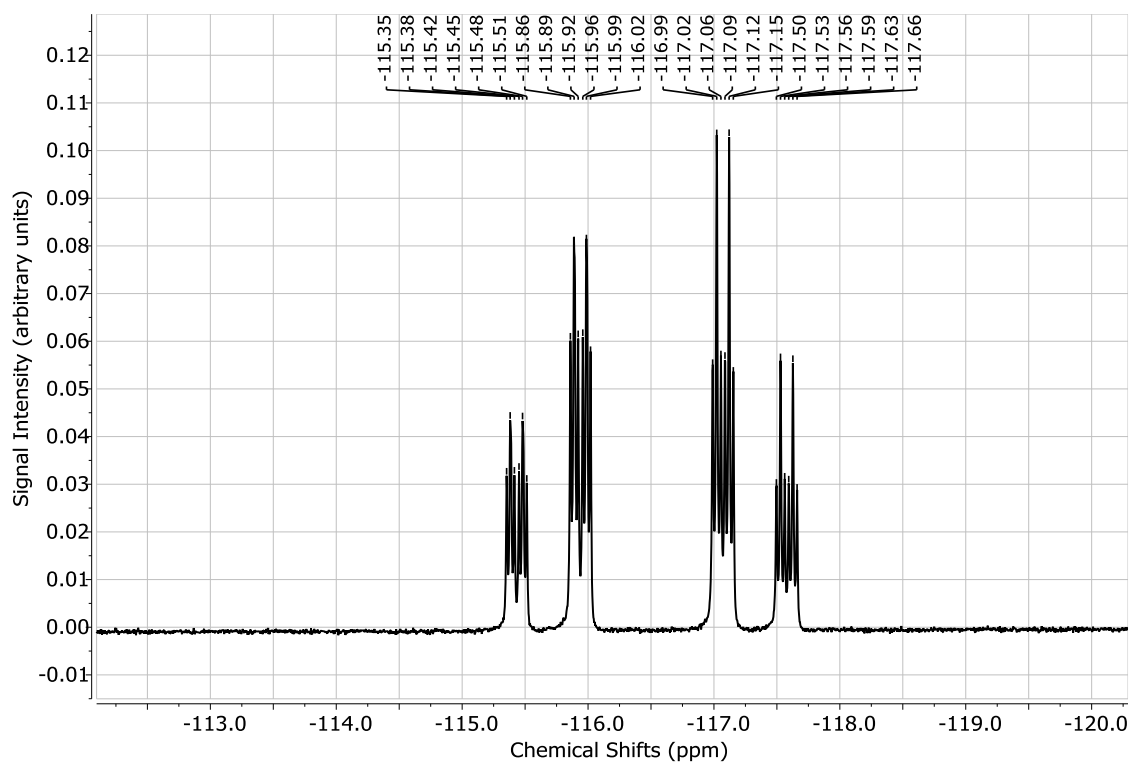


Figure 8.4 $^{19}\text{F-NMR}$ (565 MHz) spectrum of H-DfeGly-OH.

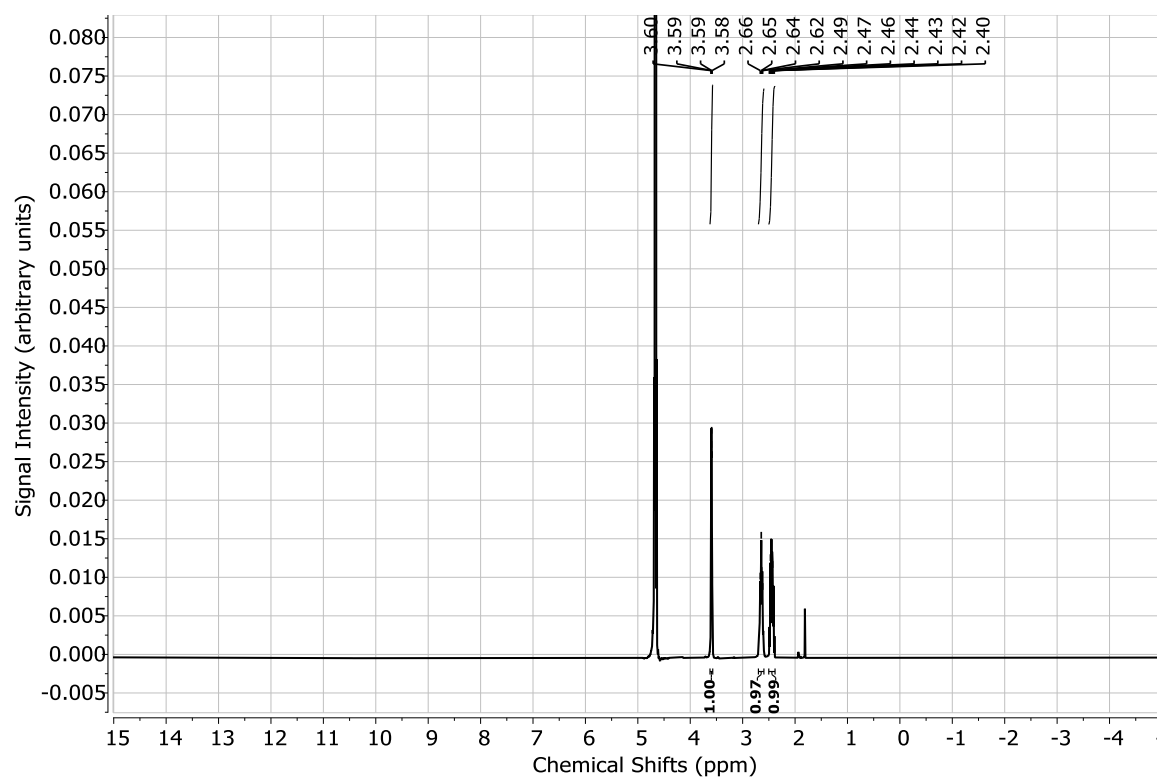


Figure 8.5 $^1\text{H-NMR}$ (600 MHz) spectrum of H-TfeGly-OH.

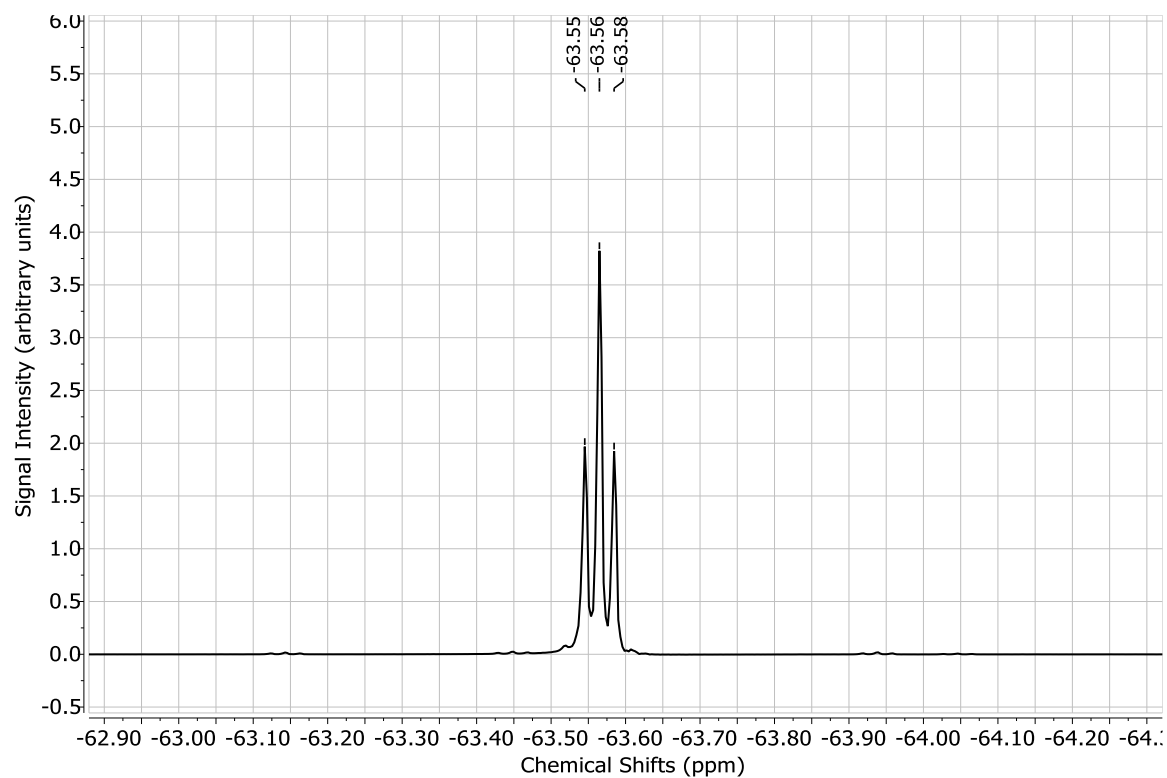


Figure 8.6 $^{19}\text{F-NMR}$ (565 MHz) spectrum of H-TfeGly-OH.

8.4 Solid-phase peptide synthesis (Section 7.1-2)

The amphipathic peptides AbuK16, MfeGlyK16, DfeGlyK16 and TfeGlyK16 were synthesized with a microwave-equipped Liberty Blue™ peptide synthesizer (CEM, Matthews, NC, USA) according to a published protocol by Chowdhary *et al.*²³⁸ After successful synthesis, the peptides were cleaved from the resin by treatment with a mixture of TFA/TIPS/H₂O (90/5/5). The crude batches were purified on a low-pressure and semi-preparative RP-HPLC system (Knauer GmbH, Berlin, Germany) with H₂O+0.1% TFA and ACN+0.1% TFA as HPLC solvents. Analytical HPLC was performed either on a Chromaster 600 bar DAD-system (VWR/Hitachi, Darmstadt, Germany) or a Hitachi Primaide™ DAD-system (VWR/Hitachi, Darmstadt, Germany) with both H₂O+0.1% TFA and ACN+0.1% TFA as HPLC solvents. The essential data for validation of peptide purity (HPLC chromatograms and HRMS spectra) can be found in **Figure 8.7**.

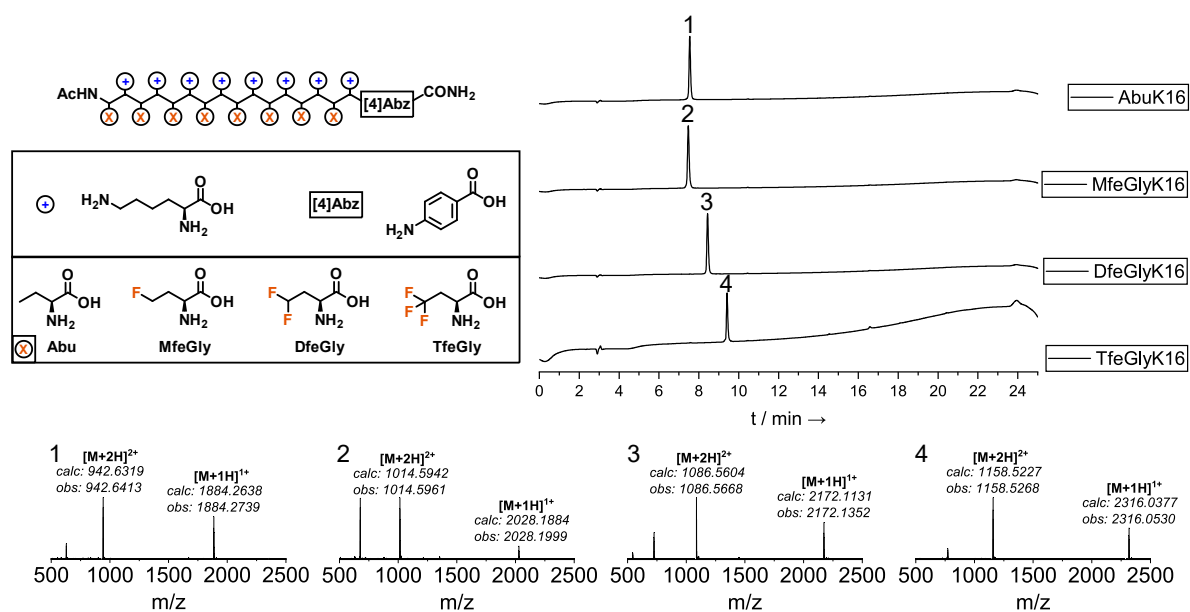


Figure 8.7 Successful synthesis (SPPS) and purification (HPLC and HRMS) of AbuK16, MfeGlyK16, DfeGlyK16 and TfeGlyK16 was confirmed *via* HPLC chromatograms and ESI-ToF mass spectrometry. HPLC conditions: (A) H₂O + 0.1% TFA / (B) ACN + 0.1% TFA with a gradient of 10 - 80% (B) over 18 min.

8.5 CD spectroscopy (Section 7.1)

Circular dichroism experiments were performed using a Jasco J-810 spectropolarimeter. Data were recorded using 0.1 mm Quartz Suprasil® cuvettes (Hellma). Spectra were recorded at 37 °C from 190 to 250 nm at 0.2 nm intervals, 1 nm bandwidth, 4 s response time and a scan speed of 100 nm min⁻¹ with baseline subtraction.

8.6 Proteolytic digestion studies of amphipathic peptides (Section 7.1)

Freeze-dried peptides were dissolved in 50 mM Bis-tris propane + 20 mM CaCl₂, pH 8.0 (100 µL, 500 µM). 10 µL of an enzyme solution in the same buffer (trypsin: 0.075 µM / elastase: 0.45 µM / proteinase k: 0.075 µM / bromelain: 4.5 µM) was added and the solutions were again gently mixed for 5 seconds. After that, the samples were incubated with constant shaking (300 rpm) at 30-37 °C. At fixed time points, aliquots (15 µL) were quenched with 90 µl of 30% (v/v) AcOH in H₂O containing 133 µM Ac-[4]Abz-Gly-OH as a reference. Peptide degradation was monitored and determined by HPLC analysis in real-time (DAD-280 nm). All experiments were performed in triplicates.

8.7 Microbial degradation of fluorinated peptides and amino acids (Section 7.1)

These experiments were performed by Dr. Mohd Faheem Khan under the supervision of Prof. Dr. Cormac D. Murphy (University College Dublin, Ireland). The soil microbial consortium was collected from approximately 1 g of Irish garden soil (53°16'50.0"N / 6°16'05.0"W) through incubation in tryptone soya broth (TSB, 50 mL) at 30 °C. This culture was inoculated in fresh TSB containing 15% glycerol. Aliquots (1 mL) were stored at -80°C as stocks for further experiments. *P. fluorescens* DSM 8341 were obtained from Leibniz-Institut DSMZ - Deutsche Sammlung von Mikroorganismen und Zellkulturen GmbH.

As a general procedure for the **biodegradation experiments**, a microbial aliquot (200 µL) was inoculated to TSB media (20 mL) and incubated for 24 h at 30 °C at regular shaking (200 ppm). After that, the fluorinated peptides and amino acids (each 2 mg) were added and further incubation for 48 h at 30 °C took place. The supernatants were collected by centrifugation of the microbes.

Resting cells of the soil microbes were prepared by harvesting the cells after 24 h growth in TSB media (30 °C) *via* centrifugation and resuspension in HEPES buffer (pH 7.0) to the

original volume. Afterwards, the fluorinated substrate (each 2 mg) was added and incubation at 30 °C for 48 h took place. Subsequently, the supernatants were collected by centrifugation.

Cell free (CF) extracts were obtained by harvesting the cells *via* centrifugation, then resuspending in HEPES buffer (pH 7.0) and subsequent membrane lysis by sonication [Sonics 130 W ultrasonic processor] at 30% amplitude, 10 s pulse on and 15 s pulse off for a total of 5 min. After centrifugation of the cell pellets (16.000 rpm, 4 °C, 20 min), the supernatants were collected and used as CF extracts. For sample preparation, 0.2 mg of fluorinated amino acid were diluted with 1 mL CF extract and incubated for 6 h at 30 °C. For **enrichment culture** experiments, molten agar (2 %) supplemented with 20 mM MfeGly was poured onto a petri dish, inoculated with the soil microbe inoculum (100 µl) and incubated at 30 °C for 48 h. One grown bacteria colony (Strain B) was re-streaked onto separate tryptic soy agar (TSA) plates and incubated at 30 °C for 24 h. After subsequent cultivation in TSB media, the bacteria cells were treated as mentioned above for obtaining a single bacterial strain-based CF extract in HEPES buffer (CF Strain B).

For comparing the **defluorinating activity** of *P. fluorescens* DSM 8341 and the isolated strain B, the bacterial microbes in TSB (10 mL) were supplemented with either fluoroacetate or MfeGly (both 1 mg) and incubated at 30 °C for 48 h. After that, the cells were harvested by centrifugation, washed with HEPES buffer (pH 7.0), and resuspended in the same buffer (1mL). To test the defluorinating activities, the substrates fluoroacetate or MfeGly (both 0.2 mg) were added, and the solution was incubated at 30 °C for 6 h with regular shaking (300 rpm). Then, the supernatants were separated from the cells.

Sample analysis was executed by redissolving the freeze-dried supernatants in D₂O and, after separation through centrifugation, further analysis through ¹⁹F NMR spectroscopy [Varian 400 MHz] with NaF as internal control. For RP-HPLC [Primaide™ DAD-System] experiments, the dried samples were dissolved in MilliQ-H₂O containing 0.1% TFA (v/v), collected through centrifugation and filtered with 0.2 µm PTFE syringe filters. GC-MS measurements were performed according to a protocol by Khan *et al.* that includes the derivatization of the samples *via* silylation.²⁴⁹ Fluoride ion release was measured through a colorimetric assay described in depth by Bygd *et al.* using an Epoch 2 Microplate Spectrophotometer.²⁴⁶ The determination of fluoride ion concentration was done as published by Khan *et al.*²⁴⁹

8.8 CCK-8 cytotoxicity assays for the determination of cell viability (Section 7.2)

These experiments were performed by Elisa Quaas (Freie Universität Berlin). Cell viability was determined using a CCK-8 Kit (Sigma-Aldrich) according to the manufacturer's instructions. HeLa cells were cultured in DMEM and L929 in RPMI medium. Both media were supplemented with 10% (v/v) FBS, 100 U/mL penicillin and 100 µg/mL streptomycin. Both cells were seeded in a 96-well plate at a density of 5×10^4 cells/mL in 90 µl DMEM/RPMI medium per well over night at 37 °C and 5% CO₂. 10 µl of SAPs (solved in 50 mM Bis-tris propane + 150 mM NaCl, pH 7.4) were added in serial dilutions including positive (1% SDS) and negative controls (medium, buffer) and incubated for another 24 h at 37 °C and 5% CO₂. For background subtraction, also wells containing no cells but only sample were used. After 24 h incubation the CCK-8 solution was added (10 µl/well) and the UV absorbance (450 nm/650 nm) was measured after approximately 3 h incubation of the dye using a Tecan plate reader (Infinite pro200, TECAN-reader Tecan Group Ltd.). Measurements were performed in triplicates and repeated three times.

8.9 Hemolytic assay for determining blood-disrupting properties (Section 7.2)

These experiments were performed by **Suvrat Chowdhary**. Purification of the erythrocytes derived from human red blood cells (hRBCs) was performed according to a published protocol by Thota *et al.*²⁵⁰ After that, a 2% (v/v) RBC solution in PBS buffer was established. For sample preparation, 100 µL peptide solution in PBS buffer in serial dilutions bearing two-fold concentrations were added to 100 µL 2% (v/v) RBC solution and then incubated at 37 °C for 45 min. A 2% Triton X-100 solution in PBS buffer was added as a positive control and a sole 1% (v/v) RBC solution served as a negative control. After incubation, the samples were centrifuged (3000 rpm, 3 min) and the UV absorbance of the supernatants was measured at 540 nm for determining the extent of hemolysis. All measurements were done in triplicates. Erythrocytes were purchased from DRK Blutspendendienst Nord-Ost Berlin.

9 Summary and outlook

The rational design of highly fluorinated peptides holds translational potential for developing artificial biomaterials with unique chemical and biological properties in foreseeable future. In this doctoral thesis, the development & characterization of polyfluorinated oligopeptides is subdivided into three main projects focusing on the multiple incorporation of fluorine-containing amino acids in different peptides motifs (β -sheet SAPs, β -hairpin AMPs, homooligopeptides [fluoropeptides]) that are illustrated in **Figure 9.1**.

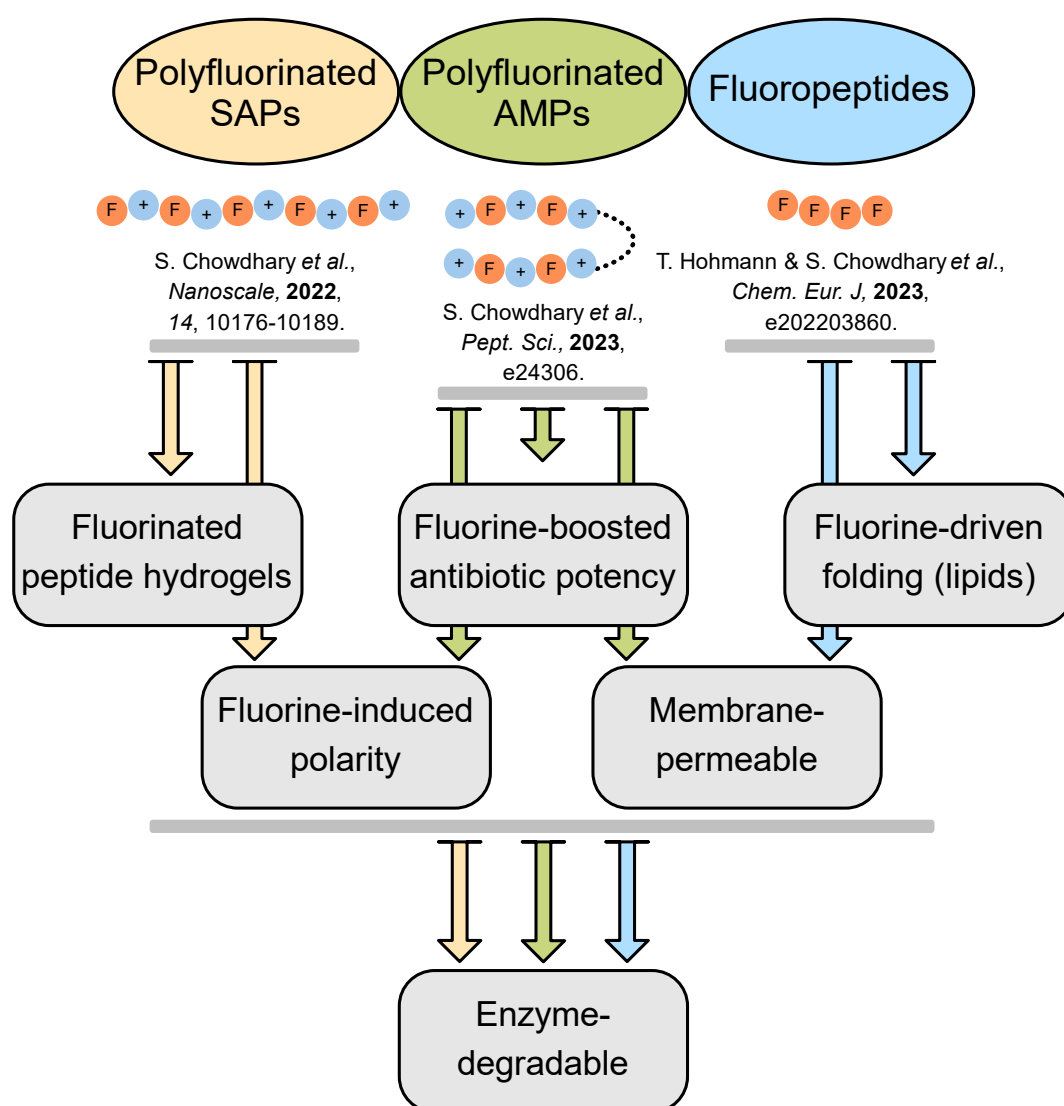


Figure 9.1 Schematic illustration of the published work in terms of this doctoral thesis.

In each project, a distinctive library of highly fluorinated peptides was established for investigating the influence of tailor-made fluorinated amino acids on secondary structure

formation, self-assembly properties, bioactivity, and proteolytic stability. In fact, an entirely new class of synthetic yet enzyme-degradable biomolecules was described with fluorination-boosted benefits on the supramolecular formation of fibrillar architectures, mechanical stiffness of water-swollen hydrogel materials, or bactericidal potencies towards a variety of pathogenic microbes. Thus, these versatile peptide scaffolds equipped with fluorine-driven physiochemical properties and bioactivities bear promising potential to serve as degradable alternatives to bio-inert & fluorocarbon-based fluoropolymers in biomaterial research. Therefore, ongoing cooperation studies with Prof. Dr. Cormac D. Murphy (University College Dublin, Ireland) are anticipated to provide deeper insights into the metabolic and excretion mechanisms during soil microbial degradation of these fluoruous peptides in near future.

Furthermore, the progressing research of the Kokschi laboratory aims to extend this novel class of polyfluorinated peptides by developing (fluoro)-peptide amphiphile micelles (PAMs) as artificial but bio-responsive carrier systems (**Figure 9.2**). As reported by Liang *et al.*, the micellular self-assembly could be initially studied by FL-based investigations after addition of the water-insoluble probe pyrene.²⁵¹ An enhancement in fluorescence intensity, consequently, would indicate the encapsulation & solubilization of pyrene in a hydrophobic inner micellar core.

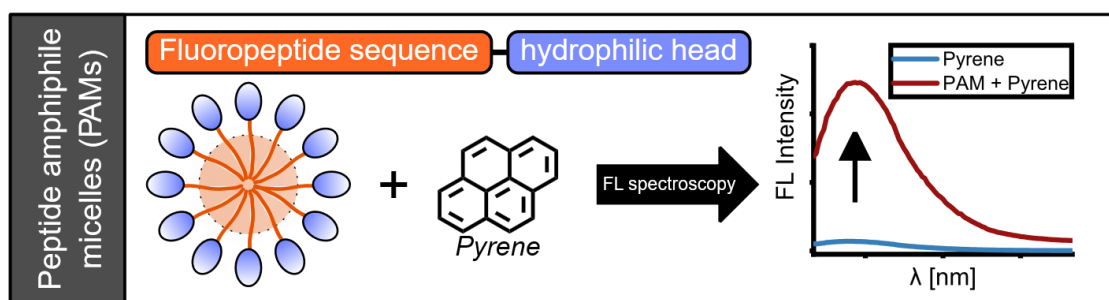


Figure 9.2 Expanding the portfolio of polyfluorinated peptides by the development of fluoruous peptide amphiphile micelles (PAMs). The micellization behavior, as schematically illustrated, can be studied by FL-monitored solubilization of the hydrophobic probe pyrene by the PAMs.²⁵¹

The following sections will summarize these individual projects and provide an outlook on future studies:

1. Rational design of amphiphilic fluorinated peptides: evaluation of self-assembly properties and hydrogel formation

Summary: Supramolecular β -sheet hydrogelators composed of amphiphilic self-assembling peptides (SAPs) have received emerging interest in biomedical and pharmaceutical research. In fact, the molecular self-assembly of nanofibrillar SAP networks, as well as the viscoelastic stability of resulting hydrogel matrices are dictated by diverse non-covalent driving forces like hydrophobic, electrostatic or vdW interactions. The impact of fluorine-specific interactions, however, has been barely studied and only a small portfolio of β -sheet SAPs containing fluorinated amino acids is available till date.

Given to this background, a library of polyfluorinated SAPs with solely aliphatic fluorinated amino acids as hydrophobic components was systematically designed and characterized. The first-of-its-kind aliphatic oligopeptides AbuK16, MfeGlyK16, DfeGlyK16 and TfeGlyK16 served as models to study fluorine-specific interactions in β -sheet formation, peptide self-assembly and hydrogel formation. Successive enhancement of fluorine-substitution, as given for DfeGlyK16 & TfeGlyK16 compared to AbuK16, was found to promote amyloid-like fibrillization and the rheological stiffness of peptide hydrogels in physiological conditions. Vice versa, a combined set of experimental and theoretical data emphasized the innating side chain polarity in the hydrophobic domain of MfeGlyK16 to impede β -sheet assembly. Therefore, MD simulations found electrostatic repulsions through protruding Lys residues of head-to-head MfeGlyK16 dimers to prevent hydrophobicity-driven self-assembly. Thus, fluorine-specific interactions were quantified as an interplay of the side chains' polarity and hydrophobicity, both induced differentially by varying degrees of fluorination.

Unpublished work (summary): In ongoing studies discussed in **Section 7**, the SAPs AbuK16, MfeGlyK16, DfeGlyK16 and TfeGlyK16 were assessed for their biodegradability. Incubation with commercially available serine and cysteine proteases confirmed all peptides to be enzymatically degradable despite the degree of side chain fluorination. The degree of digestion differed in varying magnitudes depending on the type of fluorinated amino acids and enzyme. Further experiments on the soil microbial degradation [in collaboration with Dr. Mohd Faheem Khan & Prof. Dr. Cormac D. Murphy, (University College Dublin, Ireland)] conducted with the polyfluorinated peptides MfeGlyK16,

DfeGlyK16 and TfeGlyK16 and their individual fluorinated amino acids MfeGly, DfeGly and TfeGly depicted subsequent fluoride ion release as an indication of enzyme-catalyzed C-F bond cleavage. Also, the enrichment of a microbial consortium with MfeGly as sole carbon source led to the particular isolation of a grown bacterium (strain B). Enzymatic defluorination of MfeGly (and subsequent detection of homoserine) was further achieved with cell free extracts from both the soil microbial consortium and the isolated strain B. That emphasized a similar mechanism on proteolytic C-F bond cleavage as known for common *fluoroacetate dehalogenases*. At last, cell viability tests were executed and gave insights into fluorine-induced toxicity above a respective threshold concentration. Also, higher degrees of side chain fluorination were found to cause enhanced rates of human blood cell hemolysis.

Outlook: Future work is supposed to explore the conformational alterations in peptide folding & β -sheet assembly upon fluorine-substitution by applying NMR spectroscopy. Also, the biocompatibility of the polyfluorinated SAPs should be elucidated in depth. In order to examine the potential applicability of these hydrogels as, for example, synthetic ECM mimics with fluorine-functionalized stiffness, further toxicity tests with a wide range of fibroblast cell lines (e.g. NIH/3T3 or C3H10t1/2) are to be considered.

Moreover, further attempts should pursue on the identification of the isolated bacterium “strain B” by genome sequencing. In the case of its successful isolation and purification, the newly discovered hydrolase could be tested against a larger scope of fluorinated compounds to get a more detailed insight into potential substrate specificities.

2. Fine-tuning the antimicrobial activity of β -hairpin peptides with fluorinated amino acids

Summary: A multitude of naturally occurring antimicrobial peptides (AMPs) possess the β -hairpin conformation. Their bactericidal potency towards a variety of pathogenic strains is predominantly depending on an overall balance of positively charged and hydrophobic residues. Thus, the selective fluorination of AMP scaffolds can serve as an useful approach to alter the peptides' hydrophobic nature for tuning their bioactivity.

In this study, the influence of aliphatic side chain fluorination on the antimicrobial activities of artificial β -hairpin peptides was elucidated. Implementation of the *D-Phe-[2]Abz* β -turn motif served to develop two distinctive series of amphipathic & polyfluorinated peptide libraries (XR14 & SAJO). Minimal inhibitory concentration (MIC) screenings revealed a synergy between fluorine-enhanced hydrophobicity and antimicrobial potency. Ultimately, the peptide SAJO-PfpGly equipped with two pentafluoro-alkylated residues was identified as the most potent agent among this work. All peptides were found with near to zero values of blood cell hemolysis and cytotoxicity, serving as indispensable criterions for potential therapeutical applications. Most interestingly, incorporation of fluorinated amino acids into these amphipathic peptides was proven to maintain peptide proteolysis while causing notable changes in enzyme-substrate recognition. These results underline the tremendous perspective tailor-made fluorinated amino acids bear as orthogonal tool in modern peptide engineering to develop next-generation peptide-based antimicrobial agents.

Outlook: Further systematic studies should be directed on improving the proteolytic stability of the XR14/SAJO-scaffold. In fact, an urgent problem causing the limited success of AMPs in clinical applications is constituted by their poor bioavailability. Among various chemical, side chain and backbone modifications (e.g. cyclization) to refine the peptide design towards enzymatic digestion, the stepwise substitution of L-amino acids by their corresponding D- and/or β -derivatives should be firstly tested. A growing replacement of the L-amino acids Arg and Trp in both motifs with their commercially available D-enantiomers is proposed to mask the predominant cleaving sites on the amphipathic β -strands, thus increasing the proteolytic stability of these AMPs.

3. Introducing Aliphatic Fluoropeptides: Perspectives on Folding Properties, Membrane Partition and Proteolytic Stability

Summary: In this work, a new class of artificial peptides mainly built-up from fluorinated aliphatic amino acids (fluoropeptides) was developed and characterized. The structural properties of these peptide foldamers were studied regarding the degree of fluorination and the peptide length. Structural investigations revealed a fluorine-induced β -strand to α -helix transition in the presence of SDS or artificial liposomes. In the case of TfeGly-derived fluoropeptides, an unusual formation of PPII helices was observed. The insertion of these fluoropeptides into POPC:POPG unilamellar vesicles were further studied using CD spectroscopy, SEIRAS IR-spectroscopy and FL-based leaking assays. Membrane partition was estimated as a comparably slow process in which the highest helical secondary structure content in the peptide/POPC:POPG mixture was given for the nonfluorinated Abu₁₃GY(K)₄ but decreased in the order of TfeGly₁₃GY(K)₄, DfeGly₁₃GY(K)₄, and MfeGly₁₃GY(K)₄. Furthermore, this work describes the first study on the proteolytic hydrolysis of peptide sequences consisting exclusively of fluorinated amino acids. Unexpectedly, all fluoropeptides were enzymatically degraded regardless of the degree of fluorination. MS-assisted analysis confirmed a predominant P1-P1' cleaving site at which all fluorinated amino acids in this work were validated for occupying the P1 & P1' positions. In consequence, the artificial amino acids comply with the primary specificity of both serine proteases (elastase and proteinase k). These pioneering results may play an intriguing role in the development of fluorinated peptide-based biomaterials as enzyme-degradable alternatives to otherwise bio-persistent fluoropolymers.

Outlook: Future studies should focus on expanding the repertoire of fluorinated amino acids on the further development of fluoropeptides. Highly fluorinated and branched amino acids like HfLeu may alter the fate of fluoropeptide proteolysis by their far higher spatial demands than given for the fluorinated variants of Abu. Also, further studies should probe the applicability of these fluoropeptides as membrane-penetrating tags for the improved cellular uptake of bioactive peptides or proteins into living cells. A *de novo* design could include a bioactive cargo peptide equipped with a truncated fluoropeptide-tag and a terminal FITC-label for applying FL-microscopic monitoring on cytosolic delivery. Based on current results, the fluorous-tagged peptides may reveal higher rates of cellular internalization than non-tagged and non-fluorinated analogs, respectively.

10 Bibliography

1. *European Journal of Biochemistry*, 1984, **138**, 9-37.
2. L. M. De Leon Rodriguez, Y. Hemar, J. Cornish and M. A. Brimble, *Chemical Society Reviews*, 2016, **45**, 4797-4824.
3. J. Kopeček and J. Yang, *Acta Biomaterialia*, 2009, **5**, 805-816.
4. L. Schnaider, L. Shimonov, T. Kreiser, D. Zaguri, D. Bychenko, I. Brickner, S. Kolusheva, A. Lichtenstein, J. Kost and E. Gazit, *ACS Applied Bio Materials*, 2020, **3**, 8395-8401.
5. K. O. Christe, *Inorganic Chemistry*, 1986, **25**, 3721-3722.
6. F. Agostini, L. Sinn, D. Petras, C. J. Schipp, V. Kubyshkin, A. A. Berger, P. C. Dorrestein, J. Rappsilber, N. Budisa and B. Koks, *ACS Central Science*, 2021, **7**, 81-92.
7. M. Salwiczek, E. K. Nyakatura, U. I. M. Gerling, S. Ye and B. Koks, *Chemical Society Reviews*, 2012, **41**, 2135-2171.
8. C. K. Smith and L. Regan, *Science*, 1995, **270**, 980-982.
9. R. R. Crichton, in *Biological Inorganic Chemistry*, ed. R. R. Crichton, Elsevier, Amsterdam, 2008, DOI: <https://doi.org/10.1016/B978-044452740-0.50004-1>, pp. 43-76.
10. A. Perczel, Z. Gáspári and I. G. Csizmadia, *Journal of Computational Chemistry*, 2005, **26**, 1155-1168.
11. M. Tsutsumi and J. M. Otaki, *Journal of Chemical Information and Modeling*, 2011, **51**, 1457-1464.
12. A. Hazari, M. R. Sawaya, N. Vlahakis, T. C. Johnstone, D. Boyer, J. Rodriguez, D. Eisenberg and J. A. Raskatov, *Chemical Science*, 2022, **13**, 8947-8952.
13. J. S. Rudra, S. H. Kelly and J. H. Collier, in *Comprehensive Biomaterials II*, ed. P. Ducheyne, Elsevier, Oxford, 2017, DOI: <https://doi.org/10.1016/B978-0-12-803581-8.10210-3>, pp. 67-89.
14. J. A. Robinson, *Accounts of Chemical Research*, 2008, **41**, 1278-1288.
15. J. Adamcik and R. Mezzenga, *Angewandte Chemie International Edition*, 2018, **57**, 8370-8382.
16. E. Gazit, *FEBS Journal*, 2005, **272**, 5971-5978.
17. N. Cremades and C. M. Dobson, *Neurobiology of Disease*, 2018, **109**, 178-190.
18. A. B. Soriaga, S. Sangwan, R. Macdonald, M. R. Sawaya and D. Eisenberg, *The journal of physical chemistry. B*, 2016, **120**, 5810-5816.
19. A. L. Boyle, in *Peptide Applications in Biomedicine, Biotechnology and Bioengineering*, ed. S. Koutsopoulos, Woodhead Publishing, 2018, DOI: <https://doi.org/10.1016/B978-0-08-100736-5.00003-X>, pp. 51-86.
20. P.-N. Cheng, J. D. Pham and J. S. Nowick, *Journal of the American Chemical Society*, 2013, **135**, 5477-5492.
21. A. Brack and L. E. Orgel, *Nature*, 1975, **256**, 383-387.
22. S. St. Pierre, R. T. Ingwall, M. S. Verlander and M. Goodman, *Biopolymers*, 1978, **17**, 1837-1848.
23. H. Yanagawa, M. Nishizawa and K. Kojima, *Origins of life*, 1984, **14**, 267-272.
24. W. A. Hiltner, A. J. Hopfinger and A. G. Walton, *Journal of the American Chemical Society*, 1972, **94**, 4324-4327.
25. S. Zhang, C. Lockshin, A. Herbert, E. Winter and A. Rich, *EMBO J*, 1992, **11**, 3787-3796.

26. S. Zhang, T. Holmes, C. Lockshin and A. Rich, *Proceedings of the National Academy of Sciences*, 1993, **90**, 3334-3338.
27. J. K. Ducett, F. C. Peterson, L. A. Hoover, A. J. Prunuske, B. F. Volkman and E. A. Craig, *Journal of molecular biology*, 2013, **425**, 19-31.
28. S. Zhang, T. C. Holmes, C. M. DiPersio, R. O. Hynes, X. Su and A. Rich, *Biomaterials*, 1995, **16**, 1385-1393.
29. G. A. Braun, B. E. Ary, A. J. Dear, M. C. H. Rohn, A. M. Payson, D. S. M. Lee, R. C. Parry, C. Friedman, T. P. J. Knowles, S. Linse and K. S. Åkerfeldt, *Biomacromolecules*, 2020, **21**, 4781-4794.
30. P. Arosio, T. P. J. Knowles and S. Linse, *Physical Chemistry Chemical Physics*, 2015, **17**, 7606-7618.
31. M. R. Sawaya, S. Sambashivan, R. Nelson, M. I. Ivanova, S. A. Sievers, M. I. Apostol, M. J. Thompson, M. Balbirnie, J. J. W. Wiltzius, H. T. McFarlane, A. Ø. Madsen, C. Riek and D. Eisenberg, *Nature*, 2007, **447**, 453.
32. R. Nelson, M. R. Sawaya, M. Balbirnie, A. Ø. Madsen, C. Riek, R. Grothe and D. Eisenberg, *Nature*, 2005, **435**, 773-778.
33. A. Bertolani, L. Pirrie, L. Stefan, N. Houbenov, J. S. Haataja, L. Catalano, G. Terraneo, G. Giancane, L. Valli, R. Milani, O. Ikkala, G. Resnati and P. Metrangolo, *Nature Communications*, 2015, **6**, 7574.
34. F. Gelain, Z. Luo, M. Rioult and S. Zhang, *npj Regenerative Medicine*, 2021, **6**, 9.
35. H. Yokoi, T. Kinoshita and S. Zhang, 2005, **102**, 8414-8419.
36. C. J. Bowerman and B. L. Nilsson, *Biopolymers*, 2012, **98**, 169-184.
37. Y. Chen, Y. Hua, W. Zhang, C. Tang, Y. Wang, Y. Zhang and F. Qiu, *Int J Nanomedicine*, 2018, **13**, 2477-2489.
38. K. S. Hellmund, B. von Lospichl, C. Böttcher, K. Ludwig, U. Keiderling, L. Noirez, A. Weiß, D. J. Mikolajczak, M. Gradzielski and B. Kocsch, *Peptide Science*, 2021, **113**, e24201.
39. B. Ozbas, J. Kretsinger, K. Rajagopal, J. P. Schneider and D. J. Pochan, *Macromolecules*, 2004, **37**, 7331-7337.
40. J. P. Schneider, D. J. Pochan, B. Ozbas, K. Rajagopal, L. Pakstis and J. Kretsinger, *Journal of the American Chemical Society*, 2002, **124**, 15030-15037.
41. K. Nagy-Smith, E. Moore, J. Schneider and R. Tycko, *Proceedings of the National Academy of Sciences*, 2015, **112**, 9816-9821.
42. C. J. Bowerman, D. M. Ryan, D. A. Nissan and B. L. Nilsson, *Molecular BioSystems*, 2009, **5**, 1058-1069.
43. I. M. Geisler and J. P. Schneider, *Advanced Functional Materials*, 2012, **22**, 529-537.
44. C. M. Micklitsch, S. H. Medina, T. Yucel, K. J. Nagy-Smith, D. J. Pochan and J. P. Schneider, *Macromolecules*, 2015, **48**, 1281-1288.
45. M. Paradís-Bas, J. Tulla-Puche, A. A. Zompra and F. Albericio, *European Journal of Organic Chemistry*, 2013, **2013**, 5871-5878.
46. M. Paradís-Bas, J. Tulla-Puche and F. Albericio, *Chemical Society Reviews*, 2016, **45**, 631-654.
47. R. B. Dyer, S. J. Maness, E. S. Peterson, S. Franzen, R. M. Fesinmeyer and N. H. Andersen, *Biochemistry*, 2004, **43**, 11560-11566.
48. L. Wang, N. Wang, W. Zhang, X. Cheng, Z. Yan, G. Shao, X. Wang, R. Wang and C. Fu, *Signal Transduction and Targeted Therapy*, 2022, **7**, 48.
49. A. G. de Brevern, *Scientific Reports*, 2016, **6**, 33191.
50. C. M. Venkatachalam, *Biopolymers*, 1968, **6**, 1425-1436.
51. J. Venkatraman, S. C. Shankaramma and P. Balaram, *Chemical Reviews*, 2001, **101**, 3131-3152.

52. M. Ramírez-Alvarado, F. J. Blanco, H. Niemann and L. Serrano, *Journal of Molecular Biology*, 1997, **273**, 898-912.
53. E. G. Hutchinson and J. M. Thornton, *Protein Science*, 1994, **3**, 2207-2216.
54. T. Blandl, A. G. Cochran and N. J. Skelton, *Protein Science*, 2003, **12**, 237-247.
55. S. Fischer, M. Lamping, M. Gold, Y. Röttger, D. Brödje, R. Dodel, R. Frantz, M. A. Mraheil, T. Chakraborty and A. Geyer, *Bioorg Med Chem*, 2017, **25**, 603-608.
56. C. A. Bush, S. K. Sarkar and K. D. Kopple, *Biochemistry*, 1978, **17**, 4951-4954.
57. C. Cantoni, M. Ponassi, R. Biassoni, R. Conte, A. Spallarossa, A. Moretta, L. Moretta, M. Bolognesi and D. Bordo, *Structure*, 2003, **11**, 725-734.
58. P. Bhat, S. Shwetha, D. K. Sharma, A. P. Joseph, N. Srinivasan and S. Das, *Nucleic Acids Research*, 2015, **43**, 2888-2901.
59. D. B. Smith and K. S. Johnson, *Gene*, 1988, **67**, 31-40.
60. A. K. Satapathy, A. B. Kochaniak, S. Mukherjee, D. J. Crampton, A. van Oijen and C. C. Richardson, *Proceedings of the National Academy of Sciences*, 2010, **107**, 6782-6787.
61. S.-n. Nishimura, K. Nishida and M. Tanaka, *Chemical Communications*, 2022, **58**, 505-508.
62. P. V. Panteleev, I. A. Bolosov, S. V. Balandin and T. V. Ovchinnikova, *Acta Naturae*, 2015, **7**, 37-47.
63. M. Zasloff, *Nature*, 2002, **415**, 389-395.
64. R. E. W. Hancock and H.-G. Sahl, *Nature Biotechnology*, 2006, **24**, 1551-1557.
65. P. Cardoso, H. Glossop, T. G. Meikle, A. Aburto-Medina, C. E. Conn, V. Sarojini and C. Valery, *Biophysical Reviews*, 2021, **13**, 35-69.
66. J. M. Ahn, K. Kassees, T. K. Lee, B. Manandhar and A. M. Yousif, in *Comprehensive Medicinal Chemistry III*, eds. S. Chackalamannil, D. Rotella and S. E. Ward, Elsevier, Oxford, 2017, DOI: <https://doi.org/10.1016/B978-0-12-409547-2.12413-8>, pp. 66-115.
67. R. L. Fahrner, T. Dieckmann, S. S. L. Harwig, R. I. Lehrer, D. Eisenberg and J. Feigon, *Chemistry & Biology*, 1996, **3**, 543-550.
68. P. J. Loll, E. C. Upton, V. Nahoum, N. J. Economou and S. Cocklin, *Biochimica et biophysica acta*, 2014, **1838**, 1199-1207.
69. J.-P. S. Powers, M. M. Martin, D. L. Goosney and R. E. W. Hancock, *Antimicrobial agents and chemotherapy*, 2006, **50**, 1522-1524.
70. I. Knyght, L. Clifton, Y. Saaka, M. J. Lawrence and D. J. Barlow, *Langmuir*, 2016, **32**, 7403-7410.
71. Y. Huan, Q. Kong, H. Mou and H. Yi, *Frontiers in Microbiology*, 2020, **11**.
72. J. Lei, L. Sun, S. Huang, C. Zhu, P. Li, J. He, V. Mackey, D. H. Coy and Q. He, *Am J Transl Res*, 2019, **11**, 3919-3931.
73. K. A. Brogden, *Nature Reviews Microbiology*, 2005, **3**, 238-250.
74. J. Li, J.-J. Koh, S. Liu, R. Lakshminarayanan, C. S. Verma and R. W. Beuerman, *Frontiers in Neuroscience*, 2017, **11**.
75. T. J. Silhavy, D. Kahne and S. Walker, *Cold Spring Harb Perspect Biol*, 2010, **2**, a000414.
76. Q.-Y. Zhang, Z.-B. Yan, Y.-M. Meng, X.-Y. Hong, G. Shao, J.-J. Ma, X.-R. Cheng, J. Liu, J. Kang and C.-Y. Fu, *Military Medical Research*, 2021, **8**, 48.
77. R. Kundu, *ChemMedChem*, 2020, **15**, 1887-1896.
78. L. Yang, T. A. Harroun, T. M. Weiss, L. Ding and H. W. Huang, *Biophysical Journal*, 2001, **81**, 1475-1485.
79. W. C. Wimley, *ACS Chemical Biology*, 2010, **5**, 905-917.

-
80. S. S. Kale, G. Priya, A. S. Kotmale, R. L. Gawade, V. G. Puranik, P. R. Rajamohanan and G. J. Sanjayan, *Chemical Communications*, 2013, **49**, 2222-2224.
 81. F. He, J. Bao, X. Y. Zhang, Z. C. Tu, Y. M. Shi and S. H. Qi, *J Nat Prod*, 2013, **76**, 1182-1186.
 82. A. J. Cameron, C. J. Squire, P. J. B. Edwards, E. Harjes and V. Sarojini, *Chemistry – An Asian Journal*, 2017, **12**, 3195-3202.
 83. A. J. Cameron, P. J. B. Edwards, E. Harjes and V. Sarojini, *Journal of Medicinal Chemistry*, 2017, **60**, 9565-9574.
 84. A. J. Cameron, K. G. Varnava, P. J. B. Edwards, E. Harjes and V. Sarojini, *Journal of Peptide Science*, 2018, **24**, e3094.
 85. K. G. Varnava, P. J. B. Edwards, A. J. Cameron, E. Harjes and V. Sarojini, *Journal of Peptide Science*, **n/a**, e3291.
 86. H. Schofield, *Journal of Fluorine Chemistry*, 1999, **100**, 7-11.
 87. D. O'Hagan, *Chemical Society Reviews*, 2008, **37**, 308-319.
 88. K. Borzutzki, J. Thienenkamp, M. Diehl, M. Winter and G. Brunklaus, *Journal of Materials Chemistry A*, 2019, **7**, 188-201.
 89. C. V. Amanchukwu, Z. Yu, X. Kong, J. Qin, Y. Cui and Z. Bao, *Journal of the American Chemical Society*, 2020, **142**, 7393-7403.
 90. M. Rautenberg, M. Gernhard, J. Radnik, J. Witt, C. Roth and F. Emmerling, *Frontiers in Chemistry*, 2022, **10**.
 91. C. Sprinz, M. Zanon, S. Altmayer, G. Watte, K. Irion, E. Marchiori and B. Hochegger, *Scientific Reports*, 2018, **8**, 2126.
 92. A. A. Berger, J.-S. Völler, N. Budisa and B. Koksich, *Accounts of Chemical Research*, 2017, **50**, 2093-2103.
 93. B. C. Buer and E. N. G. Marsh, *Protein science : a publication of the Protein Society*, 2012, **21**, 453-462.
 94. J. N. Sloand, M. A. Miller and S. H. Medina, *Peptide Science*, 2021, **113**, e24184.
 95. C. Jäckel and B. Koksich, *European Journal of Organic Chemistry*, 2005, **2005**, 4483-4503.
 96. N. C. Yoder and K. Kumar, *Chemical Society Reviews*, 2002, **31**, 335-341.
 97. J. Bégué and D. Bonnet-Delpon, in *Bioorganic and Medicinal Chemistry of Fluorine*, 2008, DOI: doi:10.1002/9780470281895.ch1, ch. 1, pp. 1-22.
 98. G. A. Patani and E. J. LaVoie, *Chemical Reviews*, 1996, **96**, 3147-3176.
 99. A. Bondi, *The Journal of Physical Chemistry*, 1964, **68**, 441-451.
 100. N. A. Meanwell, *Journal of Medicinal Chemistry*, 2018, **61**, 5822-5880.
 101. B. E. Smart, *Journal of Fluorine Chemistry*, 2001, **109**, 3-11.
 102. H.-J. Böhm, D. Banner, S. Bendels, M. Kansy, B. Kuhn, K. Müller, U. Obst-Sander and M. Stahl, *ChemBioChem*, 2004, **5**, 637-643.
 103. J. D. Dunitz, *ChemBioChem*, 2004, **5**, 614-621.
 104. J. A. K. Howard, V. J. Hoy, D. O'Hagan and G. T. Smith, *Tetrahedron*, 1996, **52**, 12613-12622.
 105. F. Leroux, *ChemBioChem*, 2004, **5**, 644-649.
 106. G. Wuitschik, E. M. Carreira, B. Wagner, H. Fischer, I. Parrilla, F. Schuler, M. Rogers-Evans and K. Müller, *Journal of Medicinal Chemistry*, 2010, **53**, 3227-3246.
 107. Q. A. Huchet, B. Kuhn, B. Wagner, H. Fischer, M. Kansy, D. Zimmerli, E. M. Carreira and K. Müller, *Journal of Fluorine Chemistry*, 2013, **152**, 119-128.
 108. J. C. Biffinger, H. W. Kim and S. G. DiMaggio, *ChemBioChem*, 2004, **5**, 622-627.
 109. I. Zivkovic, J. Moschner, B. Koksich and I. Gruic-Sovulj, *The FEBS Journal*, 2020, **287**, 800-813.

110. M. P. Krafft, *Journal of Polymer Science Part A: Polymer Chemistry*, 2006, **44**, 4251-4258.
111. M. P. Krafft and J. G. Riess, *Journal of Polymer Science Part A: Polymer Chemistry*, 2007, **45**, 1185-1198.
112. T. Song, Y. Gao, M. Song, J. Qian, H. Zhang, J. Zhou and Y. Ding, *Medicine in Drug Discovery*, 2022, **14**, 100123.
113. A. P. Dobbs and M. R. Kimberley, *Journal of Fluorine Chemistry*, 2002, **118**, 3-17.
114. C. A. Moody and J. A. Field, *Environmental Science & Technology*, 2000, **34**, 3864-3870.
115. M. P. Krafft, *Advanced Drug Delivery Reviews*, 2001, **47**, 209-228.
116. D. M. Lemal, *The Journal of Organic Chemistry*, 2004, **69**, 1-11.
117. D. W. Grainger, in *Biomaterials Science (Fourth Edition)*, eds. W. R. Wagner, S. E. Sakiyama-Elbert, G. Zhang and M. J. Yaszemski, Academic Press, 2020, DOI: <https://doi.org/10.1016/B978-0-12-816137-1.00012-X>, pp. 125-138.
118. R. Wang, G. Xu and Y. He, *e-Polymers*, 2017, **17**, 215-220.
119. L. W. McKeen, in *Introduction to Fluoropolymers (Second Edition)*, ed. S. Ebnesajjad, William Andrew Publishing, Oxford, 2021, DOI: <https://doi.org/10.1016/B978-0-12-819123-1.00019-7>, pp. 339-367.
120. V. F. Cardoso, D. M. Correia, C. Ribeiro, M. M. Fernandes and S. Lanceros-Méndez, *Polymers*, 2018, **10**, 161.
121. A. Wemhöner, I. Hackspiel, N. Hobi, A. Ravasio, T. Haller and M. Rüdiger, *Respiratory Research*, 2010, **11**, 52.
122. Z. Zhang, W. Shen, J. Ling, Y. Yan, J. Hu and Y. Cheng, *Nature Communications*, 2018, **9**, 1377.
123. A. Studer, S. Hadida, R. Ferritto, S.-Y. Kim, P. Jeger, P. Wipf and D. P. Curran, *Science*, 1997, **275**, 823-826.
124. C. C. Tzschucke, C. Markert, W. Bannwarth, S. Roller, A. Hebel and R. Haag, *Angewandte Chemie International Edition*, 2002, **41**, 3964-4000.
125. Z. Luo, Q. Zhang, Y. Oderaotoshi and D. P. Curran, *Science*, 2001, **291**, 1766-1769.
126. W. Zhang and D. P. Curran, *Tetrahedron*, 2006, **62**, 11837-11865.
127. K.-S. Ko, F. A. Jaipuri and N. L. Pohl, *Journal of the American Chemical Society*, 2005, **127**, 13162-13163.
128. F. A. Jaipuri and N. L. Pohl, *Organic & Biomolecular Chemistry*, 2008, **6**, 2686-2691.
129. M. Mizuno, K. Goto, T. Miura, D. Hosaka and T. Inazu, *Chemical Communications*, 2003, DOI: 10.1039/B300682D, 972-973.
130. M. Mizuno, K. Goto, T. Miura, T. Matsuura and T. Inazu, *Tetrahedron Letters*, 2004, **45**, 3425-3428.
131. A. G. W. Cameron, *Space Science Reviews*, 1973, **15**, 121-146.
132. N. Budisa, V. Kubyshkin and D. Schulze-Makuch, *Life*, 2014, **4**, 374-385.
133. D. O'Hagan, C. Schaffrath, S. L. Cobb, J. T. G. Hamilton and C. D. Murphy, *Nature*, 2002, **416**, 279-279.
134. K. Müller, C. Faeh and F. Diederich, *Science*, 2007, **317**, 1881-1886.
135. D. B. Harper and D. O'Hagan, *Natural Product Reports*, 1994, **11**, 123-133.
136. J. Moschner, A. A. Berger and B. Kocsch, in *The Curious World of Fluorinated Molecules*, ed. K. Seppelt, Elsevier, 2021, vol. 6, pp. 277-294.
137. W. R. Dolbier, *Journal of Fluorine Chemistry*, 2005, **126**, 157-163.
138. D. B. Harper, D. O'Hagan and C. D. Murphy, in *Natural Production of Organohalogen Compounds*, ed. G. Gribble, Springer Berlin Heidelberg, Berlin, Heidelberg, 2003, DOI: 10.1007/b10454, pp. 141-169.

139. N. V. Goncharov, R. O. Jenkins and A. S. Radilov, *Journal of Applied Toxicology*, 2006, **26**, 148-161.
140. M. Sanada, T. Miyano, S. Iwadare, J. M. Williamson, B. H. Arison, J. L. Smith, A. W. Douglas, J. M. Liesch and E. Inamine, *J Antibiot (Tokyo)*, 1986, **39**, 259-265.
141. S. Potenti, L. Spada, M. Fusè, G. Mancini, A. Gualandi, C. Leonardi, P. G. Cozzi, C. Puzzarini and V. Barone, *ACS Omega*, 2021, **6**, 13170-13181.
142. C. D. Murphy, D. O'Hagan and C. Schaffrath, *Angewandte Chemie International Edition*, 2001, **40**, 4479-4481.
143. C. D. Murphy, C. Schaffrath and D. O'Hagan, *Chemosphere*, 2003, **52**, 455-461.
144. P. F. V. Ward, R. J. Hall and R. A. Peters, *Nature*, 1964, **201**, 611-612.
145. J. T. G. Hamilton and D. B. Harper, *Phytochemistry*, 1997, **44**, 1129-1132.
146. X. M. Zhu, S. Hackl, M. N. Thaker, L. Kalan, C. Weber, D. S. Urgast, E. M. Krupp, A. Brewer, S. Vanner, A. Szawiola, G. Yim, J. Feldmann, A. Bechthold, G. D. Wright and D. L. Zechel, *ChemBioChem*, 2015, **16**, 2498-2506.
147. E. P. Gillis, K. J. Eastman, M. D. Hill, D. J. Donnelly and N. A. Meanwell, *Journal of Medicinal Chemistry*, 2015, **58**, 8315-8359.
148. B. M. Johnson, Y.-Z. Shu, X. Zhuo and N. A. Meanwell, *Journal of Medicinal Chemistry*, 2020, **63**, 6315-6386.
149. M. Inoue, Y. Sumii and N. Shibata, *ACS Omega*, 2020, **5**, 10633-10640.
150. H. Mei, J. Han, K. D. Klika, K. Izawa, T. Sato, N. A. Meanwell and V. A. Soloshonok, *European Journal of Medicinal Chemistry*, 2020, **186**, 111826.
151. H. Rosenbrock, C. Dorner-Ciossek, R. Giovannini, B. Schmid and N. Schuelert, *Journal of Pharmacology and Experimental Therapeutics*, 2022, **382**, 223-232.
152. E. J. Gane, H. J. Kim, K. Visvanathan, Y. J. Kim, A.-H. Nguyen, J. J. Wallin, D. Y. Chen, C. McDonald, P. Arora, S. K. Tan, A. Gaggar, S. K. Roberts and Y.-S. Lim, *Hepatology*, 2021, **74**, 1737-1749.
153. D. R. Owen, C. M. N. Allerton, A. S. Anderson, L. Aschenbrenner, M. Avery, S. Berritt, B. Boras, R. D. Cardin, A. Carlo, K. J. Coffman, A. Dantonio, L. Di, H. Eng, R. Ferre, K. S. Gajiwala, S. A. Gibson, S. E. Greasley, B. L. Hurst, E. P. Kadar, A. S. Kalgutkar, J. C. Lee, J. Lee, W. Liu, S. W. Mason, S. Noell, J. J. Novak, R. S. Obach, K. Ogilvie, N. C. Patel, M. Pettersson, D. K. Rai, M. R. Reese, M. F. Sammons, J. G. Sathish, R. S. P. Singh, C. M. Steppan, A. E. Stewart, J. B. Tuttle, L. Updyke, P. R. Verhoest, L. Wei, Q. Yang and Y. Zhu, *Science*, 2021, **374**, 1586-1593.
154. S. Purser, P. R. Moore, S. Swallow and V. Gouverneur, *Chemical Society Reviews*, 2008, **37**, 320-330.
155. P. Shah and A. D. Westwell, *Journal of Enzyme Inhibition and Medicinal Chemistry*, 2007, **22**, 527-540.
156. C. Bokemeyer, A. Gerl, P. Schöffski, A. Harstrick, N. Niederle, J. Beyer, J. Casper, H. J. Schmoll and L. Kanz, *J Clin Oncol*, 1999, **17**, 512-516.
157. A. Selyutina, P. Hu, S. Miller, L. M. Simons, H. J. Yu, J. F. Hultquist, K. Lee, V. N. KewalRamani and F. Diaz-Griffero, *iScience*, 2022, **25**, 103593.
158. J. A. Olsen, D. W. Banner, P. Seiler, B. Wagner, T. Tschopp, U. Obst-Sander, M. Kansy, K. Müller and F. Diederich, *ChemBioChem*, 2004, **5**, 666-675.
159. Y. N. Lamb, *Drugs*, 2022, **82**, 585-591.
160. A. Buchanan and J. D. Revell, in *Novel Approaches and Strategies for Biologics, Vaccines and Cancer Therapies*, eds. M. Singh and M. Salnikova, Academic Press, San Diego, 2015, DOI: <https://doi.org/10.1016/B978-0-12-416603-5.00008-0>, pp. 171-197.
161. Q. Wang, J. Han, A. Sorochinsky, A. Landa, G. Butler and V. A. Soloshonok, *Pharmaceuticals*, 2022, **15**, 999.

162. A. Sutherland and C. L. Willis, *Natural Product Reports*, 2000, **17**, 621-631.
163. L. F. Awad and M. S. Ayoup, *Beilstein journal of organic chemistry*, 2020, **16**, 1022-1050.
164. C. Carlier, S. Strese, K. Viktorsson, E. Velander, P. Nygren, M. Uustalu, T. Juntti, R. Lewensohn, R. Larsson, J. Spira, E. De Vlieghere, W. P. Ceelen and J. Gullbo, *Oncotarget*, 2016, **7**.
165. T. Olivier and V. Prasad, *Translational Oncology*, 2022, **18**, 101374.
166. H. R. Hoveyda, E. Marsault, R. Gagnon, A. P. Mathieu, M. Vézina, A. Landry, Z. Wang, K. Benakli, S. Beaubien, C. Saint-Louis, M. Brassard, J.-F. Pinault, L. Ouellet, S. Bhat, M. Ramaseshan, X. Peng, L. Foucher, S. Beauchemin, P. Bhérier, D. F. Veber, M. L. Peterson and G. L. Fraser, *Journal of Medicinal Chemistry*, 2011, **54**, 8305-8320.
167. J. James, S. Mair, W. Doll, E. Sandefer, D. Wurtman, A. Maurer, A. M. Deane and M. S. Harris, *Neurogastroenterol Motil*, 2020, **32**, e13784.
168. F. Narjes, K. F. Koehler, U. Koch, B. Gerlach, S. Colarusso, C. Steinkühler, M. Brunetti, S. Altamura, R. De Francesco and V. G. Matassa, *Bioorg Med Chem Lett*, 2002, **12**, 701-704.
169. R. Lohmann, I. T. Cousins, J. C. DeWitt, J. Glüge, G. Goldenman, D. Herzke, A. B. Lindstrom, M. F. Miller, C. A. Ng, S. Patton, M. Scheringer, X. Trier and Z. Wang, *Environmental Science & Technology*, 2020, **54**, 12820-12828.
170. J. Lv and Y. Cheng, *Chemical Society Reviews*, 2021, **50**, 5435-5467.
171. V. Ochoa-Herrera, J. A. Field, A. Luna-Velasco and R. Sierra-Alvarez, *Environmental Science: Processes & Impacts*, 2016, **18**, 1236-1246.
172. P. Goldman, *Journal of Biological Chemistry*, 1965, **240**, 3434-3438.
173. C. D. Murphy, *Biotechnology Letters*, 2010, **32**, 351-359.
174. J.-Q. Liu, T. Kurihara, S. Ichiyama, M. Miyagi, S. Tsunasawa, H. Kawasaki, K. Soda and N. Esaki, *Journal of Biological Chemistry*, 1998, **273**, 30897-30902.
175. L. Q. Tu, P. F. A. Wright, C. J. Rix and J. T. Ahokas, *Comparative Biochemistry and Physiology Part C: Toxicology & Pharmacology*, 2006, **143**, 59-66.
176. C. Donnelly and C. D. Murphy, *Applied Microbiology and Biotechnology*, 2007, **77**, 699-703.
177. N. K. O'Connor, D. K. Rai, B. R. Clark and C. D. Murphy, *Journal of Fluorine Chemistry*, 2012, **143**, 210-215.
178. L. P. Wackett, *Microbial Biotechnology*, 2022, **15**, 773-792.
179. Y. H. Zhao, M. H. Abraham and A. M. Zissimos, *The Journal of Organic Chemistry*, 2003, **68**, 7368-7373.
180. S. A. Samsonov, M. Salwiczek, G. Anders, B. Kokschi and M. T. Pisabarro, *The Journal of Physical Chemistry B*, 2009, **113**, 16400-16408.
181. M. Salwiczek, S. Samsonov, T. Vagt, E. Nyakatura, E. Fleige, J. Numata, H. Cölfen, M. T. Pisabarro and B. Kokschi, *Chemistry – A European Journal*, 2009, **15**, 7628-7636.
182. U. I. M. Gerling, M. Salwiczek, C. D. Cadicamo, H. Erdbrink, C. Czekelius, S. L. Grage, P. Wadhvani, A. S. Ulrich, M. Behrends, G. Haufe and B. Kokschi, *Chemical Science*, 2014, **5**, 819-830.
183. S. Chowdhary, J. Moschner, D. J. Mikolajczak, M. Becker, A. F. Thünemann, C. Kästner, D. Klemczak, A.-K. Stegemann, C. Böttcher, P. Metrangolo, R. R. Netz and B. Kokschi, *ChemBioChem*, 2020, **21**, 3544-3554.
184. B. Bilgiçer, A. Fichera and K. Kumar, *Journal of the American Chemical Society*, 2001, **123**, 4393-4399.
185. T. Gallagher, P. Alexander, P. Bryan and G. L. Gilliland, *Biochemistry*, 1994, **33**, 4721-4729.

-
186. H.-P. Chiu, B. Kokona, R. Fairman and R. P. Cheng, *Journal of the American Chemical Society*, 2009, **131**, 13192-13193.
187. A. Kapurniotu, *BIOspektrum*, 2012, **18**, 734-736.
188. S. Ye, B. Loll, A. A. Berger, U. Mülow, C. Alings, M. C. Wahl and B. Kokschi, *Chemical Science*, 2015, **6**, 5246-5254.
189. J. Leppkes, N. Dimos, B. Loll, T. Hohmann, M. Dyrks, A. Wieseke, B. G. Keller and B. Kokschi, *RSC Chemical Biology*, 2022, **3**, 773-782.
190. J. R. Robalo, S. Huhmann, B. Kokschi and A. Vila Verde, *Chem*, 2017, **3**, 881-897.
191. J. R. Robalo and A. Vila Verde, *Physical Chemistry Chemical Physics*, 2019, **21**, 2029-2038.
192. J. Moschner, V. Stulberg, R. Fernandes, S. Huhmann, J. Leppkes and B. Kokschi, *Chemical Reviews*, 2019, **119**, 10718-10801.
193. J. Leppkes, T. Hohmann and B. Kokschi, *Journal of Fluorine Chemistry*, 2020, **232**, 109453.
194. D. Winkler and K. Burger, *Synthesis*, 1996, **1996**, 1419-1421.
195. T. Tsushima, K. Kawada, S. Ishihara, N. Uchida, O. Shiratori, J. Higaki and M. Hirata, *Tetrahedron*, 1988, **44**, 5375-5387.
196. A. E. Sorochinsky, H. Ueki, J. L. Aceña, T. K. Ellis, H. Moriwaki, T. Sato and V. A. Soloshonok, *Journal of Fluorine Chemistry*, 2013, **152**, 114-118.
197. T. T. Romoff, A. B. Palmer, N. Mansour, C. J. Creighton, T. Miwa, Y. Ejima, H. Moriwaki and V. A. Soloshonok, *Organic Process Research & Development*, 2017, **21**, 732-739.
198. J. Han, R. Takeda, X. Liu, H. Konno, H. Abe, T. Hiramatsu, H. Moriwaki and V. A. Soloshonok, *Molecules (Basel, Switzerland)*, 2019, **24**, 4521.
199. H. Mei, T. Hiramatsu, R. Takeda, H. Moriwaki, H. Abe, J. Han and V. A. Soloshonok, *Organic Process Research & Development*, 2019, **23**, 629-634.
200. S. Zhou, J. Wang, X. Chen, J. L. Aceña, V. A. Soloshonok and H. Liu, 2014, **53**, 7883-7886.
201. Y. Nian, J. Wang, H. Moriwaki, V. A. Soloshonok and H. Liu, *Dalton Transactions*, 2017, **46**, 4191-4198.
202. T. Hohmann, M. Dyrks, S. Chowdhary, M. Weber, D. Nguyen, J. Moschner and B. Kokschi, *The Journal of Organic Chemistry*, 2022, **87**, 10592-10604.
203. J. M. Monkovic, H. Gibson, J. W. Sun and J. K. Montclare, *Pharmaceuticals*, 2022, **15**, 1201.
204. D. M. Ryan, S. B. Anderson, F. T. Senguen, R. E. Youngman and B. L. Nilsson, *Soft Matter*, 2010, **6**, 475-479.
205. D. M. Ryan, S. B. Anderson and B. L. Nilsson, *Soft Matter*, 2010, **6**, 3220-3231.
206. C. J. Bowerman, W. Liyanage, A. J. Federation and B. L. Nilsson, *Biomacromolecules*, 2011, **12**, 2735-2745.
207. W. Liyanage and B. L. Nilsson, *Langmuir*, 2016, **32**, 787-799.
208. D. M. Raymond, B. L. Abraham, T. Fujita, M. J. Watrous, E. S. Toriki, T. Takano and B. L. Nilsson, *ACS Applied Bio Materials*, 2019, **2**, 2116-2124.
209. B. L. Abraham, S. G. Mensah, B. R. Gwinnell and B. L. Nilsson, *Soft Matter*, 2022, **18**, 5999-6008.
210. S. M. Hsu, Y. C. Lin, J. W. Chang, Y. H. Liu and H. C. Lin, *Angew Chem Int Ed Engl*, 2014, **53**, 1921-1927.
211. S.-M. Hsu, F.-Y. Wu, T.-S. Lai, Y.-C. Lin and H.-C. Lin, *RSC Advances*, 2015, **5**, 22943-22946.
212. F.-Y. Wu, S.-M. Hsu, H. Cheng, L.-H. Hsu and H.-C. Lin, *New Journal of Chemistry*, 2015, **39**, 4240-4243.
-

213. M. Mohammed, R. D. Chakravarthy and H.-C. Lin, *Molecular Systems Design & Engineering*, 2022, **7**, 1336-1343.
214. E. N. G. Marsh, B. C. Buer and A. Ramamoorthy, *Molecular BioSystems*, 2009, **5**, 1143-1147.
215. D. Giménez, C. Andreu, M. I. d. Olmo, T. Varea, D. Diaz and G. Asensio, *Bioorganic & Medicinal Chemistry*, 2006, **14**, 6971-6978.
216. L. M. Gottler, H. Y. Lee, C. E. Shelburne, A. Ramamoorthy and E. N. Marsh, *Chembiochem*, 2008, **9**, 370-373.
217. L. M. Gottler, R. de la Salud Bea, C. E. Shelburne, A. Ramamoorthy and E. N. G. Marsh, *Biochemistry*, 2008, **47**, 9243-9250.
218. H. Meng and K. Kumar, *Journal of the American Chemical Society*, 2007, **129**, 15615-15622.
219. S. C. Setty, S. Horam, M. Pasupuleti and W. Haq, *International Journal of Peptide Research and Therapeutics*, 2017, **23**, 213-225.
220. H. D. Glossop, G. H. De Zoysa, L. I. Pilkington, D. Barker and V. Sarojini, *Journal of Fluorine Chemistry*, 2021, **241**, 109685.
221. D. Chow, M. L. Nunalee, D. W. Lim, A. J. Simnick and A. Chilkoti, *Mater Sci Eng R Rep*, 2008, **62**, 125-155.
222. I. Schechter and A. Berger, *Biochemical and Biophysical Research Communications*, 1967, **27**, 157-162.
223. I. Schechter and A. Berger, *Biochem Biophys Res Commun*, 1968, **32**, 898-902.
224. F. J. Gisdon, E. Bombarda and G. M. Ullmann, *The Journal of Physical Chemistry B*, 2022, **126**, 4035-4048.
225. L. Hedstrom, *Chemical Reviews*, 2002, **102**, 4501-4524.
226. S. H. Hung and L. Hedstrom, *Protein Eng*, 1998, **11**, 669-673.
227. V. Schellenberger, U. Schellenberger, Y. V. Mitin and H. D. Jakubke, *Eur J Biochem*, 1990, **187**, 163-167.
228. V. Schellenberger, C. W. Turck and W. J. Rutter, *Biochemistry*, 1994, **33**, 4251-4257.
229. R. J. Swanekamp, J. J. Welch and B. L. Nilsson, *Chemical Communications*, 2014, **50**, 10133-10136.
230. J. Mangelschots, M. Bibian, J. Gardiner, L. Waddington, Y. Van Wanseele, A. Van Eeckhaut, M. M. D. Acevedo, B. Van Mele, A. Madder, R. Hoogenboom and S. Ballet, *Biomacromolecules*, 2016, **17**, 437-445.
231. Z. Lai, X. Yuan, H. Chen, Y. Zhu, N. Dong and A. Shan, *Biotechnology Advances*, 2022, **59**, 107962.
232. S. Huhmann and B. Koksich, *European Journal of Organic Chemistry*, 2018, **2018**, 3667-3679.
233. B. Koksich, N. Sewald, H.-J. Hofmann, K. Burger and H.-D. Jakubke, *Journal of Peptide Science*, 1997, **3**, 157-167.
234. R. Smits and B. Koksich, *Current topics in medicinal chemistry*, 2006, **6**, 1483-1498.
235. V. Asante, J. Mortier, H. Schlüter and B. Koksich, *Bioorganic & Medicinal Chemistry*, 2013, **21**, 3542-3546.
236. V. Asante, J. Mortier, G. Wolber and B. Koksich, *Amino Acids*, 2014, **46**, 2733-2744.
237. S. Huhmann, A. K. Stegemann, K. Folmert, D. Klemczak, J. Moschner, M. Kube and B. Koksich, *Beilstein J Org Chem*, 2017, **13**, 2869-2882.
238. S. Chowdhary, R. F. Schmidt, A. K. Sahoo, T. tom Dieck, T. Hohmann, B. Schade, K. Brademann-Jock, A. F. Thünemann, R. R. Netz, M. Gradzielski and B. Koksich, *Nanoscale*, 2022, **14**, 10176-10189.
239. T. J. Measey, R. Schweitzer-Stenner, V. Sa and K. Kornev, *Macromolecules*, 2010, **43**, 7800-7806.

-
240. S. Chowdhary, T. Pelzer, M. Saathoff, E. Quaas, J. Pendl, M. Fulde and B. Kokschi, *Peptide Science*, **n/a**, e24306.
 241. X. Bi, C. Wang, W. Dong, W. Zhu and D. Shang, *The Journal of Antibiotics*, 2014, **67**, 361-368.
 242. T. Hohmann, S. Chowdhary, K. Ataka, J. Er, G. H. Dreyhsig, J. Heberle and B. Kokschi, *Chemistry – A European Journal*, **n/a**, e202203860.
 243. J. L. Lopes, A. J. Miles, L. Whitmore and B. A. Wallace, *Protein Sci*, 2014, **23**, 1765-1772.
 244. T. J. Measey and R. Schweitzer-Stenner, *Journal of the American Chemical Society*, 2006, **128**, 13324-13325.
 245. S. Z. Sudo and M. Dworkin, in *Advances in Microbial Physiology*, eds. A. H. Rose and D. W. Tempest, Academic Press, 1973, vol. 9, pp. 153-224.
 246. M. D. Bygd, K. G. Aukema, J. E. Richman and L. P. Wackett, *Applied and Environmental Microbiology*, 2022, **88**, e00288-00222.
 247. L. Cai, X. Qin, Z. Xu, Y. Song, H. Jiang, Y. Wu, H. Ruan and J. Chen, *ACS omega*, 2019, **4**, 12036-12042.
 248. C. Wu, Z. Zheng, Y. Guo, C. Tian, Q. Xue and G. Liang, *Nanoscale*, 2017, **9**, 11429-11433.
 249. M. F. Khan and C. D. Murphy, *Applied Microbiology and Biotechnology*, 2021, **105**, 9359-9369.
 250. C. K. Thota, A. A. Berger, B. Harms, M. Seidel, C. Böttcher, H. von Berlepsch, C. Xie, R. Süßmuth, C. Roth and B. Kokschi, *Peptide Science*, 2020, **112**, e24130.
 251. J. Liang, W.-L. Wu, X.-D. Xu, R.-X. Zhuo and X.-Z. Zhang, *Colloids and Surfaces B: Biointerfaces*, 2014, **114**, 398-403.